TENASCINS: KEY PLAYERS IN TISSUE HOMEOSTASIS AND DEFENSE

EDITED BY: Kim Midwood, Gertraud Orend and Kyoko Imanaka-Yoshida
PUBLISHED IN: Frontiers in Immunology

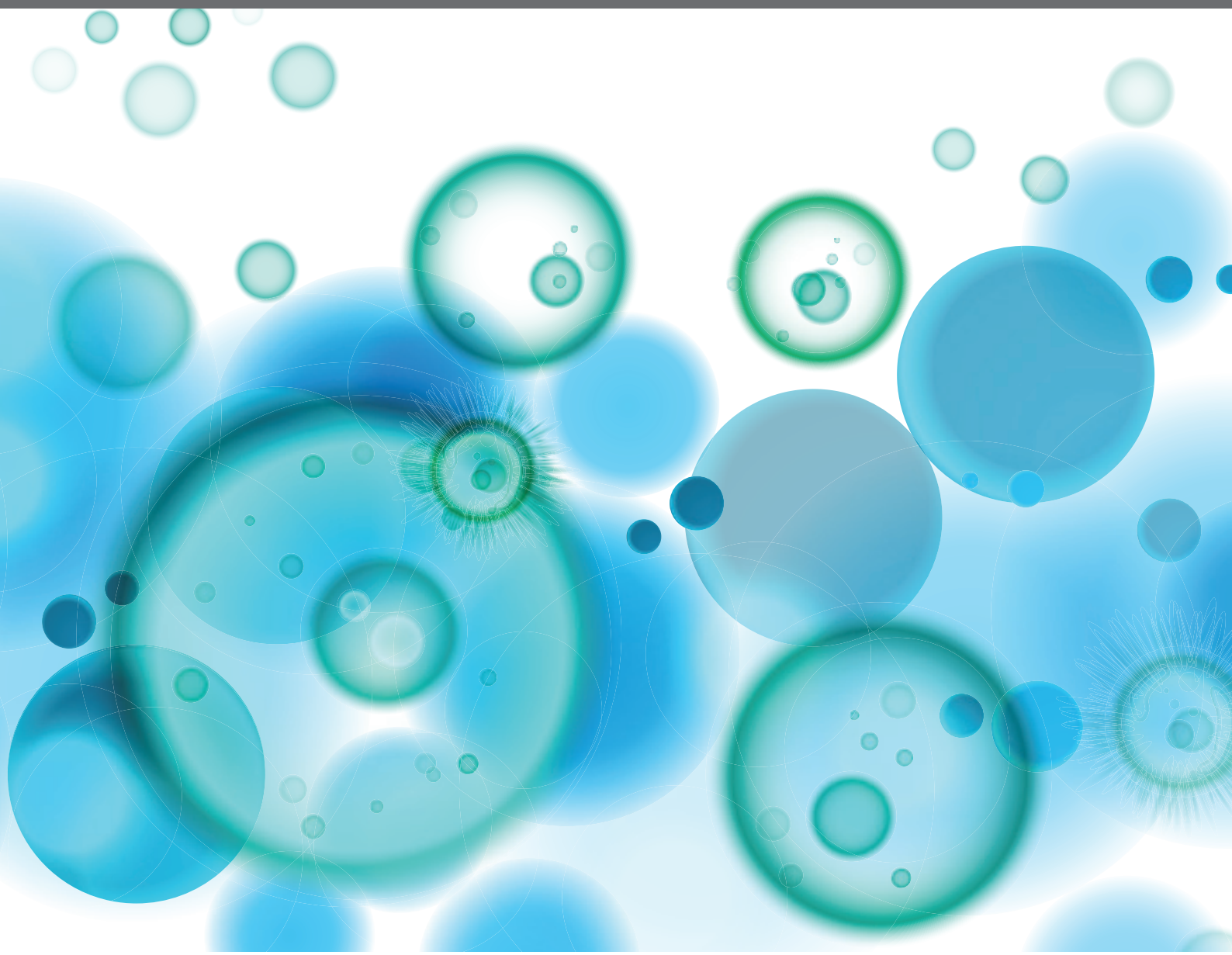

frontiers Research Topics

frontiers

ISSN 1664-8714
ISBN 978-2-88974-430-5
DOI 10.3389/978-2-88974-430-5

About Frontiers

Frontiers is more than just an open-access publisher of scholarly articles: it is a pioneering approach to the world of academia, radically improving the way scholarly research is managed. The grand vision of Frontiers is a world where all people have an equal opportunity to seek, share and generate knowledge. Frontiers provides immediate and permanent online open access to all its publications, but this alone is not enough to realize our grand goals.

Frontiers Journal Series

The Frontiers Journal Series is a multi-tier and interdisciplinary set of open-access, online journals, promising a paradigm shift from the current review, selection and dissemination processes in academic publishing. All Frontiers journals are driven by researchers for researchers; therefore, they constitute a service to the scholarly community. At the same time, the Frontiers Journal Series operates on a revolutionary invention, the tiered publishing system, initially addressing specific communities of scholars, and gradually climbing up to broader public understanding, thus serving the interests of the lay society, too.

Dedication to Quality

Each Frontiers article is a landmark of the highest quality, thanks to genuinely collaborative interactions between authors and review editors, who include some of the world's best academicians. Research must be certified by peers before entering a stream of knowledge that may eventually reach the public - and shape society; therefore, Frontiers only applies the most rigorous and unbiased reviews.
Frontiers revolutionizes research publishing by freely delivering the most outstanding research, evaluated with no bias from both the academic and social point of view. By applying the most advanced information technologies, Frontiers is catapulting scholarly publishing into a new generation.

What are Frontiers Research Topics?

Frontiers Research Topics are very popular trademarks of the Frontiers Journals Series: they are collections of at least ten articles, all centered on a particular subject. With their unique mix of varied contributions from Original Research to Review Articles, Frontiers Research Topics unify the most influential researchers, the latest key findings and historical advances in a hot research area! Find out more on how to host your own Frontiers Research Topic or contribute to one as an author by contacting the Frontiers Editorial Office: frontiersin.org/about/contact

TENASCINS: KEY PLAYERS IN TISSUE HOMEOSTASIS AND DEFENSE

Topic Editors:
Kim Midwood, University of Oxford, United Kingdom
Gertraud Orend, INSERM Immuno Rhumatologie Moléculaire (IRM), France
Kyoko Imanaka-Yoshida, Mie University, Japan

Citation: Midwood, K., Orend, G., Imanaka-Yoshida, K., eds. (2022). Tenascins: Key Players in Tissue Homeostasis and Defense. Lausanne: Frontiers Media SA.
doi: 10.3389/978-2-88974-430-5

Table of Contents

frontiers in Immunology

EDITORIAL
published: 12 January 2022
doi: 10.3389/fimmu.2021.834353

Editorial: Tenascins – Key Players in Tissue Homeostasis and Defense

Kyoko Imanaka Yoshida[1*†], *Kim S. Midwood*[2*†] *and Gertraud Orend*[3*†]

[1] Department of Pathology and Matrix Biology, Mie University Graduate School of Medicine, Tsu, Japan, [2] Kennedy Institute of Rheumatology, University of Oxford, Oxford, United Kingdom, [3] University Strasbourg, INSERM U1109, The Tumor Microenvironment Laboratory, Hôpital Civil, Institut d'Hématologie et d'Immunologie, Fédération de Médecine Translationnelle de Strasbourg (FMTS), 1 Place de l'Hopital, Strasbourg, France

Keywords: tenascins, extracellular matrix, inflammation, infection, cancer, fibrosis, tissue homeostasis, defense

Editorial on the Research Topic

Tenascins: Key Players in Tissue Homeostasis and Defense

OPEN ACCESS

Edited and reviewed by:
Pietro Ghezzi,
Brighton and Sussex Medical School, United Kingdom

***Correspondence:**
Kyoko Imanaka Yoshida
imanaka@med.mie-u.ac.jp
Kim S. Midwood
kim.midwood@kennedy.ox.ac.uk
Gertraud Orend
gertraud.orend@inserm.fr

[†]These authors have contributed equally to this work

Specialty section:
This article was submitted to Inflammation, a section of the journal Frontiers in Immunology

Received: *13 December 2021*
Accepted: *20 December 2021*
Published: *12 January 2022*

Citation:
Yoshida KI, Midwood KS and Orend G (2022) Editorial: Tenascins – Key Players in Tissue Homeostasis and Defense. Front. Immunol. 12:834353. doi: 10.3389/fimmu.2021.834353

Tenascin-C, -R, -X and -W are the four members of a family of large, multimodular, extracellular matrix molecules. By virtue of a large repertoire of binding partners, including other matrix molecules, soluble factors, and cell surface receptors, tenascins are key regulators of both tissue architecture and cell phenotype. This Research Topic looks back over the discovery of these matrix molecules over 40 years ago and highlight how our understanding of tenascin-related biology, and pathology, has exponentially progressed over this time. This issue also addressed how these molecules are being exploited for use in the diagnosis and treatment of inflammatory and fibrotic diseases, and cancer, in the context of immune checkpoint therapy and beyond.

One may ask for the justification of a Research Topic on *"Tenascins: Key Players in Tissue Homeostasis and Defense" in "Frontiers in Immunology"*. It has been some time now since the extracellular matrix has been considered merely an inert static mass of molecules that exists only to provide cells with support and stability. More recently has come the understanding of the key role that the matrix plays in general in directly controlling immune responses. In particular, the role of the tenascin family in actively communicating with cells to maintain tissue homeostasis, to signal perturbations in homeostasis and to orchestrate inflammatory and repair programmes to eliminate threat and restore homeostasis, is becoming ever more evident. Each tenascin family member exhibits a specifically restricted, largely non-overlapping, pattern of expression that is tightly controlled in healthy tissues, helping to create distinct microenvironmental niches that program localized cell behavior, for example in stem cell niches, in areas of high mechanical load, in connective tissue and in the perineural nets. The expression of these molecules is transiently upregulated in response to cellular stress and tissue injury, where they each play diverse roles in activating immune responses designed to restore homeostasis. However, misregulated expression of these molecules is associated with aberrant inflammation in inflammatory, fibrotic, and metabolic diseases, and cancer.

This Research Topic of 22 papers comprises 13 review articles and 9 original articles, co-authored by over 100 researchers in the field, that elaborate on both the history and the current state of the art in the fascinating story of the tenascins in the immune context. Indeed, the story actually starts a long way back in time. In this issue, Orend and Tucker showed that the first family member linked to a role in inflammation, tenascin-C (TNC) coevolved with adaptive immunity, and identify a "tool kit" used in cells regulating immunity and interacting with TNC. This raises the question

whether the presence and conservation of TNC amongst vertebrates may be explained by its important role in immunity. There is an ever expanding literature on the mechanisms underpinning TNC-mediated inflammation following its identification as a damage associated molecular pattern (DAMP) that drives toll-like receptor 4 activation in 2009 (1). Topically, it is also of interest to mention that binding of TNC to HIV has been shown to facilitate viral neutralization, identifying how milk from breast feeding mothers can protect their infants from infection (2). Moreover, TNC was recently found to be elevated in COVID19 patients, specifically those with severe symptoms (3), thus opening opportunities to examine a novel role for TNC in immunity upon viral infection.

We are delighted that in this issue, in 5 short reviews, researchers who were amongst those center stage in the discoveries of the respective tenascin family members set out their views on the early days of tenascin work. These historical perspectives are written by Sakakura and Chiquet (TNC), Rathjen and Hodge (TNR), Miller (TNX) and Degen et al.

This glance into the past, at the very beginning of our examination of the extracellular matrix, reveals the discovery of TNC, the first tenascin family member to emerge, and also the first matrix molecule to be sequenced. TNC was named after its presence in developing (nascent) tissues and at places with physical tension (tendons). Depending on its discovery it received different names such as GMEM (glial mesenchymal extracellular matrix, 1983) by Boudon and collaborators (4), "myotendinous antigen" (1984) by Chiquet and colleagues (5), "hexabrachion" (1984) by Erickson and Ingelsias (6), "Cytotactin" (1985) by Grumet and colleagues (7), before R. Chiquet-Ehrismann coined the term tenascin (1986) (8), that then turned into tenascin-C (1993) (9). The smallest family member, TNR, was first identified in the late 1980s as an axonal associated molecule, and was called restrictin by Rathjen and colleaugues, due to its very specific localization not only within the CNS and spinal cord but also its expression pattern in discrete niches of the neural system (10) or J1-160/180 by Schachner and colleagues (5, 11). The discovery of TNX in the late 1980s occurred entirely by serendipity by investigators hunting for the gene that causes congential adrenal hyperplasia. This was eventually mapped to the *CYP21A2* gene, encoding steroid 21-hydroxylase, but which locus was overlapped by an unknown gene, gene X (12). Upon comparison with existing TNC cDNA sequences, gene X soon became tenascin-X, and its archetypal domain organization and oligomerization established, alongside a key role in dermal collagen organization, and beyond. With unification across these three molecules, and phylogenetic confirmation of tenascin-Y as the chicken homolog of tenascin-X, this triad of the tenascin family was born (13). It was not until 1998, that the baby of the family, TNW, came along. Often cited as the least understood tenascin, TNW was identified and eponymously named by Weber and colleagues using a Zebra fish cDNA library to screen for tenascin related molecules (14), with the mammalian homolog, named TNN, identified in mice by Niehardt et al. in 2003 (15). Confusion, likely caused by different numbers of alternatively spliced domains in TNW and TNN, and lack of consensus around the expression of this molecule made this a difficult birth, and still to date little is known about the biological role of TNW, making it arguably the most intriguing family member.

These perspectives also touch on the generation of the first tenascin knockout animals; key tools in the field, but with an interesting history. For example, the TNC knockout mouse was generated 3 times independently (16–18) as it was hard to reconcile how these animals could be viable and apparently healthy. Although it was clearly shown that tenascins-C, R and W play a role in tissue development and homeostasis (although this is still insufficiently understood) they became more "famous" for the roles they adopted when expressed during disease, rather than in healthy tissue. Knockout mice for each tenascin alone or even in combination (triple knockout for TNC, TNW and TNR (19)) are viable and overtly normal. However closer inspection of both mouse and man revealed that these molecules are not entirely indispensable. For example, deficiency of TNX, and point mutations in TNR and TNC are associated with diseases such as the Ehlers Danlos syndrome (TNX) (20) and neurological aberrations (TNR) (21) and hearing loss and tendinopathy (TNC) (22, 23).

Despite these examples, it is remarkable that the sequence of all tenascins is highly conserved amongst vertebrates suggesting a selection pressure for their maintenance which is not understood at all. In tenascin knockout conditions the different responses to the loss of the respective tenascin protein raises questions about potential compensatory mechanisms. In most knockout mice the respective protein is missing due to deletion of an exon, however most of the remaining mRNA is still expressed. It is intriguing to speculate that the remaining mRNA may have an impact on miR and long non coding (lnc) RNA networks as recently shown for the lncRNA ET20 that plays a role in EMT and was induced by TGFβ. The authors discovered that the ET20 locus is located within the TNC locus in antisense orientation and that ablation of ET20 inhibited TNC expression and TNC-induced EMT (24), altogether opening a new view on how results from knockout mice can be interpreted. It will be important to consider the methodology of tenascin family gene manipulation going forward, and indeed these data may help to interpret other *in vivo* studies.

Here, for the first time, the phenotype of the TNW/TNN knockout mouse is presented. This mouse shows an aberrant tooth (incisor) developmental phenotype amongst other deficits, described by Imhof et al. TNN/TNW deficiency affects periodontal remodeling and increases nerve fiber branching *via* sonic hedghog signaling, presumably increasing pain that led to reduced food intake and lower body weight. In contrast to knockout generation, in this Research Topic, Hendaoui et al. showed over expression of TNW in extrahepatic cancers of the billiary system and propose high expression TNW as potential means to detect this type of cancer earlier that stays too long asymptomatic showing already metastasis at the time of diagnosis. Moreover, in this Research Topic, new insights into the role of TNC are reviewed, including in joint disease (Hasegawa et al.), myocarditis/cardiomyopathy (Tajiri et al.), glaucoma (Wiemann et al.), sepsis (Meijer et al.), stroke (Okada and Suzuki), glial scar formation (Bijelić et al.) and pancreatic cancer (Liot et al.).

All tenascins have context dependent functions. This has clearly been shown for TNC in joint disease. Of note in this Research Topic the role of TNC as DAMP in rheumatoid arthritis (RA) and as a regulator of tissue repair in osteoarthritis (OA) is discussed by Hasegawa et al., who emphasize the importance of considering the context specific action of this matrix molecule in different disease settings even within the same tissue. More recently, pro- and anti-inflammatory roles for TNC have been reported in cancer (25–29) and it is clear that we need good *in vivo* models to better understand the functions of tenascins in space and time, and in a cell type specific manner. Four novel murine models have been described here; a sepsis model using Klebsiella in wildtype and TNC knockout animals, revealing a moderately lower bacterial load in lungs and blood, that does not translate to impact on severity of the disease symptoms (Meijer et al.), the first inducible TNC over expression mouse ectopically expressing TNC in heart, increasing expression of inflammatory cytokines and increasing mortality during the acute stage after myocardial infarction (Yonebayashi et al.), a model of autoimmune glaucoma (Wiemann et al.) and a novel orthotopic tongue squamous cell carcinoma cell grafting model that is sensitive to radiotherapy (Spenlé et al.).

In search of the underlying mechanisms of tenascin action, attention has focused on the different proteoforms of these extensively alternatively spliced genes. Iyoda et al. review results on the generation and actions of the alternatively spliced, and cryptic, TNIIIA2 domain in the malignancy of glioblastoma (GBM). This involves MMP9 secretion by TNC-activated macrophages generating TNIIIA2 from intact TNC, activating β1 integrin signaling in conjunction with syndecan-4 enhancing cell adhesion and malignancy of GBM cells. In this Research Topic, Bijelić et al. used recombinantly expressed proteins representing different domains of TNC to interrogate regulation of astrocyte behaviour *in vitro* and *in vivo*. *In vitro*, TNC fragments induced pro-inflammatory cytokine production. Alternatively spliced TNIIID, TNIIIA and their combination strongly decreased proliferation and delayed gap closure of scratch wound assay of cultured astrocytes. *In vivo*, TNIIID or TNIII(D+A) led to higher expression of GFAP in the wild type mice than TNC knockout mice. Addition of TNIIID to TNC knockout mice increased the activated microglia although overall cell proliferation in injured sites were not affected. Aubert et al. focus on another domain, conserved in all family members and revealed a TGFβ pathway-promoting function of the FBG domain of all four tenascins, where binding of the latent form of TGFβ and its activation are addressed. These results are intriguing and reveal that in addition to thrombospondin 1, connective tissue factor (CTGF, CCN2) and previously shown TNX also the FBG of TNC, TNW and TNR can bind TGFβ and activate TGFβ receptor signaling. Finally, Albacete-Albacete et al. review the transportation of ECM components by extracellular vesicles. Exosomal secretion is particularly critical for extracellular release and deposition of TNC (30) and has been shown to follow rhinovirus infection of epithelial airways (31). Circulating exosomes from cancer patients frequently carry TNC and exosomal TNC is fully functional, which may induce a proinflammatory state and contribute to premetastatic niche formation.

While understanding the roles of a particular tenascin requires models that enable correlation between phenotype to high and no expression of the respective tenascin, it is obvious that tenascins form networks with other molecules which may define their highly context dependent actions. In this Research Topic, Liot et al. summarize the roles of TNC in context of other known matrisomal molecules impacting disease severity of pancreatic ductal adenocarcinoma. Okada and Suzuki review literature on TNC-induced roles on inflammation in context of other matrix molecules on stroke-related pathologies while Matsumoto and Aoki review the roles of TNC in conjunction with TNX in the cardiovascular system. TNX and TNC have distinct roles in physiological and pathological conditions. TNX is involved in the structural integrity of collagen fibrils, activation and its absence causes classical-like Ehlers-Danlos syndrome. In contrast, the role of TNC can be detrimental or beneficial also in a context-dependent manner. TNC may prevent aortic dissection and rupture of cerebral aneurysm, while it may exacerbate acute vasospastic response and cerebral injury.

Finally, it has been evident for some time now that tenascins may be reliable biomarkers for disease diagnosis and targets for new therapies. Dhaouadi et al. developed nanobodies against TNC and showed binding in the central constant TNIII domains of the molecule. These nanobodies recognized human and murine TNC in paraffin embedded tumor tissue (useful for the clinical practice) and blocked cell rounding and chemoretention of dendritic cells by TNC potentially thus being valuable for therapy. Other nanobodies specific for TNC have recently been proposed to be also valuables tools in particular for imaging tumors (US 2019/0225693 A1 patent by RO Hynes).

Altogether despite the discovery of TNC more than 4 decades ago, followed by the identification and characterization of the other 3 family members, it is clear that we still are at the beginning of our understanding of the molecular and structural networks in which the respective tenascin molecule is expressed and what each member is doing there. Moreover, as all members can be regulated by splicing and modified by glycosylation more research has to be done to identify which proteoform is expressed when and where and what roles these different molecules have. Novel tools and a broader understanding of tenascin expression and functions as described in this Research Topic are valuable and may help to prepare a future application of this knowledge in diagnosis and therapy.

AUTHOR CONTRIBUTIONS

All authors listed have made a substantial, direct, and intellectual contribution to the work and approved it for publication.

FUNDING

GO was supported by ANR-MatrixNash, INCa-PLBIO TENMAX, Aviesan Radio 3R, Ligue contre le Cancer CCIRGE.

REFERENCES

1. Midwood K, Sacre S, Piccinini AM, Inglis J, Trebaul A, Chan E, et al. Tenascin-C Is an Endogenous Activator of Toll-Like Receptor 4 That Is Essential for Maintaining Inflammation in Arthritic Joint Disease. *Nat Med* (2009) 15(7):774–80. doi: 10.1038/nm.1987
2. Fouda GG, Jaeger FH, Amos JD, Ho C, Kunz EL, Anasti K, et al. Tenascin-C is an Innate Broad-Spectrum, HIV-1-Neutralizing Protein in Breast Milk. *Proc Natl Acad Sci USA* (2013) 110(45):18220–5. doi: 10.1073/pnas.1307336110
3. Zeng HL, Chen D, Yan J, Yang Q, Han Q-Q, Li S-S, et al. Proteomic Characteristics of Bronchoalveolar Lavage Fluid in Critical COVID-19 Patients. *FEBS J* (2021) 288(17):5190–200. doi: 10.1111/febs.15609
4. Bourdon MA, Wikstrand CJ, Furthmayr H, Matthews TJ, Bigner DD. Human Glioma-Mesenchymal Extracellular Matrix Antigen Defined by Monoclonal Antibody. *Cancer Res* (1983) 43(6):2796–805.
5. Chiquet M, Fambrough DM. Chick Myotendinous Antigen. I. A Monoclonal Antibody as a Marker for Tendon and Muscle Morphogenesis. *J Cell Biol* (1984) 98(6):1926–36. doi: 10.1083/jcb.98.6.1926
6. Erickson HP, Inglesias JL. A Six-Armed Oligomer Isolated From Cell Surface Fibronectin Preparations. *Nature* (1984) 311(5983):267–9. doi: 10.1038/311267a0
7. Grumet M, Hoffman S, Crossin KL, Edelman GM. Cytotactin, an Extracellular Matrix Protein of Neural and non-Neural Tissues That Mediates Glia-Neuron Interaction. *Proc Natl Acad Sci USA* (1985) 82 (23):8075–9. doi: 10.1073/pnas.82.23.8075
8. Chiquet-Ehrismann R, Mackie EJ, Pearson CA, Sakakura T. Tenascin: An Extracellular Matrix Protein Involved in Tissue Interactions During Fetal Development and Oncogenesis. *Cell* (1986) 47(1):131–9. doi: 10.1016/0092-8674(86)90374-0
9. Erickson HP. Tenascin-C, Tenascin-R and Tenascin-X: A Family of Talented Proteins in Search of Functions. *Curr Opin Cell Biol* (1993) 5(5):869–76. doi: 10.1016/0955-0674(93)90037-q
10. Rathjen FG, Wolff JM, Chiquet-Ehrismann R. Restrictin: A Chick Neural Extracellular Matrix Protein Involved in Cell Attachment Co-Purifies With the Cell Recognition Molecule F11. *Development* (1991) 113(1):151–64. doi: 10.1242/dev.113.1.151
11. Kruse J, Keilhauer G, Faissner A, Timpl R, Schachner M. The J1 Glycoprotein—a Novel Nervous System Cell Adhesion Molecule of the L2/HNK-1 Family. *Nature* (1985) 316(6024):146–8. doi: 10.1038/316146a0
12. Morel Y, Bristow J, Gitelman SE, Miller WL. Transcript Encoded on the Opposite Strand of the Human Steroid 21-Hydroxylase/Complement Component C4 Gene Locus. *Proc Natl Acad Sci USA* (1989) 86(17):6582–6. doi: 10.1073/pnas.86.17.6582
13. Bristow J, Tee MK, Gitelman SE, Mellon SH, Miller WL. Tenascin-X: A Novel Extracellular Matrix Protein Encoded by the Human XB Gene Overlapping P450c21B. *J Cell Biol* (1993) 122(1):265–78. doi: 10.1083/jcb.122.1.265
14. Weber P, Montag D, Schachner M, Bernhardt RR. Zebrafish Tenascin-W, a New Member of the Tenascin Family. *J Neurobiol* (1998) 35(1):1–16. doi: 10.1002/(SICI)1097-4695(199804)35:1<1::AID-NEU1>3.0.CO;2-9
15. Dawson MR, Polito A, Levine JM, Reynolds R. NG2-Expressing Glial Progenitor Cells: An Abundant and Widespread Population of Cycling Cells in the Adult Rat CNS. *Mol Cell Neurosci* (2003) 24(2):476–88. doi: 10.1016/s1044-7431(03)00210-0
16. Evers MR, Salmen B, Bukalo O, Rollenhagen A, Bösl MR, Morellini F, et al. Impairment of L-Type Ca2+ Channel-Dependent Forms of Hippocampal Synaptic Plasticity in Mice Deficient in the Extracellular Matrix Glycoprotein Tenascin-C. *J Neurosci* (2002) 22(16):7177–94. doi: 10.1523/JNEUROSCI.22-16-07177.2002
17. Forsberg E, Hirsch E, Fröhlich L, Meyer M, Ekblom P, Aszodi A, et al. Skin Wounds and Severed Nerves Heal Normally in Mice Lacking Tenascin-C. *Proc Natl Acad Sci USA* (1996) 93(13):6594–9. doi: 10.1073/pnas.93.13.6594
18. Saga Y, Yagi T, Ikawa Y, Sakakura T, Aizawa S. Mice Develop Normally Without Tenascin. *Genes Dev* (1992) 6(10):1821–31. doi: 10.1101/gad.6.10.1821
19. Rauch U, Zhou XH, Roos G. Extracellular Matrix Alterations in Brains Lacking Four of its Components. *Biochem Biophys Res Commun* (2005) 328 (2):608–17. doi: 10.1016/j.bbrc.2005.01.026
20. Schalkwijk J, Zweers MC, Steijlen PM, Dean WB, Taylor G, van Vlijmen IM, et al. A Recessive Form of the Ehlers-Danlos Syndrome Caused by Tenascin-X Deficiency. *N Engl J Med* (2001) 345(16):1167–75. doi: 10.1056/NEJMoa002939
21. Dufresne D, Hamdan FF, Rosenfeld JA, Torchia B, Rosenblatt B, Michaud JL, et al. Homozygous Deletion of Tenascin-R in a Patient With Intellectual Disability. *J Med Genet* (2012) 49(7):451–4. doi: 10.1136/jmedgenet-2012-100831
22. Mokone GG, Gajjar M, September AV, Schwellnus MP, Greenberg J, Noakes TD, et al. The Guanine-Thymine Dinucleotide Repeat Polymorphism Within the Tenascin-C Gene is Associated With Achilles Tendon Injuries. *Am J Sports Med* (2005) 33(7):1016–21. doi: 10.1177/0363546504271986
23. Zhao Y, Zhao F, Zong L, Zhang P, Guan L, Zhang J, et al. Exome Sequencing and Linkage Analysis Identified Tenascin-C (TNC) as a Novel Causative Gene in Nonsyndromic Hearing Loss. *PloS One* (2013) 8(7):e69549. doi: 10.1371/journal.pone.0069549
24. Saxena M, Hisano M, Neutzner M, Diepenbruck M, Ivanek R, Sharma K, et al. The Long non-Coding RNA ET-20 Mediates EMT by Impairing Desmosomes in Breast Cancer Cells. *J Cell Sci* (2021) 134(21):jcs258418. doi: 10.1242/jcs.258418
25. Deligne C, Murdamoothoo D, Gammage AN, Gschwandtner M, Erne W, Loustau T, et al. Matrix-Targeting Immunotherapy Controls Tumor Growth and Spread by Switching Macrophage Phenotype. *Cancer Immunol Res* (2020) 8(3):368–82. doi: 10.1158/2326-6066.CIR-19-0276
26. Jachetti E, Caputo S, Mazzoleni S, Brambillasca CS, Parigi SM, Grioni M, et al. Tenascin-C Protects Cancer Stem-Like Cells From Immune Surveillance by Arresting T-Cell Activation. *Cancer Res* (2015) 75(10):2095–108. doi: 10.1158/0008-5472.CAN-14-2346
27. Murdamoothoo D, Sun Z, Yilmaz A, Riegel G, Abou-Faycal C, Deligne C, et al. Tenascin-C Immobilizes Infiltrating T Lymphocytes Through CXCL12 Promoting Breast Cancer Progression. *EMBO Mol Med* (2021) 13(6):e13270. doi: 10.15252/emmm.202013270
28. Pires A, Greenshields-Watson A, Jones E, Smart K, Lauder SN, Somerville M, et al. Immune Remodeling of the Extracellular Matrix Drives Loss of Cancer Stem Cells and Tumor Rejection. *Cancer Immunol Res* (2020) 8(12):1520–31. doi: 10.1158/2326-6066.CIR-20-0070
29. Spenle C, Loustau T, Murdamoothoo D, Erne W, Beghelli-de la Forest Divonne S, Veber R, et al. Tenascin-C Orchestrates an Immune-Suppressive Tumor Microenvironment in Oral Squamous Cell Carcinoma. *Cancer Immunol Res* (2020) 8(9):1122–38. doi: 10.1158/2326-6066.CIR-20-0074
30. Albacete-Albacete L, Navarro-Lérida I, López JA, Martín-Padura I, Astudillo AM, Ferrarini A, et al. ECM Deposition is Driven by Caveolin-1-Dependent Regulation of Exosomal Biogenesis and Cargo Sorting. *J Cell Biol* (2020) 219 (11):e202006178. doi: 10.1083/jcb.202006178
31. Mills JT, Schwenzer A, Marsh EK, Edwards MR, Sabroe I, Midwood KS, et al. Airway Epithelial Cells Generate Pro-Inflammatory Tenascin-C and Small Extracellular Vesicles in Response to TLR3 Stimuli and Rhinovirus Infection. *Front Immunol* (2019) 10:1987. doi: 10.3389/fimmu.2019.01987

Conflict of Interest: The authors declare that the research was conducted in the absence of any commercial or financial relationships that could be construed as a potential conflict of interest.

frontiers in Immunology

MINI REVIEW
published: 30 September 2020
doi: 10.3389/fimmu.2020.577015

Tenascin-C in Osteoarthritis and Rheumatoid Arthritis

Masahiro Hasegawa[1]*, *Toshimichi Yoshida*[2] *and Akihiro Sudo*[1]

[1] Department of Orthopaedic Surgery, Mie University Graduate School of Medicine, Tsu, Japan, [2] Department of Pathology & Matrix Biology, Mie University Graduate School of Medicine, Tsu, Japan

Tenascin-C (TNC) is a large multimodular glycoprotein of the extracellular matrix that consists of four distinct domains. Emerging evidence suggests that TNC may be involved in the pathogenesis of osteoarthritis (OA) and rheumatoid arthritis (RA). In this review, we summarize the current understanding of the role of TNC in cartilage and in synovial biology, across both OA and RA. TNC is expressed in association with the development of articular cartilage; the expression decreases during maturation of chondrocytes and disappears almost completely in adult articular cartilage. TNC expression is increased in diseased cartilage, synovium, and synovial fluid in OA and RA. In addition, elevated circulating TNC levels have been detected in the blood of RA patients. Thus, TNC could be used as a novel biochemical marker for OA and RA, although it has no specificity as a biochemical marker for these joint disorders. In a post-traumatic OA model of aged joints, TNC deficiency was shown to enhance cartilage degeneration. Treatment with TNC domains results in different, domain-specific effects, which are also dose-dependent. For instance, some TNC fragments including the fibrinogen-like globe domain might function as endogenous inducers of synovitis and cartilage matrix degradation through binding with toll-like receptor-4, while full-length TNC promotes cartilage repair and prevents the development of OA without exacerbating synovitis. The TNC peptide TNIIIA2 also prevents cartilage degeneration without causing synovial inflammation. The clinical significance of TNC effects on cartilage and synovium is unclear and understanding the clinical significance of TNC is not straightforward.

Keywords: tenascin-C, osteoarthritis, rheumatoid arthritis, cartilage, repair, synovitis, animal model

OPEN ACCESS

Edited by:
Kim Midwood,
University of Oxford, United Kingdom

Reviewed by:
Ali Mobasheri,
State Research Institute Center for Innovative Medicine, Lithuania
Yasser Mohamed El-Sherbiny,
Nottingham Trent University, United Kingdom

***Correspondence:**
Masahiro Hasegawa
masahase@clin.medic.mie-u.ac.jp

Specialty section:
This article was submitted to Inflammation, a section of the journal Frontiers in Immunology

Received: *28 June 2020*
Accepted: *15 September 2020*
Published: *30 September 2020*

Citation:
Hasegawa M, Yoshida T and Sudo A (2020) Tenascin-C in Osteoarthritis and Rheumatoid Arthritis. Front. Immunol. 11:577015. doi: 10.3389/fimmu.2020.577015

INTRODUCTION

Osteoarthritis (OA) is a well-known cause of disability, with an estimated global prevalence of more than 30% (1). Further, its prevalence is increasing because of rapid population aging. Risk factors for OA include person factors (age, sex, obesity, and genetics) and joint factors (deformity, malalignment, and injury) that interact in a complex manner (2). Rheumatoid arthritis (RA) is a chronic inflammatory disease that can cause joint destruction as well as disability (3). The global prevalence of RA is around 1%, and genetics are the principal risk factor for developing RA, while smoking is the main environmental risk factor. RA is most typically found in elderly women (3, 4). The pathogenesis of RA and periodontitis might be similar, with both diseases involving chronic inflammation and bone erosion (5).

Tenascin-C (TNC) is a non-structural extracellular matrix (ECM) protein that is highly expressed in morphogenesis and tissue remodeling, and has many effects on cellular responses (6). Emerging evidence suggests that TNC might be involved in the pathogenesis of OA and RA. In this review, we present the current understanding of the role of TNC in cartilage and in synovial biology, across both OA and RA.

STRUCTURE AND DISTRIBUTION OF TENASCIN-C

TNC is a hexameric glycoprotein component of the ECM. The TNC molecule is composed of large molecular weight subunits (220–400 kDa) consisting of four distinct domains, with each TNC subunit consisting of a tenascin assembly (TA) domain that forms a coil at the N-terminus, 14.5 epidermal growth factor-like (EGF-L) repeats, up to 17 fibronectin type III (FNIII) -like repeats, and a C-terminal fibrinogen-like globe (FBG) domain. The FNIII-like repeats undergo alternative splicing to bind different ECM proteins, such as fibronectin, syndecan-4, and integrins αVβ3 and α8β1 (7–10). Furthermore, the FNIII-like repeats bind to a number of growth factors including fibroblast growth factor (FGF), platelet-derived growth factor (PDGF), and the transforming growth factor-β (TGF-β) family. The FBG domain binds to αVβ3 integrin and receptor-type tyrosine-protein phosphatase zeta, and activates toll-like receptor-4 (TLR4) (9, 11). TNC can drive a range of processes including cell migration, attachment, proliferation, and synthesis of proteases and proinflammatory cytokines (9). Growth factors, such as TGF-β, FGF, and PDGF, can induce TNC expression. TNC is transiently expressed in the mesenchyme around developing organs, such as mammary glands, teeth, and kidneys. TNC is also expressed during embryo development in cartilage, ligament, tendon, periosteum, myotendinous junction, smooth muscle, and perichondrium. Expression of TNC is generally low in adult tissues, but is transiently elevated following tissue injury. Once the damaged tissue is repaired, TNC expression is inhibited. TNC shares a structural relationship with fibronectin (12); although fibronectin is adhesive in nature while TNC is only weakly adhesive (13). Functional inhibition of syndecan-4 suppresses TNC activity. In contrast, overexpression of syndecan-4 neutralizes the effect of TNC. Thus TNC and syndecan-4 work together to control fibroblast signaling and morphology, and to regulate the contraction of the matrix, including tissue repair (14, 15). TNC expression is regulated by mechanical stress, and is elevated in tissues that experience high tensile stress, such as smooth muscle, ligaments, and tendons (16).

CARTILAGE

Articular cartilage is an aneural, avascular, alymphatic and viscoelastic tissue. It's extremely low coefficient of friction contributes to the lubrication of joint movement. Water accounts for up to 85% of the wet weight of cartilage (17). By dry weight, the large aggregating proteoglycan aggrecan and type II collagen are the main ECM components of cartilage (18). Chondrocytes produce ECM with scant cell turnover (19). During the first stage of joint development, an interzone emerges at the presumptive joint site. Joint cavitation subsequently occurs at the center of the interzone, and cells within the interzone form the joint and cartilage (20). TNC participates in chondrogenesis and cartilage development (7, 8). At the early stage of articular cartilage formation the Indian hedgehog (Ihh), Erg, noggin, Wnt9a, and Gdf5 genes are expressed strongly. At the later stage, the expression of these early regulatory genes is downregulated, and the expression of structural genes, including proteoglycan (Prg) 4, type II collagen, CD44, and TNC, becomes preponderant (20, 21). In comparison, TGF-β, FGF18, and parathyroid hormone-related protein are continuously expressed during articular cartilage formation (20). In the newborn mouse knee, articular cartilage is a thin, dense tissue consisting of small, randomly oriented Prg4- and TNC-expressing cells (22). In mature cartilage, TNC is only present in the perichondrium (23), and disappears almost completely in adult articular cartilage (24). When the articular cartilage of TNC-knockout mice at a postnatal age of 8 weeks was compared to that of age-matched wild-type (WT) mice, the tangential/transitional zone was thicker and the density of chondrocytes was lower in WT mice than in the TNC-knockout mice. This observation in mice implies that TNC plays a role in increasing articular cartilage volume as well as producing ECM from birth to 2 months of age (25).

CARTILAGE REPAIR

Articular cartilage has a limited potential for repair and damaged cartilage is associated with the development of OA. Many strategies to repair cartilage have been proposed including bone marrow stimulation techniques, osteochondral graft, cell-based cartilage repair procedures, and the use of growth factors, such as TGF-β, bone morphogenetic protein-2, and FGF (26, 27). Autologous chondrocyte implantation offers great promise with good long-term results; however, its applicability for large defects is limited (28). Although local administration of growth factors could be easily implemented, this strategy has not been used in clinical trials (26). Notably, TNC appears to be capable of mediating repair in human OA cartilage *in vitro* (29). During *in vivo* cartilage repair, TNC expression was found at the early phase with expression disappearing at the late phase with cartilage maturation (30). In TNC-knockout BALB/c mice, cartilage repair was found to be significantly delayed compared to WT mice, and the deficiency of TNC accelerated degeneration of cartilage (30). When examining the effects of intra-articular TNC administration on the repair of full-thickness cartilage defects in rabbits using scaffolding matrices, full-length TNC (10 μg/mL) was found to promote the repair of cartilage *in vivo* (27). However, scaffold impregnated with a higher concentration (100 μg/mL) of TNC did not facilitate cartilage repair. In a

BALB/c mouse model, full-length TNC (100 μg/mL) promoted cartilage repair in the absence of scaffold (31) (**Table 1**).

OSTEOARTHRITIS

Pathologic alterations in cartilage, bone, synovium, ligament, and meniscus are observed in OA, revealing OA to be a whole joint disease, with synovitis being one of the common features of OA. Synoviocytes synthesize hyaluronic acid and lubricin, which contribute to normal joint function (39). During progression of OA, the synovium can be a source of matrix metalloproteinase (MMP) and aggrecanase, which contributes to the degradation of the cartilage matrix. OA has historically been categorized as a non-inflammatory form of arthritis; however, the role of the development of synovitis in OA pathogenesis has been demonstrated (40–42). The synovium can produce soluble inflammatory mediators, including cytokines and chemokines, that are detected in joint tissues and synovial fluid in OA, and contribute to cartilage degeneration (40). Animal models of OA have been categorized into spontaneous and induced models, and the post-traumatic OA (PTOA) model is the most widely studied. Methods for inducing PTOA models include anterior cruciate ligament transection, medial collateral ligament transection, meniscectomy, and destabilization of the medial meniscus. In chemically induced models, sodium monoiodoacetate (MIA) is most commonly used to induce OA (43).

In clinical practice, the severity of OA is generally assessed with plain radiographs (44). Biochemical markers, however, provide an opportunity to better diagnose and stratify patients. Although cartilage oligomeric matrix protein in serum and C-terminal telopeptide of collagen type II in urine are the most widely investigated markers of tissue degradation, no marker has been well validated in clinical use for the diagnosis and monitoring of OA (39). It is not possible to determine the site of origin when biochemical markers are measured in serum or urine, but markers present in synovial fluid can provide insight into the damage in an individual joint (39). TNC levels in the synovial fluid were shown to be significantly increased in patients with knee OA (34, 45). In addition, TNC levels correlated with

TABLE 1 | Effect of tenascin-C domain on cartilage and synovial responses.

Tissue	Addition of TNC	Domain	Response	Cell type/species	Reference
Cartilage	*in vitro*	EGF-L domain and FNIII 3–8	Aggrecan-degrading ability	Human chondrocyte	Sofat et al. (32)
		TNIIIA2	Upregulating TNF-α, MMP-3, bFGF	Human chondrocyte	Hattori et al. (33)
		Full-length	Inducing IL-6, PGE2, nitrate release, upregulating ADAMTS4	Bovine and human chondrocytes	Patel et al. (34)
		Full-length	Cartilage proliferation	Human chondrocyte	Nakoshi et al. (29)
		Full-length	Upregulating TNF-α, IL-1β, ADAMTS4, MMP-3, MMP-13, TGF-β, TIMP3 Downregulating ADAMTS5	Human chondrocyte	Unno et al. (31)
	in vivo	FBG	Inducing cartilage proteoglycan loss	129/SV mouse	Midwood et al. (35)
		TNIIIA2	Preventing cartilage degeneration	BALB/c mouse	Hattori et al. (33)
		Full-length	Preventing cartilage degeneration	BALB/c mouse	Matsui et al. (36)
		Full-length	Repairing cartilage defects	Japanese white rabbit	Ikemura et al. (27)
		Full-length	Repairing cartilage defects	BALB/c mouse	Unno et al. (31)
Synovium	*in vitro*	Full-length FBG	Upregulating IL-6	Human synovial fibroblast	Midwood et al. (35)
		FNIII 3	Upregulating TNF-α, IL-1α, IL-1β, IL-6, CCL2, CCL3, CCL4, CXCL2, CXCL5, CXCL12, MMP-9 Downregulating MMP-2	Mouse synovial macrophage, Mouse synovial fibroblast	Kanayama et al. (37)
	in vivo	FBG	Inducing synovitis	129/SV mouse	Midwood et al. (35)
		FNIII 1-5	Antibody directed against FNIII1-5 reducing synovitis	BALB/c mouse	Mehta et al. (38)
		TNIIIA2	No enhancement of synovitis	BALB/c mouse	Hattori et al. (33)
		Full-length	No enhancement of synovitis	BALB/c mouse	Unno et al. (31)

TNC, tenascin-C; EGF-L, epidermal growth factor–like; FNIII, fibronectin type III; FBG, fibrinogen-like globe; TNF, tumor necrosis factor.
MMP, matrix metalloproteinase; FGF, fibroblast growth factor; IL, interleukin; PGE, prostaglandin E.
ADAMTS, a disintegrin and metalloproteinase with thrombospondin motifs; TGF, transforming growtfactor.
TIMP, tissue inhibitor of metalloprotease; CCL, chemokine (C-C motif) ligand; CXCL, chemokine (C-X-C motif) ligand.

the radiographic grading levels (45), and TNC in the synovial fluid has been demonstrated to be a useful marker of OA progression (45). In a canine PTOA model, TNC levels increased markedly during the acute phase and then decreased over time, but remained elevated relative to the control group, even after 12 months (46).

Immunohistochemical analysis of TNC expression revealed that TNC staining intensity increased with the degeneration of cartilage in comparison with normal cartilage (29). TNC staining is observed on the OA cartilage surface overlying chondroitin sulfate (CS)-positive areas (29), and enhanced TNC staining is associated with clusters of chondrocytes (47). These results suggest that the distribution of TNC is correlated with CS production and chondrocyte proliferation in OA cartilage. In cultured human OA chondrocytes, treatment with TNC induced chondrocyte proliferation and increased aggrecan levels (29). Tumor necrosis factor (TNF)-α stimulates TNC expression through nuclear factor-κB signaling with RelA subunit activation, which could affect cell proliferation. TNC is reported to have a potential role in remodeling of cartilage (47); however, elevated levels of TNC could induce inflammatory mediators and promote degradation of matrix in OA cartilage (34). TNC plays dual roles in synovial fluid, where it not only acts as a marker of joint damage, but also stimulates joint degradation (46). These two opposing roles of TNC in synovial fluid may stem from the versatile nature of this glycoprotein (48). Full-length TNC prevented cartilage degeneration in a PTOA model using BALB/c mice (36). In contrast, recombinant TNC fragments induced aggrecanase activity and mediated cartilage degeneration. The EGF-L and FNIII-like domains 3–8 of TNC showed high aggrecan-degrading activity, which was not observed with either full-length TNC or other TNC domains (32) (**Table 1**, **Figure 1**). TNIIIA2 is a 22-mer peptide of TNC that induces β1 integrin activation through syndecan-4, and intra-articular injection of TNIIIA2 prevented degeneration of articular cartilage in a PTOA model using BALB/c mice (33). The inflammatory effects of TNC were identified through binding with TLR4, and integrins α9β1 and αVβ3 (49), but further work is required to clarify whether TNC contributes to OA pathogenesis *via* integrins. In cultured human and bovine chondrocytes, treatment with TNC upregulated interleukin (IL)-6, prostaglandin E_2, nitrate release, and disintegrin and metalloproteinase with thrombospondin motifs-4 (34). Treatment with TNC decreased the amount of proteoglycan present in cartilage explants (32, 34). The FBG domain was reported to be an endogenous inducer of cartilage matrix degradation (32), while full-length TNC did not cause the severe inflammation observed with the FBG domain (27, 31, 36). Animal OA models using TNC-knockout mice have generated mixed results. Intra-articular injection of TNC induced synovitis in a TLR4-dependent manner using 129/SV mice (35) (**Table 1**). TLR4 activates the Fcγ receptor, and regulate the early onset of joint inflammation and cartilage damage during immune complex-mediated arthritis (50). TNC is not involved in the early onset of joint inflammation but is required for maintenance of inflammatory processes (35). The damage-associated molecular patterns CD14 ligand appears to contribute to cartilage repair in

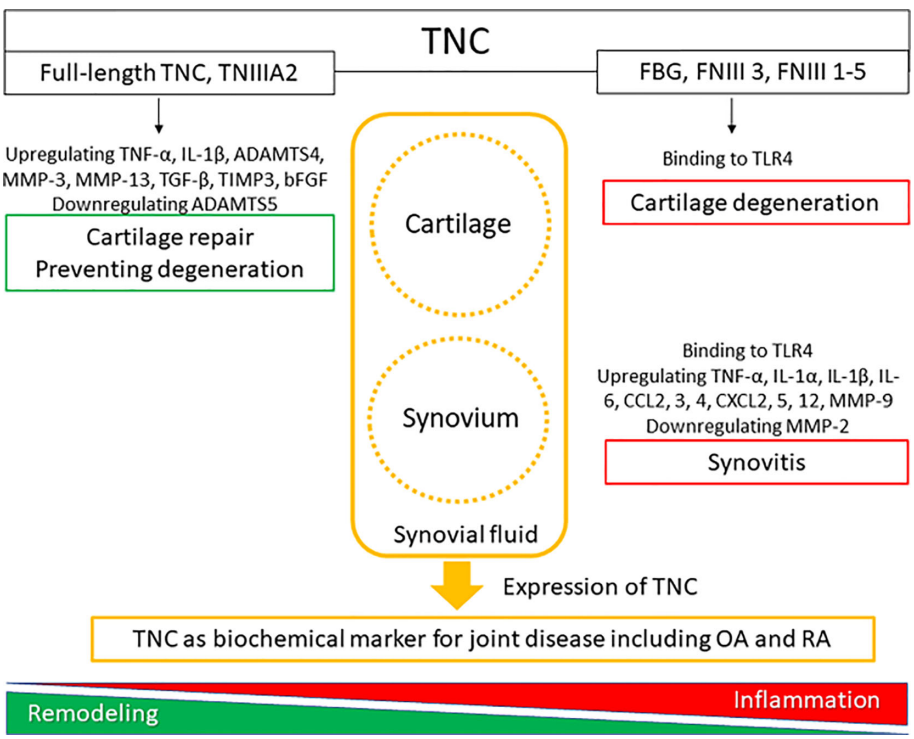

FIGURE 1 | The roles of tenascin-C (TNC) in synovial joint biology. TNC expression is upregulated in degenerated cartilage and inflamed synovial tissue.

OA (51), although CD14 is a modulator of innate inflammatory signaling that acts as a receptor for bacterial lipopolysaccharide with TLR4 (52). There are reports of beneficial effects for joint tissues (31, 36) in BALB/c mice, while deleterious effects for joint tissues were found in a different mouse species (129/SV).

Genetic variations might play a role in the differential responses in cartilage and synovium. For example, the MRL/MpJ strain mouse has an impaired inflammatory response and no susceptibility to OA (53). Moreover, MRL/MpJ mice showed lower levels of IL-1 and higher levels of IL-4 and IL-10 compared with C57BL/6 mice in a PTOA model (53). STR/ort mice are highly susceptible to OA, while C57BL/6J mice are only moderately susceptible (54).

RHEUMATOID ARTHRITIS

RA is characterized by swelling, tenderness, and destruction of joints due to synovitis, inflammation, and autoantibodies, particularly to rheumatoid factor and citrullinated peptide, which can cause cartilage and bone damage and consequent disability (3, 4). The 2010 American College of Rheumatology/European League Against Rheumatism RA classification criteria are widely used for clinical diagnosis (55). The increased risk for RA in patients with the shared epitope is associated with seropositivity for autoantibodies against rheumatoid factor, which are autoantibodies against IgG and citrullinated peptide (ACPA). The inflammatory milieu in the synovial joint is regulated by a complex cytokine and chemokine network. TNF-α and IL-6 are essential to the process, whereas IL-1 and various chemokines may be less important (3, 56). Serum biomarkers are routinely used in monitoring of disease progression including erythrocyte sedimentation rate (ESR), C-reactive protein (CRP), and MMP-3 (57). Interaction of TNC and α9β1 integrin induced the expression of IL-6 and MMPs in synovial fibroblasts, and IL-1β and TNF-α in synovial macrophages (58).

Zymosan can be used to induce acute synovitis in 129/SV mice, where synovitis and cartilage proteoglycan loss were observed at 4 days in WT mice. In contrast, TNC-knockout mice did not exhibit any synovitis or loss of cartilage proteoglycan (35) (**Table 1**). TNC induced the synthesis of proinflammatory cytokines *via* endogenous activation of TLR4 (35). Using 129/SV mice, intra-articular injection of 1 or 3 μg FBG induced synovitis, inflammatory cell infiltration, pannus formation, and loss of cartilage proteoglycan; in contrast, 100 ng FBG injection did not induce any inflammation or proteoglycan loss (35) (**Table 1**). However, intra-articular administration of full-length TNC to BALB/c mice induced similar synovial inflammation compared to no TNC administration (31, 36). In a PTOA model using BALB/c mice, low-grade synovitis occurred at 2 weeks, but these changes improved at 4 weeks in mice with and without intra-articular injection of TNIIIA2 (33) (**Table 1**). While the FBG domain of TNC could be a critical driver of synovial inflammation in 129/SV mice, administration of full-length TNC and TNIIIA2 had no role in synovial inflammation in BALB/c mice (**Figure 1**). The capacity of TNC to exert both beneficial and deleterious effects on joint tissues is fascinating, and the mechanism underlying the dual nature of TNC remains poorly understood. Moreover, the dose of TNC administered appears to be an important factor in determining the *in vivo* effects of TNC.

TNC plays an important role in physiological tissue repair but also drives pathological inflammation and fibrosis (49). Intense TNC immunoreactivity was found in the RA synovium with strong chronic inflammation and fibrosis (59). Elevated circulating TNC levels have been detected in the blood of RA patients, and patients with late stage RA have higher TNC levels compared to those with early stage RA (60). TNC levels in blood and synovial fluid were not reported to correlate with CRP (59, 60). Moreover, blood levels of TNC did not correlate with other biomarkers, such as ESR and ACPA (60). However, TNC levels in blood correlated positively with erosion scores determined by ultrasound in early stage RA (60). TNC concentrations in synovial fluid were reported to be fourfold higher in RA compared with OA (59). Multiple citrullination sites exist in the FBG domain of TNC, and citrullinated TNC (cTNC) 5 was recognized as a biochemical marker that can be detected years before the onset of RA (61). Periodontitis is a risk factor for RA, and antibodies to cytokeratin 13 were found to correlate with anti-cTNC5 (62). The TN64 antibody is directed against the FNIII-like repeats 1-5 (TNfnIII 1-5) of TNC, and has been observed to prevent fibroblast-mediated cartilage destruction. The TN64 antibody was evaluated in collagen-induced arthritis in BALB/c mice, and TN64 was found to prevent the induction of arthritis by downregulation of TNF-α, IL-6, IL-10, IL-12, and IFN-γ (38). Both full-length TNC and the FBG domain induced synthesis of IL-6 in synovial fibroblasts (35). Mapping the active domain within TNC demonstrated a unique structural FBG epitope, essential for binding to and activating TLR4 (63). Monoclonal antibodies recognizing the FBG domain of TNC inhibited release of TNF-α, IL-6, and IL-8 by RA synovium (64). Blocking inflammatory signals from the ECM including TNC domains represents a potential novel therapeutic strategy for treating RA that may avoid global immune suppression.

It is not clear how the different domains in TNC interact with each other at a functional level and knowledge of different ligand binding modes of TNC is also limited (49). Moreover, it remains unclear whether activation of TLR4 by the FBG domain occurs in isolation from or in synergy with other TNC domains. Similarly, little is known about how tissue-specific responses to TNC are mediated (64). The clinical significance of TNC effects on cartilage and synovium is unclear and understanding the clinical significance of TNC is not straightforward, as it appears to contribute to both beneficial and deleterious effects in a context-dependent manner (65). However, TNC is clearly an important molecule involved in controlling cellular activity during tissue remodeling and inflammation (**Figure 1**). TNC does not have any specificity as a biochemical marker for OA and RA but has been shown to be a potential marker for other diseases. Elevated TNC expression was reported to predict poor prognosis among patients with various cancers, and TNC can be a serum biochemical marker for cancer (66). Serum TNC levels

in patients with asthma was associated with clinical features of asthma, suggesting that serum TNC can be a biochemical for asthma (67). Circulating TNC levels were also elevated in patients with ankylosing spondylitis, systemic lupus erythematosus, psoriatic arthritis, ulcerative colitis, and Crohn's disease (60, 68).

CONCLUSION

TNC is a key molecule in tissue remodeling and is associated with OA and RA. TNC could be used as a novel biochemical marker for OA and RA, although it has no specificity as a biochemical marker for these joint disorders. Administration of TNC showed both beneficial and deleterious effects across different joint tissues and different TNC domains, and it's *in vivo* effects were clearly dose-dependent. Full-length TNC and TNIIIA2 prevented the development of OA in a PTOA model using BALB/c mice, suggesting that TNC domains and animal species might influence the type and nature of the responses obtained in pre-clinical studies. Thus, the clinical significance of TNC effects on cartilage and synovium awaits further clarification.

AUTHOR CONTRIBUTIONS

MH and TY designed and reviewed the paper and contributed in drafting the manuscript. AS reviewed the manuscript. All authors contributed to the article and approved the submitted version.

REFERENCES

1. Vina ER, Kwoh CK. Epidemiology of osteoarthritis: literature update. *Curr Opin Rheumatol* (2018) 30:160–7. doi: 10.1097/BOR.0000000000000479
2. Palazzo C, Nguyen C, Lefevre-Colau MM, Rannou F, Poiraudeau S. Risk factors and burden of osteoarthritis. *Ann Phys Rehabil Med* (2016) 59:134–8. doi: 10.1016/j.rehab.2016.01.006
3. Smolen JS, Aletaha D, McInnes IB. Rheumatoid arthritis. *Lancet* (2016) 388:2023–38. doi: 10.1016/S0140-6736(16)30173-8
4. Scott DL, Wolfe F, Huizinga TW. Rheumatoid arthritis. *Lancet* (2010) 376:1094–108. doi: 10.1016/S0140-6736(10)60826-4
5. Potempa J, Mydel P, Koziel J. The case for periodontitis in the pathogenesis of rheumatoid arthritis. *Nat Rev Rheumatol* (2017) 13:606–20. doi: 10.1038/nrrheum.2017.132
6. Imanaka-Yoshida K, Aoki H. Tenascin-C and mechanotransduction in the development and diseases of cardiovascular system. *Front Physiol* (2014) 5:283. doi: 10.3389/fphys.2014.00283
7. Chiquet M, Fambrough DM. Chick myotendinous antigen. I. A monoclonal antibody as a marker for tendon and muscle morphogenesis. *J Cell Biol* (1984) 98:1926–36. doi: 10.1083/jcb.98.6.1926
8. Chiquet M, Fambrough DM. Chick myotendinous antigen. II. A novel extracellular glycoprotein complex consisting of large disulfide-linked subunits. *J Cell Biol* (1984) 98:1937–46. doi: 10.1083/jcb.98.6.1937
9. Giblin SP, Midwood KS. Tenascin-C: Form versus function. *Cell Adh. Migr* (2015) 9:48–82. doi: 10.4161/19336918.2014.987587
10. Tucker RP, Chiquet-Ehrismann R. Tenascin-C: Its functions as an integrin ligand. *Int J Biochem Cell Biol* (2015) 65:165–8. doi: 10.1016/j.biocel.2015.06.003
11. Yoshida T, Akatsuka T, Imanaka-Yoshida K. Tenascin-C and integrins in cancer. *Cell Adh Migr* (2015) 9:96–104. doi: 10.1080/19336918.2015.1008332
12. Halper J, Kjaer M. Basic components of connective tissues and extracellular matrix: elastin, fibrillin, fibulins, fibrinogen, fibronectin, laminin, tenascins and thrombospondins. *Adv Exp Med Biol* (2014) 802:31–47. doi: 10.1007/978-94-007-7893-1_3
13. Chiquet-Ehrismann R, Kalla P, Pearson CA, Beck K, Chiquet M. Tenascin interferes with fibronectin action. *Cell* (1988) 53:383–90. doi: 10.1016/0092-8674(88)90158-4
14. Huang W, Chiquet-Ehrismann R, Moyano JV, Garcia-Pardo A, Orend G. Interference of tenascin-C with syndecan-4 binding to fibronectin blocks cell adhesion and stimulates tumor cell proliferation. *Cancer Res* (2001) 61(23):8586–94.
15. Midwood KS, Valenick LV, Hsia HC, Schwarzbauer JE. Coregulation of fibronectin signaling and matrix contraction by tenascin-C and syndecan-4. *Mol Biol Cell* (2004) 15:5670–7. doi: 10.1091/mbc.e04-08-0759
16. Kreja L, Liedert A, Schlenker H, Brenner RE, Fiedler J, Friemert B, et al. Effects of mechanical strain on human mesenchymal stem cells and ligament fibroblasts in a textured poly(l-lactide) scaffold for ligament tissue engineering. *J Mater Sci Mater Med* (2012) 23:2575–82. doi: 10.1007/s10856-012-4710-7
17. Krishnan Y, Grodzinsky AJ. Cartilage diseases. *Matrix Biol* (2018) 71-72:51–69. doi: 10.1016/j.matbio.2018.05.005
18. Tian J, Zhang FJ, Lei GH. Role of integrins and their ligands in osteoarthritic cartilage. *Rheumatol Int* (2015) 35:787–98. doi: 10.1007/s00296-014-3137-5
19. Decker RS. Articular cartilage and joint development from embryogenesis to adulthood. *Semin Cell Dev Biol* (2017) 62:50–6. doi: 10.1016/j.semcdb.2016.10.005
20. Chijimatsu R, Saito T. Mechanisms of synovial joint and articular cartilage development. *Cell Mol Life Sci* (2019) 76:3939–52. doi: 10.1007/s00018-019-03191-5
21. Koyama E, Shibukawa Y, Nagayama M, Sugito H, Young B, Yuasa T, et al. A distinct cohort of progenitor cells participates in synovial joint and articular cartilage formation during mouse limb skeletogenesis. *Dev Biol* (2008) 316:62–73. doi: 10.1016/j.ydbio.2008.01.012
22. Decker RS, Um HB, Dyment NA, Cottingham N, Usami Y, Enomoto-Iwamoto M, et al. Cell origin, volume and arrangement are drivers of articular cartilage formation, morphogenesis and response to injury in mouse limbs. *Dev Biol* (2017) 426:56–68. doi: 10.1016/j.ydbio.2017.04.006
23. Mackie EJ, Thesleff I, Chiquet-Ehrismann R. Tenascin is associated with chondrogenic and osteogenic differentiation in vivo and promotes chondrogenesis in vitro. *J Cell Biol* (1987) 105:2569–79. doi: 10.1083/jcb.105.6.2569
24. Chevalier X, Groult N, Larget-Piet B, Zardi L, Hornebeck W. Tenascin distribution in articular cartilage from normal subjects and from patients with osteoarthritis and rheumatoid arthritis. *Arthritis Rheumatol* (1994) 37:1013–22. doi: 10.1002/art.1780370706
25. Gruber BL, Mienaltowski MJ, MacLeod JN, Schittny J, Kasper S, Flück M. Tenascin-C expression controls the maturation of articular cartilage in mice. *BMC Res Notes* (2020) 13:78. doi: 10.1186/s13104-020-4906-8
26. Goldberg A, Mitchell K, Soans J, Kim L, Zaidi R. The use of mesenchymal stem cells for cartilage repair and regeneration: a systematic review. *J Orthop Surg Res* (2017) 12:39. doi: 10.1186/s13018-017-0534-y
27. Ikemura S, Hasegawa M, Iino T, Miyamoto K, Imanaka-Yoshida K, Yoshida T, et al. Effect of tenascin-C on the repair of full-thickness osteochondral defects of articular cartilage in rabbits. *J Orthop Res* (2015r) 33:563–71. doi: 10.1002/jor.22794
28. Peterson L, Vasiliadis HS, Brittberg M, Lindahl A. Autologous chondrocyte implantation: a long-term follow-up. *Am J Sports Med* (2010) 38:1117–24. doi: 10.1177/0363546509357915
29. Nakoshi Y, Hasegawa M, Akeda K, Iino T, Sudo A, Yoshida T, et al. Distribution and role of tenascin-C in human osteoarthritic cartilage. *J Orthop Sci* (2010) 15:666–73. doi: 10.1007/s00776-010-1513-x
30. Okamura N, Hasegawa M, Nakoshi Y, Iino T, Sudo A, Imanaka- Yoshida K, et al. Deficiency of tenascin-C delays articular cartilage repair in mice. *Osteoarthritis Cartilage* (2010) 18:839–48. doi: 10.1016/j.joca.2009.08.013
31. Unno H, Hasegawa M, Suzuki Y, Iino T, Imanaka-Yoshida K, Yoshida T, et al. Tenascin-C promotes the repair of cartilage defects in mice. *J Orthop Sci* (2020) 25:324–30. doi: 10.1016/j.jos.2019.03.013

32. Sofat N, Robertson SD, Hermansson M, Jones J, Mitchell P, Wait R. Tenascin-C fragments are endogenous inducers of cartilage matrix degradation. *Rheumatol Int* (2012) 32:2809–17. doi: 10.1007/s00296-011-2067-8
33. Hattori T, Hasegawa M, Unno H, Iino T, Fukai F, Yoshida T, et al. TNIIIA2, The Peptide of Tenascin-C, as a Candidate for Preventing Articular Cartilage Degeneration. *Cartilage* (2020). doi: 10.1177/1947603520912300. Online ahead of print.
34. Patel L, Sun W, Glasson SS, Morris EA, Flannery CR, Chockalingam PS. Tenascin-C induces inflammatory mediators and matrix degradation in osteoarthritic cartilage. *BMC Musculoskelet Disord* (2011) 12:164. doi: 10.1186/1471-2474-12-164
35. Midwood K, Sacre S, Piccinini AM, Inglis J, Trebaul A, Chan E, et al. Tenascin-C is an endogenous activator of Toll-like receptor 4 that is essential for maintaining inflammation in arthritic joint disease. *Nat Med* (2009) 15:774–80. doi: 10.1038/nm.1987
36. Matsui Y, Hasegawa M, Iino T, Imanaka-Yoshida K, Yoshida T, Sudo A. Tenascin-C Prevents Articular cartilage degeneration in murine osteoarthritis models. *Cartilage* (2018) 9:80–8. doi: 10.1177/1947603516681134
37. Kanayama M, Kurotaki D, Morimoto J, Asano T, Matsui Y, Nakayama Y, et al. Alpha9 integrin and its ligands constitute critical joint microenvironments for development of autoimmune arthritis. *J Immunol* (2009) 182(12):8015–25. doi: 10.4049/jimmunol.0900725
38. Mehta BB, Tiwari A, Sharma S, Shukla A, Sharma M, Vasishta RK, et al. Amelioration of collagen antibody induced arthritis in mice by an antibody directed against the fibronectin type III repeats of tenascin-C: Targeting fibronectin type III repeats of tenascin-C in rheumatoid arthritis. *Int Immunopharmacol* (2018) 58:15–23. doi: 10.1016/j.intimp.2018.02.022
39. Glyn-Jones S, Palmer AJ, Agricola R, Price AJ, Vincent TL, Weinans H, et al. Osteoarthritis. *Lancet* (2015) 386:376–87. doi: 10.1016/S0140-6736(14)60802-3
40. Scanzello CR, Goldring SR. The role of synovitis in osteoarthritis pathogenesis. *Bone* (2012) 51:249–57. doi: 10.1016/j.bone.2012.02.012
41. Oehler S, Neureiter D, Meyer-Scholten C, Aigner T. Subtyping of osteoarthritic synoviopathy. *Clin Exp Rheumatol* (2002) 20:633–40.
42. Krenn V, Morawietz L, Burmester GR, Kinne RW, Mueller-Ladner U, Muller B, et al. Synovitis score: discrimination between chronic low-grade and high-grade synovitis. *Histopathology* (2006) 49:358–64. doi: 10.1111/j.1365-2559.2006.02508.x
43. Kuyinu EL, Narayanan G, Nair LS, Laurencin CT. Animal models of osteoarthritis: classification, update, and measurement of outcomes. *J Orthop Surg Res* (2016) 11:19. doi: 10.1186/s13018-016-0346-5
44. Kellgren JH, Lawrence JS. Radiological assessment of osteoarthrosis. *Ann Rheum Dis* (1957) 16:494–502. doi: 10.1136/ard.16.4.494
45. Hasegawa M, Hirata H, Sudo A, Kato K, Kawase D, Kinoshita N, et al. Tenascin-C concentration in synovial fluid correlates with radiographic progression of knee osteoarthritis. *J Rheumatol* (2004) 31:2021–6.
46. Chockalingam PS, Glasson SS, Lohmander LS. Tenascin-C levels in synovial fluid are elevated after injury to the human and canine joint and correlate with markers of inflammation and matrix degradation. *Osteoarthritis Cartilage* (2013) 21:339–45. doi: 10.1016/j.joca.2012.10.016
47. Nakoshi Y, Hasegawa M, Sudo A, Yoshida T, Uchida A. Regulation of tenascin-C expression by tumor necrosis factor-alpha in cultured human osteoarthritis chondrocytes. *J Rheumatol* (2008) 35:147–52.
48. Spring J, Beck K, Chiquet-Ehrisman R. Two contrary functions of tenascin: dissection of the active sites by recombinant tenascin fragments. *Cell* (1989) 59:325–34. doi: 10.1016/0092-8674(89)90294-8
49. Marzeda AM, Midwood KS. Internal Affairs: Tenascin-C as a Clinically Relevant, Endogenous Driver of Innate Immunity. *J Histochem Cytochem* (2018) 66:289–304. doi: 10.1369/0022155418757443
50. van Lent PL, Blom AB, Grevers L, Sloetjes A, van den Berg WB. Toll-like receptor 4 induced FcgammaR expression potentiates early onset of joint inflammation and cartilage destruction during immune complex arthritis: Toll-like receptor 4 largely regulates FcgammaR expression by interleukin 10. *Ann Rheum Dis* (2007) 66:334–40. doi: 10.1136/ard.2006.057471
51. Liu-Bryan R, Terkeltaub R. The growing array of innate inflammatory ignition switches in osteoarthritis. *Arthritis Rheumatol* (2012) 64:2055–8. doi: 10.1002/art.34492
52. Lévêque M, Simonin-Le Jeune K, Jouneau S, Moulis S, Desrues B, Belleguic C, et al. Soluble CD14 acts as a DAMP in human macrophages: origin and involvement in inflammatory cytokine/chemokine production. *FASEB J* (2017) 31:1891–902. doi: 10.1096/fj.201600772R
53. Ward BD, Furman BD, Huebner JL, Kraus VB, Guilak F, Olson SA. Absence of posttraumatic arthritis following intraarticular fracture in the MRL/MpJ mouse. *Arthritis Rheumatol* (2008) 58:744–53. doi: 10.1002/art.23288
54. Sebastian A, Chang JC, Mendez ME, Murugesh DK, Hatsell S, Economides AN, et al. Comparative Transcriptomics Identifies Novel Genes and Pathways Involved in Post-Traumatic Osteoarthritis Development and Progression. *Int J Mol Sci* (2018) 19:pii: E2657. doi: 10.3390/ijms19092657
55. Kay J, Upchurch KS. ACR/EULAR 2010 rheumatoid arthritis classification criteria. *Rheumatol (Oxford)* (2012) 51(Suppl 6):vi5–9. doi: 10.1093/rheumatology/kes279
56. Feldmann M, Maini SR. Role of cytokines in rheumatoid arthritis: an education in pathophysiology and therapeutics. *Immunol Rev* (2008) 223:7–19. doi: 10.1111/j.1600-065X.2008.00626.x
57. Miossec P, Verweij CL, Klareskog L, Pitzalis C, Barton A, Lekkerkerker F, et al. Biomarkers and personalised medicine in rheumatoid arthritis: a proposal for interactions between academia, industry and regulatory bodies. *Ann Rheum Dis* (2011) 70:1713–8. doi: 10.1136/ard.2011.154252
58. Asano T, Iwasaki N, Kon S, Kanayama M, Morimoto J, Minami A, et al. α9β1 integrin acts as a critical intrinsic regulator of human rheumatoid arthritis. *Rheumatol (Oxford)* (2014) 53:415–24. doi: 10.1093/rheumatology/ket371
59. Hasegawa M, Nakoshi Y, Muraki M, Sudo A, Kinoshita N, Yoshida T, et al. Expression of large tenascin-C splice variants in synovial fluid of patients with rheumatoid arthritis. *J Orthop Res* (2007) 25:563–8. doi: 10.1002/jor.20366
60. Page TH, Charles PJ, Piccinini AM, Nicolaidou V, Taylor PC, Midwood KS. Raised circulating tenascin-C in rheumatoid arthritis. *Arthritis Res Ther* (2012) 14:R260. doi: 10.1186/ar4105
61. Schwenzer A, Jiang X, Mikuls TR, Payne JB, Sayles HR, Quirke AM, et al. Identification of an immunodominant peptide from citrullinated tenascin-C as a major target for autoantibodies in rheumatoid arthritis. *Ann Rheum Dis* (2016) 75:1876–83. doi: 10.1136/annrheumdis-2015-208495
62. Schwenzer A, Quirke AM, Marzeda AM, Wong A, Montgomery AB, Sayles HR, et al. Association of distinct fine specificities of anti-citrullinated peptide antibodies with elevated immune responses to Prevotella intermedia in a Subgroup of patients with rheumatoid arthritis and periodontitis. *Arthritis Rheumatol* (2017) 69:2303–13. doi: 10.1002/art.40227
63. Zuliani-Alvarez L, Marzeda AM, Deligne C, Schwenzer A, McCann FE, Marsden BD, et al. Mapping tenascin-C interaction with toll-like receptor 4 reveals a new subset of endogenous inflammatory triggers. *Nat Commun* (2017) 8:1595. doi: 10.1038/s41467-017-01718-7
64. Aungier SR, Cartwright AJ, Schwenzer A, Marshall JL, Dyson MR, Slavny P, et al. Targeting early changes in the synovial microenvironment: a new class of immunomodulatory therapy? *Ann Rheum Dis* (2019) 78:186–91. doi: 10.1136/annrheumdis-2018-214294
65. Imanaka-Yoshida K, Yoshida T, Miyagawa-Tomita S. Tenascin-C in development and disease of blood vessels. *Anat Rec (Hoboken)* (2014) 297:1747–57. doi: 10.1002/ar.22985
66. Ming X, Qiu S, Liu X, Li S, Wang Y, Zhu M, et al. Prognostic Role of Tenascin-C for Cancer Outcome: A Meta-Analysis. *Technol Cancer Res Treat* (2019) 18. doi: 10.1177/1533033818821106
67. Yasuda M, Harada N, Harada S, Ishimori A, Katsura Y, Itoigawa Y, et al. Characterization of tenascin-C as a novel biomarker for asthma: utility of tenascin-C in combination with periostin or immunoglobulin E. *Allergy Asthma Clin Immunol* (2018) 14:72. doi: 10.1186/s13223-018-0300-7
68. Ning L, Li S, Gao J, Ding L, Wang C, Chen W, et al. Tenascin-C Is Increased in Inflammatory Bowel Disease and Is Associated with response to Infliximab Therapy. *BioMed Res Int* (2019) 2019:1475705. doi: 10.1155/2019/1475705

Conflict of Interest: The authors declare that the research was conducted in the absence of any commercial or financial relationships that could be construed as a potential conflict of interest.

frontiers in Immunology

ORIGINAL RESEARCH
published: 09 October 2020
doi: 10.3389/fimmu.2020.566279

Loss of the Extracellular Matrix Molecule Tenascin-C Leads to Absence of Reactive Gliosis and Promotes Anti-inflammatory Cytokine Expression in an Autoimmune Glaucoma Mouse Model

Susanne Wiemann[1], Jacqueline Reinhard[1], Sabrina Reinehr[2], Zülal Cibir[1], Stephanie C. Joachim[2†] and Andreas Faissner[1*†]*

[1] Department of Cell Morphology and Molecular Neurobiology, Faculty of Biology and Biotechnology, Ruhr University Bochum, Bochum, Germany, [2] Experimental Eye Research Institute, University Eye Hospital, Ruhr University Bochum, Bochum, Germany

OPEN ACCESS

Edited by:
Kim Midwood,
University of Oxford, United Kingdom

Reviewed by:
Martin Degen,
Universität Bern, Switzerland
Anna Maria Piccinini,
University of Nottingham,
United Kingdom

***Correspondence:**
Stephanie C. Joachim
stephanie.joachim@rub.de
Andreas Faissner
andreas.faissner@rub.de

[†] These authors have contributed equally to this work

Specialty section:
This article was submitted to Inflammation, a section of the journal Frontiers in Immunology

Received: 27 May 2020
Accepted: 26 August 2020
Published: 09 October 2020

Citation:
Wiemann S, Reinhard J, Reinehr S, Cibir Z, Joachim SC and Faissner A (2020) Loss of the Extracellular Matrix Molecule Tenascin-C Leads to Absence of Reactive Gliosis and Promotes Anti-inflammatory Cytokine Expression in an Autoimmune Glaucoma Mouse Model. Front. Immunol. 11:566279. doi: 10.3389/fimmu.2020.566279

Previous studies demonstrated that retinal damage correlates with a massive remodeling of extracellular matrix (ECM) molecules and reactive gliosis. However, the functional significance of the ECM in retinal neurodegeneration is still unknown. In the present study, we used an intraocular pressure (IOP) independent experimental autoimmune glaucoma (EAG) mouse model to examine the role of the ECM glycoprotein tenascin-C (Tnc). Wild type (WT ONA) and Tnc knockout (KO ONA) mice were immunized with an optic nerve antigen (ONA) homogenate and control groups (CO) obtained sodium chloride (WT CO, KO CO). IOP was measured weekly and electroretinographies were recorded at the end of the study. Ten weeks after immunization, we analyzed retinal ganglion cells (RGCs), glial cells, and the expression of different cytokines in retina and optic nerve tissue in all four groups. IOP and retinal function were comparable in all groups. Although RGC loss was less severe in KO ONA, WT as well as KO mice displayed a significant cell loss after immunization. Compared to KO ONA, less βIII-tubulin$^+$ axons, and downregulated oligodendrocyte markers were noted in WT ONA optic nerves. In retina and optic nerve, we found an enhanced GFAP$^+$ staining area of astrocytes in immunized WT. A significantly higher number of retinal Iba1$^+$ microglia was found in WT ONA, while a lower number of Iba1$^+$ cells was observed in KO ONA. Furthermore, an increased expression of the glial markers *Gfap*, *Iba1*, *Nos2*, and *Cd68* was detected in retinal and optic nerve tissue of WT ONA, whereas comparable levels were observed in KO ONA. In addition, pro-inflammatory *Tnfa* expression was upregulated in WT ONA, but downregulated in KO ONA. Vice versa, a significantly increased anti-inflammatory

Tgfb1 expression was measured in KO ONA animals. We conclude that Tnc plays an important role in glial and inflammatory response during retinal neurodegeneration. Our results provide evidence that Tnc is involved in glaucomatous damage by regulating retinal glial activation and cytokine release. Thus, this transgenic EAG mouse model for the first time offers the possibility to investigate IOP-independent glaucomatous damage in direct relation to ECM remodeling.

Keywords: autoimmune glaucoma model, cytokines, microglia, optic nerve demyelination, reactive gliosis, tenascin-C

INTRODUCTION

Glaucomatous neurodegeneration is characterized by a progressive loss of retinal ganglion cells (RGCs) and their axons, which form the optic nerve. The molecular mechanisms of RGC degeneration are still not fully understood. In addition to increased intraocular pressure (IOP), immunological processes, glial activation, and remodeling of extracellular matrix (ECM) constituents are associated with glaucoma. In regard to the immune system, studies also indicate an alteration in serum antibodies against various retinal proteins in glaucoma patients with a normal IOP (1–3). The connection between an immune response and glaucoma disease with the characteristic loss of RGCs was already demonstrated in an experimental autoimmune glaucoma (EAG) rat model. Here, glaucomatous damage was induced by immunization with ocular proteins (4, 5). Furthermore, a pathological upregulation of specific ECM components could be demonstrated in this model (6). However, the relationship between a change in ECM components and glaucoma pathogenesis needs to be investigated.

The ECM consists of several molecules, including proteoglycans and glycoproteins and controls cellular key events such as adhesion, differentiation, migration, proliferation as well as survival (7–12). During development of the central nervous system (CNS), tenascin-C (Tnc) is strongly expressed by radial glial cells, immature astrocytes, and oligodendrocyte precursor cells (OPCs). It regulates axonal as well as neurite outgrowth and glial cells differentiation (11, 13–17). In this regard, axonal growth is modulated by specific Tnc isoforms, which contain a different combination of fibronectin type III domains (18). Moreover, Tnc expression is associated with the stem cell niche and regulates stem cell maintenance in addition to differentiation (19).

In the diseased brain, Tnc is highly re-expressed (11). For example, Tnc immunoreactivity is directly linked to amyloid-β plaques in Alzheimer's disease patients (20). A lack of Tnc leads to reduced deposits of amyloid-β plaques and protects from Alzheimer's disease (21). Furthermore, an immunomodulatory impact of Tnc was described by regulating the Th17 cell differentiation and activation (22, 23). Here, Tnc deficiency ameliorates experimental autoimmune encephalomyelitis in mice (24).

In the context of retinal neurodegenerative processes, Tnc also plays an important role (25). During retinal development, Tnc is found in the inner neuroblastic layer at embryonic day 13 (26). In the adult retina, Tnc is highly enriched in the outer and inner plexiform layers and is prominently expressed by amacrine and horizontal cells (27, 28). Additionally, optic nerve astrocytes synthesize Tnc (29, 30). ECM molecules can provide an inhibitory environment for neural regeneration and migration in the retina (30). A dramatic remodeling of ECM constituents was already described after ischemia and glaucomatous damage (25, 31). An upregulation of Tnc has been noted in a glaucoma animal model (32) as well as in open-angle glaucoma patients (33).

Tnc is a key regulator of the immune system and plays an important role during neuroinflammation and glial response (34–36). Moreover, expression of Tnc by astrocytes is regulated by cytokines secreted by microglia (37, 38). Microglia play an important role during neurodegenerative and neuroinflammatory processes (39). Their activation is characterized by an enhanced proliferation, migration, phagocytosis, and increased expression levels of neuroinflammatory molecules (40, 41). The neurotoxic M1-subtype has an amoeboid morphology and releases pro-inflammatory signaling molecules, like tumor necrosis factor-alpha (TNF-α) and inducible nitric oxide synthase (iNOS) (42–44). In contrast, the M2-phenotype is characterized by a morphology with ramified processes and the expression of anti-inflammatory cytokines, such as the transforming growth factor-beta (TGF-β) (45–47).

In this study, we used a Tnc deficient EAG mouse model to further analyze the importance of Tnc during retinal neurodegeneration and neuroinflammatory outcomes. We immunized wild type (WT) and Tnc knockout (KO) mice with an optic nerve antigen (ONA) homogenate and examined retinal and optic nerve damage as well as macro- and microglial activity. Furthermore, we determined the expression pattern of pro- and anti-inflammatory cytokines. The present study

Abbreviations: Brn3a, brain-specific homeobox/POU domain protein 3a; CC1, coiled coil-1; Cd68, cluster of differentiation 68; EAG, experimental autoimmune glaucoma; ECM, extracellular matrix; ERG, electroretinogram; GCL, ganglion cell layer; GFAP, glial fibrillary acidic protein; Iba1, ionized calcium-binding adapter molecule 1; INL, inner nuclear layer; iNOS, inducible nitric oxide synthase; IOP, intraocular pressure; IPL, inner plexiform layer; KO, knockout; KO CO, control group tenascin-C knockout; KO ONA, immunized tenascin-C knockout; MBP, myelin basic protein; NFL, nerve fiber layer; Nos2, nitric oxide synthase 2; Olig2, oligodendrocyte transcription factor 2; ONA, optic nerve antigen; ONL, outer nuclear layer; OPC, oligodendrocytes precursor cell; OPL, outer plexiform layer; RGC, retinal ganglion cell; *Tgfb*/TGF-β, transforming growth factor-beta; Tnc, tenascin-C; TLR4, toll-like receptor 4; *Tnfa*/TNF-α, tumor necrosis factor-alpha; WT, wild type; WT CO, control group wild type; WT ONA, immunized wild type.

was undertaken to address the role of Tnc in glaucomatous damage, retinal glial activation, myelination, and inflammatory cytokine release.

MATERIALS AND METHODS

Animals

Animals were housed under a 12 h light-dark cycle and had free access to chow and water. All procedures were approved by the animal care committee of North Rhine-Westphalia, Germany and performed according to the ARVO statement for the use of animals in ophthalmic and vision research. For the experiments, male and female littermates of 129/Sv WT and *Tnc* KO mice (48) were used at 6 weeks of age.

Immunization

WT (WT ONA) and KO (KO ONA) mice were immunized intraperitoneally with ONA (1 mg/ml) mixed with incomplete Freund's adjuvants (FA; 50 µl) and 1 µg pertussis toxin (PTx; both Sigma Aldrich, St. Louis, MO, USA) as described (49). To generate the ONA homogenate, fresh bovine eyes were obtained from a local slaughterhouse (Schlachthaus Wuppertal, Germany). As previously described, optic nerves were cut off behind the optic nerve head, cleaned from surrounding tissue and the dura mater was removed. Nerves were pulverized in a cooled mortar and then suspended in phosphate-buffered saline (PBS) (5). A final concentration of 1 mg/ml was set. FA acted as an immunostimulatory and PTx was given to ensure the permeability of the blood retina barrier. Intraperitoneal PTx-application was repeated 2 days after immunization. Booster injections containing half of the initial dose were given intraperitoneally 4 and 8 weeks after initial immunization. The control groups (WT CO; KO CO) were injected with 1 ml sodium chloride (B. Braun Melsungen AG, Melsungen, Germany), FA and PTx. Ten weeks after immunization, retinae, and optic nerves were explanted for immunohistochemistry, quantitative real time PCR (RT-qPCR), and Western blot analyses. For RT-qPCR and Western blot, retinal as well as optic nerve tissue of both eyes from one animal were pooled.

Intraocular Pressure Measurements

Before IOP measurement, mice were anesthetized with a ketamine/xylazine mixture (120/16 mg/kg). Both eyes were analyzed and 10 readings of each eye were averaged. IOP measurements were performed before immunization in WT and KO mice at 5 weeks of age with a rebound tonometer (TonoLab; Icare; Oy; Finland; $n = 16$/group) as previously described (50, 51). After immunization, IOP was measured weekly in all four groups until the end of the study ($n = 8$/group).

Electroretinogram Recordings

Scotopic full-field flash electroretinograms (ERG) recordings (HMsERG system, OcuScience, Henderson, NV, USA) were taken 10 weeks after immunization in all groups ($n = 5$/group)

TABLE 1 | List of primary and secondary antibodies to examine RGCs, macro-, and microglial cell types as well as Tnc in retinae and optic nerves via immunohistochemistry.

Primary antibody	Species, clonality/type	Dilution	Source (stock no.)/RRID	Secondary antibody	Species, type	Dilution/ source
Brn-3a (flat-mount/ retina)	Goat, polyclonal, IgG	1:300	Santa Cruz (Sc-31984) RRID:AB_2167511	Anti-goat Cy3	Donkey, IgG	1:250/ Dianova
CC1 (optic nerve)	Mouse, monoclonal, IgG	1:100	Abcam (Ab16794) RRID:AB_443473	Anti-mouse Cy2	Goat, IgG	1:250/ Dianova
GFAP (retina/optic nerve)	Mouse, monoclonal, IgG	1:300	Sigma-Aldrich (G3893) RRID:AB_477010	Anti-mouse Cy2	Goat, IgG	1:250/ Dianova
Iba1 (flat-mount)	Rabbit, polyclonal, IgG	1:250	WAKO (019-19741) RRID:AB_839504	Anti-rabbit Cy2	Donkey, IgG	1:250/ Dianova
MBP (optic nerve)	Rat, monoclonal, IgG	1:250	Bio-Rad (MCA409) RRID:AB_325004	Anti-rat Cy2	Goat, IgG	1:250/ Dianova
Olig2 (optic nerve)	Rabbit, polyclonal, IgG	1:400	Merck (AB9610) RRID:AB_570666	Anti-rabbit Cy3	Goat, IgG	1:250/ Dianova
Tnc (Kaf12) (retina)	Rabbit, polyclonal, IgG	1:250	(52)	Anti-rabbit Cy3	Goat, IgG	1:250/ Dianova
βIII-tubulin (optic nerve)	Mouse, monoclonal, IgG2b	1:300	Sigma-Aldrich (T 8660) RRID:AB_477590	Anti-mouse Cy2	Goat, IgG	1:250/ Dianova

Primary and secondary antibodies, including species, clonality/type, dilution, and source/stock number were shown.

TABLE 2 | Adjustments for the ImageJ macro.

Protein	Tissue	Background subtraction	Lower threshold	Upper threshold
βIII-tubulin	Optic nerve	50	29.45	82.18
GFAP	Retina	20	25.00	76.54
	Optic nerve	50	27.50	78.00
MBP	Optic nerve	50	7.62	62.45
Tnc	Retina	50	6.79	78.68

Data of background subtractions and upper/lower thresholds were present to determine the immunoreactive area [%].

as previously described (51). Mice were dark-adapted and anesthetized with a ketamine/xylazine mixture (120/16 mg/kg). Scotopic flash series with flash intensities at 0.1, 0.3, 1.0, 3.0, 10.0, and 25.0 cd/m^2 were recorded. Electrical potentials were analyzed with the ERGView 4.380R software (OcuScience) using a 150 Hz filter before evaluating a- and b-wave amplitudes.

Immunohistochemistry and Confocal Laser Scanning Microscopy

Eyes and optic nerves were dissected and fixed in paraformaldehyde (PFA) for 1 day, dehydrated in sucrose (30%) and embedded in Tissue-Tek freezing medium (Thermo Fisher Scientific, Cheshire, UK). Retinal cross-sections and optic nerve longitudinal sections (16 µm) were cut with a cryostat (CM3050 S, Leica) and transferred onto Superfrost plus object slides (Menzel-Glaeser, Braunschweig, Germany). First, slices were blocked with 1% bovine serum albumin (BSA; Sigma-Aldrich), 3% goat serum (Dianova, Hamburg, Germany), and 0.5 % Triton™-X-100 (Sigma-Aldrich) in PBS for 1 hour (h) at room temperature (RT). Afterwards, the primary antibodies were diluted in blocking solution and incubated at RT overnight (**Table 1**). Sections were washed 3 times in PBS and incubated for 2 h with adequate secondary antibody (Dianova, Hamburg, Germany; **Table 1**) solution without Triton™-X-100. Cell nuclei were detected with TO-PRO-3 (1:400; Thermo Fisher Scientific). The retinal and optic nerve slices were analyzed with a confocal laser-scanning microscope (LSM 510 META; Zeiss, Göttingen, Germany). Two sections per slide, 4 images per retina (400x magnification), and 3 images per optic nerve (200x magnification) were captured (n = 4–5/group). In addition, a 630x magnification was used for colocalization staining in optic nerve sections with antibodies against CC1 (coiled-coil 1) and Olig2 (oligodendrocyte transcription factor 2). Accordingly, 4 images were taken per slide (n = 5/group).

Laser lines and emission filters were adjusted using the Zeiss ZEN black software. Cropping of the images was done using Coral Paint Shop Pro X8 (Coral Corporation, Ottawa, Canada). Masked evaluation of the staining signal was performed with ImageJ software (ImageJ 1.51w, National Institutes of Health; Bethesda, MD, USA) as previously described (6, 53). Images were converted into gray scales and the background was subtracted. Then, the lower and upper threshold values was determined for each image (**Table 2**). The percentage of the area fraction was measured using an ImageJ macro as previously described (53). This analysis was performed for immunohistochemical stainings against βIII-tubulin, glial fibrillary acidic protein (GFAP), myelin basic protein (MBP), and Tnc. Cell countings were done for immunopositive Brn3a$^+$ cells in retinal cross-sections and for Olig2$^+$/CC1$^+$ cells in optic nerve slices. Values were transferred to Statistica software and the WT CO group was set to 100% (V13.3; StatSoft (Europe), Hamburg, Germany).

Quantification of RGCs and Microglia in Retinal Flat-Mounts

Eyes were enucleated and fixed in 4% PFA at 4°C for 1 h. The retinae were dissected from the eye and prepared as flat-mounts (n = 9/group). The tissue was fixed again in 4% PFA for 5 min and washed 3 times in PBS. Flat-mounts were blocked in 1% BSA, 3% donkey serum, and 2% Triton™-X-100 in PBS at RT for 1 h. Next, incubation was performed with the RGC specific marker Brn3a [brain-specific homeobox/POU domain protein 3a; (54, 55)] and microglia marker Iba1 [ionized calcium-binding adapter molecule 1; (56)] for 2 days at 4°C. Following PBS washing (3 × 20 min), flat-mounts were incubated with secondary antibodies donkey anti-goat Cy3, donkey anti-rabbit Alexa Fluor 488, and TO-PRO-3 (1:400) in blocking solution without Triton™-X-100 at RT for 2 h. Microscopic images were captured using Axio Zoom.V16 (Zeiss, Göttingen, Germany). Flat-mounts were divided into 16 quadrants (200 × 200 µm) and Brn3a$^+$ and Iba1$^+$ cells were counted. Groups were compared using two-way ANOVA followed by Tukey's *post-hoc* test. The WT CO group was set to 100%.

Western Blotting

Retinal tissue (n = 5/group) was homogenized in 150 µl and optic nerve tissue (n = 5/group) in 100 µl lysis buffer (60 mM n-octyl-β-D-glucopyranoside, 50 mM sodium acetate, 50 mM Tris chloride, pH 8.0 and 2 M urea) containing a protease inhibitor cocktail (Sigma-Aldrich) on ice for 1 h. Prior to lysis, the optic nerve tissue was incubated in liquid nitrogen. Subsequently, all samples were centrifuged at 14.000 × g at 4°C for 30 min and the supernatant was applied to determine the protein concentration. A BCA Protein Assay kit (Pierce, Thermo Fisher Scientific, Rockford, IL, USA) was used for retinal tissue. For optic nerves, the Qubit® Protein Assay kit (Life Technologies GmbH, Darmstadt, Germany) was used according to manufacturer's instructions. 4x SDS buffer was added to each protein sample (20 µg) and denaturized at 94°C for 5 min. After separation via SDS-PAGE (10% gels, respectively, 4–12% polyacrylamide gradient gels), proteins were transferred to a polyvinylidene difluoride (PVDF) membrane (Roth, Karlsruhe, Germany) by Western blotting (1–2 h and 75 mA). Membranes were blocked (5% w/v milk powder in TRIS-buffered saline (TBS) with 0.05% Tween®20; TBST) at RT for 1 h and incubated with the primary antibody (**Table 3**) in blocking solution at 4°C overnight. On the next day, membranes were washed with TBST and incubated with horseradish peroxidase (HRP) coupled secondary antibodies (**Table 3**) in blocking solution at RT for 2 h. Excess antibody was washed off with TBST. ECL Substrate (Bio-Rad Laboratories GmbH, München,

TABLE 3 | List of primary and secondary antibodies for western blotting.

Primary antibody	Species, clonality, type	Dilution	Source (stock no.)/RRID	Secondary antibody, species, type	Dilution	Source	kDa
Actin	Mouse, monoclonal, IgG	1:5,000	BD Bioscience (612657) RRID:AB_399901	Anti-mouse, IgG + IgM HRP	1:5,000	Dianova	42
GFAP	Rabbit, polyclonal, IgG	1:10,000	Dako (Z0334) RRID:AB_10013382	Anti-rabbit, IgG HRP	1:10,000	Dianova	50
MBP	Rat, monoclonal, IgG	1:1,000	Bio-Rad (MCA409) RRID:AB_325004	Anti-rat, IgG HRP	1:5,000	Dianova	20
Olig2	Rabbit, polyclonal, IgG	1:500	Merck (AB9610) RRID:AB_570666	Anti-rabbit, IgG HRP	1:5,000	Dianova	32 and 50
Tnc (Kaf12)	Rabbit, polyclonal, IgG	1:5,000	(52)	Anti-rabbit, IgG HRP	1:5,000	Dianova	∼ 250 and > 250
Vinculin	Mouse, monoclonal, IgG1	1:200	Sigma-Aldrich (V 9131) RRID:AB_477629	Anti-mouse, IgG + IgM HRP	1:5,000	Dianova	116

Primary and secondary antibodies, including species, clonality, type, dilution, source, and stock number are listed. Relative quantification of band intensity was done against the housekeeping proteins actin or vinculin. HRP, horseradish peroxidase; kDa, Kilodalton.

Germany) was applied to develop the membrane (mixed 1:1 for 5 min). Finally, protein immunoreactivity was detected with a MicroChemi Chemiluminescence Reader (Biostep, Burkhardtsdorf, Germany). Band intensity was analyzed using ImageJ software and normalized to a corresponding reference protein (actin/vinculin). The normalized values of the Western blot results were given in arbitrary units (a.u.).

RNA Isolation, cDNA Synthesis, and RT-qPCR

Retinal tissue was homogenized by trituration using a pipette ($n = 5$/group). The RNA isolation of the retina was carried out according to the manufacturer's introduction using the Gene Elute Mammalian Total RNA Miniprep Kit (Sigma-Aldrich, St. Louis, MO, USA). For total RNA isolation of optic nerve tissue, the ReliaPrepTM RNA Tissue Miniprep System (Promega, Madison, WI, USA) was taken. Prior to isolation, optic nerve tissue was incubated in liquid nitrogen and then homogenized with a pestle ($n = 5$/group). An additional DNase digestion at RT for 15 min ensured that no genomic DNA contaminated RNA was obtained. The concentration and purity of the isolated RNA was determined photometrically using the BioSpectrometer® (Eppendorf, Hamburg, Germany). One microgram RNA and random hexamer primers were applied for reverse transcription using a cDNA synthesis kit (Thermo Fisher Scientific, Waltham, MA, USA). RT-qPCR experiments were done with SYBR Green I in a Light Cycler 96® (Roche Applied Science, Mannheim, Germany). For each primer pair (**Table 4**), efficiencies were determined by a dilution series of 5, 25, and 125 ng cDNA. Expression in retina and optic nerve tissue was normalized against the housekeeping genes *β-actin* (*Actb*) and *18S ribosomal RNA (Rn18S)*, respectively.

Statistical Analysis

Immunohistological, Western blot, IOP, and ERG data of control WT (WT CO) and KO (KO CO) as well as ONA-immunized WT (WT ONA) and KO (KO ONA) were analyzed by two-way ANOVA followed by Tukey's *post-hoc* test using Statistica software (V13.3; StatSoft (Europe), Hamburg, Germany). Results of IOP measurements were presented as mean ± standard error mean (SEM) ± standard deviation (SD). ERG recordings, immunohistochemical, and Western blot data were shown as mean ± SEM. Analyses of Tnc protein levels in WT mice via immunohistochemistry and Western blot were analyzed via Student *t*-test and presented as mean ± SEM. For RT-qPCR results, groups were compared using the pairwise fixed reallocation and randomization test (REST© software) and were presented as median ± quartile ± minimum/maximum (57).

RESULTS

No Changes in IOP and Retinal Functionality in the EAG Mouse Model

IOP measurements were performed before immunization in 5-week-old WT (WT CO) and KO (KO CO; **Figure 1A**). After immunization, IOP was measured weekly in control and immunized WT (WT ONA) and KO (KO ONA) animals until the end of the study. At 5 weeks of age (−1), we observed no significant differences in the IOP of WT CO (9.8 ± 0.2 mmHg) and KO CO (9.7 ± 0.1 mmHg; $p = 1.0$). Furthermore, no changes in the IOP were found in control and immunized groups throughout the study (**Supplementary Table 1**).

To determine possible retinal function deficits, induced by ONA-immunization, we performed ERG recordings of control and immunized WT and KO mice. Under scotopic

TABLE 4 | List of primer pairs used for mRNA analyses by RT-qPCR.

Gene	Primer sequence	Amplicon size (bp)	Primer efficiency, retina/ optic nerve	GenBank accession number
*Rn18S*_for	GCAATTATTCC CCATGAACG	68	–/1	NR_003278.3
*Rn18S*_rev	GGGACTTAAT CAACGCAAGC			
*Actb*_for	CTAAGGCCAA CCGTGAAAAG	104	0.84/–	NM_007393.3
*Actb*_rev	ACCAGAGGCAT ACAGGGACA			
*Cd68*_for	GGACCCACAAC TGTCACTCA	60	0.89/1	NM_001291058.1
*Cd68*_rev	AATTGTGGCAT TCCCATGAC			
*Gfap*_for	ACAGACTTTCTC CAACCTCCAG	63	0.84/1	NM_001131020
*Gfap*_rev	CCTTCTGACAC GGATTTGGT			
*Iba1*_for	GGATTTGCAG GGAGGAAAAG	92	0.80/0.91	NM_019467.3
*Iba1*_rev	TGGGATCATC GAGGAATTG			
*Nos2*_for	CTTTGCCAC GGACGAGAC	66	1/0.70	NM_010927.3
*Nos2*_rev	TCATTGTACTCT GAGGGCTGAC			
*Tgfb1*_for	TGGAGCAACA TGTGGAACTC	73	1/0.91	NM_011577.2
*Tgfb1*_rev	GTCAGCAGC CGGTTACCA			
*Tnfa*_for	TCTTCTCATTCC TGCTTGTGG	101	1/0.97	NM_013693.3/ NM_001278601.1
*Tnfa*_rev	GAGGCCATTTG GGAACTTCT			

For evaluation of mRNA-levels, Actb, and Rn18S served as housekeeping genes. Primer sequence, predicted amplicon size, primer efficiency for retinae and optic nerves and GenBank accession number are listed. Bp, base pairs; for, forward; rev, reverse.

conditions, a-wave responses arise from rod-photoreceptors, while b-waves represent the rod bipolar and Müllerglia cell response. In all four conditions no significant differences were observed between control and immunized WT and KO animals (**Figures 1B,C**; **Supplementary Table 2**). Therefore, we concluded that photoreceptor and bipolar cell function was not affected in this EAG mouse model.

Significant RGC Loss Following Immunization

Previous studies of an EAG rat model showed a significant reduction of RGC numbers 4 weeks post immunization with ONA (4, 58). Additionally, an upregulation of Tnc was found before significant RGC loss occurred (6). In our EAG mouse model, we detected unaltered Tnc protein levels 10 weeks after immunization (**Supplementary Table 3, Supplementary Figure 1**). Based on these findings, immunohistochemical stainings of RGCs were performed with an antibody against Brn3a, which specifically detects RGCs (**Figure 2**, **Supplementary Table 4**). The evaluation of RGCs in retinal cross-sections showed a significant reduction in the percentage of $Brn3a^+$ cells in WT ONA compared to WT CO as well as to KO CO (WT ONA: 73.1 ± 6.1% $Brn3a^+$ cells vs. WT CO: 100.0 ± 4.2% $Brn3a^+$ cells; $p = 0.004$ and KO CO: 92.2 ± 3.9% $Brn3a^+$ cells, $p = 0.04$, **Figures 2A,B**). Interestingly, no significant differences were detected between control and immunized KO in horizontal cross-sections (KO CO: 92.2 ± 3.9% $Brn3a^+$ cells vs. KO ONA: 83.7 ± 8.7% $Brn3a^+$ cells, $p = 0.57$, **Figures 2A,B**).

To further characterize the RGC population, we counted $Brn3a^+$ cells in retinal flat-mounts (**Figure 2C**). We determined the total amount (**Figure 2D**) as well as the number of $Brn3a^+$ cells within the central (**Figure 2E**) and peripheral (**Figure 2F**) area of the retina. A significant reduction in the total number was observed in immunized WT compared to both control genotypes (WT ONA: 80.3 ± 1.5% $Brn3a^+$ cells vs. WT CO: 100.0 ± 2.0% $Brn3a^+$ cells, $p < 0.001$, KO CO: 98.2 ± 3.3% $Brn3a^+$ cells, $p < 0.001$). Also, a significant loss of RGCs was detected in KO ONA mice (86.9 ± 3.1% $Brn3a^+$ cells) compared to KO CO ($p = 0.02$) and WT CO ($p = 0.01$). A comparable percentage of $Brn3a^+$ cells was also observed in the central retina. So, immunized WT and KO animals showed a significant decline of RGCs compared to the corresponding control groups (WT ONA: 82.7 ± 1.7% $Brn3a^+$ cells vs. WT CO: 100.0 ± 2.5% $Brn3a^+$ cells, $p < 0.001$ and KO ONA: 86.3 ± 3.7% $Brn3a^+$ cells vs. KO CO: 97.8 ± 2.9% $Brn3a^+$ cells, $p = 0.03$). No significant differences were found between both immunized genotypes ($p = 0.80$). Furthermore, a decrease in the RGC density was verified in the peripheral area. Retinae of the WT ONA group (77.0 ± 1.8% $Brn3a^+$ cells) displayed a loss of about 25% RGCs compared to WT CO (100.0 ± 1.7% $Brn3a^+$ cells, $p < 0.001$). A significant reduction was also found in the comparison of KO CO and KO ONA (KO CO: 99.0 ± 4.1% $Brn3a^+$ cells vs. KO ONA: 87.1 ± 2.8% $Brn3a^+$ cells, $p = 0.02$). However, KO ONA showed a decrease of about 15 % in the peripheral part compared to WT CO group ($p = 0.01$).

Although not statistically significant, we found a trend to a weaker RGC damage in immunized KO compared to WT ONA.

Optic Nerve Degeneration Post ONA-Immunization in WT Mice

To analyze a possible degeneration of RGC axons, immunoreactivity of βIII-tubulin was examined in optic nerve longitudinal sections of control and immunized WT and KO animals (**Figure 3A**). The immunopositive βIII-tubulin area was significantly reduced in immunized WT (30.85 ± 8.55% βIII-$tubulin^+$ area) compared to WT CO (100.00 ± 18.35% βIII-$tubulin^+$ area, $p = 0.04$, **Figure 3B**). Also, the βIII-$tubulin^+$ area was decreased in WT ONA compared to both KO conditions (KO CO: 93.66 ± 19.18% βIII-$tubulin^+$ area, $p = 0.06$ and KO ONA: 119.93 ± 13.48% βIII-$tubulin^+$ area, $p < 0.01$).

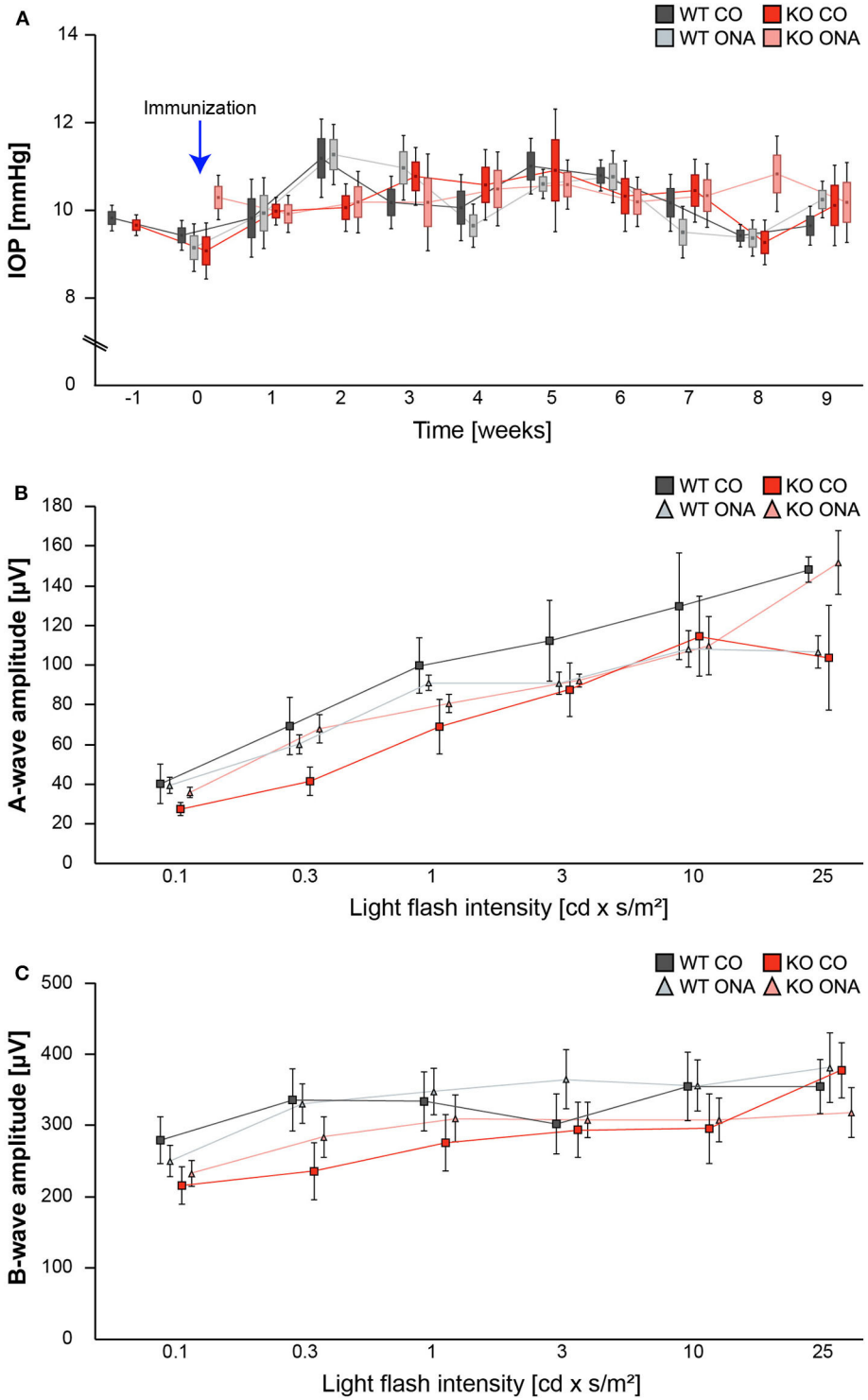

FIGURE 1 | IOP and ERG recordings were not altered after immunization of WT and KO mice. **(A)** IOP measurements were performed before immunization in 5 weeks old WT and KO mice (−1; $n = 16$/group). Then, IOP was determined weekly in immunized and control WT and KO until the end of the study ($n = 8$/group). No significant changes could be detected between all groups. **(B,C)** ERG recordings 10 weeks after initial immunization in control and immunized WT and KO mice. No changes in a-wave **(B)** and b-wave **(C)** amplitudes could be detected in control and immunized WT and KO mice ($n = 5$/group). Data were analyzed using two-way ANOVA followed by Tukey's *post-hoc* test and present as mean ± SEM ± SD in **(A)** and mean ± SEM in **(B,C)**. cd, candela; IOP, intraocular pressure; µV, micro volt; m, minutes; s, seconds.

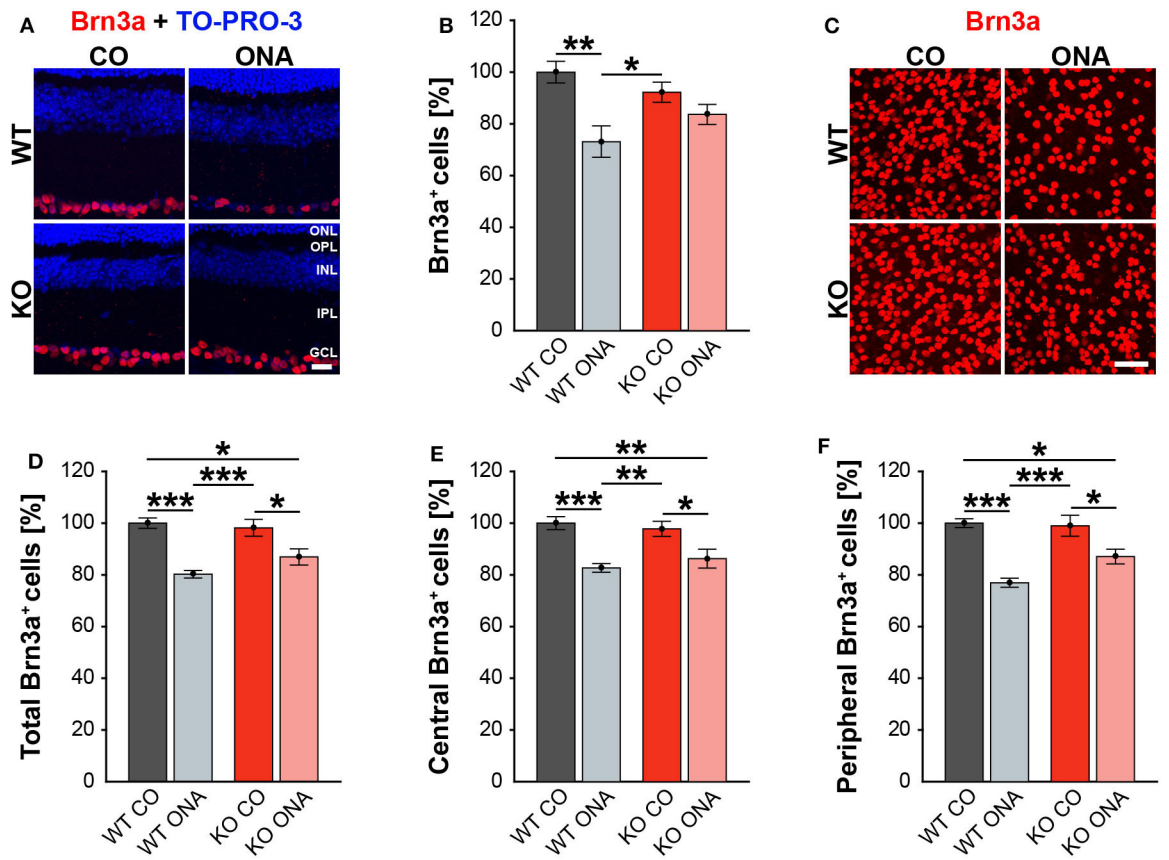

FIGURE 2 | Less RGC loss in immunized KO animals. **(A)** Retinal cross-sections from WT CO, WT ONA, KO CO, and KO ONA mice were stained with an antibody against Brn3a (red) and nuclei were detected with TO-PRO-3 (blue). **(B)** A decline of RGC numbers was detected in WT ONA compared to the control groups (n = 5/group). **(C)** Representative pictures of Brn3a$^+$ cells in retinal flat-mounts. **(D–F)** Quantification of the total RGC number as well as in central and peripheral parts (n = 9/group). A significant loss of RGCs was detected in immunized WT and KO in comparison to the control groups. It was also shown that the RGC number in KO ONA RGCs were significantly decreased compared to WT CO. Furthermore, WT ONA RGC numbers were significantly reduced compared to KO CO. Data were analyzed using two-way ANOVA followed by Tukey's *post-hoc* test and values were shown as mean ± SEM. *$p < 0.05$; **$p < 0.01$; ***$p < 0.001$. Scale bar = 20 μm in **(A)** and 50 μm in **(C)**. ONL, outer nuclear layer; OPL, outer plexiform layer; INL, inner nuclear layer; IPL, inner plexiform layer; GCL, ganglion cell layer.

Extenuated Macroglial Reactivity After Immunization in KO Mice

Our results showed a decrease in the RGC number 10 weeks after immunization in WT and KO animals. Next, we investigated, if this glaucomatous neurodegeneration is associated with an altered macroglial response. Therefore, we analyzed the immunoreactivity of GFAP$^+$ astrocytes in retinal cross-sections. GFAP stained astrocytes were mainly localized in the ganglion cell layer (GCL; **Figure 4A**). The GFAP$^+$ area was increased in WT ONA (167.22 ± 18.61% GFAP$^+$ area) compared to the control groups (WT CO: 100.00 ± 9.28% GFAP$^+$ area, $p = 0.01$ and KO CO: 105.81 ± 4.54% GFAP$^+$ area, $p = 0.02$, **Figure 4B**). Interestingly, no changes in the GFAP signal area were found in KO ONA (142.49 ± 8.19% GFAP$^+$ area) compared to KO CO ($p = 0.18$) as well as to WT CO ($p = 0.11$). The statistical comparison of both immunized genotypes showed no significant differences ($p = 0.46$).

Then, we evaluated GFAP protein levels via Western blot. For GFAP, a prominent band was detected at 50 kDa (**Figure 4C**). Relative quantification verified a slight, but not statistically significant, increase in the GFAP protein concentration in WT after immunization (WT ONA: 1.15 ± 0.25 a.u. vs. WT CO: 0.76 ± 0.11 a.u., $p = 0.73$ and KO CO: 0.91 ± 0.40 a.u., $p = 0.92$, **Figure 4D**). No changes were observed in the GFAP level of control and immunized KO animals (KO ONA: 0.98 ± 0.23 a.u., $p = 0.99$).

We also analyzed the mRNA expression of *Gfap* in retinae via RT-qPCR (**Figures 4E–G**, **Supplementary Table 5**). Analysis revealed comparable levels of *Gfap* in KO CO and WT CO (1.4-fold, $p = 0.11$, **Figure 4E**). A significant increase of *Gfap* mRNA expression levels was observed in WT ONA (WT CO vs. WT ONA: 1.7-fold, $p = 0.04$, **Figure 4F**), whereas no differences could be detected in KO ONA (KO CO vs. KO ONA: 1.2-fold, $p = 0.40$, **Figure 4F**). The expression was comparable in both immunized genotypes (1.0-fold, $p = 0.99$, **Figure 4G**).

For GFAP, a thread-like staining pattern was observed in optic nerve slices (**Figure 5A**). The evaluation of the GFAP immunoreactivity in optic nerve sections also showed no

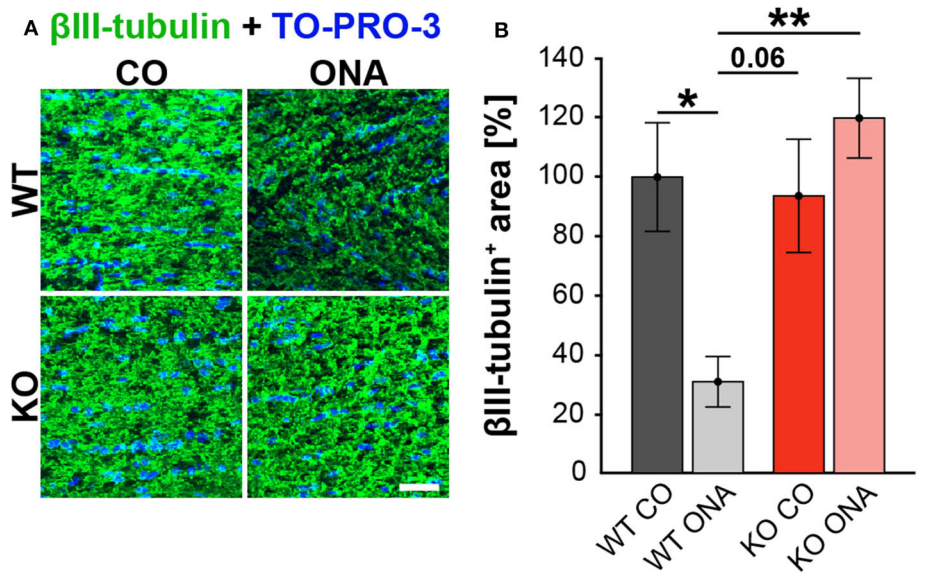

FIGURE 3 | No optic nerve degeneration in KO post immunization. **(A)** Optic nerve slices were stained with βIII-tubulin (green) and cell nuclei were marked with TO-PRO-3 (blue). **(B)** WT ONA mice showed a significantly decreased βIII-tubulin$^+$ area compared to WT CO as well as to KO ONA group. Data were analyzed using two-way ANOVA followed by Tukey's *post-hoc* test and presented as mean ± SEM. $^*p < 0.05$; $^{**}p < 0.01$. $n = 4$/group. Scale bar = 20 μm.

increased macroglial area in KO post immunization (KO ONA: 134.30 ± 23.57% GFAP$^+$ area vs. KO CO: 147.18 ± 31.27% GFAP$^+$ area, $p = 0.98$ and WT CO: 100.00 ± 17.72% GFAP$^+$ area, $p = 0.70$, **Figure 5B**). Moreover, a nearly doubled GFAP intensity was observed in WT ONA (196.70 ± 13.60% GFAP$^+$ area) compared to the corresponding control group ($p = 0.04$).

Furthermore, protein levels of GFAP via Western blot analyses were comparable between all four groups (**Figure 5C**). However, the band intensity in WT ONA group was tendentially increased compared to the control group (WT ONA: 1.36 ± 0.29 a.u. vs. WT CO: 1.02 ± 0.27 a.u., $p = 0.68$, **Figure 5D**). Equal protein levels were found between control and KO ONA animals (KO CO: 0.82 ± 0.11 a.u. vs. KO ONA: 0.84 ± 0.10 a.u., $p = 0.99$).

Finally, the RT-qPCR results of the optic nerve tissue showed no changes in *Gfap* expression between both control groups (WT CO vs. KO CO: 1.1-fold, $p = 0.54$, **Figure 5E**, **Supplementary Table 5**). In line with the immunohistochemical results, we found a slightly enhanced mRNA level in WT ONA (WT CO vs. WT ONA: 1.4-fold, $p = 0.07$, **Figure 5F**), whereas the KO ONA animals exhibited a reduction of *Gfap* expression (KO CO vs. KO ONA: 0.5-fold, $p < 0.05$). Interestingly, in a direct comparison of the two immunized groups, *Gfap* expression was significantly reduced in KO animals (WT ONA vs. KO ONA: 0.4-fold, $p = 0.02$, **Figure 5G**).

In summary, we concluded that Tnc deficiency resulted in a diminished macroglial reaction during retinal and optic nerve degeneration in the EAG mouse model.

Decreased Demyelination After ONA-Immunization in KO Mice

Our study demonstrates RGC degeneration in WT and KO animals after immunization. Furthermore, we noted that Tnc deficiency resulted in a diminished macroglial response. Finally, we analyzed the impact of ONA-immunization on oligodendroglia in optic nerve tissue. The oligodendrocytes appear in two different populations, as immature OPCs and as myelinating, mature oligodendrocytes. To analyze both oligodendrocyte populations separately, an immunohistochemical colocalization staining was performed using the markers Olig2 and CC1. Olig2 is expressed by oligodendrocytes of all stages (59). In contrast, CC1 is only expressed by mature oligodendrocytes (60). Colocalization identified double positive cells as mature and single Olig2$^+$ cells as immature oligodendrocytes. Immunohistochemical stainings revealed fewer Olig2$^+$ cells in the WT ONA group compared to the other groups. Interestingly, there were more Olig2$^+$ cells in KO ONA than in WT ONA (**Figure 6A**). 76.3 ± 1.6% Olig2$^+$ cells were found in WT ONA, which indicates a significant oligodendrocyte loss over 25% compared to control WT (100.0 ± 3.5% Olig2$^+$ cells, $p < 0.001$, **Figure 6B**). The number of Olig2$^+$ cells was also significantly decreased in WT ONA compared to KO CO ($p = 0.04$). No differences were observed between both Tnc deficient groups (KO CO: 90.2 ± 2.4% Olig2$^+$ cells vs. KO ONA: 95.2 ± 4.9% Olig2$^+$ cells, $p = 0.71$). Most interestingly, we verified significant differences between both immunized groups ($p < 0.01$). The number of double-positive (Olig2$^+$/CC1$^+$) mature oligodendrocytes was clearly reduced in WT ONA compared to all other groups (**Figure 6A**). The statistical evaluation demonstrated only 64.7 ± 5.8% Olig2$^+$/CC1$^+$ cells in WT ONA, whereas KO ONA exhibited 107.8 ± 8.9% Olig2$^+$/CC1$^+$ cells in optic nerve slices ($p = 0.002$, **Figure 6C**). Also, immunized WT showed a significant loss of mature oligodendrocytes compared to WT CO (100.0 ± 8.3% Olig2$^+$/CC1$^+$ cells,

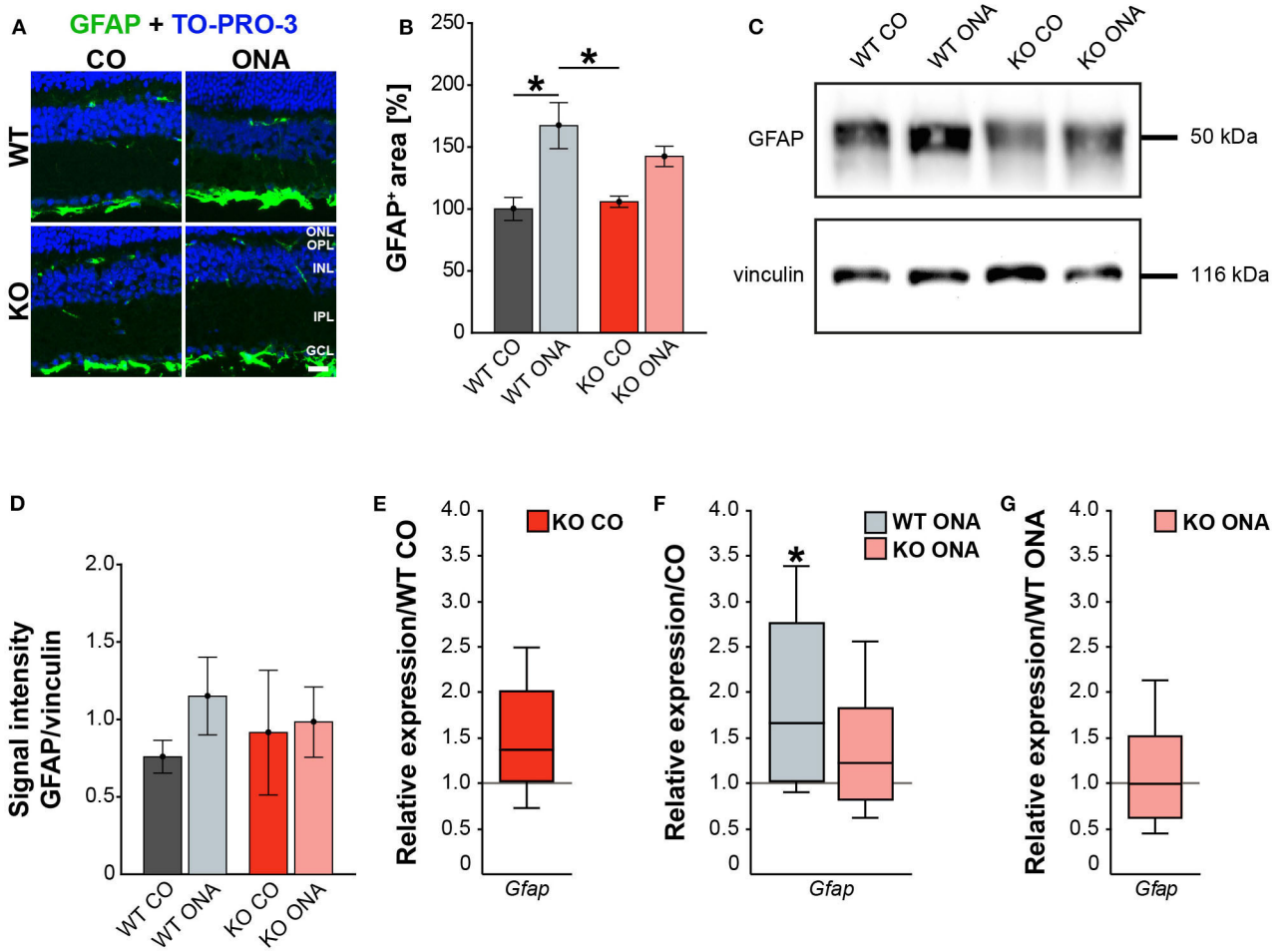

FIGURE 4 | Reduced astrogliosis after immunization in KO mice. **(A)** Images of GFAP stained macroglia cells in retinal cross-section from control and immunized WT and KO animals. Immunohistochemistry revealed a prominent signal for GFAP$^+$ cells (green) in the GCL. Cell nuclei were detected with TO-PRO-3 (blue). **(B)** GFAP$^+$ area was significantly increased in WT ONA compared to WT CO. No changes of the GFAP signal area were found in KO ONA compared to the control groups. **(C)** Western blot analyses of GFAP protein in retinal tissue. **(D)** Quantification revealed slightly more GFAP in WT ONA, whereas a comparable level was observed in KO ONA. **(E)** No differences of *Gfap* expression were noted in KO CO compared to WT CO. **(F)** A significant upregulation of *Gfap* mRNA expression was seen in WT ONA in comparison to WT CO. **(G)** WT ONA and KO ONA animals showed similar *Gfap* levels. Data were analyzed using two-way ANOVA followed by Tukey's *post-hoc* test and present as mean ± SEM in **(B,D)**. For RT-qPCR results, groups were compared using the pairwise fixed reallocation and randomization test and were shown as median ± quartile ± minimum/maximum in **(E–G)**. $^*p < 0.05$. $n = 5$/group. Scale bar = 20 µm. ONL, outer nuclear layer; OPL, outer plexiform layer; INL, inner nuclear layer; IPL, inner plexiform layer; GCL, ganglion cell layer.

$p = 0.01$) and KO CO (118.4 ± 3.5% Olig2$^+$/CC1$^+$ cells, $p < 0.001$).

To consolidate the immunohistochemistry results, we analyzed the Olig2 protein level in optic nerves by Western blot analyses (**Figure 6D**). For Olig2, we observed two bands at 32 and 50 kDa. A slight but not significantly decrease of the band intensity was found in WT ONA (0.36 ± 0.10 a.u.) compared to the corresponding control group (0.86 ± 0.41 a.u., $p = 0.41$, **Figure 6E**). Equal Olig2 protein levels were observed in KO CO (0.62 ± 0.10 a.u.) and KO ONA (0.67 ± 0.12 a.u., $p = 0.99$). Missing of Tnc resulted in an equal Olig2 protein level in both immunized groups ($p = 0.76$).

Finally, we also investigated MBP on protein level via immunohistochemistry and Western blot. This protein is specifically expressed by myelinating oligodendrocytes (61). Immunohistochemical staining revealed significantly reduced MBP immunoreactivity in WT ONA (**Figure 7A**). Statistical analyses discovered a decreased MBP signal in WT ONA (46.22 ± 11.30% MBP$^+$ area) compared to WT CO (100.00 ± 7.47% MBP$^+$ area, $p = 0.001$), KO CO (88.76 ± 4.93% MBP$^+$ area, $p = 0.01$) and KO ONA (109.79 ± 7.01% MBP$^+$ area $p < 0.001$, **Figure 7B**).

MBP was examined on protein level via Western blot analyses and a prominent protein band was detected at 20 kDa (**Figure 7C**). Quantitative analyses revealed comparable MBP protein levels in control (WT CO: 0.76 ± 0.07 a.u., KO CO: 0.56 ± 0.09 a.u.) and ONA mice (WT ONA: 0.52 ± 0.09 a.u., KO ONA: 0.51 ± 0.1 a.u., **Figure 7D**).

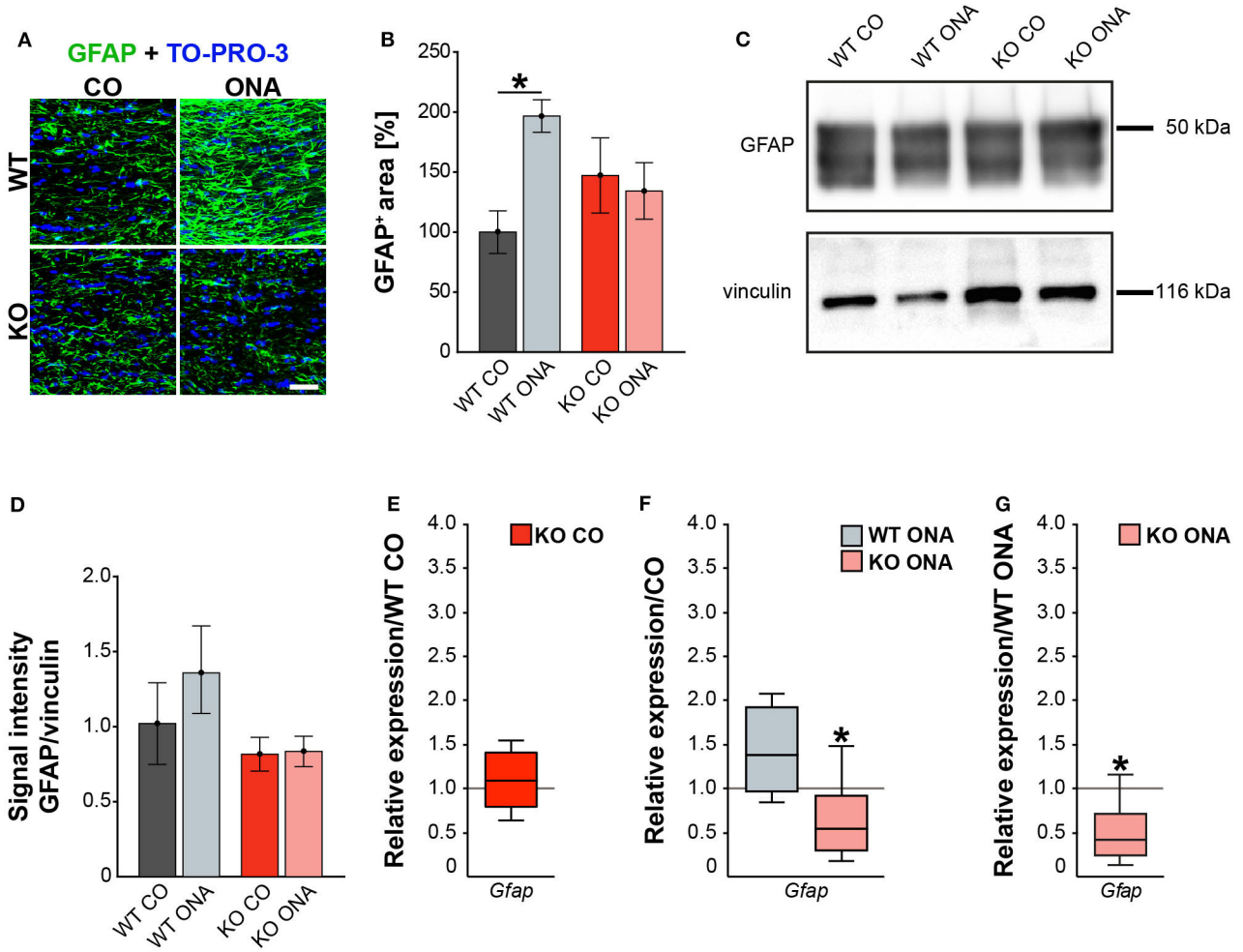

FIGURE 5 | Diminished macroglial response post ONA-immunization in optic nerve tissue of KO animals. **(A)** Representative pictures of optic nerve sections of control and immunized WT and KO mice stained against GFAP (green). Nuclear staining was done with TO-PRO-3 (blue). **(B)** WT ONA animals showed a larger GFAP$^+$ staining area then WT CO. No differences between KO mice could be detected. **(C)** Western blot analyses of relative GFAP protein levels in optic nerve tissue. **(D)** Protein quantification revealed slightly enhanced band intensity in WT ONA, whereas KO ONA exhibit no increased GFAP level. **(E)** No differences of *Gfap* expression were noted in KO CO compared to WT CO. **(F)** A slight upregulation of *Gfap* mRNA expression was seen in WT ONA in comparison to WT CO, but in KO ONA decreased expression was verified compared to KO CO. **(G)** A downregulation of *Gfap* in KO ONA in comparison to WT ONA was noted. Data were analyzed using two-way ANOVA followed by Tukey's *post-hoc* test and were shown as mean ± SEM in **(B,D)**. For RT-qPCR, groups were compared using the pairwise fixed reallocation and randomization test and were shown as median ± quartile ± minimum/maximum in **(E–G)**. *$p < 0.05$. $n = 5$/group. Scale bar = 20 μm.

In conclusion, we found a significant decrease in mature as well as immature oligodendroglia in WT after immunization. Remarkably, immunized Tnc deficient mice showed no demyelination.

Decreased Number of Microglia and Declined Microglial Response in KO ONA Mice

Neurodegeneration is often accompanied by reactive microgliosis. In order to analyze the microglia population in the EAG mouse model and the effects of immunization, we performed immunohistochemical staining of retinal flat-mounts using an Iba1 antibody (**Figure 8A**, **Supplementary Table 4**). The number of Iba1$^+$ cells in the total as well as in the central and peripheral area of the retina was evaluated (**Figures 8B–D**). A significant increase in microglia numbers was detected in WT ONA (123.0 ± 2.4% Iba1$^+$ cells) compared to control WT and KO in the total retina (WT CO: 100.0 ± 2.9% Iba1$^+$ cells, $p < 0.001$ and vs. KO CO: 102.3 ± 5.7% Iba1$^+$ cells; $p = 0.002$, **Figure 8B**). No differences were found between both control groups ($p = 0.97$). Remarkably, a significantly lower number of Iba1$^+$ cells was observed after immunization in KO ONA (KO ONA: 84.5 ± 2.7% Iba1$^+$ cells) compared to WT ONA ($p < 0.001$), WT CO ($p = 0.03$), and KO CO ($p < 0.01$). Also, in the central part of the retina 20% more Iba1$^+$ cells were detected in WT ONA (122.5 ± 2.9% Iba1$^+$ cells) compared to the corresponding control group (WT CO: 100.0 ± 3.5% Iba1$^+$ cells, $p < 0.01$, **Figure 8C**). Immunized WT

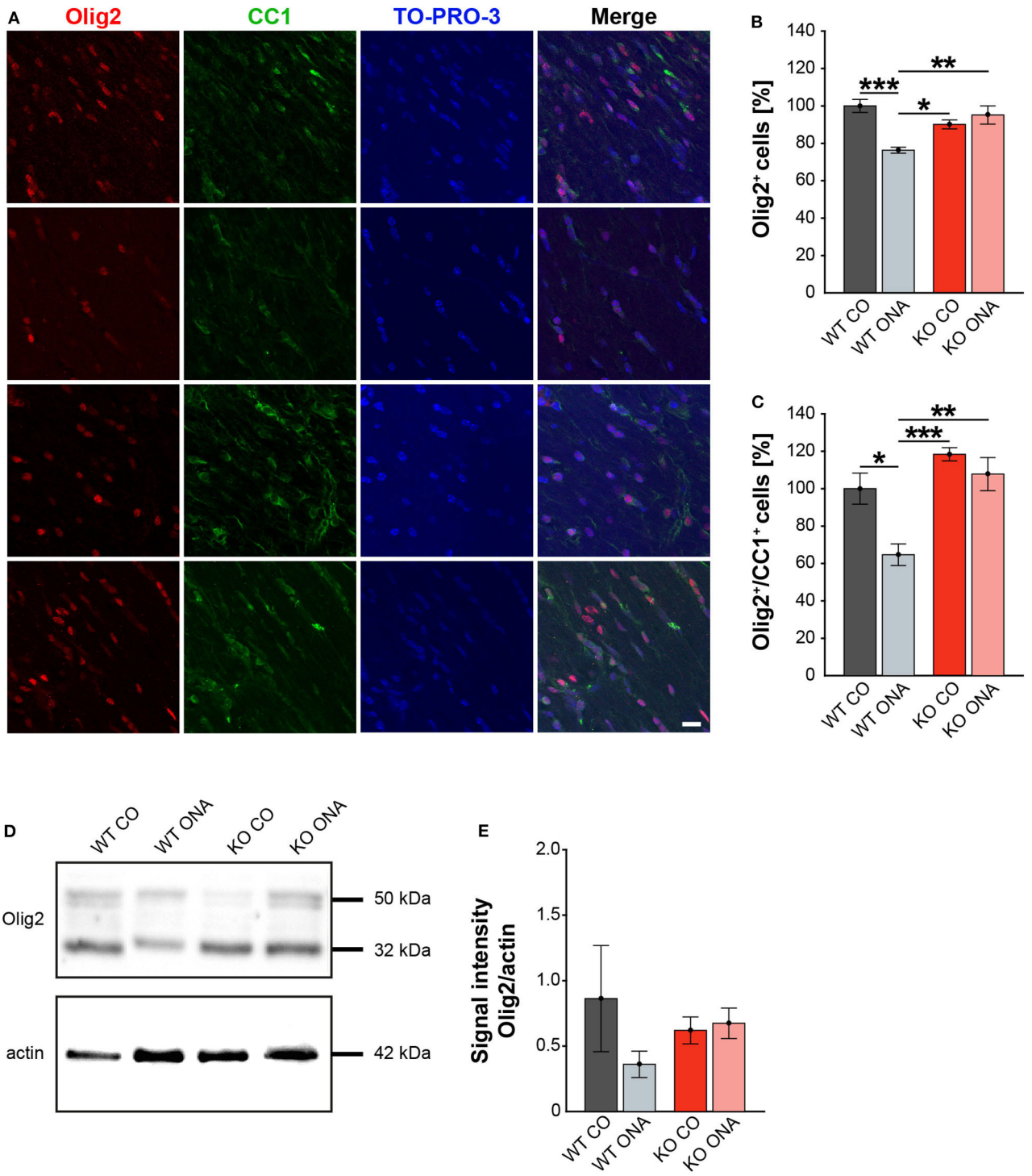

FIGURE 6 | No demyelination after immunization in KO mice. **(A)** Olig2 (red) and CC1 (green) staining of optic nerve sections. Cell nuclei were labeled with TO-PRO-3 (blue). **(B)** Quantification of Olig2$^+$ cells revealed a significant decrease of oligodendroglia in WT ONA compared to WT CO and KO CO. Interestingly, the statistical comparison of both immunized groups showed a significant loss of Olig2$^+$ cells in WT compared to KO mice. **(C)** WT ONA nerves displayed a significantly decrease of mature oligodendrocytes in comparison to both control groups. A significantly higher amount of double positive oligodendrocytes was observed in KO ONA compared to WT ONA. **(D)** An exemplary Western blot of Olig2. **(E)** Relative protein quantification revealed a slightly decreased band intensity of the Olig2 protein in WT ONA, whereas KO ONA nerves exhibited no reduction of the Olig2 protein level. Data were analyzed using two-way ANOVA followed by Tukey's *post-hoc* test and values were shown as mean ± SEM. $^*p < 0.05$; $^{**}p < 0.01$, $^{***}p < 0.001$. $n = 5$/group. Scale bar = 20 μm.

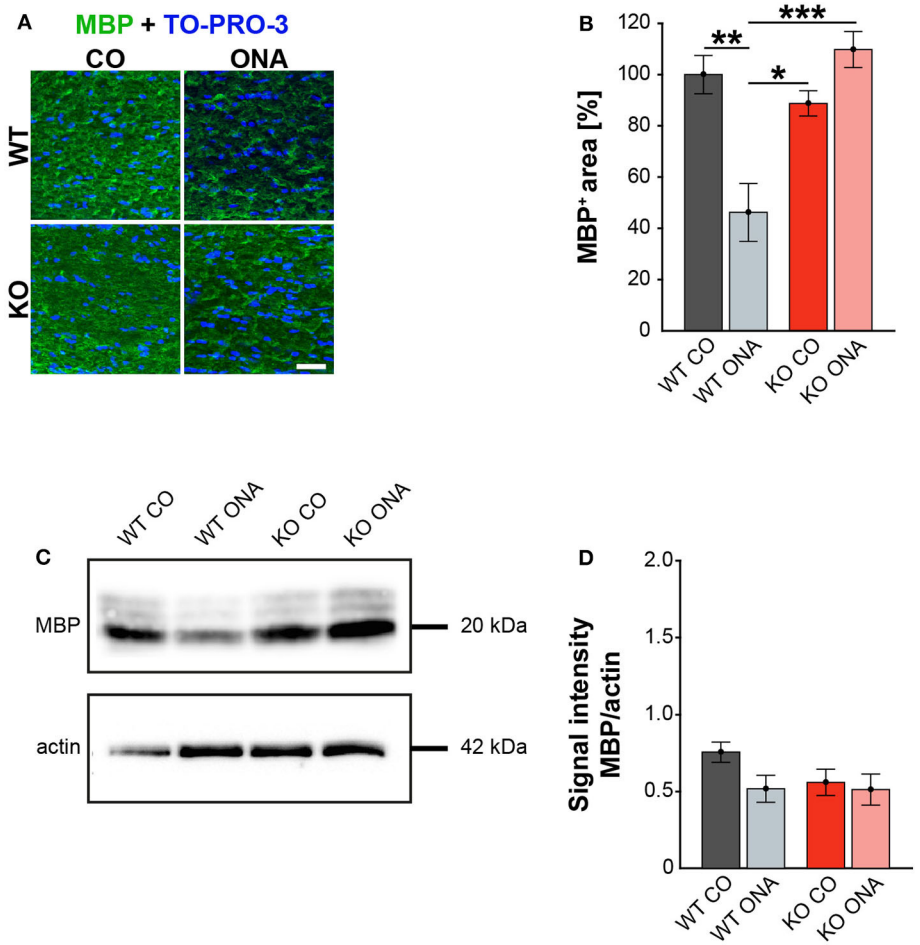

FIGURE 7 | Unaltered MBP immunoreactivity post immunization in KO mice. **(A)** MBP (green) was stained in optic nerve tissue. In blue TO-PRO-3 detected cell nuclei. Immunohistochemistry indicates a reduced MBP signal in WT ONA. **(B)** A significant downregulation of MBP was noted in WT ONA compared to WT CO. Furthermore, the MBP signal was significantly reduced in WT ONA compared to control as well as to immunized KO mice. **(C)** Western blot analyses of MBP of optic nerve tissue. **(D)** Comparable MBP protein levels were observed in all groups. Data were analyzed using two-way ANOVA followed by Tukey's *post-hoc* test and values were indicated as mean ± SEM. $^{*}p < 0.05$; $^{**}p < 0.01$; $^{***}p < 0.001$. $n = 5$/group. Scale bar = 20 μm.

also showed significantly more microglial cells compared to control ($p < 0.001$) and immunized KO mice ($p < 0.001$). In KO CO, we counted 98.1 ± 5.8% Iba1$^+$ cells, whereas KO ONA only has 84.0 ± 2.9% Iba1$^+$ cells ($p = 0.08$). A reduced microglia number was noted in KO ONA compared to WT CO ($p = 0.04$). Equal numbers of microglial cells were seen in both control groups ($p = 0.99$). Similarly, the number of microglia in WT ONA (123.6 ± 3.4% Iba1$^+$ cells) was significantly enhanced compared to WT CO (100.0 ± 3.2% Iba1$^+$ cells, $p = 0.002$, **Figure 8D**) and KO CO (107.2 ± 6.4% Iba1$^+$ cells, $p < 0.05$) in peripheral regions of the retinal. Also, the number of Iba1$^+$ cells was lower in KO ONA (85.1 ± 3.1% Iba1$^+$ cells) compared to KO CO ($p < 0.01$) and WT CO ($p = 0.08$) in the periphery. Additionally, a significantly reduced microglial response was detected in immunized KO and WT animals ($p < 0.001$). Regarding the quantification of Iba1$^+$ cells in the periphery, both control groups had similar cell counts ($p = 0.63$).

In the next step, RT-qPCR was used to investigate whether microglia have reactive phenotypes. Besides *Iba1*, we also examined the markers *Nos2* and *Cd68* in retinal tissue (**Figures 8E–G**, **Supplementary Table 5**). No differences could be detected in the *Iba1* expression between control WT and KO mice (1.3-fold, $p = 0.2$, **Figure 8E**). However, KO CO mice showed significantly elevated levels of *Nos2* (1.7-fold; $p = 0.013$) and *Cd68* (1.3-fold; $p = 0.017$) compared to WT CO. The comparison of immunized and non-immunized WT illustrated a significantly increased expression of *Iba1* (1.5-fold, $p = 0.048$) as well as of the reactive markers *Nos2* (1.4-fold, $p = 0.021$) and *Cd68* (1.3-fold, $p = 0.032$, **Figure 8F**). Interestingly, comparable expression levels of these microglial markers were found in immunized KO and KO CO (p

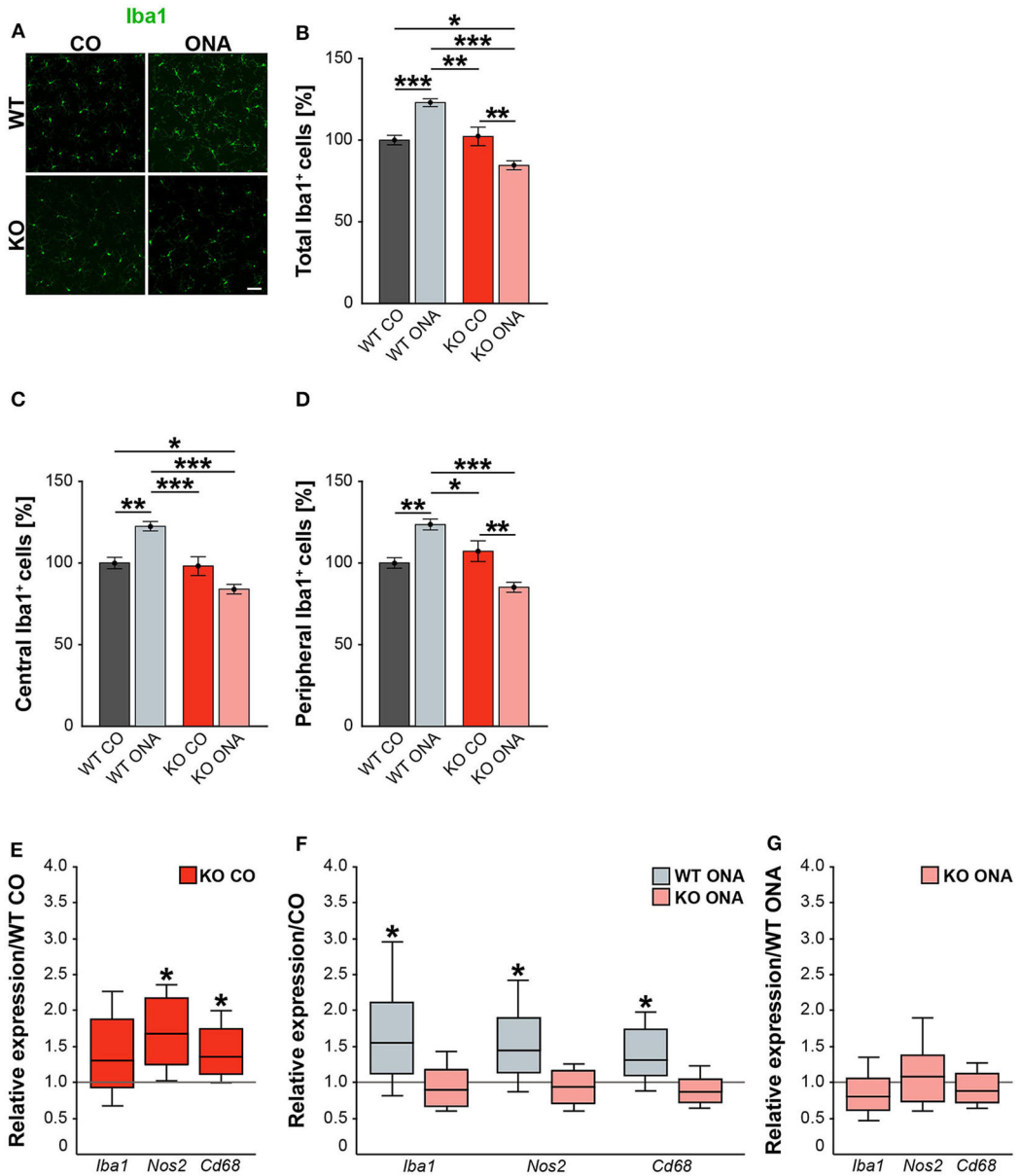

FIGURE 8 | Decreased microglia response after immunization in KO mice. **(A)** Representative pictures of Iba1$^+$ cells (green) in retinal flat-mounts of immunized and non-immunized WT and KO mice. **(B–D)** Quantification of Iba1$^+$ microglia in control and immunized WT and KO animals in the total, central and peripheral retina (n = 9/group). WT ONA group exhibited clearly more microglia. In contrast, KO ONA animals displayed fewer Iba1$^+$ cells. **(E)** RT-qPCR analyses (n = 5/group) of the relative *Iba1*, *Nos2*, and *Cd68* mRNA expression showed a significant increase of *Nos2* and *Cd68* in KO CO compared to WT CO retinae. No differences were observed for *Iba1* mRNA expression. **(F)** Compared to WT CO, a significant upregulation of *Iba1*, *Nos2*, and *Cd68* levels were found in WT ONA. No significant changes were detected regarding the expression levels of these markers in KO ONA compared to KO CO. **(G)** After immunization, a comparable mRNA level of *Iba1, Cd68*, and *Nos2* was detected in KO ONA compared to WT ONA. Data were analyzed using two-way ANOVA followed by Tukey's *post-hoc* test and present as mean ± SEM in **(B–D)**. For RT-qPCR, groups were compared using the pairwise fixed reallocation and randomization test and were shown as median ± quartile ± minimum/maximum in **(E–G)**. *$p < 0.05$; **$p < 0.01$; ***$p < 0.001$. Scale bar = 50 μm.

> 0.05, **Figure 8F**). RT-qPCR analyses revealed comparable mRNA levels in KO ONA compared to WT ONA ($p > 0.05$, **Figure 8G**).

In line with the RT-qPCR results of retinal tissue, we found a similar expression pattern of microglial markers in the optic nerve of control and immunized WT and KO mice (**Supplementary Table 5, Supplementary Figure 2**).

In summary, WT ONA animals showed a significantly increased microglia infiltration and glial marker expression, indicating an increased microglial response. Remarkably,

a significantly reduced invasion and reactivity of microglia were observed in KO ONA, suggesting that Tnc signaling is an important modulator of microglia in glaucomatous neurodegeneration.

Altered Expression Pattern of Pro- and Anti-inflammatory Cytokines in Immunized WT Compared to Immunized KO Animals

In our study, we noted a reactive gliosis and an increased microglial response after immunization in WT mice. Interestingly, these effects could not be detected in Tnc deficient animals.

Next, we analyzed the pro- and anti-inflammatory responses of the microglial phenotypes in retinae and optic nerves (**Figure 9**, **Supplementary Table 5**). Here, *Tnfa* was used to study M1 pro-inflammatory microglia, while *Tgfb1* is expressed by M2 anti-inflammatory microglia. RT-qPCR experiments revealed comparable mRNA level of *Tnfa* (1.4-fold, $p = 0.132$) and *Tgfb1* (1.4-fold, $p = 0.071$) in KO CO mice compared to WT CO mice (**Figure 9A**). After ONA-immunization, *Tnfa* was significantly upregulated in WT and interestingly downregulated in KO compared to the corresponding control groups (WT CO vs. WT ONA: 1.7-fold, $p = 0.026$ and KO CO vs. KO ONA: 0.4-fold, $p = 0.031$, **Figure 9B**). Statistical comparable *Tgfb1* mRNA levels were found in WT CO and WT ONA (1.0-fold; $p = 0.807$) as well as in KO CO and KO ONA (0.9-fold, $p = 0.415$; **Figure 9B**). The evaluation of both immunized genotypes showed a significant reduction of *Tnfa* (0.5-fold, $p = 0.036$) and a significant increase of *Tgfb1* (1.2-fold, $p = 0.005$) after immunization in KO mice (**Figure 9C**).

Finally, we examined, which microglial subtypes are altered due to an increased microglial reactivity in the optic nerve tissue of immunized and non-immunized WT and KO mice (**Figures 9D–F**, **Supplementary Table 5**). Equal mRNA levels of *Tnfa* (1.4-fold, $p = 0.07$) and *Tgfb1* (0.9-fold, $p = 0.659$) were seen in WT and KO controls (**Figure 9D**). A significantly enhanced *Tnfa* expression (2.1-fold, $p = 0.008$) and an unchanged *Tgfb1* expression (0.9-fold, $p = 0.71$) were detected in WT ONA compared to WT CO (**Figure 9E**). No changes of these markers were found in KO CO in comparison to KO ONA mice (*Tnfa*: 0.8-fold, $p = 0.443$ and *Tgfb1*: 0.9-fold, $p = 0.575$). In line with the RT-qPCR results of retinal tissue, we found a slightly reduced *Tnfa* (0.6-fold, $p = 0.101$) and an unaltered *Tgfb1* (0.8-fold, $p = 0.297$) expression between both immunized groups (**Figure 9F**).

In conclusion, missing Tnc resulted in a reduced mRNA level of pro-inflammatory *Tnfa*, but an enhanced expression of anti-inflammatory *Tgfb1*. The increased expression of the pro-inflammatory cytokine in WT after immunization points toward an enhanced presence of reactive M1 microglia.

DISCUSSION

Glaucoma involves a progressive degeneration of RGCs and their axons leading to visual field loss (62–64). Developing glaucoma is often associated with elevated IOP, but RGC damage can also occur without IOP changes. Previous studies provided evidence that an altered immune response is involved in glaucoma pathology (2, 65–68). In addition, a remodeling of ECM constituents was found in several retinal neurodegenerative diseases, including glaucoma (31–33, 69, 70).

In glaucoma pathology the mechanisms are currently poorly understood, especially the relationship between RGC loss and the role of the immune system as well as ECM molecules. Hence, we characterized glaucomatous damage associated with the absence of the ECM glycoprotein Tnc in an IOP-independent EAG mouse model for the first time. Therefore, we immunized WT and KO mice with ONA to induce retinal damage and analyzed IOP, retinal functionality, RGC degeneration, glial activation, and pro- and anti-inflammatory cytokine expression.

In a previous study, we already successfully transferred the EAG glaucoma model from rats to mice (49). Here, glaucomatous neurodegeneration was observed 6 weeks post ONA-immunization. However, in order to provoke a possible more robust glaucomatous macro- and microgliosis in our transgenic Tnc EAG mouse model, the duration of our study was extended to 10 weeks post immunization. Accordingly, we observed significantly increased GFAP levels and a higher number of $Iba1^+$ infiltrating microglia cells in the WT, suggesting an induction of glaucomatous gliosis.

Our analyses revealed that the IOP of WT and KO stayed in normal ranges. Previous studies of the EAG animal model also showed no alteration in the IOP (49, 58). Comparable IOP in control and immunized animals points to the fact that the EAG model can be considered a suitable model for normal tension glaucoma.

Analyses of retinal functionality via ERG recordings revealed no differences in a- and b-wave responses in control and immunized WT and KO mice, which indicates that photoreceptor cells as well as bipolar and Müller glia cells are not affected in our model.

We found a significant loss of $Brn3a^+$ RGCs in both genotypes following immunization. Interestingly, immunized KO mice displayed ∼15% more RGCs in retinal flat-mounts compared to immunized WT mice. Moreover, a comparable number of RGCs was found in retinal cross-sections of KO ONA animals. We also verified a severe optic nerve damage by diminished βIII-tubulin staining in immunized WT, while no alterations were found in the KO ONA mice. Previous studies of the EAG rat model showed that antibody deposits are accompanied by apoptotic RGC death (71). Furthermore, activation of the complement system via the lectin pathway seems to trigger retinal degeneration in this model (72). In our present study, we demonstrate that Tnc deficiency results in an extenuated loss of RGCs. Accordingly, we suggest that beside immunological alterations, Tnc-mediated signaling pathways are involved in glaucoma pathology.

In an EAG rat model a significant loss of RGCs could be detected 22 days after immunization (71). While an early upregulation of Tnc and its interaction partner RPTPβ/ζ/phosphacan was observed already at 7 days (6). Additionally, we noted an increased Tnc immunoreactivity in the retina 14 days post immunization. However, we did not reveal any differences regarding the Tnc protein level at later

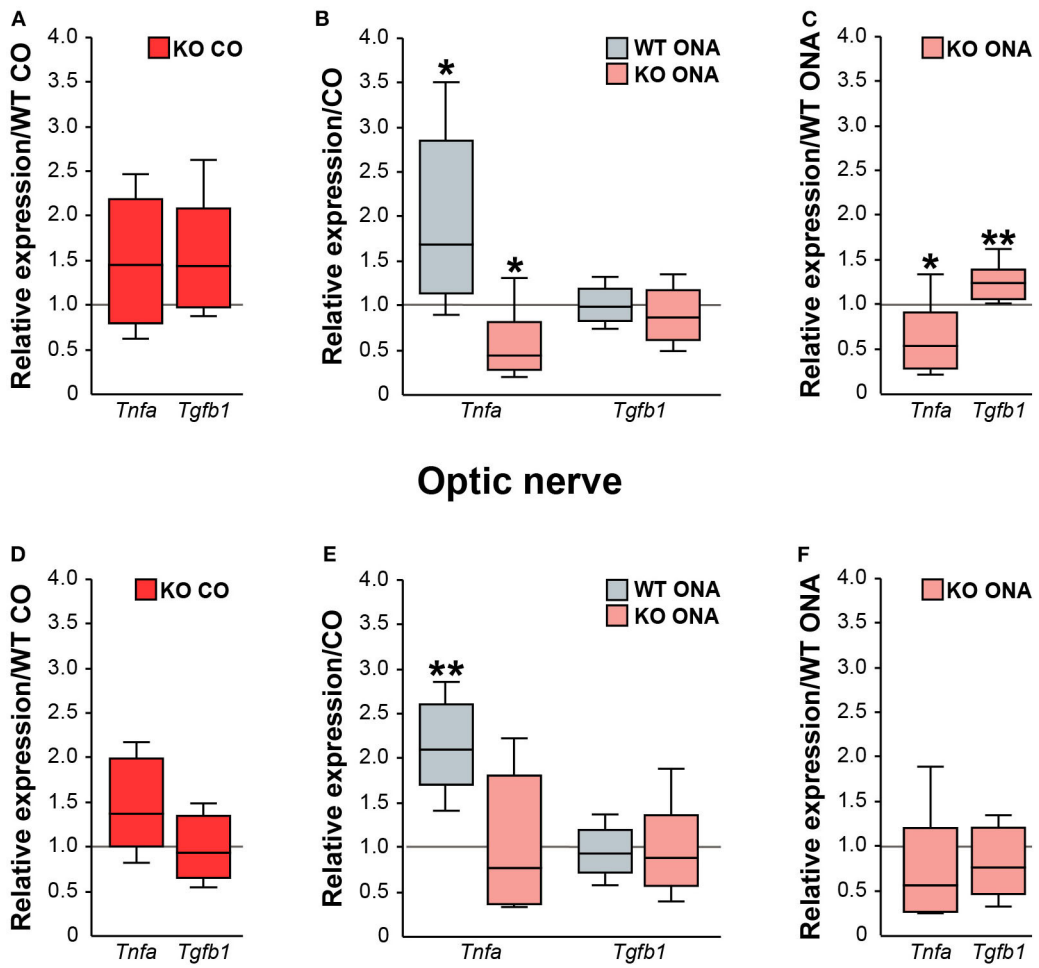

FIGURE 9 | Reduced pro-inflammatory and enhanced anti-inflammatory cytokine expression in immunized KO mice. Relative expression of pro-inflammatory *Tnfa* and anti-inflammatory *Tgfb1* was examined via RT-qPCR in control and immunized WT and KO retinae **(A–C)** and optic nerves **(D–F)**. **(A)** Analysis revealed comparable levels of *Tnfa* and *Tgfb1* in KO CO compared to WT CO. **(B)** *Tnfa* expression level was significantly increased in WT ONA compared to WT CO. Strikingly, a reduced *Tnfa* mRNA level was found in KO ONA compared to the corresponding control group. Regarding *Tgfb1,* the expression was comparable in both genotypes. **(C)** Comparison of WT ONA and KO ONA. Here, the pro-inflammatory factor was downregulated and the anti-inflammatory cytokine was significantly upregulated in KO mice after immunization. **(D–F)** Quite similar expression patterns of both examined cytokines were noted in optic nerve tissue. Only, a significantly enhanced *Tnfa* expression was detected in WT ONA compared to WT CO **(E)**. Groups were compared using the pairwise fixed reallocation and randomization test and values were shown as median ± quartile ± maximum/minimum. $^{*}p < 0.05$; $^{**}p < 0.01$. $n = 5$/group.

points in time, namely 28 days after immunization. Therefore, we assume that alterations of Tnc levels occurred at an early point in time, shortly after immunization and then returned to normal values. Due to the fact that glaucomatous degeneration in both rodent EAG models is temporally comparable, we also assume that Tnc induction takes place at similar points in time. However, the precise timeline of Tnc induction should be determined in a future follow-up project. Ten weeks after immunization, we observed Tnc immunoreactivity in horizontal and amacrine cells as well as in the outer and inner plexiform layers (27, 28). The quantification of the Tnc signal intensity revealed comparable protein levels in control and immunized WT mice. This is in line with results from the EAG rat model, were no differences in the Tnc protein levels were noted at later points in time (6).

In regard to the temporal induction, *Tnc* expression levels were enhanced 3 days post injury and returned to normal levels 7 and 14 days after the induction of brain laser lesion (73). In the CNS, *Tnc* is re-expressed under pathological conditions and represents an important component of the glial scar (11, 25, 36, 74–76). In Alzheimer's disease, Tnc immunoreactivity is highly associated with amyloid-β plaques (20). In multiple sclerosis, Tnc has an immunomodulatory function and loss of Tnc protects from experimental autoimmune encephalopathy (24). In regard to brain injury it was demonstrated that Tnc

isoforms that contain the fibronectin type III domains B and D as well as the smallest splice variants, were specifically upregulated after cortical lesion (77). Future studies should focus on comprehensive analyses of specific Tnc isoforms in our glaucoma model. Due to these and our results, we conclude that Tnc induction occurred at early points in time and returned to normal levels at later points in time after immunization with ocular antigens. We speculate that upregulation of Tnc may serve as an early indicator for neurodegenerative processes before retinal damage is detectable. Finally, we assume that Tnc is a key mediator of inflammatory responses in our glaucoma mouse model.

Studies reported that Tnc is involved in the pathogenesis of CNS autoimmunity and astrocytes are a main Tnc source (24, 29, 30, 34–36). Astrocytes are the major glial cells in the optic nerve head and provide neurotrophic as well as mechanical support for RGC axons. Furthermore, astrocytes influence survival and functionality of neurons (78, 79). Neuroinflammatory processes, characterized by altered functional properties and distribution of glial cells, appear to have an obvious function in glaucomatous optic neuropathy (80–82). In addition, an enhanced astrocyte reactivity in response to inflammatory signals is directly regulated by the ECM (83). Furthermore, RGC degeneration is accompanied by reactive astrogliosis, which results in a higher GFAP expression (51, 58, 84–86). In our study, we observed an upregulated *Gfap* expression and an increased GFAP immunostaining in retinal and optic nerve tissue of immunized WT mice, whereas absence of Tnc led to a missing reactive gliosis. Therefore, severe glaucomatous damage induced by immunization seems to be triggered by Tnc expressing reactive astrocytes in the WT condition. We assume that the increase of astrocytic Tnc results in an enhanced glial cell proliferation, infiltration and cytokine release.

We noted a reduced population of mature oligodendrocytes and OPCs after immunization in WT mice. Also, a reduced MBP immunoreactivity demonstrated a demyelination of the optic nerve in the WT condition. Furthermore, no evidence of a decreased oligodendroglia density and demyelination was detected after ONA-immunization in KO animals. Interestingly, the fraction of mature Olig2/CC1 double immunopositive oligodendrocytes was significantly increased in the KO, in agreement with findings that Tnc inhibits the maturation of oligodendrocytes (17, 87). In addition, a strong expression of Tnc in the optic nerve head inhibits the migration of oligodendrocytes from the optic nerve into the retina (88). Based on our results and the mentioned studies, we suggest that Tnc has an impact on demyelination processes. Missing of Tnc leads to no alteration in oligodendroglia but has a protective effect on myelination of optic nerve fibers in our EAG mouse model.

Microglia are the main resident immune cells of the CNS and play a crucial role during retinal neurodegeneration (89). They change their morphology to a reactive ameboid cell type after injury and neuroinflammatory changes in the retina occur during glaucomatous damage (81). Microglial activation is a very early event in glaucoma, often before significant loss of RGCs takes place (47, 90, 91). Analyses of microglial cells showed that Tnc deficiency results in a diminished microglial response characterized by a reduced number and reactivity. Furthermore, we detected enhanced levels of the anti-inflammatory factor *Tgfb1* and a decreased expression of the pro-inflammatory *Tnfa*. This is consistent with the study by Piccinini, which demonstrated that the deletion of Tnc reduced TNF-α production (92). In the retina, TGF-β signaling has an important role in neuronal differentiation and survival (93). In microglia, TGF-β regulates homeostasis and lack of TGF-β signaling promotes retinal degeneration (94, 95). Additionally, TGF-β inhibits pro-inflammatory cytokines and regulates proliferation and activity of microglia (96). Our results indicate that the loss of Tnc signaling in microglia may promote the neuroprotective M2-subtype, resulting in a weaker RGC loss as well as axonal fiber damage in immunized KO animals.

The WT condition exhibited unaltered *Tgfb1* expression and it is known that Tnc is able to bind this growth factor (97). In a pilocarpine seizure model it was shown that TGF-β signaling is accompanied by Tnc upregulation (98). Here, an increase of the *Tgfb1* level occurred shortly after pilocarpine application, whereas the rise of *Tgfb*1 was less pronounced over time. Based on this date, we suggest that TGF-β dependent signaling in WT mice is associated with an early upregulation of Tnc and becomes less efficient at later points in time.

An enhanced microglial infiltration and marker expression revealed an increased glial response in WT post immunization in our study. Moreover, we found a significantly increased expression of the pro-inflammatory cytokine *Tnfa*. In glaucoma, a glia-derived neuronal death was described through TNF-α (99–102). The indirect neurotoxicity of this pro-inflammatory factor is based on TNF receptor 2-mediated activation of microglia, whereas blocking of TNF-α results in an extenuated microglial response (101). Moreover, TNF-α does not directly induce RGC death but leads to an upregulation of the microglial Fas ligand, where the membrane-bound form elicits RGC apoptosis (103, 104). However, in an early phase after injury a neuroprotective effect of TNF-α was found in an optic nerve crush animal model (105).

Microglia are involved in time-dependent astrocytic reactivity and this cross-talk is mediated by cytokines such as TNF-α (106–108). Previous studies noted that resting microglia switched to a M1-like phenotype, which can lead to neurotoxic effects by producing high levels of pro-inflammatory cytokines (43, 109, 110). Based on this, we speculate that microglia are the first glial cells that react after immunization as a driving force of reactive gliosis in the EAG mouse model. Our investigations of immunized WT and Tnc deficient mice lead to the assumption that Tnc promotes immunomodulatory processes of the neurotoxic M1-subtype in turns of higher activity. This is in line with previous reports that Tnc supports the activity of M1-microglia (36, 111).

Astrocytes as well as microglia express the toll-like receptor 4 (TLR4) and its expression is maintained by the extracellular environment (112, 113). Tnc activates TLR4 via its fibrinogen-like globe domain and thereby regulates the production of pro-inflammatory cytokines, such as IL-6, IL-8, and TNF-α (114, 115). In primary microglia, Tnc induced the synthesis of *Tnfa* and regulated the expression of *iNOS* via TLR4

signaling (38). Besides microglia, activated macrophages can also produce TNF-α (116). In human macrophages, specific alternatively spliced Tnc isoforms stimulate IL-6 and TNF-α release via TLR4 activation (117). In an experimental model of retinal degeneration, infiltration of peripheral monocytes occurred very early on, before microglia activation could be observed (118). Accordingly, we conclude that enhanced *Tnfa* expression, 10 weeks after immunization, is caused by Tnc-induced microglial TLR4 activation. Furthermore, we speculate that microglial TNF-α release and Tnc itself may regulate astrocytic *Tnc* expression, which results in a subsequently harmful astrogliosis in glaucomatous WT mice.

Our study could show that Tnc signaling pathways modulate both microglia and astrocyte response during glaucomatous damage. This might lead to a feedback loop by which increased levels of M1-microglial factors impact astrocytic Tnc release and vice versa. Finally, we propose that Tnc acts as an endogenous TLR4 ligand and represents an alarmin in our glaucoma model. However, it is possible that other receptors, for instance integrins, have an impact on inflammatory effects of Tnc (119, 120). In this regard, also other ECM components and Tnc interaction partners might be involved. Here, e.g., the extra domain A of fibronectin was recently described to elevate IOP through TLR4 signaling in a TGFβ2-induced ocular hypertension mouse model (121). Hence, future studies should focus on the downstream signaling cascade of TLR4 in our IOP-independent EAG mouse model.

CONCLUSION

Taken together, our study demonstrated that Tnc influences glial response, migration, and inflammation during glaucomatous damage. This model is ideally suited for a better understanding of the molecular mechanisms between retinal neurodegeneration and ECM remodeling in order to develop future therapeutic options.

DATA AVAILABILITY STATEMENT

All datasets generated for this study are included in the article/**Supplementary Material**.

ETHICS STATEMENT

The animal study was reviewed and approved by Landesamt für Natur, Umwelt und Verbraucherschutz, North Rhine-Westphalia.

AUTHOR CONTRIBUTIONS

SW performed experiments, analyzed data, and wrote the manuscript. JR designed the study, analyzed data, and revised the manuscript. SR and ZC performed experiments and analyzed data. SCJ and AF designed the study and revised the manuscript. All authors read and approved the final manuscript.

FUNDING

AF received grant support from the German Research Foundation (DFG, FA-159/24-1). SW was supported by the Konrad-Adenauer-Foundation (200520593).

ACKNOWLEDGMENTS

This manuscript has been released as a pre-print at bioRxiv, (122). The authors thank Stephanie Chun, Anja Coenen, Sabine Kindermann, Franziska Mennes, Annalena Pamp, and Marion Voelzkow for excellent technical assistance.

SUPPLEMENTARY MATERIAL

The Supplementary Material for this article can be found online at: https://www.frontiersin.org/articles/10.3389/fimmu.2020.566279/full#supplementary-material

REFERENCES

1. Tezel G, Seigel GM, Wax MB. Autoantibodies to small heat shock proteins in glaucoma. *Invest Ophthalmol Vis Sci*. (1998) 39:2277–87.
2. Wax MB, Yang J, Tezel G. Serum autoantibodies in patients with glaucoma. *J Glaucoma*. (2001) 10:S22–24. doi: 10.1097/00061198-200110001-00009
3. Wax MB. The case for autoimmunity in glaucoma. *Exp Eye Res*. (2011) 93:187–90. doi: 10.1016/j.exer.2010.08.016
4. Laspas P, Gramlich OW, Muller HD, Cuny CS, Gottschling PF, Pfeiffer N, et al. Autoreactive antibodies and loss of retinal ganglion cells in rats induced by immunization with ocular antigens. *Invest Ophthalmol Vis Sci*. (2011) 52:8835–48. doi: 10.1167/iovs.10-6889
5. Joachim SC, Reinehr S, Kuehn S, Laspas P, Gramlich OW, Kuehn M, et al. Immune response against ocular tissues after immunization with optic nerve antigens in a model of autoimmune glaucoma. *Mol Vis*. (2013) 19:1804–14.
6. Reinehr S, Reinhard J, Wiemann S, Stute G, Kuehn S, Woestmann J, et al. Early remodelling of the extracellular matrix proteins tenascin-C and phosphacan in retina and optic nerve of an experimental autoimmune glaucoma model. *J Cell Mol Med*. (2016) 20:2122–37. doi: 10.1111/jcmm.12909
7. Hynes RO. The extracellular matrix: not just pretty fibrils. *Science*. (2009) 326:1216–9. doi: 10.1126/science.1176009
8. Theocharidis U, Long K, Ffrench-Constant C, Faissner A. Regulation of the neural stem cell compartment by extracellular matrix constituents. *Prog Brain Res*. (2014) 214:3–28. doi: 10.1016/B978-0-444-63486-3.00001-3
9. Faissner A, Reinhard J. The extracellular matrix compartment of neural stem and glial progenitor cells. *Glia*. (2015) 63:1330–49. doi: 10.1002/glia.22839
10. Krishnaswamy VR, Benbenishty A, Blinder P, Sagi I. Demystifying the extracellular matrix and its proteolytic remodeling in the brain: structural and functional insights. *Cell Mol Life Sci*. (2019) 76:3229–48. doi: 10.1007/s00018-019-03182-6
11. Roll L, Faissner A. Tenascins in CNS lesions. *Semin Cell Dev Biol*. (2019) 89:118–24. doi: 10.1016/j.semcdb.2018.09.012
12. Theocharis AD, Manou D, Karamanos NK. The extracellular matrix as a multitasking player in disease. *FEBS J*. (2019) 286:2830–69. doi: 10.1111/febs.14818

13. Garcion E, Faissner A, Ffrench-Constant C. Knockout mice reveal a contribution of the extracellular matrix molecule tenascin-C to neural precursor proliferation and migration. *Development*. (2001) 128:2485–96.
14. Joester A, Faissner A. The structure and function of tenascins in the nervous system. *Matrix Biol*. (2001) 20:13–22. doi: 10.1016/S0945-053X(00)00136-0
15. Garwood J, Garcion E, Dobbertin A, Heck N, Calco V, Ffrench-Constant C, et al. The extracellular matrix glycoprotein Tenascin-C is expressed by oligodendrocyte precursor cells and required for the regulation of maturation rate, survival and responsiveness to platelet-derived growth factor. *Eur J Neurosci*. (2004) 20:2524–40. doi: 10.1111/j.1460-9568.2004.03727.x
16. Loers G, Schachner M. Recognition molecules and neural repair. *J Neurochem*. (2007) 101:865–82. doi: 10.1111/j.1471-4159.2006.04409.x
17. Czopka T, Von Holst A, Ffrench-Constant C, Faissner A. Regulatory mechanisms that mediate tenascin C-dependent inhibition of oligodendrocyte precursor differentiation. *J Neurosci*. (2010) 30:12310–22. doi: 10.1523/JNEUROSCI.4957-09.2010
18. Rigato F, Garwood J, Calco V, Heck N, Faivre-Sarrailh C, Faissner A. Tenascin-C promotes neurite outgrowth of embryonic hippocampal neurons through the alternatively spliced fibronectin type III BD domains via activation of the cell adhesion molecule F3/contactin. *J Neurosci*. (2002) 22:6596–609. doi: 10.1523/JNEUROSCI.22-15-06596.2002
19. Faissner A, Roll L, Theocharidis U. Tenascin-C in the matrisome of neural stem and progenitor cells. *Mol Cell Neurosci*. (2017) 81:22–31. doi: 10.1016/j.mcn.2016.11.003
20. Mi Z, Halfter W, Abrahamson EE, Klunk WE, Mathis CA, Mufson EJ, et al. Tenascin-C is associated with cored amyloid-beta plaques in Alzheimer disease and pathology burdened cognitively normal elderly. *J Neuropathol Exp Neurol*. (2016) 75:868–76. doi: 10.1093/jnen/nlw062
21. Xie K, Liu Y, Hao W, Walter S, Penke B, Hartmann T, et al. Tenascin-C deficiency ameliorates Alzheimer's disease-related pathology in mice. *Neurobiol Aging*. (2013) 34:2389–98. doi: 10.1016/j.neurobiolaging.2013.04.013
22. Ruhmann M, Piccinini AM, Kong PL, Midwood KS. Endogenous activation of adaptive immunity: tenascin-C drives interleukin-17 synthesis in murine arthritic joint disease. *Arthritis Rheum*. (2012) 64:2179–90. doi: 10.1002/art.34401
23. Machino-Ohtsuka T, Tajiri K, Kimura T, Sakai S, Sato A, Yoshida T, et al. Tenascin-C aggravates autoimmune myocarditis via dendritic cell activation and Th17 cell differentiation. *J Am Heart Assoc*. (2014) 3:e001052. doi: 10.1161/JAHA.114.001052
24. Momcilovic M, Stamenkovic V, Jovanovic M, Andjus PR, Jakovcevski I, Schachner M, et al. Tenascin-C deficiency protects mice from experimental autoimmune encephalomyelitis. *J Neuroimmunol*. (2017) 302:1–6. doi: 10.1016/j.jneuroim.2016.12.001
25. Reinhard J, Roll L, Faissner A. Tenascins in retinal and optic nerve neurodegeneration. *Front Integr Neurosci*. (2017) 11:30. doi: 10.3389/fnint.2017.00030
26. Klausmeyer A, Garwood J, Faissner A. Differential expression of phosphacan/RPTPbeta isoforms in the developing mouse visual system. *J Comp Neurol*. (2007) 504:659–79. doi: 10.1002/cne.21479
27. D'alessandri L, Ranscht B, Winterhalter KH, Vaughan L. Contactin/F11 and tenascin-C co-expression in the chick retina correlates with formation of the synaptic plexiform layers. *Curr Eye Res*. (1995) 14:911–26. doi: 10.3109/02713689508995131
28. Sanchez-Lopez A, Cuadros MA, Calvente R, Tassi M, Marin-Teva JL, Navascues J. Radial migration of developing microglial cells in quail retina: a confocal microscopy study. *Glia*. (2004) 46:261–73. doi: 10.1002/glia.20007
29. Bartsch U, Pesheva P, Raff M, Schachner M. Expression of janusin. (J1-160/180) in the retina and optic nerve of the developing and adult mouse. *Glia*. (1993) 9:57–69. doi: 10.1002/glia.440090108
30. Reinhard J, Joachim SC, Faissner A. Extracellular matrix remodeling during retinal development. *Exp Eye Res*. (2015) 133:132–40. doi: 10.1016/j.exer.2014.07.001
31. Reinhard J, Renner M, Wiemann S, Shakoor DA, Stute G, Dick HB, et al. Ischemic injury leads to extracellular matrix alterations in retina and optic nerve. *Sci Rep*. (2017) 7:43470. doi: 10.1038/srep43470
32. Johnson EC, Jia L, Cepurna WO, Doser TA, Morrison JC. Global changes in optic nerve head gene expression after exposure to elevated intraocular pressure in a rat glaucoma model. *Invest Ophthalmol Vis Sci*. (2007) 48:3161–77. doi: 10.1167/iovs.06-1282
33. Pena JD, Varela HJ, Ricard CS, Hernandez MR. Enhanced tenascin expression associated with reactive astrocytes in human optic nerve heads with primary open angle glaucoma. *Exp Eye Res*. (1999) 68:29–40. doi: 10.1006/exer.1998.0577
34. Jakovcevski I, Miljkovic D, Schachner M, Andjus PR. Tenascins and inflammation in disorders of the nervous system. *Amino Acids*. (2013) 44:1115–27. doi: 10.1007/s00726-012-1446-0
35. Dzyubenko E, Manrique-Castano D, Kleinschnitz C, Faissner A, Hermann DM. Role of immune responses for extracellular matrix remodeling in the ischemic brain. *Ther Adv Neurol Disord*. (2018) 11:1756286418818092. doi: 10.1177/1756286418818092
36. Wiemann S, Reinhard J, Faissner A. Immunomodulatory role of the extracellular matrix protein tenascin-C in neuroinflammation. *Biochem Soc Trans*. (2019) 47:1651–60. doi: 10.1042/BST20190081
37. Smith GM, Hale JH. Macrophage/Microglia regulation of astrocytic tenascin: synergistic action of transforming growth factor-beta and basic fibroblast growth factor. *J Neurosci*. (1997) 17:9624–33. doi: 10.1523/JNEUROSCI.17-24-09624.1997
38. Haage V, Elmadany N, Roll L, Faissner A, Gutmann DH, Semtner M, et al. Tenascin C regulates multiple microglial functions involving TLR4 signaling and HDAC1. *Brain Behav Immun*. (2019) 81:1–672. doi: 10.1016/j.bbi.2019.06.047
39. Glass CK, Saijo K, Winner B, Marchetto MC, Gage FH. Mechanisms underlying inflammation in neurodegeneration. *Cell*. (2010) 140:918–34. doi: 10.1016/j.cell.2010.02.016
40. Langmann T. Microglia activation in retinal degeneration. *J Leukoc Biol*. (2007) 81:1345–51. doi: 10.1189/jlb.0207114
41. Wolf SA, Boddeke HW, Kettenmann H. Microglia in Physiology and Disease. *Annu Rev Physiol*. (2017) 79:619–43. doi: 10.1146/annurev-physiol-022516-034406
42. Harms AS, Lee JK, Nguyen TA, Chang J, Ruhn KM, Trevino I, et al. Regulation of microglia effector functions by tumor necrosis factor signaling. *Glia*. (2012) 60:189–202. doi: 10.1002/glia.21254
43. Varnum MM, Ikezu T. The classification of microglial activation phenotypes on neurodegeneration and regeneration in Alzheimer's disease brain. *Arch Immunol Ther Exp*. (2012) 60:251–66. doi: 10.1007/s00005-012-0181-2
44. Silverman SM, Wong WT. Microglia in the retina: roles in development, maturity, and disease. *Annu Rev Vis Sci*. (2018) 4:45–77. doi: 10.1146/annurev-vision-091517-034425
45. De Simone R, Ajmone-Cat MA, Minghetti L. Atypical antiinflammatory activation of microglia induced by apoptotic neurons: possible role of phosphatidylserine-phosphatidylserine receptor interaction. *Mol Neurobiol*. (2004) 29:197–212. doi: 10.1385/MN:29:2:197
46. Colton CA. Heterogeneity of microglial activation in the innate immune response in the brain. *J Neuroimmune Pharmacol*. (2009) 4:399–418. doi: 10.1007/s11481-009-9164-4
47. Ramirez AI, De Hoz R, Salobrar-Garcia E, Salazar JJ, Rojas B, Ajoy D, et al. The Role of Microglia in Retinal Neurodegeneration: Alzheimer's Disease, Parkinson, and Glaucoma. *Front Aging Neurosci*. (2017) 9:214. doi: 10.3389/fnagi.2017.00214
48. Forsberg E, Hirsch E, Frohlich L, Meyer M, Ekblom P, Aszodi A, et al. Skin wounds and severed nerves heal normally in mice lacking tenascin-C. *Proc Natl Acad Sci USA*. (1996) 93:6594–9. doi: 10.1073/pnas.93.13.6594
49. Reinehr S, Reinhard J, Wiemann S, Hesse K, Voss C, Gandej M, et al. Transfer of the experimental autoimmune glaucoma model from rats to mice-new options to study glaucoma disease. *Int J Mol Sci*. (2019) 20. doi: 10.3390/ijms20102563
50. Schmid H, Renner M, Dick HB, Joachim SC. Loss of inner retinal neurons after retinal ischemia in rats. *Invest Ophthalmol Vis Sci*. (2014) 55:2777–87. doi: 10.1167/iovs.13-13372
51. Reinhard J, Wiemann S, Joachim SC, Palmhof M, Woestmann J, Denecke B, et al. Heterozygous Meg2 ablation causes intraocular pressure elevation and progressive glaucomatous neurodegeneration. *Mol Neurobiol*. (2019) 56:4322–45. doi: 10.1007/s12035-018-1376-2

52. Faissner A, Kruse J. J1/tenascin is a repulsive substrate for central nervous system neurons. *Neuron*. (1990) 5:627–37. doi: 10.1016/0896-6273(90)90217-4
53. Reinehr S, Kuehn S, Casola C, Koch D, Stute G, Grotegut P, et al. HSP27 immunization reinforces AII amacrine cell and synapse damage induced by S100 in an autoimmune glaucoma model. *Cell Tissue Res*. (2018) 371:237–49. doi: 10.1007/s00441-017-2710-0
54. Xiang M, Zhou H, Nathans J. Molecular biology of retinal ganglion cells. *Proc Natl Acad Sci USA*. (1996) 93:596–601. doi: 10.1073/pnas.93.2.596
55. Nadal-Nicolas FM, Jimenez-Lopez M, Sobrado-Calvo P, Nieto-Lopez L, Canovas-Martinez I, Salinas-Navarro M, et al. Brn3a as a marker of retinal ganglion cells: qualitative and quantitative time course studies in naive and optic nerve-injured retinas. *Invest Ophthalmol Vis Sci*. (2009) 50:3860–8. doi: 10.1167/iovs.08-3267
56. Ito D, Imai Y, Ohsawa K, Nakajima K, Fukuuchi Y, Kohsaka S. Microglia-specific localisation of a novel calcium binding protein, Iba1. *Brain Res Mol Brain Res*. (1998) 57:1–9. doi: 10.1016/S0169-328X(98)00040-0
57. Pfaffl MW, Horgan GW, Dempfle L. Relative expression software tool. (REST) for group-wise comparison and statistical analysis of relative expression results in real-time PCR. *Nucleic Acids Res*. (2002) 30:e36. doi: 10.1093/nar/30.9.e36
58. Noristani R, Kuehn S, Stute G, Reinehr S, Stellbogen M, Dick HB, et al. Retinal and optic nerve damage is associated with early glial responses in an experimental autoimmune glaucoma model. *J Mol Neurosci*. (2016) 58:470–82. doi: 10.1007/s12031-015-0707-2
59. Gautier HO, Evans KA, Volbracht K, James R, Sitnikov S, Lundgaard I, et al. Neuronal activity regulates remyelination via glutamate signalling to oligodendrocyte progenitors. *Nat Commun*. (2015) 6:8518. doi: 10.1038/ncomms9518
60. Bin JM, Harris SN, Kennedy TE. The oligodendrocyte-specific antibody 'CC1' binds Quaking 7. *J Neurochem*. (2016) 139:181–6. doi: 10.1111/jnc.13745
61. Pohl HB, Porcheri C, Mueggler T, Bachmann LC, Martino G, Riethmacher D, et al. Genetically induced adult oligodendrocyte cell death is associated with poor myelin clearance, reduced remyelination, and axonal damage. *J Neurosci*. (2011) 31:1069–80. doi: 10.1523/JNEUROSCI.5035-10.2011
62. Tochel CM, Morton JS, Jay JL, Morrison JD. Relationship between visual field loss and contrast threshold elevation in glaucoma. *BMC Ophthalmol*. (2005) 5:22. doi: 10.1186/1471-2415-5-22
63. Shon K, Wollstein G, Schuman JS, Sung KR. Prediction of glaucomatous visual field progression: pointwise analysis. *Curr Eye Res*. (2014) 39:705–10. doi: 10.3109/02713683.2013.867353
64. Mcmonnies CW. Glaucoma history and risk factors. *J Optom*. (2017) 10:71–8. doi: 10.1016/j.optom.2016.02.003
65. Wax MB, Tezel G, Edward PD. Clinical and ocular histopathological findings in a patient with normal-pressure glaucoma. *Arch Ophthalmol*. (1998) 116:993–1001. doi: 10.1001/archopht.116.8.993
66. Tezel G, Edward DP, Wax MB. Serum autoantibodies to optic nerve head glycosaminoglycans in patients with glaucoma. *Arch Ophthalmol*. (1999) 117:917–24. doi: 10.1001/archopht.117.7.917
67. Joachim SC, Grus FH, Pfeiffer N. Analysis of autoantibody repertoires in sera of patients with glaucoma. *Eur J Ophthalmol*. (2003) 13:752–8. doi: 10.1177/1120672103013009-1003
68. Grus FH, Joachim SC, Bruns K, Lackner KJ, Pfeiffer N, Wax MB. Serum autoantibodies to alpha-fodrin are present in glaucoma patients from Germany and the United States. *Invest Ophthalmol Vis Sci*. (2006) 47:968–76. doi: 10.1167/iovs.05-0685
69. Hernandez MR, Andrzejewska WM, Neufeld AH. Changes in the extracellular matrix of the human optic nerve head in primary open-angle glaucoma. *Am J Ophthalmol*. (1990) 109:180–8. doi: 10.1016/S0002-9394(14)75984-7
70. Hernandez MR. Ultrastructural immunocytochemical analysis of elastin in the human lamina cribrosa. changes in elastic fibers in primary open-angle glaucoma. *Invest Ophthalmol Vis Sci*. (1992) 33:2891–903.
71. Joachim SC, Mondon C, Gramlich OW, Grus FH, Dick HB. Apoptotic retinal ganglion cell death in an autoimmune glaucoma model is accompanied by antibody depositions. *J Mol Neurosci*. (2014) 52:216–24. doi: 10.1007/s12031-013-0125-2
72. Reinehr S, Reinhard J, Gandej M, Kuehn S, Noristani R, Faissner A, et al. Simultaneous complement response via lectin pathway in retina and optic nerve in an experimental autoimmune glaucoma model. *Front Cell Neurosci*. (2016) 10:140. doi: 10.3389/fncel.2016.00140
73. Roll L, Eysel UT, Faissner A. Laser lesion in the mouse visual cortex induces a stem cell niche-like extracellular matrix, produced by immature astrocytes. *Front Cell Neurosci*. (2020) 14:102. doi: 10.3389/fncel.2020.00102
74. Fawcett JW, Asher RA. The glial scar and central nervous system repair. *Brain Res Bull*. (1999) 49:377–91. doi: 10.1016/S0361-9230(99)00072-6
75. Roll L, Mittmann T, Eysel UT, Faissner A. The laser lesion of the mouse visual cortex as a model to study neural extracellular matrix remodeling during degeneration, regeneration and plasticity of the CNS. *Cell Tissue Res*. (2012) 349:133–45. doi: 10.1007/s00441-011-1313-4
76. Bradbury EJ, Burnside ER. Moving beyond the glial scar for spinal cord repair. *Nat Commun*. (2019) 10:3879. doi: 10.1038/s41467-019-11707-7
77. Dobbertin A, Czvitkovich S, Theocharidis U, Garwood J, Andrews MR, Properzi F, et al. Analysis of combinatorial variability reveals selective accumulation of the fibronectin type III domains B and D of tenascin-C in injured brain. *Exp Neurol*. (2010) 225:60–73. doi: 10.1016/j.expneurol.2010.04.019
78. Russo R, Varano GP, Adornetto A, Nucci C, Corasaniti MT, Bagetta G, et al. Retinal ganglion cell death in glaucoma: Exploring the role of neuroinflammation. *Eur J Pharmacol*. (2016) 787:134–42. doi: 10.1016/j.ejphar.2016.03.064
79. De Hoz R, Rojas B, Ramirez AI, Salazar JJ, Gallego BI, Trivino A, et al. Retinal macroglial responses in health and disease. *Biomed Res Int*. (2016) 2016:2954721. doi: 10.1155/2016/2954721
80. Soto I, Howell GR. The complex role of neuroinflammation in glaucoma. *Cold Spring Harb Perspect Med*. (2014) 4. doi: 10.1101/cshperspect.a017269
81. Williams PA, Marsh-Armstrong N, Howell GR, Lasker IIOA, Glaucomatous Neurodegeneration P. Neuroinflammation in glaucoma: a new opportunity. *Exp Eye Res*. (2017) 157:20–7. doi: 10.1016/j.exer.2017.02.014
82. Melik Parsadaniantz S, Reaux-Le Goazigo A, Sapienza A, Habas C, Baudouin C. Glaucoma: a degenerative optic neuropathy related to neuroinflammation? *Cells*. (2020) 9:535. doi: 10.3390/cells9030535
83. Johnson KM, Milner R, Crocker SJ. Extracellular matrix composition determines astrocyte responses to mechanical and inflammatory stimuli. *Neurosci Lett*. (2015) 600:104–9. doi: 10.1016/j.neulet.2015.06.013
84. Senatorov V, Malyukova I, Fariss R, Wawrousek EF, Swaminathan S, Sharan SK, et al. Expression of mutated mouse myocilin induces open-angle glaucoma in transgenic mice. *J Neurosci*. (2006) 26:11903–14. doi: 10.1523/JNEUROSCI.3020-06.2006
85. Inman DM, Horner PJ. Reactive nonproliferative gliosis predominates in a chronic mouse model of glaucoma. *Glia*. (2007) 55:942–53. doi: 10.1002/glia.20516
86. Johnson EC, Morrison JC. Friend or foe? Resolving the impact of glial responses in glaucoma. *J Glaucoma*. (2009) 18:341–53. doi: 10.1097/IJG.0b013e31818c6ef6
87. Czopka T, Von Holst A, Schmidt G, Ffrench-Constant C, Faissner A. Tenascin C and tenascin R similarly prevent the formation of myelin membranes in a RhoA-dependent manner, but antagonistically regulate the expression of myelin basic protein via a separate pathway. *Glia*. (2009) 57:1790–801. doi: 10.1002/glia.20891
88. Bartsch U, Faissner A, Trotter J, Dorries U, Bartsch S, Mohajeri H, et al. Tenascin demarcates the boundary between the myelinated and nonmyelinated part of retinal ganglion cell axons in the developing and adult mouse. *J Neurosci*. (1994) 14:4756–68. doi: 10.1523/JNEUROSCI.14-08-04756.1994
89. Rashid K, Akhtar-Schaefer I, Langmann T. Microglia in retinal degeneration. *Front Immunol*. (2019) 10:1975. doi: 10.3389/fimmu.2019.01975
90. Ebneter A, Casson RJ, Wood JP, Chidlow G. Microglial activation in the visual pathway in experimental glaucoma: spatiotemporal characterization and correlation with axonal injury. *Invest Ophthalmol Vis Sci*. (2010) 51:6448–60. doi: 10.1167/iovs.10-5284
91. Bosco A, Steele MR, Vetter ML. Early microglia activation in a mouse model of chronic glaucoma. *J Comp Neurol*. (2011) 519:599–620. doi: 10.1002/cne.22516

92. Piccinini AM, Midwood KS. Endogenous control of immunity against infection: tenascin-C regulates TLR4-mediated inflammation via microRNA-155. *Cell Rep*. (2012) 2:914–26. doi: 10.1016/j.celrep.2012.09.005
93. Braunger BM, Pielmeier S, Demmer C, Landstorfer V, Kawall D, Abramov N, et al. TGF-beta signaling protects retinal neurons from programmed cell death during the development of the mammalian eye. *J Neurosci*. (2013) 33:14246–58. doi: 10.1523/JNEUROSCI.0991-13.2013
94. Zoller T, Schneider A, Kleimeyer C, Masuda T, Potru PS, Pfeifer D, et al. Silencing of TGFbeta signalling in microglia results in impaired homeostasis. *Nat Commun*. (2018) 9:4011. doi: 10.1038/s41467-018-06224-y
95. Ma W, Silverman SM, Zhao L, Villasmil R, Campos MM, Amaral J, et al. Absence of TGFbeta signaling in retinal microglia induces retinal degeneration and exacerbates choroidal neovascularization. *Elife*. (2019) 8. doi: 10.7554/eLife.42049
96. Piras F, Salani F, Bossu P, Caltagirone C, Spalletta G. High serum levels of transforming growth factor beta1 are associated with increased cortical thickness in cingulate and right frontal areas in healthy subjects. *J Neuroinflammation*. (2012) 9:42. doi: 10.1186/1742-2094-9-42
97. De Laporte L, Rice JJ, Tortelli F, Hubbell JA. Tenascin C promiscuously binds growth factors via its fifth fibronectin type III-like domain. *PLoS ONE*. (2013) 8:e62076. doi: 10.1371/journal.pone.0062076
98. Mercado-Gomez O, Landgrave-Gomez J, Arriaga-Avila V, Nebreda-Corona A, Guevara-Guzman R. Role of TGF-beta signaling pathway on Tenascin C protein upregulation in a pilocarpine seizure model. *Epilepsy Res*. (2014) 108:1694–704. doi: 10.1016/j.eplepsyres.2014.09.019
99. Tezel G, Li LY, Patil RV, Wax MB. TNF-alpha and TNF-alpha receptor-1 in the retina of normal and glaucomatous eyes. *Invest Ophthalmol Vis Sci*. (2001) 42:1787–94.
100. Kitaoka Y, Kitaoka Y, Kwong JM, Ross-Cisneros FN, Wang J, Tsai RK, et al. TNF-alpha-induced optic nerve degeneration and nuclear factor-kappaB p65. *Invest Ophthalmol Vis Sci*. (2006) 47:1448–57. doi: 10.1167/iovs.05-0299
101. Nakazawa T, Nakazawa C, Matsubara A, Noda K, Hisatomi T, She H, et al. Tumor necrosis factor-alpha mediates oligodendrocyte death and delayed retinal ganglion cell loss in a mouse model of glaucoma. *J Neurosci*. (2006) 26:12633–41. doi: 10.1523/JNEUROSCI.2801-06.2006
102. Cueva Vargas JL, Osswald IK, Unsain N, Aurousseau MR, Barker PA, Bowie D, et al. Soluble tumor necrosis factor alpha promotes retinal ganglion cell death in glaucoma via calcium-permeable AMPA receptor activation. *J Neurosci*. (2015) 35:12088–102. doi: 10.1523/JNEUROSCI.1273-15.2015
103. Gregory MS, Hackett CG, Abernathy EF, Lee KS, Saff RR, Hohlbaum AM, et al. Opposing roles for membrane bound and soluble Fas ligand in glaucoma-associated retinal ganglion cell death. *PLoS ONE*. (2011) 6:e17659. doi: 10.1371/journal.pone.0017659
104. Krishnan A, Kocab AJ, Zacks DN, Marshak-Rothstein A, Gregory-Ksander M. A small peptide antagonist of the Fas receptor inhibits neuroinflammation and prevents axon degeneration and retinal ganglion cell death in an inducible mouse model of glaucoma. *J Neuroinflammation*. (2019) 16:184. doi: 10.1186/s12974-019-1576-3
105. Mac Nair CE, Fernandes KA, Schlamp CL, Libby RT, Nickells RW. Tumor necrosis factor alpha has an early protective effect on retinal ganglion cells after optic nerve crush. *J Neuroinflammation*. (2014) 11:194. doi: 10.1186/s12974-014-0194-3
106. Liu W, Tang Y, Feng J. Cross talk between activation of microglia and astrocytes in pathological conditions in the central nervous system. *Life Sci*. (2011) 89:141–6. doi: 10.1016/j.lfs.2011.05.011
107. Pekny M, Pekna M. Astrocyte reactivity and reactive astrogliosis: costs and benefits. *Physiol Rev*. (2014) 94:1077–98. doi: 10.1152/physrev.00041.2013
108. Norden DM, Trojanowski PJ, Villanueva E, Navarro E, Godbout JP. Sequential activation of microglia and astrocyte cytokine expression precedes increased Iba-1 or GFAP immunoreactivity following systemic immune challenge. *Glia*. (2016) 64:300–16. doi: 10.1002/glia.22930
109. Block ML, Zecca L, Hong JS. Microglia-mediated neurotoxicity: uncovering the molecular mechanisms. *Nat Rev Neurosci*. (2007) 8:57–69. doi: 10.1038/nrn2038
110. Tang Y, Le W. Differential Roles of M1 and M2 Microglia in Neurodegenerative Diseases. *Mol Neurobiol*. (2016) 53:1181–94. doi: 10.1007/s12035-014-9070-5
111. Claycomb KI, Winokur PN, Johnson KM, Nicaise AM, Giampetruzzi AW, Sacino AV, et al. Aberrant production of tenascin-C in globoid cell leukodystrophy alters psychosine-induced microglial functions. *J Neuropathol Exp Neurol*. (2014) 73:964–74. doi: 10.1097/NEN.0000000000000117
112. Jack CS, Arbour N, Manusow J, Montgrain V, Blain M, Mccrea E, et al. TLR signaling tailors innate immune responses in human microglia and astrocytes. *J Immunol*. (2005) 175:4320–30. doi: 10.4049/jimmunol.175.7.4320
113. Rosenberger K, Derkow K, Dembny P, Kruger C, Schott E, Lehnardt S. The impact of single and pairwise Toll-like receptor activation on neuroinflammation and neurodegeneration. *J Neuroinflammation*. (2014) 11:166. doi: 10.1186/s12974-014-0166-7
114. Midwood K, Sacre S, Piccinini AM, Inglis J, Trebaul A, Chan E, et al. Tenascin-C is an endogenous activator of Toll-like receptor 4 that is essential for maintaining inflammation in arthritic joint disease. *Nat Med*. (2009) 15:774–80. doi: 10.1038/nm.1987
115. Zuliani-Alvarez L, Marzeda AM, Deligne C, Schwenzer A, Mccann FE, Marsden BD, et al. Mapping tenascin-C interaction with toll-like receptor 4 reveals a new subset of endogenous inflammatory triggers. *Nat Commun*. (2017) 8:1595. doi: 10.1038/s41467-017-01718-7
116. Parameswaran N, Patial S. Tumor necrosis factor-alpha signaling in macrophages. *Crit Rev Eukaryot Gene Expr*. (2010) 20:87–103. doi: 10.1615/CritRevEukarGeneExpr.v20.i2.10
117. Giblin SP, Schwenzer A, Midwood KS. Alternative splicing controls cell lineage-specific responses to endogenous innate immune triggers within the extracellular matrix. *Matrix Biol*. (2020). doi: 10.1016/j.matbio.2020.06.003
118. Paschalis EI, Lei F, Zhou C, Kapoulea V, Thanos A, Dana R, et al. The role of microglia and peripheral monocytes in retinal damage after corneal chemical injury. *Am J Pathol*. (2018) 188:1580–96. doi: 10.1016/j.ajpath.2018.03.005
119. Midwood KS, Chiquet M, Tucker RP, Orend G. Tenascin-C at a glance. *J Cell Sci*. (2016) 129:4321–7. doi: 10.1242/jcs.190546
120. Marzeda AM, Midwood KS. Internal affairs: Tenascin-C as a clinically relevant, endogenous driver of innate immunity. *J Histochem Cytochem*. (2018) 66:289–304. doi: 10.1369/0022155418757443
121. Roberts AL, Mavlyutov TA, Perlmutter TE, Curry SM, Harris SL, Chauhan AK, et al. Fibronectin extra domain A. (FN-EDA) elevates intraocular pressure through Toll-like receptor 4 signaling. *Sci Rep*. (2020) 10:9815. doi: 10.1038/s41598-020-66756-6
122. Wiemann S, Reinhard J, Reinehr S, Cibir Z, Joachim SC, Faissner A. Loss of extracellular matrix molecule tenascin-C leads to absence of reactive gliosis and promotes anti-inflammatory cytokine expression in an autoimmune glaucoma model. *bioRxiv*. (2020). doi: 10.1101/2020.04.28.064758

Conflict of Interest: The authors declare that the research was conducted in the absence of any commercial or financial relationships that could be construed as a potential conflict of interest.

frontiers in Immunology

OPINION
published: 26 November 2020
doi: 10.3389/fimmu.2020.611789

Tenascin-C: From Discovery to Structure-Function Relationships

Matthias Chiquet *

Laboratory for Oral Molecular Biology, Department of Orthodontics and Dentofacial Orthopedics, University of Bern, Bern, Switzerland

Keywords: recombinant protein, cDNA sequencing, electron microscopy, monoclonal antibodies, extracellular matrix, fibronectin, tenascin-C, rotary shadowing

INTRODUCTION: HOW TO ISOLATE AN ECM PROTEIN IN 1980

Forty years ago, the tremendous complexity of extracellular matrix (ECM) was still largely an uncharted area, mainly because many of its components could only be solubilized by denaturing agents. Known were just five types of collagens, elastin, a couple of proteoglycans, and a few ECM glycoproteins, among them fibronectin, thrombospondin-1, and laminin-111 (1). The best studied was fibronectin (2), which became notorious for promoting specific cell adhesion to collagens. In parallel, the search for yet undetected large ECM glycoproteins continued. In 1981-82, Carter (3) observed several novel glycoproteins in human fibroblast ECM extracts. Among them, "GP250" was shown to be distinct from fibronectin but resisted isolation. However, between 1983-85 several research groups independently discovered and characterized a similar ECM glycoprotein that later became known as tenascin-C (see below). Its subunits were comparable in size to fibronectin but instead of dimers formed large (>10^6 kDa) disulfide-linked oligomers. In the following paragraphs, the history and context of the individual discoveries of tenascin-C is briefly recounted. I then describe how a combination of methods available at the time lead to a detailed structural model of tenascin-C. This was the basis for trying to assign functions to different parts of the molecule. For reasons outlined below, this turned out to be more difficult than for fibronectin.

OPEN ACCESS

Edited by:
Kim Midwood,
University of Oxford, United Kingdom

Reviewed by:
Richard P. Tucker,
University of California, Davis, United States

***Correspondence:**
Matthias Chiquet
matthias.chiquet@zmk.unibe.ch

Specialty section:
This article was submitted to Inflammation, a section of the journal Frontiers in Immunology

Received: *29 September 2020*
Accepted: *05 November 2020*
Published: *26 November 2020*

Citation:
Chiquet M (2020) Tenascin-C: From Discovery to Structure-Function Relationships. Front. Immunol. 11:611789. doi: 10.3389/fimmu.2020.611789

DISCOVERIES OF TENASCIN-C

Glial Mesenchymal Extracellular Matrix (GMEM) Protein

Working on brain cancer, Bourdon et al. (4) aimed at finding a glioma-specific cell surface marker. They used the new tool of generating a monoclonal antibody (mAb) library, which they screened for mAbs binding specifically to U-251 glioma cells. One mAb, 81C6, also strongly reacted with the ECM of these cells. The antigen recognized by this mAb was detected in human glioblastoma but few other neural cancers, and was absent from normal human brain. The novel ECM component was also present in restricted mesenchymal areas of normal adult tissues. Interestingly, "glial mesenchymal extracellular matrix" (GMEM) antigen was practically absent from normal skin, but was strongly expressed by fibrosarcomas and human fibroblast lines in culture. By radioimmunoassays, mAb 81C6 did not react with plasma fibronectin, collagen types I-V, and glycosaminoglycans. Immunoprecipitation of radiolabeled U-251 cell extracts revealed two bands of 230 and 210 kDa on reducing SDS gels. The authors concluded to have identified a novel human ECM protein of glial

and mesenchymal origin that differed from fibronectin and any other ECM component known at the time.

Myotendinous Antigen

Tenascin-C was discovered a second time due to its appearance in the developing vertebrate musculoskeletal system. Chiquet and Fambrough (5) aimed at finding mesenchymal ECM components that connect muscle fibers to tendons at the myotendinous junctions. Again a mAb library was generated, this time against chick skeletal muscle ECM, and screened for antibodies that specifically labeled tendons and myotendinous junctions in embryonic and adult limbs. The most promising, mAb M1, recognized a "myotendinous antigen" that was also present in restricted areas of a few other developing organs. After immunoprecipitation, a major band at 220 kDa and two minor (splice) variants at 200 and 190 kDa were observed. Despite of similar size, there were clear differences to fibronectin. First, proteolytic cleavage patterns of myotendinous antigen were distinct from fibronectin. Second, on non-reducing SDS gels the antigen had an Mr of $>10^6$, indicating that it was a disulfide-linked oligomer instead of a dimer. Third, contrary to fibronectin, myotendinous antigen did not bind to gelatin but co-purified with proteoglycan, pointing to functional differences (6). In conclusion, a novel ECM protein presumably involved in muscle-tendon interactions was isolated.

Hexabrachion

Erickson and Inglesias (7) investigated cell surface fibronectin preparations after rotary shadowing in the electron microscope (EM). The majority of particles in their samples had the typical V-shape of fibronectin dimers, but in addition they found molecules of a peculiar six-armed, gnat-like appearance that they called "hexabrachions". In contrast to the rather uniform fibronectin subunits, hexabrachion arms showed distinct structural features. The authors therefore concluded that hexabrachions were not higher-order fibronectin oligomers, but represented a novel ECM protein contaminating fibronectin preparations.

J1 Glycoproteins

The mAbs L2 and HNK-1 recognize a specific oligosaccharide epitope present on certain neural adhesion molecules. To identify unknown neural components carrying this epitope, Kruse et al. (8) used a mAb L2 column to enrich for L2/HNK-1 positive proteins from mouse brain. After removing N-CAM, L1, and MAG, they produced an antiserum against the "rest L2 fraction". Interestingly, this antiserum inhibited neuron-astrocyte interactions in culture. On immunoblots, it reacted with a mixture of ECM proteins present in brain. According to their size in kDa, these proteins were called "J1-200/220" and "J1-160/180", respectively. Later, collaborations established that J1-200/220 was identical to tenascin-C (9), and J1-160/180 to its paralog tenascin-R (10).

Cytotactin

Grumet et al. (11) published a similar approach to isolate "cytotactin" from embryonic chicken brain. They purified the protein from a crude fraction of HNK-1-positive components by ion exchange chromatography, and showed it to be a disulfide-linked complex of 220, 200 and 190 kDa polypeptides like myotendinous antigen. Purified cytotactin blocked the activity of an antiserum that inhibited the adhesion of neurons to glial cells, again indicating that the novel ECM protein was involved in the interaction between the two cell types. Grumet et al. (11) also showed the distribution of cytotactin in the chick embryo, which agreed with the results for myotendinous antigen (5).

Tenascin-C

Exchange of reagents and collaborations quickly established that the novel ECM protein described independently was in fact one molecular species (12). Eventually, the new name "tenascin" coined by Chiquet-Ehrismann et al. (13) became generally accepted. After discovery of the additional family members tenascin-R (14), -X (15), and -W/N (16), the original tenascin was amended to tenascin-C (17).

TOWARDS A STRUCTURAL MODEL OF TENASCIN-C

A crude model of tenascin-C was already laid out in the first publications. The molecule consisted of several similar or identical 220 kDa subunits that were linked together at one end by disulfide bridges (6). EM images of rotary-shadowed molecules revealed an intriguing hexabrachion structure (**Figure 1**). From opposite sides of a central globule, two triplets of arms were emanating that showed distinct features. Each arm had a thin proximal rod fused to a thicker, flexible middle region and ended in a distal globular domain (7, 18, 19). From expression cloning using the new antibodies against tenascin/cytotactin, its first cDNA sequences were published in 1988 (20, 21). Fortunately, the tenascin-C cDNA contained sequence repeats coding for some small protein modules for which X-ray structures were already available. These were (from N- to C-terminus) an alpha-helical coiled coil domain suitable for oligomerization, epidermal growth factor (EGF)-like modules, a series of fibronectin type III (FN3) domains, and a single globular domain related to the fibrinogen gamma-chain (**Figure 1A**).

It was tempting to correlate the tenascin-C cDNA sequence with the structural features of hexabrachion particles as observed by EM. The N-terminal coiled-coil domain with adjacent cysteines could link two triplets of subunits at the central globe via disulfide bridges. The EGF-like repeats might correspond to the proximal rod domain of each hexabrachion arm, the stretch of FN3 domains to the flexible middle part, and the fibrinogen-like domain to the distal globule (**Figure 1A**). To prove this hypothesis for avian tenascin-C, two approaches were used. First, a library of monoclonal antibodies was generated against the purified molecule (18). Individual antibodies were tested for their binding to different recombinant tenascin-C fragments that were derived from various parts of the sequence (22). Simultaneously, individual mAbs were incubated with intact tenascin-C, and the

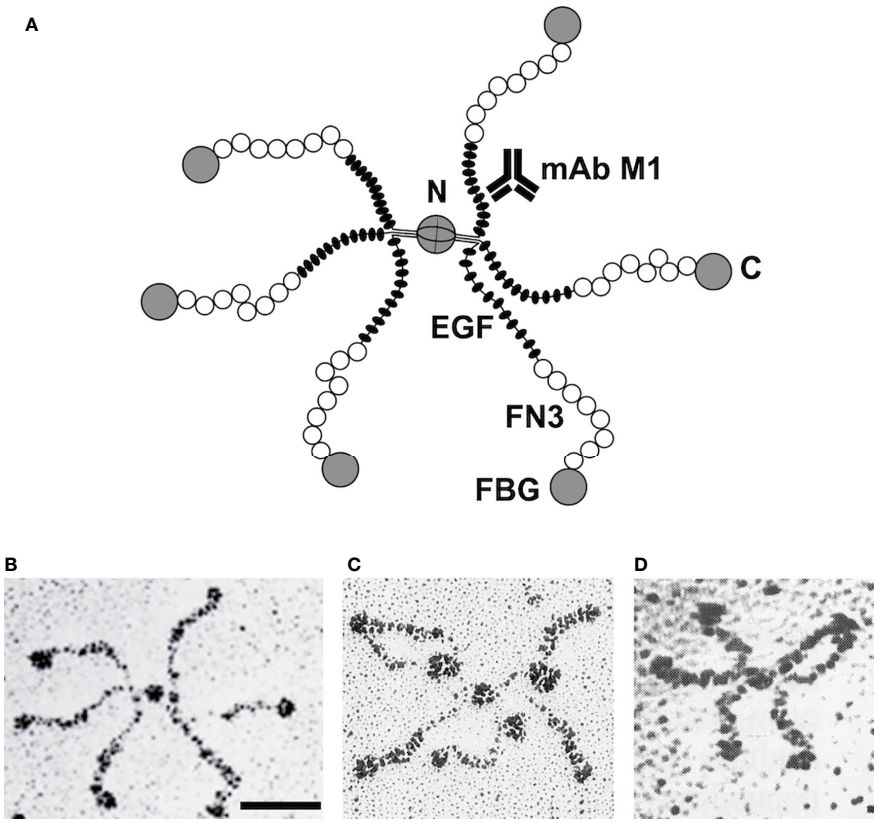

FIGURE 1 | Correlation of tenascin-C domain structure with electron micrographic images. Model of the hexameric tenascin-C molecule derived from cDNA sequencing. Each arm corresponds to one subunit: two triplets of arms are connected by disulfide bridges at the central globular domain. C, C-terminus; N, N-terminus; EGF, EGF-like domains; FN3, fibronectin type III repeats; FBG, fibrinogen-like domain; mAb M1, monoclonal antibody binding site **(A)**. EM image of a single tenascin-C (hexabrachion) molecule after rotary shadowing. Bar, 50 nm **(B)**. EM image of tenascin-C molecule with three mAb M1 particles binding to the inner rod domain (EGF repeats) of its arms **(C)**. Recombinant tenascin-C mutant with a deletion of the EGF-like repeats. Note that the arms are shortened because their inner rod domain is missing **(D)**. Original micrographs **(B, C)** from Chiquet-Ehrismann et al. (18), and **(D)** from Fischer et al. (19) with permission.

mixture was examined in the EM after rotary shadowing. IgG molecules attached to hexabrachion particles could easily be identified and their binding sites mapped from such images (**Figure 1C**). For example, mAb M1 reacted with a recombinant chick tenascin-C fragment containing the N-terminal EGF-like repeats, and mAb Tn68 with a fragment comprising the C-terminal FN3 repeats (22). On EM images, mAb M1 bound to the proximal thin rod region of tenascin-C particles (**Figure 1C**), and mAb Tn68 to the flexible middle region close to the distal globe. Similarly, mAbs against other parts of the molecule were mapped by EM on intact tenascin-C.

Later, a complementary approach derived from analyzing recombinant deletion variants of full-length tenascin-C by EM. Fischer et al. (19) expressed and purified chick tenascin-C subunits that lacked specific parts of the intact molecule, but still assembled correctly into hexabrachion particles. Reactivity of such tenascin-C variants with antibodies matched with the specific deletions. A variant missing the EGF-like domains reacted with all tenascin-C specific mAbs except mAb M1, and when examined in the EM, it lacked the proximal rod-like part of the hexabrachion arms (**Figure 1D**). A FN3 deletion variant did not react with mAb Tn68, and missed the flexible middle region from the hexabrachion structure. Similarly, when the fibrinogen-like domain was deleted, hexabrachions without the distal globe of the arms were observed by EM. By these means, it was possible to generate a precise model of the hexameric chick tenascin-C molecule (19, 22) (**Figure 1**). Knowing the X-ray structures of the various modules from those of the original proteins, on paper the model of $1.3x10^6$ kDa hexameric tenascin-C could be extrapolated essentially to atomic resolution.

DISCUSSION: THE TRICKY PATH FROM STRUCTURE TO FUNCTION

Elucidation of the structure of a complex protein is rightly considered the basis for understanding its interactions and functions. In the ECM field in the early 1980s, fibronectin was the role model. Once its general structure was known, various

defined functions could be assigned to distinct parts of the molecule, among them cell/integrin, gelatin/collagen, and heparin/glycosaminoglycan binding sites. In fibronectin, all these sites fully retained their individual functions as small proteolytic or recombinant fragments. Fibronectin appeared like an interface with independent functional units plugged in, enabling it to connect cells with ECM (23). However, the example of fibronectin spoiled us. For other large ECM proteins, the structure-function relationships turned out to be much more complex, and tenascin-C is a puzzling example. It has been classified as an adhesion-modulating "matricellular" protein with seemingly context-dependent activities. On the one hand, it is a poor adhesion molecule for many cells and notorious for inhibiting spreading of fibroblasts on fibronectin (18). On the other hand, it binds proteoglycans and promotes neurite outgrowth [for review, see (24)]. However, it proved difficult to assign these functions to specific parts of the molecule. Partially conflicting results were reported from using small recombinant tenascin-C fragments (22, 25, 26). In a reciprocal approach, Fischer et al. (19) instead analyzed avian tenascin-C deletion mutants for function. In this case, tenascin-C lacking the C-terminal fibrinogen-like domain completely lost its ability to inhibit fibroblast spreading. However, deletion of other regions (primarily adjacent FN3 repeats) diminished this activity as well. Similarly, the neurite-promoting activity of full-length tenascin-C disappeared completely by removing just the fibrinogen globe. However, when the FN3 repeats were omitted in addition, a strong neurite-promoting activity became unmasked in the EGF-like region, which was not seen with intact tenascin-C and did not depend on the fibrinogen domain. Thus in contrast to fibronectin, distinct activities of tenascin-C appear to depend on strong crosstalks between its various domains (19). Such interactions can also affect functions (such as glycosaminoglycan binding) that are observed with certain fragments but hidden in the full-length molecule (27). Intact tenascin-C is clearly much more than just the sum of its parts, which complicates the analysis of structure-function relationships. This should be taken into account when studying the more recently discovered roles of tenascins in the immune system (28), which are the topic of this special issue.

AUTHOR CONTRIBUTIONS

MC designed the article, assembled the literature, drafted and edited the manuscript, and prepared the figure.

FUNDING

Own work on tenascin-C was supported by a postdoctoral fellowship of the Bay Foundation, and by a career development award (START fellowship #9060) and research grants #9474, #31007, #45952, #55551, #67029, and #107515 from the Swiss National Science Foundation.

ACKNOWLEDGMENTS

Electron micrographs in **Figure 1** were originally generated by Konrad Beck and Therese Schulthess, then at the Biocenter, University of Basel. I would like to thank all my colleagues with whom I collaborated during my work with tenascins. They are too numerous to mention, but they know how much I appreciated their support and friendship over the years. This article is dedicated to Ruth Chiquet-Ehrismann, tenascin pioneer and my best colleague and partner both in science and life. Ruth died on September 4, 2015.

REFERENCES

1. Hay ED. Extracellular matrix. *J Cell Biol* (1981) 91:205s–23s. doi: 10.1083/jcb.91.3.205s
2. Hynes RO, Yamada KM. Fibronectins: multifunctional modular glycoproteins. *J Cell Biol* (1982) 95:369–77. doi: 10.1083/jcb.95.2.369
3. Carter WG. Transformation-dependent alterations in glycoproteins of extracellular matrix of human fibroblasts. Characterization of GP250 and the collagen-like GP140. *J Biol Chem* (1982) 257:13805–15. doi: 10.1016/B978-0-12-333320-9.50030-1
4. Bourdon MA, Wikstrand CJ, Furthmayr H, Matthews TJ, Bigner DD. Human glioma-mesenchymal extracellular matrix antigen defined by monoclonal antibody. *Cancer Res* (1983) 43:2796–805.
5. Chiquet M, Fambrough DM. Chick myotendinous antigen. I. A monoclonal antibody as a marker for tendon and muscle morphogenesis. *J Cell Biol* (1984) 98:1926–36. doi: 10.1083/jcb.98.6.1926
6. Chiquet M, Fambrough DM. Chick myotendinous antigen. II. A novel extracellular glycoprotein complex consisting of large disulfide-linked subunits. *J Cell Biol* (1984) 98:1937–46. doi: 10.1083/jcb.98.6.1937
7. Erickson HP. Inglesias JL. A six-armed oligomer isolated from cell surface fibronectin preparations. *Nature* (1984) 311:267–9. doi: 10.1038/311267a0
8. Kruse J, Keilhauer G, Faissner A, Timpl R, Schachner M. The J1 glycoprotein — a novel nervous system cell adhesion molecule of the L2/HNK-1 family. *Nature* (1985) 316:146–8. doi: 10.1038/316146a0
9. Faissner A, Kruse J, Chiquet-Ehrismann R, Mackie E. The high-molecular-weight J1 glycoproteins are immunochemically related to tenascin. *Differentiation* (1988) 37:104–14. doi: 10.1111/j.1432-0436.1988.tb00802.x
10. Pesheva P, Probstmeier R, Skubitz AP, McCarthy JB, Furcht LT, Schachner M. Tenascin-R (J1 160/180) inhibits fibronectin-mediated cell adhesion—functional relatedness to tenascin-C. *J Cell Sci* (1994) 107:2323–33.
11. Grumet M, Hoffman S, Crossin KL, Edelman GM. Cytotactin, an extracellular matrix protein of neural and non-neural tissues that mediates glia-neuron interaction. *Proc Natl Acad Sci U S A* (1985) 82:8075–9. doi: 10.1073/pnas.82.23.8075
12. Erickson HP, Taylor HC. Hexabrachion proteins in embryonic chicken tissues and human tumors. *J Cell Biol* (1987) 105:1387–94. doi: 10.1083/jcb.105.3.1387
13. Chiquet-Ehrismann R, Mackie EJ, Pearson CA, Sakakura T. Tenascin: an extracellular matrix protein involved in tissue interactions during fetal development and oncogenesis. *Cell* (1986) 47:131–9. doi: 10.1016/0092-8674(86)90374-0
14. Nörenberg U, Hubert M, Brümmendorf T, Tárnok A, Rathjen FG. Characterization of functional domains of the tenascin-R (restrictin) polypeptide: cell attachment site, binding with F11, and enhancement of F11-mediated neurite outgrowth by tenascin-R. *J Cell Biol* (1995) 130:473–84. doi: 10.1083/jcb.130.2.473
15. Bristow J, Tee MK, Gitelman SE, Mellon SH, Miller WL. Tenascin-X: a novel extracellular matrix protein encoded by the human XB gene overlapping P450c21B. *J Cell Biol* (1993) 122:265–78. doi: 10.1083/jcb.122.1.265

16. Weber P, Montag D, Schachner M, Bernhardt RR. Zebrafish tenascin-W, a new member of the tenascin family. *J Neurobiol* (1998) 35:1–16. doi: 10.1002/(SICI)1097-4695(199804)35:1<1::AID-NEU1>3.0.CO;2-9
17. Erickson HP. Tenascin-C, tenascin-R and tenascin-X: a family of talented proteins in search of functions. *Curr Opin Cell Biol* (1993) 5:869–76. doi: 10.1016/0955-0674(93)90037-q
18. Chiquet-Ehrismann R, Kalla P, Pearson CA, Beck K, Chiquet M. Tenascin interferes with fibronectin action. *Cell* (1988) 53:383–90. doi: 10.1016/0092-8674(88)90158-4
19. Fischer D, Brown-Lüdi M, Schulthess T, Chiquet-Ehrismann R. Concerted action of tenascin-C domains in cell adhesion, anti-adhesion and promotion of neurite outgrowth. *J Cell Sci* (1997) 110:1513–22.
20. Jones FS, Burgoon MP, Hoffman S, Crossin KL, Cunningham BA, Edelman GM. A cDNA clone for cytotactin contains sequences similar to epidermal growth factor- like repeats and segments of fibronectin and fibrinogen. *Proc Natl Acad Sci U S A* (1988) 85:2186–90. doi: 10.1073/pnas.85.7.2186
21. Pearson CA, Pearson D, Shibahara S, Hofsteenge J, Chiquet-Ehrismann R. Tenascin: cDNA cloning and induction by TGF-beta. *EMBO J* (1988) 7:2977–82. doi: 10.1002/j.1460-2075.1988.tb03160.x
22. Spring J, Beck K, Chiquet-Ehrismann R. Two contrary functions of tenascin: dissection of the active sites by recombinant tenascin fragments. *Cell* (1989) 59:325–34. doi: 10.1016/0092-8674(89)90294-8
23. Ruoslahti E. Fibronectin and its receptors. *Annu Rev Biochem* (1988) 57:375–413. doi: 10.1146/annurev.bi.57.070188.002111
24. Midwood KS, Chiquet M, Tucker RP, Orend G. Tenascin-C at a glance. *J Cell Sci* (2016) 129:4321–7. doi: 10.1242/jcs.190546
25. Aukhil I, Joshi P, Yan Y, Erickson HP. Cell- and heparin-binding domains of the hexabrachion arm identified by tenascin expression proteins. *J Biol Chem* (1993) 268:2542–53.
26. Prieto AL, Edelman GM, Crossin KL. Multiple integrins mediate cell attachment to cytotactin/tenascin. *Proc Natl Acad Sci U S A* (1993) 90:10154–8. doi: 10.1073/pnas.90.21.10154
27. Fischer D, Chiquet-Ehrismann R, Bernasconi C, Chiquet M. A single heparin binding region within the fibrinogen-like domain is functional in chick tenascin-C. *J Biol Chem* (1995) 270:3378–84. doi: 10.1074/jbc.270.7.3378
28. Marzeda AM, Midwood KS. Internal Affairs: Tenascin-C as a clinically relevant, endogenous driver of innate immunity. *J Histochem Cytochem* (2018) 66:289–304. doi: 10.1369/0022155418757443

Conflict of Interest: The author declares that the research was conducted in the absence of any commercial or financial relationships that could be construed as a potential conflict of interest.

frontiers in Immunology

MINI REVIEW
published: 01 December 2020
doi: 10.3389/fimmu.2020.609752

The Roles of Tenascins in Cardiovascular, Inflammatory, and Heritable Connective Tissue Diseases

Ken-ichi Matsumoto[1]* *and Hiroki Aoki*[2]*

[1] Department of Biosignaling and Radioisotope Experiment, Interdisciplinary Center for Science Research, Organization for Research and Academic Information, Shimane University, Izumo, Japan, [2] Cardiovascular Research Institute, Kurume University, Kurume, Japan

Tenascins are a family of multifunctional extracellular matrix (ECM) glycoproteins with time- and tissue specific expression patterns during development, tissue homeostasis, and diseases. There are four family members (tenascin-C, -R, -X, -W) in vertebrates. Among them, tenascin-X (TNX) and tenascin-C (TNC) play important roles in human pathologies. TNX is expressed widely in loose connective tissues. TNX contributes to the stability and maintenance of the collagen network, and its absence causes classical-like Ehlers-Danlos syndrome (clEDS), a heritable connective tissue disorder. In contrast, TNC is specifically and transiently expressed upon pathological conditions such as inflammation, fibrosis, and cancer. There is growing evidence that TNC is involved in inflammatory processes with proinflammatory or anti-inflammatory activity in a context-dependent manner. In this review, we summarize the roles of these two tenascins, TNX and TNC, in cardiovascular and inflammatory diseases and in clEDS, and we discuss the functional consequences of the expression of these tenascins for tissue homeostasis.

Keywords: tenascin-C, tenascin-X, cardiovascular disease, fibrosis, inflammation, Ehlers-Danlos syndrome

OPEN ACCESS

Edited by:
Gertraud Orend,
INSERM Immuno Rhumatologie Moléculaire (IRM), France

Reviewed by:
Marcus Franz,
University Hospital Jena, Germany
Hiromi Yanagisawa,
University of Tsukuba, Japan
Hidenori Suzuki,
Mie University, Japan

***Correspondence:**
Ken-ichi Matsumoto
matumoto@med.shimane-u.ac.jp
Hiroki Aoki
haoki@med.kurume-u.ac.jp

Specialty section:
This article was submitted to Inflammation, a section of the journal Frontiers in Immunology

Received: *24 September 2020*
Accepted: *03 November 2020*
Published: *01 December 2020*

Citation:
Matsumoto K-i and Aoki H (2020) The Roles of Tenascins in Cardiovascular, Inflammatory, and Heritable Connective Tissue Diseases. Front. Immunol. 11:609752. doi: 10.3389/fimmu.2020.609752

INTRODUCTION

An important component of the extracellular environment is the extracellular matrix (ECM), which is comprised of glycoproteins, proteoglycans, and fibrillar proteins. The ECM offers not only structural support for cells but also influences cell adhesion, proliferation, differentiation, and survival through specific receptor-mediated interactions (1). Within the ECM, the tenascins comprise an attractive glycoprotein family with distinct features for each member.

Abbreviations: BDNF, brain-derived neurotrophic factor; BNP, B-type natriuretic peptide; circRNA, circular RNA; clEDS, classical-like Ehlers-Danlos syndrome; CNS, central nervous system; DRG, dorsal root ganglion; ECM, extracellular matrix; EDS, Ehlers-Danlos syndrome; EGF, epidermal growth factor; EMT, epithelial-mesenchymal transition; FBG, fibrinogen; FGFs, fibroblast growth factors; FNIII, fibronectin type III; HFCD, high levels of phosphorus and calcium; HFpEF, heart failure with preserved ejection fraction; lncRNA, long non-coding RNA; MMPs, matrix metalloproteinases; PDGFs, platelet-derived growth factors; PNS, peripheral nervous system; SLE, systemic lupus erythematosus; SNPs, single nucleotide polymorphisms; sTNX, serum form of TNX; TGF-β, transforming growth factor-β; TLR4, Toll-like receptor 4; TNC, tenascin-C; TNR, tenascin-R; TNW, tenascin-W; TNX, tenascin-X; *Tnxb*, mouse tenascin-X gene; *TNXB*, human tenascin-X gene; TNY, tenascin-Y; VEGF-B, vascular endothelial growth factor, B; VEGFR-1, vascular endothelial growth factor receptor 1; VUR, vesicoureteral reflux.

Tenascins comprise four members in vertebrates: tenascin-C (TNC), tenascin-R (TNR), tenascin-X (TNX) [referred to as tenascin-Y (TNY) in chickens], and tenascin-W (TNW) (originally named tenascin-N in mice) (2, 3). The tenascin family members have a common structure with heptad repeats, epidermal growth factor (EGF)-like repeats, fibronectin type III (FNIII)-like repeats, and a fibrinogen (FBG)-related domain. This modular structure allows tenascins to interact with multiple binding partners, including cell surface receptors, cytokines, and extracellular matrix molecules. Each of tenascins shows a unique time- and tissue specific expression pattern both during development and in adulthood (4–8). On the other hand, tenascins are also subjected to dynamic remodeling during a number of pathological conditions such as inflammation, fibrotic disorders, cardiovascular diseases, and cancer progression (9). Transcriptional control of tenascin family members for their specific expression patterns has recently been reviewed (10). Such an expression pattern of tenascins is one of the features of all matricellular proteins including tenascins (11, 12).

TNX

Expression of TNX in Physiological and Pathological Conditions

Regulation of TNX Expression

TNX expression is undetectable during early embryonic stages, but its expression increases ubiquitously in various tissues, especially in heart, skeletal muscle, and skin, during the middle embryonic stage and after birth (13–15). TNX is associated with blood vessels in most tissues and its distribution is often reciprocal to that of TNC, particularly in the skin and tissues of the digestive tract (13). Interestingly, by the analyses of TNC-deficient mice it was found that TNX does not compensate for the loss of TNC, at least in the brain (16) and during early heart development (17).

As for the regulation of TNX expression by the cellular microenvironment, brain-derived neurotrophic factor (BDNF) stimulates its mRNA expression in endothelial cells (18), whereas TNX is subjected to downregulation by glucocorticoids in fibroblasts (19). Sp1, which is a widely distributed transcription factor, is essential for expression of the mouse TNX gene (*Tnxb*) (20). Recently, microRNA miR-30b (21), long non-coding RNA (lncRNA) LINC01305 (22, 23), and circular RNA (circRNA) circRNA_14940 (24) have also been revealed to be key regulators of TNX expression.

TNX Expression in the Nervous System

Recently, the expression pattern and significance of TNX in the nervous system have become apparent. In the nervous system, TNX is localized in the perineurium and endoneurium of the peripheral nervous system (PNS) such as sciatic nerves (15, 25). Indeed, patients with TNX-deficient type EDS (classical-like EDS: clEDS) show abnormal peripheral nerves (26). TNX has been expressed in Schwann cells but not in axons (27). TNX has been mainly detected in the leptomeninges in the spinal cord and in the pia matter of the dorsal root ganglion (DRG). In the DRG, TNX is localized in satellite cells surrounding primary sensory neurons (27). In the central nervous system (CNS), TNX has been detected in the leptomeninges and choroid plexus of the adult cerebral cortex (28). Avian TNX (TNY) has been shown to inhibit neurite outgrowth and reduce the spread of growth cones (29).

TNX Expression in Cancers

Although there have been fewer reports on TNX expression in cancer compared with reports on the expression of TNC and TNW in cancer, reports on TNX expression have been increasing. TNX has been shown to be highly expressed in malignant mesothelioma (30, 31) and ovarian cancer (32), indicating the possibility of TNX being a novel diagnostic maker of these cancers. On the other hand, there have been several reports of TNX expression being downregulated during tumor progression in astrocytomas (33), cutaneous melanoma (34), and neurofibromatosis type 1 (35), findings that are mostly opposite to those for TNC. Intriguingly, it has also been reported that TNX has a tumor suppressor role in cervical cancer *via* LINC01305 expression which modulates TNX expression (22), esophageal squamous-cell carcinoma (36), and lung cancer *via* LINC01305 expression (23) and that TNX is downregulated in these tumors. In agreement with the tumor suppressor role of TNX in cancer progression, TNX-deficient mice with grafted melanoma cells exhibited promotion of tumor invasion and metastasis because of increased activities of matrix metalloproteinases (MMPs) (37, 38). Interestingly, by the analyses of TNX and TNC single and/or double deficient mice, we found out that TNX deficiency-induced tumor cell proliferation in the primary tumor site is repressed by the lack of TNC, while TNX deficiency-induced invasion to neighboring tissues is not promoted by the lack of TNC (39).

Physiological Functions of TNX

The results of a number of studies on abnormalities in mice with targeted deletion in *Tnxb* (40) and in clEDS patients (26, 41) have suggested structural roles of TNX in tissue integrity (7, 42). TNX possesses elastic properties in the FNIII-like domain (43) and increases the stiffness of collagen gels (44). TNX is associated with collagen fibrils within tissues and regulates collagen fibril spacing (42) *via* direct interaction with types I, III and V fibrillar collagens (45), types XII (46) and XIV fibril-associated collagens (45), and decorin (47). It has also been shown that TNX increases both the rate and extent of fibril formation *in vivo*, indicating a crucial role of TNX in collagen fibrillogenesis (48, 49). Taken together, the findings suggest that TNX regulates collagen deposition, collagen fiber stability and collagen mechanical properties. In addition, it has been shown that TNX binds to tropoelastin (49). Coarse and fragmented immature elastin fibers have been detected in clEDS patients, suggesting that TNX is also involved in the stability and maintenance of elastin fibers (50).

Other Functions of TNX

Fragments of TNX, especially its EGF-like repeats and FNIII-like repeats, have profound proangiogenic properties (51). Furthermore, we have shown that TNX interacts with vascular endothelial growth factor B (VEGF-B) and stimulates endothelial

cell proliferation *via* simultaneous binding to VEGF receptor 1 (VEGFR-1) and VEGF-B (52). Indeed, results of *in vivo* studies using TNX-deficient mice have shown that TNX plays a crucial role in blood vessel formation in sciatic nerves (53) and in injury-induced stromal angiogenesis in the cornea (54). Recently, we have reported that TNX-deficient mice display upregulation of osteoclast marker gene expression and promoted bone resorption activities due to increased multinucleated osteoclasts (55). These results provide the first evidence for the essential functions of TNX in bone metabolism such as osteoclast differentiation. These non-structural functions of TNX may be related to the structural roles of this ECM glycoprotein. The modification of the composition and organization of extracellular environment due to TNX deficiency might cause the alteration of mechanical stress to the surrounding cells, leading to the non-structural aberrations.

Alcaraz *et al* (56). demonstrated that the C-terminal FBG-related domain of TNX activates the latent transforming growth factor-β (TGF-β) into the active molecule and that integrin α11β1 is required as a cell surface receptor for TNX for this activation. They also showed that the FBG-related domain-mediated TGF-β activation elicits the TGF-β/Smad signaling pathway and causes epithelial-mesenchymal transition (EMT) in epithelial cells (56).

So far, a number of important phenotypes have been observed by studying TNX-deficient mice (**Table 1**).

TABLE 1 | Tenascin-X-deficient mouse phenotypes.

Phenotypes		References
clEDS-related phenotypes	Hyperextensible skin, reduced tensile strength, reduced collagen deposition and stability, reduced fibrillar collagen, increased elastic fibers	(40, 48, 49, 57),
	Muscle weakness, myopathic changes	(58, 59),
	Reduced diameter of myelinated fibers in sciatic nerves	(59)
	Abnormal wound healing	(60, 61),
	Gastrointestinal pain and dysfunction, increased colonic afferent sensitivity and increased sensory neuronal sprouting	(62, 63),
	Mechanical allodynia and hypersensitivity to chemical stimuli	(27)
	Abnormal location of vaginal plug, rectal prolapse	(64)
Behavior	Increased anxiety, superior memory retention, increased sensorimotor coordination	(65)
Blood vessel formation and neovascularization	Abnormal blood vessel formation and less neovascularization	(53, 54),
Triglyceride synthesis	Accumulation of triglycerides and altered composition of triglyceride-associated fatty acids	(66)
Bone homeostasis	Bone loss due to increased osteoclastogenesis	(55)
Tumor progression	Promotion of invasion and metastasis of melanoma cells, increased activities of MMPs	(37, 38),
Liver fibrosis	Suppression of hepatic dysfunction by administration of a high-fat diet	(67)

clEDS Caused by TNX Deficiency

Ehlers-Danlos syndrome (EDS) is a group of clinically and genetically heritable connective tissue disorders characterized by joint hypermobility, skin hyperextensibility, and generalized connective tissue fragility (68). So far, EDS has been classified into 14 distinct subtypes caused by defects in 20 different genes encoding fibrillar collagens and collagen-modifying proteins and ECM proteins (69, 70). Among the subtypes, classical-like EDS (clEDS) is caused by a complete lack of TNX due to homozygous or compound heterozygous TNX gene (*TNXB*) mutations with autosomal recessive inheritance, leading to nonsense-mediated decay of the mutant RNA (41). clEDS shows typical clinical hallmarks characterized by soft/velvety hyperextensible skin without atrophic scarring, generalized joint hypermobility and easy bruising as its major clinical features (41). TNX is also present in sera. The serum form of TNX (sTNX) with a molecular size of 140 kDa is generated by cleavage of the 450-kDa mature form of TNX (41). The measurement of sTNX concentration is useful for the diagnosis of clEDS (71).

Mitral valve abnormality (24%) and hypertension (24%) have been reported as cardiovascular complications in clEDS patients (72). It has also been reported that clEDS patients exhibit rectal prolapse (18%) and diverticulosis or diverticulitis (18%) as gastrointestinal complications (72). Currently, these gastrointestinal complications are considered to be more common in clEDS patients (73, 74).

Nearly 90% of patients with EDS show chronic pain (75). clEDS patients frequently complain of chronic back pain, chronic myalgia and chronic arthralgia (72). Recent investigations of TNX-deficient mice have shown that there is a direct link between TNX deficiency and pain. For example, Aktar *et al.* showed that TNX-deficient mice have hypersensitive colonic nociceptive afferents and increased sensory neuronal sprouting, leading to gastrointestinal pain and dysfunction (62). In addition, we recently reported that TNX-deficient mice exhibit mechanical allodynia and hypersensitivity to chemical stimuli and hypersensitization of myelinated Aδ and Aβ fibers (27).

TNX and Fibrosis

In a previous study, we showed that TNX contributes to liver fibrosis in TNX-deficient mice administered a high-fat and high-cholesterol diet with high levels of phosphorus and calcium (HFCD) (67). Inflammation assessed by inflammatory cell infiltrates and levels of type I collagen was suppressed in TNX-deficient mice compared with that in wild-type mice. On the other hand, the TGF-β pathway is a well-known key signaling pathway associated with hepatic stellate cell activation and fibrosis progression (76). As mentioned above, TNX affects latent TGF-β activation and signaling (56). Thus, it is reasonable to assume that TNX, especially its FBG-related domain, contributes to liver fibrosis and inflammatory responses *via* the TGF-β pathway in combination with integrin α11β1.

Other Diseases Associated With Mutations or SNPs in *TNXB*

It has been reported that another disease associated with heterozygous mutations in *TNXB* is primary vesicoureteral reflux (VUR) (77). There is also some evidence that single

nucleotide polymorphisms (SNPs) in *TNXB* are associated with other diseases. For example, genomic studies with SNPs in genome-wide association studies revealed that two closely linked SNPs in the coding region of *TNXB* are associated with schizophrenia risk in a Japanese population by a case-control study (78). On the other hand, an SNP in the 5' flanking region of *TNXB* has been reported to be associated with systemic lupus erythematosus (SLE) (79). However, the functional implications of SNPs in *TNXB* relevant to these diseases remain uncertain and warrant further investigation.

TNC

Context-Dependent Function of TNC

TNC is a prototypical and most well-characterized member of the tenascin family. TNC has a variety of biological functions including regulation of cell adhesion, migration, growth and differentiation by binding through its modular structure to multiple cell surface receptors including integrins, Toll-like receptor 4 (TLR4) and syndecan-4 (80, 81). TNC also binds to cytokines such as fibroblast growth factors (FGFs), platelet-derived growth factors (PDGFs) and TGF-β family members among others, thus regulating the cellular behavior and organization of the extracellular matrix.

The expression of TNC is regulated during embryonic development with a specific time and spatial pattern, and its expression is greatly diminished in adult tissue. Although the specific expression pattern of TNC was suggestive of its role in embryogenesis, mice with genetic deletion of TNC were born and grew without any gross abnormality and were fertile (16). Later, it was demonstrated that TNC-deficient mice exhibit abnormalities in their behavior and in the cytoarchitecture of the brain (82). Considering the extensive expression of TNC during embryogenesis, TNC may have more roles in fine tuning animal development that are yet to be clarified.

TNC is transiently and specifically re-expressed upon acute inflammation and is persistently expressed upon chronic inflammation (83–85). Growing evidence has suggested that TNC is a proinflammatory factor and plays a deleterious role in fibrotic diseases (86–88). Interestingly, several lines of evidence have suggested that TNC also acts as an anti-inflammatory factor. For example, it was shown that the first two alternative spliced FNIII-like repeats suppress *in vitro* T cell activation (89). The results of *in vivo* studies showed that chemically induced inflammatory dermatitis (90) and Habu-snake venom-induced glomerulonephritis (91) develop more severely in TNC-deficient mice than in wild-type mice. Such bimodal activities, namely proinflammatory or anti-inflammatory activities, of TNC can have paradoxical effects and may influence many aspects of the immune response in a context-dependent manner.

The context-dependent function of TNC seems to be derived from its multidomain structure, which allows TNC to interact with multiple extracellular matrix and cytokines (81). In addition, TNC gene can generate multiple variants of TNC protein by alternative splicing of mRNA in tissue- and disease-specific manners (92), and proteolytic processing by various proteases, of which significance has been demonstrated by experiments with domain-specific antibodies and recombinant proteins.

Pathophysiological Role of TNC in Cardiac Diseases

TNC is reported to be involved in a variety of cardiovascular diseases (83, 93, 94). In the pathogenesis of myocardial damage and cardiac dysfunction, animal experiments have demonstrated that TNC is involved in adverse remodeling of myocardium due to myocardial infarction (95, 96) and myocarditis (97). TNC has been reported to promote myocardial hypertrophy, fibrosis (98, 99) and cardiac dysfunction (100) in animal models of cardiac hypertrophy and myocardial infarction. Being consistent with those findings, TNC has been shown to promote cardiac fibrosis in an angiotensin II-induced hypertrophy model (101). However, another study showed that TNC attenuated cardiac fibrosis due to pressure overload or angiotensin II infusion (102). These contradictory findings may be due to the fact that the adverse effect of TNC was demonstrated in a BALB/c background of the mouse strain, while its beneficial effect was shown in the background of C57BL/6. It was further speculated that the difference may reflect the predominant immune responses of Th2 in BALB/c and Th1 in C57BL/6, although this hypothesis awaits formal proof (103).

Pathophysiological Role of TNC in Vascular Diseases

With regard to vascular diseases, TNC has been reported to be atherogenic by stimulating TLR4-dependent foam cell formation (104). However, TNC has also been reported to be anti-atherogenic since TNC-deficient mice showed mast cell accumulation and intraplaque hemorrhage (105, 106). Similarly, expression of TNC may prevent the rupture of cerebral aneurysm by promoting fibrosis of the aneurysmal wall (107, 108), while it may be deleterious by exacerbating acute vasospastic response and exacerbate cerebral injury after subarachnoidal hemorrhage (109, 110). Expression of TNC by neurohumoral stress protects the aorta from acute aortic dissection (111) (**Figure 1**), while it seems to have no impact on the development of abdominal aortic aneurysm, although it was highly expressed in the aneurysmal tissue (112). Therefore, TNC can be either disease-promotive, disease-preventive or neutral in cardiovascular diseases (94), underscoring the context-dependent function of TNC, as demonstrated also in various animal models of non-cardiovascular diseases.

TNC as a Biomarker of Tissue Damage

While the role of TNC is context-dependent and can be detrimental or beneficial, it has been established that TNC is expressed in various cardiovascular diseases in clinical settings (93). TNC is elevated after myocardial injury due to myocardial infarction (113) or due to acute (114) or chronic myocarditis (115). TNC is also elevated in hypertrophic (116) and dilated cardiomyopathies (117). In addition, TNC is elevated in heart failure with preserved ejection fraction (HFpEF) (118) and in right ventricular failure (119). TNC is not only deposited in the

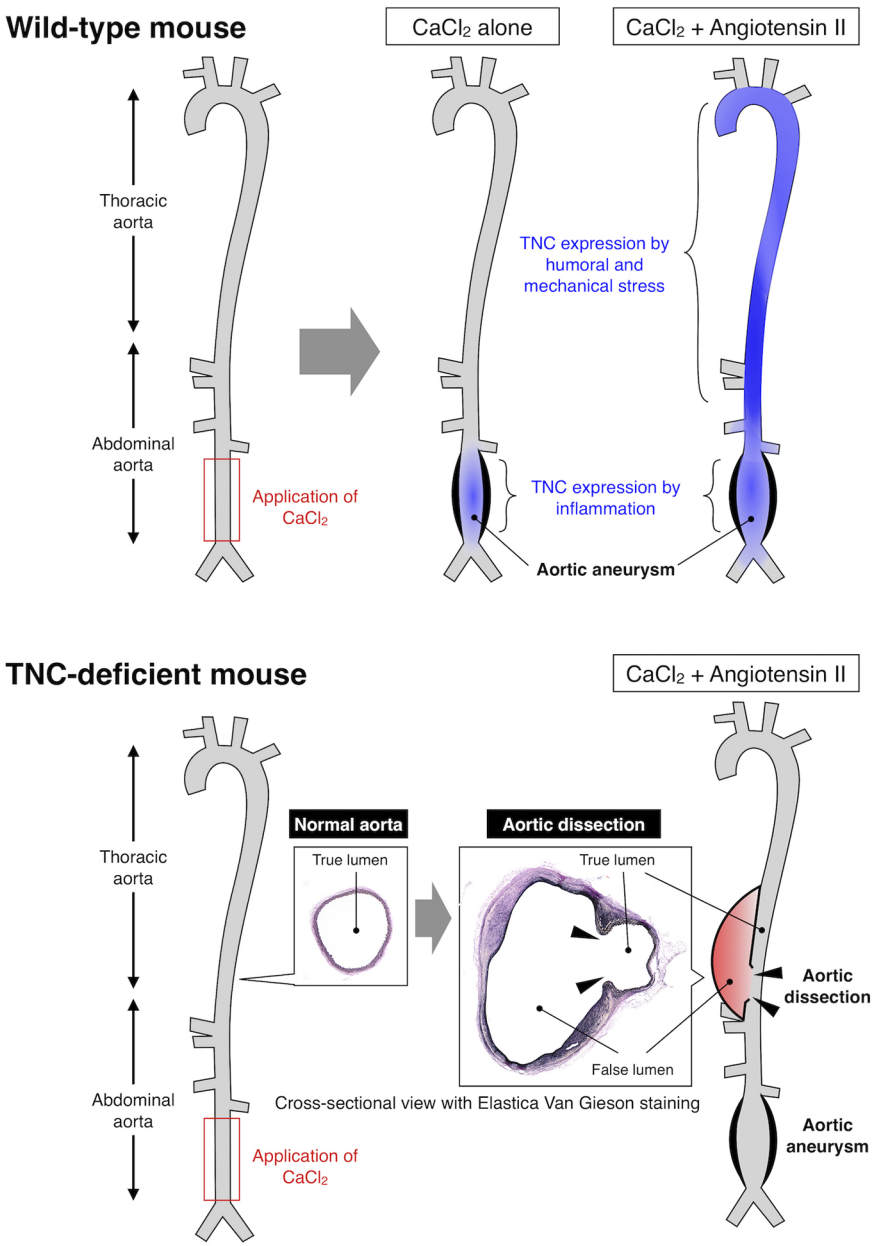

FIGURE 1 | Expression and function of TNC in mouse model of aortic diseases. Upper panel: Application of $CaCl_2$ solution to the lower abdominal aorta caused local inflammation and formation of aortic aneurysm. Continuous infusion of angiotensin II after the $CaCl_2$ application resulted in higher wall stress and formation of larger aortic aneurysm. TNC was induced in the lower abdominal aorta by $CaCl_2$-induced local inflammation, and in the thoracic and upper abdominal aorta due to the angiotensin II-induced higher wall stress, as illustrated by the blue color. Lower panel: TNC-deficient mice developed aortic aneurysm comparable to wild-type mice by $CaCl_2$ application in the presence or absence of angiotensin II. On the other hand, TNC-deficient mice developed aortic dissection in the thoracic and upper abdominal aorta that was characterized by the disruption of the aortic wall (arrowheads) and the formation of false lumen (red color). These findings indicate that TNC does not play a major role in the destructive inflammation in the aortic aneurysm, while it is critical for protecting the aortic wall from dissection, exemplifying the context-dependent function of TNC (111).

damaged tissue but also liberated in circulating blood flow. It has been proposed that TNC can serve as a prognostic marker for heart failure due to these diseases. While B-type natriuretic peptide (BNP) is an established prognostic marker for heart failure, the combination of BNP and TNC may be more precise than BNP or TNC alone for patients with dilated cardiomyopathy (120). Furthermore, reverse remodeling of the ventricle in heart failure patients due to cardiac resynchronization therapy was shown to be associated with reduction in serum TNC level, suggesting that TNC may reflect ongoing myocardial damage (121).

Since TNC is induced by various inflammatory mediators, it may also reflect the disease activities of inflammatory cardiovascular diseases including Kawasaki disease (122, 123) and cardiac sarcoidosis (124). TNC is expressed locally in the tissue of coronary atherosclerosis (125) and abdominal aortic aneurysm (112, 126), and its expression is elevated in serum of patients with these diseases (127). The serum level of TNC is elevated in patients with acute aortic dissection and its elevated level is associated with acute mortality (128), as well as chronic prognosis (129, 130). TNC is also elevated in cerebrospinal fluid after subarachnoidal hemorrhage and may predict the development of cerebral vasospasm (131). Elevated serum TNC is not only associated with specific diseases but also with the mortality and the development of cardiovascular diseases in patients with chronic kidney disease (132) and it is also associated with major adverse cardiovascular events and death in individuals with type 2 diabetes mellitus (133). In addition to the serum level, local deposition of TNC may serve as a marker of tissue damage, as demonstrated in animal models of myocarditis (134) and myocardial infarction (135). Therefore, quantitative detection of systemic and local levels of TNC may have a clinical value for monitoring inflammation and tissue damage both in acute and chronic diseases in order to realize precision medicine for better outcomes by optimizing the clinical practice for individual requirement.

Considering the fact that the structure of TNC can be altered in a disease-specific manner, domain-specific detection of TNC may also have a clinical value (92). For example, isoform-specific expression of TNC was demonstrated in the lung tissue of experimental pulmonary hypertension (136) and in the serum of the patients (137). This means that care should be taken which isoform of TNC is being measured to evaluate its significance as a biomarker in a particular clinical setting, as well as the normal range of TNC concentration. Because of the significance of the different TNC isoforms, domain-specific monoclonal antibodies for TNC would have potential clinical values both as diagnostic tools to evaluate the disease conditions, and as therapeutic tools to target a particular function of TNC or a particular tissue that expresses the corresponding TNC isoform (92).

CONCLUSIONS

TNX and TNC have distinct roles in physiological and pathological conditions. In a physiological condition, TNX is involved in the structural integrity of collagen fibrils. TNX also has a tumor suppressor role, a proangiogenic property, a role in osteoclast differentiation, and a role in TGF-β activation. On the other hand, in a pathological condition such as TNX deficiency, its absence causes clEDS with major clinical features such as hyperextensible skin without atrophic scarring, generalized joint hypermobility and easy bruising. Interestingly, TNX deficiency is involved in pain and fibrosis. The underlying molecular mechanisms for pain and suppression of fibrosis caused by TNX deficiency need to be elucidated in more detail.

The physiological role of TNC is yet to be clarified. Although genetic deletion of TNC in mice resulted in no gross abnormality of the animals, the possibility remains that TNC plays a role in cell differentiation and tissue organization during embryogenesis. On the other hand, accumulating evidence indicates that TNC is re-expressed and actively participates in the pathogenesis of various diseases with tissue damage. The context-dependent function of TNC, possibly due to its modular structure and multiple binding partners, makes it difficult to interpret the experimental results as to whether expression of TNC is detrimental or beneficial. Nonetheless, expression of TNC seems to be a sensitive marker for tissue damage both in cardiovascular and non-cardiovascular diseases including cancer. Considering the wide range of physiological and pathophysiological functions of tenascins and their specific expression patterns, basic and clinical studies of tenascin family would be fruitful for delineating their precise roles and their clinical implications both in normal and abnormal conditions.

AUTHOR CONTRIBUTIONS

KM and HA designed and wrote this manuscript. All authors contributed to the article and approved the submitted version.

FUNDING

This work was supported by the Japan Society for the Promotion of Science KAKENHI grant number 19K08470 to KM and 19H03743 to HA from the Ministry of Education, Culture, Sports, Science and Technology of Japan.

REFERENCES

1. Adams JC, Watt FM. Regulation of development and differentiation by the extracellular matrix. *Development* (1993) 117:1183–98.
2. Chiquet-Ehrismann R, Tucker RP. Tenascins and the importance of adhesion modulation. *Cold Spring Harb Perspect Biol* (2011) 3:a004960. doi: 10.1101/cshperspect.a004960
3. Adams JC, Chiquet-Ehrismann R, Tucker RP. The evolution of tenascins and fibronectin. *Cell Adh Migr* (2015) 9:22–33. doi: 10.4161/19336918.2014.970030
4. Tucker RP, Chiquet-Ehrismann R. The regulation of tenascin expression by tissue microenvironments. *Biochim Biophys Acta* (2009) 1793:888–92. doi: 10.1016/j.bbamcr.2008.12.012
5. Chiquet-Ehrismann R, Orend G, Chiquet M, Tucker RP, Midwood KS. Tenascins in stem cell niches. *Matrix Biol* (2014) 37:112–23. doi: 10.1016/j.matbio.2014.01.007
6. Jakovcevski I, Miljkovic D, Schachner M, Andjus PR. Tenascins and inflammation in disorders of the nervous system. *Amino Acids* (2013) 44:1115–27. doi: 10.1007/s00726-012-1446-0
7. Valcourt U, Alcaraz LB, Exposito JY, Lethias C, Bartholin L. Tenascin-X: beyond the architectural function. *Cell Adh Migr* (2015) 9:154–65. doi: 10.4161/19336918.2014.994893
8. Tucker RP, Degen M. The expression and possible functions of tenascin-W during development and disease. *Front Cell Dev Biol* (2019) 7:53. doi: 10.3389/fcell.2019.00053

9. Chiquet-Ehrismann R, Chiquet M. Tenascins: regulation and putative functions during pathological stress. *J Pathol* (2003) 200:488–99. doi: 10.1002/path.1415
10. Chiovaro F, Chiquet-Ehrismann R, Chiquet M. Transcriptional regulation of tenascin genes. *Cell Adh Migr* (2015) 9:34–47. doi: 10.1080/19336918.2015.1008333
11. Bornstein P. Diversity of function is inherent in matricellular proteins: an appraisal of thrombospondin 1. *J Cell Biol* (1995) 130:503–6. doi: 10.1083/jcb.130.3.503
12. Bornstein P, Sage EH. Matricellular proteins: extracellular modulators of cell function. *Curr Opin Cell Biol* (2002) 14:608–16. doi: 10.1016/s0955-0674(02)00361-7
13. Matsumoto K, Saga Y, Ikemura T, Sakakura T, Chiquet-Ehrismann R. The distribution of tenascin-X is distinct and often reciprocal to that of tenascin-C. *J Cell Biol* (1994) 125:483–93. doi: 10.1083/jcb.125.2.483
14. Burch GH, Bedolli MA, McDonough S, Rosenthal SM, Bristow J. Embryonic expression of tenascin-X suggests a role in limb, muscle, and heart development. *Dev Dyn* (1995) 203:491–504. doi: 10.1002/aja.1002030411
15. Geffrotin C, Garrido JJ, Tremet L, Vaiman M. Distinct tissue distribution in pigs of tenascin-X and tenascin-C transcripts. *Eur J Biochem* (1995) 231:83–92. doi: 10.1111/j.1432-1033.1995.tb20673.x
16. Saga Y, Yagi T, Ikawa Y, Sakakura T, Aizawa S. Mice develop normally without tenascin. *Genes Dev* (1992) 6:1821–31. doi: 10.1101/gad.6.10.1821
17. Imanaka-Yoshida K, Matsumoto K, Hara M, Sakakura T, Yoshida T. The dynamic expression of tenascin-C and tenascin-X during early heart development in the mouse. *Differentiation* (2003) 71:291–8. doi: 10.1046/j.1432-0436.2003.7104506.x
18. Takeda K, Shiba H, Mizuno N, Hasegawa N, Mouri Y, Hirachi A, et al. Brain-derived neurotrophic factor enhances periodontal tissue regeneration. *Tissue Eng* (2005) 11:1618–29. doi: 10.1089/ten.2005.11.1618
19. Sakai T, Furukawa Y, Chiquet-Ehrismann R, Nakamura M, Kitagawa S, Ikemura T, et al. Tenascin-X expression in tumor cells and fibroblasts: glucocorticoids as negative regulators in fibroblasts. *J Cell Sci* (1996) 109(Pt 8):2069–77.
20. Minamitani T, Ariga H, Matsumoto K. Transcription factor Sp1 activates the expression of the mouse tenascin-X gene. *Biochem Biophys Res Commun* (2000) 267:626–31. doi: 10.1006/bbrc.1999.2006
21. Tafazzoli A, Forstner AJ, Broadley D, Hofmann A, Redler S, Petukhova L, et al. Genome-wide microRNA analysis implicates miR-30b/d in the etiology of alopecia areata. *J Invest Dermatol* (2018) 138:549–56. doi: 10.1016/j.jid.2017.09.046
22. Yan SP, Chu DX, Qiu HF, Xie Y, Wang CF, Zhang JY, et al. LncRNA LINC01305 silencing inhibits cell epithelial-mesenchymal transition in cervical cancer by inhibiting TNXB-mediated PI3K/Akt signalling pathway. *J Cell Mol Med* (2019) 23:2656–66. doi: 10.1111/jcmm.14161
23. Yan F, Liu SW, Li XY, Li CC, Wu Y. Silencing LncRNA LINC01305 inhibits epithelial mesenchymal transition in lung cancer cells by regulating TNXB-mediated PI3K/Akt signaling pathway. *J Biol Regul Homeost Agents* (2020) 34:499–508. doi: 10.23812/20-73-a-33
24. Wu L, Zhou R, Diao J, Chen X, Huang J, Xu K, et al. Differentially expressed circular RNAs in orbital adipose/connective tissue from patients with thyroid-associated ophthalmopathy. *Exp Eye Res* (2020) 196:108036. doi: 10.1016/j.exer.2020.108036
25. Matsumoto K, Sawa H, Sato M, Orba Y, Nagashima K, Ariga H. Distribution of extracellular matrix tenascin-X in sciatic nerves. *Acta Neuropathol* (2002) 104:448–54. doi: 10.1007/s00401-002-0577-x
26. Burch GH, Gong Y, Liu W, Dettman RW, Curry CJ, Smith L, et al. Tenascin-X deficiency is associated with Ehlers-Danlos syndrome. *Nat Genet* (1997) 17:104–8. doi: 10.1038/ng0997-104
27. Okuda-Ashitaka E, Kakuchi Y, Kakumoto H, Yamanishi S, Kamada H, Yoshidu T, et al. Mechanical allodynia in mice with tenascin-X deficiency associated with Ehlers-Danlos syndrome. *Sci Rep* (2020) 10:6569. doi: 10.1038/s41598-020-63499-2
28. Imura K, Sato I. Novel localization of tenascin-X in adult mouse leptomeninges and choroid plexus. *Ann Anat* (2008) 190:324–8. doi: 10.1016/j.aanat.2008.04.003
29. Tucker RP, Hagios C, Santiago A, Chiquet-Ehrismann R. Tenascin-Y is concentrated in adult nerve roots and has barrier properties in vitro. *J Neurosci Res* (2001) 66:439–47. doi: 10.1002/jnr.1236
30. Yuan Y, Nymoen DA, Stavnes HT, Rosnes AK, Bjørang O, Wu C, et al. Tenascin-X is a novel diagnostic marker of malignant mesothelioma. *Am J Surg Pathol* (2009) 33:1673–82. doi: 10.1097/PAS.0b013e3181b6bde3
31. Nakayama K, Seike M, Noro R, Takeuchi S, Matsuda K, Kunugi S, et al. Tenascin XB is a novel diagnostic marker for malignant mesothelioma. *Anticancer Res* (2019) 39:627–33. doi: 10.21873/anticanres.13156
32. Kramer M, Pierredon S, Ribaux P, Tille JC, Petignat P, Cohen M. Secretome identifies tenascin-X as a potent marker of ovarian cancer. *BioMed Res Int* (2015) 2015:208017. doi: 10.1155/2015/208017
33. Hasegawa K, Yoshida T, Matsumoto K, Katsuta K, Waga S, Sakakura T. Differential expression of tenascin-C and tenascin-X in human astrocytomas. *Acta Neuropathol* (1997) 93:431–7. doi: 10.1007/s004010050636
34. Geffrotin C, Horak V, Créchet F, Tricaud Y, Lethias C, Vincent-Naulleau S, et al. Opposite regulation of tenascin-C and tenascin-X in MeLiM swine heritable cutaneous malignant melanoma. *Biochim Biophys Acta* (2000) 1524:196–202. doi: 10.1016/s0304-4165(00)00158-6
35. Lévy P, Ripoche H, Laurendeau I, Lazar V, Ortonne N, Parfait B, et al. Microarray-based identification of tenascin C and tenascin XB, genes possibly involved in tumorigenesis associated with neurofibromatosis type 1. *Clin Cancer Res* (2007) 13:398–407. doi: 10.1158/1078-0432.Ccr-06-0182
36. Yang N, Tian J, Wang X, Mei S, Zou D, Peng X, et al. A functional variant in TNXB promoter associates with the risk of esophageal squamous-cell carcinoma. *Mol Carcinog* (2020) 59:439–46. doi: 10.1002/mc.23166
37. Matsumoto K, Takayama N, Ohnishi J, Ohnishi E, Shirayoshi Y, Nakatsuji N, et al. Tumour invasion and metastasis are promoted in mice deficient in tenascin-X. *Genes Cells* (2001) 6:1101–11. doi: 10.1046/j.1365-2443.2001.00482.x
38. Matsumoto K, Minamitani T, Orba Y, Sato M, Sawa H, Ariga H. Induction of matrix metalloproteinase-2 by tenascin-X deficiency is mediated through the c-Jun N-terminal kinase and protein tyrosine kinase phosphorylation pathway. *Exp Cell Res* (2004) 297:404–14. doi: 10.1016/j.yexcr.2004.03.041
39. Matsumoto K, Takahashi K, Yoshiki A, Kusakabe M, Ariga H. Invasion of melanoma in double knockout mice lacking tenascin-X and tenascin-C. *Jpn J Cancer Res* (2002) 93:968–75. doi: 10.1111/j.1349-7006.2002.tb02472.x
40. Mao JR, Taylor G, Dean WB, Wagner DR, Afzal V, Lotz JC, et al. Tenascin-X deficiency mimics Ehlers-Danlos syndrome in mice through alteration of collagen deposition. *Nat Genet* (2002) 30:421–5. doi: 10.1038/ng850
41. Schalkwijk J, Zweers MC, Steijlen PM, Dean WB, Taylor G, van Vlijmen IM, et al. A recessive form of the Ehlers-Danlos syndrome caused by tenascin-X deficiency. *N Engl J Med* (2001) 345:1167–75. doi: 10.1056/NEJMoa002939
42. Bristow J, Carey W, Egging D, Schalkwijk J. Tenascin-X, collagen, elastin, and the Ehlers-Danlos syndrome. *Am J Med Genet C Semin Med Genet* (2005) 139c:24–30. doi: 10.1002/ajmg.c.30071
43. Jollymore A, Lethias C, Peng Q, Cao Y, Li H. Nanomechanical properties of tenascin-X revealed by single-molecule force spectroscopy. *J Mol Biol* (2009) 385:1277–86. doi: 10.1016/j.jmb.2008.11.038
44. Margaron Y, Bostan L, Exposito JY, Malbouyres M, Trunfio-Sfarghiu AM, Berthier Y, et al. Tenascin-X increases the stiffness of collagen gels without affecting fibrillogenesis. *Biophys Chem* (2010) 147:87–91. doi: 10.1016/j.bpc.2009.12.011
45. Lethias C, Carisey A, Comte J, Cluzel C, Exposito JY. A model of tenascin-X integration within the collagenous network. *FEBS Lett* (2006) 580:6281–5. doi: 10.1016/j.febslet.2006.10.037
46. Veit G, Hansen U, Keene DR, Bruckner P, Chiquet-Ehrismann R, Chiquet M, et al. Collagen XII interacts with avian tenascin-X through its NC3 domain. *J Biol Chem* (2006) 281:27461–70. doi: 10.1074/jbc.M603147200
47. Elefteriou F, Exposito JY, Garrone R, Lethias C. Binding of tenascin-X to decorin. *FEBS Lett* (2001) 495:44–7. doi: 10.1016/s0014-5793(01)02361-4
48. Minamitani T, Ikuta T, Saito Y, Takebe G, Sato M, Sawa H, et al. Modulation of collagen fibrillogenesis by tenascin-X and type VI collagen. *Exp Cell Res* (2004) 298:305–15. doi: 10.1016/j.yexcr.2004.04.030
49. Egging D, van den Berkmortel F, Taylor G, Bristow J, Schalkwijk J. Interactions of human tenascin-X domains with dermal extracellular

matrix molecules. *Arch Dermatol Res* (2007) 298:389–96. doi: 10.1007/s00403-006-0706-9
50. Zweers MC, van Vlijmen-Willems IM, van Kuppevelt TH, Mecham RP, Steijlen PM, Bristow J, et al. Deficiency of tenascin-X causes abnormalities in dermal elastic fiber morphology. *J Invest Dermatol* (2004) 122:885–91. doi: 10.1111/j.0022-202X.2004.22401.x
51. Demidova-Rice TN, Geevarghese A, Herman IM. Bioactive peptides derived from vascular endothelial cell extracellular matrices promote microvascular morphogenesis and wound healing in vitro. *Wound Repair Regen* (2011) 19:59–70. doi: 10.1111/j.1524-475X.2010.00642.x
52. Ikuta T, Ariga H, Matsumoto K. Extracellular matrix tenascin-X in combination with vascular endothelial growth factor B enhances endothelial cell proliferation. *Genes Cells* (2000) 5:913–27. doi: 10.1046/j.1365-2443.2000.00376.x
53. Sakai H, Yokota S, Kajitani N, Yoneyama T, Kawakami K, Yasui Y, et al. A potential contribution of tenascin-X to blood vessel formation in peripheral nerves. *Neurosci Res* (2017) 124:1–7. doi: 10.1016/j.neures.2017.06.003
54. Sumioka T, Iwanishi H, Okada Y, Nidegawa Y, Miyajima M, Matsumoto KI, et al. Loss of tenascin X gene function impairs injury-induced stromal angiogenesis in mouse corneas. *J Cell Mol Med* (2018) 22:948–56. doi: 10.1111/jcmm.13397
55. Kajitani N, Yamada T, Kawakami K, Matsumoto KI. TNX deficiency results in bone loss due to an increase in multinucleated osteoclasts. *Biochem Biophys Res Commun* (2019) 512:659–64. doi: 10.1016/j.bbrc.2019.03.134
56. Alcaraz LB, Exposito JY, Chuvin N, Pommier RM, Cluzel C, Martel S, et al. Tenascin-X promotes epithelial-to-mesenchymal transition by activating latent TGF-β. *J Cell Biol* (2014) 205:409–28. doi: 10.1083/jcb.201308031
57. Minamitani T, Ariga H, Matsumoto K. Deficiency of tenascin-X causes a decrease in the level of expression of type VI collagen. *Exp Cell Res* (2004) 297:49–60. doi: 10.1016/j.yexcr.2004.03.002
58. Huijing PA, Voermans NC, Baan GC, Buse TE, van Engelen BG, de Haan A. Muscle characteristics and altered myofascial force transmission in tenascin-X-deficient mice, a mouse model of Ehlers-Danlos syndrome. *J Appl Physiol (1985)* (2010) 109:986–95. doi: 10.1152/japplphysiol.00723.2009
59. Voermans NC, Verrijp K, Eshuis L, Balemans MC, Egging D, Sterrenburg E, et al. Mild muscular features in tenascin-X knockout mice, a model of Ehlers-Danlos syndrome. *Connect Tissue Res* (2011) 52:422–32. doi: 10.3109/03008207.2010.551616
60. Egging D, van Vlijmen-Willems I, van Tongeren T, Schalkwijk J, Peeters A. Wound healing in tenascin-X deficient mice suggests that tenascin-X is involved in matrix maturation rather than matrix deposition. *Connect Tissue Res* (2007) 48:93–8. doi: 10.1080/03008200601166160
61. Hashimoto K, Kajitani N, Miyamoto Y, Matsumoto KI. Wound healing-related properties detected in an experimental model with a collagen gel contraction assay are affected in the absence of tenascin-X. *Exp Cell Res* (2018) 363:102–13. doi: 10.1016/j.yexcr.2017.12.025
62. Aktar R, Peiris M, Fikree A, Cibert-Goton V, Walmsley M, Tough IR, et al. The extracellular matrix glycoprotein tenascin-X regulates peripheral sensory and motor neurones. *J Physiol* (2018) 596:4237–51. doi: 10.1113/jp276300
63. Aktar R, Peiris M, Fikree A, Eaton S, Kritas S, Kentish SJ, et al. A novel role for the extracellular matrix glycoprotein-Tenascin-X in gastric function. *J Physiol* (2019) 597:1503–15. doi: 10.1113/jp277195
64. Egging DF, van Vlijmen-Willems I, Choi J, Peeters AC, van Rens D, Veit G, et al. Analysis of obstetric complications and uterine connective tissue in tenascin-X-deficient humans and mice. *Cell Tissue Res* (2008) 332:523–32. doi: 10.1007/s00441-008-0591-y
65. Kawakami K, Matsumoto K. Behavioral alterations in mice lacking the gene for tenascin-X. *Biol Pharm Bull* (2011) 34:590–3. doi: 10.1248/bpb.34.590
66. Matsumoto K, Sato T, Oka S, Orba Y, Sawa H, Kabayama K, et al. Triglyceride accumulation and altered composition of triglyceride-associated fatty acids in the skin of tenascin-X-deficient mice. *Genes Cells* (2004) 9:737–48. doi: 10.1111/j.1356-9597.2004.00755.x
67. Yamaguchi S, Kawakami K, Satoh K, Fukunaga N, Akama K, Matsumoto KI. Suppression of hepatic dysfunction in tenascin−X−deficient mice fed a high −fat diet. *Mol Med Rep* (2017) 16:4061–7. doi: 10.3892/mmr.2017.7052
68. De Paepe A, Malfait F. The Ehlers-Danlos syndrome, a disorder with many faces. *Clin Genet* (2012) 82:1–11. doi: 10.1111/j.1399-0004.2012.01858.x
69. Malfait F, Francomano C, Byers P, Belmont J, Berglund B, Black J, et al. The 2017 international classification of the Ehlers-Danlos syndromes. *Am J Med Genet C Semin Med Genet* (2017) 175:8–26. doi: 10.1002/ajmg.c.31552
70. Malfait F, Castori M, Francomano CA, Giunta C, Kosho T, Byers PH. The Ehlers-Danlos syndromes. *Nat Rev Dis Primers* (2020) 6:64. doi: 10.1038/s41572-020-0194-9
71. Yamada K, Watanabe A, Takeshita H, Matsumoto KI. A method for quantification of serum tenascin-X by nano-LC/MS/MS. *Clin Chim Acta* (2016) 459:94–100. doi: 10.1016/j.cca.2016.05.022
72. Demirdas S, Dulfer E, Robert L, Kempers M, van Beek D, Micha D, et al. Recognizing the tenascin-X deficient type of Ehlers-Danlos syndrome: a cross-sectional study in 17 patients. *Clin Genet* (2017) 91:411–25. doi: 10.1111/cge.12853
73. Sakiyama T, Kubo A, Sasaki T, Yamada T, Yabe N, Matsumoto K, et al. Recurrent gastrointestinal perforation in a patient with Ehlers-Danlos syndrome due to tenascin-X deficiency. *J Dermatol* (2015) 42:511–4. doi: 10.1111/1346-8138.12829
74. Green C, Ghali N, Akilapa R, Angwin C, Baker D, Bartlett M, et al. Classical-like Ehlers-Danlos syndrome: a clinical description of 20 newly identified individuals with evidence of tissue fragility. *Genet Med* (2020) 22:1576–82. doi: 10.1038/s41436-020-0850-1
75. Voermans NC, Knoop H, Bleijenberg G, van Engelen BG. Pain in Ehlers-Danlos syndrome is common, severe, and associated with functional impairment. *J Pain Symptom Manage* (2010) 40:370–8. doi: 10.1016/j.jpainsymman.2009.12.026
76. Xu F, Liu C, Zhou D, Zhang L. TGF-β/SMAD pathway and its regulation in hepatic fibrosis. *J Histochem Cytochem* (2016) 64:157–67. doi: 10.1369/0022155415627681
77. Gbadegesin RA, Brophy PD, Adeyemo A, Hall G, Gupta IR, Hains D, et al. TNXB mutations can cause vesicoureteral reflux. *J Am Soc Nephrol* (2013) 24:1313–22. doi: 10.1681/asn.2012121148
78. Tochigi M, Zhang X, Ohashi J, Hibino H, Otowa T, Rogers M, et al. Association study between the TNXB locus and schizophrenia in a Japanese population. *Am J Med Genet B Neuropsychiatr Genet* (2007) 144b:305–9. doi: 10.1002/ajmg.b.30441
79. Kamatani Y, Matsuda K, Ohishi T, Ohtsubo S, Yamazaki K, Iida A, et al. Identification of a significant association of a single nucleotide polymorphism in TNXB with systemic lupus erythematosus in a Japanese population. *J Hum Genet* (2008) 53:64–73. doi: 10.1007/s10038-007-0219-1
80. Imanaka-Yoshida K, Aoki H. Tenascin-C and mechanotransduction in the development and diseases of cardiovascular system. *Front Physiol* (2014) 5:283:283. doi: 10.3389/fphys.2014.00283
81. Midwood KS, Chiquet M, Tucker RP, Orend G. Tenascin-C at a glance. *J Cell Sci* (2016) 129:4321–7. doi: 10.1242/jcs.190546
82. Mackie EJ, Tucker RP. The tenascin-C knockout revisited. *J Cell Sci* (1999) 112(Pt 22):3847–53.
83. Midwood KS, Hussenet T, Langlois B, Orend G. Advances in tenascin-C biology. *Cell Mol Life Sci* (2011) 68:3175–99. doi: 10.1007/s00018-011-0783-6
84. Midwood KS, Orend G. The role of tenascin-C in tissue injury and tumorigenesis. *J Cell Commun Signal* (2009) 3:287–310. doi: 10.1007/s12079-009-0075-1
85. Marzeda AM, Midwood KS. Internal affairs: tenascin-C as a clinically relevant, endogenous driver of innate immunity. *J Histochem Cytochem* (2018) 66:289–304. doi: 10.1369/0022155418757443
86. Kasprzycka M, Hammarström C, Haraldsen G. Tenascins in fibrotic disorders-from bench to bedside. *Cell Adh Migr* (2015) 9:83–9. doi: 10.4161/19336918.2014.994901
87. El-Karef A, Yoshida T, Gabazza EC, Nishioka T, Inada H, Sakakura T, et al. Deficiency of tenascin-C attenuates liver fibrosis in immune-mediated chronic hepatitis in mice. *J Pathol* (2007) 211:86–94. doi: 10.1002/path.2099
88. Carey WA, Taylor GD, Dean WB, Bristow JD. Tenascin-C deficiency attenuates TGF-ß-mediated fibrosis following murine lung injury. *Am J Physiol Lung Cell Mol Physiol* (2010) 299:L785–93. doi: 10.1152/ajplung.00385.2009
89. Puente Navazo MD, Valmori D, Rüegg C. The alternatively spliced domain TnFnIII A1A2 of the extracellular matrix protein tenascin-C suppresses

activation-induced T lymphocyte proliferation and cytokine production. *J Immunol* (2001) 167:6431–40. doi: 10.4049/jimmunol.167.11.6431
90. Koyama Y, Kusubata M, Yoshiki A, Hiraiwa N, Ohashi T, Irie S, et al. Effect of tenascin-C deficiency on chemically induced dermatitis in the mouse. *J Invest Dermatol* (1998) 111:930–5. doi: 10.1046/j.1523-1747.1998.00401.x
91. Nakao N, Hiraiwa N, Yoshiki A, Ike F, Kusakabe M. Tenascin-C promotes healing of Habu-snake venom-induced glomerulonephritis: studies in knockout congenic mice and in culture. *Am J Pathol* (1998) 152:1237–45.
92. Giblin SP, Midwood KS. Tenascin-C: Form versus function. *Cell Adh Migr* (2015) 9:48–82. doi: 10.4161/19336918.2014.987587
93. Golledge J, Clancy P, Maguire J, Lincz L, Koblar S. The role of tenascin C in cardiovascular disease. *Cardiovasc Res* (2011) 92:19–28. doi: 10.1093/cvr/cvr183
94. Imanaka-Yoshida K. Tenascin-C in cardiovascular tissue remodeling: from development to inflammation and repair. *Circ J* (2012) 76:2513–20. doi: 10.1253/circj.cj-12-1033
95. Nishioka T, Onishi K, Shimojo N, Nagano Y, Matsusaka H, Ikeuchi M, et al. Tenascin-C may aggravate left ventricular remodeling and function after myocardial infarction in mice. *Am J Physiol Heart Circ Physiol* (2010) 298: H1072–8. doi: 10.1152/ajpheart.00255.2009
96. Santer D, Nagel F, Goncalves IF, Kaun C, Wojta J, Fagyas M, et al. Tenascin-C aggravates ventricular dilatation and angiotensin-converting enzyme activity after myocardial infarction in mice. *ESC Heart Fail* (2020) 7:2113–22. doi: 10.1002/ehf2.12794
97. Machino-Ohtsuka T, Tajiri K, Kimura T, Sakai S, Sato A, Yoshida T, et al. Tenascin-C aggravates autoimmune myocarditis via dendritic cell activation and Th17 cell differentiation. *J Am Heart Assoc* (2014) 3:e001052. doi: 10.1161/jaha.114.001052
98. Podesser BK, Kreibich M, Dzilic E, Santer D, Forster L, Trojanek S, et al. Tenascin-C promotes chronic pressure overload-induced cardiac dysfunction, hypertrophy and myocardial fibrosis. *J Hypertens* (2018) 36:847–56. doi: 10.1097/HJH.0000000000001628
99. Nishioka T, Suzuki M, Onishi K, Takakura N, Inada H, Yoshida T, et al. Eplerenone attenuates myocardial fibrosis in the angiotensin II-induced hypertensive mouse: involvement of tenascin-C induced by aldosterone-mediated inflammation. *J Cardiovasc Pharmacol* (2007) 49:261–8. doi: 10.1097/FJC.0b013e318033dfd4
100. Abbadi D, Laroumanie F, Bizou M, Pozzo J, Daviaud D, Delage C, et al. Local production of tenascin-C acts as a trigger for monocyte/macrophage recruitment that provokes cardiac dysfunction. *Cardiovasc Res* (2018) 114:123–37. doi: 10.1093/cvr/cvx221
101. Shimojo N, Hashizume R, Kanayama K, Hara M, Suzuki Y, Nishioka T, et al. Tenascin-C may accelerate cardiac fibrosis by activating macrophages via the integrin αVβ3/nuclear factor-κB/interleukin-6 axis. *Hypertension* (2015) 66:757–66. doi: 10.1161/hypertensionaha.115.06004
102. Song L, Wang L, Li F, Yukht A, Qin M, Ruther H, et al. Bone marrow-derived tenascin-C attenuates cardiac hypertrophy by controlling inflammation. *J Am Coll Cardiol* (2017) 70:1601–15. doi: 10.1016/j.jacc.2017.07.789
103. Park WJ, Jeong D, Oh JG. Tenascin-C in cardiac hypertrophy and fibrosis: friend or foe? *J Am Coll Cardiol* (2017) 70:1616–7. doi: 10.1016/j.jacc.2017.08.014
104. Liu R, He Y, Li B, Liu J, Ren Y, Han W, et al. Tenascin-C produced by oxidized LDL-stimulated macrophages increases foam cell formation through Toll-like receptor-4. *Mol Cells* (2012) 34:35–41. doi: 10.1007/s10059-012-0054-x
105. Wang L, Shah PK, Wang W, Song L, Yang M, Sharifi BG. Tenascin-C deficiency in Apo E-/- mouse increases eotaxin levels: implications for atherosclerosis. *Atherosclerosis* (2013) 227:267–74. doi: 10.1016/j.atherosclerosis.2013.01.039
106. Wang L, Wang W, Shah PK, Song L, Yang M, Sharifi BG. Deletion of tenascin-C gene exacerbates atherosclerosis and induces intraplaque hemorrhage in Apo-E-deficient mice. *Cardiovasc Pathol* (2012) 21:398–413. doi: 10.1016/j.carpath.2011.12.005
107. Hamada K, Miura Y, Toma N, Miyamoto K, Imanaka-Yoshida K, Matsushima S, et al. Gellan sulfate core platinum coil with tenascin-C promotes intra-aneurysmal organization in rats. *Transl Stroke Res* (2014) 5:595–603. doi: 10.1007/s12975-014-0352-z
108. Suzuki H, Kawakita F. Tenascin-C in aneurysmal subarachnoid hemorrhage: deleterious or protective? *Neural Regener Res* (2016) 11:230–1. doi: 10.4103/1673-5374.177721
109. Fujimoto M, Shiba M, Kawakita F, Liu L, Shimojo N, Imanaka-Yoshida K, et al. Effects of tenascin-C knockout on cerebral vasospasm after experimental subarachnoid hemorrhage in mice. *Mol Neurobiol* (2018) 55:1951–8. doi: 10.1007/s12035-017-0466-x
110. Shiba M, Suzuki H, Fujimoto M, Shimojo N, Imanaka-Yoshida K, Yoshida T, et al. Imatinib mesylate prevents cerebral vasospasm after subarachnoid hemorrhage via inhibiting tenascin-C expression in rats. *Neurobiol Dis* (2012) 46:172–9. doi: 10.1016/j.nbd.2012.01.005
111. Kimura T, Shiraishi K, Furusho A, Ito S, Hirakata S, Nishida N, et al. Tenascin C protects aorta from acute dissection in mice. *Sci Rep* (2014) 4:4051. doi: 10.1038/srep04051
112. Kimura T, Yoshimura K, Aoki H, Imanaka-Yoshida K, Yoshida T, Ikeda Y, et al. Tenascin-C is expressed in abdominal aortic aneurysm tissue with an active degradation process. *Pathol Int* (2011) 61:559–64. doi: 10.1111/j.1440-1827.2011.02699.x
113. Sato A, Aonuma K, Imanaka-Yoshida K, Yoshida T, Isobe M, Kawase D, et al. Serum tenascin-C might be a novel predictor of left ventricular remodeling and prognosis after acute myocardial infarction. *J Am Coll Cardiol* (2006) 47:2319–25. doi: 10.1016/j.jacc.2006.03.033
114. Morimoto S, Imanaka-Yoshida K, Hiramitsu S, Kato S, Ohtsuki M, Uemura A, et al. Diagnostic utility of tenascin-C for evaluation of the activity of human acute myocarditis. *J Pathol* (2005) 205:460–7. doi: 10.1002/path.1730
115. Tsukada B, Terasaki F, Shimomura H, Otsuka K, Otsuka K, Katashima T, et al. High prevalence of chronic myocarditis in dilated cardiomyopathy referred for left ventriculoplasty: expression of tenascin C as a possible marker for inflammation. *Hum Pathol* (2009) 40:1015–22. doi: 10.1016/j.humpath.2008.12.017
116. Kitaoka H, Kubo T, Baba Y, Yamasaki N, Matsumura Y, Furuno T, et al. Serum tenascin-C levels as a prognostic biomarker of heart failure events in patients with hypertrophic cardiomyopathy. *J Cardiol* (2012) 59:209–14. doi: 10.1016/j.jjcc.2011.11.008
117. Terasaki F, Okamoto H, Onishi K, Sato A, Shimomura H, Tsukada B, et al. Higher serum tenascin-C levels reflect the severity of heart failure, left ventricular dysfunction and remodeling in patients with dilated cardiomyopathy. *Circ J* (2007) 71:327–30. doi: 10.1253/circj.71.327
118. Kanagala P, Arnold JR, Khan JN, Singh A, Gulsin GS, Chan DS, et al. Plasma Tenascin-C: a prognostic biomarker in heart failure with preserved ejection fraction. *Biomarkers* (2020) 25:556–65. doi: 10.1080/1354750X.2020.1810319
119. Hessel M, Steendijk P, den Adel B, Schutte C, van der Laarse A. Pressure overload-induced right ventricular failure is associated with re-expression of myocardial tenascin-C and elevated plasma tenascin-C levels. *Cell Physiol Biochem* (2009) 24:201–10. doi: 10.1159/000233246
120. Fujimoto N, Onishi K, Sato A, Terasaki F, Tsukada B, Nozato T, et al. Incremental prognostic values of serum tenascin-C levels with blood B-type natriuretic peptide testing at discharge in patients with dilated cardiomyopathy and decompensated heart failure. *J Card Fail* (2009) 15:898–905. doi: 10.1016/j.cardfail.2009.06.443
121. Hessel MH, Bleeker GB, Bax JJ, Henneman MM, den Adel B, Klok M, et al. Reverse ventricular remodelling after cardiac resynchronization therapy is associated with a reduction in serum tenascin-C and plasma matrix metalloproteinase-9 levels. *Eur J Heart Fail* (2007) 9:1058–63. doi: 10.1016/j.ejheart.2007.07.007
122. Okuma Y, Suda K, Nakaoka H, Katsube Y, Mitani Y, Yoshikane Y, et al. Serum tenascin-C as a novel predictor for risk of coronary artery lesion and resistance to intravenous immunoglobulin in Kawasaki disease- a multicenter retrospective study. *Circ J* (2016) 80:2376–81. doi: 10.1253/circj.CJ-16-0563
123. Yokouchi Y, Oharaseki T, Enomoto Y, Sato W, Imanaka-Yoshida K, Takahashi K. Expression of tenascin C in cardiovascular lesions of Kawasaki disease. *Cardiovasc Pathol* (2019) 38:25–30. doi: 10.1016/j.carpath.2018.10.005
124. Kul S, Ozcelik HK, Uyarel H, Karakus G, Guvenc TS, Yalcinsoy M, et al. Diagnostic value of strain echocardiography, galectin-3, and tenascin-C levels for the identification of patients with pulmonary and cardiac sarcoidosis. *Lung* (2014) 192:533–42. doi: 10.1007/s00408-014-9586-5

125. Wallner K, Li C, Shah PK, Fishbein MC, Forrester JS, Kaul S, et al. Tenascin-C is expressed in macrophage-rich human coronary atherosclerotic plaque. *Circulation* (1999) 99:1284–9. doi: 10.1161/01.cir.99.10.1284
126. Satta J, Soini Y, Pollanen R, Paakko P, Juvonen T. Tenascin expression is associated with a chronic inflammatory process in abdominal aortic aneurysms. *J Vasc Surg* (1997) 26:670–5. doi: 10.1016/s0741-5214(97)70068-5
127. Gao W, Li J, Ni H, Shi H, Qi Z, Zhu S, et al. Tenascin C: a potential biomarker for predicting the severity of coronary atherosclerosis. *J Atheroscler Thromb* (2019) 26:31–8. doi: 10.5551/jat.42887
128. Guo T, Zhou X, Zhu A, Peng W, Zhong Y, Chai X. The role of serum tenascin-C in predicting in-hospital death in acute aortic dissection. *Int Heart J* (2019) 60:919–23. doi: 10.1536/ihj.18-462
129. Trescher K, Thometich B, Demyanets S, Kassal H, Sedivy R, Bittner R, et al. Type A dissection and chronic dilatation: tenascin-C as a key factor in destabilization of the aortic wall. *Interact Cardiovasc Thorac Surg* (2013) 17:365–70. doi: 10.1093/icvts/ivt204
130. Nozato T, Sato A, Hikita H, Takahashi A, Imanaka-Yoshida K, Yoshida T, et al. Impact of serum tenascin-C on the aortic healing process during the chronic stage of type B acute aortic dissection. *Int J Cardiol* (2015) 191:97–9. doi: 10.1016/j.ijcard.2015.05.009
131. Suzuki H, Kanamaru K, Shiba M, Fujimoto M, Imanaka-Yoshida K, Yoshida T, et al. Cerebrospinal fluid tenascin-C in cerebral vasospasm after aneurysmal subarachnoid hemorrhage. *J Neurosurg Anesthesiol* (2011) 23:310–7. doi: 10.1097/ANA.0b013e31822aa1f2
132. Liabeuf S, Barreto DV, Kretschmer A, Barreto FC, Renard C, Andrejak M, et al. High circulating levels of large splice variants of tenascin-C is associated with mortality and cardiovascular disease in chronic kidney disease patients. *Atherosclerosis* (2011) 215:116–24. doi: 10.1016/j.atherosclerosis.2010.11.038
133. Gellen B, Thorin-Trescases N, Thorin E, Gand E, Sosner P, Brishoual S, et al. Serum tenascin-C is independently associated with increased major adverse cardiovascular events and death in individuals with type 2 diabetes: a French prospective cohort. *Diabetologia* (2020) 63:915–23. doi: 10.1007/s00125-020-05108-5
134. Sato M, Toyozaki T, Odaka K, Uehara T, Arano Y, Hasegawa H, et al. Detection of experimental autoimmune myocarditis in rats by ^{111}In monoclonal antibody specific for tenascin-C. *Circulation* (2002) 106:1397–402. doi: 10.1161/01.cir.0000027823.07104.86
135. Ageyama N, Kurosawa H, Fujimoto O, Uehara T, Hiroe M, Arano Y, et al. Successful inflammation imaging of non-human primate hearts using an antibody specific for tenascin-C. *Int Heart J* (2019) 60:151–8. doi: 10.1536/ihj.17-734
136. Lipke DL, Aziz SM, Fagerland JA, Majesky M, Arcot SS. Tenascin synthesis, deposition, and isoforms in monocrotaline-induced pulmonary hypertensive rat lungs. *Am J Physiol* (1996) 271:L208–15. doi: 10.1152/ajplung.1996.271.2.L208
137. Rohm I, Grun K, Muller LM, Kretzschmar D, Fritzenwanger M, Yilmaz A, et al. Increased serum levels of fetal tenascin-C variants in patients with pulmonary hypertension: novel biomarkers reflecting vascular remodeling and right ventricular dysfunction? *Int J Mol Sci* (2017) 18:2371–81. doi: 10.3390/ijms18112371

Conflict of Interest: The authors declare that the research was conducted in the absence of any commercial or financial relationships that could be constructed as a potential conflict of interest.

frontiers in Immunology

REVIEW
published: 09 December 2020
doi: 10.3389/fimmu.2020.610096

Biologically Active TNIIIA2 Region in Tenascin-C Molecule: A Major Contributor to Elicit Aggressive Malignant Phenotypes From Tumors/Tumor Stroma

Takuya Iyoda[1*†], *Motomichi Fujita*[2†] *and Fumio Fukai*[2*]

[1] Department of Pharmacy, Faculty of Pharmaceutical Sciences, Sanyo-Onoda City University, Sanyo-Onoda, Japan,
[2] Department of Molecular Patho-Physiology, Faculty of Pharmaceutical Sciences, Tokyo University of Science, Noda, Japan

OPEN ACCESS

Edited by:
Kyoko Imanaka-Yoshida,
Mie University, Japan

Reviewed by:
Shigeyuki Kon,
Fukuyama University, Japan
Koyu Ito,
Tohoku University, Japan

***Correspondence:**
Takuya Iyoda
iyoda@rs.socu.ac.jp
Fumio Fukai
fukai@rs.tus.ac.jp

[†]These authors have contributed equally to this work

Specialty section:
This article was submitted to Cancer Immunity and Immunotherapy, a section of the journal Frontiers in Immunology

Received: 25 September 2020
Accepted: 06 November 2020
Published: 09 December 2020

Citation:
Iyoda T, Fujita M and Fukai F (2020) Biologically Active TNIIIA2 Region in Tenascin-C Molecule: A Major Contributor to Elicit Aggressive Malignant Phenotypes From Tumors/Tumor Stroma. Front. Immunol. 11:610096. doi: 10.3389/fimmu.2020.610096

Tenascin (TN)-C is highly expressed specifically in the lesions of inflammation-related diseases, including tumors. The expression level of TN-C in tumors and the tumor stroma is positively correlated with poor prognosis. However, no drugs targeting TN-C are currently clinically available, partly because the role of TN-C in tumor progression remains controversial. TN-C harbors an alternative splicing site in its fibronectin type III repeat domain, and its splicing variants including the type III-A2 domain are frequently detected in malignant tumors. We previously identified a biologically active region termed TNIIIA2 in the fibronectin type III-A2 domain of TN-C molecule and showed that this region is involved in promoting firm and persistent cell adhesion to fibronectin. In the past decade, through the exposure of various cell lines to peptides containing the TNIIIA2 region, we have published reports demonstrating the ability of the TNIIIA2 region to modulate distinct cellular activities, including survival/growth, migration, and invasion. Recently, we reported that the signals derived from TNIIIA2-mediated β1 integrin activation might play a crucial role for inducing malignant behavior of glioblastoma (GBM). GBM cells exposed to the TNIIIA2 region showed not only exacerbation of PDGF-dependent proliferation, but also acceleration of disseminative migration. On the other hand, we also found that the pro-inflammatory phenotypic changes were promoted when macrophages are stimulated with TNIIIA2 region in relatively low concentration and resulting MMP-9 upregulation is needed to release of the TNIIIA2 region from TN-C molecule. With the contribution of TNIIIA2-stimulated macrophages, the positive feedback spiral loop, which consists of the expression of TN-C, PDGF, and β1 integrin, and TNIIIA2 release, seemed to be activated in GBM with aggressive malignancy. Actually, the growth of transplanted GBM grafts in mice was significantly suppressed *via* the attenuation of β1 integrin activation. In this review, we thus introduce that the TNIIIA2 region has a significant impact on malignant progression of tumors by regulating cell adhesion. Importantly, it has been demonstrated that the TNIIIA2 region exerts unique biological functions through the extremely strong

activation of β1-integrins and their long-lasting duration. These findings prompt us to develop new therapeutic agents targeting the TNIIIA2 region.

Keywords: tenascin-C, TNIIIA2, β1-integrin, macrophage, solid tumor, glioblastoma, PDGF

INTRODUCTION

Tenascin (TN)-C, a cell adhesion-modulatory matricellular protein, is characterized by its unique expression pattern. TN-C is transiently highly expressed during embryogenesis, wound healing, and tumorigenesis, whereas its expression in normal tissue is relatively low (1–5). Notably, TN-C is frequently found in most malignant tumors at high levels, with its expression showing a positive correlation with poor disease-free survival in patients with different cancers, such as lung and breast carcinomas and glioma (4, 5). Nonetheless, the role of TN-C in malignant tumor progression remains largely unclear.

As criteria for evaluating tumor cell malignancy, several cellular activities are frequently examined such as proliferation, survival, migration, and differentiation. Any of these cellular activities are strongly linked to cell adhesion. However, the effect of TN-C on cell adhesion control is particularly complex. This is because the TN-C substrate supports the attachment of some cell types but is non-adhesive for others (6–8). Therefore, TN-C is classified as an "adhesion modulatory" ECM protein and is called a "matricellular" protein (9, 10). Because of this antithetical property in cell adhesion control, understanding the role played by TN-C in pathological events is complicated and difficult.

TN-C has various isoforms, which are generated by alternative mRNA splicing within its fibronectin type III-like repeat (FNIII) domain A1 to D. The bioactivities of each TN-C isoform are thought to depend on the domains included. Because frequent detection of TN-C containing the FNIII-A2 domain has been reported within tumor-associated pathological lesions (11, 12), it has been presumed that the FNIII-A2 domain may play a role in tumor formation and progression. About 15 years ago, we found a biologically active region in the FNIII-A2 domain of TN-C (**Figure 1**) and gave the responsible 8-amino acid sequence YTITIRGV the name TNIIIA2 (13). This region appeared to be cryptic but was exposed by MMP-2/-9–mediated processing of TN-C (13–15). It has been shown that the released TNIIIA2 region is capable of enhancing cell adhesion to fibronectin (FN) through induction of β1 integrin activation.

Integrin superfamily members act as adhesive transmembrane receptors mediating the cell-to-ECM interaction. Integrins can alter ligand binding and signal transduction activities. Given that integrin-mediated cell-to-ECM interactions play key roles in the induction of appropriate cellular functions in normal cells, including macrophages, changes in the affinity or specificity of the interaction between integrins on the cell surface and the surrounding ECM might be critical for anchorage-dependent cellular processes. Because tumor malignancy is characterized by abnormalities in cell survival, growth, and migration, all of which involve anchorage-dependent cellular processes, there is a possibility that aberrant β1 integrin activation induced by the TNIIIA2 region might be a trigger for eliciting malignancy from tumors and/or the tumor stroma.

In this review, we introduce our recent observations concerning the effect of the TNIIIA2 region on the construction of inflammatory environments and the subsequent elicitation of malignancy from an aggressive tumor type, glioblastoma (GBM). Furthermore, we show that the bioactivity of the TNIIIA2 region might become a fruitful anti-tumor target in the clinical setting.

BIOLOGICAL PROPERTIES OF THE TNIIIA2 REGION IN TN-C AND ITS EFFECT ON MACROPHAGES

The TNIIIA2 region was first identified as an accelerator of cell adhesion to FN substrate. It has been shown that WI38VA cells

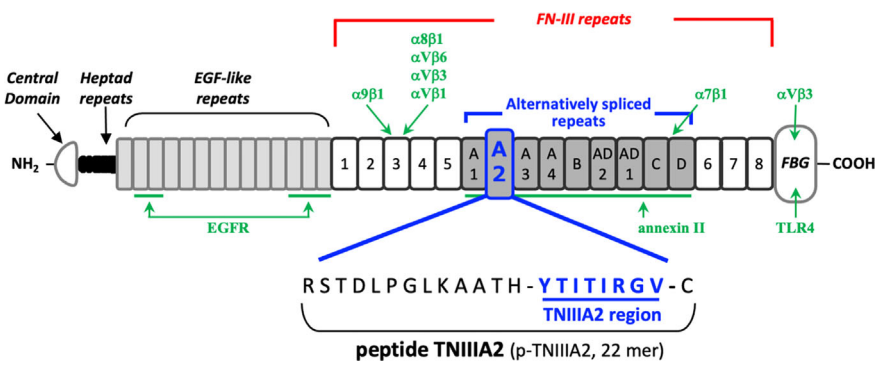

FIGURE 1 | Schematic illustration of the domain structure of tenascin-C and its intramolecular bioactive region TNIIIA2. The sites responsible for receptor binding or ligand binding are shown in green arrow, with the name of corresponding interaction molecules in green text.

stimulated with a peptide containing the TNIIIA2 region (p-TNIIIA2) attached and spread rapidly to the FN substrate (13). Ability of p-TNIIIA2 to induce potentiated and sustained activation of β1 integrin has been shown (13). It has also been demonstrated that cell surface sydecan-4 is needed for the expression of pro-adhesive activity of TNIIIA2 region (13). Syndecan-4 is a member of cell surface proteoglycans that affect numerous cellular processes including growth and migration through activation of various signaling pathways. As for the relationship with β1 integrins, syndecan-4 works not only as an intracellular signal transducer but also for regulating integrin turn over expressed on cell surface and maintain focal adhesion functionality (16–21). Versatility of syndecan-4 in cell regulation depends on their ability to bind numerous molecules to their intracellular domain. Integrin turnover is also achieved by sydecan-4-induced activation of PKCα and/or ARF6 signaling pathways (16, 18). However, in our case, it was identified that the ectodomain of syndecan-4 plays an important role in β1 integrin activation in response to TNIIIA2 region because conformational change of β1 integrin was still observed even with both deletion of the cytoplasmic domains of syndecan-4 and addition of PKCα inhibitor (13). Therefore, as illustrated in **Figure 2**, it was predicted that TNIIIA2 region of TN-C binds to syndecan-4 ectodomain, nestles close to β1 integrin in inactive form, and then, forces change β1 integrin conformation to active in a lateral "outside-out" interaction (14, 15).

Activated integrins could interact with ECM proteins, and transmit signals into cells. Intracellular signaling derived from cell adhesion receptors plays a role in regulating various cellular functions. Even in macrophages, it is generally well-known that integrin-derived signal is critical for inducing phagocytosis, cytokine release, ROS production and chemotaxis (22, 23). When we stimulated macrophage cell lines with p-TNIIIA2, upregulation of inflammatory genes including IL-1β was observed (**Figure 3A**). Western blotting analysis revealed that the upregulated IL-1β seems to be cleaved to its active form (**Figure 3B**) and is accompanied by increases in both expression and activation of caspase-1 (**Figure 3B**). Consistent with the elevation of IL-1β and caspase-1 expression in active form, NLRP3, which is a component of caspase-1-activating multiprotein complex called NLRP3-inflammasome, was also elevated in p-TNIIIA2 stimulated macrophages (**Figure 3A**). These observations suggest that the TNIIIA2 region would force macrophages to establish an inflammatory environment through elevation of IL-1β expression and following its secretion in active form. On the other hand, increased expression of TN-C, which is the parental molecule of TNIIIA2, was not detected in macrophages stimulated with p-TNIIIA2, despite the significant upregulation of MMP-9 which is needed for the release of the cryptic TNIIIA2 region from TN-C was detected (**Figure 3A**). Almost the same observation was obtained using PMA-differentiated THP-1 human macrophages (**Figures 3C, D**). These observations let us presume that macrophages have to be present in the lesion sites where parental TN-C was abundantly provided by other cells, if assuming that the macrophages stimulated by TNIIIA2 region play a role in disease progression.

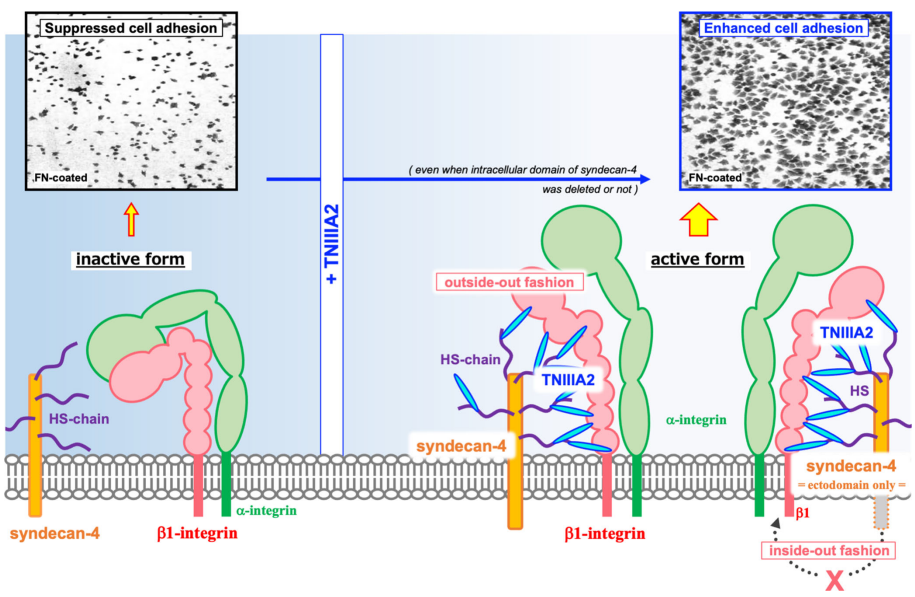

FIGURE 2 | Schematic illustration of the β1 integrin activation induced by TNIIIA2. Integrin heterodimer containing β1 integrin in inactive form is shown in left side. Accompanied with the release of TNIIIA2 region from TN-C by proteolysis, TN-C fragment containing TNIIIA2 region forms complex with cell surface syndecan-4 through heparan sulfate chain. Then, conformation change of β1 integrin to active form will be occurred by lateral interaction of formed TNIIIA2/syndecan-4 complex with β1 integrin (right side). Representative image of enhanced cell adhesion induced by p-TNIIIA2 addition is shown in upper part.

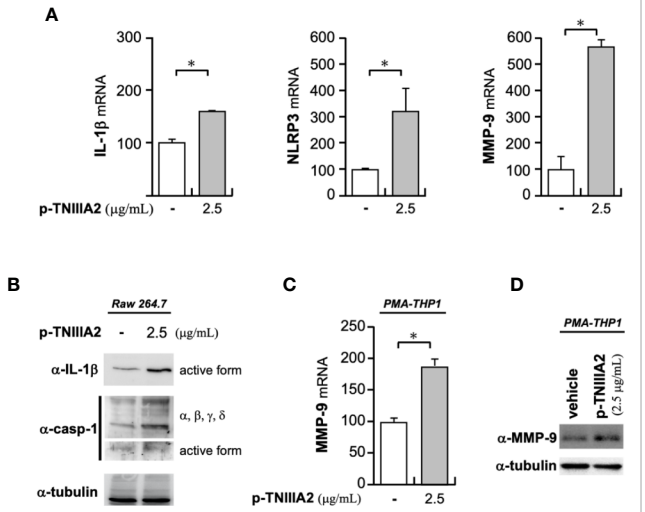

FIGURE 3 | Pro-inflammatory effects of p-TNIIIA2 in macrophages. **(A)** mRNA expression in p-TNIIIA2-stimulated Raw 264.7 cells was evaluated by real-time PCR. **(B)** Western blotting analysis of IL-1β and caspase-1 in p-TNIIIA2-stimulated Raw 264.7 cells. **(C, D)** MMP-9 expression in p-TNIIIA2-stimulated THP-1 cells differentiated with PMA was evaluated by real-time PCR **(C)** and western blotting analysis **(D)**. Results are shown in the mean ± S.D. *$p < 0.01$ vs. p-TNIIIA2(-) control group.

CONTRIBUTION OF THE TNIIIA2 REGION TO ABERRANT CELL SURVIVAL AND GROWTH

As described above, TN-C expression in normal adult tissue is relatively low. However, transient overexpression of TN-C has been frequently observed in various types of tumor progression and the particularly high expression of TN-C in GBM, an aggressive glial tumor in adults, has been reported (24, 25). Therapeutic efficacy of anti-TN-C monoclonal antibody has been demonstrated in glioma xenograft model (26) and the positive correlation between high TN-C levels and poor prognosis in GBM patients has also been reported (5). Therefore, expression in GBM is considered a negative prognostic factor. Since, parallelism between association of proteolytic degradation of TN-C and poor prognosis in cancer including glioma (27, 28), we decided to focus on GBM next and tried to make it clear whether TNIIIA2 region, which is presumed to be released from TN-C digested by macrophage-derived MMP-9, play some roles in leading aggressive progression of tumor or not.

As described above, the function of the TNIIIA2 region is mainly based on their ability to induce conformational change of β1 integrins from inactive to active. Therefore, we first tested the effect of a β1 integrin inactivator on GBM progression *in vivo*. Fortunately, we previously identified a potent β1 integrin inactivation tool termed p-FNIII14, which is a peptide derived from 14th type III segment of FN (29). β1 integrins in active form would be forced to change their conformation to inactive form when cells were exposed to p-FNIII14 (20). We also reported that the eEF1A on cell surface act as a membrane receptor for p-FNIII14 and functional inactivation of β1 integrin was carried out by the interaction of integrins with p-FNIII14/eEF1A complex in "outside-out" fashion (30). The point is that the effect of p-FNIII14 on β1 integrin is quite the contrary to that of p-TNIIIA2 and we showed that the excessive β1 integrin activation induced by p-TNIIIA2 was able to be attenuated by addition of p-FNIII14 (31–35). When inactivation of β1 integrins was promoted in animals transplanted with GBM cells, by injection of p-FNIII14, significant suppression in the growth of GBM xenograft was observed, whereas it was continuously grown in the animals injected with biologically inactive control peptide (tumor volume on p-FNIII14 injected mice vs. control peptide injected mice = 2289.5 ± 172.5 mm^3 vs. 5567.0 ± 779.0 mm^3) (34). This result suggests that the malignant progression of GBM would be abrogated by β1 integrin inactivation. Because GBM cells abundantly express TN-C, MMP-mediated release of the TNIIIA2 region from TN-C appears to be a key event underlying the expression of malignancy in GBM cells, through its ability to activate β1 integrins. If so, macrophage-derived MMPs may contribute to TNIIIA2 exposure from GBM cell-derived TN-C molecules.

To investigate the TNIIIA2-mediated regulation of GBM malignancy in detail, we next evaluated the effect of p-TNIIIA2 on a GBM cell line *in vitro*. One of the characteristics of GBM cells is a high degree of proliferation and significant activation in mitogenic PDGF signaling has been reported in proneural GBM (36, 37). Given that we have previously shown that hyperstimulation of PDGF-dependent proliferation is induced when NIH3T3 cells are exposed to both p-TNIIIA2 and PDGF (14), we hypothesized that PDGF-dependent proliferation in GBM cells could also be accelerated by TNIIIA2-derived signaling. Hence, we first tested the effects of PDGF stimuli on T98G GBM cells and confirmed that T98G cell proliferation was accelerated by PDGF in a dose-dependent manner but reached a plateau at over 10 ng/ml (34). When p-TNIIIA2 was added to the culture medium of T98G cells stimulated with a submaximal dose of PDGF, the proliferation of these cells was further accelerated. The p-TNIIIA2–dependent hyperproliferation observed in PDGF-stimulated T98G cells was abrogated by the addition of function-blocking antibodies against α5 and β1 integrin, whereas anti-α4, αv, and β3 integrin antibodies showed no effect (34). We have also observed that the β1 integrin-activating antibody HUTS-4 can boost PDGF-dependent GBM cell proliferation, similar to p-TNIIIA2 (34). From these observations, PDGF-secured GBM cell proliferation is strongly stimulated further by α5β1 integrin activation, which involves binding of the TNIIIA2 region to GBM cells. TN-C, which is highly expressed in GBM lesions, would be a source of the release of TNIIIA2 region.

The effect of p-TNIIIA2 on the hyperstimulation of PDGF-dependent GBM cell growth was further proved through validation of anchorage-independent cell proliferation. As determined with a soft agar colony formation assay, the number of colonies formed was significantly elevated in T98G cells stimulated with both PDGF and p-TNIIIA2, whereas the

colony number for the cells stimulated with PDGF or p-TNIIIA2 alone showed just a slight elevation (34). The β1 integrin-inactivating peptide p-FNIII14 can rescue T98G cells from an aberrant acceleration in both adhesion-dependent and -independent cell survival/growth induced by p-TNIIIA2 stimulation combined with PDGF (34). From these observations, it was suggested that the TNIIIA2 region in TN-C is responsible for inducing the hyperstimulation of GBM cell survival and proliferation, with its bioactivity inducing potent and prolonged activation of β1 integrins.

Regarding parental TN-C molecule, its ability to stimulate tumor cell growth has been reported by several groups (38–45). As a molecular mechanism for this effect of TN-C, Huang et al. demonstrated that TN-C is capable of interfering in the ligation of cell surface sydecan-4, which works as a co-receptor of integrins, to FNIII-13 domain of FN (46). They showed that the intracellular signaling pathway activated by syndecan-4 ligated to FNIII-13 domain is responsible for suppressing tumor cell proliferation (46). TN-C has ability to bind to the same FNIII-13 domain of FN. Therefore, TN-C is able to neutralize anti-proliferative signal derived from FN-ligated syndecan-4, result in vigorous cell growth accompanied by the suppression of cell adhesion in spread form (46). Consistent with this report, Orend et al. also reported that the inhibition of interaction between FNIII-13 domain of FN and sydecan-4 by TN-C leads cell cycle arrest in fibroblast (47). Moreover, inhibition of tumor cell growth by exogeneous addition of TN-C in soluble phase has been reported (48). Among these reports referred above, TN-C seems to work as an inhibitor for cell adhesion to FN. On the other hand, TNIIIA2 region acted as an inducer of cell adhesion to FN. p-TNIIIA2 could promote β1 integrin activation even when intracellular domain of its receptor syndecan-4 was deleted, and when PKCα signaling that is activated by FN-ligated sydecan-4 was inhibited (13). Since TNIIIA2 region is usually fold inside in intact TN-C molecule and exposed when TN-C was digested by inflammatory proteinase like MMPs, the mechanisms responsible for the proliferation-stimulatory effect of TNIIIA2 region seems to be different and independent from that underlying expression of TN-C's effects at least on growth activity.

EFFECT OF THE TNIIIA2 REGION ON GBM CELL MIGRATION AND SCATTERED PROLIFERATION

Similar to its aggressive proliferation, GBM is also characterized by frequent dissemination throughout the brain parenchyma. Therefore, we next tested whether p-TNIIIA2 has ability to affect cell migratory and showed that the migratory activity of GBM cell lines in an *in vitro* scratch assay was significantly accelerated by p-TNIIIA2 administration (34). p-TNIIIA2-mediated elevation in cell migration activity was completely abrogated by the addition of the β1 integrin-inactivating peptide p-FNIII14 (34). Moreover, we recently reported that binding of the FN substrate to α5β1 integrin, but not α4β1 integrin, might be a key event underlying the accelerated GBM cell migration induced by p-TNIIIA2 (34). These results suggest that activation of α5β1 integrin is responsible for the augmented migratory activity observed in p-TNIIIA2–treated GBM cells.

During the experiments described above, we found that T98G cells cultured on the 2D FN substrate proliferate with a cobblestone-like cell sheet formation (**Figure 4**). Interestingly, the cell-to-cell adhesive interactions of T98G cells seemed to be arrested by the addition of TNIIIA2, resulting in a mesenchymal morphology (**Figure 4**). This "EMT-like" change induced by TNIIIA2 was completely blocked by not only a peptide that leads inactivation of β1 integrin, p-FNIII14 (**Figure 4**), but also a function-blocking antibody to β1 integrin, BV7 (34). Concomitant with the promotion of cell scattering from the cobblestone-like sheet, we also found that one of the EMT-related markers, β-catenin, was localized around the cell-to-cell contact area in GBM cells without p-TNIIIA2 stimulation, and this localization was markedly reduced and became diffuse in the cytosol when p-TNIIIA2 was added to GBM cell culture (34). These observations suggest that β1 integrin activation by the TNIIIA2 region might also be implicated in more aggressive GBM cell migration, which is one of the important characteristics of malignant disseminative behavior in GBM.

As for the parental TN-C molecule, migration-stimulatory effect has been broadly reported not only in tumor cells (4, 38, 45, 48–55) but also in non-tumor cells (56–58). Of note, Tsunoda et al. demonstrated that TN-C substrates containing FNIII-A1, -A2, -A4, -B, and -D repeat is capable of enhancing tumor cell migration whereas TN-C without alternative splicing domain showed no effect (45). They also mentioned that large variants of TN-C without FNIII-B repeat is also effective for acceleration of tumor cell migration (45). Contribution of β1-integrin in TN-C-mediated acceleration of cell migration has also been demonstrated (55, 57). Since bioactive TNIIIA2 region has been found from FNIII-A2 repeat and works as a potent inducer of β1-integrin activation, there is a possibility that the migration promotive nature of TN-C might be retained by TNIIIA2.

On the other hand, deep relationship between TN-C expression and EMT promotion has also been reported (59–65). Among them, Yoneura et al. demonstrated that the

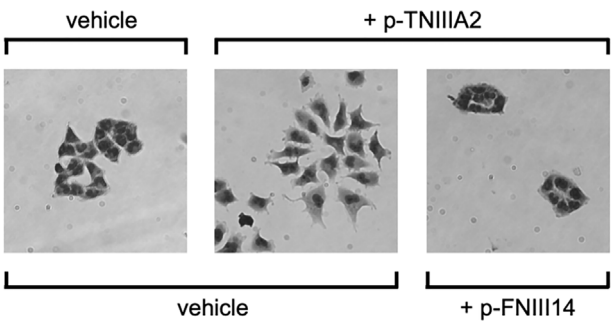

FIGURE 4 | TNIIIA2-mediated acceleration of GBM cell dissemination. p-TNIIIA2-stimulated GBM cells were cultured with or without p-FNIII14. Then, the disseminative activity of these cells was evaluated by microscopic analysis.

interaction of TN-C with annexin II, which is known to be able to bind to alternative splicing domain of TN-C, is capable of driving EMT and following acquisition of anoikis resistance in pancreatic cancer (61). Since TNIIIA2 region has been found from FNIII-A2 alternative splicing repeat of TN-C, and this region has ability to added anoikis resistance to GBM cell (34), the EMT-promotive effect of TN-C seems to be expressed through exposure of TNIIIA2 region. However, Katoh et al. showed that the binding of αVβ1 and αVβ6 integrins, both of which could bind to FNIII-3 domain of TN-C, is responsible for TN-C-mediated EMT promotion in breast cancer cells (62, 63). Mamuya et al. and Tiwari et al. has also showed a contribution of FNIII-1 to 5 domains to EMT promotion in lens epithelial cells (64, 65). Thus, release of TNIIIA2 region might plays a role in EMT promotion, at least in part, depend on cellular context.

POSITIVE FEEDBACK LOOP BETWEEN TNIIIA2 RELEASE AND THE EXPRESSION OF TN-C, β1 INTEGRIN, AND PDGF

In addition to the above-described experiments, we found that the PDGF-B expression in p-TNIIIA2-treated T98G cells was significantly higher than that cultured without p-TNIIIA2 (**Figure 5A**). Moreover, the expression of β1 integrin in p-TNIIIA2-treated T98G cells was also 3 to 4 times higher than untreated cells (35). Interestingly, PDGF-BB, which is upregulated in TNIIIA2-stimulated GBM cells (**Figure 5A**), can accelerate both the expression and secretion of TN-C, the TNIIIA2 parental protein (**Figure 5B**). These observations suggest that TNIIIA2 can stimulate PDGF production and that subsequent binding of PDGF to PDGF receptor on GBM cells in an autocrine/paracrine manner leads to upregulation of TN-C protein. Moreover, the TNIIIA2-derived signals would be further reinforced by TNIIIA2-mediated upregulation of β1 integrin (35), which is the molecule responsible for the bioactivity of TNIIIA2. These results suggest that there is a feedback loop between the upregulation of TN-C, TNIIIA2, β1 integrin, and PDGF (**Figure 5C**). Because MMP-9 expression in macrophages was significantly upregulated by p-TNIIIA2 at 2.5 μg/ml (**Figures 3A, C, D**), which is 10 times lower than that was needed for eliciting GBM cell malignancy, macrophages might contribute to this feedback loop and elicit the aggressive malignancy of GBM cells through promotion of the continuous release and accumulation of the TNIIIA2 region by MMP-9-mediated cleavage of TN-C, result in subsequent PDGF production from GBM cells and make this feedback loop effectively work.

CONTRIBUTION OF β1 INTEGRIN ACTIVATION TO DRUG RESISTANCE

For newly diagnosed GBM patients, temozolomide (TMZ), an oral alkylating agent, is the first-line chemotherapeutic agent. However, more than half of all GBM patients show resistance to TMZ. One of the reasons for the acquisition of drug resistance in GBM is upregulation of the DNA repair protein MGMT (66). Thus, the development of new clinical strategies to overwhelm TMZ resistance is warranted. Recently, Janouskova et al. (67)

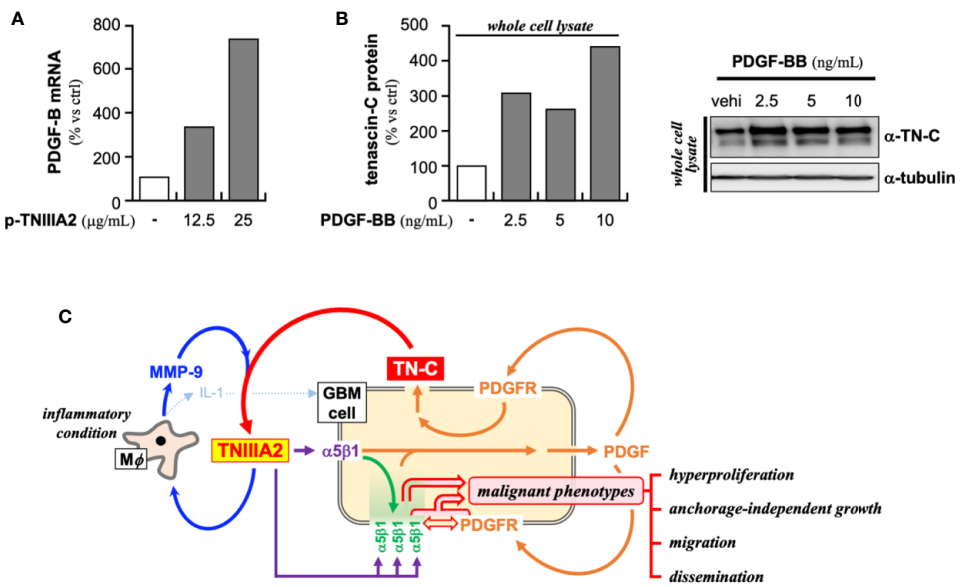

FIGURE 5 | Presumed positive feedback loop in the malignant progression of GBM through TNIIIA2-derived signal transmission. **(A)** PDGF-B expression in p-TNIIIA2-stimulated GBM cells was evaluated by RT-PCR. **(B)** TN-C expression in PDGF-BB-stimulated GBM cells was evaluated by western blotting analysis. **(C)** Schematic illustration of the putative positive feedback loop underlying the acceleration of GBM aggressiveness.

showed that GBM cells with α5 integrin overexpression develop TMZ resistance and that depletion of α5 integrin sensitizes GBM cells to TMZ. α5 and β1 integrin can form a heterodimer, which would contribute to cell adhesion as a FN receptor, and we recently demonstrated that the inactivation of β1 integrins *via* p-FNIII14 administration can significantly reduce the EC_{50} of TMZ against T98G cells (34). In our experimental conditions, downregulation of MGMT appeared to be the one of underlying mechanisms for the restoration of chemosensitivity observed in FNIII14-treated GBM cells. This MGMT downregulation was not depend on the enhanced MGMT promoter methylation (34). Likewise, Wang et al. also reported a methylation independent regulation of MGMT expression (68), although the level of MGMT promotor methylation has been reported as a marker of response to TMZ in glioma (68–71). On the other hand, we have also reported previously that p-FNIII14-mediated β1 integrin inactivation can sensitize solid tumor cells to various chemotherapeutic drugs through activation of pro-apoptotic Bim (72). Taken together, although the molecular mechanisms underlying FNIII14-induced MGMT downregulation require further investigation, β1 integrin activation promoted by the TNIIIA2 region might also play a role in the acquisition of drug resistance in tumor cells.

DISCUSSION

In this review, we focused on GBM and proposed the existence of a positive feedback loop comprising TN-C, TNIIIA2, β1 integrin, and PDGF that can stimulate hyperproliferation, enhanced migration, and active dissemination. GBM cells can also become resistant to chemotherapeutic drugs when β1 integrin is activated. Thus, TNIIIA2-mediated potent and sustained β1 integrin activation would be a key event in eliciting the aggressive malignant phenotype of GBM. Because proliferation of GBM cells was stimulated by PDGF but reached a plateau, signals derived from PDGF binding would be insufficient to instigate the positive feedback loop mentioned above. Notably, the tumor-beneficial action of macrophages was stimulated by 2.5 μg/ml of p-TNIIIA2 whereas malignant phenotypes in GBM cell was enhanced by 25 μg/ml of p-TNIIIA2. This indicates that macrophages exposed to low levels of TNIIIA2 in the early stage of the tumor lesion establishment might contribute to the elicitation of an aggressive malignant phenotype from GBM cells *via* enhanced MMP-9 expression and subsequent digestion of TN-C and exposure of TNIIIA2 region. By the macrophage-mediated elevation in the level of the exposed TNIIIA2 region, hypothesized positive feedback loop (**Figure 5C**) can be pushed result in promotion of aggressive malignancy in GBM cells.

When focused onto the effect of parental TN-C on macrophages, accumulated evidence indicates that TN-C is capable of adding inflammatory phenotype on macrophages. Acceleration of inflammatory cytokine production promoted by FBG domain of TN-C molecule through binding to TLR4 has been shown (73, 74). Moreover, it has also been reported that the αVβ3 integrin mediated interaction of macrophages with TN-C leads production of inflammatory cytokines, such as IL-1β, IL-6, and TNF (75). However, there are no report showing MMP-2/9 upregulation in macrophages stimulated with TN-C. Moreover, both FBG and FNIII-3 domain is not defined as an alternative spliced domain. Thus, TNIIIA2-mediated polarization of macrophages toward inflammatory phenotype might be a newly acquired function of TN-C expressed through its limited digestion. In our observations, macrophages were 10 times more susceptible to p-TNIIIA2 than GBM cells. This fact let us presume that macrophages would be stimulated earlier than GBM cells during progression of tumors. If so, which cells are responsible for the "first" released of TNIIIA2 region. One of the answers to this question might be macrophages because basal expression of MMP-2 is frequently observed although it is in relatively low level. Tumor cell is also candidates because various type of tumor cells has ability to produce MMPs, especially on their way to express metastatic activity. There is a possibility that fibroblast acts as a source of MMPs, since Kanayama et al. has previously shown that MMP-9 production is upregulated when fibroblast was stimulated with FNIII-3 domain of TN-C (76). Although further examination is needed, it is supposed that the environmental MMP-2/9 level which would be drastically elevated through inflammatory activation of macrophages might be one of the key events for adding aggressive metastatic phenotypes on tumor cells.

On the other hand, as shown in **Figures 3A, B**, p-TNIIIA2 is able to stimulate IL-1β production in macrophages. IL-1β has been reported to be the factor that makes the tissue environment favorable for solid tumor progression through the acceleration of tumor cell growth, invasion, and neovascularization (77–79). In addition, regarding GBM progression, Paugh et al. reported that IL-1 can boost GBM cell survival and invasion through sphingosine kinase 1 upregulation (80). Moreover, we recently reported that the acceleration of survival and proliferation in preneoplastic cells was induced by soluble paracrine factors secreted from TNIIIA2-stimulated fibroblasts (33). Furthermore, we have also reported that TNIIIA2 is able to increase the invasive and metastatic activity of colon cancer cell lines (81). The contribution of β1 integrin activation to the acquisition of drug resistance is not limited to GBM cells but broadly observed in various solid tumor cell lines, although the suggested underlying mechanisms differ between GBM and other cell types (34, 72). These observations led us to presume that the released TNIIIA2 region might be able to elicit malignant phenotypes from tumor cells universally. The macrophage-mediated splicing of TN-C seems to be a key event for eliciting aggressive malignant phenotypes from tumor cells.

In any case, the accumulated evidence suggests that the TNIIIA2 region in TN-C might be a powerful initiator for the elicitation of aggressive properties from tumors through potentiated and sustained activation of β1 integrins. Macrophages, which are present in or infiltrate into the tumor stroma and can react to TNIIIA2 region at low levels, play a key role in ensuring that the level of released TNIIIA2 region is sufficient to promote the aggressive properties of tumors. Therefore, inactivation of β1 integrin would provide a useful strategy to abrogate the acquisition of aggressive behaviors by tumors, including GBM. The combined administration of the

peptide FNIII14 and chemotherapeutic drugs would be a promising strategy for clinical cancer treatment. Actually, Matsunaga et al. previously reported that β1 integrin-mediated adhesion of AML cells is crucial for the formation or minimal residual disease at bone marrow which is the major cause of relapse after chemotherapy in AML patient (82) and showed the therapeutic efficacy of combined administration of β1 integrin inactivator p-FNIII14 with chemotherapeutic drug to eradicate MRD and suppress AML relapse in mice (83). Although further investigation and more detailed information is needed, TNIIIA2 region itself of releasing mechanism of this region might become a fruitful target for establishing new therapeutic strategies targeting TN-C.

In addition, as described in this review, since TNIIIA2 region was found as a potent and sustained activator of β1 integrin, and since β1 integrin-mediated cell adhesion is broadly observed in various types of cells, it is likely that the pathological and physiological properties of TNIIIA2 region would not be restricted to tumors. Actually, investigations examining the role of TNIIIA2 region in other pathological conditions are being performed by several groups lately (84–87). Further advances in the research focused on TNIIIA2 region are expected and would be of interest.

AUTHOR CONTRIBUTIONS

TI and MF wrote, reviewed, and proofread the manuscript. FF reviewed and proofread the manuscript. All authors contributed to the article and approved the submitted version.

REFERENCES

1. Chiquet-Ehrismann R, Mackie EJ, Pearson CA, Sakakura T. Tenascin: an extracellular matrix protein involved in tissue interactions during fetal development and oncogenesis. *Cell* (1986) 47:131–9. doi: 10.1016/0092-8674(86)90374-0
2. Lightner VA, Slemp CA, Erickson HP. Localization and quantitation of hexabrachion (tenascin) in skin, embryonic brain, tumors, and plasma. *Ann N Y Acad Sci* (1990) 580:260–75. doi: 10.1111/j.1749-6632.1990.tb17935.x
3. Chiquet-Ehrismann R, Chiquet M. Tenascins: regulation and putative functions during pathological stress. *J Pathol* (2003) 200:488–99. doi: 10.1002/path.1415
4. Orend G, Chiquet-Ehrismann R. Tenascin-C induced signaling in cancer. *Cancer Lett* (2006) 244:143–63. doi: 10.1016/j.canlet.2006.02.017
5. Midwood KS, Hussenet T, Langlois B, Orend G. Advances in tenascin-C biology. *Cell Mol Life Sci* (2011) 68:3175–99. doi: 10.1007/s00018-011-0783-6
6. Chiquet-Ehrismann R, Kalla P, Pearson CA, Beck K, Chiquet M. Tenascin interferes with fibronectin action. *Cell* (1988) 53:383–90. doi: 10.1016/0092-8674(88)90158-4
7. Bourdon MA, Ruoslahti EJ. Tenascin mediates cell attachment through an RGD-dependent receptor. *Cell Biol* (1989) 108:1149–55. doi: 10.1083/jcb.108.3.1149
8. Joshi P, Chung CY, Aukhil I, Erickson HP. Endothelial cells adhere to the RGD domain and the fibrinogen-like terminal knob of tenascin. *J Cell Sci* (1993) 106:389–400.
9. Murphy-Ullrich JE. The de-adhesive activity of matricellular proteins: is intermediate cell adhesion an adaptive state? *J Clin Investi* (2001) 107:785–90. doi: 10.1172/JCI12609
10. Bornstein P, Sage EH. Matricellular proteins: extracellular modulators of cell function. *Curr Opin Cell Biol* (2002) 14:608–16. doi: 10.1016/s0955-0674(02)00361-7
11. Brosicke N, van Landeghem FKH, Scheffler B, Faissner A. Tenascin-C is expressed by human glioma in vivo and shows a strong association with tumor blood vessels. *Cell Tissue Res* (2013) 354:409–30. doi: 10.1007/s00441-013-1704-9
12. Dueck M, Riedl S, Hinz U, Tandara A, Moller P, Herfarth C, et al. Detection of tenascin-C isoforms in colorectal mucosa, ulcerative colitis, carcinomas and liver metastases. *Int J Cancer* (1999) 82:477–83. doi: 10.1002/(sici)1097-0215(19990812)82:4<477::aid-ijc2>3.0.co;2-5
13. Saito Y, Imazeki H, Miura S, Yoshimura T, Okutsu H, Harada Y, et al. Peptide derived from tenascin-C induces beta1 integrin activation through syndecan-4. *J Biol Chem* (2007) 282:34929–37. doi: 10.1074/jbc.M705608200
14. Tanaka R, Seki Y, Saito Y, Kamiya S, Fujita M, Okutsu H, et al. Tenascin-C derived peptide TNIIIA2 highly enhances cell survival and platelet-derived growth factor (PDGF)-dependent cell proliferation through potentiated and sustained activation of integrin α5β1. *J Biol Chem* (2014) 289:17699–708. doi: 10.1074/jbc.M113.546622
15. Fujita M, Sasada M, Iyoda T, Fukai F. Regulation of integrin activation by bioactive peptides derived from tenascin-C and fibronectin: Involvement in cancer aggression and application to anticancer strategy. *Molecules* (2020) 25:3239–54. doi: 10.3390/molecules25143239
16. Mostafavi-Pour Z, Askari JA, Parkinson SJ, Parker PJ, Ng TTC, Humphries MJ. Integrin-specific signaling pathway controlling focal adhesion formation and cell migration. *J Cell Biol* (2003) 161:155–67. doi: 10.1083/jcb.200210176
17. Bass MD, Williamson RC, Nunan RD, Humphries JD, Byron A, Morgan MR, et al. A syndecan-4 hair trigger initiates wound healing through caveolin- and RhoD-regulated integrin endocytosis. *Dev Cell* (2011) 21:681–93. doi: 10.1016/j.devcel.2011.08.007
18. Brooks R, Williamson R, Bass M. Sundecan-4 independently regulates multiple small GTPase to promote fibroblast migration during wound healing. *Small GTPases* (2012) 3:73–9. doi: 10.4161/sgtp.19301
19. Morgan MR, Hamidi H, Bass MD, Warwood S, Ballestrem C, Humphries MJ. Syndecan-4 phosphorylation is a control point for integrin recycling. *Dev Cell* (2013) 24:472–85. doi: 10.1016/j.devcel.2013.01.027
20. Turner CE. Paxillin and focal adhesion signaling. *Nat Cell Biol* (2000) 2:E231–6. doi: 10.1038/35046659
21. Denhez F, Wilcox-Adelman SA, Baciu PC, Saoncella S, Lee S, French B, et al. Syndesmos, a syndecan-4 cytoplasmic domain interactor, bind to the focal adhesion adaptor proteins paxillin and Hic-5. *J Biol Chem* (2002) 277:12270–4. doi: 10.1074/jbc.M110291200
22. Berton G. Lowell CA. Integrin signaling in neutrophils and macrophages. *Cell Signal* (1999) 11:621–35. doi: 10.1016/s0898-6568(99)00003-0
23. Mocsai A, Abram CL, Jakus Z, Hu Y, Lanier LL, Lowell CA. Integrin signaling in neutrophil and macrophages uses adaptors containing immunoreceptor tyrosine-based activation motifs. *Nat Immunol* (2006) 7:1326–33. doi: 10.1038/ni1407
24. Leins A, Riva P, Lindstedt R, Davidoff MS, Mehraein P, Weis S. Expression of tenascin-C in various human brain tumors and its relevance for survival in patients with astrocytoma. *Cancer* (2003) 98:2430–9. doi: 10.1002/cncr.11796
25. Brosicke N, Faissner A. Role of tenascins in the ECM of gliomas. *Cell Adh Migr* (2015) 9:131–40. doi: 10.1080/19336918.2014.1000071
26. Lee YS, Bullard DE, Zalutsky MR, Coleman RE, Wikstrand CJ, Friedman HS, et al. Therapeutic efficacy of antiglioma mesenchymal extracellular matrix ^{131}I-radiolabeled murine monoclonal antibody in a human glioma xenograft model. *Cancer Res* (1988) 48:559–66.
27. Mai J, Sameni M, Mikkelsen T, Sloane B. Degradation of extracellular matrix protein tenascin-C by cathepsin B: an interaction involved in the progression of gliomas. *Biol Chem* (2002) 389:1407–13. doi: 10.1515/BC.2002.159
28. Cai M, Onoda K, Takao M, Imanaka-Yoshida K, Shimpo H, Yoshida T, et al. Degradation of tenascin-C and activity of matrix metalloproteinase-2 are associated with tumor recurrence in early stage no-small cell lung cancer. *Clin Cancer Res* (2002) 8:1152–6.
29. Fukai F, Hasebe S, Ueki M, Mutoh M, Ohgi C, Takahashi H, et al. Identification of the anti-adhesive site buried within the heparin-binding domain of fibronectin. *J Biochem (Tokyo)* (1997) 121:189–92.

30. Itagaki K, Naito T, Iwakiri R, Haga M, Miura S, Saiyo Y, et al. Eukaryotic translation elongation factor 1A induces anoikis by triggering cell dedtachiment. *J Biol Chem* (2012) 287:16037–46. doi: 10.1074/jbc.M111.308122
31. Saito Y, Shiota Y, Nishisaka M, Owaki T, Shimamura M, Fukai F. Inhibition of angiogenesis by tenascin-C peptide which is capable of activating beta1-integrins. *Biol Pharm Bull* (2008) 31:1003–7. doi: 10.1248/bpb.31.1003
32. Tanaka R, Owaki T, Kamiya S, Matsunaga T, Shimoda K, Kodama H, et al. VLA-5-mediated adhesion to fibronectin accelerates hemin-stimulated erythroid differentiation of K562 cells through induction of VLA-4 expression. *J Biol Chem* (2009) 284:19817–25. doi: 10.1074/jbc.M109.009860
33. Fujita M, Ito-Fujita Y, Iyoda T, Sasada M, Okada Y, Ishibashi K, et al. Peptide TNIIIA2 derived from tenascin-C contributes to malignant progression in colitis-associated colorectal cancer via β1-integrin activation in fibroblasts. *Int J Mol Sci* (2019) 20:2752. doi: 10.3390/ijms20112752
34. Fujita M, Yamamoto T, Iyoda T, Fujisawa T, Sasada M, Nagai R, et al. Aggressive Progression in Glioblastoma Cells through Potentiated Activation of Integrin α5β1by the Tenascin-C-Derived Peptide TNIIIA2. *Mol Cancer Ther* (2019) 9:1649–58. doi: 10.1158/1535-7163.MCT-18-1251
35. Fujita M, Yamamoto T, Iyoda T, Fujisawa T, Nagai R, Kudo C, et al. Autocrine production of PDGF stimulated by the tenascin-C-derived peptide TNIIIA2 induces hyperproliferation in glioblastoma cells. *Int J Mol Sci* (2019) 20:3183. doi: 10.3390/ijms20133183
36. Brennan C, Momota H, Hambardzumyan D, Ozawa T, Tandon A, Pedraza A, et al. Glioblastoma subclasses can be defined by activity among signal transduction pathways and associated genomic alterations. *PLoS One* (2009) 4:e7752. doi: 10.1371/journal.pone.0007752
37. Ozawa T, Riester M, Cheng YK, Huse JT, Squatrito M, Helmy K, et al. Most human non-GCIMP glioblastoma subtypes evolve from a common proneural-like precursor glioma. *Cancer Cell* (2014) 26:288–300. doi: 10.1016/j.ccr.2014.06.005
38. Yoshida T, Yoshimura E, Numata H, Sakakura Y, Sakakura T. Involvement of tenascin-C in proliferation and migration of laryngeal carcinoma cells. *Virchows Arch* (1999) 435:496–500. doi: 10.1007/s004280050433
39. Kim CH, Bak KH, Kim YS, Kim JM, Ko Y, Oh SJ, et al. Expression of tenascin-C in astrocytic tumors: its relevance to proliferation and angiogenesis. *Surg Neurol* (2000) 54:235–40. doi: 10.1016/s0090-3019(00)00307-4
40. Herold-Mende C, Mueller MM, Bonsanto MM, Schmtt HP, Kunze S, Steiner HH. Clinical impact and functional aspects of tenascin-C expression during glioma progression. *Int J Cancer* (2002) 98:362–9. doi: 10.1002/ilc.10233
41. Ruiz C, Huang W, Hegi ME, Lange K, Hamou MF, Fluri E, et al. Differential gene expression analysis reveals activation of growth promoting signaling pathway by tenascin-C. *Cancer Res* (2004) 64:7377–85. doi: 10.1158/0008-5472.CAN-04-1234
42. Behrem S, Zarkovic K, Eskinja N, Jonjic N. Distribution pattern of tenascin-C in glioblastoma: Correlation with angiogenesis and tumor cell proliferation. *Pathol Oncol Res* (2005) 11:229–35. doi: 10.1007/BF02893856
43. Orend G. Potential oncogenic action of tenascin-c in tumorigenesis. *Int J Biochem Cell Biol* (2005) 37:1066–83. doi: 10.1016/j.biocel.2004.12.002
44. Sarkar S, Mirzaei R, Zemp FJ, Wei W, Senger DL, Robbins SM, et al. Activation of Notch signaling by tenascin-C promotes growth of human brain tumor-initiating cells. *Cancer Res* (2017) 77:3231–43. doi: 10.1158/0008-5472.CAN-16-2171
45. Tsunoda T, Inada H, Kalembeyi I, Imanaka-Yoshida K, Sakakibara M, Okada R, et al. Involvement of large tenascin-C splice variants in breast cancer progression. *Am J Pathol* (2003) 162:1857–66. doi: 10.1016/S0002-9440(10)64320-9
46. Huang W, Chiquet-Ehrismann R, Moyano JV, Garcia-Pardo A, Orend G. Interference of tenascin-C with syndecan-4 binding to fibronectin blocks cell adhesion and stimulates tumor cell proliferation. *Cancer Res* (2001) 61:8586–94.
47. Orend G, Huang W, Olayioye MA, Hynes NE, Chiquet-Ehrismann R. Tenascin-C blocks cell-cycle progression of anchorage-dependent fibroblasts on fibronectin through inhibition of syndecan-4. *Oncogene* (2003) 22:3917–26. doi: 10.1038/sj.onc.1206618
48. Paron I, Berchtold S, Voros J, Shamarla M, Erkan M, Hofler H, et al. Tenascin-C enhances pancreatic cancer cell growth and motility and affects cell adhesion through activation of the integrin pathway. *PLoS One* (2011) 6: e21684. doi: 10.1371/journal.pone.0021684
49. Deryugina EI, Burdon MA. Tenascin mediates human glioma cell migration and modulates cell migration on fibronectin. *J Cell Sci* (1996) 109:643–52.
50. Hirata E, Arakawa Y, Shirahata M, Yamaguchi M, Kishi Y, Okada T, et al. Endogenous tenascin-C enhances glioblastoma invasion with reactive change of surrounding brain tissue. *Cancer Sci* (2009) 100:1451–9. doi: 10.1111/j.1349-7006.2009.01189.x
51. Grahovac J, Becker D, Wells A. Melanoma cell invasiveness is promoted at least in part by the epidermal growth factor-like repeats on tenascin-C. *J Invest Dermatol* (2013) 133:210–2. doi: 10.1038/jid.2012.263
52. Sakar S, Zemp FJ, Senger D, Robbins SM, Yong VW. ADAM-9 is a novel mediator of tenascin-C-stimulated invasiveness of brain tumor-initiating cells. *Neuro Oncol* (2015) 17:1095–105. doi: 10.1093/neuonc/nou362
53. Berndt A, Richter P, Kosmehi H, Franz M. Tenascin-C and carcinoma cell invasion in oral and urinary bladder cancer. *Cell Adh Migr* (2015) 9:105–11. doi: 10.1080/19336918.2015.1005463
54. Cai J, Du S, Wang H, Xin B, Wang J, Shen W, et al. Tenascin-C induces migration and invasion through JNK/c-Jun signaling in pancreatic cancer. *Oncotarget* (2017) 8:74406–22. doi: 10.18632/oncotarget.20160
55. Sun Z, Schwenzer A, Rupp T, Murdamoothoo D, Vegliante R, Lefebre O, et al. Tenascin-C promote tumor cell migration and metastasis through integrin α9β1-mediated YAP inhibition. *Cancer Res* (2017) 78:950–61. doi: 10.1158/0008-5472.CAN-17-1597
56. Tamaoki M, Imanaka-Yoshida K, Yokoyama K, Nishioka T, Inada H, Hiroe M, et al. Tenascin-C regulates recruitment of myofibroblasts during tissue repair after myocardial injury. *Am J Pathol* (2005) 167:71–80. doi: 10.1016/S0002-9440(10)62954-9
57. Zhang Z, Yu B, Gu Y, Zhou S, Qian T, Wang Y, et al. Fibroblast-derived tenascin-C promotes schwann cell migration through β1-integrin dependent pathway during peripheral nerve regeneration. *Glia* (2016) 64:374–85. doi: 10.1002/glia.22934
58. Harman RM, He MK, Zhang S, Van de Walle GR. Plasminogen activator inhibitor-1 and tenascin-C secreted by equine mesenchymal stromal cells stimulate dermal fibroblast migration in vitro and contribute to wound healing in vivo. *Cytotherapy* (2018) 20:1061–76. doi: 10.1016/j.cjcyt.2018.06.005
59. Takahashi Y, Sawada G, Kurashige J, Matsumura T, Uchi R, Ueo H, et al. Tumor-derived tenascin-C promotes the epithelial-mesenchymal transition in colorectal cancer cells. *Anticancer Res* (2013) 33:1927–34.
60. Yang Z, Zhang C, Qi W, Cui C, Cui Y, Xuan Y. Tenascin-C as a prognostic determinant of colorectal cancer through induction of epithelial-to-mesenchymal transition and proliferation. *Exp Mol Pathol* (2018) 105:216–22. doi: 10.1016/j.yexmp.2018.08.009
61. Yoneura N, Takano S, Yoshitomi H, Nakata Y, Shimazaki R, Kagawa S, et al. Experession od annexin II and stromal tenascin C promotes epithelial to mesenchymal transition and correlates with distant metastasis in pancreatic cancer. *Int J Mol Med* (2018) 42:821–30. doi: 10.3892/ijmm.2018.3652
62. Nagaharu K, Zhang X, Yoshida T, Katoh D, Hanamura N, Kozuka Y, et al. Tenascin C induces epithelial-mesenchymal transition-like change accompanied by SRC activation and focal adhesion kinase phosphorylation in human breast cancer cells. *Am J Pathol* (2011) 178:754–63. doi: 10.1016/j.ajpath.2010.10.015
63. Katoh D, Nagaharu K, Shimojo N, Hanamura N, Yamashita M, Kozuka Y, et al. Binding of αVβ1 and αVβ6 integrins to tenascin-C induces epithelial-mesenchymal transition-like change of breast cancer cells. *Oncogenesis* (2013) 2:e65. doi: 10.1038/oncsis.2013.27
64. Mamuya FA, Wang Y, Roop VH, Scheiblin DA, Zajac JC, Duncan MK. The role of αV integrins in lens EMT and posterior capsular opacification. *J Cell Mol Med* (2014) 18:656–70. doi: 10.111/jcmm.12213
65. Tiwari A, Ram J. Luthra-Guptasarma. Targeting the fibronectin type III repeats in tenascin-C inhibit epithelial-mesenchymal transition in the context of posterior capsular opacification. *Invest Ophthalmol Vis Sci* (2015) 565:272–83. doi: 10.1167/iovs.14-14934
66. Hegi ME, Liu L, Herman JG, Stupp R, Wick W, Weller M, et al. Correlation of O6-methylguanine methyltransferase (MGMT) promoter methylation with clinical outcomes in glioblastoma and clinical strategies to modulate MGMT activity. *J Clin Oncol* (2008) 26:4189–99. doi: 10.1200/JCO.2007.11.5964
67. Janouskova H, Maglott A, Leger DY, Bossert C, Noulet F, Guerin E, et al. Integrin α5β1 plays a critical role in resistance to temozolomide by interfering with the p53 pathway in high-grade glioma. *Cancer Res* (2012) 72:3463–70. doi: 10.1158/0008-5472.CAN-11-4199

68. Wang K, Chen D, Qian Z, Cui D, Gao L, Lou M. Hedgehog/Gli1 signaling pathway regulates MGMT expression and chemoresistance to temozolomide in human glioblastoma. *Cancer Cell Int* (2017) 17:117. doi: 10.1186/s12935-017-0491-x
69. Everhard S, Kaloshi G, Criniere E, Benouaich-Amiel A, Lejeune J, Marie Y, et al. MGMT methylation: a marker of response to temozolomide in low grade gliomas. *Ann Neurol* (2006) 60:740–3. doi: 10.1002/ana.21044
70. Dunn J, Baborie A, Alam F, Joyce K, Moxham M, Sibson R, et al. Extent of MGMT promoter methylation correlates with outcome in glioblastomas given temozolomide and radiotherapy. *Br J Cancer* (2009) 101:124–31. doi: 10.1038/sj.bjc.6605127
71. Weller M, Stupp R, Reifenberger G, Brandes AA, van den Bent MJ, Wick W, et al. MGMT promoter methylation in malignant gliomas: ready for personalized medicine? *Nat Rev Neurol* (2010) 6:39–51. doi: 10.1038/nrneurol.2009.197
72. Iyoda T, Nagamine Y, Nakane Y, Tokita Y, Akari S, Otsuka K, et al. Coadministration of the FNIII14 peptide synergistically augments the anticancer activity of chemotherapeutic drugs by activating pro-apoptotic Bim. *PLoS One* (2016) 11:e0162525. doi: 10.1371/journal.pone.0162525
73. Midwood K, Sacre S, Piccinini AM, Inglis J, Trebaul A, Chan E, et al. Tenascin-C is an endogenous activator of tall-like recceptor 4 that is essential for maintaining inflammation in artheritic joint disease. *Nat Med* (2009) 15:774–81. doi: 10.1038/nm.1987
74. Benbow HH, Thompson KJ, Cope HL, Brandon-Waener E, Culberson CR, Bossi KL. et al. Diet-induced obesity enhances progression of hepatocellular carcinoma through tenascin-C/toll-loke receptor 4 signaling. *Am J Pathol* (2016) 186:145–58. doi: 10.1016/j.ajpath.2015.09.015
75. Shimojo N, Hashizume R, Kanayama K, Hara M, Suzuki Y, Nishioka T, et al. Tenascin-C may accelerate cardiac fibrosis by activating macrophages via the integrin αVβ3/nuclear factor-κB/inter-leukin-6 axis. *Hypertension* (2015) 66:751–66. doi: 10.1161/HYPERTENTIONAHA.115.06004
76. Kanayama M, Kurotanki D, Morimoto J, Asano T, Matsui Y, Nakayama Y, et al. α9 integrin and its ligands constitute critical joint microenvironments for development of autoimmune artheritis. *J Immunol* (2009) 182:8015–25. doi: 10.4049/jimmunol.0900725
77. Voronov E, Shouval DS, Krelin Y, Cagnano E, Benharroch D, Iwakura Y, et al. IL-1 is required for tumor invasiveness and angiogenesis. *Proc Natl Acad Sci USA* (2003) 100:2645–50. doi: 10.1073/pnas.0437939100.Epub2003Feb21
78. Dinarello CA. Biologic basis for interleukin-1 in disease. *Blood* (1996) 87:2095–147. doi: 10.1182/blood.V87.6.2095.bloodjournal8762095
79. Elaraj DM, Weinreich DM, Varghese S, Puhlmann M, Hewitt SM, Carroll NM, et al. The role of interleukin 1 in growth and metastasis of human cancer xenografts. *Clin Cancer Res* (2006) 12:1088–96. doi: 10.1158/1078-0432.CCR-05-1603
80. Paugh BS, Bryan L, Paugh SW, Wilczynka KM, Alvarez SM, Singh SK, et al. Interleukin-1 regulates the expression of sphingosine kinase 1 in glioblastoma cells. *J Biol Chem* (2009) 284:3408–17. doi: 10.1074/jbc.M807170200
81. Suzuki H, Sasada M, Kamiya S, Ito Y, Watanabe H, Okada Y, et al. The promoting effect of the extracellular matrix peptide TNIIIA2 derived from tenascin-C in colon cancer cell infiltration. *Int J Mol Sci* (2017) 18:181. doi: 10.3390/ijms18010181
82. Matsunaga T, Takemoto N, Sato T, Takimoto R, Tanaka I, Fujimi A, et al. Interaction between leukemic-cell VLA-4 and stromal fibronectin is a decisive factor for minimal residual disease of acute myelogenous leukemia. *Nat Med* (2003) 9:1158–65. doi: 10.1038/nm909
83. Matsunaga T, Fukai F, Miura S, Nakane Y, Owaki T, Kodama H, et al. Combination therapy of an anticancer drug with the FNIII14 peptide of fibronectin effectivily overcomes cell adhesion-mediated drug resistance of acute myelogenous leukwmia. *Leukemia* (2008) 22:353–60. doi: 10.1038/sj.leu.24050017
84. Hattori T, Hasegawa M, Unno H, Iino T, Fukai F, Yoshida T, et al. TNIIIA2, The Peptide of Tenascin-C, as a Candidate for Preventing Articular Cartilage Degeneration. *Cartilage* (2020). doi: 10.1177/1947603520912300
85. Iyoda T, Fukai F. Promotion or macrophage foam cell formation by the peptide derived from tenascin-C. *Pept Sci* (2016) 2015:203–6.
86. Otsuka K, Sasada M, Hirano Y, Nohara Y, Iyoda T, Higami Y, et al. Acyclic retinoid combined with tenascin-C-derived peptide reduces the malignant phenotype of neuroblastoma cells through N-Myc degradation. *Anticancer Res* (2019) 39:3487–92. doi: 10.21873/anticanres.13494
87. Otsuka K, Sasada M, Iyoda T, Nohara Y, Sakai S, Asayama T, et al. Combining peptide TNIIIA2 with all-trans retinoic acid accelerates N-Myc protein degradation and neuronal differentiation in MYCN-amplified neuroblastoma cells. *Am J Cancer Res* (2019) 9:434–48.

Conflict of Interest: The authors declare that the research was conducted in the absence of any commercial or financial relationships that could be constructed as a potential conflict of interest.

frontiers in Immunology

OPINION
published: 08 January 2021
doi: 10.3389/fimmu.2020.612482

Early Days of Tenascin-R Research: Two Approaches Discovered and Shed Light on Tenascin-R

Fritz G. Rathjen * *and Russell Hodge*

Department of Neuroscience, Max-Delbrück-Center for Molecular Medicine, Berlin, Germany

Keywords: tenascin-R, tenascin-C, human diseases, perineuronal nets, scaffolding

THE PATH TO TENASCIN-R

It has taken nearly 30 years. But finally, studies on cohorts of patients seem to be shedding some light on a protein that has been surfaced from time to time in the neurobiological literature. Tenascin-R, as it is now known, has proven a slippery quarry. That almost works as a pun, given the fact that in certain contexts, the molecule interferes with cell adhesion.

The protein was first identified in chicken and rodents in the late 1980s among a large number of molecules associated with axons. Significant efforts were being made to untangle the mysteries of axon growth, fasciculation and pathfinding (1). Monoclonal antibody approaches turned up a number of immunoglobulin (Ig)-like cell adhesion proteins (2) which, introduced into cell cultures, influenced the development of neurites (3). One of these was an IgCAM that interacted with the plasma membrane *via* covalently linked glycosylphosphatidylinositol; it was variously termed F11 protein, F3 or contactin—nowadays contactin1 (4–9). Immunoaffinity isolates of contactin1 yielded a complex of at least two polypeptides. The major component was contactin1, at 130 kDa, and along with it a minor partner at about 170 kDa. Further biochemical and immunological experiments showed that the minor component was unrelated to the 130 kDa contactin1, suggesting they had copurified (5, 10).

Antibodies to the 170 kDa protein revealed that it was expressed in the developing nervous system, in a pattern partly overlapping with that of contactin1 but spatially much more restricted. In the spinal cord, for example, it was found on the ventral side around motor neurons during embryonic development. This position suggested a name: restrictin (11). Independently, the same protein was discovered in the Schachner laboratory through different means: using the L2 monoclonal antibody directed to the L2/HNK-1 carbohydrate moiety (12), which captured several glycosylated proteins from neural tissues. These included, IgCAMs, tenascin-C (initially named J1-200/220) and tenascin–R (christened J1-160/180 or janusin by Schachner and her colleagues) (13).

STRUCTURAL FEATURES AND THE TENASCIN FAMILY

The experiments in chick and rodents had turned up homologs, as became clear through molecular cloning and sequencing of the chick and rat cDNAs. This showed that the components of restrictin and J1-160/180 represented the products of a common gene, and proteins were based on a set of structural motifs found in tenascin-C (14–18). These include an N-terminal cysteine-rich segment with three heptad repeats, followed by 4.5 EGF-like domains, nine fibronectin type III domains, and a C-terminal knob. The latter consists of a globular domain similar to the carboxyl terminal portion of the β- and

OPEN ACCESS

Edited by:
Gertraud Orend,
INSERM Immuno Rhumatologie Moléculaire (IRM), France

Reviewed by:
Andreas Faissner,
Ruhr University Bochum, Germany

****Correspondence:***
Fritz G. Rathjen
rathjen@mdc-berlin.de

Specialty section:
This article was submitted to Inflammation, a section of the journal Frontiers in Immunology

Received: *30 September 2020*
Accepted: *07 December 2020*
Published: *08 January 2021*

Citation:
Rathjen FG and Hodge R (2021) Early Days of Tenascin-R Research: Two Approaches Discovered and Shed Light on Tenascin-R. Front. Immunol. 11:612482. doi: 10.3389/fimmu.2020.612482

γ-chains of fibrinogen (19, 20). The N-terminal cysteine-rich region serves as an oligomerization domain. Three heptad repeats of hydrophobic amino acids fold in an α helix and generate a triple-stranded coiled coil to form a trimer which is stabilized by the surrounding cysteines. The related tenascin-C forms hexamers, which may also be the case for tenascin-R (21–23). So far, however, it has only been found as trimers, dimers and monomers in isolates of brain tissues (**Figure 1**) (13, 19). The N-terminal oligomerization domain of the pre-mRNA also contains one alternative splicing site; the 6th fibronectin type III domain is also alternatively spliced. Based on these overall similarities, James Bristow and colleagues suggested renaming restrictin and J1-160/180 to tenascin-R; the proposal was promptly supported in a review article by Harold Erickson (24, 26). Subsequently the nomenclature has been universally adopted. Tenascin-R is the smallest member of the family, and the relationship of its sequence and those to TN-C, TN-X, TN-Y, and TN-W suggests that they arose from a primordial gene that most closely resembled TN-R (26, 27).

TEASING OUT THE FIRST INTERACTION PARTNERS

The complex, modular structure of tenascin-R clearly indicated a potential for diverse molecular interactions, most likely with other proteins on the cell surface. An early goal was to identify receptors that might interact with it and to map regions that could be essential for binding (28). In addition to contactin1, the partner responsible for its discovery, tenascin-R was found in complexes with the IgCAM members neurofascin and contactin2 (previously called axonin-1 or TAG1) (29). An additional cell surface receptor was found in a molecular interaction screen: the transmembrane protein CSPG5 (previously termed CALEB, or neuroglycan C). CSPG5 contains an EGF domain, an acidic stretch and chondroitin-sulfate chains, and it binds to the fibrinogen-like globular domain of tenascin-R (30–34).

More support for a physiological interaction between tenascin-R and contactin1 has come from molecular mapping studies. Immunoglobulin domains 2–4 of the latter molecule are sufficient for the interaction (35), and binding occurs to the second and third fibronectin type III domain of tenascin-R. This region is also important for interactions with neurofascin and contactin2 (29, 36). Tenascin-R interacts with other ECM proteins including fibronectin, β1-integrins (37) and it binds with high affinity to phosphacan and a class of extracellular chondroitin sulfate proteoglycans collectively called lecticans (aggrecan, versican, brevican, and neurocan) (38–43). Later work demonstrated that tenascin-R also contains chondroitinsulfate chains of its own (25, 44).

Most of the interaction partners of tenascin-R have been defined primarily *in vitro* and through cell adhesion assays. Light microscopy work supports the colocalization of tenascin-R with

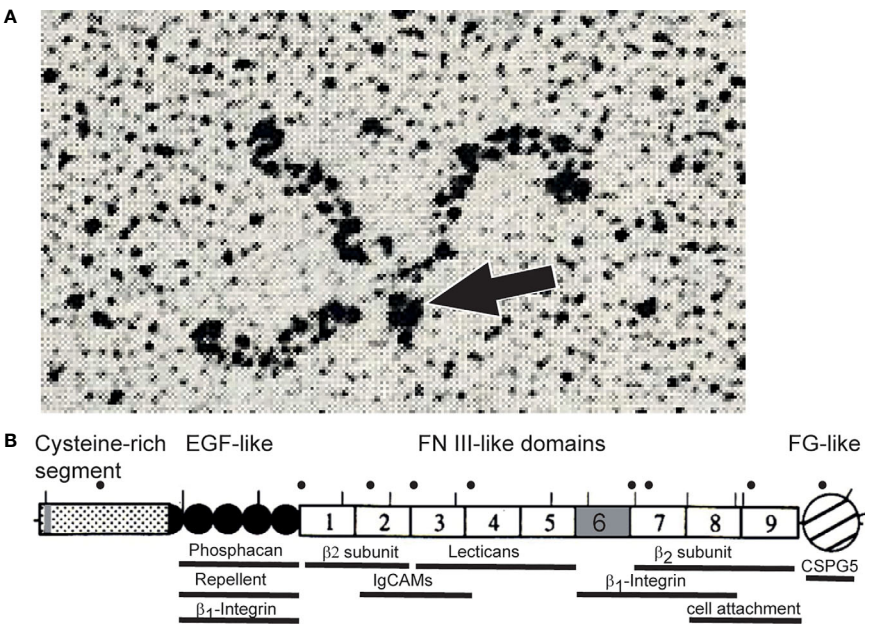

FIGURE 1 | **(A)** Rotary shadowing electron micrograph of tenascin-R purified from brains revealing a trimeric structure. Dimeric and monomeric but no hexameric forms were seen in these electron micrographs (13, 19). The TN-R polypeptide contains a single cysteine amino-terminal to the trimer-forming segment. This cysteine might connect two trimers into hexamers, the hexabrachion structure. It is therefore likely that TN-R might also form hexabrachions in tissues as found for tenascin-C (24). However, alternative splicing or proteolytical cleavage in the N-terminal segment might affect multimer formation of tenascin-R (19, 25). The arrow points to the N-terminal knob formed by a triple-stranded coiled coil. **(B)** Scheme of tenascin-R polypeptide. Lines above the scheme indicate putative N-glycosylation sites of the chicken protein. Human disease mutations are marked by dots above the scheme and regions that bind to cell surface receptors, extracellular matrix proteins or indicate cellular activities are marked by bars below the scheme (please see text). Alternative splice sites of the pre-mRNA encoding TN-R are colored in grey. "β2-subunit" refers to the β2-subunit of sodium channels.

these proteins in some contexts, but for the most part, there is a lack of *in vivo* evidence of direct binding.

THE SEARCH FOR BIOLOGICAL FUNCTIONS OF TENASCIN-R

Cell culture experiments in the early days of tenascin-R research hinted at a number of putative functions through adhesion or neurite outgrowth assays. While many extracellular matrix glycoproteins are known to promote the attachment and spreading of cells, tenascin-R promotes only weak cell adhesion and does not affect cell spreading. For example, the 8th to 9th FNIII domains of tenascin-R serve as a weak cell attachment site for neural cells, which can be specifically blocked by mAb 23-14 (19). In some culture systems, tenascin-R even repels axons or inhibits their regeneration (45–47). A number of *in vitro* studies have also shown that tenascin-R modulates homophilic and heterophilic interactions between IgCAMs and extracellular matrix glycoproteins on neural cells (6, 29, 36, 39, 46, 48–54).

Obviously, the results of such *in vitro* studies have to be taken with a grain of salt, given that they may not accurately reflect the situation in the intact organism or provide true insights into the functions of tenascin-R *in vivo*. Here, further insights can come through studies of expression patterns. TN-R is apparently restricted to the central nervous system, but is absent from the peripheral—with the exception of transient expression on Schwann cells (11, 20, 55–58). Around 2000 came a breakthrough with observations that tenascin-R is localized at perineuronal nets (59, 60). These structures were long known, having been described by several authors at the turn of the 20th century. They surround groups of neurons and synapses on cell bodies primarily in the mature brain, comprising a specialized form of the extracellular matrix; constituents include hyaluronan, lecticans, and several other kinds of CSPGs (61, 62). Perineuronal nets attracted particular interest as brain structures that appear to be implicated in terminating the critical period for neuronal plasticity (63). Here a crucial function for tenascin-R began to emerge; it appears to be essential for the normal development of perineuronal nets. Tenascin-R-deficient mice exhibit an abnormal aggregation of perineuronal CSPGs (59, 64, 65). In electron microscopy images, purified tenascin-R appears to crosslinks aggrecan complexes, which suggests that within the nets, tenascin-R might provide a molecular scaffolding for lecticans (40).

Knockouts of tenascin-R produced a number of phenotypes that might be traceable to this scaffolding function. At the cellular and functional levels, deficiencies lead to mild abnormalities in synaptic transmission and architecture (66, 67). These might arise through disruptions of structures involving lecticans or IgCAMs and CSPG5 (32, 33, 68, 69). Ultimately, the effects on the mature brain involve both structural and functional abnormalities. Consequently, tenascin-R deficient mice exhibit behavioral deficits such as severe impairments in locomotion and hippocampal-associated learning impairments (70).

Another interesting feature of tenascin-R emerged: *in situ* hybridization experiments revealed a dominant colocalization with oligodendrocytes during the period of active myelination (20, 71, 72). In tenascin-R knockout mice, the nodes of Ranvier appear normal, but an analysis of compound action potential recordings from optic nerves revealed a decrease in the conduction velocity. A potential reason for this might be the lack of expression of tenascin-R on oligodendrocytes, which appears to be essential for their differentiation (48, 72); another could be that under normal conditions, the protein might associate with sodium channels to modulate their function (65, 73, 74).

Very recently, a few studies on mouse knockouts combined with cell culture experiments have also shown that tenascin-R modulates the differentiation of neural stem cells during developmental and adult stages. In the olfactory bulb—a structure with a continuous flow of newborn neurons from the subventricular zone of the lateral ventricles—tenascin-R acts as a molecular cue that initiates a radial migration of neuroblasts toward the outer cell layers of the olfactory bulb. Consequently, an absence of tenascin-R affects the recruitment of neuroblasts in the olfactory bulb (37, 75, 76). In the dentate gyrus of the hippocampus, tenascin-R is required for the fate determination of neural stem or progenitor cells. Its absence leads to an increase in the number of GABAergic neurons was increased (77, 78). In summary, these findings point to a role of tenascin-R on neurogenesis.

DISCUSSION

Insights From Human Disease Mutations

Recently, an extensive exome sequencing study by a consortium identified 13 patients from eight unrelated families with biallelic variants in the human tenascin-R gene. Combined with two case studies already in the literature, this represents an important chance to investigate functions of the human form of the gene. So far, all of the patients affected have shared some common traits, particularly delays in motor development. The severity varies, ranging from spastic para- or tetraparesis, axial muscular hypotonia, to dyspraxia and transient opisthotonus (79–81). For example, compared to healthy counterparts, patients with the mutation take longer to develop unsupported sitting or standing. In line with these observations are data on mouse knockouts of tenascin-R or its cellular receptor CSPG5, which also exhibit motor deficits (33, 70). These problems in motor development in human patients can most likely be traced to the brain, given current evidence suggesting that tenascin-R expression is primarily restricted to the central nervous system (11, 19, 20, 55–58). And roughly half of the 13 patients revealed mild or moderately impaired cognitive development, including delayed language progression. Once again, there were differences in the degree to which patients were affected.

Overall, tenascin-R associated mutations led to health issues generally considered to be nonprogressive—which is in line with a pattern of expression in which tenascin-R predominantly appears during early brain development (79). MRI of patients' brains showed delayed myelination consistent with observations

on tenascin-R mouse knockouts (48, 72) and, in a few cases, abnormalities in the structure of the corpus callosum. Both observations might be explained if humans follow the pattern observed in the mouse, where tenascin-R is expressed in developing oligodendrocytes (20, 71). The precise effects of the human missense mutations have yet to be determined: whether they affect the overall expression of tenascin-R or interactions with some of the interaction partners mentioned above. Some of these issues may be resolved with further binding assays and the generation of mouse models that replicate mutations specific to the in human patients. It would be particularly interesting to introduce mutations that interfere with molecular interactions of tenascin-R during the formation of perineuronal nets. If this impaired synaptic plasticity or disrupted the normal maturation and maintenance of neuronal circuits during critical periods of brain development, we would stand to learn much about the function of these complex intercellular structures.

As has been the case with many other diseases, the study of mutations in the human tenascin-R gene will likely prove to be a game changer, stimulating research into tenascin-R and clarifying aspects of its functions that go beyond the molecule itself. Insights into its functions could redirect studies performed on the current mouse models. For example, tenascin-R might give scientists a handle on particular brain regions and their complex interactions at highly specific moments in development. The fact that human patients exhibit delays in motor development mean that this approach might serve as a wedge into this highly complex system within the central nervous system. It is interesting that in MRI examinations of the patients, the cerebellum appears normal (79). What would be the result of specifically inactivating tenascin-R in the mouse cerebellum? This might reveal whether the cerebellum plays a role in the axial hypotonia or spasticity observed in patients with mutations in the tenascin-R gene—or whether these deficits are related to changes in perineuronal inhibition at the level of the spinal cord or basal ganglia. At the very least, this might offer a new perspective on how cells and structures in the developing nervous system intertwine at various levels to produce, on the one hand, a marvelously functioning organism—or on the other, a patient burdened by the symptoms of motor diseases.

AUTHOR CONTRIBUTIONS

All authors contributed to the article and approved the submitted version.

FUNDING

The work of the author was supported by the Max-Delbrück-Center and grant SFB665 by the DFG.

ACKNOWLEDGMENTS

The critical reading of Dr Dirk Montag (Magdeburg) is greatly acknowledged. The authors regret that not all publications on TN-R members could be cited in this article due to space limitations. FR thanks Dr Carmen Birchmeier (MDC, Berlin) for generous support and insightful discussions. FR is an emeritus professor, and RH is a science writer at the MDC.

REFERENCES

1. Tessier-Lavigne M, Goodman CS. The molecular biology of axon guidance. *Sci (80-)* (1996) 274:1123–33. doi: 10.1126/science.274.5290.1123
2. Rajewsky K. The advent and rise of monoclonal antibodies. *Nature* (2019) 575:47–9. doi: 10.1038/d41586-019-02840-w
3. Sonderegger P, Rathjen FG. Regulation of axonal growth in the vertebrate nervous system by interactions between glycoproteins belonging to two subgroups of the immunoglobulin superfamily. *J Cell Biol* (1992) 119:1387–94. doi: 10.1083/jcb.119.6.1387
4. Gennarini G, Durbec P, Boned A, Rougon G, Goridis C. Transfected F3/F11 neuronal cell surface protein mediates intercellular adhesion and promotes neurite outgrowth. *Neuron* (1991) 6:595–606. doi: 10.1016/0896-6273(91)90062-5
5. Rathjen FG, Wolff JM, Frank R, Bonhoeffer F, Rutishauser U. Membrane glycoproteins involved in neurite fasciculation. *J Cell Biol* (1987) 104:343–53. doi: 10.1083/jcb.104.2.343
6. Brümmendorf T, Wolff JM, Frank R, Rathjen FG. Neural cell recognition molecule F11: homology with fibronectin type III and immunoglobulin type C domains. *Neuron* (1989) 2:1351–61. doi: 10.1016/0896-6273(89)90073-1
7. Wolff JM, Brümmendorf T, Rathjen FG. Neural cell recognition molecule F11: Membrane interaction by covalently attached phosphatidylinositol. *Biochem Biophys Res Commun* (1989) 161:931–38. doi: 10.1016/0006-291X(89)92688-0
8. Ranscht B, Moss DJ, Thomas C. A neuronal surface glycoprotein associated with the cytoskeleton. *J Cell Biol* (1984) 99:1803–13. doi: 10.1083/jcb.99.5.1803
9. Sanes JR, Zipursky SL. Synaptic Specificity, Recognition Molecules, and Assembly of Neural Circuits. *Cell* (2020) 181:536–56. doi: 10.1016/j.cell.2020.04.008
10. Wolff JM, Rathjen FG, Frank R, Roth S. Biochemical characterization of polypeptide components involved in neurite fasciculation and elongation. *Eur J Biochem* (1987) 168:551–61. doi: 10.1111/j.1432-1033.1987.tb13453.x
11. Rathjen FG, Wolff JM, Chiquet-Ehrismann R. Restrictin: a chick neural extracellular matrix protein involved in cell attachment co-purifies with the cell recognition molecule F11. *Development* (1991) 113:151–64.
12. Kruse J, Keilhauer G, Faissner A, Timpl R, Schachner M. The J1 glycoprotein–a novel nervous system cell adhesion molecule of the L2/HNK-1 family. *Nature* (1985) 316:146–8. doi: 10.1038/316146a0
13. Pesheva P, Spiess E, Schachner M. J1-160 and J1-180 are oligodendrocyte-secreted nonpermissive substrates for cell adhesion. *J Cell Biol* (1989) 109:1765–78. doi: 10.1083/jcb.109.4.1765
14. Spring J, Beck K, Chiquet-Ehrismann R. Two contrary functions of tenascin: dissection of the active sites by recombinant tenascin fragments. *Cell* (1989) 59:325–34. doi: 10.1016/0092-8674(89)90294-8
15. Jones FS, Hoffman S, Cunningham BA, Edelman GM. A detailed structural model of cytotactin: protein homologies, alternative RNA splicing, and binding regions. *Proc Natl Acad Sci USA* (1989) 86:1905–9. doi: 10.1073/pnas.86.6.1905
16. Chiquet M, Fambrough DM. Chick myotendinous antigen. I. A monoclonal antibody as a marker for tendon and muscle morphogenesis. *J Cell Biol* (1984) 98:1926–36. doi: 10.1083/jcb.98.6.1926
17. Chiquet M, Fambrough DM. Chick myotendinous antigen. II. A novel extracellular glycoprotein complex consisting of large disulfide-linked subunits. *J Cell Biol* (1984) 98:1937–46. doi: 10.1083/jcb.98.6.1937

18. Grumet M, Hoffman S, Crossin KL, Edelman GM. Cytotactin, an extracellular matrix protein of neural and non-neural tissues that mediates glia-neuron interaction. *Proc Natl Acad Sci USA* (1985) 82:8075–9. doi: 10.1073/pnas.82.23.8075
19. Nörenberg U, Wille H, Michael Wolff J, Frank R, Rathjen FGG, Norenberg U, et al. The chicken neural extracellular matrix molecule restrictin: similarity with EGF-, fibronectin type III-, and fibrinogen-like motifs. *Neuron* (1992) 8:849–63. doi: 10.1016/0896-6273(92)90199-N
20. Fuss B, Wintergerst ES, Bartsch U, Schachner M. Molecular characterization and in situ mRNA localization of the neural recognition molecule J1-160/180: A modular structure similar to tenascin. *J Cell Biol* (1993) 120:1237–50. doi: 10.1083/jcb.120.5.1237
21. Erickson HP, Taylor HC. Hexabrachion proteins in embryonic chicken tissues and human tumors. *J Cell Biol* (1987) 105:1387–94. doi: 10.1083/jcb.105.3.1387
22. Erickson HP, Inglesias JL. A six-armed oligomer isolated from cell surface fibronectin preparations. *Nature* (1984) 311:267–9. doi: 10.1038/311267a0
23. Kammerer RA, Schulthess T, Landwehr R, Lustig A, Fischer D, Engel J. Tenascin-C hexabrachion assembly is a sequential two-step process initiated by coiled-coil α-helices. *J Biol Chem* (1998) 273:10602–8. doi: 10.1074/jbc.273.17.10602
24. Erickson HP. Tenascin-C, tenascin-R and tenascin-X: a family of of talented proteins in search of functions. *Curr Opin Cell Biol* (1993) 5:869–76. doi: 10.1016/0955-0674(93)90037-Q
25. Woodworth A, Pesheva P, Fiete D, Baenziger JU. Neuronal-specific Synthesis and Glycosylation of Tenascin-R. *J Biol Chem* (2004) 279:10413–21. doi: 10.1074/jbc.M312466200
26. Bristow J, Meng Kian T, Gitelman SE, Mellon SH, Miller WL. Tenascin-X: A novel extracellular matrix protein encoded by the human XB gene overlapping P450c21B. *J Cell Biol* (1993) 122:265–78. doi: 10.1083/jcb.122.1.265
27. Erickson HP. Evolution of the tenascin family–implications for function of the C-terminal fibrinogen-like domain. *Perspect Dev Neurobiol* (1994) 2:9–19. doi: 10.1080/0907676x.1994.9961218
28. Jones FS, Jones PL. The tenascin family of ECM glycoproteins: Structure, function, and regulation during embryonic development and tissue remodeling. *Dev Dyn* (2000) 218:235–59. doi: 10.1002/(SICI)1097-0177(200006)218:2<235::AID-DVDY2>3.0.CO;2-G
29. Volkmer H, Zacharias U, Nörenberg U, Rathjen FG. Dissection of complex molecular interactions of neurofascin with axonin- 1, F11, and tenascin-R, which promote attachment and neurite formation of tectal cells. *J Cell Biol* (1998) 142:1083–93. doi: 10.1083/jcb.142.4.1083
30. Schumacher S, Volkmer H, Buck F, Otto A, Tarnok A, Roth S, et al. Chicken acidic leucine-rich EGF-like domain containing brain protein (CALEB), a neural member of the EGF family of differentiation factors, is implicated in neurite formation. *J Cell Biol* (1997) 136:895–906. doi: 10.1083/jcb.136.4.895
31. Schumacher S, Jung M, Nörenberg U, Dorner A, Chiquet-Ehrismann R, Stuermer CAO, et al. CALEB Binds via Its Acidic Stretch to the Fibrinogen-like Domain of Tenascin-C or Tenascin-R and Its Expression Is Dynamically Regulated after Optic Nerve Lesion. *J Biol Chem* (2001) 276:7337–45. doi: 10.1074/jbc.M007234200
32. Juttner R, More MI, Das D, Babich A, Meier J, Henning M, et al. Impaired synapse function during postnatal development in the absence of CALEB, an EGF-like protein processed by neuronal activity. *Neuron* (2005) 46:233–45. doi: 10.1016/j.neuron.2005.02.027
33. Jüttner R, Montag D, Craveiro RBB, Babich A, Vetter P, Rathjen FG. Impaired presynaptic function and elimination of synapses at premature stages during postnatal development of the cerebellum in the absence of CALEB (CSPG5/neuroglycan C). *Eur J Neurosci* (2013) 38:3270–80. doi: 10.1111/ejn.12313
34. Pintér A, Hevesi Z, Zahola P, Alpár A, Hanics J. Chondroitin sulfate proteoglycan-5 forms perisynaptic matrix assemblies in the adult rat cortex. *Cell Signal* (2020) 74:109710. doi: 10.1016/j.cellsig.2020.109710
35. Brümmendorf T, Hubert M, Treubert U, Leuschner R, Tarnok A, Rathjen FG. The axonal recognition molecule F11 is a multifunctional protein: specific domains mediate interactions with Ng-CAM and restrictin. *Neuron* (1993) 10:711–27. doi: 10.1016/0896-6273(93)90172-N
36. Norenberg U, Hubert M, Brummendorf T, Tarnok A, Rathjen FG. Characterization of functional domains of the tenascin-R (restrictin) polypeptide: Cell attachment site, binding with F11, and enhancement of F11- mediated neurite outgrowth by tenascin-R. *J Cell Biol* (1995) 130:473–48. doi: 10.1083/jcb.130.2.473
37. Liao H, Huang W, Schachner M, Guan Y, Guo J, Yan J, et al. β 1 integrin-mediated effects of tenascin-R domains EGFL and FN6-8 on neural stem/progenitor cell proliferation and differentiation in vitro. *J Biol Chem* (2008) 283:27927–36. doi: 10.1074/jbc.M804764200
38. Yamaguchi Y. Lecticans: Organizers of the brain extracellular matrix. *Cell Mol Life Sci* (2000) 57:276–89. doi: 10.1007/PL00000690
39. Xiao ZC, Bartsch U, Margolis RK, Rougon G, Montag D, Schachner M. Isolation of a tenascin-R binding protein from mouse brain membranes: A phosphacan-related chondroitin sulfate proteoglycan. *J Biol Chem* (1997) 272:32092–101. doi: 10.1074/jbc.272.51.32092
40. Lundell A, Olin AI, Mörgelin M, Al-Karadaghi S, Aspberg A, Logan DT. Structural basis for interactions between tenascins and lectican C-type lectin domains: Evidence for a crosslinking role for tenascins. *Structure* (2004) 12:1495–506. doi: 10.1016/j.str.2004.05.021
41. Aspberg A, Binkert C, Ruoslahti E. The versican C-type lectin domain recognizes the adhesion protein tenascin-R. *Proc Natl Acad Sci USA* (1995) 92:10590–4. doi: 10.1073/pnas.92.23.10590
42. Aspberg A, Miura R, Bourdoulous S, Shimonaka M, Heinegård D, Schachner M, et al. The C-type lectin domains of lecticans, a family of aggregating chondroitin sulfate proteoglycans, bind tenascin-R by protein-protein interactions independent of carbohydrate moiety. *Proc Natl Acad Sci USA* (1997) 94:10116–21. doi: 10.1073/pnas.94.19.10116
43. Margolis RK, Rauch U, Maurel P, Margolis RU. Neurocan and phosphacan: two major nervous tissue-specific chondroitin sulfate proteoglycans. *Perspect Dev Neurobiol* (1996) 3:273–90.
44. Okuda H, Tatsumi K, Morita S, Shibukawa Y, Korekane H, Horii-Hayashi N, et al. Chondroitin sulfate proteoglycan tenascin-R regulates glutamate uptake by adult brain astrocytes. *J Biol Chem* (2014) 289:2620–31. doi: 10.1074/jbc.M113.504787
45. Becker T, Anliker B, Becker CG, Taylor J, Schachner M, Meyer RL, et al. Tenascin-R inhibits regrowth of optic fibers in vitro and persists in the optic nerve of mice after injury. *Glia* (2000) 29:330–46. doi: 10.1002/(SICI)1098-1136(20000215)29:4<330::AID-GLIA4>3.0.CO;2-L
46. Lochter A, Taylor J, Fuss B, Schachner M. The Extracellular Matrix Molecule Janusin Regulates Neuronal Morphology in a Substrate- and Culture Time-dependent Manner. *Eur J Neurosci* (1994) 6:597–606. doi: 10.1111/j.1460-9568.1994.tb00304.x
47. Taylor J, Pesheva P, Schachner M. Influence of janusin and tenascin on growth cone behavior in vitro. *J Neurosci Res* (1993) 35:347–62. doi: 10.1002/jnr.490350402
48. Pesheva P, Gloor S, Schachner M, Probstmeier R. Tenascin-R is an intrinsic autocrine factor for oligodendrocyte differentiation and promotes cell adhesion by a sulfatide-mediated mechanism. *J Neurosci* (1997) 17:4642–51. doi: 10.1523/jneurosci.17-12-04642.1997
49. Pesheva P, Gennarini G, Goridis C, Schachner M. The F3/11 cell adhesion molecule mediates the repulsion of neurons by the extracellular matrix glycoprotein J1-160/180. *Neuron* (1993) 10:69–82. doi: 10.1016/0896-6273(93)90243-K
50. Xiao ZC, Taylor J, Montag D, Rougon G, Schachner M. Distinct effects of recombinant tenascin-R domains in neuronal cell functions and identification of the domain interacting with the neuronal recognition molecule F3/11. *Eur J Neurosci* (1996) 8:766–82. doi: 10.1111/j.1460-9568.1996.tb01262.x
51. Pesheva P, Probstmeier R, Skubitz APN, McCarthy JB, Furcht LT, Schachner M. Tenascin-R (J1 160/180) inhibits fibronectin-mediated cell adhesion functional relatedness to tenascin-C. *J Cell Sci* (1994) 107:2323–33.
52. Zacharias U, Nörenberg U, Rathjen FG. Functional interactions of the immunoglobulin superfamily member F11 are differentially regulated by the extracellular matrix proteins tenascin-R and tenascin-C. *J Biol Chem* (1999) 274:24357–65. doi: 10.1074/jbc.274.34.24357
53. Yang H, Xiao ZC, Becker B, Hillenbrand R, Rougon G, Schachner M. Role for myelin-associated glycoprotein as a functional tenascin-R receptor. *J Neurosci Res* (1999) 55:687–701. doi: 10.1002/(SICI)1097-4547(19990315)55:6<687::AID-JNR4>3.0.CO;2-6
54. Angelov DN, Walther M, Streppel M, Guntinas-Lichius O, Neiss WF, Probstmeier R, et al. Tenascin-R is antiadhesive for activated microglia that induce downregulation of the protein after peripheral nerve injury: A new role

in neuronal protection. *J Neurosci* (1998) 18:6218–29. doi: 10.1523/jneurosci.18-16-06218.1998
55. Wintergerst ES, Rathjen FG, Schwaller B, Eggli P, Celio MR. Tenascin-R associates extracellularly with parvalbumin immunoreactive neurones but is synthesised by another neuronal population in the adult rat cerebral cortex. *J Neurocytol* (2001) 30:293–301. doi: 10.1023/A:1014452212067
56. Wintergerst ES, Fuss B, Bartsch U. Localization of Janusin mRNA in the Central Nervous System of the Developing and Adult Mouse. *Eur J Neurosci* (1993) 5:299–310. doi: 10.1111/j.1460-9568.1993.tb00497.x
57. Dauth S, Grevesse T, Pantazopoulos H, Campbell PH, Maoz BM, Berretta S, et al. Extracellular matrix protein expression is brain region dependent. *J Comp Neurol* (2016) 524:1309–36. doi: 10.1002/cne.23965
58. Probstmeier R, Nellen J, Gloor S, Wernig A, Pesheva P. Tenascin-R is expressed by Schwann cells in the peripheral nervous system. *J Neurosci Res* (2001) 64:70–8. doi: 10.1002/jnr.1055
59. Bruckner G, Grosche J, Schmidt S, Hartig W, Margolis RU, Delpech B, et al. Postnatal development of perineuronal nets in wild-type mice and in a mutant deficient in tenascin-R. *JComp Neurol* (2000) 428:616–29. doi: 10.1002/1096-9861(20001225)428:4<616::AID-CNE3>3.0.CO;2-K
60. Hagihara K, Miura R, Kosaki R, Berglund E, Ranscht B, Yamaguchi Y. Immunohistochemical evidence for the brevican-tenascin-R interaction: Colocalization in perineuronal nets suggests a physiological role for the interaction in the adult rat brain. *J Comp Neurol* (1999) 410:256–64. doi: 10.1002/(SICI)1096-9861(19990726)410:2<256::AID-CNE7>3.0.CO;2-5
61. Celio MR, Spreafico R, De Biasi S, Vitellaro-Zuccarello L. Perineuronal nets: Past and present. *Trends Neurosci* (1998) 21:510–5. doi: 10.1016/S0166-2236(98)01298-3
62. Reichelt AC, Hare DJ, Bussey TJ, Saksida LM. Perineuronal Nets: Plasticity, Protection, and Therapeutic Potential. *Trends Neurosci* (2019) 42:458–70. doi: 10.1016/j.tins.2019.04.003
63. Berardi N, Pizzorusso T, Ratto GM, Maffei L. Molecular basis of plasticity in the visual cortex. *Trends Neurosci* (2003) 26:369–78. doi: 10.1016/S0166-2236(03)00168-1
64. Haunsoø A, Ibrahim M, Bartsch U, Letiembre M, Celio MR, Menoud PA. Morphology of perineuronal nets in tenascin-R and parvalbumin single and double knockout mice. *Brain Res* (2000) 864:142–5. doi: 10.1016/S0006-8993(00)02173-9
65. Weber P, Bartsch U, Rasband MN, Czaniera R, Lang Y, Bluethmann H, et al. Mice deficient for tenascin-R display alterations of the extracellular matrix and decreased axonal conduction velocities in the CNS. *J Neurosci* (1999) 19:4245–62. doi: 10.1523/jneurosci.19-11-04245.1999
66. Nikonenko A, Schmidt S, Skibo G, Brückner G, Schachner M. Tenascin-R-deficient mice show structural alterations of symmetric perisomatic synapses in the CA1 region of the hippocampus. *J Comp Neurol* (2003) 456:338–49. doi: 10.1002/cne.10537
67. Saghatelyan AK, Dityatev A, Schmidt S, Schuster T, Bartsch U, Schachner M. Reduced perisomatic inhibition, increased excitatory transmission, and impaired long-term potentiation in mice deficient for the extracellular matrix glycoprotein tenascin-R. *Mol Cell Neurosci* (2001) 17:226–40. doi: 10.1006/mcne.2000.0922
68. Murai KK, Misner D, Ranscht B. Contactin supports synaptic plasticity associated with hippocampal long-term depression but not potentiation. *Curr Biol* (2002) 12:181–90. doi: 10.1016/S0960-9822(02)00680-2
69. Bukalo O, Schachner M, Dityatev A. Hippocampal metaplasticity induced by deficiency in the extracellular matrix glycoprotein tenascin-R. *J Neurosci* (2007) 27:6019–28. doi: 10.1523/JNEUROSCI.1022-07.2007
70. Montag-Sallaz M, Montag D. Severe cognitive and motor coordination deficits in tenascin-R-deficient mice. *Genes Brain Behav* (2003) 2:20–31. doi: 10.1034/j.1601-183X.2003.00003.x
71. Bartsch U, Pesheva P, Raff M, Schachner M. Expression of janusin (J1–160/180) in the retina and optic nerve of the developing and adult mouse. *Glia* (1993) 9:57–69. doi: 10.1002/glia.440090108
72. Czopka T, Von Holst A, Schmidt G, Ffrench-Constant C, Faissner A, Tenascin C. and tenascin R similarly prevent the formation of myelin membranes in a RhoA-dependent manner, but antagonistically regulate the expression of myelin basic protein via a separate pathway. *Glia* (2009) 57:1790–801. doi: 10.1002/glia.20891
73. Xiao ZC, Ragsdale DS, Malhotra JD, Mattei LN, Braun PE, Schachner M, et al. Tenascin-R is a functional modulator of sodium channel β subunits. *J Biol Chem* (1999) 274:26511–7. doi: 10.1074/jbc.274.37.26511
74. Srinivasan J, Schachner M, Catterall WA. Interaction of voltage-gated sodium channels with the extracellular matrix molecules tenascin-C and tenascin-R. *Proc Natl Acad Sci USA* (1998) 95:15753–7. doi: 10.1073/pnas.95.26.15753
75. David LS, Schachner M, Saghatelyan A. The extracellular matrix glycoprotein tenascin-R affects adult but not developmental neurogenesis in the olfactory bulb. *J Neurosci* (2013) 33:10324–39. doi: 10.1523/JNEUROSCI.5728-12.2013
76. Saghatelyan A, De Chevigny A, Schachner M, Lledo PM. Tenascin-R mediates activity-dependent recruitment of neuroblasts in the adult mouse forebrain. *Nat Neurosci* (2004) 7:347–56. doi: 10.1038/nn1211
77. Xu JC, Xiao MF, Jakovcevski I, Sivukhina E, Hargus G, Cui YF, et al. The extracellular matrix glycoprotein tenascin-R regulates neurogenesis during development and in the adult dentate gyrus of mice. *J Cell Sci* (2014) 127:641–52. doi: 10.1242/jcs.137612
78. Hargus G, Cui Y, Schmid J-S, Xu J, Glatzel M, Schachner M, et al. Tenascin-R promotes neuronal differentiation of embryonic stem cells and recruitment of host-derived neural precursor cells after excitotoxic lesion of the mouse striatum. *Stem Cells* (2008) 26:1973–84. doi: 10.1634/stemcells.2007-0929
79. Wagner M, Lévy J, Jung-Klawitter S, Bakhtiari S, Monteiro F, Maroofian R, et al. Loss of TNR causes a nonprogressive neurodevelopmental disorder with spasticity and transient opisthotonus. *Genet Med* (2020) 22:1061–8. doi: 10.1038/s41436-020-0768-7
80. Dufresne D, Hamdan FF, Rosenfeld JA, Torchia B, Rosenblatt B, Michaud JL, et al. Homozygous deletion of Tenascin-R in a patient with intellectual disability. *J Med Genet* (2012) 49:451–4. doi: 10.1136/jmedgenet-2012-100831
81. Lynch DS, Rodrigues Brandão De Paiva A, Zhang WJ, Bugiardini E, Freua F, Tavares Lucato L, et al. Clinical and genetic characterization of leukoencephalopathies in adults. *Brain* (2017) 140:1204–11. doi: 10.1093/brain/awx045

Conflict of Interest: The authors declare that the research was conducted in the absence of any commercial or financial relationships that could be construed as a potential conflict of interest.

frontiers in Immunology

OPINION
published: 11 January 2021
doi: 10.3389/fimmu.2020.612497

Tenascin-X—Discovery and Early Research

*Walter L. Miller**

Department of Pediatrics, Center for Reproductive Sciences, and Institute of Human Genetics, University of California, San Francisco, CA, United States

Keywords: adrenal, 21-hydroxylase, human leukocyte antigen locus, extracellular matrix, Ehlers-Danlos syndrome, major histocompatibility locus, CYP21, cytochrome P450

OPEN ACCESS

Edited by:
Sermin Genc,
Dokuz Eylul University, Turkey

Reviewed by:
Deborah Merke,
National Institutes of Health Clinical Center (NIH), United States
Delfien Syx,
Ghent University, Belgium

***Correspondence:**
Walter L. Miller
wlmlab@ucsf.edu

Specialty section:
This article was submitted to Inflammation, a section of the journal Frontiers in Immunology

Received: *30 September 2020*
Accepted: *04 December 2020*
Published: *11 January 2021*

Citation:
Miller WL (2021) Tenascin-X—Discovery and Early Research. Front. Immunol. 11:612497. doi: 10.3389/fimmu.2020.612497

INTRODUCTION

Tenascin-X (TNX) is a large extracellular matrix protein discovered because its *TNXB* gene overlaps the *CYP21A2* gene encoding steroid 21-hydroxylase (P450c21), whose mutations cause congenital adrenal hyperplasia (CAH). In the 1980s, several laboratories worked to clone the "CAH gene". We sought a P450c21 clone in a cDNA library prepared from a CAH adrenal and identified a transcript larger than P450c21 cDNA; sequencing indicated it was encoded by an unknown ("X") gene overlapping *CYP21A2* on the opposite DNA strand. Extensive genomic sequencing revealed the structure of a tenascin: N-terminal EGF-like repeats, multiple fibronectin-III repeats, and a C-terminal fibrinogen-like domain; we named this "Tenascin-X" (TNX). To study TNX function, we postulated a "contiguous gene syndrome"—a single mutation affecting both *CYP21A2* and *TNXB*, causing CAH plus another disorder that might suggest the role of TNX. A patient with CAH and Ehlers-Danlos syndrome (EDS) had partial deletions encompassing both genes. With collaborators, we described patients with recessive TNX-deficient EDS (now termed "classic-like EDS"), which was clinically distinct from dominant EDS caused by collagen mutations. TNX haploinsufficiency causes the mild "hypermobility form" of EDS, often associated with CAH, comprising the unique CAH-X syndrome. The discovery of TNX illustrates scientific serendipity and the value of pursuing unexpected results.

STUMBLING ONTO "GENE X"—AN UNEXPECTED FINDING IN AN ENDOCRINE STUDY

The discovery of TNX and its associated deficiency disease (a form of Ehlers-Danlos Syndrome) was done in studies of human steroidogenesis and its disorders rather than in studies of connective tissues. In the 1980s, application of then-new molecular biologic techniques revolutionized understanding of steroidogenesis (1). A driving force behind this early work was steroid 21-hydroxylase deficiency (21OHD), a form of congenital adrenal hyperplasia (CAH) causing cortisol deficiency, potentially-lethal aldosterone deficiency, and androgen excess with prenatal virilization of affected females. There are many forms of CAH, but 21OHD, with an incidence of ~1:15,000 (2) was responsible for >90% of cases; 21OHD is now well understood, but requires intensive management (3). Adrenal 21-hydroxylation is catalyzed by P450c21 (CYP21), a microsomal cytochrome P450 enzyme. In 1986, we reported the bovine *Cyp21* gene sequence (4) and others (5, 6) reported the human gene. The gene

lay in the human leukocyte antigen (HLA) locus (major histocompatibility locus, MHC) on chromosome 6p21.33, the most gene-dense and highly recombinogenic region of the human genome. Duplicated 30-kb units contained the functional *CYP21A2* gene and a non-functional *CYP21A1P* pseudogene duplicated in tandem with the *C4A* and *C4B* genes encoding the fourth component of serum complement (7–9) (**Figure 1**). *CYP21A1P* is transcribed (10, 11), but is considered a pseudogene because its RNAs do not encode protein. Human *CYP21A2* encodes P450c21, in mice the *cyp21a1* gene corresponding to *CYP21A1P* is active (12, 13), in cattle both genes function (4, 14), and some other mammals have single copies of this locus (15); thus the gene duplication post-dates mammalian speciation (16).

There was great interest in studying *CYP21* genes in patients with 21OHD. We obtained adrenal mRNA from an abortus with 21OHD, prepared a cDNA library, and screened it with radiolabeled double-stranded P450c21 cDNA to obtain the cDNA for the responsible mutant gene (17). Both the known cDNA sequence and RNA blotting showed that the full-length cDNA would be 2.0 kb, but several clones were longer than that, suggesting that the 21OHD might have arisen by an RNA splicing error. Restriction endonuclease mapping of the longest (2.7 kb) clone indicated that it contained only the 3' end of *CYP21*. A 2.7 kb clone might have been a cloning artifact, a recombination between *CYP21* and something else (as sometimes happened with the reagents then available), but because we had screened the cDNA library with a double-stranded probe, we considered that the 2.7 kb clone could have arisen from a transcript on the opposite strand of DNA from the *CYP21* genes. DNA sequencing showed that the 2.7 kb clone had a 3' poly(A) tail with upstream DNA that matched the predicted opposite-strand sequence of final exon of *CYP21*. The complete 2.7 kb sequence showed an open reading frame with repeating units whose structural significance was not clear (17). Because the CYP21/C4 locus is duplicated, we knew that this new "gene X" must also be duplicated as "XA" and "XB" genes with the arrangement 5'-C4A-21A-XA-C4B-21B-XB-3' (**Figure 1**). Deletions in the gene causing 21OHD did not appear to extend into the XB gene, but deletions of the XA region were found in 14% of human chromosomes (18, 19), suggesting that the 2.7-kb cDNA arose from the XB gene (17). But the nature of the gene encoding the 2.7-kb cDNA was unknown—the operational name "gene X" thus became the source of the name "Tenascin-X".

GENE X BECOMES TENASCIN-X

The publication of the 2.7 kb cDNA led us and others to study its gene structure. In 1989, Dr. Russell Doolittle (UC-San Diego), told us that the sequence of our 2.7 kb cDNA resembled chicken tenascin, and published a paper describing a fibrinogen-like sequence in an invertebrate, saying "The sea cucumber protein also corresponds exactly with a segment found as part of the previously unidentified gene product found in human adrenals" (20). Our 2.7 kb cDNA sequence had domains for fibrinogen and fibronectin type III (Fn-III) repeats, thus resembling tenascin (16). Matsumoto et al. confirmed the identification of fibrinogen and Fn-III domains, identified tenascin-like EGF-like domains

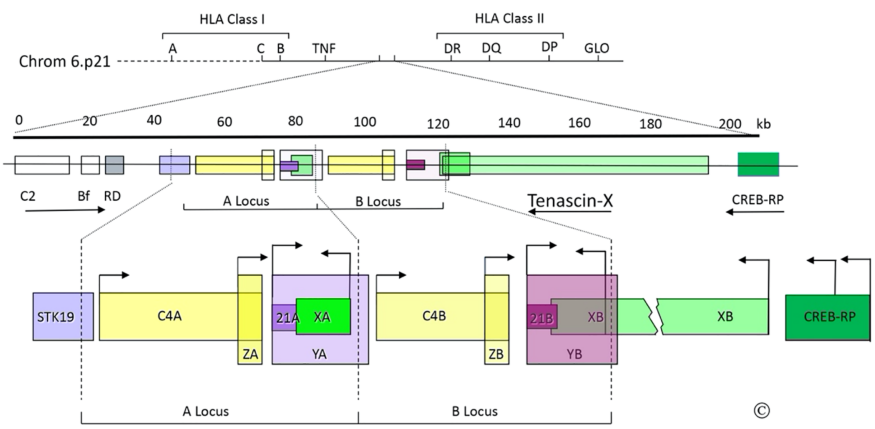

FIGURE 1 | The C4/CYP21/TNX gene locus. Top: Diagram of the short arm of chromosome 6; the telomere is to the left and the centromere is to the right. The MHC Class I and Class II regions are indicated with their principal human leukocyte antigen (HLA) genes; the ~1 megabase region between these is the "Class III region", which includes the gene for tumor necrosis factor (TNF). Middle: Scale bar in kilobases (kb) and enlarged view of a portion of the Class III region (chrom 6p21.33); the arrows indicate transcriptional orientations. C2, complement factor C2; Bf, properedin factor Bf; RD is now known as NEFLE, negative elongation factor subunit E; CREB-RP, CREB-related protein. Bottom: The duplicated 30 kb C4/CYP21/TNX units and adjacent regions: STK19, serine/threonine kinase 19; C4A and C4B, genes for complement component 4; 21A, *CYP21A1P* pseudogene; 21B *CYP21A2* gene; XA, YA, and YB, adrenal transcripts that lack open reading frames; XB, the *TNXB* gene; XB-S the short, adrenal-specific form of TNX, arises from the leftward transcription arrow within the XB gene, analogously to XA; ZA and ZB, adrenal-specific transcripts with open reading frames arising from promoters within the C4 genes; the ZA and ZB promoters are enhancer elements of the *CYP21A1P* and *CYP21A2* promoters. Most TNX transcription arises from the untranslated exon at the 5'end of *TNXB*, but some also arises from two sites within CREB-RP. The vertical dotted lines designate the boundaries of the gene duplication event. © WL Miller.

and provided additional information about exonic organization (21, 22). To determine how this locus was duplicated, we sequenced genomic DNA at the predicted duplication boundaries and through the entire 7 kb between 21A and C4B that had to comprise the XA locus, providing the entire XA gene sequence and the precise boundaries of the human gene duplication (16). These boundaries were substantially different from the corresponding duplication loci in the mouse genome, as expected for independent duplication events that post-dated mammalian speciation. Although XA was abundantly expressed in the adrenal, its gene was truncated at its 5' end (compared to XB) by the gene duplication (16), suggesting that it is a pseudogene and that XB would be the more important locus.

Manual sequencing of overlapping genomic clones revealed the nearly complete structure of the XB gene: 39 exons spanning 65 kb encoding a protein of >400-kDa (23). Some Fn-III repeats underwent alternative splicing; current data show 44 exons spanning 68 kb encoding 4,244 amino acids totaling 458,220 Da (24). The structure contained the five domains expected of a tenascin. First, the N-terminus comprised a 22AA signal peptide that directs the protein to the secretory pathway, used by extracellular matrix proteins. Second is a hydrophobic domain containing three heptad repeats that encode the tenascin "head piece", which permits polymerization of tenascin monomers into multi-armed "brachion" structures. The three heptad repeats suggested that TNX should form a "tri-brachion", similar to the hexabrachion structure of chicken (25) and human (26) tenascin. TNX lacked the additional cysteine residues in this domain of tenascin and restrictin, which permit two tri-brachions to pair into a hexabrachion. The tri-brachion structure of TNX was subsequently confirmed (27); with glycosylation, a TNX tri-brachion is ~1.5 million Da. Third, a single exon encoded a series of 18.5 EGF-like repeats having 55% similarity to the 13.5 EGF-like repeats of human tenascin/cytotactin. Fourth, a series of evolutionarily duplicated exons encoded 32 Fn-III repeats, including the cell-binding domain identified in chicken tenascin (25). Finally, the last five exons encode the carboxy-terminal fibrinogen-like domain and the 3'-untranslated region, including the domains that overlap *CYP21A2* (17). The carboxy-terminal fibrinogen-like domain was widely conserved in evolution (20, 28), and the sequence and intron/exon arrangement of the 3' end of XB were very similar to the β- and γ- chains of fibrinogen (29). Thus, the product of the XB gene was a member of the family of tenascins. We said "We suggest that this category of proteins be termed 'brachions' or 'tenascins'. We favor the latter. Tenascin, the first-described member, which is also widely termed 'cytotactin', would be termed tenascin-C or TN-C to designate tenascin-cytotactin; restrictin would be termed tenascin-R or TN-R; and the product of the XB gene described in this paper would be tenascin-X or TN-X. This system would emphasize the relatedness among the monomeric units of these proteins and would, to the extent possible, incorporate terminologies and letterings favored by various groups. It seems unlikely that the number of tenascins will exceed the confines of the alphabet." (23). Thus, the currently used nomenclature for the tenascins, TNC, TNR, and TNX, was established, soon to be followed by TNW (30, 31).

ADDITIONAL STUDIES AND GENES IN THE *TNX* GENE LOCUS

The structure of TNX is conserved in mice, with subunits of ~500 kD expressed in a pattern distinct from TNC (32). Expression of *TNXB* is tissue-specific and developmentally regulated (33, 34). In fetal adrenal, fetal muscle, and skin HT1080 cells, *TNXB* transcription begins with an untranslated exon ~10 kb upstream from the first coding exon (35). The *CREB-RP* gene encoding the transcription factor CREB-related protein lies immediately upstream from *TNXB* (36). *TNXB* transcripts arise from multiple Sp1/Sp3 sites near to and within *CREB-BP* (35, 37); thus, both ends of *TNXB* overlap other genes (**Figure 1**). Because *XA* is transcribed despite lacking promoter sequences comparable to those of *TNXB*, we characterized the 128 bp *XA* promoter lying between *XA* and *C4B* (38). This sequence is identical in *TNXB* and drives the adrenal-specific expression of a truncated 74 kDa form of TNX, called XB-Short (XB-S), which is identical to the carboxy-terminal 673 amino acids of TNX (38) (**Figure 1**). Expression of XB-S is induced by hypoxia (39), and XB-S associates with mitotic motor kinesin Eg5 (40), but its precise function remains unclear. Additional transcripts termed YA and YB arise from the *CYP21A1P* and *CYP21A2* promoters, but do not encode protein (10), and transcripts termed ZA and ZB arise from a promoter element within intron 35 of the *C4* genes, but it is not clear whether these open reading frames encode protein (41). The ZB promoter is an upstream adrenal enhancer element for *CYP21A2* (42). The location of this essential *CYP21A2* element within *C4B* (also seen in the mouse) (43), explains why the *C4*, *CYP21*, and *TNX* genes remain intimately linked in mammalian genomes.

TENASCIN-X DEFICIENCY CAUSES AN AUTOSOMAL RECESSIVE FORM OF EHLERS-DANLOS SYNDROME

Developmental expression of *TNXB* showed a recurring pattern, appearing first in connective tissue surrounding muscle and then in a subset of intramuscular cells, suggesting roles in muscle morphogenesis (33). To find a biological role for TNX, we hypothesized that an HLA-linked deficiency disease for TNX might exist, but no clinical candidates emerged. Another approach was to postulate existence of a "contiguous gene syndrome" comprising a partial deletion of both the *CYP21A2* and *TNXB* genes, so we sought a patient with 21OHD "and something else". Serendipitously, Dr. Cynthia Curry (Fresno CA), asked us about a patient with 21OHD and a connective tissue disorder that resembled Ehlers-Danlos Syndrome (EDS). EDS was then known as an autosomal dominant disorder of collagen deposition, with rare recessive forms in collagen-modifying enzymes, (lysyl hydroxylase or pro-collagen N-proteinase) (44), hence TNX was not an obvious candidate. The patient's skin had ultrastructural findings atypical for known forms of EDS. An antiserum that recognized multiple TNX epitopes detected TNX in cultured dermal fibroblasts from

controls and from the obligately-heterozygous parents, but not in the patient's fibroblasts; similarly, control, but not patient fibroblasts contained TNX mRNA, confirming TNX-deficiency. Because the protein-coding regions of *CYP21A2* and *TNXB* do not overlap, we sought gene deletions rather than point mutations. Genomic PCR and Southern blotting identified a deletion extending from *XA* through *CYP21A2* to the corresponding point in *TNXB*, demonstrating that TNX deficiency causes EDS (45). In collaboration with Prof. Joost Schalkwijk (U. Nijmegen, Netherlands), we found an immunoassayable TNX fragment in the sera of 146 of 151 patients with EDS; the five patients lacking serum TNX had *TNXB* mutations, none of which encompassed *CYP21A2* (46). Subsequent work has confirmed that TNX deficiency causes a clinically distinct, severe form of EDS (47, 48). Similarly, *Tnxb*-knockout mice had skin hyperextensibility, reduced skin tensile strength and reduced skin collagen content (49); whereas mouse knockouts of TNC and TNR lacked abnormal phenotypes (50–52). TNX appears to associate with and stabilize newly produced collagen fibrils (27, 53, 54), thus all recessive forms of EDS concern post-translational modification of collagens.

CONGENITAL ADRENAL HYPERPLASIA AND TENASCIN-X—THE CAH-X SYNDROME

TNX has functions beyond EDS (55); it promotes epithelial-mysenchymal transitions in development (56), and may be associated with tumor invasion (57–59). TNX-deficiency has been associated with primary myopathy (60, 61), recurrent gastrointestinal perforation (62), and vesicoureteral reflux (63, 64). TNX is expressed in leptomeninges and choroid plexus (34, 65), suggesting neurologic roles: *TNXB* single nucleotide polymorphisms are associated with schizophrenia (66, 67), and *Tnxb*-knockout mice have increased anxiety, improved memory, and higher sensorimotor coordination than controls (68).

While TNX-deficient EDS is autosomal recessive, heterozygous *TNXB* mutations cause TNX haploinsufficiency, with joint hypermobility, recurring joint dislocations and joint pain—the "hypermobility type EDS". Among 20 obligate heterozygotes for a severely defective *TNXB* allele, 9 of 14 females but no males had hypermobility EDS (69). Dr. Deborah Merke (NIH, Bethesda MD) found that 7% of patients with 21OHD had symptomatic TNX haploinsufficiency (70, 71), and a recent study reported 14% (72); this association is now regarded as a subtype of 21OHD termed CAH-X (73). Thus, studies of 21OHD and TNX, like their genes, have been linked from the beginning and continue together.

AUTHOR CONTRIBUTIONS

WLM assembled the literature, wrote and edited the manuscript, drew the figure, and approved it for publication.

FUNDING

WLM's research was supported in the past by grants from the NIH and the March of Dimes.

ACKNOWLEDGMENTS

I thank James Bristow for his indispensable role in the discovery and functional elucidation of Tenascin-X, first in my laboratory and then independently.

REFERENCES

1. Miller WL. Molecular biology of steroid hormone synthesis. *Endocr Rev* (1988) 9:295–318. doi: 10.1210/edrv-9-3-295
2. Miller WL, Levine LS. Molecular and clinical advances in congenital adrenal hyperplasia. *J Pediatr* (1987) 111:1–17. doi: 10.1016/S0022-3476(87)80334-7
3. Speiser PW, Arlt W, Auchus RJ, Baskin LS, Conway GS, Merke DP, et al. Congenital adrenal hyperplasia due to steroid 21-hydroxylase deficiency: An Endocrine Society clinical practice guideline. *J Clin Endocrinol Metab* (2018) 103:4043–88. doi: 10.1210/jc.2018-01865
4. Chung B, Matteson KJ, Miller WL. Structure of the bovine gene for P450c21 (steroid 21-hydroxylase) defines a novel cytochrome P450 gene family. *Proc Natl Acad Sci USA* (1986) 83:4243–7. doi: 10.1073/pnas.83.12.4243
5. Higashi Y, Yoshioka H, Yamane M, Gotoh O, Fujii-Kuriyama Y. Complete nucleotide sequence of two steroid 21-hydroxylase genes tandemly arranged in human chromosome: A pseudogene and genuine gene. *Proc Natl Acad Sci USA* (1986) 83:2841–5. doi: 10.1073/pnas.83.9.2841
6. White PC, New MI, Dupont B. Structure of the human steroid 21-hydroxylase genes. *Proc Natl Acad Sci USA* (1986) 83:5111–5. doi: 10.1073/pnas.83.14.5111
7. Amor M, Tosi M, Duponchel C, Steinmetz M, Meo T. Liver cDNA probes disclose two cytochrome P450 genes duplicated in tandem with the complement C4 loci of the mouse H-2S region. *Proc Natl Acad Sci USA* (1985) 82:4453–7. doi: 10.1073/pnas.82.13.4453
8. Carroll MC, Campbell RD, Porter RR. Mapping of steroid 21-hydroxylase genes to complement component C4 genes in HLA, the major histocompatibility locus in man. *Proc Natl Acad Sci USA* (1985) 82:521–5. doi: 10.1073/pnas.82.2.521
9. White PC, Grossberger D, Onufer BJ, Chaplin DD, New MI, Dupont B, et al. Two genes encoding steroid 21-hydroxylase are located near the genes encoding the fourth component of complement in man. *Proc Natl Acad Sci USA* (1985) 82:1089–93. doi: 10.1073/pnas.82.4.1089
10. Bristow J, Gitelman SE, Tee MK, Staels B, Miller WL. Abundant adrenal-specific transcription of the human P450c21A "pseudogene". *J Biol Chem* (1993) 268:12919–24.
11. Chang SF, Chung BC. Difference in transcriptional activity of two homologous CYP21A genes. *Mol Endocrinol* (1995) 9:1330–6. doi: 10.1210/me.9.10.1330
12. Parker KL, Chaplin DD, Wong M, Seidman JG, Smith JA, Schimmer BP. Expression of murine 21-hydroxylase in mouse adrenal glands and in transfected Y1 adrenocortical tumor cells. *Proc Natl Acad Sci USA* (1985) 82:7860–4. doi: 10.1073/pnas.82.23.7860
13. Chaplin DD, Galbraith LJ, Seidman JG, White PC, Parker KL. Nucleotide sequence analysis of murine 21-hydroxylase genes: mutations affecting gene

expression. *Proc Natl Acad Sci USA* (1986) 83:9601–5. doi: 10.1073/pnas.83.24.9601
14. John ME, Okamura T, Dee A, Adler B, John MC, White PC, et al. Bovine steroid 21-hydroxylase: Regulation of biosynthesis. *Biochemistry* (1986) 25:2846–53. doi: 10.1021/bi00358a016
15. Geffrotin C, Chardon P, DeAndres-Cara DR, Feil R, Renard C, Vaiman M. The swine steroid 21-hydroxylase gene (CYP21): Cloning and mapping within the swine leukocyte antigen locus. *Anim Genet* (1990) 21:1–13. doi: 10.1111/j.1365-2052.1990.tb03202.x
16. Gitelman SE, Bristow J, Miller WL. Mechanism and consequences of the duplication of the human C4/P450c21/gene X locus. *Mol Cell Biol* (1992) 12:2124–34. doi: 10.1128/MCB.12.5.2124. Correction: Mol Cell Biol (1992) 12:3313-3314.
17. Morel Y, Bristow J, Gitelman SE, Miller WL. Transcript encoded on the opposite strand of the human steroid 2l-hydroxylase/complement component C4 gene locus. *Proc Natl Acad Sci USA* (1989) 86:6582–6. doi: 10.1073/pnas.86.17.6582
18. Miller WL, Morel Y. The molecular genetics of 21-hydroxylase deficiency. *Annu Rev Genet* (1989) 23:371–93. doi: 10.1146/annurev.genet.23.1.371
19. Morel Y, Miller WL. Clinical and molecular genetics of congenital adrenal hyperplasia due to 21-hydroxylase deficiency. *Adv Hum Genet* (1991) 20:1–68. doi: 10.1007/978-1-4684-5958-6_1
20. Xu X, Doolittle RF. Presence of a vertebrate fibrinogen-like sequence in an echinoderm. *Proc Natl Acad Sci USA* (1990) 87:2097–101. doi: 10.1073/pnas.87.6.2097
21. Matsumoto K, Arai M, Ishihara N, Ando A, Inoko H, Ikemura T. Cluster of fibronectin type III repeats found in the human major histocompatibility complex class III region shows the highest homology with the repeats in an extracellular matrix protein, tenascin. *Genomics* (1992) 12:485–91. doi: 10.1016/0888-7543(92)90438-X
22. Matsumoto K, Ishihara N, Ando A, Inoko H, Ikemura T. Extracellular matrix protein tenascin-like gene found in human MHC class III region. *Immunogenetics* (1992) 36:400–3. doi: 10.1007/BF00218048
23. Bristow J, Tee MK, Gitelman SE, Mellon SH, Miller WL. Tenascin-X: A novel extracellular matrix protein encoded by the human XB gene overlapping P450c21B. *J Cell Biol* (1993) 122:265–78. doi: 10.1083/jcb.122.1.265
24. ncbi.nlm.nih.gov/gene?Db=gene&Cmd=DetailsSearch&Term=7148
25. Spring J, Beck K, Chiquet-Ehrismann R. Two contrary functions of tenascin: dissection of the active sites by recombinant tenascin fragments. *Cell* (1989) 59:325–34. doi: 10.1016/0092-8674(89)90294-8
26. Gulcher JR, Nies DE, Alexakos MJ, Ravikant NA, Sturgill ME, Marten LS, et al. Structure of the human hexabrechion (tenascin) gene. *Proc Natl Acad Sci USA* (1991) 88:9438–42. doi: 10.1073/pnas.86.5.1588
27. Lethias C, Carisey A, Comte J, Cluzel C, Exposito J-Y. A model of tenascin-X integration within the collagenous network. *FEBS Lett* (2006) 80:6281–5. doi: 10.1016/j.febslet.2006.10.037
28. Baker NE, Mlodzik M, Rubin GM. Spacing differentiation in the developing Drosophila eye: a fibrinogen-related lateral inhibitor encoded by *scabrous*. *Science* (1990) 250:1370–7. doi: 10.1126/science.2175046
29. Pan Y, Doolittle RF. cDNA sequence of a second fibrinogen α chain in lamprey: an archetypal version aliguable with full-length β- and γ- chains. *Proc Natl Acad Sci USA* (1992) 89:2066–70. doi: 10.1073/pnas.89.6.2066
30. Weber P, Montag D, Schachner M, Bernhardt RR, Zebrafish tenascin- W. a new member of the tenascin family. *J Neurobiol* (1998) 35:1–16. doi: 10.1002/(SICI)1097-4695(199804)35:1<1::AID-NEU1>3.0.CO;2-9
31. Scherberich A, Tucker RP, Samandari E, Brown-Luedi M, Martin D, Chiquet-Ehrismann R. Murine tenascin-W: a novel mammalian tenascin expressed in kidney and at sites of bone and smooth muscle development. *J Cell Sci* (2004) 17:571–81. doi: 10.1242/jcs.00867
32. Matsumoto K, Saga Y, Ikemura T, Sakakura T, Chiquet-Ehrismann R. The distribution of tenascin-X is distinct and often reciprocal to that of tenascin-C. *J Cell Biol* (1994) 125:483–93. doi: 10.1083/jcb.125.2.483
33. Burch GH, Bedolli MA, McDonough S, Rosenthal SM, Bristow J. Embryonic expression of tenascin-X suggests a role in limb, muscle, and heart development. *Dev Dynamics* (1995) 203:491–504. doi: 10.1038/ng0997-104
34. Geffrotin C, Garrido JJ, Tremet L, Vaiman M. Distinct tissue distribution in pigs of Tenascin-X and Tenascin-C transcripts. *Eur J Biochem* (1995) 231:83–92. doi: 10.1111/j.1432-1033.1995.0083f.x
35. Speek M, Barry F, Miller WL. Alternate promoters and alternate splicing of human Tenascin-X, a gene with 5' and 3' ends buried in other genes. *Hum Mol Genet* (1996) 5:1749–58. doi: 10.1093/hmg/5.11.1749
36. Min J, Shukla H, Kozono H, Bronson SK, Weissman SM, Chaplin DD. A novel Creb family gene telomeric of HLA-DRA in the HLAcomplex. *Genomics* (1995) 30:149–56. doi: 10.1006/geno.1995.9891
37. Wijesuriya SD, Bristow J, Miller WL. Localization and analysis of the principal promoter for human Tenascin-X. *Genomics* (2002) 80:443–52. doi: 10.1006/geno.2002.6852
38. Tee MK, Thomson AA, Bristow J, Miller WL. Sequences promoting the transcription of the human XA gene overlapping P450c21A correctly predict the presence of a novel, adrenal-specific, truncated form of Tenascin-X. *Genomics* (1995) 28:171–8. doi: 10.1006/geno.1995.1128
39. Kato A, Endo T, Abiko S, Ariga H, Matsumoto K. Induction of truncated form of Tenascin-X (XB-S) through dissociation of HDAC1 from SP-1/HDAC1 complex in response to hypoxic conditions. *Exp Cell Res* (2008) 314:2661–73. doi: 10.1016/j.yexcr.2008.05.019
40. Endo T, Ariga H, Matsumoto K. Truncated form of Tenascin-X, XB-S, interacts with mitotic motor kinesin Eg5. *Mol Cell Biochem* (2009) 320:53–66. doi: 10.1007/s11010-008-9898-y
41. Tee MK, Babalola GO, Aza-Blanc P, Speek M, Gitelman SE, Miller WL. A promoter within intron 35 of the human C4A gene initiates adrenal-specific transcription of a 1kb RNA: location of a cryptic CYP21 promoter element? *Hum Mol Genet* (1995) 4:2109–16. doi: 10.1093/hmg/4.11.2109
42. Wijesuriya SD, Zhang G, Dardis A, Miller WL. Transcriptional regulatory elements of the human gene for cytochrome P450c21 (steroid 21-hydroxylase) lie within intron 35 of the linked C4B gene. *J Biol Chem* (1999) 274:38097–106. doi: 10.1074/jbc.274.53.38097
43. Milstone DS, Shaw SK, Parker KL, Szyf M, Seidman JG. An element regulating adrenal-specific steroid 21-hydroxylase expression is located within the slp gene. *J Biol Chem* (1992) 267:21924–7.
44. Byers PH. Ehlers-Danlos syndrome: recent advances and current understanding of the clinical and genetic heterogeneity. *J Invest Dermatol* (1994) 103:475–525. doi: 10.1038/jid.1994.9
45. Burch GH, Gong Y, Liu W, Dettman RW, Curry CJ, Smith L, et al. Tenascin-X deficiency is associated with Ehlers-Danlos syndrome. *Nat Genet* (1997) 17:104–8. doi: 10.1038/ng0997-104
46. Schalkwijk J, Zweers MC, Steijlen PM, Dean WB, Taylor G, von Vlijmen IM, et al. A recessive form of Ehlers-Danlos syndrome caused by Tenascin-X deficiency. *New Engl J Med* (2001) 345:1167–75. doi: 10.1056/NEJMoa002939
47. Lindor NM, Bristow J. Tenascin-X deficiency in autosomal recessive Ehlers-Danlos syndrome. *Am J Med Genet* (2005) 135A:75–80. doi: 10.1002/ajmg.a.30671
48. Demirdas S, Dulfer E, Robert L, Kempers M, van Beek D, Micha D, et al. Recognizing the tenascin-X deficient type of Ehlers–Danlos syndrome: a cross-sectional study in 17 patients. *Clin Genet* (2017) 91:411–25. doi: 10.1111/cge.12853
49. Mao JR, Taylor G, Dean WB, Wagner DR, Afzal V, Lotz JC, et al. Tenascin-X deficiency mimics Ehlers–Danlos syndrome in mice through alteration of collagen deposition. *Nat Genet* (2002) 30:421–5. doi: 10.1038/ng850
50. Saga Y, Yagi T, Ikawa Y, Sakakura T, Aizawa S. Mice develop normally without tenascin. *Genes Dev* (1992) 6:1821–31. doi: 10.1101/gad.6.10.1821
51. Forsberg E, Hirsch E, Frohlich L, Meyer M, Ekblom P, Aszodi A, et al. Skin wounds and severed nerves heal normally in mice lacking tenascin-C. *Proc Natl Acad Sci USA* (1996) 93:6594–9. doi: 10.1073/pnas.93.13.6594
52. Weber P, Bartsch U, Rasband MN, Czaniera R, Lang Y, Bluethmann H, et al. Mice deficient for tenascin-R display alterations of the extracellular matrix and decreased axonal conduction velocities in the CNS. *J Neurosci* (1999) 19:4245–62. doi: 10.1523/jneurosci.19-11-04245.1999
53. Elefteriou F, Exposito JY, Garrone R, Lethias C. Characterization of the bovine Tenascin-X. *J Biol Chem* (1997) 272:22866–74. doi: 10.1074/jbc.272.36.22866
54. Mao JR, Bristow J. The Ehlers-Danlos syndrome: on beyond collagens. *J Clin Invest* (2001) 107:1063–9. doi: 10.1172/JCI12881
55. Valcourt U, Alcaraz LB, Esposito JY, Lethias C, Bartholin L. Tenascin-X: beyond the architectural function. *Cell Adhesion Migration* (2015) 9:154–65. doi: 10.4161/19336918.2014.994893
56. Alcaraz LB, Exposito JY, Chuvin N, Pommier RM, Cluzel C, Martel S, et al. Tenascin-X promotes epithelial-to-mesenchymal transition by activating latent TGF-β. *J Cell Biol* (2014) 205:409–28. doi: 10.1083/jcb.201308031

57. Geffrotin C, Horak V, Crechet F, Tricaud Y, Lethias C, Vincent-Naulleau S, et al. Opposite regulation of tenascin-C and tenascin-X in MeLiM swine heritable cutaneous malignant melanoma. *Biochim Biophys Acta* (2000) 1524:196–202. doi: 10.1016/S0304-4165(00)00158-6
58. Matsumoto K, Takayama N, Ohnishi J, Ohnishi E, Shirayoshi Y, Nakatsuji N, et al. Tumour invasion and metastasis are promoted in mice deficient in tenascin-X. *Genes Cells* (2001) 6:1101–11. doi: 10.1046/j.1365-2443.2001.00482.x
59. Levy P, Ripoche H, Laurendeau I, Lazar V, Ortonne N, Parfait B, et al. Microarray-based identification of *Tenascin C* and *Tenascin XB*, genes possibly involved in tumorigenesis associated with neurofibromatosis type 1. *Clin Cancer Res* (2007) 13:398–407. doi: 10.1158/1078-0432.CCR-06-0182
60. Voermans NC, van Alfen N, Pillen S, Lammens M, Schalkwijk J, Zwarts MJ, et al. Neuromuscular involvement in various types of Ehlers-Danlos syndrome. *Ann Neurol* (2009) 65:687–97. doi: 10.1002/ana.21643
61. Penisson-Besnier I, Allamand V, Beurrier P, Martin L, Schalkwijk J, van Vlijmen-Willems I, et al. Compound heterozygous mutations of the TNXB gene cause primary myopathy. *Neuromuscular Disord* (2013) 23:664–9. doi: 10.1016/j.nmd.2013.04.009
62. Sakiyama T, Kubo A, Sasaki T, Yamada T, Yabe N, Matsumoto K, et al. Recurrent gastrointestinal perforation in a patient with Ehlers–Danlos syndrome due to tenascin-X deficiency. *J Dermatol* (2015) 42:511–4. doi: 10.1111/1346-8138.12829
63. Gbadegesin RA, Brophy PD, Adeyemo A, Hall G, Gupta IR, Hains D, et al. *TNXB* mutations can cause vesicoureteral reflux. *J Am Soc Nephrol* (2013) 24:1313–22. doi: 10.1681/ASN.2012121148
64. Tokhmafshan F, Brophy PD, Gbadegesin RA, Gupta IR. Vesicoureteral reflux and the extracellular matrix connection. *Pediatr Nephrol* (2017) 32:565–76. doi: 10.1007/s00467-016-3386-5
65. Imura K, Sato I. Identification of the novel localization of tenascin X in the monkey choroid plexus and comparison with the mouse. *Euro J Histochem* (2009) 53:225–31. doi: 10.4081/ejh.2009.225
66. Wei J, Hemmings GP. *TNXB* locus may be a candidate gene predisposing to schizophrenia. *Am J Med Genet B Neuropsychiatr Genet* (2004) 125:43–9. doi: 10.1002/ajmg.b.20093
67. Tochigi M, Zhang X, Ohashi J, Hibino H, Otowa T, Rogers M, et al. Association study between the TNXB locus and schizophrenia in a Japanese population. *Am J Med Genet B Neuropsychiatr Genet* (2007) 144B:305–9. doi: 10.1002/ajmg.b.30441
68. Kawakami K, Matsumoto K. Behavioral alterations in mice lacking the gene for Tenascin-X. *Biol Pharm Bull* (2011) 34:590–3. doi: 10.1248/bpb.34.590
69. Zweers MC, Bristow J, Steijlen PM, Dean WB, Hamel BC, Otero M, et al. Haploinsufficiency of *TNXB* is associated with hypermobility type of Ehlers-Danlos Syndrome. *Am J Hum Genet* (2003) 73:214–7. doi: 10.1086/376564
70. Merke DP, Chen W, Morissette R, Xu Z, Van Ryzin C, Sachdev V, et al. Tenascin-X haploinsufficiency associated with Ehlers-Danlos syndrome in patients with congenital adrenal hyperplasia. *J Clin Endocrinol Metab* (2013) 98:E379–87. doi: 10.1210/jc.2012-3148
71. Morissette R, Chen W, Perritt AF, Dreiling JL, Arai AE, Sachdev V, et al. Broadening the spectrum of Ehlers Danlos syndrome in patients with congenital adrenal hyperplasia. *J Clin Endocrinol Metab* (2015) 100:E1143–52. doi: 10.1210/jc.2015-2232
72. Gao Y, Lu L, Yu B, Mao J, Wang X, Ni M, et al. The prevalence of chimeric *TNXA/TNXB* gene and clinical symptoms of Ehlers-Danlos syndrome with 21-hydroxylase deficiency. *J Clin Endocrinol Metab* (2020) 105:2288–99. doi: 10.1210/clinem/dgaa199
73. Miller WL, Merke DP. Tenascin-X, congenital adrenal hyperplasia, and the CAH-X syndrome. *Horm Res Ped* (2018) 89:352–61. doi: 10.1159/000481911

Conflict of Interest: The author declares that the research was conducted in the absence of any commercial or financial relationships that could be construed as a potential conflict of interest.

frontiers in Immunology

REVIEW
published: 21 January 2021
doi: 10.3389/fimmu.2020.607587

The Role of Tenascin-C in Tissue Injury and Repair After Stroke

Takeshi Okada[1,2] *and Hidenori Suzuki*[1]*

[1] Department of Neurosurgery, Mie University Graduate School of Medicine, Tsu, Japan, [2] Department of Neurosurgery, Kuwana City Medical Center, Kuwana, Japan

Stroke is still one of the most common causes for mortality and morbidity worldwide. Following acute stroke onset, biochemical and cellular changes induce further brain injury such as neuroinflammation, cell death, and blood-brain barrier disruption. Matricellular proteins are non-structural proteins induced by many stimuli and tissue damage including stroke induction, while its levels are generally low in a normal physiological condition in adult tissues. Currently, a matricellular protein tenascin-C (TNC) is considered to be an important inducer to promote neuroinflammatory cascades and the resultant pathology in stroke. TNC is upregulated in cerebral arteries and brain tissues including astrocytes, neurons, and brain capillary endothelial cells following subarachnoid hemorrhage (SAH). TNC may be involved in blood-brain barrier disruption, neuronal apoptosis, and cerebral vasospasm *via* the activation of mitogen-activated protein kinases and nuclear factor-kappa B following SAH. In addition, post-SAH TNC levels in cerebrospinal fluid predicted the development of delayed cerebral ischemia and angiographic vasospasm in clinical settings. On the other hand, TNC is reported to promote fibrosis and exert repair effects for an experimental aneurysm *via* macrophages-induced migration and proliferation of smooth muscle cells. The authors review TNC-induced inflammatory signal cascades and the relationships with other matricellular proteins in stroke-related pathology.

Keywords: biomarker, blood-brain barrier disruption, cerebral vasospasm, matricellular protein, neuroinflammation, neuronal apoptosis, stroke, subarachnoid hemorrhage

OPEN ACCESS

Edited by:
Gertraud Orend,
INSERM Immuno Rhumatologie Moléculaire (IRM), France

Reviewed by:
Thomas N. Wight,
Benaroya Research Institute, United States
Rui Li,
University of Pennsylvania, United States

***Correspondence:**
Hidenori Suzuki
suzuki02@clin.medic.mie-u.ac.jp

Specialty section:
This article was submitted to Inflammation, a section of the journal Frontiers in Immunology

Received: *17 September 2020*
Accepted: *04 December 2020*
Published: *21 January 2021*

Citation:
Okada T and Suzuki H (2021) The Role of Tenascin-C in Tissue Injury and Repair After Stroke. Front. Immunol. 11:607587. doi: 10.3389/fimmu.2020.607587

INTRODUCTION

Stroke is a large public concern in terms of both human and financial resources (1, 2). In the United States, annual stroke expenses have reached approximately 33.9 billion dollars (2). Although recent research has been clarifying pathological changes in the brain following stroke, therapeutic options for these patients remain limited.

Neuroinflammation is a key pathologic change arising from stroke. Findings from both clinical and animal studies have indicated that inflammatory reactions may contribute to the development of brain injury following stroke (3–5). Post-stroke tissue damage releases secondary breakdown products of brain tissue and blood components. Damage-associated molecular patterns (DAMPs) are endogenous molecules released as a result of tissue damage that rapidly activate the innate immune response by interacting with a number of pattern recognition receptors (PRRs) located primarily on microglia and macrophages (6, 7). Activated microglia and macrophages release inflammatory cytokines and mediators *via* activation of signaling pathways downstream of the

PRRs. The PRRs include Toll-like receptors (TLRs), cytosolic NOD-like receptors and inflammasomes, receptors for advanced glycation end products, and other scavenger receptors (8–10). Following stroke, the TLR4 signaling pathway is involved in the initial steps of neuroinflammation cascades, which result in brain injury such as vasogenic and cytotoxic edema and blood-brain barrier (BBB) disruption (11). Furthermore, neuroinflammation recruits more DAMPs, accelerating the inflammatory response. The secondary brain injury includes early brain injury (EBI), cerebral vasospasm (CVS), and delayed cerebral ischemia (DCI) after subarachnoid hemorrhage (SAH). Neuroinflammation is currently considered to be a critical factor contributing to morbidity and mortality in stroke patients who survive the initial brain damage and needs to be addressed in order to improve clinical outcomes (11–13).

Matricellular proteins (MCPs) are extracellular matrix (ECM) components upregulated and released by tissue damage, exerting both beneficial and harmful effects through binding to receptors, other matrix proteins, growth factors (GFs), and cytokines (14). Recent studies have demonstrated the efficacy of treatments targeting MCPs in preclinical stroke neuroinflammation models (15, 16).

In this review, we focus on a MCP tenascin-C (TNC) involved in neuroinflammation following stroke, and highlight current evidence for its use as a clinical biomarker and a therapeutic target.

WHAT ARE MCPS?

The concept of MCPs was introduced in 1995 due to their characteristics which differ from classical ECM proteins (17). MCPs are currently considered important inducers that regulate the expression of inflammatory mediators and are involved in diverse pathological changes such as cell death, immunomodulation, inflammation, fibrosis, vascular permeability, and angiogenesis *via* modulation of the molecular functions or cellular responses to the molecules (18, 19). MCPs can work on the plasma membrane, intracellularly, in body fluids, or in the ECM, and also act as reservoirs of the bioactive molecules (18, 19). The level of protein expression is low in normal physiological conditions in adult tissues in general, and MCP knockout mice undergo normal development (18, 20). Almost all tissues and cell types produce MCPs following various stimuli which disappear after stimulus removal. MCPs do not provide a scaffold for stable cell adhesion, but induce cell motility and tissue remodeling *via* modulation of cell surface receptors, other matrix proteins, GFs, and cytokines (**Table 1**) (18). Accumulating evidence suggests that many types of MCPs, such as TNC, periostin, galectin-3, and osteopontin, contribute to aggravation or improvement of neuroinflammation in stroke at least partly by influencing the expression of each other (15, 18–23).

TNC: THE STRUCTURE AND ISOFORMS

Tenascins (TNs) are representative of MCPs and are comprised of a family of four homologs, that is, TNC, TNR, TNW, and TNX (22–24). Among the TNs, only TNC has been investigated in stroke (20). TNC was discovered in the early 1980s and initially referred to by different terms such as myotendinous antigen, glioma mesenchymal ECM, hexabrachion, TN, J1-200/220, cytotactin, and neuronectin (25, 26). TNC is a pleiotropic ECM glycoprotein with a large molecular weight (180–400 kDa). Its N-terminal contains highly conserved heptad repeats, followed by 14 epidermal growth factor (EGF)-like repeats and up to 15 fibronectin type III (FN III) repeats comprised of universal repeats and alternatively spliced repeats; and a fibrinogen repeat domain is located at the C-terminal (25, 27–30). Alternatively spliced repeats in the FN III domain are comprised of a combination of A1, A2, A3, A4, B, AD2, AD1, C, and D domains in humans and A1, A2, A4, B, C, and/or D domains in mice, which are inserted between domains 5 and 6 in universal FN III repeats (20, 23, 29–34). TNC generally forms a disulfide-linked hexamer mediated by the N-terminal domain in which six flexible arms emanate from a central globular particle (**Figure 1**) (20, 22, 29, 30, 35). In humans, TNC is encoded at a single gene located at 9q33 (20).

TNC exhibits a diverse range of isoforms in various tissues, the splicing of which is regulated by intracellular pH. Under exposure to basic pH ~7.30–7.50 as observed with fetal cells and aggressive tumors, the level of longer or larger TNC isoforms is enhanced (33). Isoforms with a large molecular mass (≥200 kDa) contain at least one alternatively spliced FN III repeat. Each alternatively spliced FN III repeat has unique functions (33). Larger TNC isoforms induce cell proliferation and migration, and control cell spreading, resulting in promotion of destruction or remodeling of local tissues (33). In addition, larger TNC isoforms can be easily degraded by matrix metalloproteinases (MMPs), leukocyte elastase, and possibly other serine proteases (33). MMPs usually cleave the sites located within the alternatively spliced region (23, 33). In contrast, TNC isoforms with a lower molecular mass (<200 kDa) lack A1-D domains in alternatively spliced FN III repeats and seem to be more stable in dense connective tissues and to be expressed at low levels in a physiologically normal tissue (33). Under physiological pH <7.0, the level of small TNC isoforms is increased (33). Different TNC isoforms seem to be produced by proteolytic processing of a large multimodular TNC isoform. The proteolytic destruction may impart novel functions to TNC by destroying existing binding

TABLE 1 | Characteristics of matricellular proteins compared with classical extracellular matrix (ECM) proteins.

Classical ECM protein	Matricellular protein
- Structural protein	- Soluble non-structural protein - Low expression level under normal physiological conditions in adult tissues - Induced in almost any tissue by stimuli and disappear after stimulus removal
- Provide a scaffold for stable cell adhesion	- Induce cell motility and tissue remodeling - Various functions *via* interacting with cell surface receptors, other matrix proteins, growth factors, and cytokines - Knockout mice basically undergo normal development

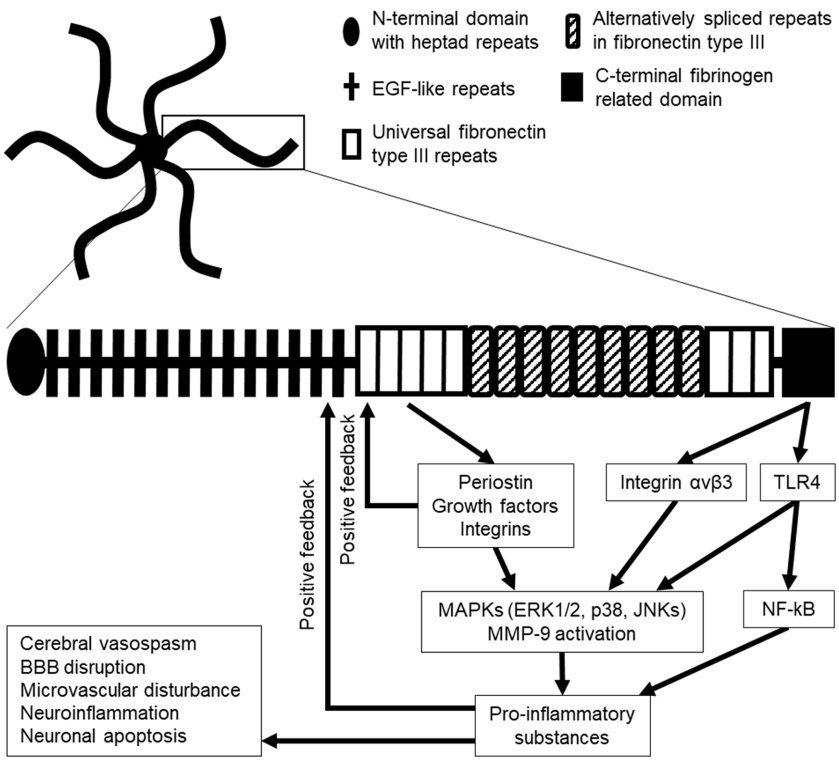

FIGURE 1 | Hexamer structure of tenascin-C (TNC; upper), monomer structure of TNC (lower), and the possible downstream signaling pathway in stroke. Six TNC monomers combine to a hexamer at their N-terminal domains. EGF, epidermal growth factor; ERK1/2, extracellular signal-regulated kinase 1/2; JNKs, c-Jun N-terminal kinases; MMP-9, matrix metalloproteinase-9; TLR4, Toll-like receptor 4.

sites or generating smaller fragments with new binding sites: these new functions can drive entirely novel processes compared to the previous or intact form (33). Smaller TNC fragments exert quite different reactions in various cells. Fragmented EGF-like domains of TNC induce apoptotic effects on vascular smooth muscle cells in culture, while intact or full-length TNC does not have the functions (36). Thus, respective TNC isoforms seem to have flexible physiological or pathological functions (20). However, the timing and location of distinct TNC isoforms production during inflammatory reactions have not been completely investigated. In addition, the functions of individual TNC isoforms have not yet been fully clarified (20).

TNC Expression During Developmental Stage

TNC is highly expressed during embryonic development and was first identified in developing astrocytes (37–41). Currently, TNC is considered to be primarily induced by astrocytes and radial glial progenitor cells and to play a crucial role in normal brain development: it serves as a repulsive substrate for neuronal and astrocytic growth and plays a role in proliferation and process elongation of astrocyte progenitor cells, maturation of neural progenitor cells, proliferation and maintenance of oligodendrocyte precursors, and synaptic plasticity through autocrine and paracrine regulatory mechanisms during developing stages (**Figure 2**) (28, 34, 40–47). In the spinal cord, TNC is synthesized by a subset of gliogenic precursors in the late phase of embryogenesis and influences proliferation and migration of a subpopulation of astrocytes (48). Although the expression of TNC is downregulated in the brain 2–3 weeks after birth, it is involved in hippocampal synaptic plasticity and synchronized neural network activities in the mature brain *via* control of postsynaptic L-type Ca^{2+} channels (47). Intrahippocampal injections of recombinant TNC fragments containing the FN III repeats 6–8 block the retention of memory and hippocampal formation in mice, showing the mediation in hippocampus-dependent contextual memory and hippocampal synaptic plasticity (49).

Regulation of TNC Expression in Adult Tissues

In adult tissues, the expression and the distribution of TNC are typically limited under normal physiological conditions but transiently upregulated in reaction to inflammatory responses or tissue damages (50, 51). TNC expression is controlled by several transcription factors and intracellular regulators, including T cell factor/lymphoid enhancer-binding factor, nuclear factor (NF)-κB, Notch1 and Notch2, hepatocyte NF-4α, Ets, SP1, c-myc, homeobox transcription factor Prx1, Rho, c-Jun, and extracellular signal-regulated kinases (ERKs) (29, 32). Overexpression of the transcription factors Slug and Sox9 induce TNC and periostin expression (52). However, the involvement of these transcription factors in stroke has not been investigated *in vivo*. In contrast,

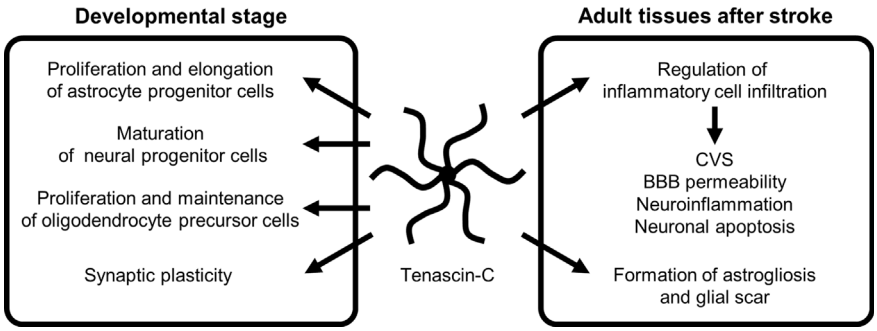

FIGURE 2 | The role of tenascin-C during developmental stage and following stroke. BBB, blood-brain barrier; CVS, cerebral vasospasm.

micro-ribonucleic acids (RNAs) such as miR-355 downregulate TNC expression in breast cancer metastases (53). Upregulation of TNC appears in reactive astrocytes, injured neurons, and glial scar formation with restricted occurrence in space and time: therefore, these cells are considered to release TNC (20, 22, 29, 47, 50, 54, 55). TNC modulates a variety of cell functions and morphologies (22, 23). Scratch wound assays induce TNC expression by astrocytes *in vitro* (56). Levels of TNC enhancement following stab-wound injury to cerebellar and cerebral cortical structures depend on the number of glial fibrillary acidic protein (GFAP)-positive cells, which represent reactive astrocytes (55). GFAP was significantly suppressed in TNC-knockout mice compared to wild-type ones one week after stab injury (57); and therefore TNC may be involved in the late acute phase formation of astrogliosis around sites of injury and failed regeneration (55). However, in another mice study, TNC exerted protective effects after brain damage (57). The study demonstrated that extravasated immunoglobulin G was considerably prolonged and RNA levels of proinflammatory cytokines tumor necrosis factor (TNF)-α, interleukins (ILs)-1β and -6 were higher in the cerebral cortex after stab-wound injury in TNC-deficient mice: TNC production might promote BBB repair or maintain the BBB integrity by the reduction of inflammatory cytokine levels (57).

TNC induces MMPs, which seem to result in a positive TNC feedback loop *via* MMP-induced TNC cleavage (29). In addition, many stimuli, including various pro- and anti-inflammatory cytokines, GFs, hypoxia, reactive oxygen species, and mechanical stress, readily but transiently upregulate TNC within several hours in various pathological conditions such as myocarditis, arteriosclerosis, and cancer, irrespective of the location or type of causative insults (**Figure 3**) (29, 58). Clinically, TNC has been reported as a plasma biomarker of neurodegenerative diseases, as significantly elevated TNC levels were found in the peripheral blood of patients with Alzheimer's disease with mild cognitive impairments and in the amniotic fluid of pregnancies affected by Down syndrome (59–61). In addition, TNC expression is induced in the hippocampi of both epileptic rats and human patients with temporal lobe epilepsy (62–64). In the brains of patients with temporal lobe epilepsy, the regions exhibiting diffuse and elevated expression of TNC were characterized by an extended area of reactive gliosis and synaptic reorganization (42). Loss of TNC in transgenic CRND8 mice caused enhanced production of anti-inflammatory cytokines and decreased production of proinflammatory cytokines, associated with reduction of β- and γ-secretase activity, Aβ oligomerization, amyloid plaque load, and synaptic impairments (65). However, another study demonstrated that TNC may be involved in the maintenance of late acute phase astrogliosis surrounding the site of severe injuries, and exert anti-inflammatory and BBB-repairing effects (57). Thus, TNC induced by reactive astrocytes may play neuroprotective, neurotoxic or other diverse roles depending on the context, including regulation of astrocyte reactivity, BBB permeability, and potentiation of inflammatory processes (**Figure 2**). TNC may also directly affect neuronal plasticity and lead to memory impairments (42).

TNC in SAH

Many experimental studies as to TNC have been reported in SAH in rats and mice. Some have demonstrated that TNC is expressed in the walls of spastic cerebral arteries (endothelial, smooth muscle, adventitial, and periarterial inflammatory cells) and in brain parenchyma (astrocytes, neurons, and brain capillary endothelial cells), primarily in the surface of the cerebral cortex between 24 and 72 h after SAH by endovascular perforation (22, 37, 66–69). In a clinical setting, TNC levels in the cerebrospinal fluid (CSF) were below the diagnostic threshold level in patients with an unruptured cerebral aneurysm but markedly increased after cerebral aneurysmal rupture (70). Elevation of TNC expression may be affected by several factors, including elevated intracranial pressure as well as brain damage resulting from local or systemic inflammatory reactions (68, 71). A previous experimental study in rats showed that even cisternal saline injections caused elevated intracranial pressure and induced slight subarachnoid inflammatory reactions, which caused TNC upregulation in the basilar artery adventitia (68, 71). TNC is a key pathological factor that promotes activation of inflammatory cell infiltration in the periarterial space, causing EBI in terms of neuroinflammation, BBB disruption, and neuronal apoptosis; and also is involved in CVS and plays an important role in the development of DCI (**Figure 2**) (3–5, 20, 29, 37, 66, 72). Recent studies demonstrated that intracisternal injections of both intact or full-length TNC and recombinant TNC fragments containing the EGF-like repeats which activate EGF receptors

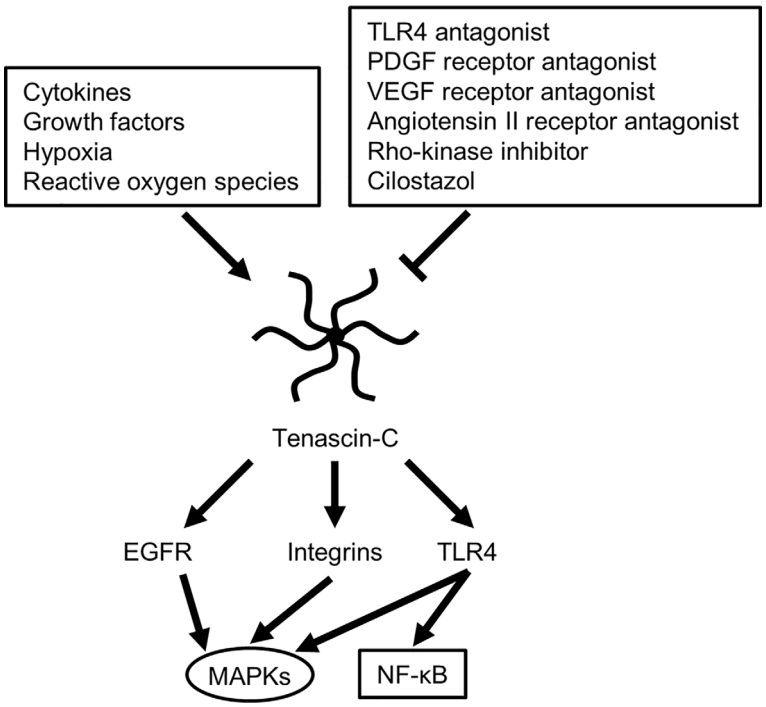

FIGURE 3 | Possible molecular mechanisms for regulating tenascin-C expression and downstream signaling cascade. EGFR, epidermal growth factor receptor; MAPKs, mitogen-activated protein kinases; NF-κB, nuclear factor-kappa B; PDGF, platelet-derived growth factor; TLR4, Toll-like receptor 4; VEGF, vascular endothelial growth factor.

activated mitogen-activated protein kinases (MAPKs) in arterial smooth muscle cells, causing prolonged CVS, but had no effects on neurobehavior, brain water content, and BBB integrity in normal healthy rats; however, in SAH rats, the TNC injections caused neurological impairments (3, 16, 22, 66, 72–77). In addition, TNC-induced activation of MAPKs is considered to upregulate MMP-9 in brain capillary endothelial cells and to cause BBB disruption in mice with SAH, although the mechanisms remain unidentified (29, 72, 73, 75, 77, 78). MAPK activation also results in a release of inflammatory mediators (18, 79). Human studies have repeatedly shown elevation of inflammatory mediators such as endothelin-1, TNF-α, and ILs-1β and -6 in CSF after SAH (37, 80–82). IL-1β induces TNC production *via* MAPK-dependent or -independent pathways, while TNC stimulates the synthesis of IL-1β (58, 77). This positive feedback mechanism upregulates TNC and the receptors in an early phase of SAH and may cause more activation of TNC signaling transduction and consequently further development or aggravation of EBI including neuronal apoptosis and BBB disruption, as well as prolonged CVS (**Figure 1**) (66, 69, 73). Post-SAH neuronal apoptosis develops through TNC-induced activation of p38 and ERK1/2 (20, 66), and the EGF-like repeats of TNC have been involved in apoptotic processes in cultured human smooth muscle cells (23). The blockage of TNC induction prevented post-SAH MAPK activation in the brain and suppressed EBI in terms of neuronal apoptosis and BBB disruption (22). Overexpression of ILs-1β and -6 itself is also known to cause apoptosis by triggering caspase cascade reactions (16).

Effects of TNC Knockout on Experimental SAH

Some studies using TNC-knockout mice have reported a relationship between TNC and EBI or CVS. In a filament perforation SAH model, TNC knockout did not change the total volume of SAH (22). However, TNC knockout alleviated neurological impairment and decreased brain water content and Evans blue dye extravasation, which were associated with inactivation of three major MAPKs (c-Jun N-terminal kinase [JNK], p38, and ERK1/2) in brain capillary endothelial cells in the cerebral cortex; and the MAPK inactivation resulted in inhibition of MMP-9 induction and retention of tight junction proteins such as zonula occludens (ZO)-1 (20, 22, 72, 83). In addition, TNC-knockout mice demonstrated prevention of CVS, which was associated with a reduction in periarterial inflammatory cells infiltration and MAPK inactivation in cerebral arterial smooth muscle cells as well as suppression of caspase-dependent neuronal apoptosis in the cerebral cortex with reduction or inactivation of TLR4, NF-κB, and ILs-1β and -6 (37, 50). TNC knockout also inhibited post-SAH upregulation of another MCP, periostin, in brain capillary endothelial cells and neurons (83). In a hepatic ischemia and reperfusion model, the protective effects of TNC knockout have been also shown in terms of a marked decrease in apoptotic hepatic cells *via* reduction of inflammatory cytokines and MMP-9 (77). Exogenous TNC treatment induced TLR4 and MMP-9 and aggravated EBI in wild-type SAH rats; and abolished the

protective effects through induction of TLR4 and MMP-9 in TNC-knockout SAH and transient hepatic ischemic models in mice (20, 22, 66, 73, 76).

TNC in Cerebral Aneurysm, Post-SAH Chronic Hydrocephalus, and Ischemic Stroke

TNC induced potent aneurysm repair through the fibrosis-promoting effects in a rat aneurysm model, possibly by recruiting macrophages, which secrete cytokines to induce migration and proliferation of smooth muscle cells (84). In contrast, the fibrosis-promoting effects of TNC may cause chronic hydrocephalus after SAH due to obstruction of circulation and reabsorption of CSF (70). Therefore, TNC induction may be protective if it is induced in the ruptured cerebral aneurysm wall but detrimental if it is induced in the brain, cerebral arteries, subarachnoid space, or CSF after SAH (22). However, no studies have investigated the role of TNC in cerebral aneurysmal genesis, growth, or rupture and the subsequent hemostasis. In addition, the effects of TNC on a ruptured cerebral aneurysm itself are unknown. Further studies are needed to clarify the role of TNC in intracranial aneurysm animal models (22).

In ischemic stroke in rats, treatment with neurotrophic factor L-serine upregulated TNC at 5 days post-ischemia and exerted neuroprotective effects by inducing the proliferation of neural stem cells and microvessels and the reconstruction of neurovascular units, resulting in neurorepair in the ischemic boundary zone (85). However, the mechanisms have not been investigated.

TLR4 Cascades and TNC in Stroke

TLRs are constituents of the innate immune system that are activated by DAMPs. At present, a total of 11 human and 13 murine TLRs have been identified (86). Since its discovery in 1998, TLR4 has been the most studied TLR family member (16, 87). TLR4 signaling is currently considered an important neuroinflammation therapeutic target because TLR4 has the unique ability to trigger two distinct signaling pathways (16, 71, 79, 86–88), the myeloid differentiation primary response protein 88 (MyD88)-dependent cascade in the acute phase and the Toll receptor-associated activator of interferon (TRIF)-dependent cascade in the late phase (86). TLR4 is expressed on the cell surface of various cells including microglia, neurons, astrocytes, brain capillary endothelial cells, endothelial and smooth muscle cells of the cerebral arteries, as well as peripheral blood cells including leukocytes, macrophages, and platelets (16, 86). TLR4 is activated by numerous DAMPs such as red blood cell breakdown products (heme, hemin, and methemoglobin), extravasated fibrinogen and fibrin, various intracellular components, and MCPs including TNC and galectin-3 (**Figure 3**) (16, 18). Activation of TLR4 induces the activation of the adaptor molecule MyD88 and subsequently the downstream signaling transcriptional factors NF-κB and activator protein (AP)-1. The process of AP-1 activation is primarily mediated by MAPKs including JNK, p38, and ERK1/2 (16, 79, 86, 89, 90). Both NF-κB and AP-1 upregulate MCPs including TNC, as well as proinflammatory cytokines or mediators such as TNF-α, IL-1β, -6, -8, and -12, intercellular adhesion molecule-1, monocyte chemoattractant protein, and MMP-9 (16, 20). These proinflammatory cytokines and mediators upregulate specific cell adhesion molecules on endothelial cells and induce neuroinflammation as well as the degradation of the inter-endothelial tight junctions and basal membrane in brain capillaries, which leads to BBB disruption and apoptosis of various cells, aggravating tissue damage after stroke (16, 20, 91). MMP-9 is a proinflammatory mediator induced by inflammatory cytokines and reactive oxygen species, and degrades components of the ECM of the cerebral microvessel basal lamina such as collagen IV, laminin, and fibronectin, as well as inter-endothelial tight junction proteins such as ZO-1, causing BBB disruption (92, 93). TNC amplifies the expression levels through positive feedback mechanisms utilizing the TLR4 signaling pathway, leading to further activation of the signaling transduction and the development or aggravation of secondary brain injury, as TNC itself is a ligand of TLR4 (16, 22). Experimental SAH studies have demonstrated that TNC induces CVS *via* activation of TLR4 and the downstream signaling MAPKs JNKs and p38 for more than 72 h in a rat cerebral artery, and that selective TLR4 antagonists LPS-RS and IAXO-102 inhibit TNC-induced CVS as well as expression of TLR4 in endothelial cells and smooth muscle cells of the arteries (**Figure 3**) (16, 17, 22, 73, 75, 76, 89). Therefore, targeting TLR4 is a potential therapeutic option against neuroinflammation after stroke. A recent study demonstrated that a selective TLR4 antagonist attenuated neurobehavioral impairments and prevented BBB disruption *via* suppression of the expression of MAPK JNK, MMP-9, MCPs such as TNC and periostin, as well as inflammatory mediators such as IL-6 and cyclooxygenase-1 in post-SAH mice (79, 89). TNC-knockout post-SAH mice showed less subarachnoid space infiltration of inflammatory cells in association with suppression of TLR4/NF-κB/IL-1β/IL-6 and the MMP-9 signaling pathway (37, 50, 67).

On the other hand, the late phase TRIF-dependent pathway in stroke induces interferon regulatory factor-3 as well as NF-κB and MAPKs, releasing interferon-β (86, 94). Interferon-β also modulates the innate immune response but exerts both anti-inflammatory and anti-apoptotic effects (94). The ligands of TLR4 interact with the receptor without distinction and induce the same downstream signaling pathways. However, the mechanisms to control the activation of respective pathways remains unclear (86).

TNC AS A CLINICAL BIOMARKER OF STROKE

In clinical settings of SAH, EBI is very difficult to be diagnosed precisely. Loss of consciousness at ictus, poor initial clinical grade, a large amount of SAH and/or intraventricular hematoma, presence of global cerebral edema, and inflammatory mediators have been generally used as surrogate markers of EBI (20).

However, these markers are neither objective nor specific to EBI (35). Highly specific biomarkers that reflect EBI and predict the development of DCI are needed to enable earlier diagnosis and treatment of EBI and DCI (67). The ideal biomarkers should be easily measured *via* simple methods and provide accurate and prompt results (95).

If TNC upregulation after stroke reflects secondary brain injury, blood and CSF TNC concentrations can be a candidate for biomarkers: both concentrations are easily measured using an enzyme-linked immunosorbent assay (35). Previous studies have shown that the level of TNC containing alternatively spliced B or C domains in both CSF and peripheral blood may be used as a diagnostic and prognostic biomarker of inflammation and tissue remodeling processes in several diseases such as cardiomyopathy, myocarditis, osteoarthritis, hepatitis, and tumor (58, 96–100).

In patients with SAH, higher plasma and CSF TNC levels may be associated with severe EBI, angiographic CVS, and DCI (22, 101). Plasma TNC level increases independent of serum levels of C-reactive protein and some proinflammatory cytokines (102). Clinically, the peripheral blood level of TNC isoforms containing a C domain in the alternatively spliced FN III repeats at 1 to 3 days from SAH onset could not predict the development of CVS (68). However, the plasma level peaked between 4 and 6 days from SAH onset and was significantly higher in patients who subsequently developed CVS (68). The plasma TNC level increased before 2.4 days of the development of CVS as determined by transcranial Doppler ultrasonography and before 3.6 days of the onset of symptomatic CVS (67, 68, 103). In intracerebral hemorrhage patients, a higher serum level of TNC containing a C domain in the FN III repeats at admission was associated with greater hematoma volume and worse initial neurological status. In addition, the elevation of TNC level was independently correlated with early neurological deterioration, hematoma growth, and worse clinical outcomes defined as modified Rankin scale score >2 at 90 days (104).

In contrast, the CSF level of TNC containing a C domain in the FN III repeats peaked within the first 3 days after SAH onset and correlated with worse neurological status and greater hematoma volume at admission; and additionally, it predicted the development of CVS and shunt-dependent chronic hydrocephalus as well as poorer functional outcomes (22, 35, 70, 101, 105, 106). The differences in the time course of TNC levels between the plasma and CSF may be because TNC in the CSF may be belatedly transferred to the plasma due to its large molecular weight, although the possibility that TNC is released by different cells between the CSF and the plasma cannot be excluded. Although the reason of different time course of peripheral blood and CSF TNC levels after SAH remains unexplained, the findings in previous studies suggest that severe hemorrhagic stroke may induce higher expressions of TNC and that both CSF and peripheral blood TNC levels could be used in predicting or diagnosing the development of CVS and DCI after SAH (20, 22, 35, 103, 107). At present, the most practical clinical application of TNC appears to be its use as a biomarker (67).

CONTRIBUTION OF OTHER MCPS TO REGULATING TNC EXPRESSION IN SAH-ASSOCIATED NEUROINFLAMMATION

Periostin

TNC directly binds to other MCPs periostin and galectin-3, and may regulate the expression levels of each other in stroke, playing diverse roles (29, 42, 54, 66, 101). Periostin is a multimodular N-glycoprotein (93 kDa) with a N-terminal cysteine-rich EMI domain, fourfold repeated fasciclin (FAS) 1 domains in the middle, and a hydrophilic C-terminal region (108). The C-terminal region interacts with other ECM proteins such as TNC, collagen, fibronectin, and heparin (15, 66, 72, 74, 107, 109–111). The FAS1 domain of periostin also directly binds to integrins (αvβ1, αvβ3, αvβ5, and α6β4) and TNC, exerting various functions (112–115). Periostin is secreted by stromal cells, which are stimulated by cytokines, transforming growth factor (TGF)-β, and other GFs which are produced in epithelial cells and other cells (112). In an experimental study, periostin was expressed in brain capillary endothelial cells and neurons in the cerebral cortex at 24 h after SAH induction (83). TNC and periostin may induce expression of each other, forming a positive feedback loop (67, 72, 83, 107, 108). MAPKs are both downstream and upstream of periostin, TNC, and IL-6; and thus activated MAPKs induce periostin, TNC, and IL-6, which in turn activate MAPKs, resulting in a positive feedback to cause and aggravate brain injury *via* various mechanisms including MMP-9 activation (54, 66, 72, 83, 107, 112). An experimental study using an endovascular perforation SAH model in mice reported that upregulated periostin enhanced the expression of TNC associated with activation of MAPKs p38 and ERK1/2 as well as MMP-9, resulting in ZO-1 degradation in brain capillary endothelial cells and the subsequent aggravation of BBB disruption (83). In addition, recombinant full-length periostin administration exacerbated post-SAH neurobehavioral impairments, brain edema, BBB disruption, and TNC induction in the post-SAH brain (83). In contrast, anti-periostin antibody prevented post-SAH neurobehavioral impairments, brain edema formation, and BBB disruption *via* downregulation of TNC, inactivation of p38, ERK1/2, and MMP-9, and the resultant retention of ZO-1 (83, 107). These findings suggest that full-length periostin strongly interacts with TNC and contributes to post-SAH BBB disruption and neurobehavioral impairments *via* the MAPK pathway, and that neutralizing full-length periostin may be an effective novel therapeutic strategy for EBI after SAH (107). TNC-knockout mice also showed the inhibition of periostin induction in the post-SAH brain and exhibited less neurobehavioral impairments (83). The interaction between periostin and TNC may play an important role in post-SAH EBI and provides a new insight for future researches (83).

Periostin also binds to integrins, leading to neuroinflammation and BBB disruption (108). In experimental SAH, the process is at least partly mediated by MAPK activation and upregulation of MMP-9 (108). However, periostin-integrin binding also induces neurogenesis *via* activation of the phosphoinositide 3-kinase

(PI3K)/Akt signaling pathway and upregulation of an anti-inflammatory cytokine TGF-β (18). The apparent discrepancy may be resolved by future studies to clarify how periostin relates with each integrin subtype in cerebrovascular diseases. In a clinical setting, a higher serum periostin level at admission was associated with worse initial neurological status, greater hemorrhage volume, more frequent development of DCI, and worse clinical outcomes in patients with aneurysmal SAH (116). In addition, plasma periostin levels increased before the development of DCI, irrespective of the presence or absence of CVS (108, 117). Therefore, periostin levels in the peripheral blood may be a predictive marker for post-SAH DCI, regardless of CVS development.

Galectin-3

Galectins are a family of MCPs comprised of more than 15 members of the β-galactoside-binding lectins and their conserved peptide sequence elements in the carbohydrate-recognition domains (CRDs) which show high affinities to β-galactoside-containing carbohydrate moieties of glycoconjugates (118). Galectins are classified into three types: proto-type (galectins-1, 2, 5, 7, 10, 11, 13–20), tandem-repeat-type (galectins-4, 6, 8, 9, 12), and chimera-type (galectin-3). Proto-type is comprised of monomers or homodimers with the sole CRD; tandem-repeat-type consists of N- and C- terminal distinct CRDs connected by a single-polypeptide-chain linker; and chimera-type has a C-terminal CRD and a N-terminal non-CRD domain which consists of proline- and glysine-rich short tandem repeats (118). The characteristics of chimera-type galectin-3 is to form a bridge between different ligands and to provide different functions (118). Recently, some studies exhibited that galectin-3 is activated through binding to TNC *via* its CRD domain (20, 118, 119). Activated galectin-3 possibly causes the development of brain injury including neuroinflammation after stroke (118–120). Galectin-3 induced by pro-inflammatory mediators contributed to brain immune responses *via* a major inflammatory signaling of Janus kinase/signal transducer and activation of transcription (STAT) and NF-κB pathways (121–123). In addition, galectin-3 is a ligand of TLR4 and activates its downstream signaling pathways as described above (18). In clinical settings, higher acute-stage plasma galectin-3 levels were associated with the development of DCI with no angiographic CVS after SAH (120). An experimental study showed that galectin-3 might cause post-SAH BBB disruption possibly by binding to TLR4 and activating ERK1/2, STAT-3, and MMP-9 (124).

Osteopontin

Osteopontin, another MCP, seems to have inhibitory effects against TNC in the setting of SAH (19). Osteopontin is an acidic phosphoglycoprotein (40–80 kDa) that contains several functional domains, allowing for integrin and CD44 receptor binding (15, 35). Osteopontin is subjected to numerous post-translational modifications including serine/threonine phosphorylation, glycosylation, tyrosine sulfation, and transglutamination, all of which regulate its functions (15). Five distinct isoforms are generated by alternative splicing (15). Thrombin and MMPs-2, -3, -7, -9, and -12 induce proteolytic cleavage of osteopontin (15). Osteopontin regulates homeostasis, angiogenesis, and immune responses through the upregulation in a variety of diverse cell types at the site of injury, stress, and inflammation (125). An intracellular form of osteopontin was expressed in dendritic cells and macrophages of the immune system in response to transient ischemic injury in the brain, and a secreted form of osteopontin promoted remodeling of the ECMs in the brain (15). After SAH induction, osteopontin binds to L-arginyl-glycyl-L-asparate (RGD)-dependent integrins and exerts neuroprotective effects by alleviating CVS and BBB disruption *via* induction of MAPK phosphatase-1, an endogenous MAPK inhibitor (22). Interestingly, both osteopontin and RGD-dependent integrin receptor antagonists significantly inhibited the vasoconstrictive effect by recombinant TNC fragments containing EGF-like repeats (20). The findings suggest that RGD-dependent integrins may be involved in CVS development, and that TNC binds to the integrins to develop CVS. Although the mechanisms of osteopontin's anti-TNC effects remain poorly understood in stroke, osteopontin and TNC share some receptors such as RGD-dependent integrins, and therefore at least partly competitive inhibition may be the mechanism (22). A novel multimodal nanoparticle, simultaneous multiple aptamers and RGD targeting, which combines triple affinity for nucleolin, RGD-containing integrins, and TNC, has been reported as a candidate for a targeted therapy against TNC (126): the nanoparticle would be well worth trying in SAH and other stroke types, considering the possible effects on both RGD-dependent integrins and TNC.

CONTRIBUTION OF GFS AND INTEGRINS TO REGULATING TNC EXPRESSION IN STROKE

The FN III domains 1–5, specifically domain 5 of TNC, have a high binding affinity for multiple GFs, such as platelet-derived GF (PDGF), vascular endothelial GF (VEGF), fibroblast GF (FGF) including FGF-2, and TGF-β1 as well as neurotrophin-3 (**Figure 1**) (27, 30, 54).

PDGF

PDGF is a homodimeric, non-glycosylated, polypeptide chain GF with a molecular weight of 28-35 kDa (127, 128). In SAH studies, PDGF is upstream of endogenous TNC and interrelated with TNC (66, 67, 69, 74). Exogenous TNC injections induce and activate PDGF receptors (PDGFRs) possibly *via* interreceptor interactions, which in turn upregulate TNC in the cerebral arteries and brain (66, 69). TNC may be further upregulated by a positive feedback on more PDGF activation *via* upregulated PDGFRs and crosstalk signaling between receptors, leading to more MAPK activation and consequent development of CVS, neuronal apoptosis, and neurological impairments in SAH rats (22). In rat SAH models, an intraperitoneal injection of imatinib mesylate, a tyrosine kinase inhibitor of PDGFR, showed the suppression of TNC induction and attenuated neurological impairments, the development of CVS and neuronal apoptosis

via inactivation of MAPKs such as JNK, p38, and ERK1/2 (22, 66, 69). In addition, a cisternal injection of recombinant TNC to imatinib mesylate-treated experimental SAH rats reactivated MAPKs to abolish the protective effects of imatinib mesylate on neuronal apoptosis and CVS, resulting in neurological aggravation (22, 66, 69). Thus, TNC downregulation was demonstrated to be involved in the neuroprotective effect mechanism of imatinib mesylate (72), and PDGFs and PDGFRs were suggested as a potential therapeutic target to regulate TNC expression and to prevent post-SAH EBI and CVS (**Figure 3**) (67).

VEGF

VEGF, a member of a family of secreted polypeptides with a highly conserved receptor-binding cystine-knot structure similar to that of the PDGF, is a homodimeric protein (34–46 kDa) that stimulates the formation of blood vessels (129). Although TNC regulates VEGF expression in tumors, no studies have reported if VEGF directly induces TNC (74, 130). In mice, VEGF enhances BBB permeability in normal brain as well as brain with inflammatory diseases (74). Neutralization of VEGF downregulated VEGF receptor-2, a major mediator of the kinase activity effects of VEGF, in association with suppression of TNC expression and MAPKs activation (69, 73, 131). Taken together, TNC may be involved in VEGF-induced BBB disruption in SAH (**Figure 3**) (72).

FGF-2

FGF-2 belongs to the FGF family and exhibits several isoforms with molecular weights ranging 18–34 kDa (132–135). FGF-2 is highly expressed in the brain and regulates a variety of cell functions including proliferation, morphogenesis, and suppression of apoptosis (27, 136, 137). FGF-2 is secreted by damaged neurons, and the synergistic action with TGF-β1, which is also upregulated in response to an injury, stimulates the expression of TNC (138). TNC binds to FGF-2 and promotes survival of oligodendrocyte precursor cells by enhancing FGF receptor-mediated signaling and blocking bone morphogenic protein signaling (139). A recent study showed that recombinant FGF-2 activated PI3K and Akt, leading to suppression of neuronal apoptosis after SAH (132). Thus, administration or augmentation of FGF-2 may be a promising therapy to reduce post-SAH neuronal apoptosis *via* activation of the FGF receptor/PI3K/Akt signaling pathway (132). However, the action of FGF-2 on TNC after stroke has not been investigated.

Integrins

Integrins are a superfamily of cell adhesion receptors that primarily recognize ECMs and cell-surface ligands, and are composed of α and β subunits that form 24 known combinations (140). Five members of the integrin family that recognize TNC as a ligand have been identified: isoforms α2β1, α8β1, α9β1, αvβ3, and αvβ6 (140, 141). All the integrins except for α9β1 bind to the FN III repeat sites of TNC, while α9β1 binds to the fibrinogen globe (20, 140). Integrin αvβ3 is expressed on endothelial cells and activates the downstream signaling that involves MAPKs, proinflammatory mediators such as ILs, and MMP-9; however, the role of the integrin αvβ3 signaling pathway in stroke has not been investigated (19, 37, 83, 106, 140, 142–145). Activated integrin αvβ3 induces internalization of ZO-1 and occludin, disrupts vascular endothelial-cadherin localization, and increases expression of MMP-9 (146). Therefore, activation of integrin αvβ3 may be involved in BBB disruption. In contrast, β1 integrins form laminin-binding, collagen-binding (α2β1), RGD-binding (α8β1), or ECMs-binding (α9β1) heterodimers (147–150). The β1 integrins are increased in cerebral blood vessels in ischemic cortex, and induce angiogenesis as well as leukocyte adhesion and migration following ischemic stroke (147, 151). In addition, increased β1 integrins in neuronal cells were associated with neuronal adhesion, and neurite outreach and regeneration (151). Thus, it has been demonstrated that β1 integrin signaling is required for neurovascular formation and recovery as well as endothelial cell migration, proliferation and blood vessel formation following transient ischemic stroke in mice (152). Therefore, β1 integrin may be a therapeutic target for ischemic stroke and other pathological conditions through modulating angiogenesis (152). On the other hand, α2 integrins have been reported to be associated with an increased risk for ischemic stroke (151). Activation of α2β1 integrin prevents endothelial cells from proliferating through binding to laminin (153). In addition, overexpression of integrin α2β1 was associated with ischemic stroke and myocardial infarction by clot formation, while its absence results in a prolonged bleeding time within safe limits (154). Therefore, inhibition of integrin α2β1 may be a potential therapy for ischemic stroke. The expression and the role of integrins α8β1, α9β1, and αvβ6 have not yet been elucidated following stroke (147). At present, it is unknown if integrins influence TNC expression.

OTHER THERAPEUTIC CANDIDATES FOR TNC-INDUCED BRAIN INJURY FOLLOWING STROKE

TNC expression can be reduced by several medications, including cilostazol, steroids, and non-steroidal anti-inflammatory drugs (NSAIDs) (**Figure 3**) (32, 103, 155). An *in vitro* study found that cilostazol, an anti-platelet and peripheral arterial vasodilating agent, is a selective inhibitor of phosphodiesterase type III with pleiotropic actions that include the inhibition of inflammatory reactions (18, 155). Blockage of phosphodiesterase type III can inhibit induction of TNC at the transcriptional level by activating the cyclic adenosine monophosphate–protein kinase A signaling pathway (103, 155). In patients with aneurysmal SAH, 300 mg/day cilostazol treatment almost completely suppressed the elevation of plasma levels of TNC variants containing alternatively spliced FN III B and C domains at days 1–12 after SAH onset, and prevented the development of DCI and chronic shunt-dependent hydrocephalus, resulting in improved clinical outcomes (103, 156). TNC is induced by inflammation, and TNC itself can

induce inflammatory reactions (58, 66, 157). Therefore, some anti-inflammatory medications are also associated with reduced TNC expression. For example, steroids and NSAIDs suppressed TNC expression in macrophages and human vascular smooth muscle cells *in vitro* and in arterial smooth muscle cells *in vivo* (32). With respect to inflammatory signaling, in a rat model of SAH, a MAPK JNK inhibitor SP600125 reversed the vasoconstrictive effects of TNC, and a MAPK p38 inhibitor SB203580 abolished TNC-induced TLR4 upregulation and TNC's vasoconstrictive effects (73).

Angiotensin II is a well-known potent inducer of TNC but the potential mechanisms have not been identified (158). Drugs that inhibit the effects of angiotensin II such as angiotensin II receptor blockers (ARBs) may block vascular TNC expression (159). In a model of carotid artery stent implantation in hypercholesterolemic rabbits, an ARB candesartan cilexetil prevented in-stent neointimal hyperplasia, which was associated with a decrease in macrophage infiltration and TNC expression in the arterial wall: the immunostaining study showed that TNC was induced in a limited area around the stent struts, but the expression disappeared by the ARB treatment (109). ARBs may suppress in-stent restenosis after carotid artery stenting *via* anti-inflammatory effects through TNC inhibition (109). Eplenerone, an aldosterone receptor antagonist, also inhibited the development of inflammation and fibrosis associated with reduced TNC expression in an angiotensin II-induced hypertension model in mice (160).

Inhibition of Rho-kinase also suppressed expression of TNC in smooth muscle cells in hypertensive rat pulmonary arteries (161). In a clinical setting, a Rho-kinase inhibitor hydroxyfasudil is commonly used to prevent CVS after SAH in Japan, although the levels of TNC have not been measured (20).

Currently, Neuradiab® (81C6 anti-TNC antibody; Bradmer Pharmaceuticals, Inc.) and double-stranded RNA directed against TNC have been reported as candidates for anti-TNC directed therapy (126). Further evidence would facilitate the development of therapeutic agents targeting TNC.

CONCLUSIONS

TNC potentially plays a key role in pathophysiological changes *via* neuroinflammation and appears to be a future therapeutic target in patients with stroke. However, the protective and detrimental roles of TNC with respect to each disease and the stage have not been completely unveiled. If TNC is set as a therapeutic molecular target, the therapeutic (time) window should also be addressed. Current evidence shows that TNC can be a biomarker to predict secondary injuries following stroke. Further studies to determine the underlying molecular mechanisms of TNC-induced pathophysiological changes and the regulation of TNC expression are warranted.

AUTHOR CONTRIBUTIONS

Both authors contributed equally to the planning, preparation, drafting, and writing of the article. All authors contributed to the article and approved the submitted version.

FUNDING

This work was funded by the Taiju Life Social Welfare Foundation (Grant Number, N/A) and the JSPS KAKENHI (Grant Number JP20K09346) to HS.

REFERENCES

1. Feigin VL, Norrving B, Mensah GA. Global Burden of Stroke. *Circ Res* (2017) 120:439–48. doi: 10.1161/CIRCRESAHA.116.308413
2. Benjamin EJ, Blaha MJ, Chiuve SE, Cushman M, Das SR, Deo R, et al. Heart Disease and Stroke Statistics—2017 Update: A Report From the American Heart Association. *Circulation* (2017) 135:e146–603. doi: 10.1161/CIR.0000000000000485
3. Miller BA, Turan N, Chau M, Pradilla G. Inflammation, vasospasm, and brain injury after subarachnoid hemorrhage. *BioMed Res Int* (2014) 2014:384342. doi: 10.1155/2014/384342
4. Provencio JJ. Inflammation in subarachnoid hemorrhage and delayed deterioration associated with vasospasm: a review. *Acta Neurochir Suppl* (2013) 115:233–8. doi: 10.1007/978-3-7091-1192-5_42
5. Carr KR, Zuckerman SL, Mocco J. Inflammation, Cerebral Vasospasm, and Evolving Theories of Delayed Cerebral Ischemia. *Neurol Res Int* (2013) 2013:1–12. doi: 10.1155/2013/506584
6. de Rooij NK, Linn FHH, van der Plas JA, Algra A, Rinkel GJE. Incidence of subarachnoid haemorrhage: a systematic review with emphasis on region, age, gender and time trends. *J Neurol Neurosurg Psychiatry* (2007) 78:1365–72. doi: 10.1136/jnnp.2007.117655
7. Moreth K, Iozzo RV, Schaefer L. Small leucine-rich proteoglycans orchestrate receptor crosstalk during inflammation. *Cell Cycle* (2012) 11:2084–91. doi: 10.4161/cc.20316
8. Shichita T, Ito M, Yoshimura A. Post-ischemic inflammation regulates neural damage and protection. *Front Cell Neurosci* (2014) 8:319. doi: 10.3389/fncel.2014.00319
9. Schaefer L. Complexity of danger: The diverse nature of damage-associated molecular patterns. *J Biol Chem* (2014) 289:35237–45. doi: 10.1074/jbc.R114.619304
10. Chaudhry SR, Hafez A, Jahromi BR, Kinfe TM, Lamprecht A, Niemelä M, et al. Role of damage associated molecular pattern molecules (DAMPs) in aneurysmal subarachnoid hemorrhage (aSAH). *Int J Mol Sci* (2018) 19:2035. doi: 10.3390/ijms19072035
11. Hayman EG, Wessell A, Gerzanich V, Sheth KN, Simard JM. Mechanisms of Global Cerebral Edema Formation in Aneurysmal Subarachnoid Hemorrhage. *Neurocrit Care* (2017) 26:301–10. doi: 10.1007/s12028-016-0354-7
12. Suzuki H. What is Early Brain Injury? *Transl Stroke Res* (2015) 6:1–3. doi: 10.1007/s12975-014-0380-8
13. Rowland MJ, Hadjipavlou G, Kelly M, Westbrook J, Pattinson KTS. Delayed cerebral ischaemia after subarachnoid haemorrhage: looking beyond vasospasm. *Br J Anaesth* (2012) 109:315–29. doi: 10.1093/bja/aes264
14. Tang D, Kang R, Coyne CB, Zeh HJ, Lotze MT. PAMPs and DAMPs: signals 0s taht spur autophagy and inmunity. *Immunol Rev* (2013) 249:158–75. doi: 10.1111/j.1600-065X.2012.01146.x.PAMPs
15. Kawakita F, Kanamaru H, Asada R, Suzuki H. Potential roles of matricellular proteins in stroke. *Exp Neurol* (2019) 322:113057. doi: 10.1016/j.expneurol.2019.113057

16. Okada T, Suzuki H. Toll-like receptor 4 as a possible therapeutic target for delayed brain injuries after aneurysmal subarachnoid hemorrhage. *Neural Regener Res* (2017) 12:193–6. doi: 10.4103/1673-5374.200795
17. Suzuki H, Shiba M, Fujimoto M, Kawamura K, Nanpei M, Tekeuchi E, et al. Matricellular Protein: A New Player in Cerebral Vasospasm Following Subarachnoid Hemorrhage. *Acta Neurochir Suppl* (2013) 115:213–8. doi: 10.1007/978-3-7091-1192-5_39
18. Okada T, Suzuki H. Mechanisms of neuroinflammation and inflammatory mediators involved in brain injury following subarachnoid hemorrhage. *Histol Histopathol* (2020) 35:18208. doi: 10.14670/HH-18-208
19. Suzuki H, Fujimoto M, Shiba M, Kawakita F, Liu L, Ichikawa N, et al. The Role of Matricellular Proteins in Brain Edema after Subarachnoid Hemorrhage. *Acta Neurochir Suppl* (2016) 121:151–6. doi: 10.1007/978-3-319-18497-5_27
20. Suzuki H, Fujimoto M, Kawakita F, Liu L, Nakatsuka Y, Nakano F, et al. Tenascin-C in brain injuries and edema after subarachnoid hemorrhage: Findings from basic and clinical studies. *J Neurosci Res* (2020) 98:42–56. doi: 10.1002/jnr.24330
21. Murphy-Ullrich JE, Sage EH. Revisiting the matricellular concept. *Matrix Biol* (2014) 37:1–14. doi: 10.1016/j.matbio.2014.07.005
22. Suzuki H, Kawakita F. Tenascin-C in aneurysmal subarachnoid hemorrhage: deleterious or protective? *Neural Regener Res* (2016) 11:230–1. doi: 10.4103/1673-5374.177721
23. Midwood KS, Chiquet M, Tucker RP, Orend G. Tenascin-C at a glance. *J Cell Sci* (2016) 129:4321–7. doi: 10.1242/jcs.190546
24. Roll L, Faissner A. Tenascins in CNS lesions. *Semin Cell Dev Biol* (2019) 89:118–24. doi: 10.1016/j.semcdb.2018.09.012
25. Erickson HP. Tenascin-C, tenascin-R and tenascin-X: a family of talented proteins in search of functions. *Curr Opin Cell Biol* (1993) 5:869–76. doi: 10.1016/0955-0674(93)90037-q
26. Rettig WJ, Triche TJ, Garin-Chesa P. Stimulation of human neuronectin secretion by brain-derived growth factors. *Brain Res* (1989) 487:171–7. doi: 10.1016/0006-8993(89)90954-2
27. De Laporte L, Rice JJ, Tortelli F, Hubbell JA. Tenascin C Promiscuously Binds Growth Factors via Its Fifth Fibronectin Type III-Like Domain. *PLoS One* (2013) 8:e62076. doi: 10.1371/journal.pone.0062076
28. Nishio T, Kawaguchi S, Iseda T, Kawasaki T, Hase T. Secretion of tenascin-C by cultured astrocytes: regulation of cell proliferation and process elongation. *Brain Res* (2003) 990:129–40. doi: 10.1016/s0006-8993(03)03448-6
29. Midwood KS, Orend G. The role of tenascin-C in tissue injury and tumorigenesis. *J Cell Commun Signal* (2009) 3:287–310. doi: 10.1007/s12079-009-0075-1
30. Reinhard J, Roll L, Faissner A. Tenascins in Retinal and Optic Nerve Neurodegeneration. *Front Integr Neurosci* (2017) 11:30. doi: 10.3389/fnint.2017.00030
31. Faissner A, Roll L, Theocharidis U. Tenascin-C in the matrisome of neural stem and progenitor cells. *Mol Cell Neurosci* (2017) 81:22–31. doi: 10.1016/j.mcn.2016.11.003
32. Golledge J, Clancy P, Maguire J, Lincz L, Koblar S. The role of tenascin C in cardiovascular disease. *Cardiovasc Res* (2011) 92:19–28. doi: 10.1093/cvr/cvr183
33. Giblin SP, Midwood KS. Tenascin-C: Form versus function. *Cell Adh Migr* (2015) 9:48–82. doi: 10.4161/19336918.2014.987587
34. Jayakumar AR, Apeksha A, Norenberg MD. Role of Matricellular Proteins in Disorders of the Central Nervous System. *Neurochem Res* (2017) 42:858–75. doi: 10.1007/s11064-016-2088-5
35. Suzuki H, Nishikawa H, Kawakita F. Matricellular proteins as possible biomarkers for early brain injury after aneurysmal subarachnoid hemorrhage. *Neural Regener Res* (2018) 13:1175–8. doi: 10.4103/1673-5374.235022
36. Wallner K, Li C, Shah PK, Wu K-J, Schwartz SM, Sharifi BG. EGF-Like Domain of Tenascin-C Is Proapoptotic for Cultured Smooth Muscle Cells. *Arterioscler Thromb Vasc Biol* (2004) 24:1416–21. doi: 10.1161/01.ATV.0000134299.89599.53
37. Fujimoto M, Shiba M, Kawakita F, Liu L, Shimojo N, Imanaka-Yoshida K, et al. Effects of Tenascin-C Knockout on Cerebral Vasospasm After Experimental Subarachnoid Hemorrhage in Mice. *Mol Neurobiol* (2018) 55:1951–8. doi: 10.1007/s12035-017-0466-x
38. Keilhauer G, Faissner A, Schachner M. Differential inhibition of neurone-neurone, neurone-astrocyte and astrocyte-astrocyte adhesion by L1, L2 and N-CAM antibodies. *Nature* (1985) 316:728–30. doi: 10.1038/316728a0
39. Kruse J, Keilhauer G, Faissner A, Timpl R, Schachner M. The J1 glycoprotein–a novel nervous system cell adhesion molecule of the L2/HNK-1 family. *Nature* (1985) 316:146–8. doi: 10.1038/316146a0
40. Meiners S, Powell EM, Geller HM. A distinct subset of tenascin/CS-6-PG-rich astrocytes restricts neuronal growth in vitro. *J Neurosci* (1995) 15:8096–108. doi: 10.1523/JNEUROSCI.15-12-08096.1995
41. Powell EM, Geller HM. Dissection of astrocyte-mediated cues in neuronal guidance and process extension. *Glia* (1999) 26:73–83. doi: 10.1002/(sici)1098-1136(199903)26:1<73::aid-glia8>3.0.co;2-s
42. Jones EV, Bouvier DS. Astrocyte-secreted matricellular proteins in CNS remodelling during development and disease. *Neural Plast* (2014) 2014:321209. doi: 10.1155/2014/321209
43. Faissner A, Kruse J. J1/tenascin is a repulsive substrate for central nervous system neurons. *Neuron* (1990) 5:627–37. doi: 10.1016/0896-6273(90)90217-4
44. Andrews MR, Czvitkovich S, Dassie E, Vogelaar CF, Faissner A, Blits B, et al. Alpha9 integrin promotes neurite outgrowth on tenascin-C and enhances sensory axon regeneration. *J Neurosci* (2009) 29:5546–57. doi: 10.1523/JNEUROSCI.0759-09.2009
45. Meiners S, Powell EM, Geller HM. Neurite outgrowth promotion by the alternatively spliced region of tenascin-C is influenced by cell-type specific binding. *Matrix Biol* (1999) 18:75–87. doi: 10.1016/s0945-053x(98)00008-0
46. Rigato F, Garwood J, Calco V, Heck N, Faivre-Sarrailh C, Faissner A. Tenascin-C Promotes Neurite Outgrowth of Embryonic Hippocampal Neurons through the Alternatively Spliced Fibronectin Type III BD Domains via Activation of the Cell Adhesion Molecule F3/Contactin. *J Neurosci* (2002) 22:6596–609. doi: 10.1523/JNEUROSCI.22-15-06596.2002
47. Song I, Dityatev A. Crosstalk between glia, extracellular matrix and neurons. *Brain Res Bull* (2018) 136:101–8. doi: 10.1016/j.brainresbull.2017.03.003
48. Karus M, Denecke B, Ffrench-Constant C, Wiese S, Faissner A. The extracellular matrix molecule tenascin C modulates expression levels and territories of key patterning genes during spinal cord astrocyte specification. *Development* (2011) 138:5321–31. doi: 10.1242/dev.067413
49. Strekalova T, Sun M, Sibbe M, Evers M, Dityatev A, Gass P, et al. Fibronectin domains of extracellular matrix molecule tenascin-C modulate hippocampal learning and synaptic plasticity. *Mol Cell Neurosci* (2002) 21:173–87. doi: 10.1006/mcne.2002.1172
50. Liu L, Fujimoto M, Nakano F, Nishikawa H, Okada T, Kawakita F, et al. Deficiency of Tenascin-C Alleviates Neuronal Apoptosis and Neuroinflammation After Experimental Subarachnoid Hemorrhage in Mice. *Mol Neurobiol* (2018) 55:8346–54. doi: 10.1007/s12035-018-1006-z
51. Udalova IA, Ruhmann M, Thomson SJP, Midwood KS. Expression and immune function of tenascin-C. *Crit Rev Immunol* (2011) 31:115–45. doi: 10.1615/critrevimmunol.v31.i2.30
52. González-González L, Alonso J. Periostin: A matricellular protein with multiple functions in cancer development and progression. *Front Oncol* (2018) 8:225. doi: 10.3389/fonc.2018.00225
53. Tavazoie SF, Alarcón C, Oskarsson T, Padua D, Wang Q, Bos PD, et al. Endogenous human microRNAs that suppress breast cancer metastasis. *Nature* (2008) 451:147–52. doi: 10.1038/nature06487
54. Tucker RP, Chiquet-Ehrismann R. The regulation of tenascin expression by tissue microenvironments. *Biochim Biophys Acta* (2009) 1793:888–92. doi: 10.1016/j.bbamcr.2008.12.012
55. Laywell ED, Dörries U, Bartsch U, Faissner A, Schachner M, Steindler DA. Enhanced expression of the developmentally regulated extracellular matrix molecule tenascin following adult brain injury. *Proc Natl Acad Sci U S A* (1992) 89:2634–8. doi: 10.1073/pnas.89.7.2634
56. Nishio T, Kawaguchi S, Yamamoto M, Iseda T, Kawasaki T, Hase T. Tenascin-C regulates proliferation and migration of cultured astrocytes in a scratch wound assay. *Neuroscience* (2005) 132:87–102. doi: 10.1016/j.neuroscience.2004.12.028
57. Ikeshima-Kataoka H, Shen J-S, Eto Y, Saito S, Yuasa S. Alteration of inflammatory cytokine production in the injured central nervous system of tenascin-deficient mice. *In Vivo (Brooklyn)* (2008) 22:409–13.

58. Chiquet-Ehrismann R, Chiquet M. Tenascins: regulation and putative functions during pathological stress. *J Pathol* (2003) 200:488–99. doi: 10.1002/path.1415
59. Soares HD, Potter WZ, Pickering E, Kuhn M, Immermann FW, Shera DM, et al. Plasma biomarkers associated with the apolipoprotein E genotype and Alzheimer disease. *Arch Neurol* (2012) 69:1310–7. doi: 10.1001/archneurol.2012.1070
60. Hall JR, Johnson LA, Barber RC, Vo HT, Winter AS, O'Bryant SE. Texas Alzheimer's Research and Care Consortium. Biomarkers of basic activities of daily living in Alzheimer's disease. *J Alzheimers Dis* (2012) 31:429–37. doi: 10.3233/JAD-2012-111481
61. Cho C-KJ, Smith CR, Diamandis EP. Amniotic fluid proteome analysis from Down syndrome pregnancies for biomarker discovery. *J Proteome Res* (2010) 9:3574–82. doi: 10.1021/pr100088k
62. Becker AJ, Chen J, Zien A, Sochivko D, Normann S, Schramm J, et al. Correlated stage- and subfield-associated hippocampal gene expression patterns in experimental and human temporal lobe epilepsy. *Eur J Neurosci* (2003) 18:2792–802. doi: 10.1111/j.1460-9568.2003.02993.x
63. Niquet J, Jorquera I, Faissner A, Ben-Ari Y, Represa A. Gliosis and axonal sprouting in the hippocampus of epileptic rats are associated with an increase of tenascin-C immunoreactivity. *J Neurocytol* (1995) 24:611–24. doi: 10.1007/BF01257376
64. Scheffler B, Faissner A, Beck H, Behle K, Wolf HK, Wiestler OD, et al. Hippocampal loss of tenascin boundaries in Ammon's horn sclerosis. *Glia* (1997) 19:35–46. doi: 10.1002/(SICI)1098-1136(199701)19:1<35::AID-GLIA4>3.0.CO;2-9
65. Xie K, Liu Y, Hao W, Walter S, Penke B, Hartmann T, et al. Tenascin-C deficiency ameliorates Alzheimer's disease-related pathology in mice. *Neurobiol Aging* (2013) 34:2389–98. doi: 10.1016/j.neurobiolaging.2013.04.013
66. Shiba M, Fujimoto M, Imanaka-Yoshida K, Yoshida T, Taki W, Suzuki H. Tenascin-C causes neuronal apoptosis after subarachnoid hemorrhage in rats. *Transl Stroke Res* (2014) 5:238–47. doi: 10.1007/s12975-014-0333-2
67. Shiba M, Suzuki H. Lessons from tenascin-C knockout mice and potential clinical application to subarachnoid hemorrhage. *Neural Regener Res* (2019) 14:262–4. doi: 10.4103/1673-5374.244789
68. Suzuki H, Kanamaru K, Suzuki Y, Aimi Y, Matsubara N, Araki T, et al. Tenascin-C is induced in cerebral vasospasm after subarachnoid hemorrhage in rats and humans: a pilot study. *Neurol Res* (2010) 32:179–84. doi: 10.1179/174313208X355495
69. Shiba M, Suzuki H, Fujimoto M, Shimojo N, Imanaka-Yoshida K, Yoshida T, et al. Imatinib mesylate prevents cerebral vasospasm after subarachnoid hemorrhage via inhibiting tenascin-C expression in rats. *Neurobiol Dis* (2012) 46:172–9. doi: 10.1016/j.nbd.2012.01.005
70. Suzuki H, Kinoshita N, Imanaka-Yoshida K, Yoshida T, Taki W. Cerebrospinal fluid tenascin-C increases preceding the development of chronic shunt-dependent hydrocephalus after subarachnoid hemorrhage. *Stroke* (2008) 39:1610–2. doi: 10.1161/STROKEAHA.107.505735
71. Suzuki H, Fujimoto M, Kawakita F, Liu L, Nakano F, Nishikawa H, et al. Toll-Like Receptor 4 and Tenascin-C Signaling in Cerebral Vasospasm and Brain Injuries After Subarachnoid Hemorrhage. *Acta Neurochir Suppl* (2020) 127:91–6. doi: 10.1007/978-3-030-04615-6_15
72. Fujimoto M, Shiba M, Kawakita F, Liu L, Shimojo N, Imanaka-Yoshida K, et al. Deficiency of tenascin-C and attenuation of blood-brain barrier disruption following experimental subarachnoid hemorrhage in mice. *J Neurosurg* (2016) 124:1693–702. doi: 10.3171/2015.4.JNS15484
73. Fujimoto M, Suzuki H, Shiba M, Shimojo N, Imanaka-Yoshida K, Yoshida T, et al. Tenascin-C induces prolonged constriction of cerebral arteries in rats. *Neurobiol Dis* (2013) 55:104–9. doi: 10.1016/j.nbd.2013.01.007
74. Liu L, Fujimoto M, Kawakita F, Nakano F, Imanaka-Yoshida K, Yoshida T, et al. Anti-Vascular Endothelial Growth Factor Treatment Suppresses Early Brain Injury After Subarachnoid Hemorrhage in Mice. *Mol Neurobiol* (2016) 53:4529–38. doi: 10.1007/s12035-015-9386-9
75. Fujimoto M, Shiba M, Kawakita F, Shimojo N, Imanaka-Yoshida K, Yoshida T, et al. Vasoconstrictive effect of tenascin-C on cerebral arteries in rats. *Acta Neurochir Suppl* (2015) 120:99–103. doi: 10.1007/978-3-319-04981-6_17
76. Fujimoto M, Shiba M, Kawakita F, Liu L, Nakasaki A, Shimojo N, et al. Epidermal growth factor-like repeats of tenascin-C-induced constriction of cerebral arteries via activation of epidermal growth factor receptors in rats. *Brain Res* (2016) 1642:436–44. doi: 10.1016/j.brainres.2016.04.034
77. Kuriyama N, Duarte S, Hamada T, Busuttil RW, Coito AJ. Tenascin-C: a novel mediator of hepatic ischemia and reperfusion injury. *Hepatology* (2011) 54:2125–36. doi: 10.1002/hep.24639
78. Cho A, Graves J, Reidy MA. Mitogen-activated protein kinases mediate matrix metalloproteinase-9 expression in vascular smooth muscle cells. *Arterioscler Thromb Vasc Biol* (2000) 20:2527–32. doi: 10.1161/01.atv.20.12.2527
79. Okada T, Kawakita F, Nishikawa H, Nakano F, Liu L, Suzuki H. Selective Toll-Like Receptor 4 Antagonists Prevent Acute Blood-Brain Barrier Disruption After Subarachnoid Hemorrhage in Mice. *Mol Neurobiol* (2018) 56:1–10. doi: 10.1007/s12035-018-1145-2
80. Suzuki K, Meguro K, Sakurai T, Saitoh Y, Takeuchi S, Nose T. Endothelin-1 concentration increases in the cerebrospinal fluid in cerebral vasospasm caused by subarachnoid hemorrhage. *Surg Neurol* (2000) 53:131–5. doi: 10.1016/s0090-3019(99)00179-2
81. Mathiesen T, Edner G, Ulfarsson E, Andersson B. Cerebrospinal fluid interleukin-1 receptor antagonist and tumor necrosis factor—α following subarachnoid hemorrhage. *J Neurosurg* (1997) 87:215–20. doi: 10.3171/jns.1997.87.2.0215
82. Hendryk S, Jarzab B, Josko J. Increase of the IL-1 beta and IL-6 levels in CSF in patients with vasospasm following aneurysmal SAH. *Neuro Endocrinol Lett* (2003) 25:141–7.
83. Liu L, Kawakita F, Fujimoto M, Nakano F, Imanaka-Yoshida K, Yoshida T, et al. Role of Periostin in Early Brain Injury After Subarachnoid Hemorrhage in Mice. *Stroke* (2017) 48:1108–11. doi: 10.1161/STROKEAHA.117.016629
84. Hamada K, Miura Y, Toma N, Miyamoto K, Imanaka-Yoshida K, Matsushima S, et al. Gellan sulfate core platinum coil with tenascin-C promotes intra-aneurysmal organization in rats. *Transl Stroke Res* (2014) 5:595–603. doi: 10.1007/s12975-014-0352-z
85. Sun L, Qiang R, Yang Y, Jiang Z-L, Wang G-H, Zhao G-W, et al. L-Serine Treatment May Improve Neurorestoration of Rats after Permanent Focal Cerebral Ischemia Potentially Through Improvement of Neurorepair. *PLoS One* (2014) 9:e93405. doi: 10.1371/journal.pone.0093405
86. Buchanan MM, Hutchinson M, Watkins LR, Yin H. Toll-like receptor 4 in CNS pathologies. *J Neurochem* (2010) 114:13–27. doi: 10.1111/j.1471-4159.2010.06736.x
87. Poltorak A, He X, Smirnova I, Liu MY, Van Huffel C, Du X, et al. Defective LPS Signaling in C3H/HeJ and C57BL/10ScCr Mice: Mutations in Tlr4 Gene. *Science (80-)* (1998) 282:2085–8. doi: 10.1126/science.282.5396.2085
88. Liu L, Suzuki H. "The Role of Matricellular Proteins in Experimental Subarachnoid Hemorrhage-Induced Early Brain Injury". In: *Cell Mol Approaches to Regen Repair*. Heidelberg, Germany: Springer (2018). p. 397–407. doi: 10.1007/978-3-319-66679-2_20
89. Kawakita F, Fujimoto M, Liu L, Nakano F, Nakatsuka Y, Suzuki H. Effects of Toll-Like Receptor 4 Antagonists Against Cerebral Vasospasm After Experimental Subarachnoid Hemorrhage in Mice. *Mol Neurobiol* (2017) 54:6624–33. doi: 10.1007/s12035-016-0178-7
90. Fang H, Wang P-F, Zhou Y, Wang Y-C, Yang Q-W. Toll-like receptor 4 signaling in intracerebral hemorrhage-induced inflammation and injury. *J Neuroinflammation* (2013) 10:27. doi: 10.1186/1742-2094-10-27
91. Kanamaru H, Suzuki H. Potential therapeutic molecular targets for blood-brain barrier disruption after subarachnoid hemorrhage. *Neural Regener Res* (2019) 14:1138–43. doi: 10.4103/1673-5374.251190
92. Peeyush Kumar T, McBride DW, Dash PK, Matsumura K, Rubi A, Blackburn SL. Endothelial Cell Dysfunction and Injury in Subarachnoid Hemorrhage. *Mol Neurobiol* (2018) 56:1992–2006. doi: 10.1007/s12035-018-1213-7
93. Guo Z, Sun X, He Z, Jiang Y, Zhang X, Zhang JH. Matrix metalloproteinase-9 potentiates early brain injury after subarachnoid hemorrhage. *Neurol Res* (2010) 32:715–20. doi: 10.1179/016164109X12478302362491
94. Akira S, Takeda K. Toll-like receptor signalling. *Nat Rev Immunol* (2004) 4:499–511. doi: 10.1038/nri1391
95. Li W, Pan R, Qi Z, Liu KJ. Current progress in searching for clinically useful biomarkers of blood-brain barrier damage following cerebral ischemia. *Brain Circ* (2018) 4:145–52. doi: 10.4103/bc.bc_11_18
96. Aso N, Tamura A, Nasu M. Circulating tenascin-C levels in patients with idiopathic dilated cardiomyopathy. *Am J Cardiol* (2004) 94:1468–70. doi: 10.1016/j.amjcard.2004.07.156

97. Hasegawa M, Hirata H, Sudo A, Kato K, Kawase D, Kinoshita N, et al. Tenascin-C concentration in synovial fluid correlates with radiographic progression of knee osteoarthritis. *J Rheumatol* (2004) 31:2021–6.
98. Imanaka-Yoshida K, Hiroe M, Yasutomi Y, Toyozaki T, Tsuchiya T, Noda N, et al. Tenascin-C is a useful marker for disease activity in myocarditis. *J Pathol* (2002) 197:388–94. doi: 10.1002/path.1131
99. Tanaka H, El-Karef A, Kaito M, Kinoshita N, Fujita N, Horiike S, et al. Circulating level of large splice variants of tenascin-C is a marker of piecemeal necrosis activity in patients with chronic hepatitis C. *Liver Int* (2006) 26:311–8. doi: 10.1111/j.1478-3231.2005.01229.x
100. Yoshida J, Wakabayashi T, Okamoto S, Kimura S, Washizu K, Kiyosawa K, et al. Tenascin in cerebrospinal fluid is a useful biomarker for the diagnosis of brain tumour. *J Neurol Neurosurg Psychiatry* (1994) 57:1212–5. doi: 10.1136/jnnp.57.10.1212
101. Suzuki H, Kanamaru K, Shiba M, Fujimoto M, Kawakita F, Imanaka-Yoshida K, et al. Tenascin-C is a possible mediator between initial brain injury and vasospasm-related and -unrelated delayed cerebral ischemia after aneurysmal subarachnoid hemorrhage. *Acta Neurochir Suppl* (2015) 120:117–21. doi: 10.1007/978-3-319-04981-6_20
102. López-Sánchez M, Muñoz-Esquerre M, Huertas D, Montes A, Molina-Molina M, Manresa F, et al. Inflammatory markers and circulating extracellular matrix proteins in patients with chronic obstructive pulmonary disease and left ventricular diastolic dysfunction. *Clin Respir J* (2017) 11:859–66. doi: 10.1111/crj.12428
103. Suzuki H, Nakatsuka Y, Yasuda R, Shiba M, Miura Y, Terashima M, et al. Dose-Dependent Inhibitory Effects of Cilostazol on Delayed Cerebral Infarction After Aneurysmal Subarachnoid Hemorrhage. *Transl Stroke Res* (2019) 10:381–8. doi: 10.1007/s12975-018-0650-y
104. Wang L-G, Huangfu X-Q, Tao B, Zhong G-J, Le Z-D. Serum tenascin-C predicts severity and outcome of acute intracerebral hemorrhage. *Clin Chim Acta* (2018) 481:69–74. doi: 10.1016/j.cca.2018.02.033
105. Suzuki H, Kanamaru K, Shiba M, Fujimoto M, Imanaka-Yoshida K, Yoshida T, et al. Cerebrospinal fluid tenascin-C in cerebral vasospasm after aneurysmal subarachnoid hemorrhage. *J Neurosurg Anesthesiol* (2011) 23:310–7. doi: 10.1097/ANA.0b013e31822aa1f2
106. Suzuki H, Hasegawa Y, Kanamaru K, Zhang JH. Mechanisms of osteopontin-induced stabilization of blood-brain barrier disruption after subarachnoid hemorrhage in rats. *Stroke* (2010) 41:1783–90. doi: 10.1161/STROKEAHA.110.586537
107. Nishikawa H, Suzuki H. Implications of periostin in the development of subarachnoid hemorrhage-induced brain injuries. *Neural Regener Res* (2017) 12:1982. doi: 10.4103/1673-5374.221150
108. Kawakita F, Suzuki H. Periostin in cerebrovascular disease. *Neural Regener Res* (2020) 15:63. doi: 10.4103/1673-5374.264456
109. Ichikawa N, Toma N, Kawakita F, Matsushima S, Imanaka-Yoshida K, Yoshida T, et al. Angiotensin II type 1 receptor blockers suppress neointimal hyperplasia after stent implantation in carotid arteries of hypercholesterolemic rabbits. *Neurol Res* (2015) 37:147–52. doi: 10.1179/1743132814Y.0000000436
110. Kii I, Nishiyama T, Li M, Matsumoto K, Saito M, Amizuka N, et al. Incorporation of Tenascin-C into the Extracellular Matrix by Periostin Underlies an Extracellular Meshwork Architecture. *J Biol Chem* (2010) 285:2028–39. doi: 10.1074/jbc.M109.051961
111. Norris RA, Moreno-Rodriguez RA, Sugi Y, Hoffman S, Amos J, Hart MM, et al. Periostin regulates atrioventricular valve maturation. *Dev Biol* (2008) 316:200–13. doi: 10.1016/j.ydbio.2008.01.003
112. Liu AY, Zheng H, Ouyang G. Periostin, a multifunctional matricellular protein in inflammatory and tumor microenvironments. *Matrix Biol* (2014) 37:150–6. doi: 10.1016/j.matbio.2014.04.007
113. Kudo A. Introductory review: periostin—gene and protein structure. *Cell Mol Life Sci* (2017) 74:4259–68. doi: 10.1007/s00018-017-2643-5
114. Horiuchi K, Amizuka N, Takeshita S, Takamatsu H, Katsuura M, Ozawa H, et al. Identification and Characterization of a Novel Protein, Periostin, with Restricted Expression to Periosteum and Periodontal Ligament and Increased Expression by Transforming Growth Factor β. *J Bone Miner Res* (1999) 14:1239–49. doi: 10.1359/jbmr.1999.14.7.1239
115. Bonnet N, Garnero P, Ferrari S. Periostin action in bone. *Mol Cell Endocrinol* (2016) 432:75–82. doi: 10.1016/j.mce.2015.12.014
116. Luo W, Wang H, Hu J. Increased concentration of serum periostin is associated with poor outcome of patients with aneurysmal subarachnoid hemorrhage. *J Clin Lab Anal* (2018) 32:e22389. doi: 10.1002/jcla.22389
117. Kanamaru H, Kawakita F, Nakano F, Miura Y, Shiba M, Yasuda R, et al. Plasma Periostin and Delayed Cerebral Ischemia After Aneurysmal Subarachnoid Hemorrhage. *Neurotherapeutics* (2019) 16:480–90. doi: 10.1007/s13311-018-00707-y
118. Nishikawa H, Suzuki H. Possible Role of Inflammation and Galectin-3 in Brain Injury after Subarachnoid Hemorrhage. *Brain Sci* (2018) 8:30. doi: 10.3390/brainsci8020030
119. Yang R-Y, Rabinovich GA, Liu F-T. Galectins: structure, function and therapeutic potential. *Expert Rev Mol Med* (2008) 10:e17. doi: 10.1017/S1462399408000719
120. Nishikawa H, Nakatsuka Y, Shiba M, Kawakita F, Fujimoto M, Suzuki H. Increased Plasma Galectin-3 Preceding the Development of Delayed Cerebral Infarction and Eventual Poor Outcome in Non-Severe Aneurysmal Subarachnoid Hemorrhage. *Transl Stroke Res* (2018) 9:110–9. doi: 10.1007/s12975-017-0564-0
121. Yip PK, Carrillo-Jimenez A, King P, Vilalta A, Nomura K, Chau CC, et al. Galectin-3 released in response to traumatic brain injury acts as an alarmin orchestrating brain immune response and promoting neurodegeneration. *Sci Rep* (2017) 7:41689. doi: 10.1038/srep41689
122. Venkatraman A, Hardas S, Patel N, Singh Bajaj N, Arora G, Arora P. Galectin-3: an emerging biomarker in stroke and cerebrovascular diseases. *Eur J Neurol* (2018) 25:238–46. doi: 10.1111/ene.13496
123. Shin T. The pleiotropic effects of galectin-3 in neuroinflammation: a review. *Acta Histochem* (2013) 115:407–11. doi: 10.1016/j.acthis.2012.11.010
124. Nishikawa H, Liu L, Nakano F, Kawakita F, Kanamaru H, Nakatsuka Y, et al. Modified citrus pectin prevents blood-brain barrier disruption in mouse Subarachnoid hemorrhage by inhibiting Galectin-3. *Stroke* (2018) 49:2743–51. doi: 10.1161/STROKEAHA.118.021757
125. Rogall R, Rabenstein M, Vay S, Bach A, Pikhovych A, Baermann J, et al. Bioluminescence imaging visualizes osteopontin-induced neurogenesis and neuroblast migration in the mouse brain after stroke. *Stem Cell Res Ther* (2018) 9:182. doi: 10.1186/s13287-018-0927-9
126. Midwood KS, Hussenet T, Langlois B, Orend G. Advances in tenascin-C biology. *Cell Mol Life Sci* (2011) 68:3175–99. doi: 10.1007/s00018-011-0783-6
127. Heldin C-H, Westermark B. Mechanism of Action and In Vivo Role of Platelet-Derived Growth Factor. *Physiol Rev* (1999) 79:1283–316. doi: 10.1152/physrev.1999.79.4.1283
128. Ying H-Z, Chen Q, Zhang W-Y, Zhang H-H, Ma Y, Zhang S-Z, et al. PDGF signaling pathway in hepatic fibrosis pathogenesis and therapeutics. *Mol Med Rep* (2017) 16:7879–89. doi: 10.3892/mmr.2017.7641
129. Thomas KA. Vascular endothelial growth factor, a potent and selective angiogenic agent. *J Biol Chem* (1996) 271:603–6. doi: 10.1074/jbc.271.2.603
130. Tanaka K, Hiraiwa N, Hashimoto H, Yamazaki Y, Kusakabe M. Tenascin-C regulates angiogenesis in tumor through the regulation of vascular endothelial growth factor expression. *Int J Cancer* (2004) 108:31–40. doi: 10.1002/ijc.11509
131. Li W, Lu Z-F, Man X-Y, Li C-M, Zhou J, Chen J-Q, et al. VEGF upregulates VEGF receptor-2 on human outer root sheath cells and stimulates proliferation through ERK pathway. *Mol Biol Rep* (2012) 39:8687–94. doi: 10.1007/s11033-012-1725-6
132. Okada T, Enkhjargal B, Travis ZD, Ocak U, Tang J, Suzuki H, et al. FGF-2 Attenuates Neuronal Apoptosis via FGFR3/PI3k/Akt Signaling Pathway After Subarachnoid Hemorrhage. *Mol Neurobiol* (2019) 56:8203–19. doi: 10.1007/s12035-019-01668-9
133. Sørensen V, Nilsen T, Wiedłocha A. Functional diversity of FGF-2 isoforms by intracellular sorting. *BioEssays* (2006) 28:504–14. doi: 10.1002/bies.20405
134. Kardami E, Jiang Z-S, Jimenez SK, Hirst CJ, Sheikh F, Zahradka P, et al. Fibroblast growth factor 2 isoforms and cardiac hypertrophy. *Cardiovasc Res* (2004) 63:458–66. doi: 10.1016/j.cardiores.2004.04.024
135. Nugent MA, Iozzo RV. Fibroblast growth factor-2. *Int J Biochem Cell Biol* (2000) 32:115–20. doi: 10.1016/S1357-2725(99)00123-5
136. Noda M, Takii K, Parajuli B, Kawanokuchi J, Sonobe Y, Takeuchi H, et al. FGF-2 released from degenerating neurons exerts microglial-induced

neuroprotection via FGFR3-ERK signaling pathway. *J Neuroinflammation* (2014) 11:1–11. doi: 10.1186/1742-2094-11-76
137. Wang Z, Zhang H, Xu X, Shi H, Yu X, Wang X, et al. BFGF inhibits ER stress induced by ischemic oxidative injury via activation of the PI3K/Akt and ERK1/2 pathways. *Toxicol Lett* (2012) 212:137–46. doi: 10.1016/j.toxlet.2012.05.006
138. Smith GM, Hale JH. Macrophage/Microglia Regulation of Astrocytic Tenascin: Synergistic Action of Transforming Growth Factor-β and Basic Fibroblast Growth Factor. *J Neurosci* (1997) 17:9624–33. doi: 10.1523/JNEUROSCI.17-24-09624.1997
139. Garcion E, Halilagic A, Faissner A, Ffrench-Constant C. Generation of an environmental niche for neural stem cell development bythe extracellular matrix molecule tenascin C. *Development* (2004) 131:3423–32. doi: 10.1242/dev.01202
140. Takada Y, Ye X, Simon S. The integrins. *Genome Biol* (2007) 8:215. doi: 10.1186/gb-2007-8-5-215
141. Tucker RP, Chiquet-Ehrismann R. Tenascin-C: Its functions as an integrin ligand. *Int J Biochem Cell Biol* (2015) 65:165–8. doi: 10.1016/j.biocel.2015.06.003
142. Soung YH, Clifford JL, Chung J. Crosstalk between integrin and receptor tyrosine kinase signaling in breast carcinoma progression. *BMB Rep* (2010) 43:311–8. doi: 10.5483/BMBRep.2010.43.5.311
143. Chong HC, Tan CK, Huang R-L, Tan NS. Matricellular proteins: a sticky affair with cancers. *J Oncol* (2012) 2012:351089. doi: 10.1155/2012/351089
144. Rivera LB, Bradshaw AD, Brekken RA. The regulatory function of SPARC in vascular biology. *Cell Mol Life Sci* (2011) 68:3165–73. doi: 10.1007/s00018-011-0781-8
145. Smyth SS, Patterson C. Tiny dancers: The integrin-growth factor nexus in angiogenic signaling. *J Cell Biol* (2002) 158:17–21. doi: 10.1083/jcb.200202100
146. Edwards DN, Bix GJ. Roles of blood-brain barrier integrins and extracellular matrix in stroke. *Am J Physiol Physiol* (2019) 316:C252–63. doi: 10.1152/ajpcell.00151.2018
147. Edwards DN, Bix GJ. The Inflammatory Response After Ischemic Stroke: Targeting β2 and β1 Integrins. *Front Neurosci* (2019) 13:540. doi: 10.3389/fnins.2019.00540
148. Caimi G, Canino B, Ferrara F, Montana M, Musso M, Porretto F, et al. Granulocyte integrins before and after activation in acute ischaemic stroke. *J Neurol Sci* (2001) 186:23–6. doi: 10.1016/s0022-510x(01)00495-6
149. Campanero MR, Sánchez-Mateos P, del Pozo MA, Sánchez-Madrid F. ICAM-3 regulates lymphocyte morphology and integrin-mediated T cell interaction with endothelial cell and extracellular matrix ligands. *J Cell Biol* (1994) 127:867–78. doi: 10.1083/jcb.127.3.867
150. Hynes RO. Integrins: bidirectional, allosteric signaling machines. *Cell* (2002) 110:673–87. doi: 10.1016/s0092-8674(02)00971-6
151. Wu X, Reddy DS. Integrins as receptor targets for neurological disorders. *Pharmacol Ther* (2012) 134:68–81. doi: 10.1016/j.pharmthera.2011.12.008
152. Lathia JD, Chigurupati S, Thundyil J, Selvaraj PK, Mughal MR, Woodruff TM, et al. Pivotal role for beta-1 integrin in neurovascular remodelling after ischemic stroke. *Exp Neurol* (2010) 221:107–14. doi: 10.1016/j.expneurol.2009.10.007
153. Mettouchi A, Klein S, Guo W, Lopez-Lago M, Lemichez E, Westwick JK, et al. Integrin-specific activation of Rac controls progression through the G (1) phase of the cell cycle. *Mol Cell* (2001) 8:115–27. doi: 10.1016/s1097-2765(01)00285-4
154. Miller MW, Basra S, Kulp DW, Billings PC, Choi S, Beavers MP, et al. Small-molecule inhibitors of integrin α 2 β 1 that prevent pathological thrombus formation via an allosteric mechanism. *Proc Natl Acad Sci* (2009) 106:719–24. doi: 10.1073/pnas.0811622106
155. Fujinaga K, Onoda K, Yamamoto K, Imanaka-Yoshida K, Takao M, Shimono T, et al. Locally applied cilostazol suppresses neointimal hyperplasia by inhibiting tenascin-C synthesis and smooth muscle cell proliferation in free artery grafts. *J Thorac Cardiovasc Surg* (2004) 128:357–63. doi: 10.1016/j.jtcvs.2003.11.015
156. Nakatsuka Y, Kawakita F, Yasuda R, Umeda Y, Toma N, Sakaida H, et al. Preventive effects of cilostazol against the development of shunt-dependent hydrocephalus after subarachnoid hemorrhage. *J Neurosurg* (2017) 127:319–26. doi: 10.3171/2016.5.JNS152907
157. Ma S, Yang D, Li D, Tang B, Sun M, Yang Y. Cardiac extracellular matrix tenascin-C deposition during fibronectin degradation. *Biochem Biophys Res Commun* (2011) 409:321–7. doi: 10.1016/j.bbrc.2011.05.013
158. Sharifi BG, LaFleur DW, Pirola CJ, Forrester JS, Fagin JA. Angiotensin II regulates tenascin gene expression in vascular smooth muscle cells. *J Biol Chem* (1992) 267:23910–5.
159. Fischer JW. Tenascin-C: A key molecule in graft stenosis. *Cardiovasc Res* (2007) 74:335–6. doi: 10.1016/j.cardiores.2007.04.001
160. Nishioka T, Suzuki M, Onishi K, Takakura N, Inada H, Yoshida T, et al. Eplerenone Attenuates Myocardial Fibrosis in the Angiotensin II-Induced Hypertensive Mouse: Involvement of Tenascin-C Induced by Aldosterone-Mediated Inflammation. *J Cardiovasc Pharmacol* (2007) 49:261–8. doi: 10.1097/FJC.0b013e318033dfd4
161. Chapados R, Abe K, Ihida-Stansbury K, McKean D, Gates AT, Kern M, et al. ROCK controls matrix synthesis in vascular smooth muscle cells: coupling vasoconstriction to vascular remodeling. *Circ Res* (2006) 99:837–44. doi: 10.1161/01.RES.0000246172.77441.f1

Conflict of Interest: The authors declare that the research was conducted in the absence of any commercial or financial relationships that could be construed as a potential conflict of interest.

frontiers in Immunology

ORIGINAL RESEARCH
published: 22 January 2021
doi: 10.3389/fimmu.2020.608223

Pivotal Role of Tenascin-W (-N) in Postnatal Incisor Growth and Periodontal Ligament Remodeling

Thomas Imhof[1,2], Anamaria Balic[3], Juliane Heilig[2,4], Ruth Chiquet-Ehrismann[5†], Matthias Chiquet[6], Anja Niehoff[4,7], Bent Brachvogel[2,8], Irma Thesleff[3] and Manuel Koch[1,2,9]*

[1] Faculty of Medicine and University Hospital Cologne, Institute for Dental Research and Oral Musculoskeletal Biology, University of Cologne, Cologne, Germany, [2] Center for Biochemistry, Faculty of Medicine and University Hospital Cologne, University of Cologne, Cologne, Germany, [3] Institute of Biotechnology, HiLIFE, University of Helsinki, Helsinki, Finland, [4] Cologne Center for Musculoskeletal Biomechanics, Faculty of Medicine and University Hospital Cologne, University of Cologne, Cologne, Germany, [5] Friedrich Miescher Institute for Biomedical Research, Novartis Res. Foundation, Basel, Switzerland, [6] Department of Orthodontics and Dentofacial Orthopedics, School of Dental Medicine, University of Bern, Bern, Switzerland, [7] Institute of Biomechanics and Orthopaedics, German Sport University Cologne, Cologne, Germany, [8] Department of Pediatrics and Adolescent Medicine, Experimental Neonatology, Faculty of Medicine and University Hospital Cologne, University of Cologne, Cologne, Germany, [9] Center for Molecular Medicine Cologne (CMMC), University of Cologne, Cologne, Germany

OPEN ACCESS

Edited by:
Kim Midwood, University of Oxford, United Kingdom

Reviewed by:
Richard P. Tucker, University of California, Davis, United States
Alicia Wong, University of Oxford, United Kingdom

***Correspondence:**
Manuel Koch
Manuel.Koch@uni-koeln.de

[†]*Deceased*

Specialty section:
This article was submitted to Inflammation, a section of the journal Frontiers in Immunology

Received: *19 September 2020*
Accepted: *07 December 2020*
Published: *22 January 2021*

Citation:
Imhof T, Balic A, Heilig J, Chiquet-Ehrismann R, Chiquet M, Niehoff A, Brachvogel B, Thesleff I and Koch M (2021) Pivotal Role of Tenascin-W (-N) in Postnatal Incisor Growth and Periodontal Ligament Remodeling. Front. Immunol. 11:608223. doi: 10.3389/fimmu.2020.608223

The continuously growing mouse incisor provides a fascinating model for studying stem cell regulation and organ renewal. In the incisor, epithelial and mesenchymal stem cells assure lifelong tooth growth. The epithelial stem cells reside in a niche known as the cervical loop. Mesenchymal stem cells are located in the nearby apical neurovascular bundle and in the neural plexus. So far, little is known about extracellular cues that are controlling incisor stem cell renewal and guidance. The extracellular matrix protein tenascin-W, also known as tenascin-N (TNN), is expressed in the mesenchyme of the pulp and of the periodontal ligament of the incisor, and is closely associated with collagen 3 fibers. Here, we report for the first time the phenotype of tenascin-W/TNN deficient mice, which in a C57BL/6N background exhibit a reduced body weight and lifespan. We found major defects in the alveolar bone and periodontal ligament of the growing rodent incisors, whereas molars were not affected. The alveolar bone around the incisor was replaced by a dense scar-like connective tissue, enriched with newly formed nerve fibers likely leading to periodontal pain, less food intake and reduced body weight. Using soft food to reduce mechanical load on the incisor partially rescued the phenotype. *In situ* hybridization and Gli1 reporter mouse experiments revealed decreased hedgehog signaling in the incisor mesenchymal stem cell compartment, which coordinates the development of mesenchymal stem cell niche. These results indicate that TNN deficiency in mice affects periodontal remodeling and increases nerve fiber branching. Through periodontal pain the food intake is reduced and the incisor renewal and the neurovascular sonic hedgehog secretion rate are reduced. In conclusion, tenascin-W/TNN seems to have a primary function in rapid periodontal tissue remodeling and a secondary function in mechanosensation.

Keywords: tenascin-W, tenascin-N, bone, remodeling, periodontal ligament, pain, tenascin

INTRODUCTION

Rodent incisors, unlike human teeth, grow continuously throughout life. In young animals the entire length of the lower incisor renews every month (1). The incisor tip self-sharpens due to the asymmetrical distribution of the enamel, which covers only the labial surface of the tooth enabling abrasion of the softer dentin on the lingual surface resulting in a sharp labial enamel edge. Though the lower incisors are only visible at the most ventral aspect of the mandible, within the jaw itself the incisors occupy almost the entire length of the body of the mandible (**Figure 1A**). In the dorsal mandible, epithelial and mesenchymal stem cells reside in the incisor and they provide a continuous supply of hard tissue forming cells. The epithelial stem cell niche is morphologically clearly defined; it is localized in a loop-shaped ending of the epithelial layer called cervical loop (**Figure 1B**). Cervical loop is composed of outer and inner epithelia, which enclose loosely arranged stellate reticulum cells, including stem cells. The epithelial stem cells differentiate into enamel secreting ameloblasts. On the other hand, dentin is produced by odontoblasts, which derive from the incisor specific mesenchymal stem cells (MSCs) just recently discovered (2–4). Lineage tracing experiments showed that Schwann cell precursors, which express Sox10 and PLP1, generate a major population of dentin producing odontoblasts (3). A second, vasculature associated mesenchymal stem cell population includes slowly dividing population expressing Gli1, as well as aSMA and NG2 expressing cells (2, 4, 5). Gli1 expressing population is regulated by Hedgehog signaling which is transduced through two Hedgehog ligands; Shh and Dhh (4, 6). Proliferation and differentiation of tooth stem cells is directed toward the tip of the tooth and is controlled through epithelial-mesenchymal crosstalk (7). In recent years it became clear that extracellular matrix proteins have a key role in controlling the organization of cell compartments: they provide cell attachment sites, form barriers, present growth factors and control the mechanical properties of the tissue (8). Each tissue has an unique composition and topology of its extracellular matrix (9). The structure and function of enamel and dentin matrix proteins such as ameloblastin, amelogenin, dentin matrix protein, and dentin sialophosphoprotein are well studied. However, the microenvironmental factors that control pulp stem cell fate are less well known. In this context, tenascins are highly interesting as they are expressed in embryonic mesenchyme and stem cell niches (10). Tenascins are large multifunctional proteins, which have a common domain structure: an N-terminal assembly domain, epidermal growth factor (EGF)—like repeats, fibronectin type III domains, and a C-terminal fibrinogen-like globular domain. In mammals four tenascins are expressed: Tenascin-C, -R, -W/(-N), and –X. One well known function of tenascins is their ability to modulate cell adhesion and migration *in vitro* (11). Tenascin-C and -R bind to neural cell adhesion receptors and co-receptors such as contactin (12, 13), syndecan (14), and integrins (11). Tenascin-C is expressed in the central nervous system and in embryonic connective tissues. Mice deficient for tenascin-C were originally reported to develop normally (15), but more recently behavioral phenotypes and abnormal central nervous system development were described (16). The expression of tenascin-R is limited to the central nervous system (17) and the knockout mice show cognitive defects, reduced coordination and increased anxiety (18). In contrast, tenascin-X is widely expressed in loose connective tissues (19), and tenascin-X deficient mice show an Ehlers-Danlos syndrome-like phenotype with altered fibrillar collagen density and hyperextensible skin (20).

Tenascin-W, also known as tenascin-N, is widely expressed during embryonal development (21), but in adult mammals its expression is mainly restricted to the periodontal ligament (22), periosteum (21), and stem cell niches (10). In cancer, TNN expression is strongly induced and for breast cancer a role in migration and metastasis has been proposed (23, 24). *In vitro* experiments show that tenascin-W/TNN promotes migration of several cell types, including breast cancer cells, osteoblasts, and endothelial cells (23, 25, 26). Hence, TNN may play an important

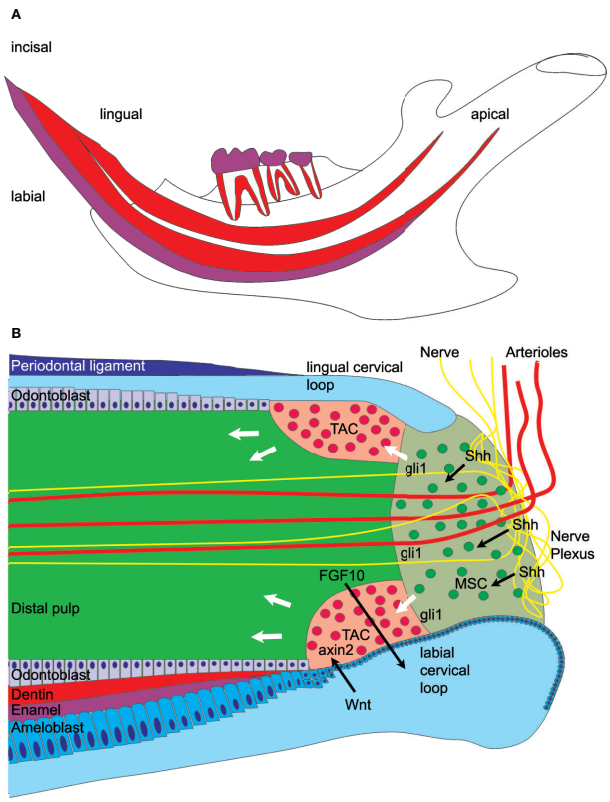

FIGURE 1 | Graphical overview of the mandibular incisor anatomy. **(A)** A large fraction of the mouse incisor is embedded in the mandible. Enamel covers (magenta) only the labial surface of the tooth. Mesenchymal stem cells (MSC) and epithelial stem cells are found in the dorsal mandible. **(B)** Mesenchymal stem cells are regulated by sonic hedgehog (Shh) released from the neurovascular bundle and express Gli1, which is a hedgehog signaling effector. Those stem cells eventually proliferate in the transient amplifying cell (TAC) zone and are regulated by epithelial-derived Wnt. Axin2, a signaling molecule from the Wnt pathway, is a marker for those highly proliferative cells. The mesenchymal TAC cells then differentiate into odontoblasts and form dentin or are differentiating into pulp stroma cells. The epithelial stem cells are found in the labial cervical loop and they differentiate into ameloblasts and form enamel.

role in cell migration and differentiation in the continuously growing incisor tooth.

In this study, we have analyzed the role of tenascin-W/TNN using a global tenascin-W/TNN deficient mouse. This first analysis of tenascin-W/TNN deficient animals showed that tenascin-W/TNN has a function in incisor periodontal ligament remodeling, in incisor eruption and in tooth renewal. Tenascin-W/TNN deficient mice show under hard pellet diet weight loss and reduced food uptake.

MATERIALS AND METHODS

Mouse Model

For the generation of tenascin-W/TNN knockout mice, the construct $Tnn^{tm1a(KOMP)Wtsi}$ was purchased from the KOMP consortium. The mice were generated and the neo-cassette has been removed by crossing with a CMV-Cre mouse line. Heterozygous mice were backcrossed 12 times with C57BL/6N wildtype animals in a specific-pathogen-free animal facility. Genotyping was performed by PCR with the following primers: TNN(-/-) fw: 5′ ttcactgcattctagttgtgg 3′, TNN(-/-) rev: 5′ caggaagatcgaggatctggc 3′, TNN WT fw: 5′ catactcccatgcacacttcc 3′, TNN WT rev: 5′ ctttgcctctagaagtatggacc 3′. The animals were fed with γ-irradiated pellet or powder form diet (1310-recipe, Altromin) and wooden gnaw sticks were placed in all cages. Gli1CreER^{T2} x R26mTmG x TNN(-/-) mice were generated by crossing heterozygous Gli1CreER^{T2} mice (27), heterozygous R26mTmG mice (28), and TNN(-/-) and control mice without neo-cassette. Genotyping was performed by PCR. For Gli1CreER^{T2} the primers fw: 5′ acctgaagatgttcgcgattatct 3′, rev: 5′ accgtcagtacgtgagatatctt 3′; and for R26mTmG the primers fw: 5′ gtgagcaagggcgaggagctg 3′, rev: 5′ ttacttgtacagctcgtccatgc 3′ were used. TNN(-/-) and WT animals of both sexes were sacrificed by cervical dislocation (1mt, 3mt, 6mt, and 12mt) or decapitation (P0 and P7 old mice). 3 month old Gli1CreER^{T2} x R26mTmG x TNN(-/-) and Gli1CreER^{T2} x R26mTmG x control mice of both sexes (mice, n = 6) were treated twice every 24 h per i.p. injection with 10 mg of tamoxifen (T5648, Sigma) dissolved in corn oil (C8267, Sigma). The lineage traced animals were sacrificed by cervical dislocation 72 h after the first injection. All experimental procedures were approved by the State Office of North-Rhine Westfalia (AZ 84-02.04.2015.A454 and AZ 81-02.04.2018.A367).

Histology

Hematoxylin-eosin (H&E) stainings, detection of endogenous alkaline phosphatase and Sirius red stainings were performed on 5 µm thick paraffin sections (mice, n = 6) as previously described (29, 30). For immunofluorescence staining tissues were dissected from animals (mice, n = 6), fixed with 4% paraformaldehyde (PFA) in PBS at 4°C overnight. After extensive washes in PBS, the samples were decalcified with 10% EDTA for 14 days under constant agitation, and with daily changes of the decalcification solution. The decalcified samples were then washed with PBS for at least 4 h, infiltrated with 30% sucrose/PBS, and embedded in OCT Compound (TissueTek, Sakura). From each animal (mice, n = 6) a comparable section was chosen for individual staining. Due the small size of this tissue, often only one perfect cryosection per mandible was obtained. Cryosections (40 µm) were permeabilized with 0.3% Triton/PBS for 2 h and blocked with 10% normal goat or donkey serum overnight at 4°C. Primary antibodies were diluted in 1% BSA/0.1% Tween/PBS and applied to the sections for 30 h at 4°C. They were: Tuj1 (ab18207, 1:1000, Abcam), CD31 (1 µg/ml, polyclonal from rabbit, own production), collagen 3 (1330-01, 1:400, Southern Biotech), Ki67 (ab16667, 1:500, Abcam), Sox10 (sc-17342, 1:500, Santa Cruz), ameloblastin (Ambn) (1 µg/ml, polyclonal from rabbit, own production), tenascin-W/TNN [1 µg/ml, polyclonal from rabbit (21)], GFP (SP3005P 3 µg/ml, Origene), and smooth muscle actin (C6198, 1:500, Sigma). Alexa dye conjugated secondary goat or donkey antibodies (Thermo Fisher Scientific) were used to detect the specific binding. Confocal images were obtained on a Leica SP8 microscope, using a 25x water objective or a 20x air objective. The images were processed with ImageJ 1.51r software (31) and brightness and contrast were adjusted.

In Situ Hybridization

Radioactive *in situ* hybridization was done on 5 µm sagittal sections (32). ^{35}S (Amersham)-labeled RNA probes were used to detect the expression of Sonic hedgehog (*Shh*), Dentin Sialophosphoprotein (*Dspp*), Ameloblastin (*Ambn*), *Axin2*, Fibroblast growth factor 10 (*Fgf10*) (33) and *Gli1* (mice, n = 3).

Micro-Computed Tomography

Micro-computed tomography (µCT) was performed using a µCT 35 Scanner (Scanco Medical). Complete mandibular bones (mice, n = 6) were scanned with an isotropic voxel size of 12 µm using 70 kVp tube voltage, 114 µA tube current, 400 ms integration time, segmentation support of 1, and a sigma correction of 0.8. For the enamel reconstruction of 6 and 12 month old mice a threshold of 27% for dentin and 60% for enamel was chosen. In 1 month old animals the threshold for dentin was selected at 23% for dentin and 60% for enamel, respectively.

Flow Cytometry

Isolated pulp tissue from 1 month old mice (mice, n = 6) was digested with 2 mg Collagenase type 1 (Worthington) and 4 mg Dispase II (Roche) in DMEM/F12 10% FCS for 1h at 37°C and constant rotation. The cells were pelleted at 2000 rpm (400g) for 5 min, resuspended in FACS staining buffer (5% FCS in PBS), incubated with the following prediluted antibodies at 1:100: CD45.2, Sca-1, CD90.2 (all Biolegend), and stained with Sytox Blue (Thermo Fisher Scientific). Data were collected on a FACScanto instrument (BD Biosciences) and analyzed using FlowJo software (TreeStar).

Statistics

The data are shown as mean ± SD. Statistical analysis was performed using GraphPad Prism 5 software. Two-tailed, paired *t*-test was used for experiments involving two groups; p values lower than 0.05 were considered significant.

RESULTS

First, we analyzed the expression of tenascin-W/TNN in the incisor pulp mesenchyme during tooth development, using immunofluorescence. The expression started at the bell stage of tooth development, marked by ameloblast and odontoblast differentiation (34) (**Supplementary Figures 1A, B**). Tenascin-W/TNN is mainly found in the distal part of the dental papilla and colocalizes with thick spiral fibers (**Figure 2A**), while it is not detected in the apical part. Co-immunostainings showed that the tenascin-W/TNN labeled fibers contain collagen 3 (**Figures 2B, B′, B′′**). In newborn mice, tenascin-W/TNN specific immunostaining is concentrated in the area of pre-odontoblasts and mature odontoblasts (**Supplementary Figure 1C**). In adult mice, only a weak signal for tenascin-W/TNN is persistent in the distal pulp (**Figure 2C**); in contrast however tenascin-W/TNN is strongly expressed in the periodontal ligament of incisors and molars (**Figures 2C, D**).

To study the *in vivo* function of tenascin-W/TNN, we generated a global tenascin-W/TNN knockout mouse line. These mice are vital and fertile, but show an increased death rate and stress intolerance. Otherwise, tenascin-W/TNN mice develop and grow normally, with the exception of visible enamel defects in the upper incisors at 12 months (**Figures 3A, B**). To determine whether the lower incisors are affected as well, we analyzed lower jaws by micro-computed tomography (μCT). There were no obvious macroscopic differences in 1 month old animals, but 6 and 12 month old tenascin-W/TNN deficient mice showed a flattening of the incisor tip, suggesting a defect in abrasion and self-sharpening and/or altered occlusion. In addition, the mandibular bone is fenestrated in 12 month old TNN(-/-) mice in the area of the apical region of the incisor (**Figures 3C, D**, upper panel, gray arrow). By 3D reconstruction of the opaque enamel (**Figures 3C, D**, lower panel), we could observe that in tenascin-W/TNN deficient animals the enamel mineralization is shifted to the apical part of the incisor. Furthermore the apical enamel layer of 6 and 12 month old TNN(-/-) animals is fragmented (**Figures 3C, D**, lower panel).

μCT of lower incisors on the height of the first molar showed that the width of the dentin was increased in 1 month old TNN (-/-) animals (**Figures 4A, D**, asterisk), and in 6 and 12 month old animals the pulp space was completely obliterated (**Figures 4B, E** and **C, F**, asterisk). In addition, the periodontal space of the 6 and 12 month old tenascin-W/TNN knockout incisors was much wider (**Figures 4B, E**, and **C, F** arrow), while it was unchanged in the first molars (**Figures 4B, E**, and **C, F**). Histological analyses has shown a dense connective tissue of the periodontal ligament within a wider periodontal space of the mutant incisors (**Figures 4G, H**, pdl). Immunofluorescence stainings for nerve fibers (Tuj1), perivascular smooth muscle cells (smooth muscle actin), and endothelial cells (CD31) revealed that blood vessels and nerve fibers disappear in the distal pulp of tenascin-W/TNN knockout mice and that there is major loss in cellularity (**Figures 4I, J, I′, J′**). Furthermore, we have found a thick nerve fiber network within the periodontal ligament (**Figures 4I, J, I′′, J′′**).

The absence of tenascin-W/TNN expression at the level of the first molar in month old TNN-/- incisors (**Supplementary Figure 1E**) indicates that the changes in dentin thickness observed at this stage must be due to a secondary effect. Next, we analyzed the morphology of the stem cell niches and no morphological changes were observed in 1 month old mice (**Figure 5A**). In 3 month old TNN(-/-) mice both the dentin and enamel formation have increased and the enamel epithelium contains cyst-like structures (**Figure 5B**). Immunohistochemical staining for ameloblastin revealed that those epithelial inclusions are composed of enamel matrix (**Figure 5B**). Next, we analyzed the position of pre-ameloblasts and mature ameloblasts, and of odontoblasts in lower incisors. In 1 month old TNN(-/-) mice dentin sialophosphoprotein (*Dspp*), sonic hedgehog (*Shh*), and ameloblastin (*Ambn*) were expressed normally as determined by *in situ* hybridization. In 3 month old mice the differentiation of both ameloblasts (*Ambn* probe) and odontoblasts (*Dspp* probe) was shifted to the apex (**Supplementary Figure 2**). Stainings for endogenous alkaline phosphatase further confirmed this shift in differentiation (**Supplementary Figure 5**), and revealed that alkaline phosphatase activity is high in 1 year old TNN(-/-) mice (**Supplementary Figure 3**).

These findings indicate either a defect in growth factor signaling or a reduced number of stem cells in TNN-deficient incisors. We therefore performed *in situ* hybridizations with *Axin2*, *Fgf10*, and *Gli1* probes (**Supplementary Figure 4**). Expression of *Axin2*, a target and negative regulator of Wnt signaling, was chosen to analyze Wnt pathway activity, which controls dentin formation. FGF10 is produced in the pulp mesenchyme and maintains epithelial stem cells. Gli1 is a transcription factor that is expressed at sites of highly active hedgehog signaling (27). We found that tenascin-W/TNN deficiency leads to reduced expression of these three factors, indicating compromised Wnt, FGF, and hedgehog signaling in the region of the mesenchymal stem cell niche of the incisors, or, alternatively, loss of specific cell stem cell populations.

We next performed lineage tracing experiments in Gli1CreER^{T2} x R26mTmG x TNN(-/-) and Gli1CreER^{T2} x R26mTmG control mice. 72 hour chase experiments showed that the pulp mesenchyme of 3 month old tenascin-W/TNN knockout mice contained only few Gli1 expressing GFP positive cells (**Figures 6A, B**) compared to controls. Ki67 immunostainings showed that the proliferation rate of putative mesenchymal stem cells was reduced in the incisors of 3 month old TNN(-/-) mice (**Figures 6C, D**).

These findings led to the question whether the mesenchymal stem cell themselves were affected or not. To resolve this issue, we performed a flow cytometry analysis of isolated apical pulp cells with CD45.2 [a general immune cell marker (35)], CD90.2 (Thy1) [a marker for immune cells and incisor mesenchymal progenitor cells (3)], and Sca1 [a general stem and progenitor cell marker (36)] antibodies. CD45.2 was used to subtract the CD45.2/CD90.2 double positive immune cells, as described in Balic and Mina (37). This experiment showed no differences in the number of CD90.2 or Sca1 positive progenitor cells in 1 month old control or knockout animals (**Supplementary Figure 5**).

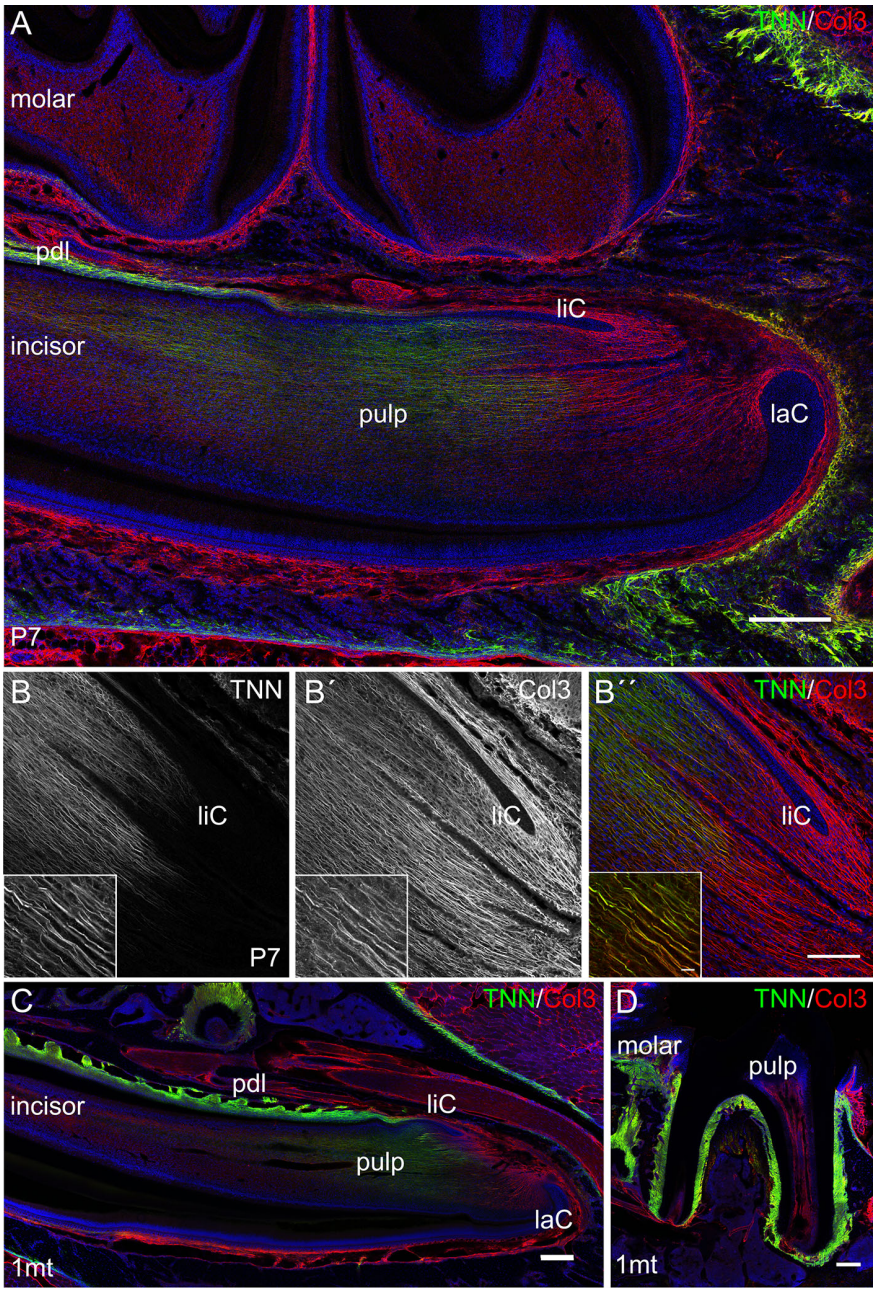

FIGURE 2 | Expression of tenascin-W/TNN in the lower incisor pulp and periodontal ligament. **(A)** In longitudinal sections, tenascin-W/TNN staining (tenascin-W/TNN in green, collagen 3 (Col3) in red) is found in the distal pulp mesenchyme and in the periodontal ligament of one week old mice. However, no expression is detected in the most apical pulp, which represents the mesenchymal stem cell niche. **(B)** In the pulp tenascin-W/TNN (B TNN in grayscale and B″ TNN in green) immunostaining co-localizes with a thick parallel fiber network, which consists of collagen 3 containing fibers (B´ Col3 in grayscale and B″ Col3 in red). In adult molars **(C)** and incisors **(D)** tenascin-W/TNN is predominantly found in the periodontal ligament, in the incisor pulp the signal intensities for both collagen 3 and tenascin-W/TNN were decreased compared to perinatal incisors (laC labial cervical loop, liC lingual cervical loop, pdl periodontal ligament, mice, n = 3, scale bar 100 µm, magnified inlet 10 µm).

Furthermore, we performed immunostainings with a CD90.2 and Sox10 antibodies. Sox10 is a marker for pluripotent neural crest cells and glia cells (38) and was used to identify nerve-derived mesenchymal stem cells in the incisor (3). The stainings showed an accumulation of Sox10 positive cells in the apical pulp mesenchyme of 3 mt old tenascin-W/TNN deficient animals; however, CD90.2 immunolocalization was not altered. This indicates that the nerve-derived mesenchymal stem cells of TNN

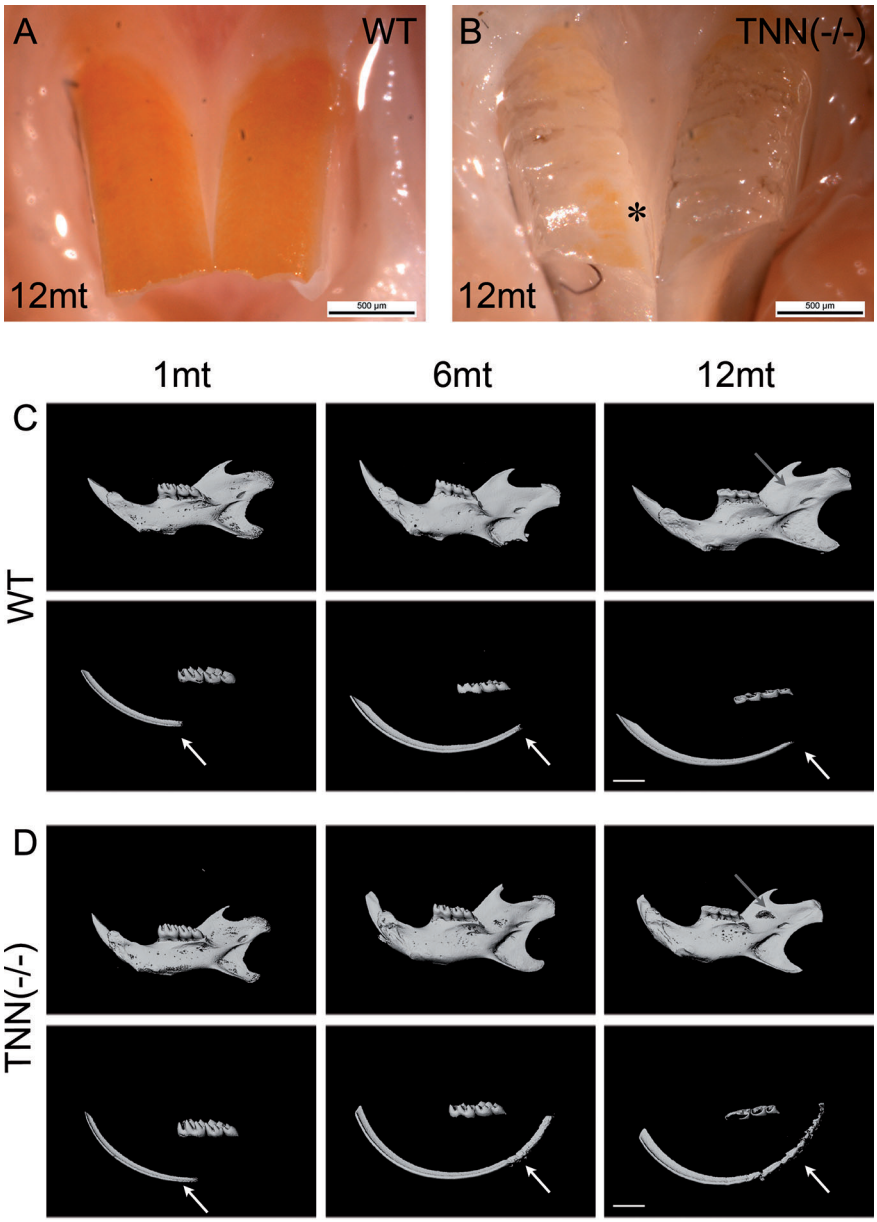

FIGURE 3 | Macroscopic phenotype **(A, B)** and µCT analysis **(C, D)** of tenascin-W/TNN deficient mouse incisors. tenascin-W/TNN knockout mice develop normally, but show enamel defects in the upper incisor at the age of 6 months. The enamel of rodents contains iron ions and is therefore yellowish. Whereas in the wildtype **(A)** the entire buccal incisor surface is covered by enamel, in TNN(-/-) animals **(B)** only few enamel spots remain (asterisk). **(C, D)** Bone and dentin (upper panels) or dentin alone (lower panels) were imaged in the lower jaw by µCT. Compared to wildtype **(C)**, aged TNN(-/-) mice **(D)** are showing flatter lower incisor tips and a lingual bone fenestration in the incisor apical region (gray arrow). The 3D reconstruction of the enamel (**C, D**; lower panels) shows a dorsal shift of enamel mineralization toward the cervical loop (shown by an arrow) and a fragmented dorsal enamel layer (mice, n = 6, scale bar µCT: 2 mm).

knockout incisors become blocked in their differentiation pathway and accumulate (**Supplementary Figure 6**).

Interestingly, aged TNN(-/-) mice never develop obesity. The body weight of 1 year old knockout animals was in both sexes significantly reduced (**Figure 7A**). We hypothesized that TNN (-/-) induced damage and tooth pain prevent proper food intake. To test this hypothesis we fed our mice with a soft food diet, which showed that the physical form of the diet was sufficient to rescue the body weight. Hence, the malformed teeth are the cause for the observed weight differences (**Figures 7A, B**). The weight of the wild type mice did not change with a soft diet. Soft food also ameliorated the incisor phenotype of knockout mice: µCT reconstructions of the enamel layer showed that the enamel layer remained continuous (**Figure 7C**), and histological sections of

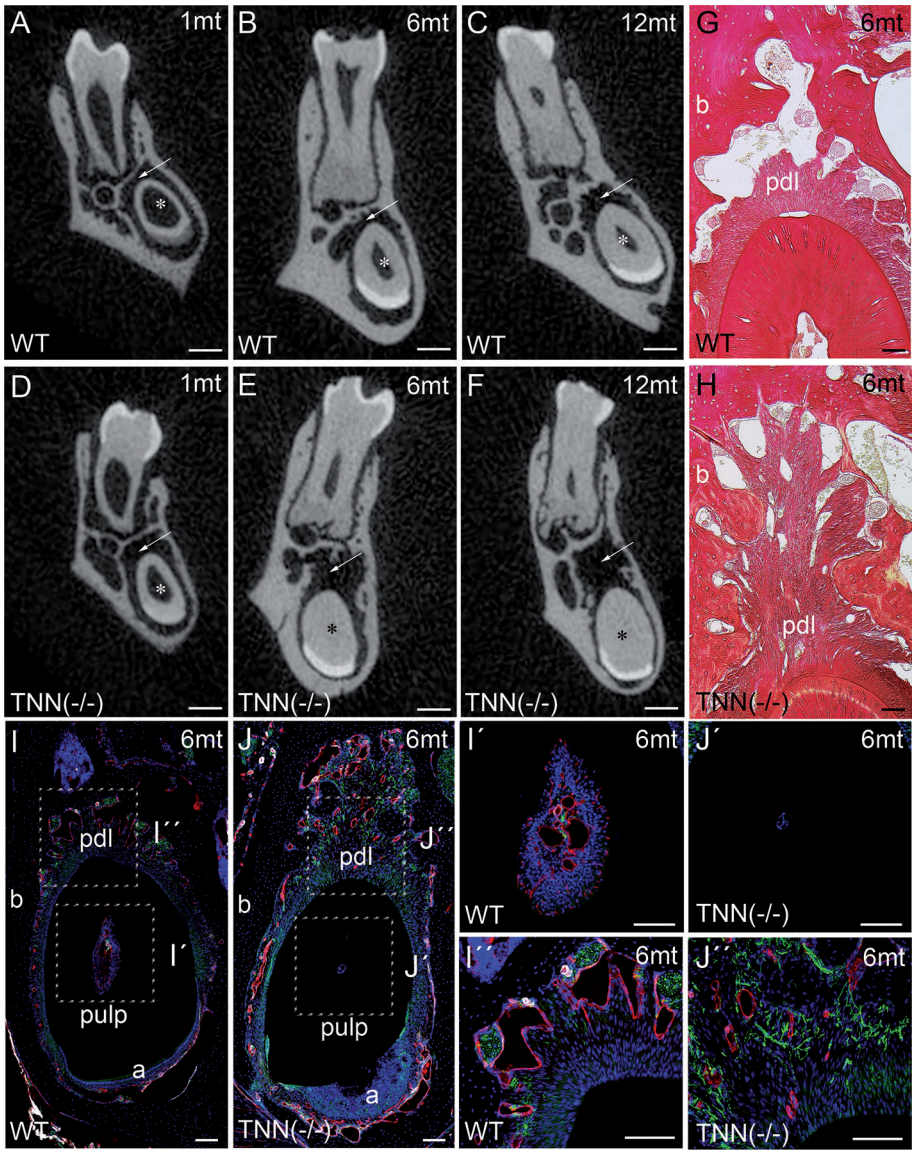

FIGURE 4 | Analysis of lower incisor cross-sections **(A–F)** µCT scans at the heights of the first molar showed that compared to wildtype **(A–C)** the incisor dentin layer is much thicker in 1 month old tenascin-W/TNN deficient mice (**D**, asterisk), in 6 and 12 month old mice the incisor pulp is completely obliterated (**E**, **F**, asterisk). A second phenotypic change in the mutant is the wider incisor periodontal space, indicated by an arrow **(D–F)**. However, the periodontal space of the molars seems normal. **(G, H)** Sirius red stainings showed a significant alveolar bone loss and a replacement by a dense connective tissue in the mutant compared to wildtype. **(I, J)** An analysis of blood vessels (CD31 in red, smooth muscle actin (SMA) in white, Tuj1 in green) and nerve fibers revealed that in TNN-deficient mice, the remaining pulp tissue does not containing any projections **(I´, J´)**; in contrast the bone replacement tissue contains a well developed network of nerve fibers **(I´´,J´´)** (a ameloblasts; pdl periodontal ligament; mice, n = 6, scale bar µCT: 0.5 mm, histology: 100 µm).

the incisor apical region showed improved epithelial and mesenchymal differentiation (**Figure 7D**). Next, we analyzed µCT cross sections of soft food fed 6 month old mice (**Figures 8A, B**). The pulp was now obliterated both in wild type and TNN deficient mice, indicating a slower tooth growth rate under soft food diet. Interestingly, the alveolar bone loss of TNN deficient mice persisted as well as the increased nerve branching under soft food diet (**Figures 8C, D**). This finding demonstrates that the periodontal ligament defect is the primary cause of the incisor eruption phenotype.

DISCUSSION

Our data reveal that tenascin-W/TNN is distinctly localized in the extracellular matrix and partially co-localizes with collagen 3

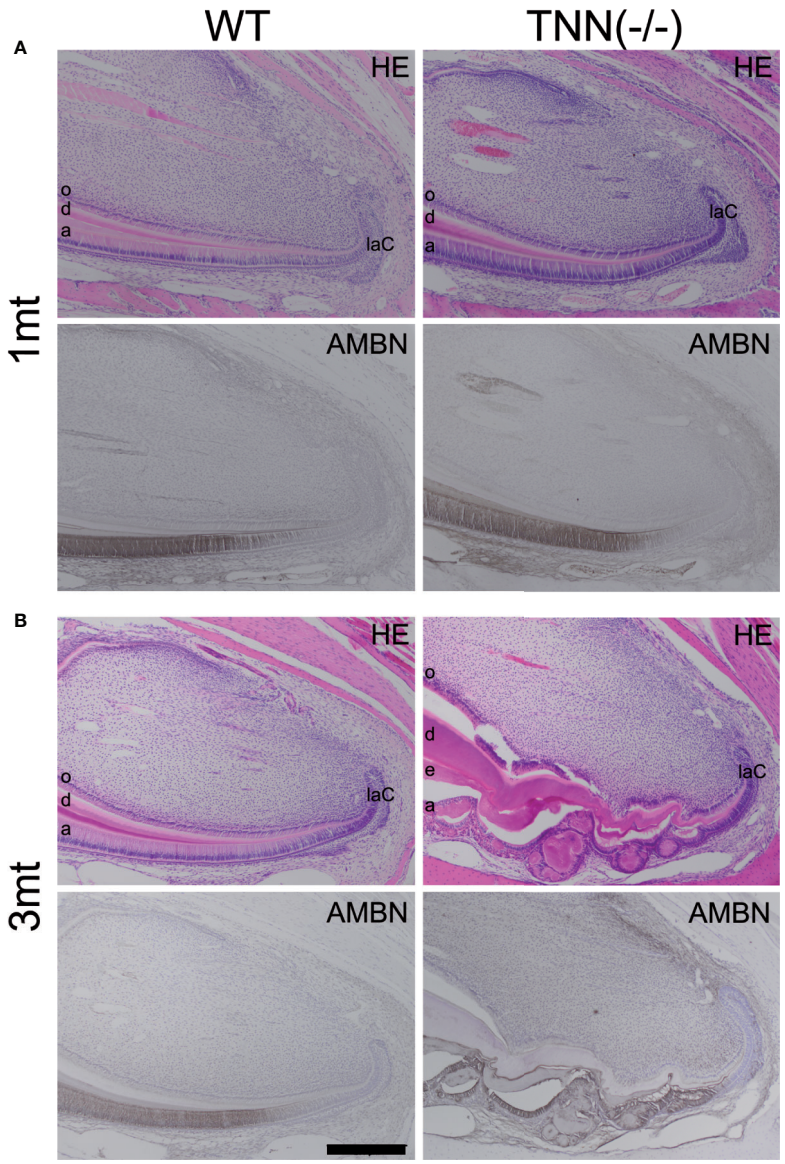

FIGURE 5 | H&E and ameloblastin stainings of the apical region of the lower incisor The pulp was longitudinally sectioned at the height of the central arterioles. **(A)** In 1 month old tenascin-W/TNN deficient mice the width of the dentin layer is increased. **(B)** Severe epithelial and mesenchymal differentiation defects are visible in the apical region of 3 month old TNN(-/-) mice. Dense eosinophilic inclusions are found in the enamel epithelium. Immunohistochemical stainings with ameloblastin antibodies (black staining) showed that those inclusions contain enamel matrix proteins (a ameloblast, laC labial cervical loop, d dentin, e enamel, o odontoblasts, mice, n = 6, scale bar 200 μm).

fibers. In teeth, this distribution pattern is different from tenascin-C, which is more diffusely distributed in the connective tissues. Earlier studies on tenascin-W/TNN have mostly focused on the *in vitro* function or tissue expression in cancer (23, 24). Here, we report the first tenascin-W/TNN deficient mouse for functional studies.

The most striking phenotype of tenascin-W/TNN deficient mice is found in the incisors, which show irregular dentin and enamel formation, while no phenotype changes are seen in molars. Furthermore, we have observed alveolar bone loss and increased nerve branching in the significantly wider periodontal ligament of TNN deficient mice. Changes in the periodontal ligament observed in the TNN-/- mice suggest that connective tissue remodeling and continuous eruption are disturbed. Initial tooth eruption in rodents relies heavily on monocyte/macrophage lineage cells as demonstrated by toothless rats (39) and in Csf1 deficient mice neither molar nor incisors erupt (40). However, little is known about the role of monocyte/macrophage lineage cells in continuous incisor eruption. The periodontal ligament is very different from the dental sac which is responsible

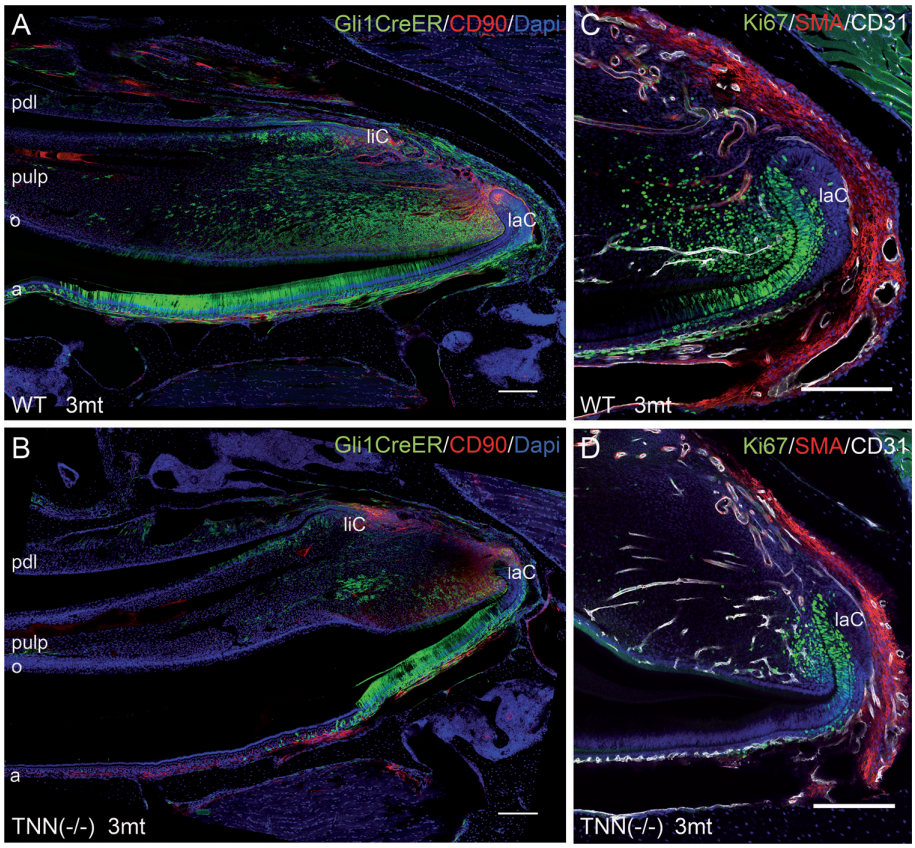

FIGURE 6 | Differentiation and proliferation defects in the TNN-/- incisor stem cell compartment **(A, B)** Gli1 lineage tracing experiments in 3mt old animals. Gli1CreER^{T2} x R26mTmG x TNN(-/-) and Gli1CreER^{T2} x R26mTmG control mice were i.p. injected twice with 10 mg tamoxifen. The animals were sacrified 72 h after the first injection. **(A, B)** Sagittal sections of the incisor pulp reveal that the GFP marked Gli1 (in green) expressing cells are reduced in number and in area. The number of CD90.2 (in red) stem cell was not affected by tenascin-W/TNN deficiency. **(C, D)** tenascin-W/TNN deficient mice have less proliferative cells (Ki67 in green) in the stem cell compartment. The blood vessels (CD31 in green, smooth muscle actin (SMA) in white) are not affected by tenascin deficiency. (a ameloblasts, laC labial cervical loop, liC lingual cervical loop, o odontoblasts, pdl periodontal ligament, mice, n = 6, scale bar 200 μm).

for initial tooth eruption. Tenascins are known to support cell migration *in vitro* (23) and to modulate macrophage activity by TLR4 binding (41). These known functions are suggesting that in TNN-deficient mice remodeling of the periodontal ligament might be affected through altered macrophage migration or activity. Another hypothesis is that tenascin-W/TNN affects the mechanical properties of the periodontal ligament and periodontal fibroblasts are differently regulated. Changes in the connective tissue stiffness are known to modulate extracellular matrix remodeling (42). Tenascin-X knockout mice have altered collagen fibers mimicking Ehlers-Danlos syndrome (20). However, in tenascin-W/TNN deficient mice ultrastructural analysis of the periodontal ligament showed normal collagen fibers (data not shown). Furthermore, we have observed alveolar bone loss and increased nerve branching in the periodontal ligament of TNN deficient mice. Since the rodent incisor periodontal ligament is rich in Ruffini- and free nerve endings (43), it is likely that this defect leads to pain or discomfort. In agreement with this assumption we found in aged tenascin-W/TNN deficient mice a significant reduction of the body weight.

Since the eruption rate of incisors is under neural and mechanical control (44) we wondered whether soft food diet accompanied with wooden gnaw sticks would rescue the body weight defect. We found that the TNN deficient mice gained weight comparably to control mice under these conditions, and the irregular dentin and enamel formation of the incisor disappeared. However, the periodontal defect including alveolar bone loss remained in the soft food treated TNN deficient animals. This important finding indicates that the odontoblast and ameloblast anomalies observed in TNN deficient incisors under standard hard food diet are secondary to a primary defect in the periodontium, and might be caused by mechanical damage to the pulp and/or pain-related processes.

Next, we examined the impact of tenascin-W/TNN deficiency on the incisor stem cell niche under standard food diet. The decreased Gli1 expression and cell proliferation suggests reduced hedgehog activity (4), and again indicate that the irregular tooth

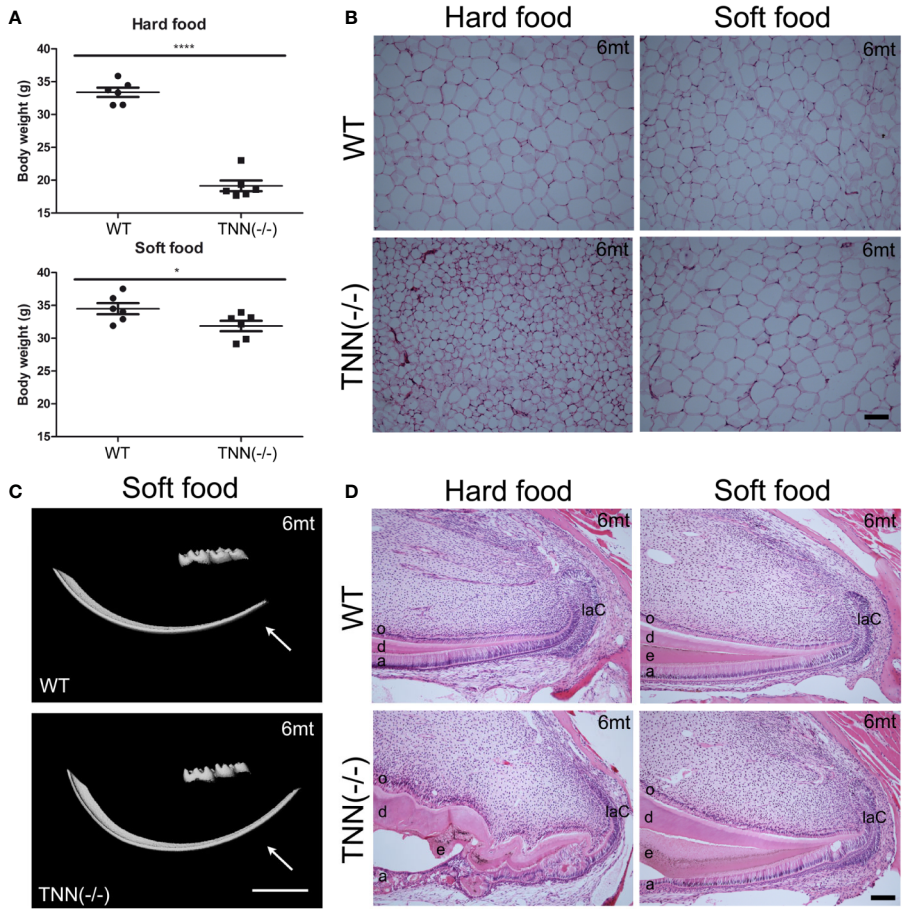

FIGURE 7 | Soft food diet ameliorates the TNN-/- incisor phenotype **(A)** Soft food diet decreases the weight loss observed in aged tenascin-W/TNN knockout mice. **(B)** tenascin-W/TNN knockout mice fed with hard food diet have significantly less white adipose tissue, soft food diet equilibrates the amount of epigonadal white adipose tissue. **(C)** The enamel layer of soft food diet fed TNN(-/-) mice is continuous. **(D)** Histological analysis of the apical region shows a significant rescue on the cellular level. (a ameloblasts, laC labial cervical loop, d dentin, e enamel, o odontoblasts, mice, n = 6, scale bar μCT: 2 mm, histology: 100 μm).

formation is of secondary nature, as tenascin-W/TNN is not expressed in the stem cell niche and the percentage of progenitor cells is not altered. Hendaoui et al. (45) proposed that tenascin-C and –W/N modulate Wnt signaling by sequestering the growth factor. However, tenascin-W/TNN is not expressed in the incisor stem cell niche itself and therefore cannot modulate growth factor signaling directly. Hence, axin2 and Gli1 expression and cell proliferation are clearly due to secondary effects. Since it is very difficult obtaining comparable sections, we decided to include only unquantified data.

Similar phenotypes in the incisors have been observed in periostin or integrin α11 deficient mouse lines; both proteins play central roles in periodontal ligament remodeling and mechanosignaling. One of them, periostin, is a characteristic extracellular matrix component of the periodontal ligament, and periostin deficiency in mice leads to periodontal defects in incisors and molars. Periostin has a known function in collagen 1 fibrillogenesis (46) by supporting proteolytic activation of lysyl oxidase (47). Furthermore, periostin plays a role in vascular smooth muscle cell migration (48) and in the migration of bone lining cells (49). Interestingly, soft chow also ameliorates the phenotype observed in periostin deficient animals (50). One major difference to the phenotype observed in TNN knockout mice is that periostin deficiency affects also the molar periodontal ligament (50), not just that of the continuously erupting incisor. The only other extracellular matrix related knockout where the incisors are affected is that of integrin α11 (51). Integrin α11β1 functions as a collagen receptor and it has been suggested that it plays a role in mechanotransduction. Interestingly, soft food diet ameliorates also the integrin α11 phenotype (51). Both periostin and integrin α11 play a role in the remodeling of collagen 1 fibers. The irregular tooth formation observed in periostin deficient mice might be due to a periodontal ligament—neurosecretory feedback mechanism. Based on published data (41), we hypothesize that tenascin-W/TNN acts on macrophages or fibroblasts directly, and that the underlying mechanism of the remodeling defect is different.

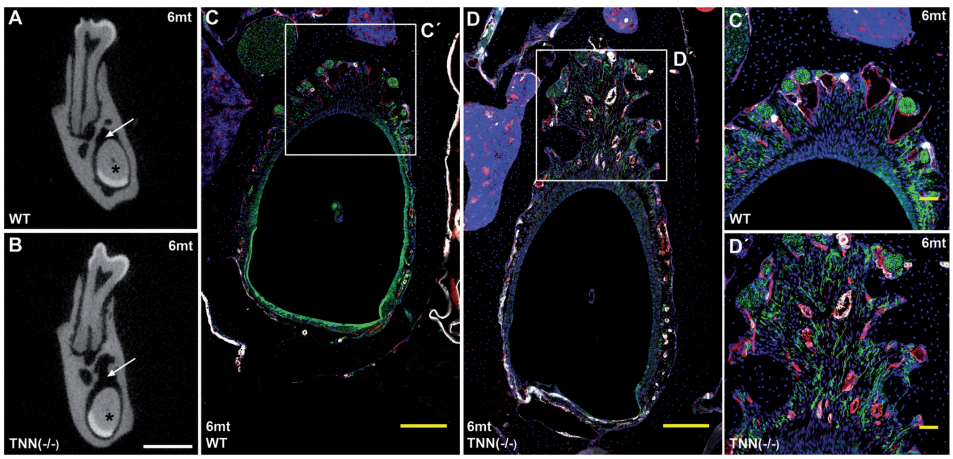

FIGURE 8 | Soft food diet does not revert the TNN-/- periodontal defect µCT cross-sectional scans at the height of the first molar showed incisor pulp obliteration in both 6 month old wildtype and tenascin-W/TNN deficient mice (**A, B**, asterisk). The wider periodontal space, indicated by an arrow (A and B, arrow) is still found in soft diet fed 6 month old tenascin-W/TNN deficient mice. Immunofluorescence stainings **(C´, D´)** confirmed the presence of branched nerve fibers (CD31 in red, smooth muscle actin (SMA) in white, Tuj1 in green) in tenascin-W/TNN deficient periodontal space. (scale bar µCT: 1 mm, mice, n = 6, histology: **(C, D)** 200 µm, **(C´, D´)** 50 µm).

In conclusion, our data show that tenascin-W/TNN co-localizes with collagen 3 fibers in the pulp and the periodontal ligament. Here, we present the first characterization of tenascin-W/TNN deficient mice and we conclude that tenascin-W/TNN plays a pivotal role in incisor periodontal remodeling and diet uptake. The periodontal remodeling phenotype is furthermore connected with nerve branching. Since soft food diet results in equal body weights, but the periodontal defect persists in these mice, we assume that nerve branching might lead to pain. Since tenascin-W/TNN itself is not expressed in the stem cell compartment nor in the proliferation zone, we hypothesize that the effect in the pulp is of secondary nature, most probably due to reduced neural input. The diminished Gli1 expression in the pulp supports this assumption. Neurovascular secreted sonic hedgehog is a known regulator in this stem cell niche and Gli1 is the main effector of activated hedgehog signaling. In summary, we report for the first time about the *in vivo* function of tenascin-W/TNN and we show that this extracellular matrix protein plays a crucial role in periodontal remodeling.

DATA AVAILABILITY STATEMENT

The raw data supporting the conclusions of this article will be made available by the authors, without undue reservation.

ETHICS STATEMENT

The animal study was reviewed and approved by Landesamt für Natur, Umwelt und Verbraucherschutz Nordrhein-Westfalen (LANUV NRW), Postfach 10 10 52, 45610 Recklinghausen.

AUTHOR CONTRIBUTIONS

Study design: TI. Animal treatment: TI. Histology, *in situ* hybridization, and immunostaining: TI, AB, IT. Tenascin W/TNN antibody production: RC-E. µCT analysis: JH and AN. FACS analysis: TI and BB. Data interpretation: TI, AB, IT, and MK. Manuscript preparation: TI, MC, and BB. All authors contributed to the article and approved the submitted version.

FUNDING

This work was supported by grants from the DFG (A2, CRC829; B2, D1, M1 FOR2722) and Köln Fortune to MK. the DFG (A2, CRC829; B2, D1, M1 FOR2722) and Köln Fortune to MK.

ACKNOWLEDGMENTS

We thank Dr. Sarah Appel, Cologne for providing mouse embryo tissues and Semra Özcelik for technical assistance. We would like to thank to Dr. Mats Paulsson for correcting the manuscript and for helpful advice.

SUPPLEMENTARY MATERIAL

The Supplementary Material for this article can be found online at: https://www.frontiersin.org/articles/10.3389/fimmu.2020.608223/full#supplementary-material

SUPPLEMENTARY FIGURE 1 | (A, B) Late expression of tenascin-W/TNN in the incisor pulp and tenascin-W/TNN expression in cross-sections Until the early bell stage (**A**; E16) no tenascin-W/TNN (TNN in green) is expressed in the incisor

pulp. Blood vessels (CD31 in red) were stained to easily distinguish the mesenchyme from the epithelium. At the late bell stage almost the entire distal pulp mesenchyme stains for tenascin-W/TNN (**B**; E19). However, tenascin-W/TNN is not expressed in the mesenchymal stem cell niche. **(C)** tenascin-W/TNN (TNN in green, CD31 in red) is strongly detected in the odontoblast layer of newborn mice. tenascin-W/TNN stains a thick spiral-shaped fiber network. **(D)** The immunostaining for tenascin-W/TNN is highly specific, in TNN(-/-) mice no signal for tenascin-W/TNN is found. (**E,E'**) tenascin-W/TNN (TNN in green) is not detected in the distal incisor pulp of 1 month old mice. In the periodontal ligament tenascin-W/TNN colocalizes with collagen 3 (Collagen (Col3) in red) (liC lingual cervical loop, laC labial cervical loop, mice, n = 3, scale bar **(A, B)** 200 μm).

SUPPLEMENTARY FIGURE 2 | *In situ* hybridization for differentiation markers Differentiation of ameloblasts and odontoblasts was further analyzed by *in situ* hybridization experiments with probes for ameloblastin (*Ambn)*, dentin sialophosphoprotein (*Dspp)*, and sonic hedgehog (*Shh)*. **(A)** Schematic overview of the incisor epithelial cell layers. Ameloblastin is expressed in pre-odontoblasts, pre-ameloblasts, and ameloblasts. Dentin sialophosphoprotein is expressed in pre-odontoblasts and odontoblasts, sonic hedgehog is expressed in pre-ameloblasts and in the stratum intermedium of the enamel organ. **(B, C)** In 1 month old mice we found no differences in the expression of differentiation markers. In 3 month old TNN-deficient mice the cells differentiate closer to the cervical loop (**C**, **D** arrow) and the cervical loop seems smaller (*Ambn* ameloblastin, *Shh* sonic hedgehog, *Dspp* dentin sialophosphoprotein, a ameloblasts, laC labial cervical loop, o odontoblasts, mice, n = 3, scale bar 100 μm).

SUPPLEMENTARY FIGURE 3 | Alkaline phosphatase staining. The epithelial and mesenchymal differentiation was analyzed by staining for endogenous alkaline phosphatase. Differentiating odontoblasts are detected in the pulp of 1 year old TNN(-/-) mice. The signal in the pre-odontoblast layer is shifted to the cervical loop region (arrow) indicating earlier differentiation. (a ameloblasts, laC labial cervical loop, o odontoblasts, mice, n = 6, scale bar 200 μm).

SUPPLEMENTARY FIGURE 4 | Defective FGF, Wnt, and Shh signaling in TNN (-/-) mice **(A–F)** *In situ* hybridization experiments for *Axin2* **(A, D)**, *Fgf10* **(B, E)**, and *Gli1* **(C, F)** showed reduced expression of these markers in the mesenchymal stem cell niche in 1 month old TNN-deficient **(D–F)** compared to wildtype **(A–C)** mice. (a ameloblasts, laC labial cervical loop, liC lingual cervical loop, o odontoblasts, pdl periodontal ligament, mice, n = 3, scale bar 200 μm).

SUPPLEMENTARY FIGURE 5 | (A) Representative FACS analysis of isolated incisor pulp cells from wildtype **(A)** and TNN(-/-) **(B)** mice. Sytox Blue dead cell stain negative and CD45 negative cells were analyzed with Sca-1 and CD90.2 markers. **(C)** FACS analysis of 1 month old mice showed that the number of CD90.2 and Sca1 positive progenitor cells is unchanged (SSC-A Side Scatter A, FSC-A Forward Scatter A, mice, n = 6).

SUPPLEMENTARY FIGURE 6 | Sox10 positive cells accumulate in the region of the neurovascular bundle **(A–H)** Cross sections of the apical region showed an accumulation of Sox10 (Sox10 in red, CD90 in white, Tuj1 in green) positive cells in the pulp of 3 month old tenascin-W/TNN knockout mice. In the knockout mice the number of Sox10 positive cells increased with ageing. **(I, J)** Sagittal sections showed that the pulp of 1 year old tenascin-W/TNN mice is full of Sox10 positive cells. CD90.2 positive cells are found in the most apical mesenchyme (a ameloblasts, laC labial cervical loop, liC lingual cervical loop, mice, n = 6, scale bar 200 μm).

REFERENCES

1. Warshawsky H, Smith CE. Morphological classification of rat incisor ameloblasts. *Anat Record* (1974) 179:423–45. doi: 10.1002/ar.1091790403
2. Feng J, Mantesso A, De Bari C, Nishiyama A, Sharpe PT. Dual origin of mesenchymal stem cells contributing to organ growth and repair. *Proc Natl Acad Sci* (2011) 108:6503–8. doi: 10.1073/pnas.1015449108
3. Kaukua N, Shahidi MK, Konstantinidou C, Dyachuk V, Kaucka M, Furlan A, et al. Glial origin of mesenchymal stem cells in a tooth model system. *Nature* (2014) 513(7519):551–4. doi: 10.1038/nature13536
4. Zhao H, Feng J, Seidel K, Shi S, Klein O, Sharpe P, et al. Secretion of Shh by a Neurovascular Bundle Niche Supports Mesenchymal Stem Cell Homeostasis in the Adult Mouse Incisor. *Cell Stem Cell* (2014) 14:160–73. doi: 10.1016/j.stem.2013.12.013
5. Vidovic I, Banerjee A, Fatahi R, Matthews BG, Dyment NA, Kalajzic I, et al. αSMA-Expressing Perivascular Cells Represent Dental Pulp Progenitors In Vivo. *J Dent Res* (2017) 96:323–30. doi: 10.1177/0022034516678208
6. Binder M, Chmielarz P, Mckinnon PJ, Biggs LC, Thesleff I, Balic A. Functionally Distinctive Ptch Receptors Establish Multimodal Hedgehog Signaling in the Tooth Epithelial Stem Cell Niche. *Stem Cells* (2019) 37:1238–48. doi: 10.1002/stem.3042
7. Jernvall J, Thesleff I. Tooth shape formation and tooth renewal: evolving with the same signals. *Development* (2012) 139:3487–97. doi: 10.1242/dev.085084
8. Gattazzo F, Urciuolo A, Bonaldo P. Extracellular matrix: A dynamic microenvironment for stem cell niche(). *Biochim Biophys Acta* (2014) 1840:2506–19. doi: 10.1016/j.bbagen.2014.01.010
9. Frantz C, Stewart KM, Weaver VM. The extracellular matrix at a glance. *J Cell Sci* (2010) 123:4195–200. doi: 10.1242/jcs.023820
10. Chiquet-Ehrismann R, Orend G, Chiquet M, Tucker RP, Midwood KS. Tenascins in stem cell niches. *Matrix Biol* (2014) 37:112–23. doi: 10.1016/j.matbio.2014.01.007
11. Chiquet-Ehrismann R, Tucker RP. Tenascins and the Importance of Adhesion Modulation. *Cold Spring Harbor Perspect Biol* (2011) 3:1–19. doi: 10.1101/cshperspect.a004960
12. Rigato F, Garwood J, Calco V, Heck N, Faivre-Sarrailh C, Faissner A. Tenascin-C Promotes Neurite Outgrowth of Embryonic Hippocampal Neurons through the Alternatively Spliced Fibronectin Type III BD Domains via Activation of the Cell Adhesion Molecule F3/Contactin. *J Neurosci* (2002) 22:6596. doi: 10.1523/JNEUROSCI.22-15-06596.2002
13. Zisch AH, D'Alessandri L, Ranscht B, Falchetto R, Winterhalter KH, Vaughan L. Neuronal cell adhesion molecule contactin/F11 binds to tenascin via its immunoglobulin-like domains. *J Cell Biol* (1992) 119:203. doi: 10.1083/jcb.119.1.203
14. Huang W, Chiquet-Ehrismann R, Moyano JV, Garcia-Pardo A, Orend G. Interference of Tenascin-C with Syndecan-4 Binding to Fibronectin Blocks Cell Adhesion and Stimulates Tumor Cell Proliferation. *Cancer Res* (2001) 61:8586.
15. Saga Y, Yagi T, Ikawa Y, Sakakura T, Aizawa S. Mice develop normally without tenascin. *Genes Dev* (1992) 6:1821–31. doi: 10.1101/gad.6.10.1821
16. Mackie EJ, Tucker RP. The tenascin-C knockout revisited. *J Cell Sci* (1999) 112:3847–53.
17. Pesheva P, Probstmeier R, Skubitz AP, McCarthy JB, Furcht LT, Schachner M. Tenascin-R (J1 160/180 inhibits fibronectin-mediated cell adhesion–functional relatedness to tenascin-C. *J Cell Sci* (1994) 107:2323–33.
18. Anlar B, Gunel-Ozcan A. Tenascin-R: Role in the central nervous system. *Int J Biochem Cell Biol* (2012) 44:1385–9. doi: 10.1016/j.biocel.2012.05.009
19. Tucker RP, Chiquet-Ehrismann R. The regulation of tenascin expression by tissue microenvironments. *Biochim Biophys Acta (BBA) - Mol Cell Res* (2009) 1793:888–92. doi: 10.1016/j.bbamcr.2008.12.012
20. Mao JR, Taylor G, Dean WB, Wagner DR, Afzal V, Lotz JC, et al. Tenascin-X deficiency mimics Ehlers-Danlos syndrome in mice through alteration of collagen deposition. *Nat Genet* (2002) 30:421–5. doi: 10.1038/ng850
21. Scherberich A, Tucker RP, Samandari E, Brown-Luedi M, Martin D, Chiquet-Ehrismann R. Murine tenascin-W: a novel mammalian tenascin expressed in kidney and at sites of bone and smooth muscle development. *J Cell Sci* (2004) 117:571–81. doi: 10.1242/jcs.00867
22. Nishida E, Sasaki T, Ishikawa SK, Kosaka K, Aino M, Noguchi T, et al. Transcriptome database KK-Periome for periodontal ligament development: Expression profiles of the extracellular matrix genes. *Gene* (2007) 404:70–9. doi: 10.1016/j.gene.2007.09.009
23. Degen M, Brellier F, Kain R, Ruiz C, Terracciano L, Orend G, et al. Tenascin-W Is a Novel Marker for Activated Tumor Stroma in Low-grade Human Breast Cancer and Influences Cell Behavior. *Cancer Res* (2007) 67:9169–79. doi: 10.1158/0008-5472.CAN-07-0666
24. Scherberich A, Tucker RP, Degen M, Brown-Luedi M, Andres A-C, Chiquet-Ehrismann R. Tenascin-W is found in malignant mammary tumors, promotes

alpha8 integrin-dependent motility and requires p38MAPK activity for BMP-2 and TNF-alpha induced expression in vitro. *Oncogene* (2004) 24:1525–32. doi: 10.1038/sj.onc.1208342
25. Brellier F, Martina E, Chiquet M, Ferralli J, van der Heyden M, Orend G, et al. The adhesion modulating properties of tenascin-W. *Int J Biol Sci* (2012) 8:187–94. doi: 10.7150/ijbs.8.187
26. Martina E, Chiquet-Ehrismann R, Brellier F. Tenascin-W: An extracellular matrix protein associated with osteogenesis and cancer. *Int J Biochem Cell Biol* (2010) 42:1412–5. doi: 10.1016/j.biocel.2010.06.004
27. Ahn S, Joyner AL. Dynamic Changes in the Response of Cells to Positive Hedgehog Signaling during Mouse Limb Patterning. *Cell* (2004) 118:505–16. doi: 10.1016/j.cell.2004.07.023
28. Muzumdar MD, Tasic B, Miyamichi K, Li L, Luo L. A global double-fluorescent Cre reporter mouse. *Genesis* (2007) 45:593–605. doi: 10.1002/dvg.20335
29. Heilig J, Paulsson M, Zaucke F. Insulin-like growth factor 1 receptor (IGF1R) signaling regulates osterix expression and cartilage matrix mineralization during endochondral ossification. *Bone* (2016) 83:48–57. doi: 10.1016/j.bone.2015.10.007
30. Zigrino P, Brinckmann J, Niehoff A, Lu Y, Giebeler N, Eckes B, et al. Fibroblast-Derived MMP-14 Regulates Collagen Homeostasis in Adult Skin. *J Invest Dermatol* (2016) 136:1575–83. doi: 10.1016/j.jid.2016.03.036
31. Schneider CA, Rasband WS, Eliceiri KW. NIH Image to ImageJ: 25 years of image analysis. *Nat Methods* (2012) 9:671. doi: 10.1038/nmeth.2089
32. Suomalainen M, Thesleff I. Patterns of Wnt pathway activity in the mouse incisor indicate absence of Wnt/β-catenin signaling in the epithelial stem cells. *Dev Dyn* (2010) 239:364–72. doi: 10.1002/dvdy.22106
33. Tummers M, Thesleff I. Root or crown: a developmental choice orchestrated by the differential regulation of the epithelial stem cell niche in the tooth of two rodent species. *Development* (2003) 130:1049–57. doi: 10.1242/dev.00332
34. Jussila M, Thesleff I. Signaling Networks Regulating Tooth Organogenesis and Regeneration, and the Specification of Dental Mesenchymal and Epithelial Cell Lineages. *Cold Spring Harbor Perspect Biol* (2012) 4:1–13. doi: 10.1101/cshperspect.a008425
35. Trowbridge IS, Thomas ML. CD45: An Emerging Role as a Protein Tyrosine Phosphatase Required for Lymphocyte Activation and Development. *Annu Rev Immunol* (1994) 12:85–116. doi: 10.1146/annurev.iy.12.040194.000505
36. Holmes C, Stanford WL. Concise Review: Stem Cell Antigen-1: Expression, Function, and Enigma. *Stem Cells* (2007) 25:1339–47. doi: 10.1634/stemcells.2006-0644
37. Balic A, Mina M. Characterization of Progenitor Cells in Pulps of Murine Incisors. *J Dental Res* (2010) 89:1287–92. doi: 10.1177/0022034510375828
38. Britsch S, Goerich DE, Riethmacher D, Peirano RI, Rossner M, Nave K-A, et al. The transcription factor Sox10 is a key regulator of peripheral glial development. *Genes Dev* (2001) 15:66–78. doi: 10.1101/gad.186601
39. Marks SC, Wojtowicz A, Szperl M, Urbanowska E, Mackay CA, Wiktor-Jedrzejczak W, et al. Administration of colony stimulating factor-1 corrects some macrophage, dental, and skeletal defects in an osteopetrotic mutation (toothless, tl) in the rat. *Bone* (1992) 13:89–93. doi: 10.1016/8756-3282(92)90365-4
40. Dai X-M, Zong X-H, Sylvestre V, Stanley ER. Incomplete restoration of colony-stimulating factor 1 (CSF-1) function in CSF-1–deficient Csf1op/Csf1op mice by transgenic expression of cell surface CSF-1. *Blood* (2004) 103:1114–23. doi: 10.1182/blood-2003-08-2739
41. Zuliani-Alvarez L, Marzeda AM, Deligne C, Schwenzer A, McCann FE, Marsden BD, et al. Mapping tenascin-C interaction with toll-like receptor 4 reveals a new subset of endogenous inflammatory triggers. *Nat Commun* (2017) 8:1595. doi: 10.1038/s41467-017-01718-7
42. Tomasek JJ, Gabbiani G, Hinz B, Chaponnier C, Brown RA. Myofibroblasts and mechano-regulation of connective tissue remodelling. *Nat Rev Mol Cell Biol* (2002) 3:349–63. doi: 10.1038/nrm809
43. Sato O, Maeda T, Kobayashi S, Iwanaga T, Fujita T, Takahashi Y. Innervation of periodontal ligament and dental pulp in the rat incisor: An immunohistochemical investigation of neurofilament protein and glia-specific S-100 protein. *Cell Tissue Res* (1988) 251:13–21. doi: 10.1007/BF00215442
44. An Z, Sabalic M, Bloomquist RF, Fowler TE, Streelman T, Sharpe PT. A quiescent cell population replenishes mesenchymal stem cells to drive accelerated growth in mouse incisors. *Nat Commun* (2018) 9:378. doi: 10.1038/s41467-017-02785-6
45. Hendaoui I, Tucker RP, Zingg D, Bichet S, Schittny J, Chiquet-Ehrismann R. Tenascin-C is required for normal Wnt/β-catenin signaling in the whisker follicle stem cell niche. *Matrix Biol* (2014) 40:46–53. doi: 10.1016/j.matbio.2014.08.017
46. Norris Russell A, Damon B, Mironov V, Kasyanov V, Ramamurthi A, Moreno-Rodriguez R, et al. Periostin regulates collagen fibrillogenesis and the biomechanical properties of connective tissues. *J Cell Biochem* (2007) 101:695–711. doi: 10.1002/jcb.21224
47. Maruhashi T, Kii I, Saito M, Kudo A. Interaction between Periostin and BMP-1 Promotes Proteolytic Activation of Lysyl Oxidase. *J Biol Chem* (2010) 285:13294–303. doi: 10.1074/jbc.M109.088864
48. Li G, Jin R, Norris RA, Zhang L, Yu S, Wu F, et al. Periostin mediates vascular smooth muscle cell migration through the integrins αvβ3 and αvβ5 and focal adhesion kinase (FAK) pathway. *Atherosclerosis* (2010) 208:358–65. doi: 10.1016/j.atherosclerosis.2009.07.046
49. Cobo T, Viloria CG, Solares L, Fontanil T, González-Chamorro E, De Carlos F, et al. Role of Periostin in Adhesion and Migration of Bone Remodeling Cells. *PLoS One* (2016) 11:e0147837. doi: 10.1371/journal.pone.0147837
50. Rios H, Koushik SV, Wang H, Wang J, Zhou H-M, Lindsley A, et al. periostin Null Mice Exhibit Dwarfism, Incisor Enamel Defects, and an Early-Onset Periodontal Disease-Like Phenotype. *Mol Cell Biol* (2005) 25:11131–44. doi: 10.1128/MCB.25.24.11131-11144.2005
51. Popova SN, Barczyk M, Tiger C-F, Beertsen W, Zigrino P, Aszodi A, et al. α11β1 Integrin-Dependent Regulation of Periodontal Ligament Function in the Erupting Mouse Incisor. *Mol Cell Biol* (2007) 27:4306–16. doi: 10.1128/MCB.00041-07

Conflict of Interest: The authors declare that the research was conducted in the absence of any commercial or financial relationships that could be construed as a potential conflict of interest.

frontiers in Immunology

PERSPECTIVE
published: 02 February 2021
doi: 10.3389/fimmu.2020.623305

Tenascin-W: Discovery, Evolution, and Future Prospects

Martin Degen[1], *Arnaud Scherberich*[2] *and Richard P. Tucker*[3]*

[1] Laboratory for Oral Molecular Biology, Department of Orthodontics and Dentofacial Orthopedics, University of Bern, Bern, Switzerland, [2] Tissue Engineering Laboratory, Department of Biomedicine, University Hospital Basel, University of Basel, Basel, Switzerland, [3] Department of Cell Biology and Human Anatomy, University of California at Davis, Davis, CA, United States

Of the four tenascins found in bony fish and tetrapods, tenascin-W is the least understood. It was first discovered in the zebrafish and later in mouse, where it was mistakenly named tenascin-N. Tenascin-W is expressed primarily in developing and mature bone, in a subset of stem cell niches, and in the stroma of many solid tumors. Phylogenetic studies show that it is the most recent tenascin to evolve, appearing first in bony fishes. Its expression in bone and the timing of its evolutionary appearance should direct future studies to its role in bone formation, in stem cell niches, and in the treatment and detection of cancer.

Keywords: extracellular matrix, cell adhesion, cell migration, cell differentiation, phylogeny

OPEN ACCESS

Edited by:
Kyoko Imanaka-Yoshida, Mie University, Japan

Reviewed by:
Ken-ichi Matsumoto, Shimane University, Japan
Anja Schwenzer, University of Oxford, United Kingdom

***Correspondence:**
Richard P. Tucker
rptucker@ucdavis.edu

Specialty section:
This article was submitted to Inflammation, a section of the journal Frontiers in Immunology

Received: *29 October 2020*
Accepted: *18 December 2020*
Published: *02 February 2021*

Citation:
Degen M, Scherberich A and Tucker RP (2021) Tenascin-W: Discovery, Evolution, and Future Prospects. Front. Immunol. 11:623305. doi: 10.3389/fimmu.2020.623305

INTRODUCTION

Tenascins are a family of extracellular matrix glycoproteins with a distinctive domain architecture (1). There are four family members: tenascin-C, tenascin-R, tenascin-X, and tenascin-W. All monomeric tenascins share a similar N-terminus comprised of heptad repeats flanked by cysteine residues. One or more epidermal growth factor (EGF)-like repeats are present near N-terminus, followed by variable numbers of fibronectin-type III (FNIII) domains. At the C-terminus is a large fibrinogen-related domain. Most tenascins form trimers *via* coiled-coil interactions within their N-terminal oligomerization domain, and some (tenascin-C and tenascin-W) can form hexamers through cysteine cross bridges. The original tenascin, and the best studied member of the family, is tenascin-C (1). The C in tenascin-C stands for cytotactin, which was one of the early names used for this protein. The second tenascin to be discovered was originally named restrictin since its expression is largely "restricted" to the nervous system. When it became clear that restrictin was closely related to tenascin-C, it was renamed tenascin-R. Tenascin-X received its name because it was encoded by the unknown "gene X", which partly overlaps the human *CYP21B* gene. The domain architecture of tenascin-X is highly variable in different taxonomic groups, so its homolog in the chicken was initially named tenascin-Y until its true identity was discovered by phylogenetic analysis (2). The fourth and final member of the tenascin gene family is tenascin-W, which is the topic of this perspective article.

THE DISCOVERY AND EXPRESSION OF TENASCIN-W

In the decades prior to genomic sequencing, many researchers attempted to discover novel members of a gene family of interest by low-stringency hybridization screening of cDNA

libraries with probes that corresponded to sequences likely to be conserved between members within the family. This approach was used by Philipp Weber and colleagues (3) to obtain the first tenascin-W sequence. In their study, a zebrafish cDNA library was screened for tenascin-related molecules using a radioactively labeled 444-bp sequence probe encoding the EGF repeats of rat tenascin-R. The 4 positive clones with sequences related to tenascins were amplified, subcloned and sequenced, and the missing 5' sequence was determined by rapid amplification. While the experimental design seemed more likely to result in the cloning of tenascin-R from zebrafish, the resulting sequence appeared novel based on low sequence homologies with known tenascins. Weber and colleagues chose the name tenascin-W, presumably after the name of the discoverer. The cDNA sequence revealed a tenascin-type domain structure: an N-terminal signal peptide, a cysteine-rich domain likely to permit oligomerization, three EGF-like repeats, five FNIII domains, and a C-terminal fibrinogen-related domain.

The presence of a novel tenascin in zebrafish led to a race to find its mammalian homologue. The first of two papers describing the discovery of murine tenascin-W was published by John Neidhardt and colleagues (4). This group used BLAST to screen mouse expressed sequence tags (ESTs) for novel sequences encoding EGF repeats and FNIII domains, and found two overlapping sequences that did not correspond to the known sequences of murine tenascin-C and tenascin-R. The complete coding sequence was then found using rapid amplification and RT-PCR, revealing a tenascin with three EGF-like repeats, 12 FNIII domains and a C-terminal fibrinogen-related domain. Phylogenetic relationships between their novel tenascin and known tenascins placed the new murine tenascin in the tenascin-W clade. However, since it had 12 FNIII domains and not five as reported in zebrafish, they concluded that they had found a new tenascin and named it tenascin-N after the paper's first author. The authors noted that many of the FNIII domains were very similar to each other, so much so that the amino acid sequences 6th and 8th FNIII domains were identical. They also reported that tenascin-N mRNA was abundant in brain, kidney and spleen, and less so in the developing embryo than in the adult mouse. The authors confirmed protein expression in the brain by immunohistochemistry.

The second paper describing tenascin-W in the mouse (5), submitted prior to the appearance of the paper by Neidhardt et al. (4), described the cloning of the homologue using PCR primers based on a human EST reported to be "similar to tenascin-R" (accession number AL049689). Overlapping cDNAs were assembled into a presumptive full-length coding sequence encoding 3 EGF-like repeats, 9 FNIII domains and a fibrinogen-related domain. The authors concluded that they found the murine homologue of tenascin-W as both the domain organization and sequence were most similar to zebrafish tenascin-W. They also noted that the similar FNIII domains (domains 3–8) corresponded to the 3rd and 4th FNIII domains of zebrafish tenascin-W, and they hypothesized that murine tenascin-W was larger than zebrafish tenascin-W due to the repetitive duplication of these domains over time. Immunohistochemistry revealed tenascin-W in developing smooth muscle and periosteum, in certain stem cell niches, as well as in the adult kidney. They did not report expression in the developing or adult central nervous system.

Why did the authors of these papers come to such different conclusions? We now know that the number of repeats or domains found in tenascins are very poor predictors of homology (1). Human tenascin-C has up to 17 FNIII domains, whereas its homologue in zebrafish (NP_570982) has nine. The human tenascin-X gene encodes 32 FNIII domains, whereas tenascin-X in some bony fish has only three. The numbers of EGF-like repeats are more similar across species, but even those repeats are highly variable in number in tenascin-X (2). The variable numbers of FNIII domains in tenascin-W (five in zebrafish and 12 in mouse) is likely to be the result of a duplication of the 3rd FNIII domain, which is encoded on a single exon (2). In the pufferfish tenascin-W has only four FNIII domains, but the 3rd domain duplicated twice in the zebrafish to give it six potential FNIII domains, one more than was sequenced by Weber et al. (3). Three copies of this domain are found in chicken tenascin-W, six in human, and nine in mouse. An exposed loop in this domain contains a potential integrin binding site, but this has yet to be demonstrated experimentally (2).

Phylogenetic tree construction is a more reliable way to identify homologues. When the fibrinogen-related domains of tenascins (the single large domain is easier to align than multiple—and variable—smaller domains) from zebrafish, chicken, mouse and human are used to establish their relationships using the phylogenetic tree-making program NGPhylogeny.fr (5), the mouse "tenascin-N" sequence clearly falls in the tenascin-W clade (**Figure 1A**). Similar results have been published by others (see below).

To date, the only evidence of tenascin-W expression in the central nervous system comes from Neidhardt et al. (4). Others found that the primary sites of expression are developing palate, bone and smooth muscle, certain stem cell niches, and in adult kidney, spleen, and periosteum (7–12). The absence of significant tenascin-W expression in brain parenchyme was confirmed by the tissue-based map of the human proteome published by Uhlén at el. (13).

Tenascin-W is also highly expressed in solid tumors (14–18). Details of tenascin-W expression in cancer can be found in a recent review (19).

How is tenascin-W expression regulated? Most of the work published to date on this subject has been done using C2C12 cells, or preosteoblast or osteo-chondroprogenitors, and these studies indicate that BMP-2 can upregulate tenascin-W expression, either directly or indirectly, through a p38-dependent signaling pathway (12, 14, 20). TNF-alpha can upregulate tenascin-W in mouse embryo fibroblasts (14), and Wnt3a, Wnt5a, and shear stress can upregulate tenascin-W expression in pre-osteoblastic MCT3T3-E1 cells (12). The regulation by Wnts is p38 dependent, but regulation by shear stress is JNK dependent. Tenascin-W expression accompanies osteoblastic differentiation in primary cultures (9), in Kusa-A1 cells (21) and in C2C12 cells (7), but not

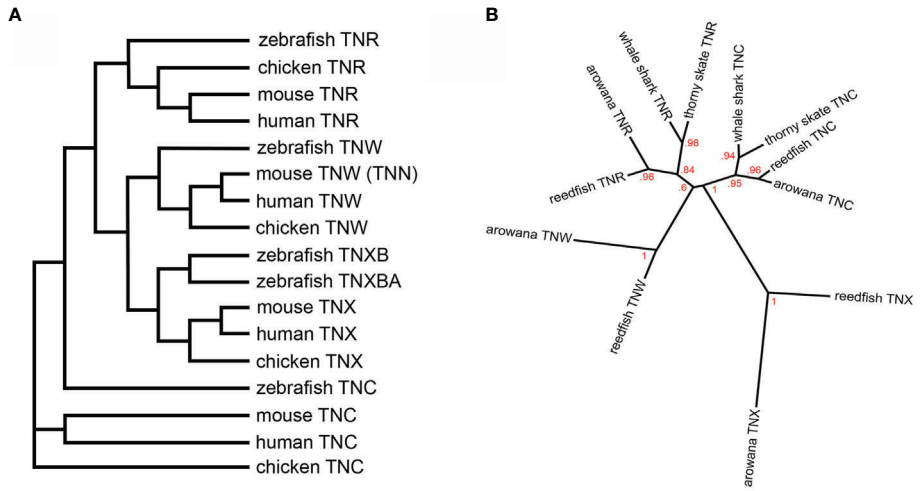

FIGURE 1 | **(A)** A dendrogram constructed using the fibrinogen-related domain amino acid sequences of zebrafish, chicken, mouse and human tenascins. The tree was constructed using the default tools and parameters at NGPhylogeny.fr (5). The murine tenascin-W (TNW), originally named tenascin-N (TNN), segregates to the TNW clade. **(B)** A phylogenetic tree constructed using the fibrinogen-related domain amino-acid sequences of tenascin-C (TNC) and tenascin-R (TNR) from the cartilaginous thorny skate and whale shark, as well as the ancient bony reedfish and arowana, and from the fibrinogen-related domains of reedfish and arowana tenascin-X (TNX) and TNW. The tree was constructed using the same parameters as Adams et al. (6) and branch support is indicated. TNW co-evolved with the bony fishes, most likely from a duplication of the TNR gene. See text for details.

in MCT3T3-E1 cells. In MCT3T3-E1 cells, tenascin-W expression dramatically decreases during osteogenic differentiation (12), and addition of exogenous tenascin-W to MCT3T3-E1 cells can inhibit their differentiation as well (20).

THE EVOLUTION OF TENASCIN-W

Tenascins are relatively modern additions to the extracellular matrix. Tenascins or tenascin-like proteins are limited to the Phylum Chordata (2, 6, 22, 23), suggesting that tenascins co-evolved with a dorsal hollow nerve cord and pharyngeal apparatus. In amphioxus and tunicates there are single tenascin genes, and phylogenetic trees constructed using the sequences of the fibrinogen-related domains do not place these tenascins from invertebrate chordates in any particular clade. Two tenascins are found in the lamprey, and in cartilaginous fish (the elephant shark *Callorhinchus milii*) there are three: tenascin-C, tenascin-R, and tenascin-X (6). Tenascin-W is present in all Euteleostomi (i.e., all chordates with bones). Since that report, the genomes of the thorny skate *Amblyraja radiata* and the whale shark *Rhincodon typus* have been reported. As with the elephant shark, these cartilaginous fish have tenascin-C (XM_033049212.1; XM_020527269.1) and tenascin-R (XM_033029137.1; XM_020515183.1), but they do not appear to have a tenascin-W.

Did tenascin-W evolve from tenascin-C or tenascin-R? Phylogenetic trees based on the amino acid sequences of the fibrinogen-related domains from bony chordates have been inconclusive (6). The addition of the skate and whale shark sequences to the analysis does suggest a closer, but still tenuous, relationship to tenascin-R of ancient Actinopterygii *Erpetoichthys calabaricus* (the reedfish) and the ancient teleost arowana *Scleropages formosus* (**Figure 1B**). The best evidence of the origin of tenascin-W is the observation that in all genomes examined tenascin-W is found adjacent to tenascin-R encoded in the opposite orientation (2). For example, in the zebrafish tenascin-W and tenascin-R are found adjacent to each other on chromosome 2, with tenascin-W on the negative strand and tenascin-R on the positive strand. In the mouse, these genes are adjacent to each other on chromosome 1, and once again tenascin-W is on the negative strand and tenascin-R is on the positive strand. This indicates that tenascin-W likely evolved from an isolated reverse tandem duplication event, and not from whole genome duplication. The latter probably resulted in the duplication of tenascin-X in the zebrafish, as tenascin-XB (XP_021323869.1) is on chromosome 19 and tenascin-XBA (XP_02132258.1) is on chromosome 16; chromosomes 19 and 16 in the zebrafish share a large number of paralogous genes (24). Interestingly, many of the genes that were duplicated in zebrafish by tandem duplication events have been linked to immune pathways (24).

FUTURE DIRECTIONS

Unlike tenascin-C, we still know very little about the basic biology of tenascin-W. It is typically abundant in solid tumors and can affect cancer cell behavior (19), but the significance of these observations is still unknown. It is possible that tenascin-W plays a role similar to tenascin-C in the creation of an immune-suppressive environment in tumor stroma (25), though this

hypothesis needs to be tested. The fibrinogen-related domain of tenascin-W, like that of tenascin-C, can bind and activate TLR4, which indicates tenascin-W may play a role in inflammation and inflammatory diseases (26). In addition, its prominent expression in the periosteum, a dense connective tissue around the bones containing progenitor cells that develop into osteoblasts, and at sites of osteogenesis, suggests a role for tenascin-W in bone repair and remodeling. The stimulating effect of tenascin-W on osteoblastic progenitors' differentiation and migration (9) seems to confirm this hypothesis, but contrary observations have also been published (20). It is likely that future studies of the role of tenascin-W in bone will not only clarify the role for this extracellular matrix in normal bone development and remodeling, but also after bone injury and in diseases. Such a function of tenascin-W remains to be demonstrated in animal models of bone fracture repair and of osteoporosis. The highly specific expression of tenascin-W in other (non-osteogenic) stem cell niches, like in the corneal limbus or cuspid niche of the aortic valve, strongly suggests a role in tissue homeostasis and repair after injury, which still requires experimental confirmation.

The authors of this perspective would also like to encourage those who study tenascin-W to use that name instead of tenascin-N, or at least include both in their descriptions. It seems more appropriate to recognize the original discover of the protein in zebrafish than to use the name that was attributed, incorrectly, by one of the first to find this protein in mouse almost 5 years later.

DATA AVAILABILITY STATEMENT

The original contributions presented in the study are included in the article/supplementary material. Further inquiries can be directed to the corresponding author.

AUTHOR CONTRIBUTIONS

Each author (MD, AS, and RT) contributed to the conception, writing, and/or final editing of this paper. All authors contributed to the article and approved the submitted version.

ACKNOWLEDGMENTS

The authors would like to acknowledge the critical roles played by our late friend, colleague, and mentor, Ruth Chiquet-Ehrismann, in the discovery and study of tenascins.

REFERENCES

1. Chiquet-Ehrismann R, Tucker RP. Tenascins and the importance of adhesion modulation. *Cold Spring Harb Perspect Biol* (2011) 3. doi: 10.1101/cshperspect.a004960
2. Tucker RP, Drabikowski K, Hess JF, Ferralli J, Chiquet-Ehrismann R, Adams JC. Phylogenetic analysis of the tenascin gene family: evidence of origin early in the chordate lineage. *BMC Evol Biol* (2006) 6:60. doi: 10.1186/1471-2148-6-60
3. Weber P, Montag D, Schachner M, Bernhardt RR. Zebrafish tenascin-W, a new member of the tenascin family. *J Neurobiol* (1998) 35:1–16.
4. Neidhardt J, Fehr S, Kutsche M, Löhler J, Schachner M. Tenascin-N: characterization of a novel member of the tenascin family that mediates neurite repulsion from hippocampal explants. *Mol Cell Neurosci* (2003) 23:193–209. doi: 10.1016/s1044-7431(03)00012-5
5. Lemoine F, Correia D, Lefort V, Doppelt-Azeroual O, Mareuil F, Cohen-Boulakia S, et al. NGPhylogeny.fr: new generation phylogenetic services for non-specialists. *Nucleic Acids Res* (2019) 47(W1):W260–5. doi: 10.1093/nar/gkz303
6. Adams JC, Chiquet-Ehrismann R, Tucker RP. The evolution of tenascins and fibronectin. *Cell Adh Migr* (2015) 9:22–33. doi: 10.4161/19336918.2014.970030
7. Scherberich A, Tucker RP, Samandari E, Brown-Luedi M, Martin D, Chiquet-Ehrismann R. Murine tenascin-W: a novel mammalian tenascin expressed in kidney and at sites of bone and smooth muscle development. *J Cell Sci* (2004) 117:571–81. doi: 10.1242/jcs.00867
8. Meloty-Kapella CV, Degen M, Chiquet-Ehrismann R, Tucker RP. Avian tenascin-W: expression in smooth muscle and bone, and effects on calvarial cell spreading and adhesion in vitro. *Dev Dyn* (2006) 235:1532–42. doi: 10.1002/dvdy.20731
9. Meloty-Kapella CV, Degen M, Chiquet-Ehrismann R, Tucker RP. Effects of tenascin-W on osteoblasts in vitro. *Cell Tissue Res* (2008) 334:445–55. doi: 10.1007/s00441-008-0715-4
10. Tucker RP, Ferralli J, Schittny JC, Chiquet-Ehrismann R. Tenascin-C and tenascin-W in whisker follicle stem cell niches: possible roles in regulating stem cell proliferation and migration. *J Cell Sci* (2013) 126:5111–15. doi: 10.1242/jcs.134650
11. Tucker RP, Peterson CA, Hendaoui I, Bichet S, Chiquet-Ehrismann R. The expression of tenascin-C and tenascin-W in human ossicles. *J Anat* (2016) 229:416–21. doi: 10.1111/joa.12496
12. Morgan JM, Wong A, Yellowley CE, Genetos DC. Regulation of tenascin expression in bone. *J Cell Biochem* (2011) 112:3354–63. doi: 10.1002/jcb.23265
13. Uhlén M, Fagerberg L, Hallström BM, Lindskog C, Oksvold P, Mardinoglu A, et al. Proteomics. Tissue-based map of the human proteome. *Science* (2015) 347:6220. doi: 10.1126/science.1260419
14. Scherberich A, Tucker RP, Degen M, Brown-Luedi M, Andres AC, Chiquet-Ehrismann R. Tenascin-W is found in malignant mammary tumors, promotes alpha8 integrin-dependent motility and requires p38MAPK activity for BMP-2 and TNF-alpha induced expression in vitro. *Oncogene* (2005) 24:1525–32. doi: 10.1038/sj.onc.1208342
15. Degen M, Brellier F, Kain R, Ruiz C, Terracciano L, Orend G, et al. Tenascin-W is a novel marker for activated tumor stroma in low-grade human breast cancer and influences cell behavior. *Cancer Res* (2007) 67:9169–79. doi: 10.1158/0008-5472.CAN-07-0666
16. Degen M, Brellier F, Schenk S, Driscoll R, Zaman K, Stupp R, et al. Tenascin-W, a new marker of cancer stroma, is elevated in sera of colon and breast cancer patients. *Int J Cancer* (2008) 122:2454–61. doi: 10.1002/ijc.23417
17. Martina E, Degen M, Ruegg C, Merlo A, Lino MM, Chiquet-Ehrismann R, et al. Tenascin-W is a specific marker of glioma-associated blood vessels and stimulates angiogenesis in vitro. *FASEB J* (2010) 24:778–87. doi: 10.1096/fj.09-140491
18. Brellier F, Martina E, Degen M, Heuze-Vourc'h N, Petit A, Kryza T, et al. Tenascin-W is a better cancer biomarker than tenascin-C for most human solid tumors. *BMC Clin Pathol* (2012) 12:14. doi: 10.1186/1472-6890-12-14
19. Tucker RP, Degen M. The expression and possible functions of tenascin-W during development and disease. *Front Cell Dev Biol* (2019) 7:53. doi: 10.3389/fcell.2019.00053
20. Kimura H, Akiyama H, Nakamura T, de Crombrugghe B. Tenascin-W inhibits proliferation and differentiation of preosteoblasts during endochondral bone formation. *Biochem Biophys Res Commun* (2007) 356:935–41. doi: 10.1016/j.bbrc.2007.03.071
21. Mikura A, Okuhara S, Saito M, Ota M, Ueda K, Iseki S. Association of tenascin-W expression with mineralization in mouse calvarial development.

Congenit Anom (Kyoto) (2009) 49:77–84. doi: 10.1111/j.1741-4520.2009.00227.x
22. Tucker RP, Chiquet-Ehrismann R. Evidence for the evolution of tenascin and fibronectin early in the chordate lineage. *Int J Biochem Cell Biol* (2009) 41:424–34. doi: 10.1016/j.biocel.2008.08.003
23. Özbek S, Balasubramanian PG, Chiquet-Ehrismann R, Tucker RP, Adams JC. The evolution of extracellular matrix. *Mol Biol Cell* (2010) 21:4300–5. doi: 10.1091/mbc.E10-03-0251
24. Howe K, Clark MD, Torroja CF, Torrance J, Berthelot C, Muffato M, et al. The zebrafish reference genome sequence and its relationship to the human genome. *Nature* (2013) 496:498–503. doi: 10.1038/nature12111
25. Spenlé C, Loustau T, Murdamoothoo D, Erne W, Beghelli-de la Forest Divonne S, Veber R, et al. Tenascin-C orchestrates an immune suppressive tumor microenvironment in oral squamous cell carcinoma. *Cancer Immunol Res* (2020) 8:1122–38. doi: 10.1158/2326-6066.CIR-20-0074
26. Zuliani-Alvarez L, Marzeda AM, Deligne C, Schwenzer A, McCann FE, Marsden BD, et al. Mapping tenascin-C interaction with toll-like receptor 4 reveals a new subset of endogenous inflammatory triggers. *Nat Commun* (2017) 8:1595. doi: 10.1038/s41467-017-01718-7

Conflict of Interest: The authors declare that the research was conducted in the absence of any commercial or financial relationships that could be construed as a potential conflict of interest.

frontiers in Immunology

OPINION
published: 03 February 2021
doi: 10.3389/fimmu.2020.620182

Serendipity; Close Encounter of Tenascin C

Teruyo Sakakura *

Department of Matrix Biology and Pathology, Mie University Graduate School of Medicine, Tsu City, Japan

Keywords: epithelial-mesenchymal interactions, morphogenesis, mammary gland, cancer, stroma

INTRODUCTION

In 1924, Hans Spemann and Hilde Mangold established the concept of embryonic induction (1). They transplanted the dorsal grey crescent region of one newt gastrula to the ventral part of another newt gastrula and found that a piece of the transplant induced the host tissue into the formation of a secondary embryo. With this as a starting point, the interactions among various tissues became the subject of follow up research during the next decade. In the 1950s, Clifford Grobstein discovered that organogenesis of glandular tissues in prenatal mice required morphogenetic interactions between epithelium and mesenchyme (2). Consequently, epithelial-mesenchymal interactions became a hot topic for developmental biologists worldwide. From 1967 to 1981, similar experiments were done on various organs such as salivary glands, kidney, pancreas, digestive tract, prostate, tooth, lung and mammary gland, etc.

In 1969, Klaus Kratochwil observed typical mammary gland morphogenesis by monopodial branching pattern in recombinant cultures of embryonic mammary epithelium with mammary mesenchyme. By contrast, mammary epithelium cultured in contact with salivary gland mesenchyme showed salivary gland like morphogenesis by dichotomous branching pattern (3). Prompted by this observation, Teruyo Sakakura and her colleagues conducted further analysis using *in vivo* system in 1976. They transplanted embryonic mammary epithelium combined with mammary or salivary mesenchyme under the kidney capsule and made the host female mice pregnant and lactating. The results were clear cut. Both grafted tissues produced milk (4). That is, mammary gland morphogenesis is mesenchyme-dependent, and cytodifferentiation is epithelium-specific. The ability to recapitulate morphogenesis persists in adult mammary epithelium. When embryonic mammary or salivary mesenchyme is transplanted into adult mammary gland, the epithelial cells in contact with the mesenchymal graft proliferate in multiple layers, forming duct-alveolar hyperplasia with nodular structure rapidly becoming cancerous (5, 6). Based upon these results, she built up a hypothesis that embryonic changes in the stroma must occur during cancer development.

DISCOVERY OF TENASCIN AS AN ONCOFETAL ECM PROTEIN

In 1984, Sakakura was invited by the director Edward Reich of the Friedrich-Miescher Institute in Basel asking her to organize a new group of breast cancer research. Ruth Chiquet-Ehrismann (Swiss), Eleanor J Mackie (Australian) and Caroline A Pearson (American) were the members of the new group. The research project was to identify stromal markers common in embryonic and malignant mammary glands. Extracellular matrix (ECM) proteins were hopeful, because the interactions

OPEN ACCESS

Edited by:
Kim Midwood,
University of Oxford, United Kingdom

Reviewed by:
Matthias Chiquet,
University of Bern, Switzerland

***Correspondence:**
Teruyo Sakakura
sakakura@houwakai.or.jp

Specialty section:
This article was submitted to Cancer Immunity and Immunotherapy, a section of the journal Frontiers in Immunology

Received: *22 October 2020*
Accepted: *31 December 2020*
Published: *03 February 2021*

Citation:
Sakakura T (2021) Serendipity; Close Encounter of Tenascin C. Front. Immunol. 11:620182. doi: 10.3389/fimmu.2020.620182

between epithelium and mesenchyme are not by diffusible factors but by matrix-bound morphogens. They had collected various antibodies against ECM substances. Sprague-Dawley rats were used in the experiments. Mammary tumors were induced by intravenous injection of N-methyl-N-nitrosourea. By fluorescent antibody method they stained embryonic mammary glands and cancers. Among them, an antibody against an ECM protein already reported as "myotendinous antigen" (7) was found to be suitable molecule and the molecule was renamed "tenascin". Ruth and her husband Matthias Chiquet (Univresity of Basel) were the godparents. Thus, the discovery of tenascin-C as an oncofetal ECM protein was indeed by serendipity. The photographs of mammary tumors stained with anti-tenascin antibody were chosen as the cover of the Cell journal (8). As for the function of tenascin, growth stimulation of tumor cells was suggested. When rat mammary tumor cells were cultured on the plates coated with several ECM proteins (tenascin, fibronectin, collagen I, collagen IV, and laminin), tenascin was a poor adhesive substrate but nevertheless the most effective in promoting cell growth after serum was removed from the culture medium (8).

In the period of 1983 to 1985, several other ECM glycoproteins had been reported independently from different laboratories: glioma-mesenchymal extracellular matrix (GMEM) (9), hexabrachion (10), J1 (11), and cytotactin (12). In terms of their gene structures and electron microscopy images, all of these molecules were considered to be identical to tenascin. The protein was renamed tenascin C (TN-C) later.

After Sakakura returned to Japan, she organized several groups at the Aichi Cancer Center Research Institute, then RIKEN and Mie University School of Medicine. These groups carried out establishment of the purification method of human TN-C and production of monoclonal antibodies against human TN-C (13), cDNA cloning of mouse TN-C (14), and generation of lines of TN-C knockout mice (15). TN-C knockout mice were initially found to be viable and fertile, but that further studies clearly showed the importance of TN-C as a disease-associated stress protein later in life.

We happened to meet tenascin by sheer serendipity. TN-C is always detected in the stroma when the tissue is under reconstruction, such as developmental morphogenesis, inflammatory process, cancer cell growth and invasion. It is just like an ambulance to appear in an accident.

AUTHOR CONTRIBUTIONS

The author confirms being the sole contributor of this work and has approved it for publication.

ACKNOWLEDGMENTS

The author thanks Dr. Yasuhiro Tomooka (Tokyo University of Science).

REFERENCES

1. Spemann H, Mangold H. Induction of embryonic primordia by implantation on organizers from a different species. *Int J Dev Biol* (1924) 45:13–38.
2. Grobstein C. Morphogenetic interaction between embryonic mouse tissues separated by membrane filter. *Nature* (1953) 172:869–71. doi: 10.1038/172869a0
3. Kratochwil K. Organ specificity in mesenchymal induction demonstrated in the embryonic development of the mammary gland of the mouse. *Dev Biol* (1969) 20:46–71. doi: 10.1016/0012-1606(69)90004-9
4. Sakakura T, Nishizuka Y, Dawe CJ. Mesenchyme-dependent morphogenesis and epithelium-specific cytodifferentiation in mouse mammary gland. *Science.* (1976) 194:1439–41. doi: 10.126/science.827022
5. Sakakura T, Sakagami Y, Nishizuka Y. Persistence of responsiveness of adult mouse mammary gland to induction by embryonic mesenchyme. *Dev Biol* (1979) 72:201–19. doi: 10.1016/0012-1606(79)90111-8
6. Sakakura T, Sakagami Y, Nishizuka Y. Accelerated mammary cancer development by fetal salivary mesenchyme isografted to adult mammary epithelium. *J Natl Cancer Inst* (1981) 66:953–9.
7. Chiquet M, Fambrough DM. Chick myotendinous antigen. I. A monoclonal antibody as a marker for tendon and muscle morphogeneis. *J Cell Biol* (1984) 98:1926–36. doi: 10.083/jcb.98.6
8. Chiquet-Ehrismann R, Mackie EJ, Pearson CA, Sakakura T. Tenascin: an extracellular matrix protein involved in tissue interactions during fetal development and oncogenesis. *Cell.* (1986) 47:131–9. doi: 10.1016/0092-8674(86)90374-0
9. Bourdon MA, Wikstrand CJ, Fruthmayr H, Matthews TJ, Bigner DD. Human glioma-mesenchymal extracellular matrix antigen defined by monoclonal antibody. *Cancer Res* (1983) 43:2796–805.
10. Erickson HP, Inglesias JL. A six-armed oligomer isolated from cell surface fibronectin preparations. *Nature* (1984) 311:267–9. doi: 10.1038/311267a0
11. Kruse J, Keihauer G, Faissner A, Timple R, Schachner M. The J1 glycoprotein : A novel nervous system cell adhesion molecule of the L2/HNK-1 family. *Nature.* (1985) 316:146–8. doi: 10.1038/316146a0
12. Grumet M, Hoffman S, Grossin KL, Edelman GM. Cytotactin, and extracellular matrix protein of neural and non-neural tissues that mediates glia-neuron interaction. *Proc Natl Acad Sci USA*. (1985) 82:8075–9. doi: 10.1073/pnas.82.23.8075
13. Oike Y, Hiraiwa N, Kawakatsu H, Nishikai M, Okinaka T, Suzuki T, et al. Isolation and characterization of human fibfroblast tenascin. An extracellular matrix plycoprotein of interest for developmental studies. *Int J Dev Biol* (1990) 34:309–17.
14. Saga Y, Tsukamoto T, Jing N, Kusakabe M, Sakakura T. Mouse tenascin: cDNA cloning and spatiotemporal expression of isoforms. *Gene.* (1991) 104:177–85. doi: 10.1016/0378-1119(91)90248-a
15. Saga Y, Yagi T, Ikawa Y, Sakakura T, Aizawa S. Mice develop normally without tenascin. *Genes Dev* (1992) 6:1821–31. doi: 10.101/gad.6.10

Conflict of Interest: The author declares that the research was conducted in the absence of any commercial or financial relationships that could be construed as a potential conflict of interest.

frontiers in Immunology

ORIGINAL RESEARCH
published: 19 February 2021
doi: 10.3389/fimmu.2020.624612

Different Functions of Recombinantly Expressed Domains of Tenascin-C in Glial Scar Formation

Dunja Bijelić[1], Marija Adžić[1], Mina Perić[1], Igor Jakovčevski[2], Eckart Förster[2], Melitta Schachner[3] and Pavle R. Andjus[1]**

[1] Centre for Laser Microscopy, Faculty of Biology, Institute of Physiology and Biochemistry "Jean Giaja", University of Belgrade, Belgrade, Serbia, [2] Institut für Neuroanatomie und Molekulare Hirnforschung, Ruhr-Universität Bochum, Bochum, Germany, [3] Keck Center for Collaborative Neuroscience and Department of Cell Biology and Neuroscience, Rutgers University, Piscataway, NJ, United States

OPEN ACCESS

Edited by:
Kyoko Imanaka-Yoshida, Mie University, Japan

Reviewed by:
Shizuya Saika, Wakayama Medical University Hospital, Japan
Hideki Kanamaru, Mie University, Japan

***Correspondence:**
Pavle R. Andjus
pandjus@bio.bg.ac.rs
Melitta Schachner
schachner@dls.rutgers.edu

Specialty section:
This article was submitted to Inflammation, a section of the journal Frontiers in Immunology

Received: 31 October 2020
Accepted: 31 December 2020
Published: 19 February 2021

Citation:
Bijelić D, Adžić M, Perić M, Jakovčevski I, Förster E, Schachner M and Andjus PR (2021) Different Functions of Recombinantly Expressed Domains of Tenascin-C in Glial Scar Formation. Front. Immunol. 11:624612. doi: 10.3389/fimmu.2020.624612

Extracellular matrix glycoprotein tenascin-C (TnC) is highly expressed in vertebrates during embryonic development and thereafter transiently in tissue niches undergoing extensive remodeling during regeneration after injury. TnC's different functions can be attributed to its multimodular structure represented by distinct domains and alternatively spliced isoforms. Upon central nervous system injury, TnC is upregulated and secreted into the extracellular matrix mainly by astrocytes. The goal of the present study was to elucidate the role of different TnC domains in events that take place after spinal cord injury (SCI). Astrocyte cultures prepared from TnC-deficient (TnC-/-) and wild-type (TnC+/+) mice were scratched and treated with different recombinantly generated TnC fragments. Gap closure, cell proliferation and expression of GFAP and cytokines were determined in these cultures. Gap closure *in vitro* was found to be delayed by TnC fragments, an effect mainly mediated by decreasing proliferation of astrocytes. The most potent effects were observed with fragments FnD, FnA and their combination. TnC-/- astrocyte cultures exhibited higher GFAP protein and mRNA expression levels, regardless of the type of fragment used for treatment. Application of TnC fragments induced also pro-inflammatory cytokine production by astrocytes *in vitro*. *In vivo*, however, the addition of FnD or Fn(D+A) led to a difference between the two genotypes, with higher levels of GFAP expression in TnC+/+ mice. FnD treatment of injured TnC-/- mice increased the density of activated microglia/macrophages in the injury region, while overall cell proliferation in the injury site was not affected. We suggest that altogether these results may explain how the reaction of astrocytes is delayed while their localization is restricted to the border of the injury site to allow microglia/macrophages to form a lesion core during the first stages of glial scar formation, as mediated by TnC and, in particular, the alternatively spliced FnD domain.

Keywords: astrocyte, glial scar, microglia/macrophages, spinal cord injury, tenascin-C

INTRODUCTION

Spinal cord injury (SCI) is a severe neurological disorder with a limited hope for recovery, thus presenting a health care and socioeconomic problem. SCI is a two-step process, primary mechanical injury is followed by secondary inflammation and apoptosis through which existing injury spreads further into the surrounding tissue (1). The hallmark of these events is the formation of the glial scar with two distinct parts. The lesion core is formed by stromal fibroblasts and inflammatory immune cells, while hypertrophic astrocytes demarcate the lesion border (2). The role of the glial scar has been often discussed, once seen as a barrier to complete regeneration (3), but often regarded as important for axonal regrowth and as the source of growth factors and other permissive molecules (4). A majority of cellular functions, signal transduction, and tissue homeostasis are maintained by extracellular matrix components (ECM) making the ECM an interesting target for modulation of the outcome of injury. It is noteworthy in this context that the ECM glycoprotein tenascin-C (TnC) is strongly upregulated after injury of central nervous system (5).

Tenascin-C (TnC) is a large multimodular glycoprotein with a hexabrahion structure (6). Each arm contains four distinct domains: amino-terminal tenascin assembly (TA) domain, epidermal growth factor-like (EGFL) repeats, fibronectin type III (FnIII) domains, and a globular fibrinogen-homology domain (FG) located at the distal end. Among FnIII repeats, eight domains are constitutively expressed (Fn1-8), while nine are alternatively spliced (FnA1, FnA2, FnA3, FnA4, FnB, FnAD2, FnAD1, FnC, and FnD). Alternative RNA splicing yields various isoforms of TnC with different numbers of domains (7, 8). Via its structurally distinct domains and by variations in domains resulting from alternative splicing, TnC is predisposed to interact with different types of cellular receptors or components of the extracellular matrix, thereby generating an impressive functional diversity (9). In the central nervous system, TnC is widely expressed at early developmental stages (10), being mainly synthesized by immature astrocytes and radial glia during neuronal migration and differentiation (11). TnC stimulates astrocyte proliferation *in vitro* (12) and contributes to regenerative processes, such as peripheral nerve regeneration and wound healing in the brain (13–15). It also regulates the phenotype of cultured astrocytes *in vitro*, thus possibly contributing to astrocytic scar formation after spinal cord injury (16). TnC is also known to interact with other extracellular matrix components, including fibronectin (17, 18) and chondroitin sulfate proteoglycans (19, 20), relevant for regeneration after injury.

Recovery of locomotor functions after spinal cord injury in constitutively TnC-deficient (TnC-/-) mice was found to be reduced when compared with their wild-type (TnC+/+) littermates. Overexpression of the FnD domain of TnC in injured spinal cords improved regeneration (21). In TnC-/- mice synaptic rearrangements in the lumbar spinal cord and the H-reflex response were both attenuated after injury when compared with wild-type littermates. It is thus conceivable that TnC exerts its beneficial effects by modifying synaptic responses to injury (21). These findings are in agreement with previous observations that TnC enhances neurite outgrowth and supports neuronal survival (22, 23).

TnC is transiently expressed in acute inflammation and may contribute to chronic inflammation in pathological conditions (24). TnC also plays a role in temporal and spatial modulation of inflammation after SCI (25). Since TnC may promote axonal regrowth during acute inflammation, but also contribute to further damage during the chronic phase, investigation of individual TnC domains at specific times and in specific cell types is much needed. Since after SCI TnC is secreted mainly by astrocytes, we examined the impact of individual TnC fragments on astrocytic physiology *in vitro* and *in vivo*.

TNC-null mice were crucial for discovering the significance of heterophilic and homophilic TNC interactions in glial scar formation. The same mice were instrumental in the initial discovery of positive effects of TNC on regeneration after spinal cord injury (21). We now report on the dissection of functional TNC domains which may allow designing structures of therapeutic value. Results of our present study indicate that gap closure *in vitro* in an astrocyte scratch assay is delayed by TnC fibronectin-like fragments, mainly due to decreasing astrocyte proliferation. Fragments also upregulated mRNA levels of pro-inflammatory cytokines in astrocyte cell cultures. In spinal cord tissue, addition of TnC fragments immediately after SCI did not alter total cell proliferation rate. TnC, and in particular fragment FnD increased the numbers of activated microglia/macrophages 7 days after injury. Altogether results may explain how astrocyte functions are restricted to the border of the injury site to allow microglia/macrophages to form a lesion core during the first stages of glial scar formation through TnC, and in particular FnD.

MATERIALS AND METHODS

Animals

Animals used in experiments were wild-type C57BL/6 (TnC+/+) mice and constitutively tenascin-C deficient (TnC-/-) mice inbred on the C57BL/6 background for more than 10 generations, and maintained in the Animal Facility of the Faculty of Biology, University of Belgrade. Animals were housed under standard conditions (21 ± 1°C, 50% humidity, 12:12 h light/dark cycle, water and food ad libitum). TnC-/- mice were derived from the original colony (26). All experimental procedures complied with the NIH Guide for Care and Use of Laboratory Animals (1985) and the European Communities Council Directive (86/609/EEC) and were approved by the Ethics Committee of the Faculty of Biology, University of Belgrade.

Treatments

Five recombinantly expressed proteins representing different domains of TnC were studied. We used all alternatively spliced fragments and some of these that are present in all variants of the tenascin-C molecule. For injury experiments, we used the alternatively spliced FnD and FnA fragments, as they were

shown to be the most promising ones in the *in vitro* experiments (23) and in a previous *in vivo* study (21). Alternatively spliced fragments are of special interest as they are upregulated upon injury (27).

Fibronectin type III-like repeats 6-8 (Fn 6-8) and epidermal growth factor-like repeats (EGFL) are constitutively expressed, whereas fibronectin type III-like repeats A, D, and C (FnA, FnD, FnC) are generated by alternative splicing. Fragments were generated as described (28). For *in vitro* experiments, treatment groups were labelled as follows: "SW" for the control group with only scratch wounding performed, "no SW" for non-injured cells, "EGFL", "FnA", "FnC", "FnD", "Fn6-8", for groups in which the fragments were individually added after SW, and "Fn(D+A)", "Fn(D+A+C)" for groups in which a combination of fragments was added. For *in vivo* experiments, all labels were the same except for the control group, which was named "Injury", indicating that only compression spinal cord injury (SCI) was performed.

Chemicals, Reagents, and Solutions

Acrylamide/Bis-acrylamide, ammonium persulfate (APS), bovine serum albumin (BSA), diethyl pyrocarbonate (DEPC), chloroform, EDTA, glucose, glycerol, Mowiol embedding medium, NP 40, paraformaldehyde (PFA), poly-L-lysine (PLL), sodium dodecyl sulphate (SDS), tetramethyl ethylenediamine (TEMED), Tris base, Triton™ X-100, trypsin, Tween 20, β-mercaptoethanol, NaCl, Na_2HPO_4, $NaHCO_3$, NaOH, HCl, KH_2PO_4, KCl were from Sigma-Aldrich (St. Louis, Missouri, USA). Leibovitz's L-15 medium, penicillin/streptomycin, foetal bovine serum (FBS), Dulbecco's modified Eagle's medium (DMEM) were from Gibco (Thermo Fisher Scientific, USA). TRIzol reagent, H_2O, Power SYBR™ Green PCR Master Mix were from Invitrogen (Thermo Fisher Scientific, USA). High Capacity cDNA Reverse Transcription Kit was from Applied Biosystems (Thermo Fisher Scientific, USA). 4,6-Diamidino-2-phenylindole (DAPI) was from Molecular Probes (Thermo Fisher Scientific, USA). Protease/phosphatase inhibitor cocktail, Pierce micro BCA Protein Assay Kit, and PAGE ruler were from Thermo Fisher Scientific, USA. Clarity ECL Substrate was from BioRad Laboratories (Hercules, CA, USA). Ethanol, isopropanol, and methanol were from Zorka Pharma (Šabac, Serbia).

Cortical Astrocyte Culture

Primary cell cultures were prepared as described (29). Briefly, for each genotype cortices from three mice, 0 to 2 days old, of both sexes were pooled. Tissue was mechanically dissociated and then centrifuged twice at 500xg for 5 min. Before the third centrifugation, the cell suspension was passed successively 3–5 times through 21G (ø 0.8 mm) and 23G (ø 0.6 mm) needles. All steps were performed in Leibowitz L-15 isolating medium supplemented with 100 IU/ml penicillin, 0.1 mg/ml streptomycin, and 0.1% BSA. Finally, cells were resuspended in growth medium (Dulbecco's modified Eagle medium-low glucose, DMEM, supplemented with 10% foetal bovine serum, D-glucose to a final concentration of 25 mmol/L, 100 IU/ml penicillin, and 100 μg/ml streptomycin), seeded in a 60 mm Petri dish and maintained in a humidified atmosphere of 5% CO_2/95% air at 37°C. The culture medium was replaced every 2 to 3 days. Upon reaching confluency, cells were trypsinized (0.25% trypsin and 0.02% EDTA) and seeded in new Petri dishes. Once confluence was reached again, cells were seeded according to the particular experimental design. Three cell cultures per genotype were prepared for all *in vitro* experiments.

Scratch Wound Assay

For the scratch wound assay (SW), astrocytes were seeded in 35 mm Petri dishes at a density of 2×10^4 cells/cm^2 and maintained until complete confluency as described (30, 31). Monolayers were scratched with a sterile 200 μl pipette tip, followed by addition of fresh culture medium containing 10 μg/ml per TnC fragments. Three to four scratches were made per Petri dish. To ensure imaging of the same fields at different times, a straight line was drawn in the middle of the Petri dish bottom. For each SW, two areas, just above and below the line, were imaged using the AxioObserver A1 inverted microscope (Carl Zeiss GmbH, Germany), EM512 CCD (Digital Camera System, Evolve, Photometrics), and 10× (A-Plan) objective. Cells were imaged immediately after scratching and addition of fragments (0 h), and later at 6, 12, 24, and 48 h. For each image a gap border was selected and the gap area (μm^2) was determined using the ImageJ software package. Relative wound closure was calculated with the formula:

$$\text{Relative } \textit{woundclosure} = [A(t_0) - A(t)]/A(t_0)$$

where A represents wound area determined at a given time point t.

Immunocytochemistry

For immunolabeling, cells were maintained on PLL-coated glass coverslips (ø 15 mm). Twenty-four h after scratching and treatment with TnC fragments, cells were fixed in 4% formaldehyde for 20 min at room temperature (RT). After several washes with phosphate-buffered saline (PBS), cells were permeabilized with 0.1% Triton in PBS for 15 min and blocked with a solution containing 5% BSA in PBS for 1 h, at RT. Following the overnight incubation with primary rabbit anti-Ki67 (1:500, Abcam, ab15580, RRID: AB_443209) or rabbit anti-GFAP (1:500, DAKO, Z0334, RRID: AB_10013382) antibodies in 1% BSA in PBS at 4°C, cells were washed and incubated with secondary donkey anti-rabbit AlexaFluor-555 antibodies for 2 h, at RT and in the dark (1:200, Invitrogen A-31572, RRID: AB_162543). Nuclei were stained with DAPI (1:4,000, for 15 min, at RT), and the glass coverslips were mounted on microscope slides with MOWIOL solution. Micrographs along the SW were acquired using AxioObserver A1 inverted microscope (Carl Zeiss GmbH, Germany), EM512 CCD (Digital Camera System, Evolve, Photometrics), and 10× (A-Plan) objective. Omission of primary antibodies did not show immunoreactivity. Images were quantified using ImageJ software. Proliferation rate was defined as the proportion of Ki67+ nuclei within the total number of DAPI+ nuclei. GFAP immunoreactivity was quantified and presented as the corrected total cell fluorescence (CTCF) of integrated density, calculated

for each frame after using the "Rolling ball" background subtraction method in ImageJ software.

Western Blot Analysis

Astrocytes seeded in 60 mm Petri dishes were scratched and treated with TnC fragments. Twenty-four h later, cultures were washed with pre-heated PBS, mechanically detached by scraping, collected in ice-cold PBS, and centrifuged for 5 min at 500×g. The pellet was resuspended in 500 µl of ice-cold RIPA lysis buffer, supplemented with 0.5% w/v protease inhibitor cocktail. Subsequently, lysates were centrifuged for 10 min at 10,000×g and 4°C. The supernatant was collected and the protein concentration was determined using the BCA protein assay kit, according to the manufacturer's instruction. Samples (5 µg protein) were mixed with 6× Laemmle sample buffer (375 mM Tris-HCl, pH 6.8, 12% SDS, 60% w/v glycerol, and 0.03% bromophenol blue). Proteins were resolved on 12% SDS-PAGE gels and electrotransferred to a PVDF support membrane (Immobilon-P transfer membrane, Millipore, Merck, Germany). Membranes were blocked with 5% BSA in Tris buffered saline/Tween 20 (TBST) and incubated overnight at 4°C with primary rabbit anti-GFAP antibodies (1:7,000, DAKO, Z0334, RRID: AB_10013382), followed by a 2 h incubation with secondary HRP-conjugated donkey anti-rabbit antibody (1:10,000, Santa Cruz, sc-2305, AB_641180). Bands were visualized with ECL solution and Chemi Doc-It imaging system (UVP, Upland, CA, USA). Membranes were then subjected to Abcam mild stripping protocol: two times in stripping buffer for 10 min, two times in PBS for 10 min, and two times in TBST for 5 min. Membranes were blocked as above-mentioned, incubated with mouse anti-β-actin (1:1,000, Santa Cruz, sc-47778, RRID: AB_2714189) overnight at 4°C, followed by secondary HRP-conjugated donkey anti-mouse antibody (1:10,000, Santa Cruz, sc-2096, RRID: AB_641168). Bands were visualized as stated above, and quantified using ImageJ software. The measured optical density of GFAP immunoreactivity was normalized to the corresponding optical density of β-actin bands serving as a loading control.

mRNA Isolation and Real-Time PCR

Astrocytes were seeded in 6-well plates at 2×10^4 cells/cm^2 density. After reaching confluence, the cultures were subjected to SW and treated with TnC fragments. Six hours later, sample lysates were collected using TRIzol reagent and the total RNA was subjected to phenol/chloroform extraction and ethanol precipitation (32). Since it has been shown that the median half-life of mRNA for all genes in mammals is up to 7 h, after which time mRNA is less stable/decays (33), we decided that 6 h would be the most appropriate time point to analyze the effects of fragments and also to not lose the information due to various signaling convergence and mRNA decay. The 6 h mRNA expression usually correlates with the protein abundance peak occurring 12–24 h later, which was confirmed in the present case. RNA concentrations were determined by measuring the absorbance at 260 nm and the purity was estimated from 260/280 nm and 260/230 nm ratios. For the synthesis of cDNA, 1 µg of total RNA was used. The real-time PCR reaction mixture contained 2 µl cDNA, 5 µl QTM SYBR Green PCR Master Mix, 0.5 µl of both reverse and forward primers (100 pmol/µl), and 2 µl RNase-free water. Amplification was carried out under the following conditions: 10 min of enzyme activation at 95°C, 40 cycles of 15 s denaturation at 95°C, 30 s annealing at 64°C, 30 s amplification at 72°C, and 5 s fluorescence measurements at 72°C. The amplification and product detection were carried out with QuantStudioTM 3 Real-Time PCR System (Applied Biosystems, Foster City, CA, USA). Relative gene expression is presented as a $\log_2$-fold change of mRNA expression. β-actin was used as a housekeeping molecule. Primer sequences are listed in **Table 1**.

Spinal Cord Injury

Compression spinal cord injury (SCI) was performed on 10- to 12-week-old mice as described (21). In short, before surgery, animals were anesthetized by intraperitoneal injections of ketamine and xylazine (100 and 5 mg/kg body weight, respectively, both from Sigma-Aldrich). Laminectomy was carried out at the T7–T9 level using mouse laminectomy forceps (Fine Science Tools, Foster City, California, USA). Then, the exposed spinal cord was compressed for 1 s using a custom-made device that consisted of watchmaker forceps mounted on a stereotaxic frame and driven by an electromagnetic device. Immediately after the injury, fragments FnD, FnA, their combination (300 µg/ml per treatment), or the vehicle control (0.9% NaCl in water) were injected into the lesion site. Injections into areas surrounding the injury site were also carried out 1 mm rostrally and caudally to the lesion site. Next, the skin was closed with a 3-0 silk suture (Ethicon, Somerville, New Jersey, USA). Mice were then kept on heating pads at 35°C for 24 h to prevent hypothermia and caged individually in a temperature-controlled room (22°C) on soft bedding with softened rodent chow and water within reach ad libitum. Bladders were manually voided twice a day. Animals were sacrificed 7 days later.

Four animals per group [vehicle control, FnA, FnD, Fn(D+A)] per each genotype (32 mice in total) underwent spinal cord injury. Criteria for the exclusion of mice from the study were, per ethical permit, weight loss of more than 20% over 24 h, passive position of animal in the cage, the lack of reaction to the experimenter, overall poor general condition as seen by the animal being immobile, cold with wet hair, and signs of severe urinary infection. Three animals were excluded for these reasons.

Tissue Preparation and Immunohistochemistry

Mice were perfused transcardially under anesthesia with saline (0.9% NaCl) for 30 s, followed by perfusion with 4% formaldehyde in 0.1 M phosphate buffer for 10 min. The spinal cord was then removed through double laminectomy

TABLE 1 | List of primer pairs for real-time PCR.

Target gene	Forward	Reverse
GFAP	CGGAGACGCATCACCTCTG	TGGAGGAGTCATTCGAGACAA
TNF-α	CTGAACTTCGGGGTGATCGG	GGCTTGTCACTCGAATTTTGAGA
Il-1β	AAAAGCCTCGTGCTGTCGGACC	TTGAGGCCCAAGGCCACAGGT
β-actin	GGGCTATGCTCTCCCTCAC	GATGTCACGCACGATTTCC

and placed in 4% formaldehyde for 2 h at 4°C. After post-fixation, tissue was cryoprotected in 0.1 M phosphate buffer supplemented with 30% sucrose at 4°C overnight and then frozen at -80°C until further use. Sagittal serial sections (25 µm thick) were cut using a LeicaCM 1850 cryostat (Leica Microsystems, Wetzlar, Germany), and sections were collected on SuperFrost®Plus slides (Menzel-Gläser, Braunschweig, Germany). After rehydration in PBS, sagittal spinal cord sections were covered with 0.1% glycine in PBS for 10 min at RT. Blocking with 10% bovine serum albumin (BSA) and 0.1% Triton X-100 was performed for 45 min at RT. Primary antibodies were diluted in 2% BSA in PBS and kept on the tissue sections overnight at 4°C. The following primary antibodies were used: mouse anti-GFAP (1:400, DAKO, Z0334), goat anti-Iba1 (1:300, Abcam) and rabbit anti-Ki67 (1:200, Abcam). After several washes in PBS, secondary antibodies diluted in PBS with 2% BSA were incubated for 2 h in the dark at RT. Secondary antibodies were donkey anti-mouse Alexa 488 (1:200, Invitrogen), donkey anti-goat Alexa 488 (1:200, Invitrogen), and donkey anti-rabbit Alexa 555 (1:200, Invitrogen). After washing with PBS, slides were incubated with TO-PRO 3 (1:40,000; Thermo Ficher Scientific T3605) to counterstain nuclei. Sections were rinsed with PBS and mounted in MOWIOL medium (Sigma Aldrich).

Confocal Imaging, Analysis of Proliferation and GFAP Immunoreactivity in Tissue Sections

Cell proliferation and GFAP immunoreactivity at the injury site were analyzed in spinal cords of three animals per group [Injury only, Injury plus FnA, FnD, or Fn(D+A)] in both genotypes. Five sections per spinal cord were examined. A confocal laser microscope (LSM 510, Carl Zeiss, Jena, Germany) equipped with 488 nm Argon, 555 and 633 nm HeNe lasers was used for obtaining images. Z-stacks were obtained in the visible zone of the injury using oil-immersion Plan Neofluar 40x 1.3 NA objective. For proliferation rates, results were expressed as the portion of Ki67+ nuclei in total DAPI+ numbers in cell cultures or TO-PRO-3 stained nuclei in tissue sections using ImageJ (Rasband, W.S., ImageJ, National Institutes of Health, Bethesda, Maryland, USA, https://imagej.nih.gov/ij/, 1997-2018.). GFAP immunoreactivity was quantified and is presented as the corrected total cell fluorescence (CTCF) of integrated density, calculated for each frame after using the "Rolling ball" background subtraction method in ImageJ software.

Stereological Analysis

The density of microglial cells in spinal cord tissue sections was obtained by stereological analysis as described (34). Counting was carried out with an Axio Imager. M1 microscope (Carl Zeiss) equipped with a motorized stage and a Stereo Investigator 9 software-controlled microscope system (MicroBrightField). First, a low-power magnification (10× objective) was used to outline the injury region and equally sized rostral and caudal regions next to it which extended for ≤1,500 µm on both sides of the injury site. In both genotypes, spinal cords from three animals were analyzed for each group (Injury, FnD). Six sections (25 µm, every 10 serial section) per spinal cord were investigated. Cells were counted based on Iba1 immunoreactivity and DAPI fluorescence and classified as activated microglia if they exhibited a polygonal shape or as resting if they showed a branched morphology. The following parameters were set: guard space depth, 2 µm, base and height of the dissector, 60x60 µm, and 10 µm; distance between the optical dissectors, 180 µm; objective 20× Plan-Neofluar 20×/0.50.

Statistical Analysis

Two-way ANOVA was used to determine the effects of treatment and genotype regarding the examined parameters in cultures or tissue sections. Three-way ANOVA was used to analyze the effect of treatment, genotype and sampling position (injury, rostral or caudal) on the density of microglia. Statistically significant interactions, simple main effects, and pairwise comparisons were determined. All pairwise comparisons were run for each simple main effect with 95% confidence intervals and p-values Bonferroni-adjusted within each simple main effect. All computations were performed using the SPSS 20 software package (SPSS Inc., Chicago, IL, USA). Data from each experiment are summarized as a box and whisker plot and shown as mean ± SD throughout the Results section. Values for p within the range of 0.001–0.05 are given as precise numbers, whereas values lower than 0.001 are presented as <0.001.

RESULTS

Tenascin-C Fragments Attenuate Gap Closure *In Vitro*

A scratch wound assay was performed in TnC+/+ and TnC-/- cortical astrocyte cultures to measure the response to mechanical injury (30). It is worth mentioning that mechanical stretching of an astrocyte monolayer is not the most adequate model for assaying glial scar formation since it lacks many components of *in vivo* injury (35). Unlike in tissues where astrocytes are confined to the lesion border, they are the only cell type in cultures.

First, we assessed whether the rate of gap closure differs between the two genotypes upon the addition of different TnC fragments. Cells were monitored at 0, 6, 12, 24, and 48 h after scratching (see an example of ImageJ measurements in **Figure 1A**). Zero h served as a reference for closure calculation, and by 48 h all gaps were closed regardless of treatment. As described (36) and observed in our present study, the most informative time point is 24 h after scratching, allowing for evaluation of fragment application, astrocytic activation, and stable progression of the astrocytic front (**Figure 1B**). Quantifications of other time points with the exception of 0 and 48 h are given as stacked bar charts (**Supplementary Figure 1**). Representative images of the gap area of the same frame taken at 0 and 24 h in control group (SW) and groups treated with FnA, FnD, and Fn(D+A) are shown in **Figure 1C**.

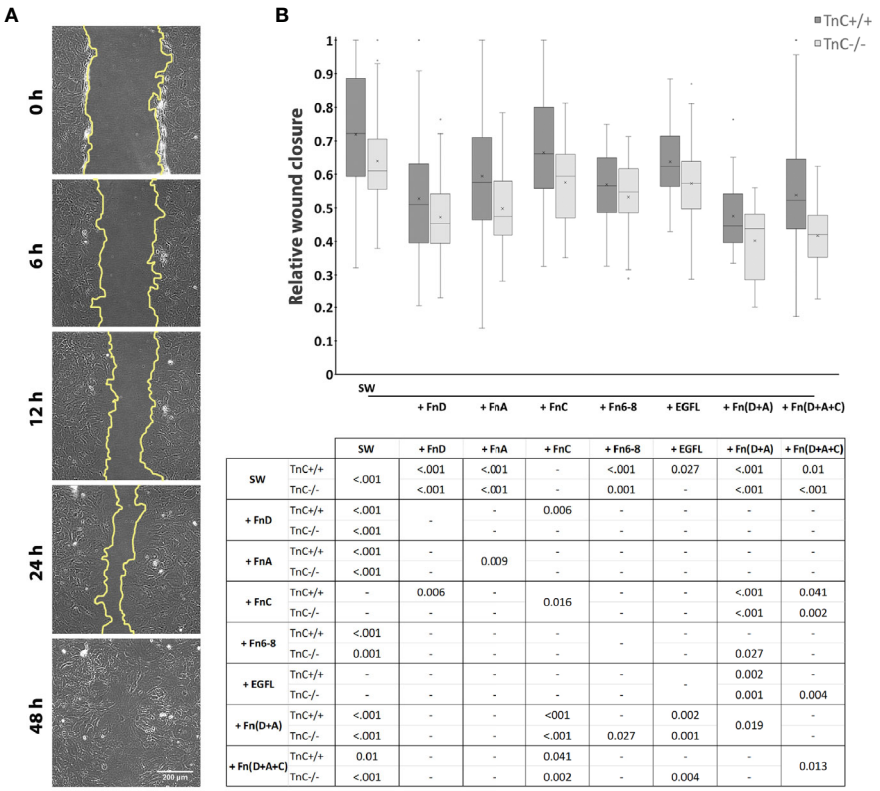

		SW	+ FnD	+ FnA	+ FnC	+ Fn6-8	+ EGFL	+ Fn(D+A)	+ Fn(D+A+C)
SW	TnC+/+	<.001	<.001	<.001	-	<.001	0.027	<.001	0.01
	TnC-/-		<.001	<.001	-	0.001	-	<.001	<.001
+ FnD	TnC+/+	<.001	-	-	0.006	-	-	-	-
	TnC-/-	<.001		-	-	-	-	-	-
+ FnA	TnC+/+	<.001	-	0.009	-	-	-	-	-
	TnC-/-	<.001	-		-	-	-	-	-
+ FnC	TnC+/+	-	0.006	-	0.016	-	-	<.001	0.041
	TnC-/-	-	-	-		-	-	<.001	0.002
+ Fn6-8	TnC+/+	<.001	-	-	-	-	-	-	-
	TnC-/-	0.001	-	-	-		-	0.027	-
+ EGFL	TnC+/+	-	-	-	-	-	-	0.002	-
	TnC-/-	-	-	-	-	-		0.001	0.004
+ Fn(D+A)	TnC+/+	<.001	-	-	<001	-	0.002	0.019	-
	TnC-/-	<.001	-	-	<.001	0.027	0.001		-
+ Fn(D+A+C)	TnC+/+	0.01	-	-	0.041	-	-	-	0.013
	TnC-/-	<.001	-	-	0.002	-	0.004	-	

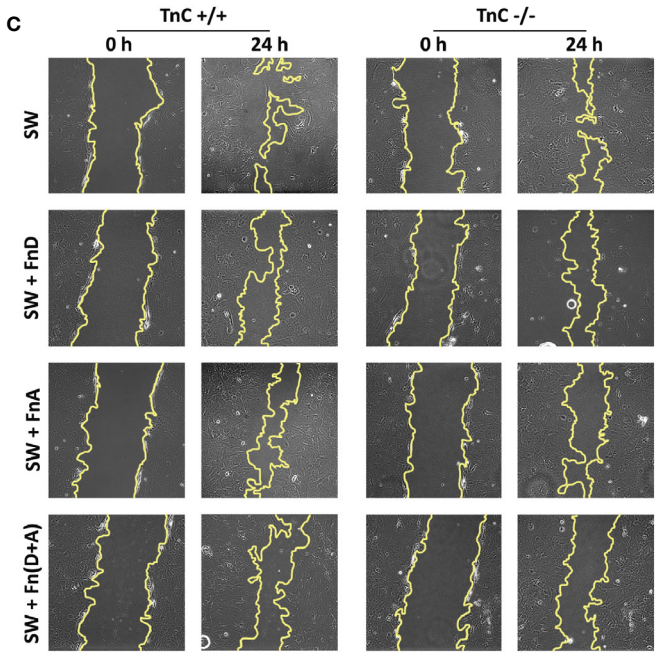

FIGURE 1 | TnC fragments attenuate wound closure in cultured astrocytes. **(A)** Representative brightfield images of five time points of the gap area measured in the ImageJ program. **(B)** Relative wound closure is presented in a box-and-whisker plot indicating the impact of TnC fragments on gap closure in TnC+/+ and TnC-/- cortical astrocyte cultures after 24 h. Two-way ANOVA analysis shows no interaction between genotype and treatment, but both the effects of treatment and genotype were significantly different ($p < 0.001$). The most potent effect was produced by FnA, FnD, and combinations Fn(D+A) and Fn(D+A+C) in both genotypes. All pairwise significance comparisons are given in the table below the box-and-whisker plot. n = 3 independent astrocyte culture preparations. **(C)** Representative images of the gap at 0 and 24 h after scratching in the control group (SW) and groups treated with FnA, FnD, and Fn(D+A).

Both the effects of treatment and genotype were significant ($p < 0.001$). The rate of injury closure reached the highest values in the control TnC+/+ group, with application of fragments retarding this process. Compared to the control group (SW), addition of FnA, FnD, Fn6-8, EGFL, Fn(D+A), and Fn(D+A+C) decreased the gap closure [p < 0.001 for FnA, FnD, Fn6-8, Fn(D+A); p = 0.027 for EGFL; p = 0.010 for Fn(D+A+C)]. Fragments FnC and EGFL did not affect gap closure. FnD decreased gap closure compared to FnC ($p = 0.006$). Combination Fn(D+A) slowed down the gap closure compared to FnC ($p < 0.001$) and EGFL ($p < 0.001$). Similarly, Fn(D+A+C) decreased gap closure compared to FnC ($p = 0.041$). In cultures of TnC-/- mice, where gap closure was most pronounced in the control group, fragments FnA, FnD, Fn6-8, Fn(D+A), and Fn (D+A+C) reduced gap closure [p < 0.001 for FnA, FnD, Fn(D+A), Fn(D+A+C); p = 0.010 for Fn6-8], while FnC and EGFL did not affect gap closure. The combined fragments Fn(D+A) also reduced gap closure when compared to FnC, Fn6-8, and EGFL ($p < 0.001$, $p = 0.027$, $p < 0.001$, respectively), while combination Fn(D+A+C) showed lower closure rates than FnC ($p < 0.001$) and EGFL ($p = 0.004$). In TnC+/+ cultures, gap closure was more pronounced than in TnC-/- cultures ($p < 0.001$). FnD and Fn6-8 attenuated gap closure in both genotypes, while FnA, FnC, Fn (D+A+C) attenuated gap closure in TnC-/- genotype (FnA: $p = 0.009$; FnC: $p = 0.016$; D+A+C: $p = 0.013$). Mean values ± standard deviations for each treatment and genotype are shown in **Table 2**.

Tenascin-C Fragments Reduce Proliferation Rate *In Vitro*

Migration and proliferation are two main processes that contribute to gap closure after scratching. Previous data show that the rate of astrocyte migration after scratching is the same as in non-injured, low density cultures used as a control group, whereas proliferation increases, making only proliferation an injury-specific response (30). On the basis of these observations, we assessed the proliferation rate (Ki67+/DAPI+ numbers) 24 h after scratching and application of fragments (**Figures 2A, B**). In this experiment another treatment group was added with no scratching and addition of fragments (no SW). There was a significant interaction between the effects of genotype and treatment on cell proliferation rate ($p = 0.005$) with both the effects of genotype and treatment being significant ($p = 0.040$, $p < 0.001$).

In TnC+/+ cultures the highest rate of proliferation was observed in the control SW group, while the addition of all fragments or their combinations decreased it [$p < 0.001$ for EGFL, FnA, FnC, FnD, Fn6-8, Fn(D+A), Fn(D+A+C)]. EGFL, FnA, FnD, Fn6-8, Fn(D+A), Fn(D+A+C) reduced proliferation compared to FnC [$p < 0.001$, except for Fn(D+A+C), $p = 0.004$]. Fn(D+A+C) led to a higher proliferation rate compared to FnD ($p = 0.012$), FnA ($p = 0.001$), Fn6-8 ($p < 0.001$), and EGFL ($p = 0.001$). The no SW group exhibited a higher proliferation rate than other treatments ($p < 0.001$), but was not different from the SW group.

Similarly, in the TnC-/- group the highest rate of proliferation was observed in the SW group, while the addition of all fragments or their combinations reduced it [$p < 0.001$ for EGFL, FnA, FnC, FnD, Fn6-8, Fn(D+A), Fn(D+A+C)]. Compared to FnC, the other treatments reduced the proliferation rate [EGFL, FnA, FnD, Fn6-8, Fn(D+A) and Fn(D+A+C), $p < 0.001$ for all]. Fragment FnA additionally reduced the proliferation rate compared to EGFL ($p = 0.039$). No SW group had a lower proliferation rate than the SW group ($p < 0.001$), but a higher proliferation rate than all other treatment groups ($p < 0.001$ for all) except for FnC. Comparisons within each treatment, between the two genotypes, showed a significant difference only in SW ($p = 0.007$), FnC ($p = 0.020$), Fn6-8 ($p = 0.052$), EGFL ($p < 0.001$) groups, where higher proliferation rates were observed in TnC-/- cultures. Mean values ± standard deviations for each treatment and genotype are shown in **Table 3**.

GFAP Expression is Upregulated in Tenascin-C-/- Astrocyte Cultures Regardless of Fragment Addition

GFAP, as a cytoskeletal marker protein of astrocytes, is upregulated after scratching (37). TnC also affects the levels of GFAP in lesion-activated astrocytes *in vitro* (38). Therefore, we examined *Gfap* mRNA (**Figure 3A**) and protein levels (**Figures 3B–D**) upon SW and treatment with TnC fragments (6 and 24 h, respectively).

Only the genotype`s effect on *Gfap* mRNA levels was significant ($p < 0.001$). *Gfap* mRNA expression levels in TnC -/- showed a $\log_2$-fold increase versus the TnC+/+ in the SW group. Compared to TnC+/+ cultures, upregulation of TnC-/- *Gfap* mRNA levels was most pronounced in the no SW group (TnC+/+ vs TnC-/-: 1.061 $\log_2$-fold change, $p = 0.041$) and in the FnC treatment group (TnC+/+ vs TnC-/-: 1.180 $\log_2$-fold change), while Fn(D+A) only tended to show upregulation (TnC+/+ vs TnC-/-: 0.680 $\log_2$-fold change, not significant).

GFAP protein expression was measured by Western blot analysis 24 h after SW and application of fragments (**Figure 3B**). Representative images of GFAP (48 kDa) and β-actin (42 kDa) are in **Figure 3C**. Only the genotype`s effect on protein levels was significant ($p < 0.001$). GFAP was more expressed in the no SW group in TnC-/- cultures compared to TnC+/+ cultures (no SW: 2.15 ± 1.14; no SW: 0.97 ± 0.30, $p < 0.001$). Scratch wounding and treatments resulted in GFAP protein upregulation in TnC-/- cultures compared to the TnC+/+ cultures in the SW, FnD, FnA, and FnC groups ($p < 0.001$; $p = 0.003$;

TABLE 2 | Mean value ± standard deviation for relative gap closure.

	SW	+EGFL	+FnA	+FnC	+FnD	+Fn6-8	+Fn(D+A)	+Fn(D+A+C)
TnC +/+	0.74 ± 0.19	0.64 ± 0.12	0.59 ± 0.19	0.66 ± 0.16	0.53 ± 0.19	0.57 ± 0.11	0.48 ± 0.11	0.54 ± 0.20
TnC -/-	0.64 ± 0.12	0.57 ± 0.13	0.50 ± .12	0.58 ± 0.11	0.47 ± 0.11	0.53 ± 0.11	0.40 ± 0.10	0.42 ± 0.09

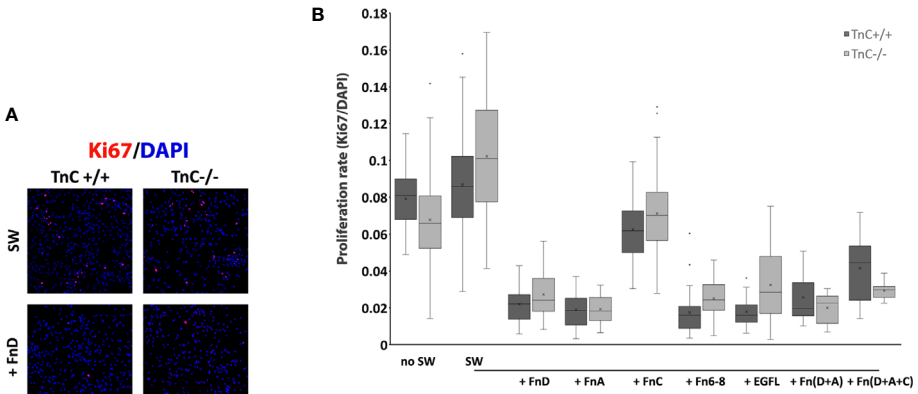

		no SW	SW	+ FnD	+ FnA	+ FnC	+ Fn6-8	+ EGFL	+ Fn(D+A)	+ Fn(D+A+C)
no SW	TnC+/+	-	-	<.001	<.001	<.001	<.001	<.001	<.001	<.001
	TnC-/-		<.001	<.001	<.001	-	<.001	<.001	<.001	<.001
SW	TnC+/+	-	0.007	<.001	<.001	<.001	<.001	<.001	<.001	<.001
	TnC-/-	<.001		<.001	<.001	<.001	<.001	<.001	<.001	<.001
+ FnD	TnC+/+	<.001	<.001	-	-	<.001	-	-	-	0.012
	TnC-/-	<.001	<.001		-	<.001	-	-	-	-
+ FnA	TnC+/+	<.001	<.001	-	-	<.001	-	-	-	0.001
	TnC-/-	<.001	<.001	-		<.001	-	0.039	-	-
+ FnC	TnC+/+	<.001	<.001	<.001	<.001	0.020	<.001	<.001	<.001	0.004
	TnC-/-	-	<.001	<.001	<.001		<.001	<.001	<.001	<.001
+ Fn6-8	TnC+/+	<.001	<.001	-	-	<.001	0.052	-	-	-
	TnC-/-	<.001	<.001	-	-	<.001		-	-	<.001
+ EGFL	TnC+/+	<.001	<.001	-	-	<.001	-	<.001	-	0.001
	TnC-/-	<.001	<.001	-	0.039	<.001	-		-	-
+ Fn(D+A)	TnC+/+	<.001	<.001	-	-	<.001	-	-	-	-
	TnC-/-	<.001	<.001	-	-	<.001	-	-		-
+ Fn(D+A+C)	TnC+/+	<.001	<.001	0.012	0.001	0.004	-	0.001	-	-
	TnC-/-	<.001	<.001	-	-	<.001	<.001	-	-	

FIGURE 2 | TnC fragments reduce proliferation in the astrocyte scratch wound assay. **(A)** Representative micrographs of Ki67+/DAPI+ immunofluorescence at 24 h after scratching in the control group and groups treated with FnA, FnD, and Fn(D+A); bar: 200 μm. **(B)** Proliferation was calculated as the number of Ki67+ nuclei compared to total DAPI+ nuclei. Results are presented as a box-and-whisker plot. Two-way ANOVA analysis shows a statistically significant interaction between the effects of genotype and treatment on cell proliferation rate ($p = 0.005$) with both the effects of genotype and treatment being significant ($p = 0.040$, $p < 0.001$, respectively). A statistically significant decrease in proliferation is seen in the presence of FnA, FnD, and Fn(D+A). All statistically significant pairwise comparisons are displayed below the box-and-whisker plot. n = 3 independent astrocyte cultures.

$p = 0.002$; $p = 0.001$, respectively). Immunostaining was performed to visually confirm Western blot GFAP protein expression levels (**Figure 3D**).

Pro-Inflammatory Tnf-α and IL-1β Levels are Upregulated by FnD, FnA, Fn6-8, and EGFL in Both Genotypes

It has been reported that TnC upregulates pro-inflammatory cytokine production in different cell types although there are no data available for astrocytes (39). Cytokine production in astrocyte cultures after scratching and addition of TnC fragments was tested in terms of mRNA levels of *Tnf-α*, *Il-1β*, *Il-6*, and *Il-10*, with *Il-6* and *Il-10* not being detectable. rtPCR results for *Tnf-α* mRNA levels showed that the treatment effect was significant ($p < 0.001$) (**Figure 4A**). In TnC+/+ cultures, addition of EGFL, FnA, FnD, and Fn6-8 fragments upregulated *Tnf-α* mRNA expression compared to SW, compared to the no SW group and compared to the FnC group. Similarly, in TnC-/- cultures, EGFL, FnA, FnD and Fn6-8 fragments increased *Tnf-α* mRNA levels compared to SW, no SW and FnC treatment group. In the case of *IL-1β* mRNA expression (**Figure 4B**) the effect of the treatment was significant ($p < 0.001$). Application of fragments EGFL, FnA, FnD and Fn6-8 upregulated *Il-1β* mRNA levels in TnC+/+ cultures compared to the SW group ($p < 0.001$ for FnA and FnD; $p = 0.001$ for EGFL and Fn6-8), no SW ($p < 0.001$ for EGFL, FnA, FnD, Fn6-8) and FnC ($p = 0.001$ for FnA and FnD; $p = 0.003$ for EGFL and Fn6-8). Similarly, in TnC-/- cultures, EGFL, FnA, FnD and Fn6-8 increased *Il-1β* mRNA expression when compared to SW ($p = 0.001$ for EGFL and FnA; $p < 0.001$ for FnD and Fn6-8), no SW ($p < 0.001$ for EGFL, FnA, FnD, Fn6-8) and FnC; ($p < 0.001$ for EGFL, FnA, FnD, Fn6-8). Mean values ± standard deviations for levels of proinflammatory cytokines TNF-α and IL-1β in astrocyte culture are presented in **Tables 4** and **5**, respectively.

TABLE 3 | Mean values ± standard deviations of proliferation rate in the astrocyte scratch wound assay.

	no SW	SW	+EGFL	+FnA	+FnC	+FnD	+Fn6-8	+Fn(D+A)	+Fn(D+A+C)
TnC +/+	0.079 ± 0.015	0.087 ± 0.026	0.018 ± 0.008	0.019 ± 0.010	0.062 ± 0.016	0.022 ± 0.010	0.017 ± 0.012	0.026 ± 0.013	0.042 ± 0.017
TnC-/-	0.078 ± 0.032	0.098 ± 0.032	0.032 ± 0.020	0.019 ± 0.007	0.071 ± 0.023	0.027 ± 0.011	0.025 ± 0.011	0.020 ± 0.008	0.029 ± 0.004

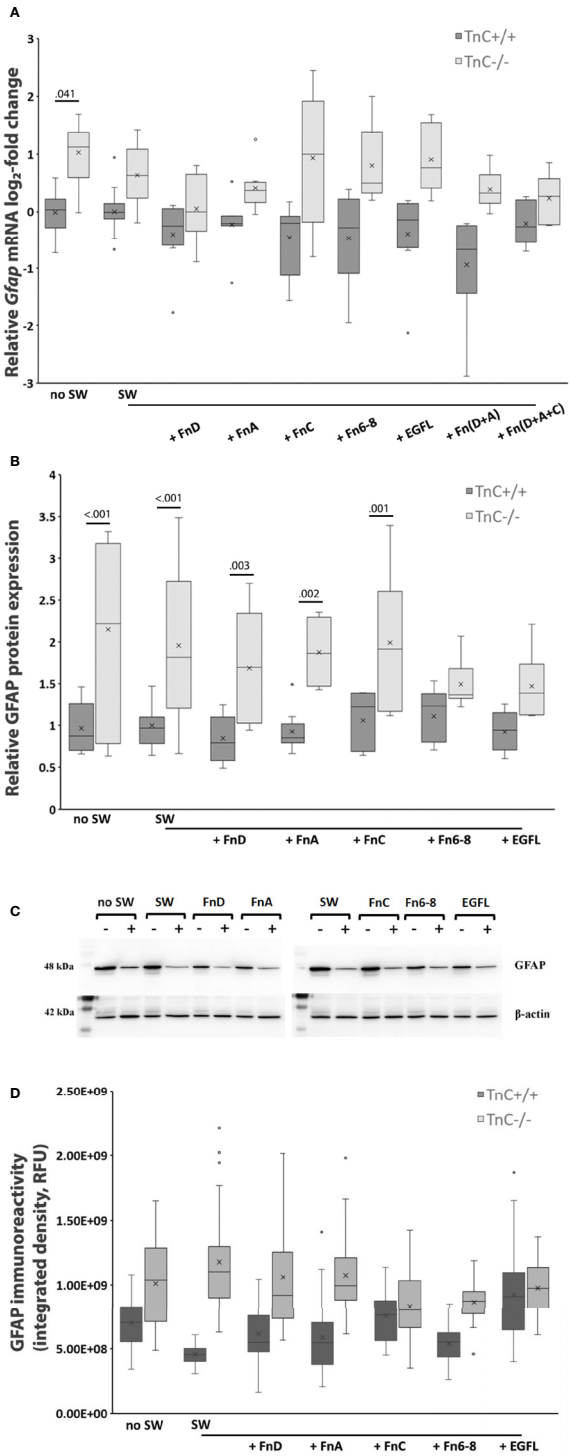

FIGURE 3 | GFAP expression is upregulated in TnC-/- astrocyte cultures both in the absence and presence of fragments. **(A)** Relative log_2-fold change of *Gfap* mRNA expression 6 h after scratching and fragment addition is shown in a box-and-whisker plot. Two-way ANOVA shows a genotype effect ($p < 0.001$). *Gfap* mRNA was significantly upregulated in TnC-/- no SW group compared to its TnC+/+ counterpart ($p = 0.041$). n = 4 independent astrocyte culture preparations. **(B)** Relative GFAP protein expression as estimated by Western blot analysis 24 h after scratching and application of fragments. Results are presented as box-and-whisker plot. Two-way ANOVA shows statistical significance of genotype ($p < 0.001$). GFAP is more expressed in the no SW group of TnC-/- versus TnC+/+ cultures ($p < 0.001$). Scratching alone and FnA, FnC, and FnD application lead to upregulation of GFAP protein levels in TnC-/- versus TnC+/+ astrocytes ($p < 0.001$; $p = 0.003$; $p = 0.002$: $p = 0.001$, respectively). n = 3 independent astrocyte culture preparations. **(C)** Representative images of Western blots for GFAP (48 kDa) and β-actin (42 kDa). **(D)** GFAP immunoreactivity is presented as Integrated density box-and-whisker plot. n = 1 astrocyte culture.

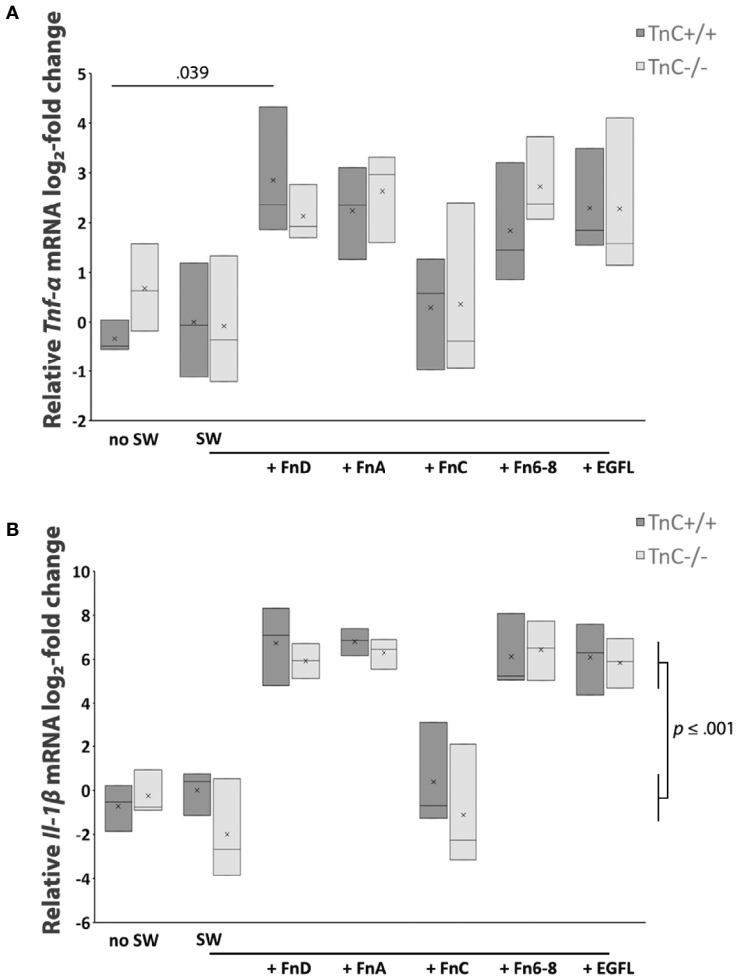

FIGURE 4 | Pro-inflammatory cytokines TNF-α and IL-1β are upregulated by FnD, FnA, Fn6-8, and EGFL fragments in astrocyte cultures of both genotypes. **(A)** Relative log_2-fold change of *Tnf-α* mRNA expression 6 h after scratching and fragment addition is presented in a box-and-whisker plot. Two-way ANOVA shows that only the treatment effect was significantly different ($p < 0.001$). In both TnC+/+ and TnC-/- genotypes, FnD, FnA, Fn6-8, and EGFL upregulate *Tnf-α* mRNA levels (~ 2 log_2-fold change for all conditions) versus the no SW, SW, and FnC groups. Only the FnD fragment statistically upregulates *Tnf-α* mRNA levels versus the no SW in TnC+/+ cultures ($p = 0.039$). n = 3 independent astrocyte culture preparation. **(B)** Relative log_2-fold change of *Il-1β* mRNA levels 6 h after scratching and fragment addition as presented in the box-and-whisker plot. Two-way ANOVA shows that only the treatment was statistically significant ($p < 0.001$). In TnC+/+ and TnC-/- cultures, addition of EGFL, FnA, FnD, and Fn6-8 upregulates *Il-1β* mRNA levels (~ 7 log_2-fold change, $p \leq 0.001$ for all conditions) versus levels of no SW, SW, and FnC. n = 3 independent astrocyte cultures.

Tenascin-C Affects Astrocytes and Microglia/Macrophages in Injured Spinal Cords

In vivo glial scar formation was induced by compression SCI. Evaluation was performed 7 days after the injury when inflammation is in its early phase and thus can be modulated *via* different mechanisms (40).

Proliferation *in vivo* was estimated in the same way as *in vitro* and in reference to all cell types in the injury region (**Figures 5A, B**). Ki67 immunolabeling indicated higher levels of proliferating cells within the region of injury and a decrease of such cells

TABLE 4 | Mean values ± standard deviations of proinflammatory cytokine TNF-α in astrocyte cultures.

	no SW	SW	+EGFL	+FnA	+FnC	+FnD	+Fn6-8
TnC +/+	-0.33 ± 0.32	0.00 ± 1.16	2.29 ± 1.04	2.24 ± 0.92	0.29 ± 1.15	2.85 ± 1.30	1.84 ± 1.22
TnC-/-	0.68 ± 0.88	-0.08 ± 1.30	2.28 ± 1.60	2.63 ± 0.91	0.36 ± 1.79	2.13 ± 0.56	2.72 ± 0.88

TABLE 5 | Mean values ± standard deviations of proinflammatory cytokine IL-1β levels in astrocyte cultures.

	no SW	SW	+EGFL	+FnA	+FnC	+FnD	+Fn6-8
TnC +/+	-0.73 ± 1.05	0.00 ± 0.99	6.09 ± 1.61	6.81 ± 0.61	0.37± 2.37	6.73 ± 1.78	6.12 ± 1.70
TnC-/-	-0.25 ± 1.02	-2.01 ± 2.27	5.84 ± 1.13	6.30 ± 0.68	-1.12 ± 2.81	5.92 ± 0.79	6.43 ± 1.35

further away, in all groups (**Figure 5A**). Even though two-way ANOVA showed that the overall effect of fragment application was significant (p = 0.043), pairwise comparisons revealed no significant difference (**Figure 5B**).

Quantification of GFAP immunoreactivity (**Figure 5C**) in the injury region revealed a statistically significant effect of genotype (p < 0.001), as well as a statistically significant interaction of genotype and treatment effects (p = 0.034). Addition of fragment

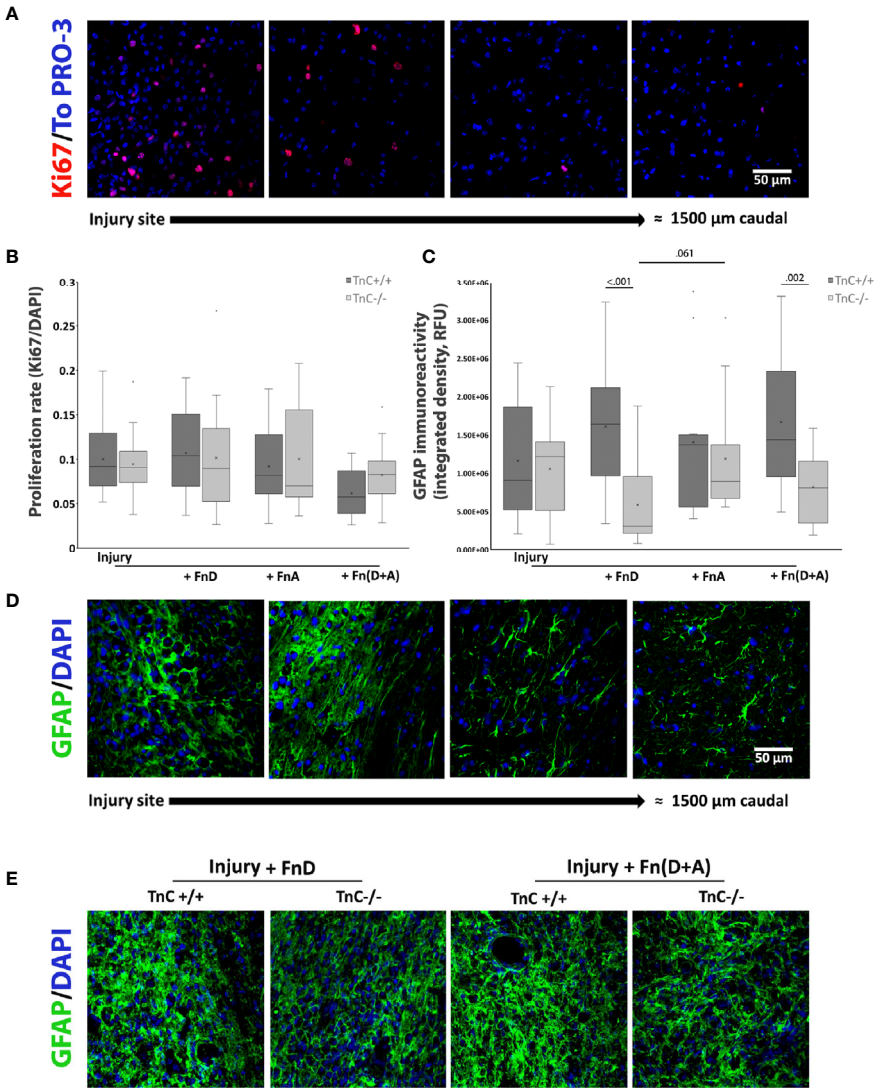

FIGURE 5 | Proliferation and GFAP expression after spinal cord injury and TnC fragment application in TnC+/+ and TnC -/- mice. **(A)** Representative images of Ki67 and TO-PRO-3 immunostainings. More proliferating cells are present at the injury region, whereas a decrease in Ki67+ cells is observed further away from the injury site. Calibration bar for all panels: 50 µm. **(B)** Proliferation is calculated as the number of Ki67+ nuclei compared to TOPRO-3+ nuclei 7 days after injury. Results are presented as box-and-whisker plots. Even though the two-way ANOVA shows that the treatments' overall effect was significant (p = 0.043), pairwise comparisons do not show significant differences. n = 3 animals per group for each genotype. **(C)** GFAP immunoreactivity at the injury region is presented as Integrated density in the box-and-whisker plot. Two-way ANOVA reveals a significant effect of genotype (p < 0.001) and significant interaction of genotype and treatment (p = 0.034). GFAP immunoreactivity is lower at 7 days after injury and application of FnD and Fn(D+A) in TnC-/- versus TnC+/+ mice. n = 3 animals per group for each genotype. **(D)** Representative images of GFAP and DAPI immunostaining reveal a change in the morphology of GFAP+ astrocytes at the injury region versus more caudal sites. Calibration bar for all panels: 50 µm. **(E)** GFAP and DAPI immunofluorescence at and around the injury site in the spinal cord of TnC+/+ and TnC-/- mice treated with FnD and Fn(D+A).

FnD to TnC-/- mice decreased GFAP immunoreactivity compared to FnD in TnC+/+ animals ($p < 0.001$). This effect was also observed with combined Fn(D+A) treatment ($p = 0.002$). Representative images of GFAP immunofluorescence at the injury site of spinal cord treated with FnD and Fn(D+A) fragments in both genotypes are presented in **Figure 5E**. In TnC-/- mice, although FnD reduced GFAP immunoreactivity compared to FnA, only a trend was observed ($p = 0.061$). Change in the morphology of GFAP positive astrocytes in the injury region compared to the more rostral or caudal regions in the spinal cord was also observed (**Figure 5D**). Astrocytes within the injury region formed a honeycomb-like structure, characteristic of the glial scar (41), whereas more distally they exhibited the fibrous quiescent phenotype (**Figure 5D**). Mean values ± standard deviations of GFAP immunoreactivity at the injury region are presented in **Table 6**.

Another typical glial scar element, especially within the first week after injury, are microglia/macrophages (40, 42). Whereas astrocyte processes overlap at the site of injury and cell bodies are difficult to distinguish individually, activated microglia/macrophages are recognized as distinct polygonal cells, being framed by astrocytes (**Figures 6A**). Thus, the density of activated and resting microglia/macrophages could be quantified throughout the injury region and surrounding rostral and caudal regions. The overall effects of genotype and sampling position on the density of activated microglia were significant ($p < 0.001$), as well as their interaction in the injury group ($p = 0.032$) (**Figure 6B**). The density of activated microglia/macrophages within the injury site was higher in TnC+/+ mice in both injury and FnD groups compared to other regions ($p < 0.001$). In FnD- treated TnC-/- mice, the density of activated microglia/macrophages in the injury region was higher than in rostral ($p = 0.003$) or caudal ($p < 0.001$) regions. When normalized to the total microglia/macrophage number, the proportion of activated microglia was higher in the injury site compared to rostral and to caudal positions in all of the conditions ($p < 0.001$) reaching the highest value in the TnC+/+ injury group (**Figure 6C**). Total microglial cell numbers were

TABLE 6 | Mean values ± standard deviations of GFAP immunoreactivity at the injury site of the spinal cord.

	Injury	+FnA	+FnD	+Fn(D+A)
TnC +/+	$1.16E^{+06} \pm 7.67E^{+05}$	$1.41E^{+06} \pm 9.47E^{+05}$	$1.61E^{+06} \pm 8.03E^{+05}$	$1.67E^{+06} \pm 8.79E^{+05}$
TnC -/-	$1.06E^{+06} \pm 5.95E^{+05}$	$1.19E^{+06} \pm 7.01E^{+05}$	$5.87E^{+05} \pm 5.42E^{+05}$	$8.21E^{+05} \pm 4.46E^{+05}$

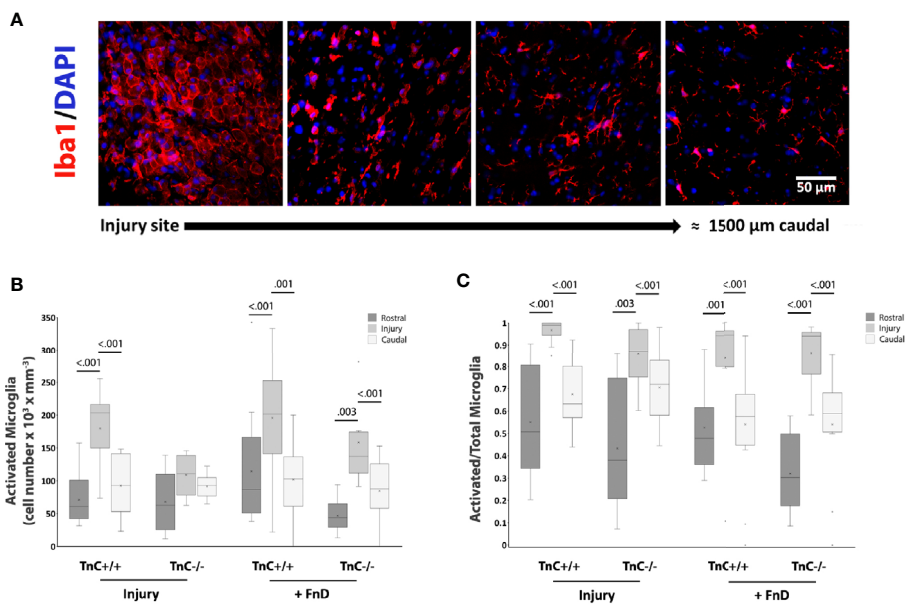

FIGURE 6 | TnC affects activation of microglia in the injury region. **(A)** Representative images of Iba1+ and DAPI immunostaining show activated, polygonal microglia framed by astrocytes, at the injury site, and a more quiescent microglia phenotype further away. Calibration bar for all panels: 50 µm. **(B)** Density of activated microglia by stereo-investigator analysis at the injury region and surrounding rostral and caudal regions of equal size 7 days after injury. Results are shown as a box-and-whisker plot. The effects of genotype and sampling position on the density of activated microglia are significant ($p < 0.001$), as well as their interaction in the Injury group ($p = 0.032$) as analyzed by three-way ANOVA. The density of activated microglia in TnC+/+ mice in the injury region is higher in TnC+/+ mice in both Injury and FnD groups compared to the other sampling positions ($p < 0.001$). FnD application in TnC-/- mice increases the density of activated microglia at the injury region more so than rostrally ($p = 0.003$) or caudally ($p < 0.001$. **(C)** A box-and-whisker plot showing Activated/(Activated + Resting) microglia numbers per region. The proportion of activated microglia is higher at the injury site than rostrally and caudally in the injury and FnD groups of both genotypes ($p < 0.001$). n = 3 animals per group for each genotype.

calculated as the sum of activated and resting microglia. Resting microglia density was a complementary image of activated microglia density (**Supplementary Figure S2**). Average numbers ± standard deviations of activated microglia in the spinal cord injury site of TnC +/+ and TnC -/- mice are presented in **Table 7**, and mean values ± standard deviations of the portion of activated microglia out of total microglia numbers is presented in **Table 8**.

DISCUSSION

We studied the effects of TnC and its fragments on the glial reaction to injury *in vitro* and *in vivo*. In the context of an astrocyte scratch assay, we found that, independent of the genotype, TnC fragments attenuated gap closure. FnD and its combination with the fragment FnA were the most effective. Proliferation of astrocytes *in vitro* was decreased upon application of alternatively spliced FnD, FnA, FnC, their combinations and constitutively expressed Fn6-8 and EGFL fragments. These results suggest that fragments delay gap closure through decreased astrocyte proliferation.

Previous observations indicate that astrocyte proliferation is enhanced in a scratch wound assay (30), while TnC is known to reduce proliferation of adult human astrocytes *in vitro* (16). Alternatively spliced region encompassing FnIII repeats from A to D binds to the cell surface annexin II receptor (43), which inhibits cell migration in the process of gap closure (44). A smaller, 190 kDa isoform of TnC, comprising only the constitutively expressed domains, binds to contactin/F11 through FnIII repeats (45) and promotes cell adhesion (46). FnIII domain can also bind to the β subunit of integrin receptors (47, 48) and affect both cell migration and proliferation through reorganization of the actin cytoskeleton. (39, 49)

A scratch wound assay elicits *in vitro* a response of a single cell type, such as astrocytes, to mechanical injury only, with astrocytes tending to close the gap through migration and proliferation. On the other hand, *in vivo*, injury includes mechanical and chemical stages, as well as heterogenous cell types, disruption of the blood brain barrier and inflammation, all contributing to a more complex reaction during glial scar formation. Seven days after SCI, pro-inflammatory cells form the lesion core, while astrocytes reside on the border of the lesion site, initially providing protection of the surroundings, and eventually forming the scar tissue (40).

Levels of pro-inflammatory cytokines *Tnf-α* and *Il-1β* were increased *in vitro* in astrocytes upon addition of EGFL, FnA, FnD, and Fn6-8 fragments, regardless of the genotype. TnC has three main binding partners in inflammatory signalling: Toll-like receptor 4 (TLR4), integrins α9β1 and αVβ3. When TLR4 is activated by TnC, the most frequent outcome is the production of soluble pro-inflammatory mediators, such as IL-6, TNF-α and IL-1β by various cell types (39). These cytokines are upregulated also in peritoneal macrophages *via* activation by TnC of integrin αVβ3 and NFκB signaling pathways (49).

In our experiments, TnC-/- astrocyte cultures exhibited consistently higher GFAP protein and mRNA expression levels, regardless of the type of fragment used for treatment. As already reported, the GFAP expression level was higher in spinal cords of TnC-/- embryos, which is not seen thereafter in adult spinal cords of non-injured mice (38). In our study, *in vivo*, 7 days after SCI, GFAP immunoreactivity was the same in TnC+/+ and TnC-/- mice treated with vehicle or FnA after injury. Injection of FnD or Fn(D+A) led to a difference between the two genotypes, with higher levels in TnC+/+ than in TnC-/- mice (40).

In vivo proliferation at the injury site of the spinal cord was the same in TnC+/+ and TnC-/- mice 7 days after SCI. Since *in vitro* proliferation of astrocytes decreased upon fragment application, regardless of the genotype, it is thus possible that FnD and FnA induce proliferation of cell types other than astrocytes or that TnC does not affect cell proliferation in the tissue during this time frame after injury. We propose that this difference is due to different binding partners on the surface of different cell types.

TnC had been implicated in regulating production of pro-inflammatory cytokines/chemokines, chemotaxis and phagocytosis through the interaction with TLR4 in cultures of microglia (50). Our results on the microglia/macrophage response to injury showed that the FnD fragment increases the number of activated microglia/macrophages at the injury site.

TABLE 7 | Average numbers ± standard deviations of activated out of total microglia in the injured spinal cord of TnC +/+ and TnC –/– mice (cell number x 10^3 x mm^{-3}).

	Injury			+FnD		
	Rostral	**Injury**	**Caudal**	**Rostral**	**Injury**	**Caudal**
TnC +/+	92.35 ± 42.79	179.70 ± 55.40	71.16 ± 39.33	101.69 ± 61.12	195.49 ± 80.70	114.49 ± 90.27
TnC-/-	91.44 ± 16.33	108.94 ± 30.62	67.95 ± 45.39	84.31 ± 47.43	158.27 ± 63.73	46.56 ± 23.80

TABLE 8 | Mean values ± standard deviations of the portion of activated microglia numbers in the injured spinal cord of TnC +/+ and TnC –/– mice.

	Injury			+FnD		
	Rostral	**Injury**	**Caudal**	**Rostral**	**Injury**	**Caudal**
TnC +/+	0.68 ± 0.14	0.97 ± 0.05	0.55 ± 0.23	0.54 ± 0.27	0.84 ± 0.24	0.53 ± 19
TnC-/-	0.71 ± 0.15	0.86 ± 0.13	0.43 ± 0.28	0.54 ± 0.24	0.86 ± 0.14	0.32 ± 0.17

Matrix metalloproteases (MMP) induce TnC turnover (46) cleaving it mostly within the alternatively spliced domains, a process through which they also generate soluble fragments which might have different functions than the whole TnC protein. In the present study, the FnD fragment was singled out as the most potent domain in mediating TnC effects on glial cells within the first week after SCI. Our results may explain how the astrocyte reaction is delayed and restricted to the border of the injury site to allow microglia/macrophages to form a lesion core during the first stages of glial scar formation through action of TnC and, in particular, FnD. Since this stage is generally regarded as a potential window for therapeutical approaches, modulation of TnC isoforms and their interaction partners could be considered to be valuable targets. Further research is needed to dissect the heterophilic interaction partners which mediate the effects of TnC fragments on astrocytes and microglia/macrophages upon injury.

DATA AVAILABILITY STATEMENT

The original contributions presented in the study are included in the article/**Supplementary Material**. Further inquiries can be directed to the corresponding authors.

ETHICS STATEMENT

The animal study was reviewed and approved by the Ethics Committee of the Faculty of Biology, University of Belgrade.

AUTHOR CONTRIBUTIONS

DB performed the *in vitro* experiments, assisted in the *in vivo* experiment data analysis, and wrote the manuscript. MA assisted in the *in vitro* experiments, data analyses, and manuscript writing. MP assisted in the *in vivo* experiments, immunohistochemistry, and data analysis. IJ conceptualized and design the study, performed the *in vivo* experiments, and wrote the manuscript. EF provided study consultation and wrote the manuscript. MS provided encouragement for the study concept, envisioned the importance of tenascin-C domains, provided study consultation, and wrote the manuscript. PA provided the study concept and design, consultation, and wrote the manuscript. All authors contributed to the article and approved the submitted version.

FUNDING

The study was funded by the DAAD/MESTD project "Involvement of Tenascin-C in Astrocyte Scarring After Spinal Cord Injury" (451-03-01766/2014-09/6) and the Ministry of Education, Science and Technological Development of the Republic of Serbia, contract number: 451-03-68/2020-14/200178.

ACKNOWLEDGMENTS

The authors thank Dr. Djordje Miljković for help with real-time PCR experiments, Dr Jelena Katić for help with the Stereo Investigator and Dr. Gabriele Loers for help with the production of fragments.

SUPPLEMENTARY MATERIAL

The Supplementary Material for this article can be found online at: https://www.frontiersin.org/articles/10.3389/fimmu.2020.624612/full#supplementary-material

Supplementary Figure 1 | Gap closure in astrocyte cultures of TnC+/+ and TnC-/- mice in the presence of different TnC fragments. Combined clustered stacked column chart displaying the relative wound closure at different time points after scratching and application of TnC fragments. Stacked columns represent the mean values of relative wound closure ± SD. n = 3 independent astrocyte culture preparations.

Supplementary Figure 2 | Density of resting microglia within the spinal cord injury region in TnC+/+ and TnC-/- mice. Box plots show the density of resting microglia within the injury region, as well as in the surrounding rostral and caudal areas obtained 7 days after the spinal cord injury. Iba1 immunolabeling was assessed by stereological analysis. n = 3 animals per group for each genotype.

REFERENCES

1. Oyinbo CA. Secondary injury mechanisms in traumatic spinal cord injury: a nugget of this multiply cascade. *Acta Neurobiol Experimentalis* (2011) 71 (2):281–99.
2. Bradbury EJ, Burnside ER. Moving beyond the glial scar for spinal cord repair. *Nat Commun* (2019) 10(1):3879. doi: 10.1038/s41467-019-11707-7
3. Windle WF, Clemente CD, Chambers WW. Inhibition of formation of a glial barrier as a means of permitting a peripheral nerve to grow into the brain. *J Comp Neurol* (1952) 96(2):359–69. doi: 10.1002/cne.900960207
4. Anderson MA, Burda JE, Ren Y, Ao Y, O'Shea TM, Kawaguchi R, et al. Astrocyte scar formation aids central nervous system axon regeneration. *Nature* (2016) 532(7598):195–200. doi: 10.1038/nature17623
5. Zhang Y, Winterbottom JK, Schachner M, Lieberman AR, Anderson PN. Tenascin-C expression and axonal sprouting following injury to the spinal dorsal columns in the adult rat. *J Neurosci Res* (1997) 49(4):433–50. doi: 10.1002/(SICI)1097-4547(19970815)49:4<433::AID-JNR5>3.0.CO;2-9
6. Taylor HC, Lightner VA, Beyer WFJr., McCaslin D, Briscoe G, Erickson HP. Biochemical and structural studies of tenascin/hexabrachion proteins. *J Cell Biochem* (1989) 41(2):71–90. doi: 10.1002/jcb.240410204
7. Nies DE, Hemesath TJ, Kim JH, Gulcher JR, Stefansson K. The complete cDNA sequence of human hexabrachion (Tenascin). A multidomain protein containing unique epidermal growth factor repeats. *J Biol Chem* (1991) 266 (5):2818–23. doi: 10.1016/S0021-9258(18)49920-6
8. Spring J, Beck K, Chiquet-Ehrismann R. Two contrary functions of tenascin: dissection of the active sites by recombinant tenascin fragments. *Cell* (1989) 59(2):325–34. doi: 10.1016/0092-8674(89)90294-8
9. Jones FS, Jones PL. The tenascin family of ECM glycoproteins: structure, function, and regulation during embryonic development and tissue remodeling. *Dev Dynamics Off Publ Am Assoc Anatomists* (2000) 218 (2):235–59. doi: 10.1002/(SICI)1097-0177(200006)218:2<235::AID-DVDY2>3.0.CO;2-G
10. Bartsch S, Bartsch U, Dörries U, Faissner A, Weller A, Ekblom P, et al. Expression of tenascin in the developing and adult cerebellar cortex. *J Neurosci*

Off J Soc Neurosci (1992) 12(3):736–49. doi: 10.1523/JNEUROSCI.12-03-00736.1992
11. Götz M, Bolz J, Joester A, Faissner A. Tenascin-C synthesis and influence on axonal growth during rat cortical development. *Eur J Neurosci* (1997) 9 (3):496–506. doi: 10.1111/j.1460-9568.1997.tb01627.x
12. Ikeshima-Kataoka H, Saito S, Yuasa S. Tenascin-C is required for proliferation of astrocytes in primary culture. *Vivo (Athens Greece)* (2007) 21(4):629–33.
13. Brodkey JA, Laywell ED, O'Brien TF, Faissner A, Stefansson K, Dörries HU, et al. Focal brain injury and upregulation of a developmentally regulated extracellular matrix protein. *J Neurosurg* (1995) 82(1):106–12. doi: 10.3171/jns.1995.82.1.0106
14. Irintchev A, Salvini TF, Faissner A, Wernig A. Differential expression of tenascin after denervation, damage or paralysis of mouse soleus muscle. *J Neurocytol* (1993) 22(11):955–65. doi: 10.1007/BF01218353
15. Martini R. Expression and functional roles of neural cell surface molecules and extracellular matrix components during development and regeneration of peripheral nerves. *J Neurocytol* (1994) 23(1):1–28. doi: 10.1007/BF01189813
16. Holley JE, Gveric D, Whatmore JL, Gutowski NJ. Tenascin C induces a quiescent phenotype in cultured adult human astrocytes. *Glia* (2005) 52 (1):53–8. doi: 10.1002/glia.20231
17. Chiquet-Ehrismann R. Anti-adhesive molecules of the extracellular matrix. *Curr Opin Cell Biol* (1991) 3(5):800–4. doi: 10.1016/0955-0674(91)90053-2
18. Chung CY, Zardi L, Erickson HP. Binding of tenascin-C to soluble fibronectin and matrix fibrils. *J Biol Chem* (1995) 270(48):29012–7. doi: 10.1074/jbc.270.48.29012
19. Chiquet M, Fambrough DM. Chick myotendinous antigen. II. A novel extracellular glycoprotein complex consisting of large disulfide-linked subunits. *J Cell Biol* (1984) 98(6):1937–46. doi: 10.1083/jcb.98.6.1937
20. Vaughan L, Huber S, Chiquet M. Winterhalter KH. A major, six-armed glycoprotein from embryonic cartilage. *EMBO J* (1987) 6(2):349–53. doi: 10.1002/j.1460-2075.1987.tb04761.x
21. Chen J, Joon Lee H, Jakovcevski I, Shah R, Bhagat N, Loers G, et al. The extracellular matrix glycoprotein tenascin-C is beneficial for spinal cord regeneration. *Mol Ther J Am Soc Gene Ther* (2010) 18(10):1769–77. doi: 10.1038/mt.2010.133
22. Lochter A, Schachner M. Tenascin and extracellular matrix glycoproteins: from promotion to polarization of neurite growth in vitro. *J Neurosci Off J Soc Neurosci* (1993) 13(9):3986–4000. doi: 10.1523/JNEUROSCI.13-09-03986.1993
23. Meiners S, Nur-e-Kamal MS, Mercado ML. Identification of a neurite outgrowth-promoting motif within the alternatively spliced region of human tenascin-C. *J Neurosci Off J Soc Neurosci* (2001) 21(18):7215–25. doi: 10.1523/JNEUROSCI.21-18-07215.2001
24. Goh FG, Piccinini AM, Krausgruber T, Udalova IA, Midwood KS. Transcriptional regulation of the endogenous danger signal tenascin-C: a novel autocrine loop in inflammation. *J Immunol (Baltimore Md 1950)* (2010) 184(5):2655–62. doi: 10.4049/jimmunol.0903359
25. Gaudet AD, Popovich PG. Extracellular matrix regulation of inflammation in the healthy and injured spinal cord. *Exp Neurol* (2014) 258:24–34. doi: 10.1016/j.expneurol.2013.11.020
26. Evers MR, Salmen B, Bukalo O, Rollenhagen A, Bösl MR, Morellini F, et al. Impairment of L-type Ca2+ channel-dependent forms of hippocampal synaptic plasticity in mice deficient in the extracellular matrix glycoprotein tenascin-C. *J Neurosci Off J Soc Neurosci* (2002) 22(16):7177–94. doi: 10.1523/JNEUROSCI.22-16-07177.2002
27. Jakovcevski I, Miljkovic D, Schachner M, Andjus PR. Tenascins and inflammation in disorders of the nervous system. *Amino Acids* (2013) 44 (4):1115–27. doi: 10.1007/s00726-012-1446-0
28. Dörries U, Taylor J, Xiao Z, Lochter A, Montag D, Schachner M. Distinct effects of recombinant tenascin-C domains on neuronal cell adhesion, growth cone guidance, and neuronal polarity. *J Neurosci Res* (1996) 43(4):420–38. doi: 10.1002/(SICI)1097-4547(19960215)43:4<420::AID-JNR4>3.0.CO;2-H
29. Bijelić DD, Milićević KD, Lazarević MN, Miljković DM, Bogdanović Pristov JJ, Savić DZ, et al. Central nervous system-infiltrated immune cells induce calcium increase in astrocytes via astroglial purinergic signaling. *J Neurosci Res* (2020) 98(11):2317–32. doi: 10.1002/jnr.24699
30. Környei Z, Czirók A, Vicsek T, Madarász E. Proliferative and migratory responses of astrocytes to in vitro injury. *J Neurosci Res* (2000) 61(4):421–9. doi: 10.1002/1097-4547(20000815)61:4<421::AID-JNR8>3.0.CO;2-4
31. Lampugnani MG. Cell Migration into a Wounded Area In Vitro. In: E Dejana, M Corada, editors. *Adhesion Protein Protocols*. Totowa, NJ: Humana Press (1999). p. 177–82. doi: 10.1385/1-59259-258-9:177
32. Rio DC, Ares MJr., Hannon GJ, Nilsen TW. Purification of RNA using TRIzol (TRI reagent). *Cold Spring Harbor Protoc* (2010) 2010(6):pdb.prot5439. doi: 10.1101/pdb.prot5439
33. Sharova LV, Sharov AA, Nedorezov T, Piao Y, Shaik N, Ko MS. Database for mRNA half-life of 19 977 genes obtained by DNA microarray analysis of pluripotent and differentiating mouse embryonic stem cells. *DNA Res Int J Rapid Publ Rep Genes Genom* (2009) 16(1):45–58. doi: 10.1093/dnares/dsn030
34. Jakovcevski I, Siering J, Hargus G, Karl N, Hoelters L, Djogo N, et al. Close homologue of adhesion molecule L1 promotes survival of Purkinje and granule cells and granule cell migration during murine cerebellar development. *J Comp Neurol* (2009) 513(5):496–510. doi: 10.1002/cne.21981
35. Yoo JY, Hwang CH, Hong HN. A Model of Glial Scarring Analogous to the Environment of a Traumatically Injured Spinal Cord Using Kainate. *Ann Rehabil Med* (2016) 40(5):757–68. doi: 10.5535/arm.2016.40.5.757
36. Adzic M, Nedeljkovic N. Unveiling the Role of Ecto-5′-Nucleotidase/CD73 in Astrocyte Migration by Using Pharmacological Tools. *Front Pharmacol* (2018) 9:153. doi: 10.3389/fphar.2018.00153
37. Gao K, Wang CR, Jiang F, Wong AY, Su N, Jiang JH, et al. Traumatic scratch injury in astrocytes triggers calcium influx to activate the JNK/c-Jun/AP-1 pathway and switch on GFAP expression. *Glia* (2013) 61(12):2063–77. doi: 10.1002/glia.22577
38. Karus M, Denecke B, ffrench-Constant C, Wiese S, Faissner A. The extracellular matrix molecule tenascin C modulates expression levels and territories of key patterning genes during spinal cord astrocyte specification. *Development* (2011) 138(24):5321. doi: 10.1242/dev.067413
39. Marzeda AM, Midwood KS. Internal Affairs: Tenascin-C as a Clinically Relevant, Endogenous Driver of Innate Immunity. *J Histochem Cytochem Off J Histochem Soc* (2018) 66(4):289–304. doi: 10.1369/0022155418757443
40. Beck KD, Nguyen HX, Galvan MD, Salazar DL, Woodruff TM, Anderson AJ. Quantitative analysis of cellular inflammation after traumatic spinal cord injury: evidence for a multiphasic inflammatory response in the acute to chronic environment. *Brain J Neurol* (2010) 133(Pt 2):433–47. doi: 10.1093/brain/awp322
41. Sun D, Jakobs TC. Structural remodeling of astrocytes in the injured CNS. *Neurosci Rev J Bringing Neurobiol Neurol Psychiatry* (2012) 18(6):567–88. doi: 10.1177/1073858411423441
42. Zhou X, Wahane S, Friedl MS, Kluge M, Friedel CC, Avrampou K, et al. Microglia and macrophages promote corralling, wound compaction and recovery after spinal cord injury via Plexin-B2. *Nat Neurosci* (2020) 23 (3):337–50. doi: 10.1038/s41593-020-0597-7
43. Chung CY, Erickson HP. Cell surface annexin II is a high affinity receptor for the alternatively spliced segment of tenascin-C. *J Cell Biol* (1994) 126(2):539–48. doi: 10.1083/jcb.126.2.539
44. Balch C, Dedman JR. Annexins II and V inhibit cell migration. *Exp Cell Res* (1997) 237(2):259–63. doi: 10.1006/excr.1997.3817
45. Weber P, Ferber P, Fischer R, Winterhalter KH, Vaughan L. Binding of contactin/F11 to the fibronectin type III domains 5 and 6 of tenascin is inhibited by heparin. *FEBS Lett* (1996) 389(3):304–8. doi: 10.1016/0014-5793(96)00609-6
46. Giblin SP, Midwood KS. Tenascin-C: Form versus function. *Cell Adhesion Migration* (2015) 9(1-2):48–82. doi: 10.4161/19336918.2014.987587
47. Giese A, Loo MA, Norman SA, Treasurywala S, Berens ME. Contrasting migratory response of astrocytoma cells to tenascin mediated by different integrins. *J Cell Sci* (1996) 109(Pt 8):2161–8.
48. Husmann K, Faissner A, Schachner M. Tenascin promotes cerebellar granule cell migration and neurite outgrowth by different domains in the fibronectin type III repeats. *J Cell Biol* (1992) 116(6):1475–86. doi: 10.1083/jcb.116.6.1475
49. Shimojo N, Hashizume R, Kanayama K, Hara M, Suzuki Y, Nishioka T, et al. Tenascin-C may accelerate cardiac fibrosis by activating macrophages via the integrin αVβ3/nuclear factor-κB/interleukin-6 axis. *Hypertension (Dallas Tex 1979)* (2015) 66(4):757–66. doi: 10.1161/HYPERTENSIONAHA.115.06004

50. Haage V, Elmadany N, Roll L, Faissner A, Gutmann DH, Semtner M, et al. Tenascin C regulates multiple microglial functions involving TLR4 signaling and HDAC1. *Brain Behav Immun* (2019) 81:470–83. doi: 10.1016/j.bbi.2019.06.047

Conflict of Interest: The authors declare that the research was conducted in the absence of any commercial or financial relationships that could be construed as a potential conflict of interest.

frontiers in Immunology

CORRECTION
published: 16 March 2021
doi: 10.3389/fimmu.2021.672476

Corrigendum: Different Functions of Recombinantly Expressed Domains of Tenascin-C in Glial Scar Formation

Dunja Bijelić[1], Marija Adžić[1], Mina Perić[1], Igor Jakovčevski[2], Eckart Förster[2], Melitta Schachner[3] and Pavle R. Andjus[1]**

[1] Centre for Laser Microscopy, Faculty of Biology, Institute of Physiology and Biochemistry "Jean Giaja", University of Belgrade, Belgrade, Serbia, [2] Institut für Neuroanatomie und Molekulare Hirnforschung, Ruhr-Universität Bochum, Bochum, Germany, [3] Keck Center for Collaborative Neuroscience and Department of Cell Biology and Neuroscience, Rutgers University, Piscataway, NJ, United States

OPEN ACCESS

Edited and reviewed by:
Kyoko Imanaka-Yoshida, Mie University, Japan

***Correspondence:**
Pavle R. Andjus
pandjus@bio.bg.ac.rs
Melitta Schachner
schachner@dls.rutgers.edu

Specialty section:
This article was submitted to Inflammation, a section of the journal Frontiers in Immunology

Received: *25 February 2021*
Accepted: *08 March 2021*
Published: *16 March 2021*

Citation:
Bijelić D, Adžić M, Perić M, Jakovčevski I, Förster E, Schachner M and Andjus PR (2021) Corrigendum: Different Functions of Recombinantly Expressed Domains of Tenascin-C in Glial Scar Formation. Front. Immunol. 12:672476. doi: 10.3389/fimmu.2021.672476

Keywords: astrocyte, glial scar, microglia/macrophages, spinal cord injury, tenascin-C

A Corrigendum on

Different Functions of Recombinantly Expressed Domains of Tenascin-C in Glial Scar Formation

Bijelić, D., Adžić, M., Perić, M., Jakovčevski, I., Förster, E., Schachner, M., and Andjus, P. R. (2021). Front. Immunol. 11(3944). doi: 10.3389/fimmu.2020.624612

In the original article, there was a mistake in **Figure 2** as published. Instead of micrograph "+ FnA", the micrograph for "+ Fn(D+A)" treatment in TnC +/+ genotype was duplicated by mistake. We have inserted the correct micrograph for "+ FnA". The corrected **Figure 2** appears below.

The authors apologize for this error and state that this does not change the scientific conclusions of the article in any way. The original article has been updated.

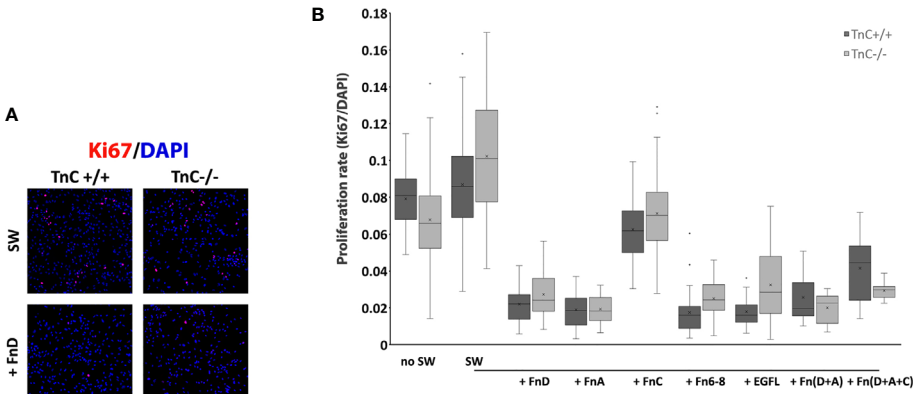

		no SW	SW	+ FnD	+ FnA	+ FnC	+ Fn6-8	+ EGFL	+ Fn(D+A)	+ Fn(D+A+C)
no SW	TnC+/+	-	-	<.001	<.001	<.001	<.001	<.001	<.001	<.001
	TnC-/-		<.001	<.001	<.001	-	<.001	<.001	<.001	<.001
SW	TnC+/+	-	0.007	<.001	<.001	<.001	<.001	<.001	<.001	<.001
	TnC-/-	<.001		<.001	<.001	<.001	<.001	<.001	<.001	<.001
+ FnD	TnC+/+	<.001	<.001	-	-	<.001	-	-	-	0.012
	TnC-/-	<.001	<.001		-	<.001	-	-	-	-
+ FnA	TnC+/+	<.001	<.001	-	-	<.001	-	-	-	0.001
	TnC-/-	<.001	<.001	-		<.001	-	0.039	-	-
+ FnC	TnC+/+	<.001	<.001	<.001	<.001	0.020	<.001	<.001	<.001	0.004
	TnC-/-	-	<.001	<.001	<.001		<.001	<.001	<.001	<.001
+ Fn6-8	TnC+/+	<.001	<.001	-	-	<.001	0.052	-	-	-
	TnC-/-	<.001	<.001	-	-	<.001		-	-	<.001
+ EGFL	TnC+/+	<.001	<.001	-	-	<.001	-	<.001	-	0.001
	TnC-/-	<.001	<.001	-	0.039	<.001	-		-	-
+ Fn(D+A)	TnC+/+	<.001	<.001	-	-	<.001	-	-	-	-
	TnC-/-	<.001	<.001	-	-	<.001	-	-		-
+ Fn(D+A+C)	TnC+/+	<.001	<.001	0.012	0.001	0.004	-	0.001	-	-
	TnC-/-	<.001	<.001	-	-	<.001	<.001	-	-	

FIGURE 2 | TnC fragments reduce proliferation in the astrocyte scratch wound assay. **(A)** Representative micrographs of Ki67+/DAPI+ immunofluorescence at 24 h after scratching in the control group and groups treated with FnA, FnD, and Fn(D+A); bar: 200 µm. **(B)** Proliferation was calculated as the number of Ki67+ nuclei compared to total DAPI+ nuclei. Results are presented as a box-and-whisker plot. Two-way ANOVA analysis shows a statistically significant interaction between the effects of genotype and treatment on cell proliferation rate ($p = 0.005$) with both the effects of genotype and treatment being significant ($p = 0.040$, $p < 0.001$, respectively). A statistically significant decrease in proliferation is seen in the presence of FnA, FnD, and Fn(D+A). All statistically significant pairwise comparisons are displayed below the box-and-whisker plot. n=3 independent astrocyte cultures.

frontiers in Immunology

MINI REVIEW
published: 22 February 2021
doi: 10.3389/fimmu.2021.624703

Immunomodulatory Role of Tenascin-C in Myocarditis and Inflammatory Cardiomyopathy

Kazuko Tajiri, Saori Yonebayashi, Siqi Li and Masaki Ieda*

Department of Cardiology, Faculty of Medicine, University of Tsukuba, Tsukuba, Japan

Accumulating evidence suggests that the breakdown of immune tolerance plays an important role in the development of myocarditis triggered by cardiotropic microbial infections. Genetic deletion of immune checkpoint molecules that are crucial for maintaining self-tolerance causes spontaneous myocarditis in mice, and cancer treatment with immune checkpoint inhibitors can induce myocarditis in humans. These results suggest that the loss of immune tolerance results in myocarditis. The tissue microenvironment influences the local immune dysregulation in autoimmunity. Recently, tenascin-C (TN-C) has been found to play a role as a local regulator of inflammation through various molecular mechanisms. TN-C is a nonstructural extracellular matrix glycoprotein expressed in the heart during early embryonic development, as well as during tissue injury or active tissue remodeling, in a spatiotemporally restricted manner. In a mouse model of autoimmune myocarditis, TN-C was detectable before inflammatory cell infiltration and myocytolysis became histologically evident; it was strongly expressed during active inflammation and disappeared with healing. TN-C activates dendritic cells to generate pathogenic autoreactive T cells and forms an important link between innate and acquired immunity.

Keywords: tenascin-C, myocarditis, inflammatory cardiomyopathy, autoimmunity, extracellular matrix

OPEN ACCESS

Edited by:
Gertraud Orend,
INSERM Immuno Rhumatologie Moléculaire (IRM), France

Reviewed by:
Przemyslaw Blyszczuk,
Jagiellonian University Medical College, Poland
Attila Kiss,
Medical University of Vienna, Austria

****Correspondence:***
Kazuko Tajiri
ktajiri@md.tsukuba.ac.jp

Specialty section:
This article was submitted to Inflammation, a section of the journal Frontiers in Immunology

Received: *01 November 2020*
Accepted: *06 January 2021*
Published: *22 February 2021*

Citation:
Tajiri K, Yonebayashi S, Li S and Ieda M (2021) Immunomodulatory Role of Tenascin-C in Myocarditis and Inflammatory Cardiomyopathy. Front. Immunol. 12:624703. doi: 10.3389/fimmu.2021.624703

INTRODUCTION

Myocarditis is an inflammatory disease of the myocardium. It represents a public health challenge worldwide, as it is one of the leading causes of dilated cardiomyopathy, particularly in young, previously healthy individuals (1). Myocarditis can be triggered by a variety of infectious and non-infectious agents (2, 3), and the subsequent autoimmune response is thought to contribute to the disease progression to inflammatory cardiomyopathy (4, 5).

Tenascin-C (TN-C) is a non-structural extracellular matrix (ECM) expressed during embryonic development in the heart, but is not present in the normal adult heart (6). In tissue injury, inflammation, or active remodeling, TN-C is re-expressed in a spatiotemporally restricted manner (6). Recently, TN-C has gained attention as a local regulator of inflammation through various molecular mechanisms (7). Several animal studies have revealed that TN-C is involved in autoimmune disorders, including myocarditis, arthritis, glaucoma, and encephalomyelitis (8–11). In autoimmune myocarditis, TN-C activates dendritic cells (DCs) to generate pathogenic autoreactive T cells and forms an important link between innate and acquired immunity (9). In this mini review, we discuss

the mechanistic insights into the development of myocarditis and its progression to inflammatory cardiomyopathy and focus on the role of TN-C in their pathology.

TRIGGERS OF MYOCARDITIS

Myocarditis can occur in association with a wide spectrum of infectious agents (such as viruses, bacteria, and protozoans), systemic immune-mediated diseases, toxic substances, and drugs (such as immune checkpoint inhibitors) (2, 3, 12, 13). Viruses have been implicated as the leading trigger of myocarditis, with cardiotropic viruses (such as coxsackievirus B3 [CVB3] and adenoviruses), vasculotropic viruses (such as parvovirus B19), and lymphotropic viruses (such as human herpesvirus 6), which are common agents identified in the myocardium of patients with myocarditis/dilated cardiomyopathy (DCM) (14–16). However, the etiologic role of the viruses detected in myocarditis patients is not evident (17). For example, a high prevalence of parvovirus B19 has been observed in hearts both with (18) and without myocarditis (19). Thus, the causative or associative link between individual viral infections and the pathogenesis of myocarditis is still under investigation (17). In Latin America, infection by the protozoan parasite *Trypanosoma cruzi* is the most common cause of inflammatory heart disease (17).

Animal models of virus-induced myocarditis with CVB3 infection have been used to study how viruses trigger myocarditis. The pathogenesis of CVB3-induced myocarditis involves both viral cytotoxicity and subsequent host immune responses (2). Initially, CVB3 enters cardiomyocytes by binding to the coxsackievirus-adenovirus receptor, and causes direct cytotoxicity to the myocardium within three to four days post-infection (16). During the early stage of CVB3 infection, innate immune cells are activated through pattern recognition receptors, such as toll-like receptors (TLRs), and produce pro-inflammatory cytokines, such as interferons (IFNs), interleukin (IL)-1β, IL-6, IL-8, and tumor necrosis factor-α (16, 20). Subsequently, antigen-specific responses in adaptive immune cells are induced, eliminating the virus by up to 14 days post-infection (16, 20). However, even after viral clearance, a subset of individuals may develop chronic myocardial inflammation with virus-triggered uncontrolled immune response and the expansion of cardiac-autoreactive T cells, leading to inflammatory cardiomyopathy.

Infection with the novel pathogen severe acute respiratory syndrome coronavirus 2 (SARS-CoV-2) may trigger myocarditis both directly and indirectly (14, 21). Several studies have suggested that the immune response triggered by the virus is the major cause of cardiomyocyte injury, rather than direct virus-mediated cytotoxicity (15, 22). In a recent series of hospitalized coronavirus disease 2019 (COVID-19) cases caused by SARS-CoV-2 infection, acute cardiac injury with serum troponin elevation occurred in 7% to 27% of patients, and elevated troponin levels were associated with increased mortality in patients with COVID-19 (23–25). However, elevated troponin can be caused not only by myocarditis but also by other heart diseases, such as ischemic heart disease, Takotsubo syndrome, or secondary cardiac injury due to systemic inflammation and hypoxemia due to respiratory dysfunction (14, 26). Recently, autopsies of 21 patients who died from COVID-19 identified multifocal lymphocytic myocarditis in three cases (14%) (26). Viral entry to cardiac cells using angiotensin converting enzyme 2 may directly induce myocarditis (27). However, the exact mechanism of SARS-CoV-2-induced myocarditis is currently unknown, and further investigations are required.

AUTOIMMUNE MYOCARDITIS AND INFLAMMATORY CARDIOMYOPATHY

Myosin heavy chain α isoform (MyHC-α) represents a major cardiac autoantigen. MyHC-α immunization with immune adjuvants or the injection of MyHC-α-loaded DCs can induce autoimmune myocarditis in mice (28, 29). MyHC-α reactive T cells have been found in patients with myocarditis and, interestingly, in healthy subjects (30), suggesting that this may be due to impaired T cell tolerance mechanisms. In the thymus, most autoreactive T cells are eliminated through central immune tolerance or negative selection. In this process, the presentation of self-peptides by antigen-presenting medullary thymic epithelial cells is crucial for determining the fate of developing T cells. Importantly, unlike other cardiac antigens, MyHC-α is not expressed in thymic cells in either mice or humans. Therefore, a lack of central T cell tolerance to this protein allows MyHC-α-reactive T cells to escape negative selection and enter the peripheral circulation (30). MyHC-α-reactive T cells were markedly increased in myocarditis, and adoptive transfer of these cells induced myocarditis in the recipients, demonstrating the effector function of MyHC-α-reactive T cells (30). Although frequency is low, MyHC-α-reactive T cells are present in the periphery of healthy individuals (30), suggesting that peripheral immune tolerance is crucial to prevent these self-reactive T cells from inducing autoimmune myocarditis (5, 31, 32). The mechanism of peripheral immune tolerance is complicated, and immune checkpoints, including cytotoxic T-lymphocyte antigen 4 (CTLA-4) and programmed cell death protein 1 (PD-1)/PD ligand 1 (PD-L1), play important roles in maintaining peripheral tolerance to cardiac antigens (33). After viral infection, MyHC-α-specific $CD4^+$ T cells expand, likely because of molecular mimicry (epitope cross-reactivity) or epitope spreading (self-antigen exposure from cardiomyocytes upon viral damage), and contribute to post-infectious myocarditis (34).

Until now, the role of gut bacteria in cardiac autoimmunity was unclear. However, recently, Gil-Cruz et al. (35) demonstrated that the commensal gut microbe *Bacteroides thetaiotaomicron* (*B. theta*) triggers a cross-immune response against the bacterial protein β-galactosidase and MyHC-α, causing inflammatory cardiomyopathy. B-galactosidase produced by *B. theta* has sequence homology to MyHC-α and

induces proliferation and T helper 17 (Th17) polarization of MyHC-α-specific $CD4^+$ T cells. Additionally, antibiotic therapy prevents lethal consequences. Patients with myocarditis have higher anti-*B. theta* antibody and circulating T cells from the patients show significantly higher IFN-γ production capacity against both MyHC-α and β-galactosidase than healthy subjects. These results suggest that targeting the microbiome could become a new therapeutic strategy.

In contrast to the well-defined cardiac antigen-specific T-cell responses, our understanding of the role of heart non-specific $CD4^+$ T cells in myocarditis is limited. Recently, Zarak-Crnkovic et al. (36) demonstrated in a proof-of-concept study that heart non-specific effector T cells did not affect the severity of myocarditis, but protected the heart from adverse post-inflammatory fibrotic remodeling and cardiac dysfunction in the chronic stage. Moreover, bystander activation of effector T cells suppressed the myofibroblast phenotype of mouse and human cardiac fibroblasts (36), suggesting a dynamic and complex role of effector T cells and the interplay between T cells and fibroblasts in autoimmune myocarditis.

TN-C IN MYOCARDITIS AND INFLAMMATORY CARDIOMYOPATHY

In the heart, TN-C is transiently expressed at several important stages during embryonic development, but TN-C-deficient mice do not show a clear phenotype (37). TN-C is rarely expressed in normal adult hearts but is upregulated under pathological conditions with tissue injury, tissue repair/regeneration, and inflammation (38, 39), including myocarditis (40, 41), DCM (42), rheumatic heart disease (43), myocardial infarction (44, 45), hypertensive heart disease (46), and Kawasaki disease (47). Serum TN-C levels appear to be useful biomarkers for assessing disease activity and predicting disease prognosis. High serum TN-C levels are a significant independent predictor for cardiac events and have an incremental predictive power with brain natriuretic peptide (BNP) in both myocardial infarctions and DCM (48, 49). BNP is secreted from cardiomyocytes in the ventricles in response to stretching caused by increased wall tension and is broadly used as a marker for the diagnosis and treatment of heart failure (50, 51). On the other hand, fibroblasts are a major source of TN-C in the pathological heart (40, 52, 53). The combination of the two biomarkers may more accurately reflect the pathological condition of the entire heart than a single biomarker (54).

The expression of TN-C is detectable in the heart before inflammatory cell infiltration and myocytolysis become histologically apparent, persists during active inflammation, and is no longer present prior to mature collagen deposition in the healing phase in a mouse model of experimental autoimmune myocarditis (5). A major source of TN-C in the pathological heart consists of residential interstitial cells, primarily fibroblasts; however, precardiac mesodermal cells, a special population of cardiomyocytes in embryonic hearts, and several cell lines of cardiomyocytes also have the potential to produce TN-C (54). Its expression level reflects the activity of myocardial inflammation (40). We previously investigated the immunomodulatory effect of TN-C in experimental autoimmune myocarditis. TN-C-deficient mice were protected from severe myocarditis with lower Th17 cell infiltration to the heart compared to wild-type mice (9). Th17 cells are closely associated with autoimmunity, and IL-17-producing Th17 cells play a major role in the initiation and development of myocarditis (2, 55, 56). In human myocarditis/inflammatory cardiomyopathy, the Th17 immunophenotype is characterized by elevated Th17 levels with increases in the Th17-related cytokines IL-6, IL-1β, transforming growth factor-β1, IL-23, and granulocyte-macrophage colony-stimulating factor (GM-CSF) (57). Moreover, patients with severe heart failure have greater proportions of Th17 than those with low severity heart failure (57). IL-6 is a key cytokine that differentiates naïve $CD4^+$ T cells into Th17 cells (58). The stimulation of DCs with exogenous TN-C produces high levels of IL-6 (9). Naive $CD4^+$ T cells co-cultured with TN-C-stimulated DCs differentiate into Th17 cells, and the IL-6 blockade inhibits Th17 polarization (9). In addition, TN-C-stimulated DCs produce high levels of IL-1β and GM-CSF, which facilitate Th17 generation and maintenance (59, 60). Taken together, TN-C may promote Th17 expansion through its ability to induce Th17-inducing cytokine production from DCs and form an important link from innate to adaptive immunity.

DCs are antigen-presenting cells essential for priming T cell responses (61). Resting tolerogenic DCs that display cardiac myosin peptides in complex with class II major histocompatibility complex (MHC) are present in a healthy heart and are trafficked to the cardiac draining lymph nodes. In the lymph nodes, DCs present cardiac myosin peptides to naïve $CD4^+$ T cells specific to those peptides, leading to deletion, anergy, or Treg induction (32). If a heart is damaged by tissue injury or inflammation, TN-C is produced by fibroblasts and stimulates myocardial DCs to migrate to the cardiac draining lymph nodes and activate cardiac myosin-specific T cells, which then differentiate into inflammatory effector T cells (**Figure 1**). In addition to presenting antigen-derived peptides on their MHCs with costimulatory molecules for naïve T cell activation and expansion, DCs release a cocktail of polarizing cytokines for the differentiation of $CD4^+$ T cells into effector cells (30, 62). In autoimmune diseases, DCs play an important role in the regulation of autoreactive $CD4^+$ T cells (30). A model of bone marrow-derived DC (BMDC)-induced autoimmune myocarditis is helpful for understanding how DCs activate autoreactive $CD4^+$ T cells (28). In this model, the activation of TLRs on BMDCs loaded with a MyHC-α peptide is essential for the induction of autoimmune myocarditis (9, 28). TLR signaling triggers innate immunity upon stimulation with microbial products or endogenous danger signals (danger-associated molecular patterns [DAMPs]) (63). In sterile inflammation, DAMPs are released from either ECM (e.g., TN-C or biglycan) or from dying cells (e.g., histones, high mobility group box 1, heat-shock proteins, DNAs, or RNAs) and stimulate TLRs (64, 65). Popovic *et al.* reported that an endogenous TLR2/4 ligand biglycan enhanced the priming of autoreactive T cells and stimulated autoimmune perimyocarditis (66). We previously showed that TN-C provides DCs to induce myocarditis *via* TLR4 activation (9). The injection of MyHC-α-

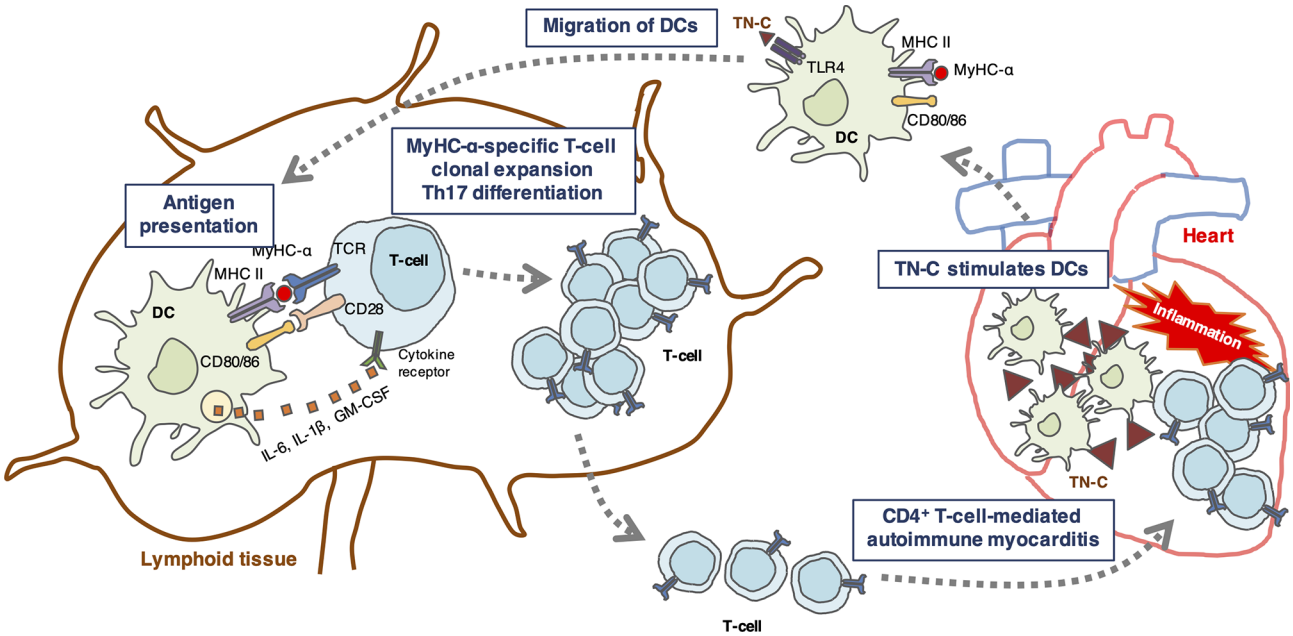

FIGURE 1 | Schematic illustration showing a hypothetical mechanism by which tenascin-C (TN-C)-stimulated dendritic cells (DCs) induce Th17 differentiation. TN-C is upregulated in the heart under pathological conditions such as tissue injury and inflammation, and stimulates myocardial dendritic cells (DCs) *via* toll-like receptor 4 (TLR4) activation in the heart. Activated DCs migrate to the cardiac draining lymph nodes where they activate cardiac myosin-specific T cells. DCs produce Th17-polarizing cytokines (IL-6, IL-1, and GM-CSF) that contribute to the generation of Th17 cells. In turn, $CD4^+$ T cells migrate back to the heart and cause autoimmune myocarditis.

loaded BMDCs stimulated with TN-C induced myocarditis in the recipient mice (9). Upon stimulation with TN-C, DCs produced large amounts of proinflammatory cytokines, including the Th17-polarizing cytokines IL-1β, IL-6, and GM-CSF (9). Naïve $CD4^+$ T cells co-cultured with TN-C-stimulated DCs differentiated into Th17 cells, but IL-6 blocking antibody inhibited Th17 polarization (9). Moreover, the blocking of TLR4 signaling reduced IL-6 secretion from DCs with less Th17 generation (9). TN-C-stimulated BMDCs from TLR4-deficient mice failed to induce myocarditis in the recipients, indicating that TN-C provides myocarditis inducibility to DCs, at least in part, *via* TLR4 interaction (**Figure 1**) (5, 9). However, this concept is based on limited experimental findings. Therefore, further studies are needed to fully determine the effect of TN-C on the onset and progression of myocarditis.

CONCLUSIONS AND PERSPECTIVES

The etiology and pathogenesis of myocarditis are not yet fully understood. TN-C may be a key extracellular modulator that controls immune responses in myocarditis and inflammatory cardiomyopathy. To date, no attempt has been made to suppress the function of TN-C during myocarditis; however, it has been reported that the administration of an antibody against a domain of TN-C to a rheumatoid arthritis model ameliorated disease severity. Thus, blocking TN-C-dependent inflammatory signals may be a potential novel therapeutic strategy for treating autoimmune myocarditis. Studies involving various animal models have provided a plethora of information, but there remains a gap in knowledge regarding how myocarditis in animal models may differ from that in humans. The prevalence of myocarditis will increase together with the expanding use of immune checkpoint inhibitors and the progression of the COVID-19 pandemic (67). As a result, sophisticated technologies, computational models, and insights are needed.

AUTHOR CONTRIBUTIONS

All authors listed have made a substantial, direct, and intellectual contribution to the work and approved it for publication. All authors contributed to the article and approved the submitted version.

FUNDING

This study was supported in part by a Grant-in-Aid for Scientific Research (Japan Society for the Promotion of Science KAKENHI grant number 20K08396) to KT.

ACKNOWLEDGMENTS

We would like to thank Editage (www.editage.jp) for English language editing.

REFERENCES

1. Corsten MF, Schroen B, Heymans S. Inflammation in viral myocarditis: Friend or foe? *Trends Mol Med* (2012) 18:426–37. doi: 10.1016/j.molmed.2012.05.005
2. Cihakova D, Rose NR. Pathogenesis of myocarditis and dilated cardiomyopathy. *Adv Immunol* (2008) 99:95–114. doi: 10.1016/S0065-2776(08)00604-4
3. Kindermann I, Barth C, Mahfoud F, Ukena C, Lenski M, Yilmaz A, et al. Update on myocarditis. *J Am Coll Cardiol* (2012) 59:779–92. doi: 10.1016/j.jacc.2011.09.074
4. Leuschner F, Katus HA, Kaya Z. Autoimmune myocarditis: past, present and future. *J Autoimmun* (2009) 33:282–9. doi: 10.1016/j.jaut.2009.07.009
5. Tajiri K, Yasutomi Y, Aonuma K. Recent advances in the management of autoimmune myocarditis: insights from animal studies. *Curr Pharm Des* (2016) 22:427–39. doi: 10.2174/1381612822666151222160702
6. Imanaka-Yoshida K, Yoshida T, Miyagawa-Tomita S. Tenascin-C in development and disease of blood vessels. *Anat Rec* (2014) 297:1747–57. doi: 10.1002/ar.22985
7. Marzeda AM, Midwood KS. Internal Affairs: Tenascin-C as a Clinically Relevant, Endogenous Driver of Innate Immunity. *J Histochem Cytochem* (2018) 66:289–304. doi: 10.1369/0022155418757443
8. Kanayama M, Morimoto J, Matsui Y, Ikesue M, Danzaki K, Kurotaki D, et al. α9β1 integrin-mediated signaling serves as an intrinsic regulator of pathogenic Th17 cell generation. *J Immunol* (2011) 187:5851–64. doi: 10.4049/jimmunol.1101524
9. Machino-Ohtsuka T, Tajiri K, Kimura T, Sakai S, Sato A, Yoshida T, et al. Tenascin-C aggravates autoimmune myocarditis via dendritic cell activation and Th17 cell differentiation. *J Am Heart Assoc* (2014) 3:e001052. doi: 10.1161/JAHA.114.001052
10. Momčilović M, Stamenković V, Jovanović M, Andjus PR, Jakovčevski I, Schachner M, et al. Tenascin-C deficiency protects mice from experimental autoimmune encephalomyelitis. *J Neuroimmunol* (2017) 302:1–6. doi: 10.1016/j.jneuroim.2016.12.001
11. Reinehr S, Reinhard J, Wiemann S, Stute G, Kuehn S, Woestmann J, et al. Early remodelling of the extracellular matrix proteins tenascin-C and phosphacan in retina and optic nerve of an experimental autoimmune glaucoma model. *J Cell Mol Med* (2016) 20:2122–37. doi: 10.1111/jcmm.12909
12. Tajiri K, Ieda M. Cardiac Complications in Immune Checkpoint Inhibition Therapy. *Front Cardiovasc Med* (2019) 6:3. doi: 10.3389/fcvm.2019.00003
13. Tajiri K, Aonuma K, Sekine I. Immune checkpoint inhibitor-related myocarditis. *Jpn J Clin Oncol* (2018) 48:7–12. doi: 10.1093/jjco/hyx154
14. Tschöpe C, Ammirati E, Bozkurt B, Caforio ALP, Cooper LT, Felix SB, et al. Myocarditis and inflammatory cardiomyopathy: current evidence and future directions. *Nat Rev Cardiol* (2020) 1–25. doi: 10.1038/s41569-020-00435-x
15. Ammirati E, Veronese G, Bottiroli M, Wang DW, Cipriani M, Garascia A, et al. Update on acute myocarditis. *Trends Cardiovasc Med* (2020). doi: 10.1016/j.tcm.2020.05.008
16. Lasrado N, Reddy J. An overview of the immune mechanisms of viral myocarditis. *Rev Med Virol* (2020) 6:1–14. doi: 10.1002/rmv.2131
17. Błyszczuk P. Myocarditis in Humans and in Experimental Animal Models. *Front Cardiovasc Med* (2019) 6:64. doi: 10.3389/fcvm.2019.00064
18. Mahrholdt H, Wagner A, Deluigi CC, Kispert E, Hager S, Meinhardt G, et al. Presentation, patterns of myocardial damage, and clinical course of viral myocarditis. *Circulation* (2006) 114:1581–90. doi: 10.1161/CIRCULATIONAHA.105.606509
19. Schenk T, Enders M, Pollak S, Hahn R, Huzly D. High prevalence of human parvovirus B19 DNA in myocardial autopsy samples from subjects without myocarditis or dilative cardiomyopathy. *J Clin Microbiol* (2009) 47:106–10. doi: 10.1128/JCM.01672-08
20. Maisch B. Cardio-Immunology of Myocarditis: Focus on Immune Mechanisms and Treatment Options. *Front Cardiovasc Med* (2019) 6:48. doi: 10.3389/fcvm.2019.00048
21. Sawalha K, Abozenah M, Kadado AJ, Battisha A, Al-Akchar M, Salerno C, et al. Systematic review of COVID-19 related myocarditis: Insights on management and outcome. *Cardiovasc Revasc Med* (2020). doi: 10.1016/j.carrev.2020.08.028
22. Wang J, Han B. Dysregulated CD4+ T Cells and microRNAs in Myocarditis. *Front Immunol* (2020) 11:539. doi: 10.3389/fimmu.2020.00539
23. Guo T, Fan Y, Chen M, Wu X, Zhang L, He T, et al. Cardiovascular Implications of Fatal Outcomes of Patients with Coronavirus Disease 2019 (COVID-19). *JAMA Cardiol* (2020) 5:811–8. doi: 10.1001/jamacardio.2020.1017
24. Shi S, Qin M, Shen B, Cai Y, Liu T, Yang F, et al. Association of Cardiac Injury with Mortality in Hospitalized Patients with COVID-19 in Wuhan, China. *JAMA Cardiol* (2020) 5:802–10. doi: 10.1001/jamacardio.2020.0950
25. Zhou F, Yu T, Du R, Fan G, Liu Y, Liu Z, et al. Clinical course and risk factors for mortality of adult inpatients with COVID-19 in Wuhan, China: a retrospective cohort study. *Lancet* (2020) 395:1054–62. doi: 10.1016/S0140-6736(20)30566-3
26. Basso C, Leone O, Rizzo S, De Gaspari M, van der Wal AC, Aubry M-C, et al. Pathological features of COVID-19-associated myocardial injury: a multicentre cardiovascular pathology study. *Eur Heart J* (2020) 41:3827–35. doi: 10.1093/eurheartj/ehaa664
27. Siripanthong B, Nazarian S, Muser D, Deo R, Santangeli P, Khanji MY, et al. Recognizing COVID-19–related myocarditis: The possible pathophysiology and proposed guideline for diagnosis and management. *Hear Rhythm* (2020) 17:1463–71. doi: 10.1016/j.hrthm.2020.05.001
28. Eriksson U, Ricci R, Hunziker L, Kurrer MO, Oudit GY, Watts TH, et al. Dendritic cell-induced autoimmune heart failure requires cooperation between adaptive and innate immunity. *Nat Med* (2003) 9:1484–90. doi: 10.1038/nm960
29. Tajiri K, Imanaka-Yoshida K, Matsubara A, Tsujimura Y, Hiroe M, Naka T, et al. Suppressor of Cytokine Signaling 1 DNA Administration Inhibits Inflammatory and Pathogenic Responses in Autoimmune Myocarditis. *J Immunol* (2012) 189:2043–53. doi: 10.4049/jimmunol.1103610
30. Lv H, Havari E, Pinto S, Gottumukkala RVSRK, Cornivelli L, Raddassi K, et al. Impaired thymic tolerance to α-myosin directs autoimmunity to the heart in mice and humans. *J Clin Invest* (2011) 121:1561–73. doi: 10.1172/JCI44583
31. Lv H, Lipes MA. Role of impaired central tolerance to α-myosin in inflammatory heart disease. *Trends Cardiovasc Med* (2012) 22:113–7. doi: 10.1016/j.tcm.2012.07.005
32. Lichtman AH. The heart of the matter: protection of the myocardium from T cells. *J Autoimmun* (2013) 45:90–6. doi: 10.1016/j.jaut.2013.05.004
33. Mueller DL. Mechanisms maintaining peripheral tolerance. *Nat Immunol* (2010) 11:21–7. doi: 10.1038/ni.1817
34. Gangaplara A, Massilamany C, Brown DM, Delhon G, Pattnaik AK, Chapman N, et al. Coxsackievirus B3 infection leads to the generation of cardiac myosin heavy chain-α-reactive CD4 T cells in A/J mice. *Clin Immunol* (2012) 144:237–49. doi: 10.1016/j.clim.2012.07.003
35. Gil-Cruz C, Perez-Shibayama C, de Martin A, Ronchi F, van der Borght K, Niederer R, et al. Microbiota-derived peptide mimics drive lethal inflammatory cardiomyopathy. *Sci (80-)* (2019) 366:881–6. doi: 10.1126/science.aav3487
36. Zarak-Crnkovic M, Kania G, Jaźwa-Kusior A, Czepiel M, Wijnen WJ, Czyż J, et al. Heart non-specific effector CD4+ T cells protect from postinflammatory fibrosis and cardiac dysfunction in experimental autoimmune myocarditis. *Basic Res Cardiol* (2020) 115:6. doi: 10.1007/s00395-019-0766-6
37. Saga Y, Yagi T, Ikawa Y, Sakakura T, Aizawa S. Mice develop normally without tenascin. *Genes Dev* (1992) 6:1821–31. doi: 10.1101/gad.6.10.1821
38. Midwood KS, Hussenet T, Langlois B, Orend G. Advances in tenascin-C biology. *Cell Mol Life Sci* (2011) 68:3175–99. doi: 10.1007/s00018-011-0783-6
39. Imanaka-Yoshida K. Tenascin-C in cardiovascular tissue remodeling: from development to inflammation and repair. *Circ J* (2012) 76:2513–20. doi: 10.1253/circj.CJ-12-1033
40. Imanaka-Yoshida K, Hiroe M, Yasutomi Y, Toyozaki T, Tsuchiya T, Noda N, et al. Tenascin-C is a useful marker for disease activity in myocarditis. *J Pathol* (2002) 197:388–94. doi: 10.1002/path.1131
41. Sato M, Toyozaki T, Odaka K, Uehara T, Arano Y, Hasegawa H, et al. Detection of experimental autoimmune myocarditis in rats by 111In monoclonal antibody specific for tenascin-C. *Circulation* (2002) 106:1397–402. doi: 10.1161/01.CIR.0000027823.07104.86
42. Tsukada B, Terasaki F, Shimomura H, Otsuka K, Otsuka K, Katashima T, et al. High prevalence of chronic myocarditis in dilated cardiomyopathy referred for left ventriculoplasty: expression of tenascin C as a possible marker for

inflammation. *Hum Pathol* (2009) 40:1015–22. doi: 10.1016/j.humpath.2008.12.017
43. Shiba M, Sugano Y, Ikeda Y, Okada H, Nagai T, Ishibashi-Ueda H, et al. Presence of increased inflammatory infiltrates accompanied by activated dendritic cells in the left atrium in rheumatic heart disease. *PloS One* (2018) 13:e0203756. doi: 10.1371/journal.pone.0203756
44. Sato A, Aonuma K, Imanaka-Yoshida K, Yoshida T, Isobe M, Kawase D, et al. Serum tenascin-C might be a novel predictor of left ventricular remodeling and prognosis after acute myocardial infarction. *J Am Coll Cardiol* (2006) 47:2319–25. doi: 10.1016/j.jacc.2006.03.033
45. Kimura T, Tajiri K, Sato A, Sakai S, Wang Z, Yoshida T, et al. Tenascin-C accelerates adverse ventricular remodelling after myocardial infarction by modulating macrophage polarization. *Cardiovasc Res* (2019) 115:614–24. doi: 10.1093/cvr/cvy244
46. Nishioka T, Suzuki M, Onishi K, Takakura N, Inada H, Yoshida T, et al. Eplerenone attenuates myocardial fibrosis in the angiotensin II-induced hypertensive mouse: involvement of tenascin-C induced by aldosterone-mediated inflammation. *J Cardiovasc Pharmacol* (2007) 49:261–8. doi: 10.1097/FJC.0b013e318033dfd4
47. Yokouchi Y, Oharaseki T, Enomoto Y, Sato W, Imanaka-Yoshida K, Takahashi K. Expression of tenascin C in cardiovascular lesions of Kawasaki disease. *Cardiovasc Pathol* (2019) 38:25–30. doi: 10.1016/j.carpath.2018.10.005
48. Sato A, Hiroe M, Akiyama D, Hikita H, Nozato T, Hoshi T, et al. Prognostic value of serum tenascin-C levels on long-term outcome after acute myocardial infarction. *J Card Fail* (2012) 18:480–6. doi: 10.1016/j.cardfail.2012.02.009
49. Fujimoto N, Onishi K, Sato A, Terasaki F, Tsukada B, Nozato T, et al. Incremental prognostic values of serum tenascin-C levels with blood B-type natriuretic peptide testing at discharge in patients with dilated cardiomyopathy and decompensated heart failure. *J Card Fail* (2009) 15:898–905. doi: 10.1016/j.cardfail.2009.06.443
50. Maisel AS, Krishnaswamy P, Nowak RM, McCord J, Hollander JE, Duc P, et al. Rapid Measurement of B-Type Natriuretic Peptide in the Emergency Diagnosis of Heart Failure. *N Engl J Med* (2002) 347:161–7. doi: 10.1056/NEJMoa020233
51. Omar HR, Guglin M. Longitudinal BNP follow-up as a marker of treatment response in acute heart failure: Relationship with objective markers of decongestion. *Int J Cardiol* (2016) 221:167–70. doi: 10.1016/j.ijcard.2016.06.174
52. Morimoto S-I, Imanaka-Yoshida K, Hiramitsu S, Kato S, Ohtsuki M, Uemura A, et al. Diagnostic utility of tenascin-C for evaluation of the activity of human acute myocarditis. *J Pathol* (2005) 205:460–7. doi: 10.1002/path.1730
53. Imanaka-Yoshida K, Hiroe M, Nishikawa T, Ishiyama S, Shimojo T, Ohta Y, et al. Tenascin-C modulates adhesion of cardiomyocytes to extracellular matrix during tissue remodeling after myocardial infarction. *Lab Invest* (2001) 81:1015–24. doi: 10.1038/labinvest.3780313
54. Imanaka-Yoshida K, Tawara I, Yoshida T. Tenascin-C in cardiac disease: A sophisticated controller of inflammation, repair, and fibrosis. *Am J Physiol Physiol* (2020) 319:C781–96. doi: 10.1152/ajpcell.00353.2020
55. Valaperti A, Marty RR, Kania G, Germano D, Mauermann N, Dirnhofer S, et al. CD11b+ monocytes abrogate Th17 CD4+ T cell-mediated experimental autoimmune myocarditis. *J Immunol* (2008) 180:2686–95. doi: 10.4049/jimmunol.180.4.2686
56. Sonderegger I, Röhn TA, Kurrer MO, Iezzi G, Zou Y, Kastelein RA, et al. Neutralization of IL-17 by active vaccination inhibits IL-23-dependent autoimmune myocarditis. *Eur J Immunol* (2006) 36:2849–56. doi: 10.1002/eji.200636484
57. Myers JM, Cooper LT, Kem DC, Stavrakis S, Kosanke SD, Shevach EM, et al. Cardiac myosin-Th17 responses promote heart failure in human myocarditis. *JCI Insight* (2016) 1:e85851. doi: 10.1172/jci.insight.85851
58. Bettelli E, Carrier Y, Gao W, Korn T, Strom TB, Oukka M, et al. Reciprocal developmental pathways for the generation of pathogenic effector TH17 and regulatory T cells. *Nature* (2006) 441:235–8. doi: 10.1038/nature04753
59. Chung Y, Chang SH, Martinez GJ, Yang XO, Nurieva R, Kang HS, et al. Critical regulation of early Th17 cell differentiation by interleukin-1 signaling. *Immunity* (2009) 30:576–87. doi: 10.1016/j.immuni.2009.02.007
60. Sonderegger I, Iezzi G, Maier R, Schmitz N, Kurrer M, Kopf M. GM-CSF mediates autoimmunity by enhancing IL-6-dependent Th17 cell development and survival. *J Exp Med* (2008) 205:2281–94. doi: 10.1084/jem.20071119
61. Van Der Borght K, Scott CL, Martens L, Sichien D, Van Isterdael G, Nindl V, et al. Myocarditis elicits dendritic cell and monocyte infiltration in the heart and self-antigen presentation by conventional type 2 dendritic cells. *Front Immunol* (2018) 9:2714. doi: 10.3389/fimmu.2018.02714
62. Hilligan KL, Ronchese F. Antigen presentation by dendritic cells and their instruction of CD4+ T helper cell responses. *Cell Mol Immunol* (2020) 17:587–99. doi: 10.1038/s41423-020-0465-0
63. Akira S, Hemmi H. Recognition of pathogen-associated molecular patterns by TLR family. *Immunol Lett* (2003) 85:85–95. doi: 10.1016/S0165-2478(02)00228-6
64. Frevert CW, Felgenhauer J, Wygrecka M, Nastase MV, Schaefer L. Danger-Associated Molecular Patterns Derived From the Extracellular Matrix Provide Temporal Control of Innate Immunity. *J Histochem Cytochem* (2018) 66:213–27. doi: 10.1369/0022155417740880
65. Zuurbier CJ, Abbate A, Cabrera-Fuentes HA, Cohen MV, Collino M, De Kleijn DPV, et al. Innate immunity as a target for acute cardioprotection. *Cardiovasc Res* (2019) 115:1131–42. doi: 10.1093/cvr/cvy304
66. Popovic ZV, Wang S, Papatriantafyllou M, Kaya Z, Porubsky S, Meisner M, et al. The proteoglycan biglycan enhances antigen-specific T cell activation potentially via MyD88 and TRIF pathways and triggers autoimmune perimyocarditis. *J Immunol* (2011) 187:6217–26. doi: 10.4049/jimmunol.1003478
67. Zaha VG, Meijers WC, Moslehi J. Cardio-Immuno-Oncology. *Circulation* (2020) 141:87–9. doi: 10.1161/CIRCULATIONAHA.119.042276

Conflict of Interest: The authors declare that the research was conducted in the absence of any commercial or financial relationships that could be construed as a potential conflict of interest.

frontiers in Immunology

ORIGINAL RESEARCH
published: 22 February 2021
doi: 10.3389/fimmu.2020.630139

Tenascin-W Is a Novel Stromal Marker in Biliary Tract Cancers

Ismaïl Hendaoui[1], Ahlem Lahmar[2,3], Luca Campo[1], Sihem Mebarki[1], Sandrine Bichet[1], Daniel Hess[1], Martin Degen[4], Nidhameddine Kchir[3,5], Leila Charrada-Ben Farhat[3,6], Rania Hefaiedh[7], Christian Ruiz[8], Luigi M. Terracciano[8], Richard P. Tucker[9], Lotfi Hendaoui[3,6‡] and Ruth Chiquet-Ehrismann[1,10†‡]*

[1] Friedrich Miescher Institute for Biomedical Research, Basel, Switzerland, [2] Department of Pathology, Mongi Slim University Hospital, La Marsa, Tunisia, [3] Medical School, University of Tunis El Manar, Tunis, Tunisia, [4] Laboratory for Oral Molecular Biology, Department of Orthodontics and Dentofacial Orthopedics, University of Bern, Bern, Switzerland, [5] Pathology Department, La Rabta University Hospital, Tunis, Tunisia, [6] Department of Diagnostic and Interventional Radiology, Mongi Slim University Hospital, La Marsa, Tunisia, [7] Department of Hepato-gastro-enterology, Mongi Slim University Hospital, Tunis, Tunisia, [8] Institute of Pathology, University Hospital Basel, Basel, Switzerland, [9] Department of Cell Biology and Human Anatomy, University of California at Davis, Davis, CA, United States, [10] Faculty of Science, University of Basel, Basel, Switzerland

Extrahepatic cancers of the biliary system are typically asymptomatic until after metastasis, which contributes to their poor prognosis. Here we examined intrahepatic cholangiocarcinomas (n = 8), carcinomas of perihilar bile ducts (n = 7), carcinomas of the gallbladder (n = 11) and hepatic metastasis from carcinomas of the gallbladder (n = 4) for the expression of the extracellular matrix glycoproteins tenascin-C and tenascin-W. Anti-tenascin-C and anti-tenascin-W immunoreactivity was found in all biliary tract tumors examined. Unlike tenascin-C, tenascin-W was not detected in normal hepatobiliary tissue. Tenascin-W was also expressed by the cholangiocarcinoma-derived cell line Huh-28. However, co-culture of Huh-28 cells with immortalized bone marrow-derived stromal cells was necessary for the formation and organization of tenascin-W fibrils *in vitro*. Our results indicate that tenascin-W may be a novel marker of hepatobiliary tumor stroma, and its absence from many normal tissues suggests that it may be a potential target for biotherapies.

Keywords: tenascin-W, tenascin-N, tenascin-C, gallbladder cancer, extracellular matrix, tumor stroma

OPEN ACCESS

Edited by:
Kyoko Imanaka-Yoshida, Mie University, Japan

Reviewed by:
Kenichiro Ishii, Mie University, Japan
Takuya Iyoda, Sanyo-Onoda City University, Japan

***Correspondence:**
Richard P. Tucker
rptucker@ucdavis.edu

†*Deceased*

‡*These authors share senior authorship*

Specialty section:
This article was submitted to Cancer Immunity and Immunotherapy, a section of the journal Frontiers in Immunology

Received: *16 November 2020*
Accepted: *30 December 2020*
Published: *22 February 2021*

Citation:
Hendaoui I, Lahmar A, Campo L, Mebarki S, Bichet S, Hess D, Degen M, Kchir N, Charrada-Ben Farhat L, Hefaiedh R, Ruiz C, Terracciano LM, Tucker RP, Hendaoui L and Chiquet-Ehrismann R (2021) Tenascin-W Is a Novel Stromal Marker in Biliary Tract Cancers. Front. Immunol. 11:630139. doi: 10.3389/fimmu.2020.630139

INTRODUCTION

Cancers originating in the epithelia of the biliary system are typically categorized as intrahepatic cholangiocarcinoma (ICC), carcinoma of perihilar bile ducts (CPHBD) or carcinoma of the gallbladder (CGB). While some early intrahepatic biliary system tumors have the potential to be treated effectively by radiotherapy, chemotherapy, local resection or liver transplantation, cancers of the extrahepatic biliary system have a particularly poor prognosis and limited options for therapy (1). In CGB the best outcomes require early diagnosis and resection, but extrahepatic lesions typically have asymptomatic development and most patients have metastatic disease by the time of surgery (2). The mean survival rate following CGB diagnosis is 6 months, and the 5-year survival rate is only 5% (3). CGB is more common in women than in men (4, 5) and while world-wide it is a

rare cancer, it is relatively common in certain populations (2, 6–9). Some of these variations are likely related to regional rates of cholelithiasis, as 74–92% of patients with CGB have gallstones (10).

Tenascins are a family of extracellular matrix glycoproteins that share a common domain architecture (11). The best studied tenascin is the hexabrachion tenascin-C, which is required for normal embryonic development and reappears in the stroma of solid tumors (12, 13). Tenascin-C is abundant in the extracellular matrix of cancers of the breast, colon, pancreas, prostate, uterus, lung, skin, and brain, to name a few (14–16). *In vitro*, tenascin-C promotes the proliferation and migration of many tumor-derived cell lines (17) and there are reduced metastases in tenascin-C knockout mice and in mice lacking factors that promote the expression of tenascin-C (16). Tenascin-C may also play a role in creating an immune suppressive tumor stroma, thus contributing to tumor growth and metastasis (18). Tenascin-C has been proposed as a marker, immunotherapy target and indicator of prognosis in many kinds of cancer (16), but its use has been limited by its presence, albeit at lower levels, in many normal adult tissues (19).

Much less is known about tenascin-W, which is also known as tenascin-N (20, 21). It is particularly abundant in the embryo, especially at sites of osteogenesis (22). In the adult, it is found in certain stem cell niches together with tenascin-C (23) but except for the kidney and spleen its expression elsewhere in the adult is sparse (24, 25). Like tenascin-C, tenascin-W can promote cell migration *in vitro*, but it typically has little or no effect on cell proliferation (21). Tenascin-W is also found in the stroma of certain solid tumors. This was first reported in murine breast carcinomas (26) and later in human breast and colon cancer (27, 28), and glioblastomas (29). Studies with normal human tissue samples suggest that the expression of tenascin-W may be more restricted in the adult than tenascin-C and may therefore be a better marker of tumor stroma and a more appropriate target for biotherapies (19).

Here we used immunohistochemistry to study the expression of tenascin-C and tenascin-W in the stroma of ICC, CPHBD and CGB, and we characterized biliary tract cancer-derived cell lines for tenascin-W expression. We also studied the expression of tenascin-W in a wide array of normal human tissues. Our goals were to determine if tenascin-W represents a novel candidate for use as a biliary tract cancer stromal marker and if tenascin-W is a potential target for adjuvant therapy to fight cancers of the biliary system.

MATERIAL AND METHODS

Cases

This study was approved by the Mongi Slim University Hospital (MSUH) Committee on Medical Ethics (La Marsa, Tunisia) and the Ethikkommission Nordwest- und Zentralschweiz (Switzerland). All methods were performed according to these approved guidelines and regulations and are consistent with the editorial and publication policies of this journal. Only MSUH patients who underwent biopsy or surgery for diagnosis or treatment purposes were asked to participate by signing an informed consent form. None of the patients received radio and/or chemotherapy before biopsy or surgery. 17/18G percutaneous needle biopsies or surgical resection were fixed in Shandon™ Formal-Fixx™ 10% Neutral Buffered Formalin (Thermo Fisher Scientific, Runcorn, UK) for 24 h and then shipped in phosphate buffered saline (PBS) at 4°C to the Friedrich Miescher Institute for Biomedical Research (Basel, Switzerland) for processing. Upon reception, samples were incubated overnight in PBS with 30% sucrose for cryoprotection before being frozen at -80°C in Tissue-Tek OCT Compound (Sakura Finetek USA, Torrance, CA, USA) using acetone precooled with dry-ice. Histological diagnosis of each biopsy/resection was performed by at least one of two pathologists (A. L. and N. K.) according to the World Health Organization classification of tumors (30). Tumors were staged according to the Union for International Cancer Control 8th TNM Classification of Malignant Tumors. Formalin-fixed and paraffin-embedded tissue samples were obtained from the Institute of Pathology of the University Hospital of Basel (Basel, Switzerland) and FDA standard human adult normal tissue frozen arrays were purchased from Biochain (Hayward, CA, USA).

Immunohistochemistry

Both monoclonal mouse anti-human tenascin-C (B28-13) and anti-human tenascin-W (56O) antibodies were generated and characterized as described previously (27, 31). Immunohistochemistry experiments were performed with a Ventana Discovery Ultra instrument (Roche Diagnostics, Manheim, Germany). For fixed-frozen material, the procedure RUO Discovery Universal was used. Sections were first fixed with 4% formaldehyde for 12 min on-line and anti-tenascin-C B28-13 (1:10000) or anti-tenascin-W 56O (1:30) were applied manually and incubated for 1 h at 37°C. For anti-tenascin-W, a blocker (Discovery antibody block, Roche Diagnostics) was applied. To detect bound antibodies, a monoclonal rabbit-anti-mouse IgG (ab133469, Abcam, Cambridge, UK) was used as a linker (0.6 µg/ml) and applied for 20 min. Antibody-antigen complexes were detected with ImmPRESS anti-rabbit Ig (peroxidase) polymer reagent (MP-7401, Vector Laboratories, Burlingame, CA, USA) applied manually and incubated for 32 min. The ChromoMap DAB kit (Roche Diagnostics) was used for detection. Finally, slides were counterstained with Hematoxylin II and Bluing Reagent (Roche Diagnostics) for 8 min.

For formalin-fixed, paraffin-embedded material, the procedure RUO Discovery Universal was used with 40 min CC1 pre-treatment. Anti-tenascin-C B28-13 (1:5000) or anti-tenascin-W 56O (1:100) were applied manually and incubated for 1 h at 37°C or 3 h at room temperature, respectively. For anti-tenascin-C, secondary antibody (ImmPRESS reagent kit peroxidase anti-mouse Ig MP-7402, Vector Laboratories) was applied manually (200 µl) and incubated for 32 min at 37°C. For anti-tenascin-W, a blocker (Dako antibody diluent with background reducing component, S3022, Dako Agilent Pathology Solutions, Santa Clara, CA, USA) was applied together with the primary antibody. Detection of bound anti-

tenascin-W antibody was achieved by incubating 20 min with anti-mouse HQ (Roche Diagnostics) and 24 min with anti-HQ HRP (Roche Diagnostics). Finally, for both anti-tenascin-C and anti-tenascin-W immunostainings, ChromoMap DAB kit (Roche Diagnostics) was used for the detection and slides were counterstained with Hematoxylin II and Bluing Reagent (Roche Diagnostics) for 8 min.

For controls, sections were processed as above but without primary antibodies. In addition, mouse IgG2A (Clone # 20102, R&D systems) and mouse IgG1 (Clone # 11711, R&D systems) were used as isotypic controls for anti-tenascin-C and anti-tenascin-W, respectively. Control slides were unlabeled.

Cell Lines

Twenty human biliary tract cancer cell lines were collected from different sources. Huh-28 (ICC), HuCCT1 (ICC), OZ (CPHBD), NOZ (CGB) and OCUG-1 (CGB) cell lines were obtained from the Japanese Collection of Research Bioresources Cell Bank. TKKK (ICC), TFK-1 (CPHBD), TGBC1TKB (CGB), TGBC2 (CGB), TGBC14TKB (CGB), TGBC24TKB (CGB) and G-415 (CGB) cell lines were obtained from the RIKEN BioResource Center. SNU-1079 (ICC), SNU-245 (CPHBD), SNU-1196 (CPHBD) and SNU-308 (CGB) cell lines were obtained from the Korean Cell Line Bank. The Egi-1 (CPHBD) cell line was obtained from the Leibniz Institute DSMZ - German Collection of Microorganisms and Cell Cultures. All cell lines were cultured as recommended by their respective cell banks. SK-ChA-1 (CPHBD), Mz-ChA-1 (CGB), Mz-ChA-2 (CGB) were obtained from Prof. Alexander Knuth (University Hospital of Zürich, Zürich, Switzerland) (32) and cultured in RPMI 1640 with 10 mM HEPES, 2 mM L-Glutamine, 1X MEM non-essential amino acids (Thermo Fisher Scientific), 100 U/ml penicillin, 100 µg/ml of streptomycin, and 10% fetal bovine serum (FBS). Human BMSCs (196hT) immortalized with the hTERT/GFP system (33) were cultured as described previously (34). The control cell line 293/hTNW that stably expresses human tenascin-W (27) was cultured in DMEM with 0.25 µg/ml of G418, 1.5 µg/ml of puromycin, and 10% FBS.

Cell Culture, Immunocytochemistry, and siRNA Transfection

For the co-culture assay, Huh-28 and 196hT cell lines were cultured in α-MEM plus 10% FBS, either alone or together at 1:1 ratio, with a total density of 27000 cells/cm². Cells were cultured in BD Falcon™ 8-well CultureSlides (BD Biosciences, Franklin Lakes, NJ, USA) pre-coated with 0.01% poly-L-lysine (Cultrex, Trevigen, Gaithersburg, MD, USA) for 2 h at 37°C. For the transwell assay, Huh-28 and 196hT cell lines were cultured in 12-well plates containing inserts separated by a polycarbonate membrane with 0.4 µm pores (Costar, Corning Amsterdam, Netherlands). Huh-28 or 196hT cells were either plated in the upper chamber (30,000 cells in 0.5 ml medium) or on 10-mm round glass coverslips pre-coated with fibronectin (50 µg/ml for 2 h at 37°C) and placed in the lower chamber (100,000 cells in 1.5 ml medium). Huh-28 or 196hT were cultured in the lower chamber either alone (with only medium in the upper chamber) or in co-culture (with 196hT or Huh-28, respectively, in the upper chamber). Cells were cultured in α-MEM plus 10% FBS. Only the cells from the lower chamber can be analyzed by immunofluorescence, thanks to their culture on the pre-coated glass coverslip. For both co-culture and transwell assays, after 4 days of culture without changing the medium, cells were fixed with 4% formaldehyde (Electron Microscopy Sciences, Hatfield, PA, USA) diluted in PBS for 10 min at room temperature, permeabilized for 5 min with 0.1% Triton X-100 (Sigma-Aldrich, St. Louis, MO, USA), washed twice with PBS, and blocked for 15 min with 3% bovine serum albumin (Sigma-Aldrich) in PBS. Cells were then incubated for 1 h with anti-tenascin-W (56O) diluted at 1:100. After 3 washes with PBS, cells were incubated for 1 h in the dark with goat anti-mouse antibody conjugated to Alexa Fluor® 568 (Thermo Fisher Scientific) diluted at 1:1000. Finally, cell nuclei were counterstained with DAPI (Sigma-Aldrich) and slides were mounted with ProLong® Diamond Antifade Mountant (Life Technologies, Waltham, MA, USA). Images were acquired with an Axio Imager Z1 microscope (Zeiss, Oberkochen, Germany).

For siRNA transfection, Huh-28 cells were seeded in 6-well plates with a density of 600,000 cells/well. The day after, cells were transfected with 25 pmol/well of different Silencer Select® SiRNAs (Thermo Fischer Scientific) using Lipofectamine RNAiMAX Transfection Reagent (Thermo Fisher Scientific) following manufacturer's instructions. SiRNA TNW 1 (sc34270), siRNA TNW 2 (sc34271) and siRNA TNW 3 (sc34272) were used to knockdown tenascin-W. SiRNA control 1 (Silencer® Negative Control #1, ref 4390843) and siRNA control 2 (Silencer® Negative Control #2, ref 4390846) were used as negative control. Cells were collected 3 days post-transfection and tenascin-W expression was analyzed by Western blot as described below.

Conditioned Media Preparation

Huh-28, 196hT and 293/hTNW cells were cultured in medium plus FBS 10% (RPMI 1640, α-MEM and DMEM, respectively) until reaching approximately 90% confluency. Then, cells were starved in their respective medium without FBS and antibiotics for 6 days (Huh-28 and 196hT cell lines) or 3 days (293/hTNW cell line) before collecting their conditioned medium. Finally, cell debris were removed by centrifugation and the conditioned medium was concentrated 15X (for Western blots) or 30X (for mass spectrometry) *via* precipitation with 10% trichloroacetic acid, before being resuspended in 4X sample buffer (0.2M Tris-HCl, 145.56mM SDS, 20% glycerol, bromophenol blue) containing 0.1M DTT.

Western Blotting

For cell lysates, cells were lysed in RIPA buffer (50 mM Tris HCl pH 7.4, 150 mM NaCl, 0.2% Na-deoxycholate, 25 mM Hepes, 5 mM $MgCl_2$) containing protease inhibitors (Complete Mini, EDTA-free, Roche Diagnostics). Protein concentration was determined with a Bradford Assay (BradfordUltra, Expedeon, San Diego, CA, USA). Cell lysates or conditioned media were separated on 7% polyacrylamide gel under reducing conditions

and blotted to polyvinyl-difluoride membranes (Thermo Fisher Scientific). Membranes were then stained with Ponceau S to control for equal protein loading and blotting efficiency. After blocking for 1 h at room-temperature with 5% Skim Milk Powder (Sigma-Aldrich) in PBS-Tween-20 0.1% (PBS-T), Blots were incubated overnight at 4°C with either anti-tenascin-W (56O) diluted at 1:1000, or anti-GAPDH (ab9485, Abcam, Cambridge, UK) diluted at 1:1000, as primary antibodies. After several washing steps with PBS-T, peroxidase-conjugated anti-mouse IgG (G21040, Life Technologies) or anti-rabbit IgG (G21234, Life Technologies) for 1 h at room temperature to detect anti-tenascin-W or anti-GAPDH, respectively. Signal from immunoblots was detected by enhanced chemiluminescence using SuperSignal™ West Dura Extended Duration Substrate (Thermo Fisher Scientific), and exposed to Super RX films (Fujifilm, Dielsdorf, Switzerland).

RNA Isolation and Gene Expression Analysis by qRT-PCR

Total RNA was isolated by using QIAshredder and RNeasy Mini Kit (QIAGEN, Hilden, Germany/Venlo, Netherlands). RNA was reverse transcribed into cDNA using the High Capacity cDNA Reverse Transcription Kit (Life Technologies) with oligo-p(dT) 15 (Roche) instead of the random primers provided in the kit. Quantitative RT-PCR assay was performed with 50 ng of cDNA from each cell line, using Platinium SYBR Green qPCR SuperMix-UDG with ROX (Invitrogen, Life Science, Carlsbad, CA, USA) on a StepOnePlus™ Real-Time PCR System (Life Technologies). Relative expression of human tenascin-W was calculated using the ΔΔCT method, normalizing values to human TBP (TATA-Box binding protein) within each sample. Primers for human tenascin-W (forward primer: 5'-ATGCCCTCACAGAAATTGACAG-3' and reverse primer: 5'-TCTCTGGTCTCTTGGTCGTC-3') and for human TBP (forward primer: 5'-TGCACAGGAGCCAAGAGTGAA-3' and reverse primer: 5'-CACATCACAGCTCCCCACCA-3') were tested for specificity and efficiency.

Mass Spectrometry

Mass spectroscopy was used to determine the identity of the high molecular weight band recognized by anti-tenascin-W on Western blots of Huh-28 cell line. For the samples, 293/hTNW cell lysate and Huh-28 serum-free conditioned medium were prepared as described above. To analyze the samples by spectrometry, 50µl of 30X concentrated serum-free Huh-28 conditioned medium and 250µg of 293/hTNW cell lysate were separated on a 7% SDS-PAGE gel and stained with InstantBlue™ (Expedeon Inc.) in order to visualize the bands of interest. The protein bands were excised from the gel, reduced with 10mM TCEP, alkylated with 20mM iodoacetamide and cleaved with 0.1 µg porcine sequencing grade trypsin (Promega) in 25mM ammonium bicarbonate (pH 8.0) at 37°C for 16 h. The extracted peptides were analyzed by capillary liquid chromatography tandem mass spectrometry with an EASY-nLC 1000 using the two-column set up (Thermo Scientific). The peptides were loaded in 0.1% formic acid, 2% acetonitrile in H_2O onto a peptide trap (Acclaim PepMap 100, 75um x 2cm, C18, 3um, 100Å) at a constant pressure of 800 bar. Then they were separated at a flow rate of 150 nl/min with a linear gradient of 2–6% buffer B (0.1% formic acid in acetonitrile) in buffer A (0.1% formic acid) for 3 min followed by an linear increase from 6–22% for 40 min, 22–28% for 9 min, 28–36% for 8 min, and 36–80% for 1 min. The column was finally washed for 12 min in 80% buffer B on a 50µm x 15cm ES801 C18, 2µm, 100Å column mounted on a DPV ion source (New Objective) connected to a Orbitrap Fusion (Thermo Scientific).

The data were acquired using 120000 resolution for the peptide measurements in the Orbitrap and a top T (3 s) method with HCD fragmentation for each precursor and fragment measurement in the LTQ. Mascot Distiller 2.5 and MASCOT 2.5 (Matrix Science, London, UK) searching the human subset of the UniProt version 2015_01 data base combined with known contaminants was used to identify the peptides. The enzyme specificity was set to trypsin allowing for up to three incomplete cleavage sites. Carbamidomethylation of cysteine (+57.0245) was set as a fixed modification, oxidation of methionine (+15.9949 Da) and acetylation of protein N-termini (+42.0106 Da) were set as variable modifications. Parent ion mass tolerance was set to 10 ppm and fragment ion mass tolerance to 0.6 Da. The decoy function in Mascot was used and the results were validated and the false discovery rate (FDR) was calculated with the program Scaffold Version 4.4 (Proteome Software, Portland, USA). The peptide threshold was set to an FDR of 0.1% and for proteins to 1%.

Cell Sorting

Huh-28 and 196hT cell lines were cultured in α-MEM plus 10% FBS, either alone or together at a ratio of 1:1, with a total density of 27,000 cells/cm². After 4 days of culture, using the ability of 196hT cells to express GFP, cells from both the co-culture and the monocultures were sorted with a BD Influx cell sorter (BD Biosciences) and BD FACS™ Sortware sorter software (Version 1.01.654). The sort was performed with a 100-mm nozzle tip, at a sheath pressure of 19.0 psi, and a frequency of 28.90 kHz. The following gates were set: gate 1 was forward scatter FSC-Area against side scatter SSC-Area, gate 2 was FSC-Width against FSC-Height, gate 3 was SSC-Width against SSC-Height, and gate 4 was 530/40 (488 nm) against 710/50 (561 nm).

RESULTS

In all, 30 tumors from patients with biliary tract cancers ranging in age from 29–79 years old were processed for histopathological examination as well as anti-tenascin-C and anti-tenascin-W immunohistochemistry. The results were compared with normal liver (all negative for HIV, hepatitis B, and hepatitis C), non-tumoral liver from a patient with ICC, and tissue from non-tumoral gallbladders that were removed due to cholecystitis. The results are summarized in **Supplementary Table 1** and **Table 1** and are illustrated in **Figures 1**–**3**.

TABLE 1 | Summary of tenascin immunostaining of normal liver, non-tumoral gallbladder, and hepatobiliary cancers.

Tissue	Anti-TNC				Anti-TNW*			
	-	+	++	+++	-	+	++	+++
Liver (n = 13)**	0/13	5/13	7/13	1/13	13/13	0/13	0/13	0/13
Gallbladder (n = 6)†	0/6	1/6	2/6	3/6	5/6	1/6¶	0/6	0/6
ICC (n = 8)‡	0/8	0/8	0/8	8/8	0/8	1/8	2/8	5/8
CPHBD (n = 7)§	0/7	0/7	1/7	6/7	0/7	2/7	2/7	3/7
CGB (n = 11)‖	0/11	0/11	0/11	11/11	0/11	1/11	3/11	7/11
CGB liver metastasis (n = 4)	0/4	0/4	0/4	4/4	0/4	0/4	2/4	2/4

Intensity of anti-tenascin-C (TNC) and anti-tenascin-W (TNW) immunostaining: -, absent; +, weak; ++, moderate; +++, high.
***Histologically normal liver, negative for HIV, hepatitis B, and hepatitis C.*
†*From cholecystectomy due to cholecystitis.*
‡*Intrahepatic cholangiocarcinoma.*
§*Carcinoma of perihilar bile ducts.*
‖*Carcinoma of the gallbladder.*
¶*Focal positivity.*

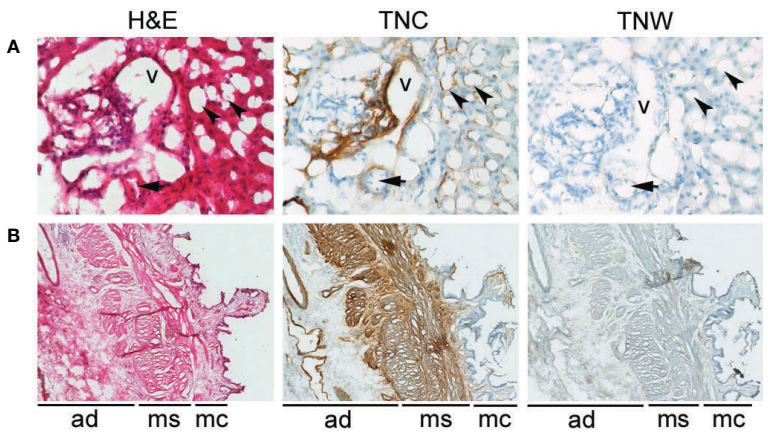

FIGURE 1 | Anti-tenascin-C (TNC) and anti-tenascin-W (TNW) immunohistochemistry of hepatobiliary tissues. **(A)** TNC immunostaining is observed around sinusoids (arrowheads) and around a vein (v) and an artery (arrow) in portal tract sections of a normal adult liver. An adjacent section is not labeled with TNW immunohistochemistry (400X). **(B)** TNC immunohistochemistry of a non-tumoral adult gallbladder (cholecystitis) shows labeling around vessels in the adventitia (ad), as well as around bundles of smooth muscle in the muscularis layer (ms). There is also patchy immunoreactivity in the mucosa (mc). In contrast, TNW does not immunolabel gallbladder tissue (40X). A third section in each series was stained with hematoxylin and eosin (H&E).

Tenascin-C immunoreactivity is seen in hepatic sinusoids and around blood vessels (vein and artery) in the portal tract of normal liver tissue (**Figure 1A**). Conversely, anti-tenascin-W does not immunostain normal hepatic tissue (**Figure 1A**). Similarly, tenascin-C immunoreactivity is seen surrounding blood vessels in the adventitia of a non-tumoral gallbladder removed from a patient with cholecystitis, around bundles of smooth muscle in the muscularis externa, and in the lamina propria of the mucosa (**Figure 1B**). Tenascin-W immunoreactivity is not detected in the non-tumoral gallbladder (**Figure 1B**) and was not detected in tissues isolated from 5 of the 6 non-tumoral gallbladders examined (**Table 1**). The anti-tenascin-W immunostaining observed in one non-tumoral gallbladder was weak (+) and only present in a single focal fibrotic area (**Table 1**). The presence of tenascin-C immunoreactivity in all the non-tumoral tissues examined, and the general absence of tenascin-W immunoreactivity in adjacent sections, led us to examine a broad array of normal human tissues with the tenascin-W antibody (**Supplementary Figure 1**). As reported by others studying tenascin-W in mice (24, 25), the anti-tenascin-W immunostains extracellular matrix in normal adult human spleen and kidney. Tenascin-W immunoreactivity is also seen in the female reproductive system (uterus, uterine tubes and ovaries) as well as in certain glands (adrenal gland, pituitary gland, thyroid and prostate). Tenascin-W immunoreactivity is not seen in heart, lung or central nervous system samples, and it is absent or weak in tissues from the gastrointestinal system (esophagus, stomach, pancreas or colon). Consistent with our findings (**Figure 1A**), tenascin-W immunoreactivity is absent from three additional normal liver samples that were part of the array.

There is strong anti-tenascin-C immunoreactivity around sinusoids in the non-tumoral region of a liver sample taken from a patient with ICC (**Figure 2A**). As in the non-tumoral liver, there is no tenascin-W immunoreactivity in this sample. However, both antibodies immunostain the stroma surrounding the ICC itself (**Figure 2B**). Both tenascin-C and tenascin-W

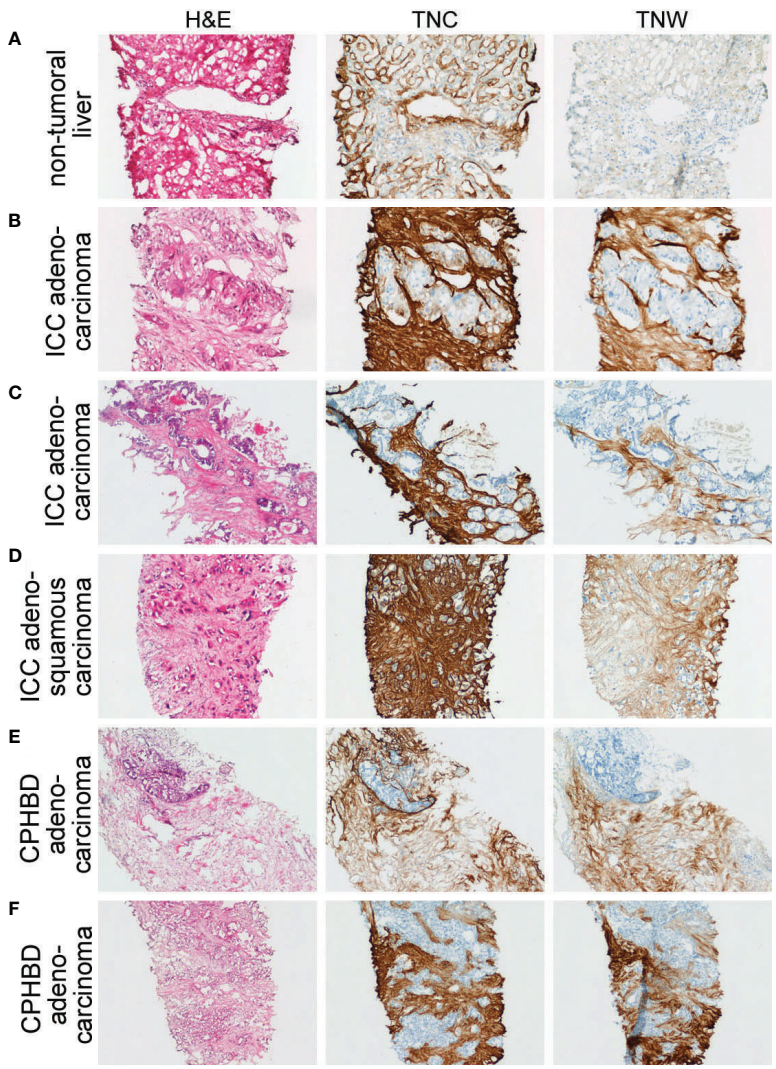

FIGURE 2 | Adjacent sections through needle biopsies of non-tumoral liver and various intrahepatic cholangiocarcinomas and carcinomas of perihilar bile ducts immunostained with anti-tenascin-C (TNC) and anti-tenascin-W (TNW). **(A)** Non-tumoral liver (patient ID 5) is immunostained with TNC, but not TNW (200X). **(B–D)** Immunohistochemical examination of intrahepatic cholangiocarcinomas (ICC). Both TNC and TNW label the stroma of a moderately differentiated adenocarcinoma **(B)** strongly (patient ID 5; 200X). Antibodies to both tenascin-C and tenascin-W label the stroma of a well differentiated adenocarcinoma (Patient ID 1; **C**; 100X) and an adenosquamous carcinoma (Patient ID 8; **D**; 100X). **(E, F)** Immunolabeling of carcinomas of perihilar bile ducts (CPHBD) with TNC and TNW. The stroma of a moderately differentiated adenocarcinoma (Patient ID 11; **E**; 100X) and a well differentiated adenocarcinoma (Patient ID 13; **F**; 100X) show expression of both tenascin-C and tenascin-W. A third section in each series was stained with hematoxylin and eosin (H&E).

antibodies labeled the stroma of each ICC (n = 8) and CPHBD (n = 7) examined (**Figure 2** and **Supplementary Table 1**). The intensity of the anti-tenascin-W immunoreactivity in ICC and CPHBD is variable, but no clear correlations could be made between the intensity of the immunostaining and the tumor grade (**Supplementary Table 1**). While most of the ICC and CPHBD examined were well or moderately differentiated adenocarcinomas (n = 13), the tenascin-W antibody also immunolabeled the stroma of a single squamous cell carcinoma (**Supplementary Table 1**) and a single adenosquamous carcinoma (**Figure 2D**).

In all, 11 cases of CGB, as well as 4 independent CGB metastases to liver, were examined with immunohistochemistry (**Figure 3** and **Supplementary Table 1**). Anti-tenascin-C and anti-tenascin-W both immunolabel the stroma of poorly (n = 3), moderately (n = 4) and well differentiated adenocarcinomas (n = 2), as well as the stroma of a single squamous cell carcinoma (**Figure 3D**) and a single mucinous carcinoma (**Figure 3E**). There is also tenascin-C and tenascin-W immunoreactivity in the stroma of CGB hepatic metastases (**Figure 3F**). As with the ICC and CPHBD immunostaining, anti-tenascin-W immunolabels the stroma of various tumors with different

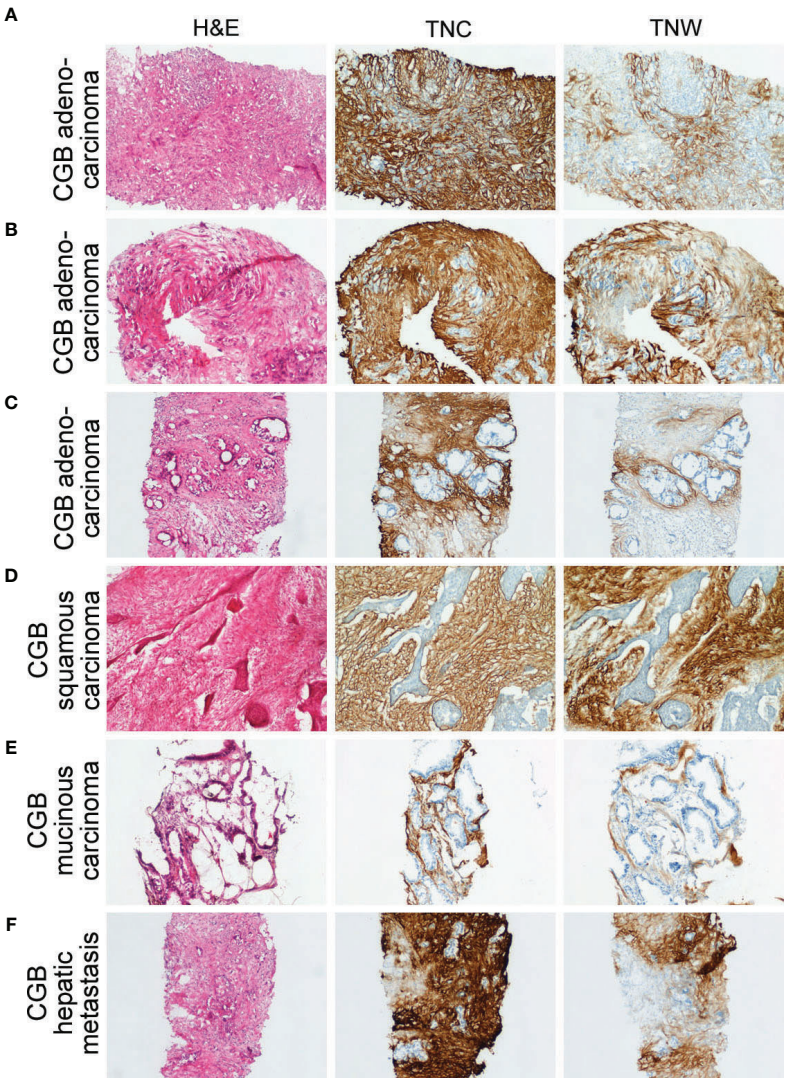

FIGURE 3 | Sections through needle biopsies of carcinomas of the gallbladder and a hepatic metastasis from a carcinoma of the gallbladder stained with hematoxylin or immunostained with anti-tenascin-C (TNC) or anti-tenascin-W (TNW). **(A–E)** Immunostaining of carcinomas of the gallbladder (CGB). The stroma of a poorly differentiated adenocarcinoma (Patient ID 18; **A**), a moderately differentiated adenocarcinoma (Patient ID 17; **B**) and a well differentiated adenocarcinoma (Patient ID 26; **C**) are immunolabeled with both TNC and TNW (100X). Both TNC and TNW label the stroma of a squamous carcinoma (Patient ID 19; **D**; 100X) and a mucinous carcinoma (Patient ID 22; **E**; 100X). **(F)** A representative section through a needle biopsy of a hepatic metastasis from a carcinoma of the gallbladder (Patient ID 27) shows strong TNC and TNW immunolabeling in the tumor stroma (100X). A third section in each series was stained with hematoxylin and eosin (H&E).

intensities, but no clear correlations could be made with the intensity of the immunostaining and the tumor grade (**Table 1**).

To maximize anti-tenascin immunostaining, the ICC, CPHBD and CGB samples shown here were processed using cryopreservation and sectioning. However, following antigen retrieval it was also possible to use the antibodies to immunostain formalin-fixed and paraffin-embedded samples of CPHBD, ICC and CGB (**Supplementary Figure 2**).

To determine the potential cellular origins of tenascin-W in biliary tract cancers and to facilitate future studies of the role of tenascin-W in these cancers, 20 different human biliary tract cell lines were examined for tenascin-W RNA expression by qRT-PCR. While many of the cell lines had low to negligible levels of expression, ICC-derived Huh-28 cells expressed significant levels of tenascin-W (**Figure 4A**). This was confirmed by western blotting of Huh-28 cell lysates and 15X concentrated Huh-28 cell conditioned medium (**Supplementary Figure 3**), and by western blotting of lysates of Huh-28 cells before and after transfection with tenascin-W-specific siRNAs (**Supplementary Figure 4**) and by mass spectrometry (**Supplementary Figure 5**). Immunocytochemistry with the anti-tenascin-W shows bright intracellular staining of cultured Huh-28 cells, but no tenascin-W-positive fibrils were observed around cells. This leads us to speculate that Huh-28 cells secrete soluble tenascin-W but are

not able to produce and organize tenascin-W-positive fibrils in the extracellular matrix, as observed in the tumor stroma of ICC, CPHBD and CGB patients (**Figure 4B**). Since bone marrow-derived stromal cells (BMSCs) represent a significant cellular source of cancer-associated fibroblasts that support tumor cell growth (35), we decided to perform co-culture between Huh-28 and the BMSC cell line 196hT in order to mimic a tumor stroma microenvironment. While 196hT cells do not express tenascin-W when cultured alone (**Figures 4A, B**), the tenascin-W labeled by immunocytochemistry in co-cultures of Huh-28 with 196hT cells is organized in fibrils surrounding nests of Huh-28 cells, mimicking the appearance of tenascin-W in the stroma surrounding nests of tumor cells in ICC. Similar results were observed with co-cultures of 196hT cells and other biliary tract cancer cell lines that express lower levels of tenascin-W: the CPHBD cell line TFK-1 and the CGB cell line G-415 (not shown). Since the 196hT cells were genetically engineered to express GFP (36), it was possible to sort the cells after co-culture and examine cell-type specific lysates for the expression of tenascin-W by western blotting (**Figure 4C**). Huh-28 cell lysates following co-culture had readily detectable tenascin-W, but 196hT cells did not (**Figure 4D**, **Supplementary Figure 6**), indicating that the source of the tenascin-W fibrils seen in the co-cultures is the Huh-28 cells and not the 196hT cells. To determine if physical contact between the cells or a secreted factor leads to the appearance of the fibrillar anti-tenascin-W immunostaining in the co-cultures, the two cells types were cultured in transwell chambers, where upper and lower

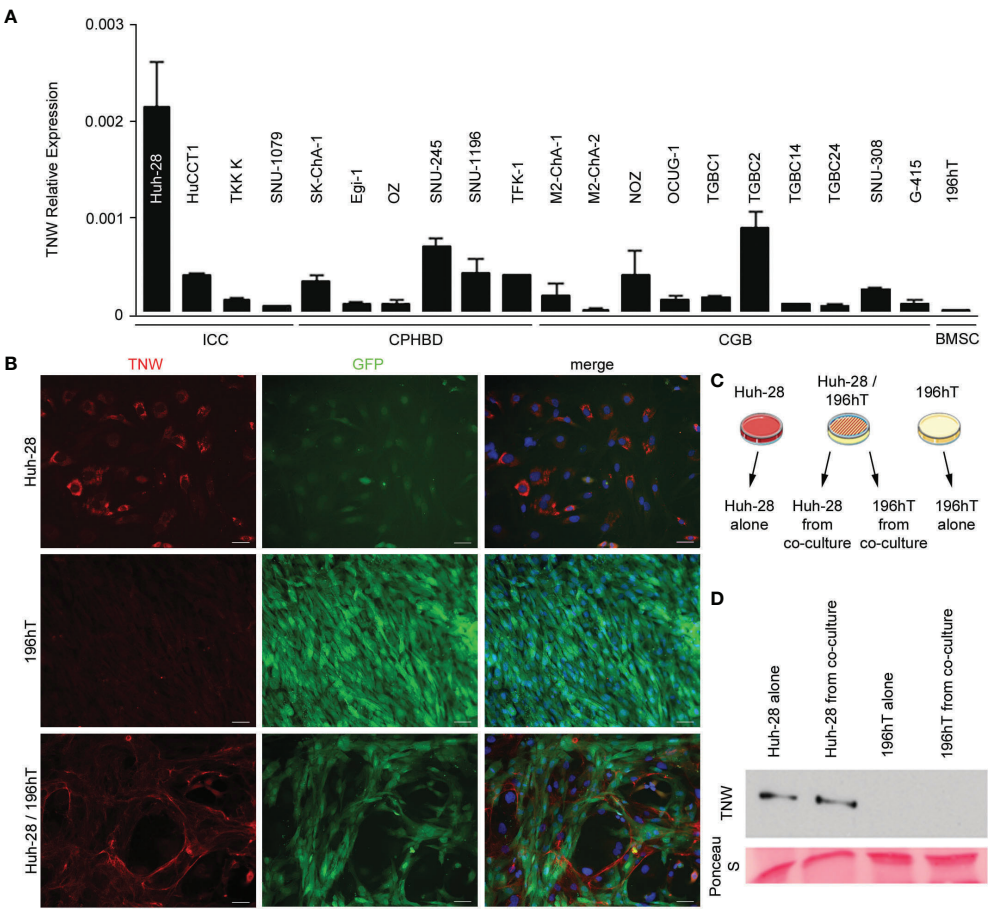

FIGURE 4 | Expression of tenascin-W by cell lines derived from biliary tract tumors. **(A)** Twenty cell lines were analyzed for tenascin-W expression using qRT-PCR. The results were plotted as expression relative to that of the housekeeping gene hTBP. Four cells lines were derived from intrahepatic cholangiocarcinomas (ICC), 6 were from carcinoma of perihilar bile ducts (CPHBD), and 10 were from carcinoma of the gallbladder (CGB). For comparison, qRT-PCR expression of tenascin-W by a bone marrow stromal cell-derived cell line (196hT) is shown. The highest level of tenascin-W expression was seen in the ICC-derived cell line Huh-28; **(B)** Immunocytochemistry with anti-tenascin-W (TNW) reveals intracellular labeling of Huh-28 cells, but not 196hT cells. The 196hT cells, but not the Huh-28 cells, express GFP. The merged images include a DAPI nuclear counterstain. When the two cell lines are co-cultured, tenascin-W-positive fibrils surround nests of Huh-28 cells, mimicking the arrangement of tenascin-W in the stroma of ICCs. Scale bars = 50 µm. **(C)** The method used for separating Huh-28 cells from GFP-positive 196hT cells following co-culture is shown schematically. Illustration was created using Servier Medical Art Powerpoint Image Bank (Servier, https://smart.servier.com/). **(D)** Tenascin-W can be detected by immunoblotting with 30µg of cell lysates of Huh-28 cells and Huh-28 cells following co-culture with 196hT cells. Tenascin-W is not detectable in the lysates of 196hT cells or 196hT cells following co-culture. Ponceau S was used as a loading control.

chambers are separated by a porous polycarbonate membrane that allows the diffusion of soluble factors, but not the transmigration of cells. If 196hT cells are in the upper chamber, tenascin-W-positive fibrils are seen around Huh-28 cells in the lower chamber, in addition to the tenascin-W cytoplasmic localization observed in Huh-28 cells (**Supplementary Figure 7**). If Huh-28 cells are in the upper chamber, tenascin-W-positive fibrils are seen in 196hT cells in the lower chamber. However, no tenascin-W immunostaining is detected in the cytoplasm of 196hT cells. Therefore, soluble tenascin-W secreted by Huh-28 cells in the upper chamber becomes associated with fibrils when it enters into contact in the lower chamber with a soluble factor secreted by 196hT cells. These results suggest that a secreted factor in the tumor microenvironment, mimicked by co-cultures of Huh-28 and 196hT cells *in vitro*, is required for the production and assembly of tenascin-W-positive fibrils in the tumor stroma, and that the cancer cells themselves can be/are the source of tenascin-W, at least in ICC.

DISCUSSION

In the current study, tenascin-C immunoreactivity was observed in the stroma of all biliary tract tumors examined. Its presence in ICC is consistent with the reports of others who studied animal models (33) and intrahepatic tumors of biliary origin in humans (37–39). Antibodies to tenascin-C have been used as an ICC stromal marker in at least one animal study (40), and in an effort to identify combinations of antibodies that could be used for prognosis, a combination of high levels of tenascin-C immunoreactivity and low levels of osteopontin immunostaining was found to correlate with low post-surgery survival rates in patients with ICC (41). Our study appears to be the first to report tenascin-C immunoreactivity in the stroma of CPHBD and CGB, though one report has described elevated levels of tenascin-C in the serum of a patient with metastatic CGB (42). Thus, CPHBD and CGB can be added to the growing list of solid tumors in which tenascin-C expression has been well documented (14–17). Here, we report anti-tenascin-C immunostaining in normal liver around sinusoids, but also around veins and arteries in the portal tract, as was shown previously (43–45).

Tenascin-C exists in multiple isoforms, and different isoforms are found in different tumors (12). While this complicates the characterization of tenascin-C in tumor stroma, it has led to the development of prospective isoform-specific tumor therapies (12). The monoclonal antibody to tenascin-C used in this study (B28-13) recognizes an epitope common to all tenascin-C isoforms (19, 31). Less is known about the possible isoforms of tenascin-W, but to date immunoblots indicate that only a single form is expressed in human tumors (19, 29). Interestingly, the tenascin-W made by the ICC-derived cell line Huh-28 runs on SDS-PAGE with a higher apparent molecular weight than expected (**Supplementary Figure 4**). While this may be the result of multimerization, it may also represent a tumor-specific form or modification of the protein. To unambiguously identify the higher molecular weight band as tenascin-W we analyzed the tryptic peptides from this region by tandem mass spectrometry and compared them to the lower molecular weight band of tenascin-W derived from 293/hTNW cells (**Supplementary Figure 5**). Seven tenascin-W peptides could be identified with good MASCOT scores and a false discovery rate of 0.1%. They were manually evaluated and had similar retention times to the peptides derived from 293/hTNW cells. They are distributed over a wide range of the tenascin-W sequence.

The anti-tenascin-W used in the current study also immunostained the stroma of all the biliary tract tumors examined. However, in contrast to anti-tenascin-C, anti-tenascin-W did not immunostain normal liver, non-tumoral liver from 3 patients with ICC, or tissues from 5 of the 6 gallbladders removed from patients with cholecystitis. This makes tenascin-W a potential candidate for identifying stromal areas associated with biliary tract tumors and a potential target for biotherapies. Similar conclusions were drawn by others who found that tenascin-W immunoreactivity was associated with glioblastomas, astrocytomas and oligodendrogliomas, but was absent from normal brain tissue (29). Tenascin-W is also found in colorectal cancer, but not in normal colon tissue (28). For a more comprehensive view of tenascin-W expression in normal human tissues, we surveyed additional normal adult human tissues using anti-tenascin-W-based immunohistochemistry and found that many, but not all, lacked tenascin-W expression. Some normal glands (e.g., prostate) and the female reproductive system (e.g., the uterus and ovaries) displayed high levels of tenascin-W expression. This would need to be considered when developing systemic therapies or using tenascin-W as a potential marker of tumor stroma in these regions. Tenascin-W is elevated in the serum of patients with breast and colorectal cancer (28). It would be interesting to see if tenascin-W is a potential serum marker for biliary tract cancers as well, as reliable serum markers for these cancers have yet to be developed (46).

What is the origin of the tenascin-W found in the stroma of biliary tract tumors? We were unable to perform *in situ* hybridization with probes for tenascin-W transcripts on the tumor samples, as the fixation protocol was optimized for immunohistochemistry. However, the expression of tenascin-W in cell lines derived from ICC (Huh-28), CGB (TGCB2) and CPHBD (SNU245) is evidence that the cancer cells themselves may express some of the tenascin-W found in the tumor stroma (**Figure 4A**). However, our results do not rule out possible origins from cancer associated fibroblasts or endothelial cells. Futures studies should address this question.

Most *in vitro* studies of tenascin-W expression have involved primary cultures of embryonic osteoblasts as few cell lines have been identified that express tenascin-W (47, 48). Here, we found that tenascin-W transcripts are relatively high in Huh-28 cells, and tenascin-W can be detected in cell lysates and conditioned medium of Huh-28 cells (**Supplementary Figure 3**). Thus, Huh-28 cells are the first cell line identified that express tenascin-W

without the addition of exogenous factors and may prove useful in future studies to elucidate tenascin-W function. The Huh-28 cell line was derived from an ICC removed with the left lobe of the liver from a 37-year-old woman in 1984 (49). They are large, spindle-shaped or polygonal cells that proliferate slowly under typical culture conditions and fail to form tumors when injected into nude mice (49). A future study could involve co-injection of BMSCs with the Huh-28 cells to see if this results in tumor formation. Because they share properties with primary cultures of cholangiocarcinoma cells, Huh-28 cells have also been used as an *in vitro* model for studying the regulation of ICC proliferation. Like primary ICC cells, Huh-28 cells express estrogen receptors and their serum-induced proliferation is inhibited with tamoxifen (50). They also proliferate in response to IGF-1 (50) and TGF-beta (51). Huh-28 cells also express relatively high levels of miR-24, a small non-coding RNA associated with oncogenesis (52). When co-cultured with immortalized BMSCs, we show here that Huh-28 cells form nests that are surrounded by fibrils that are immunostained with anti-tenascin-W, mimicking the arrangement of ICC cells surrounded by tenascin-W stroma *in situ*. This may prove to be a good model for future studies of ICC growth and the development of anti-ICC therapies. It is also important to note that as we were unable to acquire phase contrast images of the co-cultured cells, it is difficult to determine if the tenascin-W-positive fibrils were on the cell surface or were part of a broader fibrillar system. Future studies should also be directed at studying the effects of exogenous tenascin-W on Huh-28 cell proliferation and behavior, as was done with breast cancer cell lines (21).

The C-terminal fibrinogen-related domain of tenascin-W, like that of tenascin-C, can activate Toll-like receptor 4-mediated inflammatory responses (53). Moreover, tenascin-C was recently shown to contribute to immune suppression in an oral squamous cell carcinoma model (18). Future studies should be directed to determine if tenascin-W, which shares a number of features with tenascin-C, plays a similar role in tumor stroma, or if the presence of tenascin-W during cholelithiasis could contribute to tumor progression.

The extracellular matrix glycoprotein tenascin-W is found in the stroma of ICC, CPHBD and CGB. It is not expressed in normal liver or most cholecystitic gallbladders. Thus, tenascin-W is potentially a novel stromal marker for biliary tract cancers and may prove useful in the development of biotherapies.

DATA AVAILABILITY STATEMENT

The original contributions presented in the study are included in the article/**Supplementary Material**. Further inquiries can be directed to the corresponding author.

ETHICS STATEMENT

The studies involving human participants were reviewed and approved by Mongi Slim University Hospital (MSUH) Committee on Medical Ethics (La Marsa, Tunisia) and the Ethikkommission Nordwest- und Zentralschweiz (Switzerland). The patients/participants provided their written informed consent to participate in this study.

AUTHOR CONTRIBUTIONS

Study concept and design: IH, RC-E and LH. Data acquisition and analysis: IH, AL, LC, SB, NK, DH, and SM. Data interpretation and discussion: IH, RC-E, RT, AL, LC, MD, LT, LH, and CR. Patient recruitment: LH and RH. Clinical diagnosis: LH and LC-B. Taking biopsies: LH. Manuscript writing: RT, IH, and LH. Critical revision of the manuscript for important intellectual content: LT and MD. All authors contributed to the article and approved the submitted version.

FUNDING

This work was supported by funds from the Swiss National Science Foundation (31003A_156740) to RC-E.

ACKNOWLEDGMENTS

We are grateful to Prof. Alexander Knuth (University Hospital of Zürich, Switzerland) for generously providing cell lines. We thank the following people from Friedrich Miescher Institute for Biomedical Research, Basel, Switzerland: Augustyn Bogucki for technical help with histology, Hubertus Kohler for performing cell sorting experiments, Laurent Gelman for assisting with imaging, and Prof. Patrick Matthias and Prof. Nancy E. Hynes for their scientific expertise and review of the manuscript. We thank the following people from Department of Surgery, Medical School, University of Tunis El Manar, Tunisia: Prof. Zoubeir Ben Safta and Prof. Mohamed Tahar Khalfallah for their clinical expertise, and Prof. Chadli Dziri for his review of the manuscript. We thank Aurélien Lacombe (Institute of Pathology, University Hospital of Basel, Basel, Switzerland) for technical help with FFPE sections. We thank Mounira Ben Mustapha and Khadija Ben Hmida-Saad (Mongi Slim University Hospital, La Marsa, Tunisia) for administrative assistance.

SUPPLEMENTARY MATERIAL

The Supplementary Material for this article can be found online at: https://www.frontiersin.org/articles/10.3389/fimmu.2020.630139/full#supplementary-material

REFERENCES

1. Mertens JC, Rizvi S, Gores GJ. Targeting cholangiocarcinoma. *Biochim Biophys Acta* (2018) 1864:1454–60. doi: 10.1016/j.bbadis.2017.08.027
2. Hundal R, Shaffer EA. Gallbladder cancer: epidemiology and outcome. *Clin Epidemiol* (2014) 6:99–109. doi: 10.2147/CLEP.S37357
3. Henson DE, Albores-Saavedra J, Corle D. Carcinoma of the gallbladder. (1992). Histologic types, stage of disease, grade, and survival rates. *Cancer* 70:1493–7. doi: 10.1002/1097-0142(19920915)70:6<1498::aid-cncr2820700609>3.0.co;2-c
4. Randi G, Franceschi S, La Vecchia C. Gallbladder cancer worldwide: geographical distribution and risk factors. *Int J Cancer* (2006) 118:1591–602. doi: 10.1002/ijc.21683
5. Konstantinidis IT, Deshpande V, Genevay M, Berger D, Fernandez-del Castillo C, Tanabe KK, et al. Trends in presentation and survival for gallbladder cancer during a period of more than 4 decades: a single-institution experience. *Arch Surg* (2009) 144:441–7. doi: 10.1001/archsurg.2009.46
6. de Aretxabala X, Riedeman P, Burgos L, Roa I, Araya JC, Echeverría X, et al. Gallbladder cancer. Case-control study. *Rev Med Chil* (1995) 123:581–6.
7. Wi Y, Woo H, Won YJ, Jang JY, Shin A. Trends in gallbladder cancer incidence and survival in Korea. *Cancer Res Treat* (2018) 50:1444–51. doi: 10.4143/crt.2017.279
8. Kayahara M, Nagakawa T. Recent trends of gallbladder cancer in Japan: an analysis of 4,770 patients. *Cancer* (2007) 110:572–80. doi: 10.1002/cncr.22815
9. Hamdi-Cherif M, Serraino D, Mahnane A, Laouamri S, Zaidi Z, Boukharouba H, et al. Time trends of cancer incidence in Setif, Algeria, 1986-2010: an observational study. *BMC Cancer* (2014) 14:637. doi: 10.1186/1471-2407-14-637
10. Nagorney DM, McPherson GA. Carcinoma of the gallbladder and extrahepatic bile ducts. *Semin Oncol* (1988) 15:106–15.
11. Tucker RP, Drabikowski K, Hess JF, Ferralli J, Chiquet-Ehrismann R, Adams JC. Phylogenetic analysis of the tenascin gene family: evidence of origin early in the chordate lineage. *BMC Evol Biol* (2006) 6:60. doi: 10.1186/1471-2148-6-60
12. Chiquet-Ehrismann R, Tucker RP. Tenascins and the importance of adhesion modulation. *Cold Spring Harb Perspect Biol* (2011) 3:a004960. doi: 10.1101/cshperspect.a004960
13. Midwood KS, Chiquet M, Tucker RP, Orend G. Tenascin-C at a glance. *J Cell Sci* (2016) 129:4321–7. doi: 10.1242/jcs.190546
14. Orend G, Chiquet-Ehrismann R. Tenascin-C induced signaling in cancer. *Cancer Lett* (2006) 244:143–63. doi: 10.1016/j.canlet.2006.02.017
15. Midwood KS, Hussenet T, Langlois B, Orend G. Advances in tenascin-C biology. *Cell Mol Life Sci* (2011) 68:3175–99. doi: 10.1007/s00018-011-0783-6
16. Lowy CM, Oskarsson T. Tenascin C in metastasis: A view from the invasive front. *Cell Adh Migr* (2015) 9:112–24. doi: 10.1080/19336918.2015.1008331
17. Yoshida T, Akatsuka T, Imanaka-Yoshida K. Tenascin-C and integrins in cancer. *Cell Adh Migr* (2015) 9:96–104. doi: 10.1080/19336918.2015.1008332
18. Spenlé C, Loustau T, Murdamoothoo D, Erne W, Beghelli-de la Forest Divonne S, Veber R, et al. Tenascin-C orchestrates an immune suppressive tumor microenvironment in oral squamous cell carcinoma. *Cancer Immunol Res* (2020) 8:1122–38. doi: 10.1158/2326-6066.CIR-20-0074
19. Brellier F, Martina E, Degen M, Heuzé-Vourc'h N, Petit A, Kryza T, et al. Tenascin-W is a better cancer biomarker than tenascin-C for most human solid tumors. *BMC Clin Pathol* (2012) 12:14. doi: 10.1186/1472-6890-12-14
20. Martina E, Chiquet-Ehrismann R, Brellier F. Tenascin-W: an extracellular matrix protein associated with osteogenesis and cancer. *Int J Biochem Cell Biol* (2010) 42:1412–5. doi: 10.1016/j.biocel.2010.06.004
21. Tucker RP, Degen M. The expression and possible functions of tenascin-W during development and disease. *Front Cell Dev Biol* (2019) 7:53. doi: 10.3389/fcell.2019.00053
22. Meloty-Kapella CV, Degen M, Chiquet-Ehrismann R, Tucker RP. Avian tenascin-W: expression in smooth muscle and bone, and effects on calvarial cell spreading and adhesion in vitro. *Dev Dyn* (2006) 235:1532–42. doi: 10.1002/dvdy.20731
23. Chiquet-Ehrismann R, Orend G, Chiquet M, Tucker RP, Midwood KS. Tenascins in stem cell niches. *Matrix Biol* (2014) 37:112–23. doi: 10.1016/j.matbio.2014.01.007
24. Neidhardt J, Fehr S, Kutsche M, Löhler J, Schachner M. Tenascin-N: characterization of a novel member of the tenascin family that mediates neurite repulsion from hippocampal explants. *Mol Cell Neurosci* (2003) 23:193–209. doi: 10.1016/S1044-7431(03)00012-5
25. Scherberich A, Tucker RP, Samandari E, Brown-Luedi M, Martin D, Chiquet-Ehrismann R. Murine tenascin-W: a novel mammalian tenascin expressed in kidney and at sites of bone and smooth muscle development. *J Cell Sci* (2004) 117:571–81. doi: 10.1242/jcs.00867
26. Scherberich A, Tucker RP, Degen M, Brown-Luedi M, Andres AC, Chiquet-Ehrismann R. Tenascin-W is found in malignant mammary tumors, promotes alpha8 integrin-dependent motility and requires p38MAPK activity for BMP-2 and TNF-alpha induced expression in vitro. *Oncogene* (2005) 24:1525–32. doi: 10.1038/sj.onc.1208342
27. Degen M, Brellier F, Kain R, Ruiz C, Terracciano L, Orend G, et al. Tenascin-W is a novel marker for activated tumor stroma in low-grade human breast cancer and influences cell behavior. *Cancer Res* (2007) 67:9169–79. doi: 10.1158/0008-5472.CAN-07-0666
28. Degen M, Brellier F, Schenk S, Driscoll R, Zaman K, Stupp R, et al. Tenascin-W, a new marker of cancer stroma, is elevated in sera of colon and breast cancer patients. *Int J Cancer* (2008) 122:2454–61. doi: 10.1002/ijc.23417
29. Martina E, Degen M, Rüegg C, Merlo A, Lino MM, Chiquet-Ehrismann R, et al. Tenascin-W is a specific marker of glioma-associated blood vessels and stimulates angiogenesis in vitro. *FASEB J* (2010) 24:778–87. doi: 10.1096/fj.09-140491
30. Bosman FT, Carneiro FT, Hruban RH, Theise ND. *WHO classification of tumours of the digestive system*. Geneva: World Health Organization (2010).
31. Schenk S, Muser J, Vollmer G, Chiquet-Ehrismann R. Tenascin-C in serum: a questionable tumor marker. *Int J Cancer* (1995) 61:443–9. doi: 10.1002/ijc.2910610402
32. Heike M, Röhrig O, Gabbert HE, Moll R, Meyer zum Büschenfelde KH, Dippold WG, et al. New cell lines of gastric and pancreatic cancer: distinct morphology, growth characteristics, expression of epithelial and immunoregulatory antigens. *Virchows Arch* (1995) 426:375–84. doi: 10.1007/BF00191347
33. Sithithaworn P, Ando K, Limviroj W, Tesana S, Pairojkul C, Yutanawiboonchai W, et al. Expression of tenascin in bile duct cancer of hamster liver by combined treatment of dimethylnitrosamine with Opisthorchis viverrini infections. *J Helminthol* (2002) 76:261–8. doi: 10.1079/JOH2002129
34. Chiovaro F, Martina E, Bottos A, Scherberich A, Hynes NE, Chiquet-Ehrismann R. Transcriptional regulation of tenascin-W by TGF-beta signaling in the bone metastatic niche of breast cancer cells. *Int J Cancer* (2015) 137:1842–54. doi: 10.1002/ijc.29565
35. Quante M, Tu SP, Tomita H, Gonda T, Wang SS, Takashi S, et al. Bone marrow-derived myofibroblasts contribute to the mesenchymal stem cell niche and promote tumor growth. *Cancer Cell* (2011) 19:257–72. doi: 10.1016/j.ccr.2011.01.020
36. Bourgine P, Le Magnen C, Pigeot S, Geurts J, Scherberich A, Martin I. Combination of immortalization and inducible death strategies to generate a human mesenchymal stromal cell line with controlled survival. *Stem Cell Res* (2014) 12:584–98. doi: 10.1016/j.scr.2013.12.006
37. Terada T, Nakanuma Y. Expression of tenascin, type IV collagen and laminin during human intrahepatic bile duct development and in intrahepatic cholangiocarcinoma. *Histopathology* (1994) 25:143–50. doi: 10.1111/j.1365-2559.1994.tb01570.x
38. Aishima S, Taguchi K, Terashi T, Matsuura S, Shimada M, Tsuneyoshi M. Tenascin expression at the invasive front is associated with poor prognosis in intrahepatic cholangiocarcinoma. *Mod Pathol* (2003) 16:1019–27. doi: 10.1097/01.MP.0000086860.65672.73
39. Okamura N, Yoshida M, Shibuya A, Sugiura H, Okayasu I, Ohbu M. Cellular and stromal characteristics in the scirrhous hepatocellular carcinoma: comparison with hepatocellular carcinomas and intrahepatic cholangiocarcinomas. *Pathol Int* (2005) 55:724–31. doi: 10.1111/j.1440-1827.2005.01891.x
40. Mertens JC, Fingas CD, Christensen JD, Smoot RL, Bronk SF, Werneburg NW, et al. Therapeutic effects of deleting cancer-associated fibroblasts in cholangiocarcinoma. *Cancer Res* (2013) 73:897–907. doi: 10.1158/0008-5472.CAN-12-2130
41. Iguchi T, Yamashita N, Aishima S, Kuroda Y, Terashi T, Sugimachi K, et al. A comprehensive analysis of immunohistochemical studies in intrahepatic

cholangiocarcinoma using the survival tree model. *Oncology* (2009) 76:293–300. doi: 10.1159/000207506
42. Yoshida J, Wakabayashi T, Okamoto S, Kimura S, Washizu K, Kiyosawa K, et al. Tenascin in cerebrospinal fluid is a useful biomarker for the diagnosis of brain tumour. *J Neurol Neurosurg Psychiatry* (1994) 57:1212–5. doi: 10.1136/jnnp.57.10.1212
43. Van Eyken P, Geerts A, De Bleser P, Lazou JM, Vrijsen R, Sciot R, et al. Localization and cellular source of the extracellular matrix protein tenascin in normal and fibrotic rat liver. *Hepatology* (1992) 15:909–16. doi: 10.1002/hep.1840150526
44. Yamada S, Ichida T, Matsuda Y, Miyazaki Y, Hatano T, Hata K, et al. Tenascin expression in human chronic liver disease and in hepatocellular carcinoma. *Liver* (1992) 12:10–6. doi: 10.1111/j.1600-0676.1992.tb00548.x
45. Couvelard A, Bringuier AF, Dauge MC, Nejjari M, Darai E, Benifla JL, et al. Expression of integrins during liver organogenesis in humans. *Hepatology* (1998) 27:839–47. doi: 10.1002/hep.510270328
46. Macias RII, Banales JM, Sangro B, Muntané J, Avila MA, Lozano E, et al. The search for novel diagnostic and prognostic biomarkers in cholangiocarcinoma. *Biochim Biophys Acta* (2018) 1864:1468–77. doi: 10.1016/j.bbadis.2017.08.002
47. Meloty-Kapella CV, Degen M, Chiquet-Ehrismann R, Tucker RP. Effects of tenascin-W on osteoblasts in vitro. *Cell Tissue Res* (2008) 334:445–55. doi: 10.1007/s00441-008-0715-4
48. Mikura A, Okuhara S, Saito M, Ota M, Ueda K, Iseki S. Association of tenascin-W expression with mineralization in mouse calvarial development. *Congenit Anom (Kyoto)* (2009) 49:77–84. doi: 10.1111/j.1741-4520.2009.00227.x
49. Kusaka Y, Tokiwa T, Sato J. Establishment and characterization of a cell line from a human cholangiocellular carcinoma. *Res Exp Med (Berl)* (1988) 188:367–75. doi: 10.1007/BF01851205
50. Alvaro D, Barbaro B, Franchitto A, Onori P, Glaser SS, Alpini G, et al. Estrogens and insulin-like growth factor 1 modulate neoplastic cell growth in human cholangiocarcinoma. *Am J Pathol* (2006) 169:877–88. doi: 10.2353/ajpath.2006.050464
51. Shimizu T, Yokomuro S, Mizuguchi Y, Kawahigashi Y, Arima Y, Taniai N, et al. Effect of transforming growth factor-beta1 on human intrahepatic cholangiocarcinoma cell growth. *World J Gastroenterol* (2006) 12:6316–24. doi: 10.3748/wjg.v12.i39.6316
52. Ehrlich L, Hall C, Venter J, Dostal D, Bernuzzi F, Invernizzi P, et al. miR-24 Inhibition increases menin expression and decreases cholangiocarcinoma proliferation. *Am J Pathol* (2017) 187:570–80. doi: 10.1016/j.ajpath.2016.10.021
53. Zuliani-Alvarez L, Marzeda AM, Deligne C, Schwenzer A, McCann FE, Marsden BD, et al. Mapping tenascin-C interaction with toll-like receptor 4 reveals a new subset of endogenous inflammatory triggers. *Nat Commun* (2017) 8:1595. doi: 10.1038/s41467-017-01718-7

Conflict of Interest: Some of the results showed herein have been used in the patent "Tenascin-W and biliary tract cancers" (WO2017072669).

The authors declare that the research was conducted in the absence of any commercial or financial relationships that could be construed as a potential conflict of interest.

frontiers in Immunology

ORIGINAL RESEARCH
published: 08 March 2021
doi: 10.3389/fimmu.2021.620541

Generation of Transgenic Mice that Conditionally Overexpress Tenascin-C

*Saori Yonebayashi[1], Kazuko Tajiri[1], Mari Hara[2,3], Hiromitsu Saito[4], Noboru Suzuki[4], Satoshi Sakai[1], Taizo Kimura[1], Akira Sato[1], Akiyo Sekimoto[2], Satoshi Fujita[5], Ryuji Okamoto[5], Robert J. Schwartz[6], Toshimichi Yoshida[2,3] and Kyoko Imanaka-Yoshida[2,3]**

[1] Department of Cardiology, Faculty of Medicine, University of Tsukuba, Tsukuba, Japan, [2] Department of Pathology and Matrix Biology, Graduate School of Medicine, Mie University, Tsu, Japan, [3] Research Center for Matrix Biology, Mie University, Tsu, Japan, [4] Department of Animal Genomics, Functional Genomics Institute, Mie University Life Science Research Center, Tsu, Japan, [5] Department of Cardiology, Graduate School of Medicine, Mie University, Tsu, Japan, [6] Department of Biology and Biochemistry, University of Houston, Houston, TX, United States

Tenascin-C (TNC) is an extracellular matrix glycoprotein that is expressed during embryogenesis. It is not expressed in normal adults, but is up-regulated under pathological conditions. Although TNC knockout mice do not show a distinct phenotype, analyses of disease models using TNC knockout mice combined with *in vitro* experiments revealed the diverse functions of TNC. Since high TNC levels often predict a poor prognosis in various clinical settings, we developed a transgenic mouse that overexpresses TNC through Cre recombinase-mediated activation. Genomic walking showed that the transgene was integrated into and truncated the *Atp8a2* gene. While homozygous transgenic mice showed a severe neurological phenotype, heterozygous mice were viable, fertile, and did not exhibit any distinct abnormalities. Breeding hemizygous mice with Nkx2.5 promoter-Cre or α-myosin heavy chain promoter Cre mice induced the heart-specific overexpression of TNC in embryos and adults. TNC-overexpressing mouse hearts did not have distinct histological or functional abnormalities. However, the expression of proinflammatory cytokines/chemokines was significantly up-regulated and mortality rates during the acute stage after myocardial infarction were significantly higher than those of the controls. Our novel transgenic mouse may be applied to investigations on the role of TNC overexpression *in vivo* in various tissue/organ pathologies using different Cre donors.

Keywords: matricellular protein, Cre-Lox, Atp8a2, heart development, myocardial inafrction, Nkx2.5, alpha myosin heavy chain

OPEN ACCESS

Edited by:
Boris Skryabin,
University of Münster, Germany

Reviewed by:
Ilaria Bertocchi,
Neuroscience Institute Cavaleri Ottolenghi (NICO), Italy
Antonio Maurizi,
University of L'Aquila, Italy

***Correspondence:**
Kyoko Imanaka-Yoshida
imanaka@doc.medic.mie-u.ac.jp

Specialty section:
This article was submitted to Inflammation, a section of the journal Frontiers in Immunology

Received: *23 October 2020*
Accepted: *10 February 2021*
Published: *08 March 2021*

Citation:
Yonebayashi S, Tajiri K, Hara M, Saito H, Suzuki N, Sakai S, Kimura T, Sato A, Sekimoto A, Fujita S, Okamoto R, Schwartz RJ, Yoshida T and Imanaka-Yoshida K (2021) Generation of Transgenic Mice that Conditionally Overexpress Tenascin-C. Front. Immunol. 12:620541. doi: 10.3389/fimmu.2021.620541

INTRODUCTION

Tenascin-C (TNC) is a large extracellular matrix (ECM) glycoprotein and an original member of 'matricellular proteins' together with thrombosondin-1 (TSP1) and SPARC (secreted protein acidic and rich in cysteine; osteonectin) (1). Matricellular proteins are a growing family of unique ECM proteins that do not directly contribute to the formation of structural elements and are strongly up-regulated and modulate cellular functions during tissue remodeling under normal and pathological conditions (2–5). As a typical matricellular protein, TNC is transiently expressed at

several steps during embryogenesis, is weakly expressed in normal adults, and is up-regulated under pathological conditions. The essential biological roles of TNC, particularly in morphogenesis, have been suggested based on its limited spatiotemporal expression pattern. Similar to the majority of matricellular proteins, global TNC knockout mice do not show a distinct phenotype (2, 6), which facilitated the misinterpretation in the 90s that it does not have any significant role. However, with careful analyses of TNC-deficient mice, some behavioral aspects subsequently emerged and also correlated with the findings of electrophysiological and morphometric analyses (7–9). Furthermore, disease models using TNC knockout mice revealed its important roles in tissue repair after injury, inflammation and cancer invasion (10–16). Combined with the findings of *in vitro* experiments, the administration of TNC purified from culture supernatants or recombinant TNC and its fragments to animal models (17–22) or the transfection of the TNC gene into cells (16, 23) revealed multiple roles for TNC as well as its receptors and signaling cascades. Accumulating evidence suggests that TNC has diverse functions and may exert harmful and beneficial effects on tissue repair in a context-dependent manner.

In the heart, proinflammatory and profibrotic-induced dysfunctions mediated by excess TNC have attracted attention because high serum levels of TNC have been shown to predict a poor prognosis in various clinical settings, such as after myocardial infarction (MI) and dilated cardiomyopathy [reviewed in (24)].

The expression of TNC in the heart is strictly limited to specific stages and sites during early embryonic development and also to restricted lesions during the acute stage of tissue repair in adult hearts, which suggest that the rapid elimination of TNC is crucial for maintaining homeostasis in the heart.

To simulate an *in vivo* environment with excess TNC, we developed a transgenic mouse that overexpresses TNC regulated by cre-lox conditional activation. The transgene was constructed using CAG promoter-driven mouse *Tnc* cDNA, in which the loxP-tagged stuffer gene was intercalated. By breeding transgenic mice with two types of Cre mice, we successfully induced the heart-specific overexpression of TNC in both cases.

METHODS

Generation of the Mutant Strain

We utilized the *Cre/loxP* system to generate transgenic mice that conditionally overexpress tenascin-C. The insertion of 11-kb mouse tenascin-C cDNA into the PmeI site of pCAG-XstopX-polyA (25). was performed as described previously (25). Founders were made using a pronuclear injection into C57BL/6J zygotes. Mice heterozygous for the transgene were backcrossed to C57BL/6N for at least ten generations to produce the transgenic mouse strain, namely, C57BL/6N-*Tg (CAG-flox-Tnc)IYM1*.

Genomic Walking for Chromosomal Mapping of the Transgene

The genomic DNA of the transgenic mouse was extracted and purified from the tail using the High Pure PCR Template Preparation Kit (Roche Life Science). The genomic sequences that flanked the transgenes were elucidated by genomic walking using the Universal Genome Walker™ kit (BD Bioscience Clontech, Palo Alto, CA) with a slight modification. Adaptor-ligated genomic DNA libraries of the transgenic lines were constructed with tail DNA digested with six restriction enzymes: DraI, ScaI, PvuII, EcoRV, SmaI, and StuI (Takara Bio Inc., Tokyo, Japan). Primary PCR amplification was performed with an outer transgene-specific primer (5′-CCA GGC GGG CCA TTT ACC GTA AGT TAT-3′) for the CAG promoter and the outer adaptor primer provided in the kit. All PCR amplifications were performed using the HotStarTaq Master Mix (Qiagen, Tokyo, Japan) in a thermal cycler (PC806, Astec). After a 15-min incubation at 95°C for activation, primary PCR amplification was performed by 30 cycles at 94°C for 2 s and 68°C for 5 min. The primary PCR mixture diluted 100 times was used as the template for nested PCR amplification with a nested transgene-specific primer (5′-GGC GGG CCA TTT ACC GTA AGT TAT GT-3′) and the nested adaptor primer provided in the kit. Nested PCR amplification was performed at 95°C for 15 min, followed by 30 cycles at 94°C for 2 s and 68°C for 5 min. The nested PCR product was separated by electrophoresis on a 2% agarose gel in TAE buffer and visualized with ethidium bromide staining. The PCR product containing the flanking sequence was found in the Sca I library and extracted from gels using the MinElute Gel Extraction kit (Qiagen). Purified DNA was cloned using the TOPO PCR cloning kit (ThermoFisher Scientific). The nucleotide sequence of cloned DNA was elucidated by a commercial laboratory (BioMatrix Research, Nagareyama, Chiba, Japan). The transgene insertion sites in chromosomes were identified using a BLAST search via the Internet (https://blast.ncbi.nlm.nih.gov/Blast.cgi). Genomic walking analyses that proceeded backwards from the tails of the transgene were performed with two primers (5′-ACA TGG TCA TTC TCC GAG CCA GCT GT-3′ and 5′-TGG GCT GCT TCC TAA TGC AGG AGT-3′) in combination with the adapter primers provided in the kit. The PCR product containing the flanking sequence was detected in the PvuII library.

To detect the truncated forms of the gene products, the 3′ rapid amplification of cDNA ends (3′ RACE) method was performed using the 3′-Full RACE Core Set (Takara Bio Inc., Shiga, Japan) according to the manufacturer's instructions.

Genotyping of Transgenic Mice

Two primers were designed to detect the transgene of TNC cDNA (**Figure 1A**, P1: 5′-AGG GTT GCC ACC TAT TTG C-3′ and P2: 5'-GCA TCC AGG CGG GTT GTG GTT AC-3'). Primers were also employed to detect the wild allele (**Figure 1A**, P3: 5′-AGG AGG GTC ACC AAC TGG CCT G-3′, P4: 5' -GGA CAG TGC TCT CAC TTG CCT GG-3'). The genotyping of the transgenic mouse C57BL/6N-*Tg (CAG-flox-Tnc)IYM1* (Tg) was conducted using PCR analyses of tail DNA under step-down PCR conditions for the primer pair P1 and P2 (TG mix): 95°C for 15 min, 2 cycles of 95°C 20 s/65°C 20 s/72°C 1 min, 2 cycles of 95°C 20 s/62°C 20 s/72°C 1 min, 2 cycles of 95°C 20 s/59°C 20 s/72°C 1 min, and 2 cycles of 95°C 20 s/56°C 20 s/72°C 1 min, followed by 30 cycles of 95°C 20 s/55°C 20 s/72°C 1 min. The PCR conditions used for the pair P3 and P4(WT mix) were as follows: 95°C for 15 min, 30 cycles of 95°C 20 s/62°C for 1 min, and 72°C for 7 min.

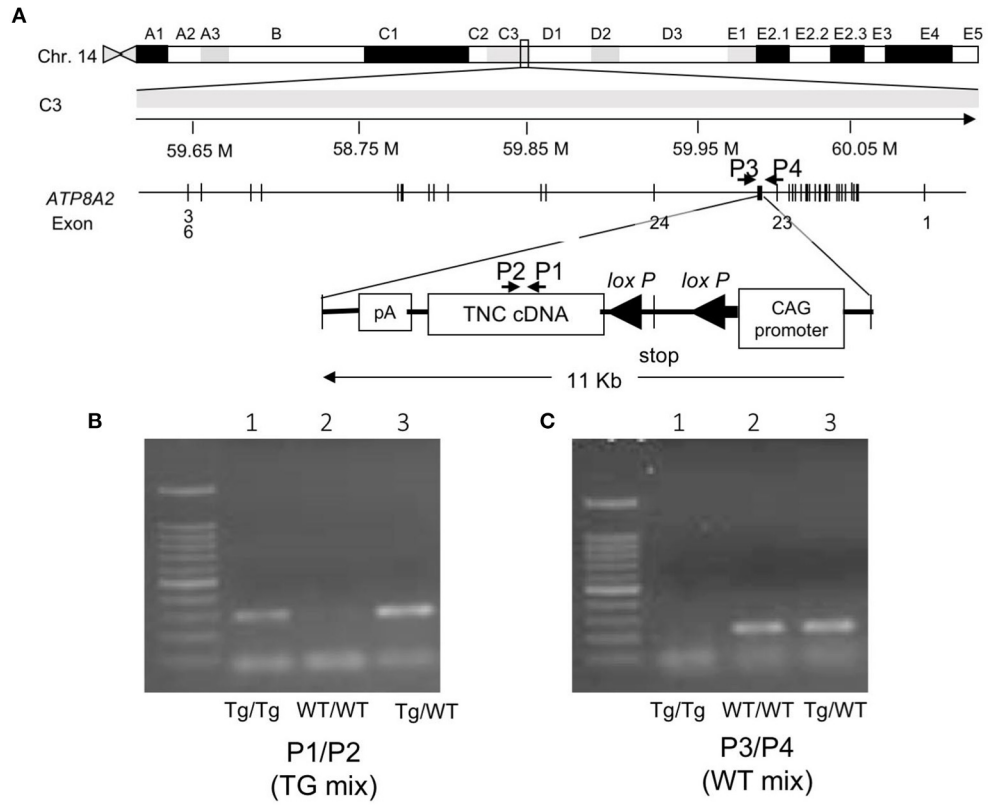

FIGURE 1 | (A) Mapping the transgene. The transgene is integrated into an intron between exons 23 and 24 of the *Atp8a2* gene, encoding the murine phosphatidylserine translocase (flippase), on chromosome 14. **(B)** Gel image of the PCR product of the genotyping of mice with the primer set P1/P2 (TG mix). Tg/Tg and Tg/WT show the amplified transgene of *Tnc* as 298 bp. **(C)** Gel image of the PCR product of the genotyping of mice with the primer set P3/P4(WT mix). Tg/ WT and WT/WT show amplified wild-type alleles as 228 bp. Tg/Tg, homozygous; Tg/WT, hemizygous; WT/WT, wild type.

Cre Mouse

Nkx2.5 ^{Cre} mice (Nkx2.5-Cre mice) were described previously (26). *Tg(Myh6-cre)2182 Md/J* mice (αMHC-Cre mice) (27) were kindly gifted from Professor M. D. Schneider.

The genotypes of mice were confirmed by a PCR analysis using the following primers: *Nkx2-5* primers (forward: 5′- CGGCATAGGACCAGAGTGATA-3′, reverse: 5′- TCCCTGAACATGTCCATCAGGTTC-3′); αMyHC Cre primer (forward: 5′-ATGACAGACAGATCCCTCCT ATCTCC-3′, 5′-reverse:-CTCATCACTCGTTGCATCAT CGAC-3′).

All animal experiments were approved by the Institutional Animal Experiment Committee of Mie University and the University of Tsukuba and conformed to the NIH Guide for the Care and Use of Laboratory Animals.

Western Blot Analysis

Heart, lung, kidney, and skeletal muscle tissues were homogenized in RIPA buffer on ice using MagNA Lyser Green Beads (Roche Diagnostics, Indianapolis, IN, USA). The homogenate was centrifuged at 13,000 rpm at 4°C for 30 min. The protein concentration of supernatants was measured using the BCA Protein Assay Kit (Pierce, Rockford, IL, USA). Samples were separated by sodium dodecyl sulfate-polyacrylamide gel electrophoresis on 7–15% polyacrylamide gradient gels and transferred onto a polyvinylidene difluoride membrane. The membrane was blocked with 3% skim milk in tris-buffered saline (TBS) containing 0.1% Tween 20 (TBST), incubated with primary antibodies (1:10,000) in TBST at 4°C overnight, and then reacted with a horseradish peroxidase-conjugated goat anti-rabbit antibody (#7074, Cell Signaling Technology, Boston, MA, USA) in TBST at 25°C for 60 min. The following primary antibodies were used: TNC (#10337 clone 4F10TT, IBL, Japan), Cre (#69050-3, Novagen, San Diego, CA, USA), and tubulin (#2148, Cell Signaling Technology, Boston, MA, USA). Blots were visualized with a chemiluminescent reagent (ImmunoStar, Wako, Osaka, Japan) and the CCD camera system (Light-Capture II, Atto Co., Tokyo, Japan).

Whole-Mount Immunostaining and Histological Examinations

Whole-mount immunostaining of mouse embryos was performed as previously described (28, 29). A polyclonal

rabbit anti-TNC antibody (30) or monoclonal rat anti-PECAM antibody (clone MEC 13.3 BD Pharmingen, San Jose, CA, USA) was used at a dilution of 1:500. Regarding histological sections, adult mouse hearts were fixed in 4% paraformaldehyde in phosphate-buffered saline (PBS) and embedded in paraffin wax. Three-micrometer-thick sections were cut, and hematoxylin and eosin (H&E) staining or picrosirius red staining was performed. Immunostaining for TNC was conducted as previously described (31). Briefly, sections were treated with 0.4% pepsin (1:60,000; Sigma Chemical Corp., St. Louis, MO, USA) in 0.01 N HCl at 37°C for 10 min for antigen retrieval.

Evaluations of interstitial collagen fibers in picrosirius red-stained sections were performed as previously described (32). Mean cardiomyocyte diameters were also measured in H&E-stained sections by tracing 100 myocytes for each heart.

RNA Extraction and Quantitative Reverse-Transcription Polymerase Chain Reaction

All hearts removed for qRT-PCR were snap-frozen and stored at −80°C. To prepare total RNA, tissue was homogenized using a bead kit (MagNA Lyser Green Beads; Roche Diagnostics, Indianapolis, IN, USA) according to the manufacturer's instructions. Total RNA samples from heart tissue and cultured cells were prepared using an RNeasy Mini Kit (Qiagen, Hilden, Germany). Complementary DNA was synthesized from 1 μg total RNA with a High Capacity cDNA Reverse Transcription kit (Applied Biosystems, Waltham, MA). The qRT-PCR analysis was performed using the LightCycler® 480 system (Roche Applied Science, Penzberg, Germany) with a Universal Probe Library (Roche Applied Science, Penzberg, Germany). Hypoxanthine-guanine phosphoribosyltransferase (*Hprt*) RNA was used as an internal control. Gene expression values were calculated using the $2^{-\Delta Ct}$ method.

Echocardiography

Transthoracic echocardiography was performed with a Vevo 2100 instrument (Fujifilm Visual Sonics, Tokyo, Japan) equipped with an MS-400 imaging transducer. Isoflurane induction was performed in an induction box with 3% isoflurane in pure medical oxygen. After the righting reflex of mice waned, they were fixed in the supine position on a heating pad to maintain normothermia, followed by the placement of electrocardiographic limb electrodes. Anesthesia was maintained using 1% isoflurane.

Induction of Myocardial Infarction

Myocardial infarction (MI) was induced using the classical MI method (33). Briefly, 10-week-old male mice weighing at least 25 g were anesthetized by an intraperitoneal injection of ketamine/xylazine (100–120 mg/kg body weight for ketamine and 7–8 mg/kg body weight for xylazine), intubated, and connected to a ventilator (Mouse Ventilator Minivent Type 845; Harvard Apparatus, Holliston, MA). The chest cavity was opened via left thoracotomy to expose the heart, which allowed the left anterior descending coronary artery to be visualized by the unaided eye or with a magnifying glass, and it was then permanently ligated with a 7-0 nylon suture at the site of its emergence from the left atrium. Complete occlusion of the vessel was confirmed by the presence of myocardial blanching in the perfusion bed. Mice that died during recovery from anesthesia were excluded from the analysis.

TABLE 1 | Histological and echocardiographic findings of the hearts of Nkx2.5C-Cre-induced TNC-overexpressing mice and TNC knockout mice (64 weeks old).

	$Tnc^{+/+}$;Tg(-); Cre(-) (Wild type)	$Tnc^{+/+}$;Tg(+);Cre(+) (excess TNC)	$Tnc^{-/-}$; Tg(-); Cre(-) (TNC defect)	*P*
Male	(*n* = 7)	(*n* = 6)	(*n* = 3)	
BW (g)	35.4 ± 2.0	42.8 ± 1.9	38.5 ± 2.3	0.04
Heart weight (mg)	200.0 ± 8.6	216.8 ± 9.3	205.7 ± 13.1	0.44
Body Heart ratio (%)	5.7 ± 0.2	5.1 ± 0.2	5.1 ± 0.2	0.13
Cardiomyocyte size (mm)	65.5 ± 1.2	66.5 ± 1.3	64.8 ± 1.7	0.74
Collagen volume fraction(%)	16.2 ± 1.8	19.5 ± 1.9	15.7 ± 2.7	0.38
Echocardiography	(*n* = 3)	(*n* = 4)	(*n* = 4)	
PWTd (mm)	1.03 ± 0.08	1.20 ± 0.07	1.13 ± 0.07	0.34
LVDd (mm)	3.67 ± 0.31	3.83 ± 0.27	3.58 ± 0.27	0.81
EF (%)	31.5 ± 5.6	37.8 ± 4.8	44.3 ± 4.8	0.28
Female	(*n* = 6)	(*n* = 6)	(*n* = 4)	
BW (g)	30.7 ± 1.7	30.8 ± 1.7	29.0 ± 2.1	0.76
Heart weight (mg)	141.5 ± 10.9	172.2 ± 10.9	149.0 ± 13.3	0.15
Body Heart ratio (%)	4.6 ± 0.2	5.6 ± 0.2	5.1 ± 0.2	0.03
Cardiomyocyte size (mm)	65.4 ± 1.1	68.0 ± 1.1	65.0 ± 1.4	0.20
Collagen volume fraction(%)	13.4 ± 1.5	16.3 ± 1.5	12.0 ± 2.2	0.25
	(*n* = 3)	(*n* = 4)	(*n* = 4)	
Echocardiography				
PWTd (mm)	0.96 ± 0.11	1.03 ± 0.10	1.08 ± 0.10	0.77
LVDd (mm)	3.53 ± 022	3.40 ± 0.19	3.30 ± 0.19	0.74
EF (%)	38.3 ± 6.6	47.8 ± 5.8	38.8 ± 5.8	0.48

Data are expressed as mean ± SEM. For multiple comparisons, one-way analysis of variance was used. BW, body weight; PWTd, posterior wall thickness in diastole; LVDd, left ventricular dimension in diastole; EF, ejection fraction.

Enzyme-Linked Immunosorbent Assay (ELISA)

Heart tissues were homogenized with RPMI-1640 containing 2.5% FBS using MagNA Lyser Green Beads (Roche Diagnostics, Indianapolis, IN, USA). Supernatants were collected after centrifugation and stored at −80°C. TN-C concentrations in the supernatants were measured using the Tenascin-C Large (FNIII-B) Assay kit (IBL, Takasaki, Japan).

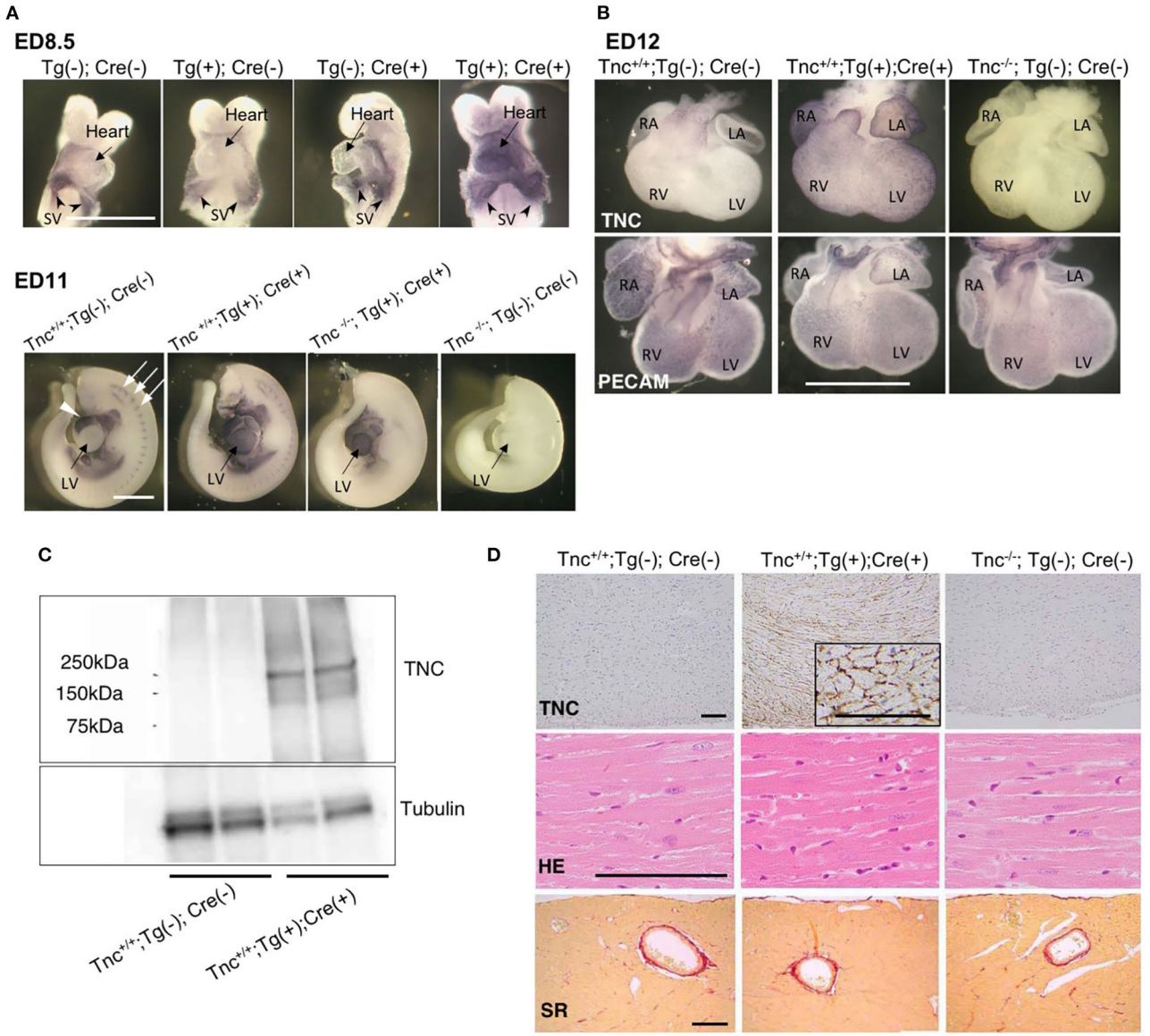

FIGURE 2 | Heart-specific overexpression of TNC in mouse embryos induced by Nkx2.5-Cre. **(A)** Whole mount immunostaining for TNC in mouse embryos on ED8.5 and ED11. The intrinsic expression of TNC is observed in sinus venosus on ED8.5. The head and pericardium were removed from ED11 embryos. In the wild type ($Tnc^{+/+}$;Tg(-); Cre(-)), the intrinsic expression of TNC was observed in the outflow tract of the heart (white arrow head) and at somites (white arrows). Scale bar = 1mm. **(B)** Whole-mount immunostaining of the mouse heart on ED12 for TNC and PECAM. Scale bar = 1 mm. **(C)** A western blot analysis of TNC protein expression in 64-week-old adult hearts. **(D)** Histological sections of the myocardium of 64-week-old mice stained with anti-TNC, H&E, and picrosirius red. Scale bar = 50 μm; SV, sinus venosus; LV, left ventricle; RV, right ventricle; LA, left atrium; RA, right atrium.

Survival Analysis

In the survival analysis after MI, we used littermates by mating C57BL/6N-*Tg (CAG-flox-Tnc)IYM1*$^{tg/+}$(Tg) with αMHC-Cre mice. Sixty-five MI mice were used in the survival analysis (-/-, $n = 19$; -/Cre, $n = 14$; Tg/-, $n = 18$; Tg/Cre, $n = 14$). After 14 days, all surviving mice were euthanized by a lethal intraperitoneal injection of sodium pentobarbital (200 mg/kg) or CO_2 inhalation.

Statistical Analysis

All data are expressed as the mean ± standard error of the mean (SEM). Normality was verified with the Shapiro-Wilk test. A one-way analysis of variance (ANOVA) with Tukey's *post hoc* test or a Kruskal-Wallis analysis with the *post-hoc* Steel-Dwass or Dunnett's test was used for multiple comparisons. Survival distributions were estimated by the Kaplan–Meier method and compared using the Log-rank test. $P < 0.05$ was considered to

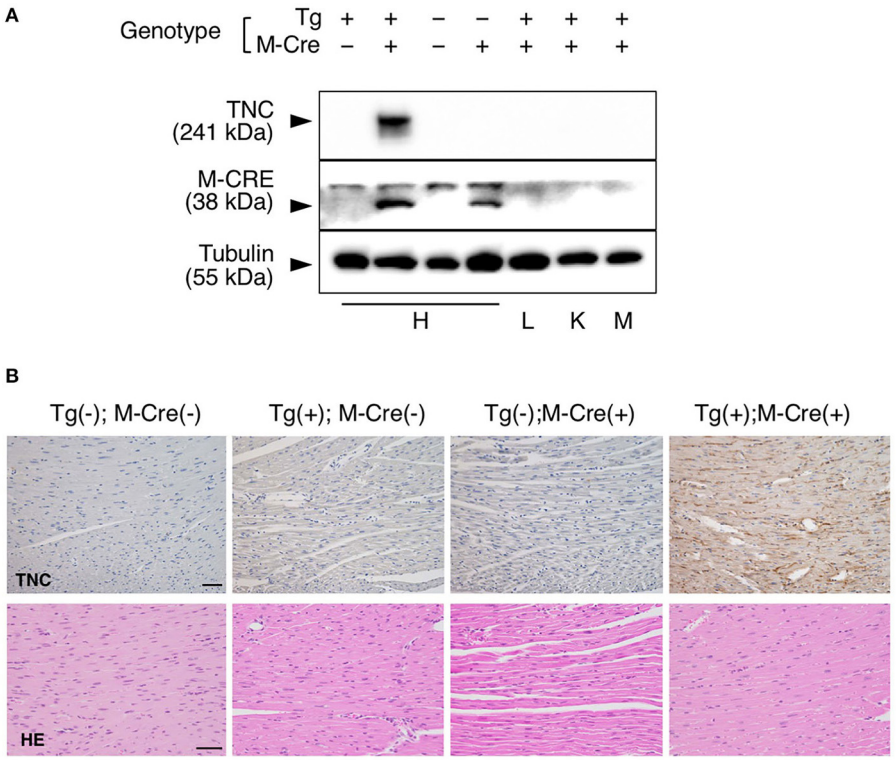

FIGURE 3 | Heart-specific overexpression of TNC in adult mice induced by αMHC-Cre. **(A)** Western blot analysis of TNC protein expression in 10-week-old mice. TNC expression is induced only in heart of Tg(+); M-Cre(**+**) mouse but not in lung, kidney or skeletal muscle. H, heart; L, lung; K, kidney; and M, muscle. **(B)** Histological section of the myocardium stained with anti-TNC, H&E and picrosirius red. Scale bar = 50 μm.

indicate significance. All statistical analyses were performed with JMP software (SAS Institute, Cary, NC).

RESULTS

Mapping and Genotyping of Transgenic Mice

A BLAST search with the 5′-flanking sequence revealed the integration of the transgene into an intron between exons 23 and 24 of the *Atp8a2* gene, encoding murine phosphatidylserine translocase (flippase), on chromosome 14 (**Figure 1A**). Primer sets of P1/P2 (TG mix) (**Figure 1B**) and P3/P4 (WT mix) (**Figure 1C**) produced transgenic and wild-type alleles as 298- and 228-bp bands, respectively. PCR analyses with the designed primers revealed the clear genotyping of three mice as homozygous (lane 1) with a transgene band only, wild-type (lane 2) with a wild band only, and heterozygous (lane 3) with both bands (**Figures 1B,C**). Several truncated forms of the gene product of *Atp8a2* were detected by a 3′ RACE analysis (data not shown).

Phenotypes of Transgenic Mice

Mice homozygous for Tg grew more slowly than their littermate controls and a prominent neurological deficit was observed. They developed body tremors, an abnormal gait, and epileptic form attacks. Despite supplementation of dry food with a soft moist diet that was placed on the cage floor to allow easy access, all homo-mutant mice died by 100 days. This phenotype is similar to that of a spontaneous mouse mutant with a mutation in the *Atp8a2* gene, which is known as wabbler-lethal (*wl*) (34). Heterozygous mice were viable, fertile, and did not show any distinct phenotype abnormalities. Therefore, we used only heterozygous mice as TG(+) in the present study.

Nkx2.5-Cre-Driven TNC-Overexpressing Mice

To examine the induction of TNC expression, we bred heterozygous C57BL/6N-*Tg (CAG-flox-Tnc)IYM1*$^{tg/+}$ (Tg(+)) with heterozygous *Nkx2.5*$^{Cre/+}$ (Cre(+)) driver mice. Nkx2.5-Cre drove efficient recombination in the embryonic heart. On embryonic day (ED) 8.5, the over-/misexpression of TNC was observed in the whole primitive heart tube of Tg(+); Cre(+) embryos, while the intrinsic expression of TNC was restricted to the sinus venosus (**Figure 2A**). TNC expression in Tg(+); Cre(-) and - Tg(-); Cre(+) mice was identical to that in the wild type Tg(-); Cre(-). Furthermore, by crossing TNC knockout mice with Tg(+); Cre(+) mice, we induced the expression of TNC only in the whole heart with the deletion of TNC in other tissues (**Figure 2A**, ED11). TNC-overexpressing embryonic mice

TABLE 2 | Echocardiographic parameters in αMHC-Cre-induced TNC-overexpressing mice (12 weeks old).

	Tg(-); M-Cre(-) (Wild type)	Tg(-); M-Cre(+)	Tg(+); M-Cre(-)	Tg(+); M-Cre(+) (excess TNC)	*P*-value
Male	(*n* = 5)	(*n* = 7)	(*n* = 9)	(*n* = 7)	
BW (g)	25.0 ± 0.9	26.1 ± 0.8	26.1 ± 0.7	24.9 ± 0.8	0.54
HR (bpm)	459 ± 22	428 ± 19	394 ± 16	403 ± 19	0.12
LVDd (mm)	3.74 ± 0.16	3.74 ± 0.14	3.66 ± 0.12	3.86 ± 0.14	0.77
LVDs (mm)	2.47± 0.11	2.50 ± 0.09	2.37 ± 0.08	2.53 ± 0.09	0.60
IVSTd(mm)	0.77 ± 0.03	0.80 ± 0.03	0.71 ± 0.03	0.77 ± 0.03	0.17
PWTd(mm)	0.85 ± 0.05	0.86 ± 0.04	0.85 ± 0.04	0.82 ± 0.04	0.93
FS (%)	33.9 ± 2.88	32.8 ± 2.44	35.0 ± 2.15	34.1 ± 2.44	0.93
EF (%)	56.7 ± 2.23	63.4 ± 1.89	61.1 ± 1.67	58.6 ± 1.89	0.12
E (mm/s)	844 ± 69	898 ± 58	936 ± 51	935 ± 58	0.71
A (mm/s)	582 ± 55	549 ± 47	571 ± 41	649 ± 47	0.47
E/A	1.49 ± 0.10	1.68 ± 0.08	1.65 ± 0.07	1.45 ± 0.08	0.17

Data are expressed as mean ± SEM. For multiple comparisons, one-way analysis of variance was used. BW, body weight; EF, ejection fraction; FS, fractional shortening; HR, heart rate; IVSTd, interventricular septal thickness in diastole; LVDd, left ventricular dimension in diastole; LVDs, left ventricular dimension in systole; PWTd, posterior wall thickness in diastole.

developed grossly normal hearts. The development of coronary arteries also appeared to be normal in TNC over-/misexpressing embryos as well as in TNC-deficient mice (**Figure 2B**). No distinct difference in the coronary vasculature was found between heterozygous TG or Nkx2.5-Cre mice and the wild type (data not shown). Heart-specific TNC-overexpressing mice were viable at least until 64 weeks. TNC expression was detected in the adult heart at 64 weeks (**Figure 2C**) and positive immunostaining for TNC was observed in the intercellular spaces of the myocardium of the (**Figure 2D**). No significant differences were observed in histology, fibrosis, or cardiac function to compare with those of wild-type and TNC knockout mice even at 64 weeks old (**Table 1**).

αMHC-Cre-Driven TNC-Overexpressing Mice

We bred heterozygous Tg mice with heterozygous *Tg(Myh6-cre)2182 Md/J*, a cardiomyocyte-specific α-myosin heavy chain promoter Cre mouse(M-Cre(+)). Tg(+);M-Cre(+)mice showed high mRNA and protein levels of myocardial TNC at 10 weeks old (**Figure 3A**). Tg(+);M-Cre(+) mice were born in Mendelian ratios, appeared healthy, and had normal cardiac function, size, and histology (**Table 2**). Although inflammatory cell infiltration was not observed in any mouse groups (Tg(+);M-Cre(+), Tg(+);M-Cre(-), Tg(-);M-Cre(+), Tg(-);M-Cre(-), **Figure 3B**). Tg(+);M-Cre(+) mice showed high mRNA expression levels of pro-inflammatory cytokines and chemokines (e.g., IL-1β, IL-6, CCL1, CCL2, and CXCL10) in the heart (**Figure 4**). Moreover, Tg(+);M-Cre(+) mice had high levels of tissue remodeling-related genes (MMP9 and TIMP2) and hypertrophy-related genes (ANP and BNP). Therefore, the hearts of mice with cardiomyocyte-specific TNC overexpression did not exhibit any morphological or functional abnormalities; however, the mRNA expression levels of pro-inflammatory cytokines, tissue remodeling-related genes, and hypertrophy-related genes were elevated.

We also investigated the effects of MI in this mouse. TNC expression levels were higher in all MI mice (Tg(+);M-Cre(+), Tg(+);M-Cre(-), Tg(-);M-Cre(+), Tg(-);M-Cre(-)) than in naïve mice; however, they were markedly higher in Tg(+);M-Cre(+) mice (**Figures 5A,B**). In wild-type MI mice, an immunohistochemical analysis of hearts on day 2 revealed that TNC was expressed at the borders between intact myocardial tissues and necrotic areas. In contrast, Tg(+);M-Cre(+) MI mice showed high TNC expression levels in both the infarct and normal areas of the heart (**Figure 5C**). Four-week survival rates were significantly lower in Tg/Cre mice than in other mice (Tg(+);M-Cre(+), 14.3% Tg(-);M-Cre(-), 57.9%; Tg(-);M-Cre(+), 50.0%; Tg(+);M-Cre(-), 44.4%, $P = 0.014$ by the Log-rank test, **Figure 5D**).

DISCUSSION

We generated a transgenic mouse that conditionally overexpresses TNC through Cre recombinase-mediated activation. By breeding heterozygous Tg mice with heterozygous Nkx2.5-Cre or αMyHC-Cre mice, we induced the heart-specific overexpression of TNC.

The *Nkx2-5* transcription factor is one of the earliest cardiogenic markers expressed in early heart mesoderm lineage progenitors and continues to be expressed in cardiomyocytes at later stages (35). The Nkx2.5-Cre mouse is often used to inactivate target genes in the early cardiac crescent on ED 7.5 (35–37).

We initially used Nkx2.5-Cre mice to examine the role of TNC during early heart development. TNC is normally expressed in precardiac mesodermal cells in the cardiac crescent; however, its expression is immediately down-regulated when mesodermal cells differentiate into cardiomyocytes, except in the outflow tract (28). We expected the prolonged expression of TNC in cardiomyocytes to perturbate heart morphogenesis. Although Nkx2.5-Cre drove TNC over-/misexpression in cardiomyocytes,

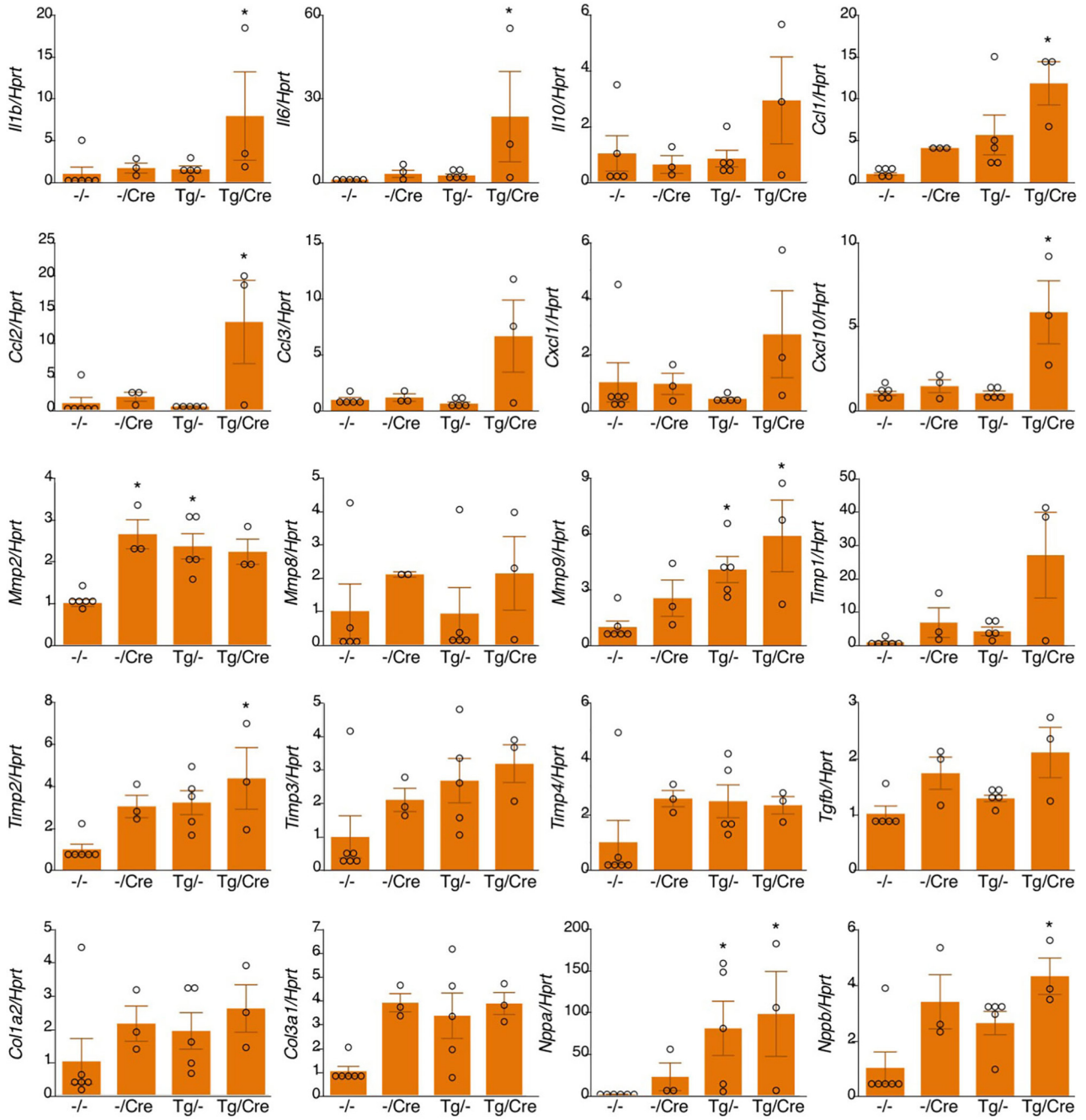

FIGURE 4 | mRNA expression in αMHC-Cre-induced TNC-overexpressing hearts. Results are shown as mean ± SEM, $n = 3$–6, $^*P < 0.05$ vs. -/- by a Kruskal-Wallis analysis with the *post-hoc* Dunnett's test. -/-, Tg(-); M-Cre(-); Tg/-, Tg(+); M-Cre(-); -/Cre, Tg(-); M-Cre(+); Tg/Cre, Tg(+); M-Cre(+).

the heart tube formed and underwent looping to produce a 4-chambered heart without any apparent abnormalities. We then focused on coronary vasculogenesis. In the normal mouse heart on ED 12, primitive coronary vascular networks are formed and cover the entire heart surface, except the TNC-positive outflow tract (24). With the shortening of the TNC-positive outflow tract, the vascular plexus gradually reaches the base of the aorta to form the proximal region of coronary arteries. This spatiotemporal relationship indicates that TNC may demarcate border zones and guide the developing vascular network. However, neither the complete deletion nor over-/mis-expression of TNC exerted apparent effects on the development of coronary vessels as shown in **Figure 2**. *Considering its pleiotropic function, excess TNC may be compensated for by other factors, particularly*

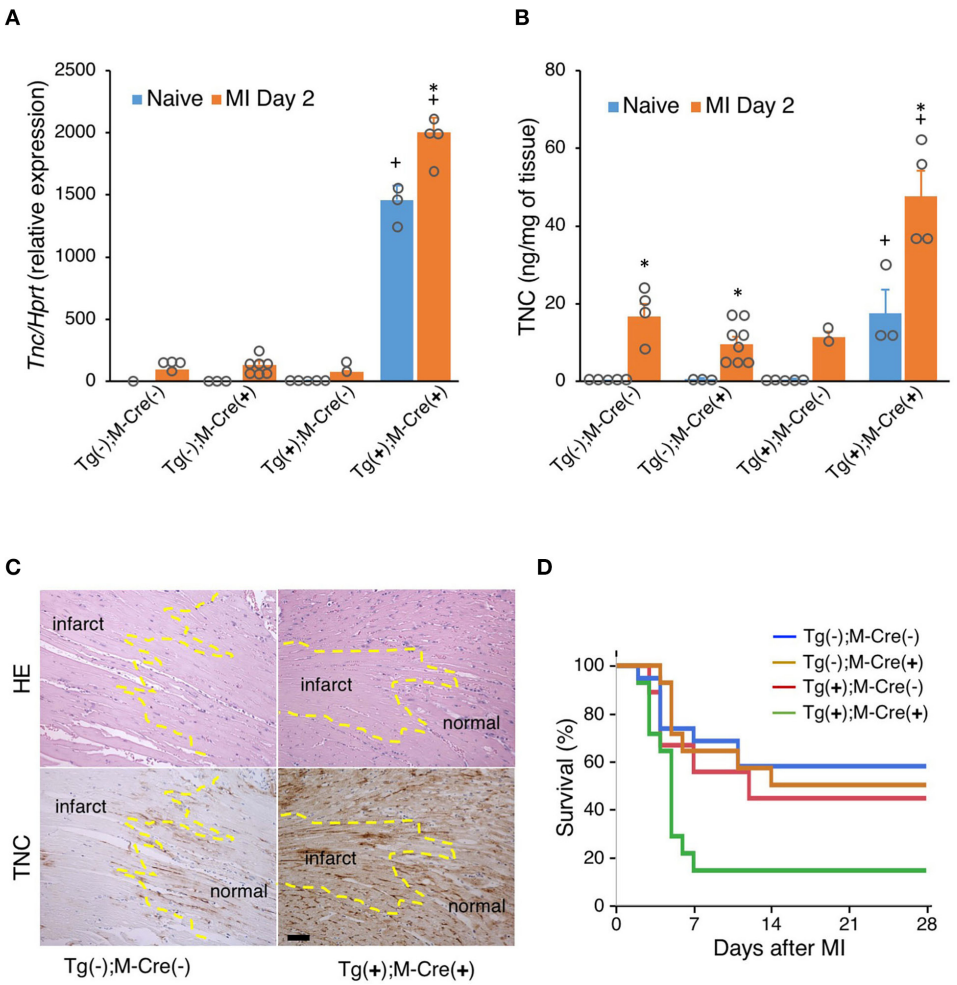

FIGURE 5 | MI in mice with the heart-specific overexpression of TNC induced by αMHC-Cre. **(A)** TNC mRNA expression in naïve hearts and on day 2 after MI (n = 1–7). **(B)** TNC protein levels in naïve hearts and on day 2 after MI (n = 2–8). Results are shown as means ± SEM. $^{+}P < 0.05$ vs Tg(-); Cre(-), $^{*}P < 0.05$ vs Native **(C)** Immunostaining for TNC expression in the heart. Scale bar = 50 μm. **(D)** Kaplan–Meier survival analysis 28 days after MI. Blue line for -/- (n = 19), brown line for -/Cre (n = 14), red line for Tg/- (n = 18), and green line for Tg/Cre (n = 14).

during development, similar to the subtle phenotype of germinal KO mice.

The Nkx2.5-Cre-driven overexpression of TNC persisted in the adult mouse heart. The deposition of TNC in the extracellular spaces of the interstitium was immunohistochemically confirmed. The TNC-overexpressing heart did not show apparent changes in cardiac function or the histology of the myocardium, such as hypertrophy or fibrosis, between wild-type and TNC knockout mice, at least at 64 weeks old, as shown in **Figure 3**.

We used another Cre mouse to induce TNC in the adult heart. The *αMyHC* promoter is activated in cardiomyocytes on ED9.5 and genetic recombination by the *αMyHC* -cre construct in the heart is initiated by ED12.5 (38–40), which is slightly later than that by Nkx2.5-Cre. *αMyHC*-Cre is one of the most frequently used Cre donors (41) inducing heart-specific recombination in adults (36).

In the Tg(+);M-Cre(+) mouse, *αMyHC* specifically drove the overexpression of TNC in the heart, and TNC synthesized in cardiomyocytes was deposited in the intercellular spaces as well as in the Nkx2.5-Cre-driven TNC-overexpressing heart. Although no apparent histological change in the myocardium or inflammatory cell infiltration was detected in the naïve Tg(+);M-Cre(+) heart, a gene expression analysis revealed the significant up-regulation of proinflammatory cytokines/chemokines and MMPs as shown in **Figures 3**, **4**. TNC is one of the proinflammatory molecules involved in myocardial tissue remodeling and activates fibroblasts (42–44) and macrophages (20, 33, 45–47) to up-regulate proinflammatory cytokines/chemokines and MMPs *in vitro*. Therefore, the present results suggest that TNC synthesized in cardiomyocytes by

genetic engineering activated interstitial cells in a paracrine manner *in vivo*. Furthermore, TNC-overexpressing mice showed significantly higher mortality rates during the acute phase after MI that were associated with greater increases in TNC levels than in the controls, which also supports TNC potentially enhancing inflammatory responses after MI by making a positive feedback loop (24, 44). These findings indicate that TNC-overexpressing mice are a good model for investigating the biological role of TNC in the microenvironment of the pathological myocardium.

However, the results obtained in TNC-overexpressing mice need to be carefully interpreted. We used cardiomyocyte-specific Cre to induce the overexpression of TNC in the adult myocardium. As discussed earlier, the expression of TNC in cardiomyocytes is limited at the very early embryonic stage, and cardiomyocytes do not synthesize TNC but interstitial cells are its source in the adult pathological myocardium. The forced expression of TNC in cardiomyocytes may induce an abnormal cellular response. In the present study, although no significant histo/morphological changes were observed in cardiomyocytes, ANP and BNP, hypertrophy/stress markers of cardiomyocytes, were elevated in the TNC-overexpressing heart. Although TNC may up-regulate ANP and BNP expression by cardiomyocytes (48, 49), this may reflect aberrant stress in cardiomyocytes, such as endoplasmic reticulum (ER) stress, in addition to the extraneous autocrine stimulation by TNC. Furthermore, several pathological phenotypes in the hearts of the heterozygous Nkx2.5 knockout status (Cre knock-in mice) (50, 51) and the cardiotoxicity of prolonged Cre expression in *αMyHC-Cre mouse* mice (41) have been reported.

It should be also mentioned that homozygous Tg mice showed a severe phenotype, which was prominent in the nervous system, due to the truncation of the ATP8a2 gene by the insertion of the transgene. Although we did not detect any significant differences, at least in the hearts of heterozygous Tg mice, we need to considered the effects of truncated ATP8a2 particularly in the nervous system.

In conclusion, our novel Tg mice may be applied to investigations on the role of TNC overexpression under a number of tissue/organ pathologies using different Cre donors; however, appropriate control animals, such as mice carrying the cre transgene only, and heterozygous Tg mice are important for comparisons.

DATA AVAILABILITY STATEMENT

The original contributions presented in the study are included in the article/supplementary material, further inquiries can be directed to the corresponding author/s.

ETHICS STATEMENT

The animal study was reviewed and approved by Institutional Animal Experiment Committee of Mice University and Institutional Animal Experiment Committee of Tsukuba University.

AUTHOR CONTRIBUTIONS

KI-Y and TY designed the study. KT, TY, and KI-Y wrote this manuscript. KI-Y, MH, and RS analyzed heart development. SF and RO analyzed cardiac function. HS and NS generated the transgenic mice. ASe and TY performed chromosomal mapping of the transgene. SY, KT, SS, TK, and ASa analyzed myocardial infarction model. All authors contributed to the article and approved the submitted version.

FUNDING

This work was supported in part by a grant from JSPS KAKENHI (Grant Number JP19H03442 to KI-Y) and a Japan Heart Foundation Research Grant on Dilated Cardiomyopathy (to KI-Y).

REFERENCES

1. Sage EH, Bornstein P. Extracellular proteins that modulate cell-matrix interactions. SPARC, tenascin, and thrombospondin. *J Biol Chem.* (1991) 266:14831–4.
2. Bornstein P, Sage EH. Matricellular proteins: extracellular modulators of cell function. *Curr Opin Cell Biol.* (2002) 14:608–16. doi: 10.1016/s0955-0674(02)00361-7
3. Murphy-Ullrich JE, Sage EH. Revisiting the matricellular concept. *Matrix Biol.* (2014) 37:1–14. doi: 10.1016/j.matbio.2014.07.005
4. Adams JC. Matricellular proteins: functional insights from non-mammalian animal models. *Curr Top Dev Biol.* (2018) 130:39–105. doi: 10.1016/bs.ctdb.2018.02.003
5. Gerarduzzi C, Hartmann U, Leask A, Drobetsky E. The matrix revolution: matricellular proteins and restructuring of the cancer microenvironment. *Cancer Res.* (2020) 80:2705–17. doi: 10.1158/0008-5472
6. Saga Y, Yagi T, Ikawa Y, Sakakura T, Aizawa S. Mice develop normally without tenascin. *Genes Dev.* (1992) 6:1821–31. doi: 10.1101/gad.6.10.1821
7. de Chevigny A, Lemasson M, Saghatelyan A, Sibbe M, Schachner M, Lledo PM. Delayed onset of odor detection in neonatal mice lacking tenascin-C. *Mol Cell Neurosci.* (2006) 32:174–86. doi: 10.1016/j.mcn.2006.04.002
8. Gurevicius K, Kuang F, Stoenica L, Irintchev A, Gureviciene I, Dityatev A, et al. Genetic ablation of tenascin-C expression leads to abnormal hippocampal CA1 structure and electrical activity in vivo. *Hippocampus.* (2009) 19:1232–46. doi: 10.002/hipo.20585
9. Morellini F, Schachner M. Enhanced novelty-induced activity, reduced anxiety, delayed resynchronization to daylight reversal and weaker muscle strength in tenascin-C-deficient mice. *Eur J Neurosci.* (2006) 23:1255–68. doi: 10.111/j.460-9568.2006.04657.x
10. Giblin SP, Midwood KS. Tenascin-C: form versus function. *Cell Adh Migr.* (2015) 9:48–82. doi: 10.4161/19336918.2014.987587
11. Midwood KS, Chiquet M, Tucker RP, Orend G. Tenascin-C at a glance. *J Cell Sci.* (2016) 129:4321–7. doi: 10.1242/jcs.190546
12. Marzeda AM, Midwood KS. Internal affairs: tenascin-c as a clinically relevant, endogenous driver of innate immunity. *J Histochem Cytochem.* (2018) 66:289–304. doi: 10.1369/0022155418757443
13. Deligne C, Murdamoothoo D, Gammage AN, Gschwandtner M, Erne W, Loustau T, et al. Matrix-targeting immunotherapy controls tumor growth and spread by switching macrophage phenotype. *Cancer Immunol Res.* (2020) 8:368–82. doi: 10.1158/2326-6066.CIR-19-0276

14. Spenlé C, Loustau T, Murdamoothoo D, Erne W, Beghelli-de la Forest Divonne S, Veber R, et al. Tenascin-C orchestrates an immune-suppressive tumor microenvironment in oral squamous cell carcinoma. *Cancer Immunol Res.* (2020) 8:1122–38. doi: 10.1158/2326-6066.CIR-20-0074
15. Sun Z, Schwenzer A, Rupp T, Murdamoothoo D, Vegliante R, Lefebvre O, et al. Tenascin-C Promotes Tumor Cell Migration And Metastasis Through Integrin α9β1-mediated YAP inhibition. *Cancer Res.* (2018) 78:950–61. doi: 10.1158/0008-5472.CAN-17-1597
16. Sun Z, Velázquez-Quesada I, Murdamoothoo D, Ahowesso C, Yilmaz A, Spenlé C, et al. Tenascin-C increases lung metastasis by impacting blood vessel invasions. *Matrix Biol.* (2019) 83:26–47. doi: 10.1016/j.matbio.2019.07.001
17. Suzuki H, Shiba M, Fujimoto M, Kawamura K, Nanpei M, Tekeuchi E, et al. Matricellular protein: a new player in cerebral vasospasm following subarachnoid hemorrhage. *Acta Neurochir Suppl.* (2013) 115:213–8. doi: 10.1007/978-3-7091-1192-5_39
18. Shiba M, Fujimoto M, Imanaka-Yoshida K, Yoshida T, Taki W, Suzuki H. Tenascin-C causes neuronal apoptosis after subarachnoid hemorrhage in rats. *Transl Stroke Res.* (2014) 5:238–47. doi: 10.1007/s12975-014-0333-2
19. Fujimoto M, Shiba M, Kawakita F, Liu L, Nakasaki A, Shimojo N, et al. Epidermal growth factor-like repeats of tenascin-C-induced constriction of cerebral arteries via activation of epidermal growth factor receptors in rats. *Brain Res.* (2016) 1642:436–41. doi: 10.1016/j.brainres.2016.04.034
20. Fujimoto M, Shiba M, Kawakita F, Liu L, Shimojo N, Imanaka-Yoshida K, et al. Deficiency of tenascin-C and attenuation of blood-brain barrier disruption following experimental subarachnoid hemorrhage in mice. *J Neurosurg.* (2016) 124:1693–702. doi: 10.3171/2015.4.JNS15484
21. Matsui Y, Hasegawa M, Iino T, Imanaka-Yoshida K, Yoshida T, Sudo A. Tenascin-C prevents articular cartilage degeneration in murine osteoarthritis models. *Cartilage.* (2018) 9:80–8. doi: 10.1177/1947603516681134
22. Unno H, Hasegawa M, Suzuki Y, Iino T, Imanaka-Yoshida K, Yoshida T, et al. Tenascin-C promotes the repair of cartilage defects in mice. *J Orthop Sci.* (2020) 25:324–30. doi: 10.1016/j.jos.2019.03.013
23. Ma JC, Huang X, Shen YW, Zheng C, Su QH, Xu JK, et al. Tenascin-C promotes migration of hepatic stellate cells and production of type I collagen. *Biosci Biotechnol Biochem.* (2016) 80:1470–7. doi: 10.1080/09168451.2016.1165600
24. Imanaka-Yoshida K, Tawara I, Yoshida T. Tenascin-C in cardiac disease: a sophisticated controller of inflammation, repair, and fibrosis. *Am J Physiol Cell Physiol.* (2020) 319:C781–C96. doi: 10.1152/ajpcell.00353.2020
25. Saito H, Tsumura H, Otake S, Nishida A, Furukawa T, Suzuki N. L7/Pcp-2-specific expression of Cre recombinase using knock-in approach. *Biochem Biophys Res Commun.* (2005) 331:1216–21. doi: 10.1016/j.bbrc.2005.04.043
26. Moses KA, DeMayo F, Braun RM, Reecy JL, Schwartz RJ. Embryonic expression of an Nkx2-5/Cre gene using ROSA26 reporter mice. *Genesis.* (2001) 31:176–80. doi: 10.1002/gene.10022
27. Agah R, Frenkel PA, French BA, Michael LH, Overbeek PA, Schneider MD. Gene recombination in postmitotic cells. Targeted expression of Cre recombinase provokes cardiac-restricted, site-specific rearrangement in adult ventricular muscle in vivo. *J Clin Invest.* (1997) 100:169–79. doi: 10.1172/JCI119509
28. Imanaka-Yoshida K, Matsumoto K, Hara M, Sakakura T, Yoshida T. The dynamic expression of tenascin-C and tenascin-X during early heart development in the mouse. *Differentiation.* (2003) 71:291–8. doi: 10.1046/j.1432-0436.2003.7104506.x
29. Imanaka-Yoshida K, Hiroe M, Nishikawa T, Ishiyama S, Shimojo T, Ohta Y, et al. Tenascin-C modulates adhesion of cardiomyocytes to extracellular matrix during tissue remodeling after myocardial infarction. Lab Invest. (2001) 81:1015–24. doi: 10.1038/labinvest.3780313
30. Hasegawa K, Yoshida T, Matsumoto K, Katsuta K, Waga S, Sakakura T. Differential expression of tenascin-C and tenascin-X in human astrocytomas. *Acta Neuropathol.* (1997) 93:431–7. doi: 10.1007/s004010050636
31. Imanaka-Yoshida K, Hiroe M, Yasutomi Y, Toyozaki T, Tsuchiya T, Noda N, et al. Tenascin-C is a useful marker for disease activity in myocarditis. *J Pathol.* (2002) 197:388–94. doi: 10.1002/path.1131
32. Nishioka T, Suzuki M, Onishi K, Takakura N, Inada H, Yoshida T, et al. Eplerenone attenuates myocardial fibrosis in the angiotensin II-induced hypertensive mouse: involvement of tenascin-C induced by aldosterone-mediated inflammation. *J Cardiovasc Pharmacol.* (2007) 49:261–8. doi: 10.1097/FJC.0b013e318033dfd4
33. Kimura T, Tajiri K, Sato A, Sakai S, Wang Z, Yoshida T, et al. Tenascin-C accelerates adverse ventricular remodelling after myocardial infarction by modulating macrophage polarization. *Cardiovasc Res.* (2019) 115:614–24. doi: 10.1093/cvr/cvy244
34. Zhu X, Libby RT, de Vries WN, Smith RS, Wright DL, Bronson RT, et al. Mutations in a P-type ATPase gene cause axonal degeneration. *PLoS Genet.* (2012) 8:e1002853. doi: 10.1371/journal.pgen.1002853
35. Shen H, Gan P, Wang K, Darehzereshki A, Wang K, Kumar SR, et al. Mononuclear diploid cardiomyocytes support neonatal mouse heart regeneration in response to paracrine IGF2 signaling. *Elife.* (2020) 9:53071. doi: 10.7554/eLife.53071
36. Zhao Q, Sun Q, Zhou L, Liu K, Jiao K. Complex regulation of mitochondrial function during cardiac development. *J Am Heart Assoc.* (2019) 8:e012731. doi: 10.1161/JAHA.119.012731
37. Fang S, Li J, Xiao Y, Lee M, Guo L, Han W, et al. Tet inactivation disrupts YY1 binding and long-range chromatin interactions during embryonic heart development. *Nat Commun.* (2019) 10:4297. doi: 10.1038/s41467-019-12325-z
38. Papanicolaou KN, Kikuchi R, Ngoh GA, Coughlan KA, Dominguez I, Stanley WC, et al. Mitofusins 1 and 2 are essential for postnatal metabolic remodeling in heart. *Circ Res.* (2012) 111:1012–26. doi: 10.1161/CIRCRESAHA.112.274142
39. Gaussin V, Van de Putte T, Mishina Y, Hanks MC, Zwijsen A, Huylebroeck D, et al. Endocardial cushion and myocardial defects after cardiac myocyte-specific conditional deletion of the bone morphogenetic protein receptor ALK3. *Proc Natl Acad Sci USA.* (2002) 99:2878–83. doi: 10.1073/pnas.042390499
40. Xu J, Ismat FA, Wang T, Lu MM, Antonucci N, Epstein JA. Cardiomyocyte-specific loss of neurofibromin promotes cardiac hypertrophy and dysfunction. *Circulation Res.* (2009) 105:304–11. doi: 10.1161/CIRCRESAHA.109.201509
41. Pugach EK, Richmond PA, Azofeifa JG, Dowell RD, Leinwand LA. Prolonged Cre expression driven by the alpha-myosin heavy chain promoter can be cardiotoxic. *J Mol Cell Cardiol.* (2015) 86:54–61. doi: 10.1016/j.yjmcc.2015.06.019
42. Maqbool A, Spary EJ, Manfield IW, Ruhmann M, Zuliani-Alvarez L, Gamboa-Esteves FO, et al. Tenascin C upregulates interleukin-6 expression in human cardiac myofibroblasts via toll-like receptor 4. *World J Cardiol.* (2016) 8:340–50. doi: 10.4330/wjc.v8.i5.340
43. Bhattacharyya S, Midwood KS, Yin H, Varga J. Toll-like receptor-4 signaling drives persistent fibroblast activation and prevents fibrosis resolution in scleroderma. *Adv Wound Care.* (2017) 6:356–69. doi: 10.1089/wound.2017.0732
44. Katoh D, Kozuka Y, Noro A, Ogawa T, Imanaka-Yoshida K, Yoshida T. Tenascin-C induces phenotypic changes in fibroblasts to myofibroblasts with high contractility through the integrin αvβ1/transforming growth factor β/SMAD signaling axis in human breast cancer. *Am J Pathol.* (2020) 190:2123–35. doi: 10.1016/j.ajpath.2020.06.008
45. Midwood K, Sacre S, Piccinini AM, Inglis J, Trebaul A, Chan E, et al. Tenascin-C is an endogenous activator of Toll-like receptor 4 that is essential for maintaining inflammation in arthritic joint disease. *Nat Med.* (2009) 15:774–80. doi: 10.1038/nm.1987
46. Piccinini AM, Zuliani-Alvarez L, Lim JMP, Midwood KS. Distinct microenvironmental cues stimulate divergent TLR4-mediated signaling pathways in macrophages. *Sci Signal.* (2016) 9:ra86. doi: 10.1126/scisignal.aaf3596
47. Zuliani-Alvarez L, Marzeda AM, Deligne C, Schwenzer A, McCann FE, Marsden BD, et al. Mapping tenascin-C interaction with toll-like receptor 4 reveals a new subset of endogenous inflammatory

triggers. *Nat Commun.* (2017) 8:1595. doi: 10.1038/s41467-017-01718-7

48. Podesser BK, Kreibich M, Dzilic E, Santer D, Forster L, Trojanek S, et al. Tenascin-C promotes chronic pressure overload-induced cardiac dysfunction, hypertrophy and myocardial fibrosis. *J Hypertens.* (2018) 36:847–56. doi: 10.1097/hjh.0000000000001628
49. Gonçalves IF, Acar E, Costantino S, Szabo PL, Hamza O, Tretter EV, et al. Epigenetic modulation of tenascin C in the heart: implications on myocardial ischemia, hypertrophy and metabolism. *J Hypertens.* (2019) 37:1861–70. doi: 10.1097/HJH.0000000000002097
50. Ashraf H, Pradhan L, Chang EI, Terada R, Ryan NJ, Briggs LE, et al. A mouse model of human congenital heart disease: high incidence of diverse cardiac anomalies and ventricular noncompaction produced by heterozygous Nkx2-5 homeodomain missense mutation. *Circ Cardiovasc Genet.* (2014) 7:423–33. doi: 10.1161/CIRCGENETICS.113.000281
51. Bousalis D, Lacko CS, Hlavac N, Alkassis F, Wachs RA, Mobini S, et al. Extracellular matrix disparities in an Nkx2-5 mutant mouse model of congenital heart disease. *Front Cardiovasc Med.* (2020) 7:93. doi: 10.3389/fcvm.2020.00093

Conflict of Interest: The authors declare that the research was conducted in the absence of any commercial or financial relationships that could be construed as a potential conflict of interest.

frontiers in Immunology

ORIGINAL RESEARCH
published: 11 March 2021
doi: 10.3389/fimmu.2021.600979

Tenascin-C Deficiency Is Associated With Reduced Bacterial Outgrowth During *Klebsiella pneumoniae*-Evoked Pneumosepsis in Mice

Mariska T. Meijer[1,2], Alex F. de Vos[1,2], Brendon P. Scicluna[1,2,3], Joris J. Roelofs[4], Chérine Abou Fayçal[5], Gertraud Orend[5], Fabrice Uhel[1,2] and Tom van der Poll[1,2,6]*

[1] Center for Experimental and Molecular Medicine, Amsterdam University Medical Centers, Location Academic Medical Center, University of Amsterdam, Amsterdam, Netherlands, [2] Amsterdam Institute for Infection and Immunity, Amsterdam University Medical Centers, Amsterdam, Netherlands, [3] Clinical Epidemiology Biostatistics and Bioinformatics, Amsterdam University Medical Centers, Location Academic Medical Center, University of Amsterdam, Amsterdam, Netherlands, [4] Department of Pathology, Amsterdam University Medical Centers, Location Academic Medical Center, University of Amsterdam, Amsterdam, Netherlands, [5] The Tumor Microenvironment Laboratory, INSERM UMR_S 1109, Université Strasbourg, Faculté de Médecine, Hopital Civil, Institut d'Hématologie et d'Immunologie, Fédération de Médecine Translationnelle de Strasbourg (FMTS), Strasbourg, France, [6] Division of Infectious Diseases, Amsterdam University Medical Centers, Location Academic Medical Center, University of Amsterdam, Amsterdam, Netherlands

OPEN ACCESS

Edited by:
Pietro Ghezzi, Brighton and Sussex Medical School, United Kingdom

Reviewed by:
Anna Maria Piccinini, University of Nottingham, United Kingdom
Colin Reardon, University of California, Davis, United States

***Correspondence:**
Mariska T. Meijer
m.t.meijer@amsterdamumc.nl

Specialty section:
This article was submitted to Inflammation, a section of the journal Frontiers in Immunology

Received: *31 August 2020*
Accepted: *22 February 2021*
Published: *11 March 2021*

Citation:
Meijer MT, de Vos AF, Scicluna BP, Roelofs JJ, Abou Fayçal C, Orend G, Uhel F and van der Poll T (2021) Tenascin-C Deficiency Is Associated With Reduced Bacterial Outgrowth During Klebsiella pneumoniae-Evoked Pneumosepsis in Mice. Front. Immunol. 12:600979. doi: 10.3389/fimmu.2021.600979

Tenascin C (TNC) is an extracellular matrix glycoprotein that recently emerged as an immunomodulator. TNC-deficient ($TNC^{-/-}$) mice were reported to have a reduced inflammatory response upon systemic administration of lipopolysaccharide, the toxic component of gram-negative bacteria. Here, we investigated the role of TNC during gram-negative pneumonia derived sepsis. $TNC^{+/+}$ and $TNC^{-/-}$ mice were infected with *Klebsiella pneumoniae* via the airways and sacrificed 24 and 42 h thereafter for further analysis. Pulmonary TNC protein levels were elevated 42 h after infection in $TNC^{+/+}$ mice and remained undetectable in $TNC^{-/-}$ mice. $TNC^{-/-}$ mice showed modestly lower bacterial loads in lungs and blood, and a somewhat reduced local—but not systemic—inflammatory response. Moreover, $TNC^{-/-}$ and $TNC^{+/+}$ mice did not differ with regard to neutrophil recruitment, lung pathology or plasma markers of distal organ injury. These results suggest that while TNC shapes the immune response during lipopolysaccharide-induced inflammation, this role may be superseded during pneumosepsis caused by a common gram-negative pathogen.

Keywords: tenascin C, sepsis, *Klebsiella pneumoniae* (*K. pneumoniae*), pneumonia, alarmins, innate immunity, immune system, mice

INTRODUCTION

Tenascin C (TNC) is a large multimeric extracellular matrix glycoprotein with binding sites for many different signaling factors. It plays a major role during embryonic development, but in adult tissues expression levels are relatively low (1, 2). However, TNC is expressed in a variety of cell types in response to both chemical and mechanical cellular stress (1, 2). Recently, TNC has drawn attention for its immunomodulatory properties (3–6).

Midwood and colleagues were the first to show that in a model of rheumatoid arthritis, inflammation could not be maintained beyond the first 24 h when mice were TNC deficient (3). Despite displaying a normal acute immune response, the Tenascin C deficient ($TNC^{-/-}$) mice did not develop the chronic inflammation displayed by TNC sufficient ($TNC^{+/+}$) mice. Moreover, it was reported that TNC can act as a direct agonist of toll-like receptor 4 (TLR4), which also serves as the main signaling receptor for lipopolysaccharide (LPS), a proinflammatory component of the gram-negative bacterial cell wall (4, 7). Thus, TNC was proposed as a putative danger associated molecular peptide (DAMP). In agreement with a role of TNC as a pro-inflammatory signaling molecule, treatment with TNC siRNA suppressed LPS-induced cytokine production by mouse macrophages (8). In accordance, $TNC^{-/-}$ mice became less severely ill after LPS injection, which was associated with decreased tumor necrosis factor (TNF)-α and interleukin (IL)-6 production (7). Together these data suggest that TNC may enhance acute and chronic inflammation.

We and others have previously shown that TNC plasma levels are increased in critically ill patients, particularly in those suffering from infection and sepsis (9, 10). Sepsis patients represent 10% of all admissions to the intensive care unit (ICU), and sepsis is the leading cause of disease in non-coronary ICUs in the developed world with a mortality rate of 20–30%. Its pathophysiology is the result of a dysregulated immune response with concurrent hyperinflammation and immune suppression (11). The most common cause of sepsis is bacterial pneumonia, and the Gram-negative bacterium *Klebsiella (K.) pneumoniae* is frequently isolated from septic patients (12). Host defense to *K. pneumoniae* pneumonia largely depends on TLR4 (13, 14). In the present study we therefore sought to determine if TNC regulates the host response during pneumonia derived sepsis caused by *K. pneumoniae*. To this end, we performed *in vivo* experiments causing pneumonia and sepsis in $TNC^{-/-}$ and $TNC^{+/+}$ mice by infection with *K. pneumoniae* via the airways.

MATERIALS AND METHODS

Ethical Statement

The experiments were reviewed and approved by the Institutional Animal Care and Use Committee of the Academic Medical Center (AMC), University of Amsterdam (identification numbers DIX21-EV-1 and DIX288-BP-1). The animal care and use protocol adhered to European Directive of 22 September 2010 (Directive 2010/63/EU) in addition to the Directive of 6 May 2009 (Directive 2009/41/EC).

Animals

$TNC^{+/+}$ and $TNC^{-/-}$ mice, bred on a C57BL/6 background for 10 generations (15), were bred in parallel from heterozygous parents. Mice were housed in individually ventilated cages enriched with disposable homes and nesting paper, and provided with food and water *at libitum*. All mice were bred and housed at the Animal Research Institute AMC under specific pathogen free conditions. Mice were acclimatized in the procedure room for at least one week before commencement of the experiment. Mice entered experiments at 8–10 weeks of age and in good health. Both genders were used for experiments and groups were sex matched. Mice were assessed on their welfare (including posture and activity) throughout their stay at the facility.

Study Design

Experimental groups consisted of 8 (24-h time point) or 12 (42-h time point) mice per genotype. This corresponds to a power of 80%, type I error of 5%, standard deviation of 35%, and effect sizes of 50% (24 h) or 35% (42 h). Home cages were placed in a random order, which was then used throughout the experiment. Pneumonia was induced by intranasal administration of 10^4 colony-forming units (CFU) of *K. pneumoniae* serotype 2 (ATCC 43816) in 50 μL sterile isotonic saline as described (13, 16). In brief, bacteria were grown for 2–3 h to a mid-logarithmic phase at 37°C using Tryptic Soy broth, harvested by centrifugation and resuspended in sterile isotonic saline so that 50 μL corresponded to 10^4 CFU. Inoculation was performed under sedation with 2–3% isoflurane in 100% O_2 to ensure calm inspiration of the inoculum. Mice were euthanized at 24 or 42 h after inoculation by intraperitoneal injection of ketamine (125 mg/kg) and dexmedetomidine (300 μg/kg) followed by cardiac puncture. Blood was collected into heparin tubes (Microtainer, BD Biosciences, NJ). Lung, spleen, and liver were harvested and homogenized in sterile saline (weight:volume, 1:5) using a tissue homogenizer (Biospec Products, Bastlesville, OK). CFU in organ homogenates and blood were determined from serial dilutions plated on blood agar plates incubated at 37°C for 14 h (13). Unless specified otherwise, data was collected from all animals.

Cytokine Quantification

Plasma TNF-α, IL-6, and chemokine (C-C motif) ligand 2 (CCL2) were measured using Cytometric Bead Array (Mouse Inflammation Kit; BD Biosciences, Franklin Lakes, NJ), according to manufacturer's instructions on a FACS Canto II with High Throughput Sampler (BD, Biosciences, Franklin Lakes, NJ). Aspartate aminotransferase (AST), alanine aminotransferase (ALT), and lactate dehydrogenase (LDH) were measured by using a c702 Roche Diagnostics (Roche Diagnostics BV, Almere, the Netherlands) (17).

To determine levels of cytokine and neutrophil products in lung tissue, homogenized lung samples were diluted with an equal volume of lysis buffer (pH 7.4) containing 1% Triton X-100, 100 mM NaCl, 15 mM Tris, 1 mM $MgCl_2$, 1 mM $CaCl_2$ and cOmplete™ Protease Inhibitor Cocktail (Roche, Basel, Switzerland), and incubated at 4°C for 30 min. Homogenates were centrifuged at 1500×g at 4°C for 15 min, and supernatants were stored at−20°C until analysis. Pulmonary TNC, as well as lung cytokines, chemokines and neutrophil products were then measured by ELISA according to the instructions of the manufacturers: TNC (large isoform containing FNIII-C, IBL International, Hamburg, Germany), TNF-α (Thermo Fisher Scientific, Waltham, MA), IL-1β, IL-6, chemokine (C-X-C motif) ligand (CXCL)1, CXCL2, myeloperoxidase (MPO) and neutrophil elastase (R&D Systems, Minneapolis, MN).

In addition to protein measurements, the mRNA expression levels of 5 cytokines were determined through quantitative

polymerase chain reaction (qPCR). RNA was isolated from long homogenate using the Nucleospin RNA isolation kit according to manufacturer's protocol (Macherey-Nagel, Düren, Germany). cDNA was synthesized using M-MLV Reverse Transcriptase with oligo(dT) primers according to manufacturer's protocol (Promega, Madigon, WI). mRNA levels were determined through quantitative polymerase chain reaction using the SensiFast^{TM} No-ROX Kit (Bioline, London, UK) measured on a LightCycler 480 (Roche, Basel, Switzerland) using the following primers: TNF-α forward: CGAGTGACAAGCCT GTAGCC, TNF-α reverse: CCTTGAAGAGAACCTGGGAGT, IL-1β forward: GGGGAACTCTGCAGACTCAA, IL-1β reverse: GGGCCTCAAAGGAAAGAATC, IL-6 forward: CTTCC TACCCCAATTTCCAATGCT, IL-6 reverse: TCTTGGTCCT TAGCCACTCCTT, CXCL1 forward: CCACTGCACCCAAAC CGAAG, CXCL1 reverse: TCCGTTACTTGGGGACACCT, mCXCL2 forward: CACTCTCAAGGGCGGTCAA and CXCL2 reverse: TCTTTGGTTCTTCCGTTGAGG. As a housekeeping gene, HPRT1 was measured using the following primers: HRPT1 forward: AGTCAAGGGCATATCCAACA and HPRT1 reverse: CAAACTTTGCTTTCCGGGT.

Histopathology

Lungs were collected and fixed in 10% formalin in PBS for at least 16 h, transferred to 70% ethanol and embedded in paraffin. Four-micrometer paraffin-embedded lung sections were stained with hematoxylin and eosin. Slides were coded and lung inflammation and damage was scored by a pathologist blinded for group identity. To score lung inflammation and damage, the entire lung surface was analyzed with respect to the following parameters: interstitial inflammation, edema, endothelialitis, bronchitis, and pleuritis. Each parameter was graded on a scale of 0–4, (0: absent; 1: mild; 2: moderate; 3: severe; 4: very severe). The percentage pneumonia was scored and graded on a scale of 0–5 (0: absent; 1: 5–20% confluent pneumonia; 2: 21–40%; 3: 41–60%; 4: 61–80%; 5: 81–100%). Lastly, the number of thrombi were counted. All parameters and corresponding scores, as present in our dataset, our illustrated in **Supplementary Figure 1**. The pathology score was expressed as the sum of the scores for each parameter (16).

Immunohistochemistry

To visualize TNC protein in the lung, paraffin-embedded lung sections were unmasked by boiling in a 10 mM pH 6 citrate solution. Slides were blocked with 5% normal goat serum in PBS and incubated with 1:100 primary anti-TNC antibody (AB19011, EMD Millipore, Temecula, CA). Slides were washed with 0.1% triton X-100 in PBS (Sigma-Aldrich, St Louis, MO) followed by 1:200 secondary anti-rabbit biotinylated antibody (Jackson ImmunoResearch, West Grove, PA). Slides were washed with 0.1% triton X-100 in PBS and treated with peroxide solution [0.6% H_2O_2 (Sigma-Aldrich, St Louis, MO) in methanol]. Slides were washed with 0.1% triton X-100 in PBS then were incubated with 3,3′-Diaminobenzidine developing solution (Vector Lab, Burlingame, CA) for 1 h at room temperature. The signal detection was done with the Elite ABC system (Vectastain, Burlingame, CA) and hematoxylin staining was performed. The sections were embedded into ProLong Gold antifade reagent (Invitrogen, Waltham, MA). Sections were examined using an Axio Imager A1. Pictures were taken with an AxioCam Icc3 camera and Axiovision software (all: Zeiss, Jena, Germany).

Statistical Analysis

Statistical analysis was performed in R 3.6.3 (18). Figures were created with ggplot2 3.3.0 (19). Data was $\log_{10}$-transformed for analysis. All data presented are back-transformed through their antilog. Tables and bar graphs show means with standard errors (SE). Figures show Tukey box-and-whisker plots, including median and interquartile range without outliers. Differences between groups over time were tested using two-way type III ANOVA, which takes into account imbalanced designs. *Post-hoc* tests were performed using Tukey's HSD. Two-group comparisons were performed using an unpaired *t*-test. Data below the lower limit of detection was imputed at the lower limit of detection. A p-value < 0.05 was considered statistically significant.

RESULTS

Pulmonary Tenascin C Modestly Impairs Antibacterial Defense During *Klebsiella* Pneumonia

TNC was detected at relatively high levels in lung homogenates of naïve $TNC^{+/+}$ mice [8.9 (3.0-26.8) ng/mL; **Figure 1A**], but not of $TNC^{-/-}$ mice, documenting constitutive presence of this protein in the lungs. Infection with *K. pneumoniae* via the airways resulted in a gradual rise in lung TNC levels that at 42 h was more than 10-fold over those measured in naïve mice [42 h: 110.8 (46.5-264.1) ng/mL, $p < 0.01$]. In contrast, plasma levels of TNC did not change during infection with *K. pneumonia* [42 hours: 1443 (1069-1948) ng/mL] compared to uninfected mice [1457 (975-2178) ng/mL, $p = 0.95$]. TNC was not detected in plasma from $TNC^{-/-}$ mice. Staining lung tissue for TNC confirmed the presence of TNC protein in the pulmonary extracellular matrix of $TNC^{+/+}$ mice after infection, while $TNC^{-/-}$ tissue remained negative (**Figure 1B**).

To determine the role of TNC in the host response during *Klebsiella* pneumonia derived sepsis we assessed bacterial burdens at the primary site of infection (lungs) and distant body sites (blood, liver and spleen) in $TNC^{+/+}$ and $TNC^{-/-}$ mice 24 and 42 h after infection (**Figure 1C**). Overall, bacterial loads were slightly lower in $TNC^{-/-}$ than in $TNC^{+/+}$ mice, which reached statistical significance for lung and blood (**Figure 1C**).

The Absence of Tenascin C Modestly Reduces Lung Inflammation During *Klebsiella* Pneumonia

TNC has been implicated as an important mediator of inflammatory responses (1, 3, 4, 7). In light of the high constitutive pulmonary TNC levels and the strong induction of TNC in the lungs during *Klebsiella* pneumonia, we considered it of interest to determine the role of TNC in lung inflammation induced by this infection. To this end, we scored lung tissue slides prepared from $TNC^{+/+}$ and $TNC^{-/-}$ mice 24 and

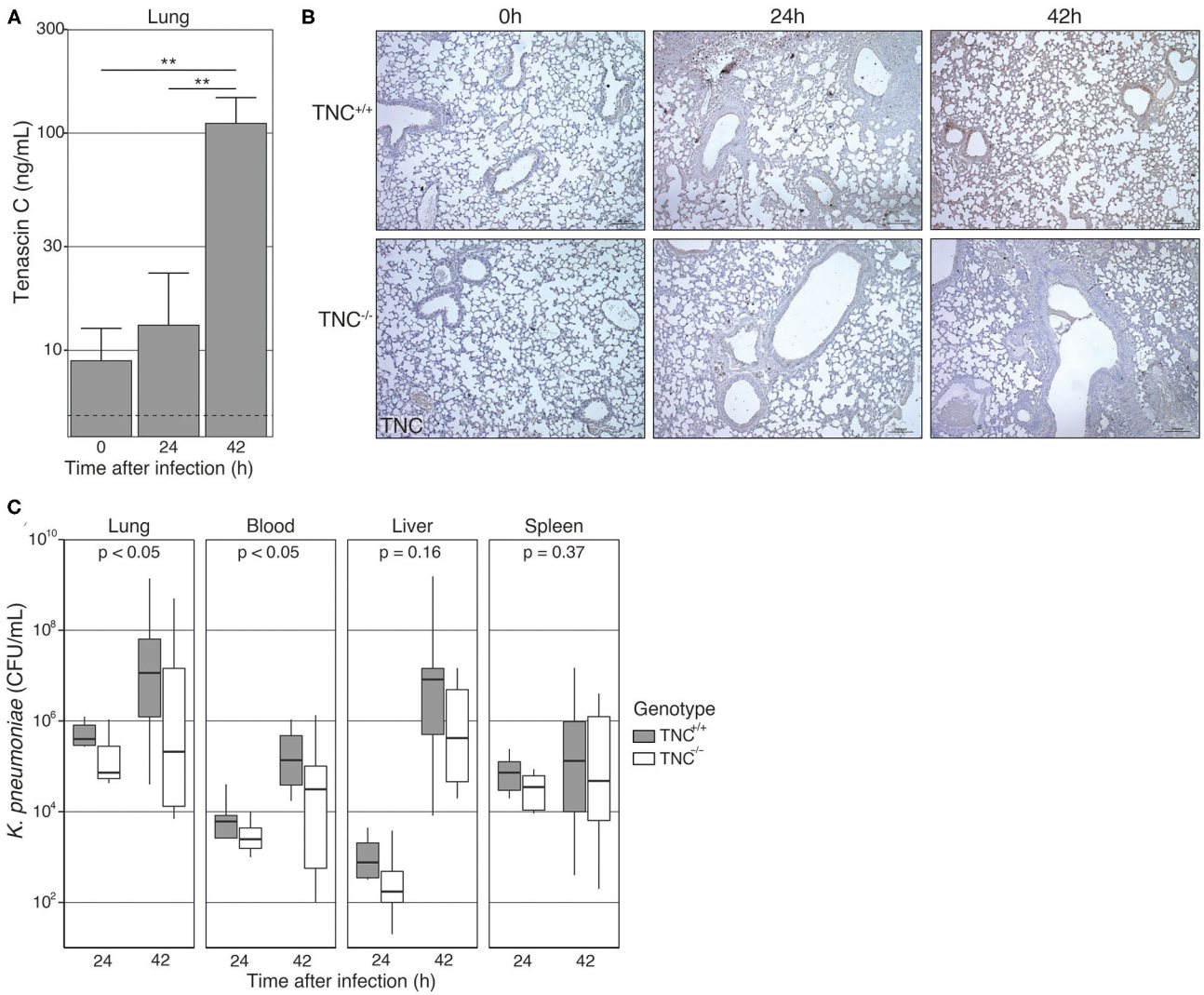

FIGURE 1 | Pulmonary Tenascin-C levels and bacterial counts during *Klebsiella* induced pneumosepsis. Tenascin C sufficient ($TNC^{+/+}$) and deficient ($TNC^{-/-}$) mice were intranasally infected with *K. pneumoniae*. **(A)** Before inoculation, and 24 and 42 h thereafter lung samples were collected and homogenized. TNC was measured in the lysate of 4 $TNC^{+/+}$ mice from each time point. Bars and whiskers show mean and SE. The dotted line represents the lower limit of quantitation. TNC was not detectable in any of the $TNC^{-/-}$ samples measured. **(B)** Lung tissue was collected, fixed and embedded in paraffin 24 and 42 h after infection, as well as in the naïve state. Tissue slides were stained for TNC protein. Depicted slides are representative of 5 independent biological replicates. **(C)** Number of colony-forming units (CFU) 24 and 42 h after infection. Data are shown as Tukey boxplots without outliers. $^{**}p < 0.01$ in an unpaired *t*-test. *P*-values **(C)** represent the effect of genotype across time-points, as indicated by a two-way type III ANOVA.

42 h after induction of infection. Overall, the extent of lung inflammation did not differ between mouse strains, although $TNC^{-/-}$ mice tended to have higher pathology scores at 24 h (**Figures 2A,B**).

The levels of neutrophil products MPO (**Figure 2C**) and elastase (**Figure 2D**) in lung homogenates did not differ between $TNC^{+/+}$ and $TNC^{-/-}$ mice, indicating similar neutrophil influx in the lung. Analysis of pulmonary cytokines (TNF-α, IL-1β, IL-6) and chemokines (CXCL1, CXCL2) revealed no significant differences between the groups (**Figure 2E**). However, at the mRNA level we did observe a decrease in cytokine expression, which reached significance for TNF-α, IL-6 and CXCL-1 (**Figure 2F**).

The Absence of Tenascin C Does Not Influence Systemic Inflammation During *Klebsiella* Pneumonia

Patients with sepsis have elevated circulating levels of TNC (9, 10) and TNC may contribute to the pro-inflammatory and injurious systemic host response in this condition (1). The model of *Klebsiella* induced pneumosepsis is associated with systemic inflammation and distant organ injury (17). To determine the role of TNC in the development of systemic inflammation, we measured the plasma levels of TNF-α, IL-6, and CCL2 as markers of systemic inflammation 24 and 42 h after the beginning of infection (**Figure 3A**). Systemic cytokine levels did

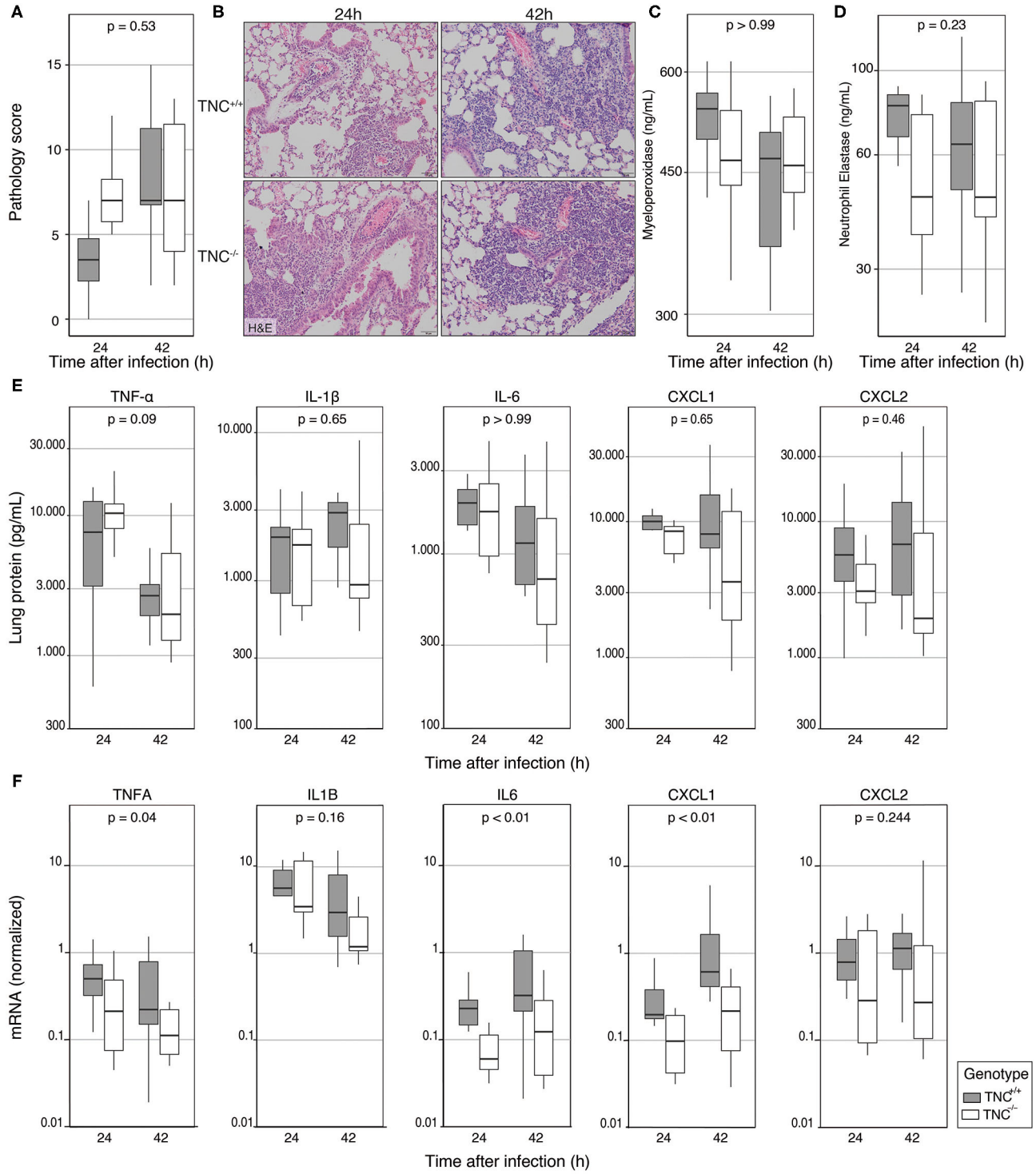

FIGURE 2 | Endogenous Tenascin-C does not impact lung inflammation during *Klebsiella* induced pneumosepsis. $TNC^{+/+}$ and $TNC^{-/-}$ mice were intranasally infected with *K. pneumoniae;* 24 and 42 h after infection, lung tissue samples were collected for histological examination or homogenization. **(A)** Lung samples of all mice were scored for interstitial inflammation, edema, endothelialitis, bronchitis, pleuritis, and the presence of thrombi by a blinded pathologist blinded for the group identity, after which the total pathology score was calculated. **(B)** Representative pictures of lung pathology at 24 h (middle panel) and 42 hours (right panel) after infection in $TNC^{+/+}$ mice (top panel) and $TNC^{-/-}$ mice (bottom panel). **(C)** Levels of MPO, **(D)** elastase, and **(E)** cytokines and chemokines were measured in lung homogenates. **(F)** Cytokine mRNA was measured in RNA isolated from lung homogenate, and is presented normalized to HPRT1 expression. Data are shown as Tukey boxplots without outliers. *p*-values represent the effect of genotype across time-points, as indicated by a two-way type III ANOVA.

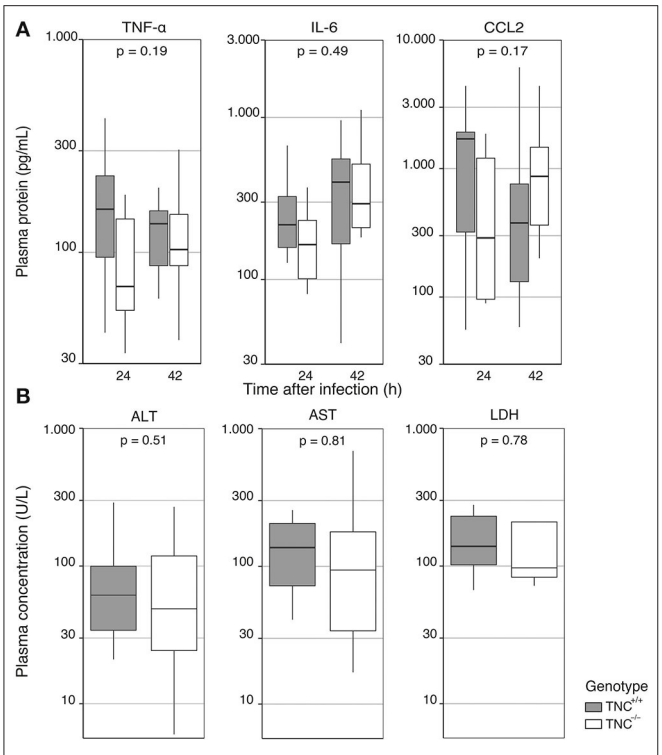

FIGURE 3 | Endogenous Tenascin-C does not impact systemic inflammation during *Klebsiella* induced pneumosepsis. $TNC^{+/+}$ and deficient $TNC^{-/-}$ mice were infected with *K. pneumoniae;* **(A)** 24 and 42 h after infection plasma was collected for measurements of TNF-α, IL-6, and CCL2. **(B)** Markers of hepatic injury (ALT, AST) and cell injury in general (LDH) were measured at 42 h. Data are shown as Tukey boxplots without outliers. *p*-values represent the effect of genotype across time-points, as indicated by a two-way type III ANOVA **(A)**, or unpaired *t*-test **(B)**.

not differ between the groups. In addition, we measured the plasma concentrations of ALT, AST and LDH as markers of hepatocellular and general cell injury (**Figure 3B**); none of these injury markers differed between $TNC^{+/+}$ and $TNC^{-/-}$ mice.

DISCUSSION

Here we investigated the hypothesis that TNC may play a role in the enhancement of inflammatory responses during sepsis. This assumption was based on multiple observations. First, TNC plasma levels are elevated in patients with sepsis. Second, TNC can induce proinflammatory cytokines by activation of TLR4 in multiple cell types, including macrophages and dendritic cells, and conversely, macrophages with reduced or no TNC expression display reduced proinflammatory cytokine production upon stimulation with LPS *in vitro* (1, 2, 7, 8). Third, $TNC^{-/-}$ mice showed attenuated proinflammatory cytokine release upon injection of LPS and the inflammation-enhancing role of TNC is further supported by mouse studies reporting a protective anti-inflammatory effect of TNC deficiency in a number of inflammatory disease models, including hepatic ischemia/reperfusion injury (20), concanavalin A–induced hepatitis (21), joint inflammation (3, 22), autoimmune encephalomyelitis (23), and Alzheimer's disease (24). Moreover, TNC has been shown to play essential proinflammatory roles in models of lung inflammation, such as ovalbumin-induced asthma (25) and bleomycin-induced pulmonary fibrosis (26, 27). As such, increased TNC levels, induced as a result of tissue damage, cellular stress, and inflammatory mediators, would be expected to be part of a positive feedback loop that amplifies the inflammatory response. However, while we detected a rise in TNC levels in lungs after airway infection with viable *K. pneumoniae,* the role of TNC in local and systemic inflammatory responses elicited by this common sepsis pathogen was very limited. Indeed, although $TNC^{-/-}$ mice showed a modest reduction in bacterial outgrowth in lungs and blood, this preceded the rise of pulmonary TNC protein levels. We found a reduced expression of TNF-α, IL-6, and CXCL1 mRNA in the lung at both timepoints. A similar trend could be seen at the protein level, although this did not reach significance.

Inhibition of TNC expression in mouse macrophages was reported to result in attenuated LPS-induced TNF-α and IL-6 release *in vitro* (8). Likewise, $TNC^{-/-}$ bone-marrow derived macrophages produced less TNF-α, IL-6 and CXLC1, and more IL-10 in response to LPS stimulation *in vitro* and $TNC^{-/-}$ mice produced less TNF-α and IL-6 shortly after systemic LPS administration *in vivo* (7). These observations were confirmed using human primary material, as reviewed in (2). We observed a similar effect at the mRNA level in lungs. At the protein level, a trend toward reduced IL-6 and CXCL1 did not reach significance, possibly because of the high variability within groups. The modest differences in bacterial loads may have influenced the extent of inflammation; vice versa differences in inflammatory responses may impact antibacterial defense mechanisms. Studies with killed bacteria or bacterial products such as LPS can provide insight in the role of TNC during non-infectious lung inflammation. As the cytokine protein levels were measured in lung homogenate, they reflect the sum of intracellular, transmembrane, and secreted protein, which could contribute to the increased variance. This holds especially for TNF-α and IL-1β, which are detected in their unprocessed cell-associated forms (before cleavage by ADAM17 and caspase-1, respectively), as well as in their secreted forms. Measurements of cytokines in bronchoalveolar lavage fluid will provide insight into secretion of mature proteins into the bronchoalveolar space, but not in tissue levels. Notably, several studies in which mediators were measured in both bronchoalveolar lavage fluid and lung homogenates reported similar results, although levels in lavage fluid were consistently lower due to the dilution factor introduced by the lavage procedure (28–32). Sampling of bronchoalveolar lavage fluid can generate information on the role of TNC in cell recruitment into the airways, which in the current study was limited to examination of lung tissue slides. Protein levels of TNF-α and IL-1β in lung homogenates may be more representative of the inflammatory potential than of active cytokine signaling. Nonetheless, it has been shown that *in vitro,* TNC post-transcriptionally regulates TNF-α production of BMDMs via the micro-RNA miR-155, and this function could not be rescued through addition of extracellular TNC protein (7). This opens up the possibility that TNC plays an intracellular role

in the innate immune system—and thus its absence may affect the innate immune response even before the tissue levels of TNC protein rise in TNC-sufficient animals. Further studies into the early innate immune response during pulmonary infection, as well as the *TNC* mRNA expression in innate immune cells at this time may further illuminate the underlying mechanisms.

Interestingly, Uddin et al. (8) show a 4-fold upregulation in serum TNC protein levels, already after 4 h of LPS injection, whereas we find no change in serum TNC and an increase in pulmonary TNC protein only after 42 h. Future studies into the early timepoints of *K. pneumoniae*-induced pneumonia could reveal if there is an early, transient peak in TNC serum levels. However, in this context, it is important to note that in our model, progression of inflammation during infection occurs over a longer time and causes the host to be exposed to a mix of pathogenic proteins, compared to an endotoxemia model where a known dose of LPS is directly injected into the peritoneum (7, 8). Thus, the two models describe a different type of immune response, during which TNC may play different roles. Indeed, LPS injection provides a standardized stimulus not subjected to variation in time due to differences in bacterial growth. While mice from different genotypes were infected with the exact same inoculum for studies at each time point, differences in bacterial loads might partially obscure the role of TNC in inflammatory responses. Finally, it should be noted that most *in vivo* work on the immunomodulatory properties of TNC was done in cells and mice on a 129/Sv genetic background (7), while we used mice on a C57/BL6 genetic background; these mouse strains differ in their immune response (33). 129/Sv mice were recently reported to lack caspase-11, which is expected to impact their responsiveness to LPS (34, 35).

A recent *in vivo* study described that the absence of TNC subtly alters the morphology of the lungs and affects transforming growth factor-β and TLR4 signaling, again in the 129/Sv background (36). In our study we did not find a difference in morphological pathology caused by infection. It has recently been reviewed that the role of TNC is highly context-dependent, and while it is often associated with an enhanced immune response and increased tissue damage, TNC can also play an immune-suppressive role depending on both the inflammatory context and the splicoform expressed (37). Thus, subtle changes in pulmonary morphology and signaling could alter the microenvironment and affect bacterial proliferation and dissemination, as well as the form and function of the TNC protein. It was recently described that the biosynthesis of TNC protein, counting over 500 splicoforms, highly varies between cell types as well as the (patho)biological context (38). The different splicoforms can vary greatly in their structure, function and location—indicating that they may regulate the microenvironment in different manners depending on the cell and context in which they were produced (38). In the current manuscript, TNC protein was quantified only in the Large FN(III)C isoform. Future studies aiming to quantify specific TNC isoforms with known immunomodulatory properties may provide more detailed information on the immune modulation of TNC during infection.

While pulmonary TNC protein levels increased at the latest stages of infection, histological staining did not reveal the source of this protein. Previous studies have indicated that immune cells are able to secrete TNC, which could then enhance inflammation in an autocrine manner (4). However, TNC expression levels remained low, and seem insufficient to explain the total increase of TNC protein observed in this study. In models of viral inflammation, poly(I:C) stimulation of TLR3 induced TNC release by bronchial epithelial cells, both *in vitro* and *in vivo* (39). However, we observed an increase in TNC protein levels only during the latest stages of infection, when both tissue injury and inflammation have become systemic. While this could be due to the time required for *de novo* synthesis and secretion of TNC, an extra-pulmonary source of TNC protein cannot be excluded, since TNC can be expressed by a wide variety of cell types in response to cellular stress (1, 2). Nonetheless, this would not explain why TNC levels would increase in the pulmonary compartment, but not in circulation. Future studies may try to elucidate the exact source of TNC protein during pulmonary infection. In addition, studies from the field of virology indicate TNC can interact directly with pathogens. For example, TNC in breastmilk binds HIV-1, and therewith neutralizes it (40). In contrast, the bacterial staphylococcal superantigen-like protein binds TNC in a manner that disrupts keratinocyte function during wound healing (41). As, in the present study, the absence of TNC affects bacterial outgrowth without large modulations to the immune system, it may be of interest to study if there is a direct interaction between the bacteria and TNC protein. Alternatively, modulations to the immune system may be very local, or affect cell populations that have not been studied in this context, such as innate lymphoid cells. Future studies into the inflammatory microenvironment might address these questions. Additionally, sampling of bronchoalveolar lavage fluid could generate information on the role of TNC in cell recruitment into the airways, which in the current study was limited to examination of lung tissue slides.

The current study is the first to investigate the functional role of TNC in experimental sepsis. The model used here resembles the clinical scenario of a local bacterial infection that subsequently disseminates to distant organs and has been utilized to obtain insight into both the early protective innate immune response and the later detrimental consequences of exaggerated inflammation (13, 16, 17). While this investigation is limited to a single model and a single causative pathogen, and the absence of TNC could be compensated through different pathways, the results reported here argue against an important role for total TNC protein as a driver in the early pathogenesis of sepsis. However, the heterogeneous function of different TNC splicoforms warrants more detailed studies that address the paradoxical nature of this protein.

DATA AVAILABILITY STATEMENT

The raw data supporting the conclusions of this article will be made available by the authors, without undue reservation.

ETHICS STATEMENT

The animal study was reviewed and approved by Institutional Animal Care and Use Committee Academic Medical Center (AMC), University of Amsterdam.

AUTHOR CONTRIBUTIONS

MM: conceptualization, analysis, investigation, methodology, funding acquisition, writing–original draft, writing–review, and editing. AV: conceptualization, methodology, supervision, writing–review, and editing. BS and FU: methodology, supervision, writing–review, and editing. JR and CA: investigation, methodology, writing–review, and editing. GO: methodology, writing–review, and editing. TP: conceptualization, methodology, supervision, funding acquisition, writing–review, and editing. All authors contributed to the article and approved the submitted version.

FUNDING

This work was supported by ZonMw (www.zonmw.nl) project MKMD (grant 114024063). The sponsors were not involved in the design or conduction of the study; nor were the sponsors involved in collection, management, analysis or interpretation of the data, or preparation, review or approval of the manuscript. The decision to submit the manuscript was not dependent on the sponsors.

ACKNOWLEDGMENTS

The authors thank J. B. Daalhuisen, M. ten Brink, and R. de Beer (Center for Experimental and Molecular Medicine, Amsterdam University Medical Centers, location AMC, Amsterdam) for technical support.

SUPPLEMENTARY MATERIAL

The Supplementary Material for this article can be found online at: https://www.frontiersin.org/articles/10.3389/fimmu.2021.600979/full#supplementary-material

REFERENCES

1. Midwood KS, Chiquet M, Tucker RP, Orend G. Tenascin-C at a glance. *J Cell Sci.* (2016) 129:4321–7. doi: 10.1242/jcs.190546
2. Marzeda AM, Midwood KS. Internal affairs: tenascin-c as a clinically relevant, endogenous driver of innate immunity. *J Histochem Cytochem.* (2018) 66:289–304. doi: 10.1369/0022155418757443
3. Midwood K, Sacre S, Piccinini AM, Inglis J, Trebaul A, Chan E, et al. Tenascin-C is an endogenous activator of Toll-like receptor 4 that is essential for maintaining inflammation in arthritic joint disease. *Nat Med.* (2009) 15:774–80. doi: 10.1038/nm.1987
4. Goh FG, Piccinini AM, Krausgruber T, Udalova IA, Midwood KS. Transcriptional regulation of the endogenous danger signal tenascin-C: a novel autocrine loop in inflammation. *J Immunol.* (2010) 184:2655–62. doi: 10.4049/jimmunol.0903359
5. Deligne C, Murdamoothoo D, Gammage AN, Gschwandtner M, Erne W, Loustau T, et al. Matrix-targeting immunotherapy controls tumor growth and spread by switching macrophage phenotype. *Cancer Immunol Res.* (2020) 8:368–82. doi: 10.1158/2326-6066.Cir-19-0276
6. Spenl,é C, Loustau T, Murdamoothoo D, Erne W, Beghelli-de la Forest Divonne S, Veber R, et al. Tenascin-C orchestrates an immune-suppressive tumor microenvironment in oral squamous cell carcinoma. *Cancer Immunol Res*. (2020) 8:1122–38. doi: 10.1158/2326-6066.Cir-20-0074
7. Piccinini AM, Midwood KS. Endogenous control of immunity against infection: tenascin-C regulates TLR4-mediated inflammation via microRNA-155. *Cell Reports.* (2012) 2:914–26. doi: 10.1016/j.celrep.2012.09.005
8. Uddin MJ, Li CS, Joe Y, Chen Y, Zhang Q, Ryter SW, et al. Carbon monoxide inhibits tenascin-C mediated inflammation via IL-10 expression in a septic mouse model. *Mediators Inflamm.* (2015) 2015:613249. doi: 10.1155/2015/613249
9. Yuan W, Zhang W, Yang X, Zhou L, Hanghua Z, Xu K. Clinical significance and prognosis of serum tenascin-C in patients with sepsis. *BMC Anesthesiol.* (2018) 18:170. doi: 10.1186/s12871-018-0634-1
10. Meijer MT, Uhel F, Cremer OL, Schultz MJ, van der Poll T. Tenascin C plasma levels in critically Ill patients with or without sepsis: a multicentre observational study. *Shock*. (2019). doi: 10.1097/shk.0000000000001481
11. van der Poll T, van de Veerdonk FL, Scicluna BP, Netea MG. The immunopathology of sepsis and potential therapeutic targets. *Nat Rev Immunol.* (2017) 17:407–20. doi: 10.1038/nri.2017.36
12. Angus DC, van der Poll T. Severe Sepsis and Septic Shock. *N Engl J Med.* (2013) 369:840–51. doi: 10.1056/NEJMra1208623
13. Wieland CW, van Lieshout MHP, Hoogendijk AJ, van der Poll T. Host defence during *Klebsiella pneumonia* relies on haematopoietic-expressed Toll-like receptors 4 and 2. *Eur Resp J.* (2011) 37:848–57. doi: 10.1183/09031936.00076510
14. Standiford LR, Standiford TJ, Newstead MJ, Zeng X, Ballinger MN, Kovach MA, et al. TLR4-dependent GM-CSF protects against lung injury in Gram-negative bacterial pneumonia. *Am J Physiol Lung Cell Mol Physiol.* (2012) 302:L447–54. doi: 10.1152/ajplung.00415.2010
15. Forsberg E, Hirsch E, Frohlich L, Meyer M, Ekblom P, Aszodi A, et al. Skin wounds and severed nerves heal normally in mice lacking tenascin-C. *Proc Natl Acad Sci USA.* (1996) 93:6594–9. doi: 10.1073/pnas.93.13.6594
16. Wieland CW, Stegenga ME, Florquin S, Fantuzzi G, van der Poll T. Leptin and host defense against Gram-positive and Gram-negative pneumonia in mice. *Shock.* (2006) 25:414–9. doi: 10.1097/01.shk.0000209524.12873.da
17. de Stoppelaar SF, Claushuis TAM, Jansen MPB, Hou B, Roelofs, J. J. T. H., et al. The role of platelet MyD88 in host response during gram-negative sepsis. *J Throm Haem.* (2015) 13:1709–20. doi: 10.1111/jth.13048
18. R Core Team. *R: A Language and Environment for Statistical Computing*. Vienna: R Foundation for Statistical Computing (2020).
19. Wickham H. *ggplot2: Elegant Graphics for Data Analysis*. New York, NY: Springer-Verlag New York (2016).
20. Kuriyama N, Duarte S, Hamada T, Busuttil RW, Coito AJ. Tenascin-C: a novel mediator of hepatic ischemia and reperfusion injury. *Hepatology.* (2011) 54:2125–36. doi: 10.1002/hep.24639
21. El-Karef A, Yoshida T, Gabazza EC, Nishioka T, Inada H, Sakakura T, et al. Deficiency of tenascin-C attenuates liver fibrosis in immune-mediated chronic hepatitis in mice. *J Pathol.* (2007) 211:86–94. doi: 10.1002/path.2099
22. Ruhmann M, Piccinini AM, Kong PL, Midwood KS. Endogenous activation of adaptive immunity: tenascin-C drives interleukin-17 synthesis in murine arthritic joint disease. *Arthritis Rheum.* (2012) 64:2179–90. doi: 10.1002/art.34401

23. Momčilovi,ć M, Stamenkovi,ć V, Jovanovi,ć M, Andjus PR, Jakovčevski I, Schachner M, et al. Tenascin-C deficiency protects mice from experimental autoimmune encephalomyelitis. *J Neuroimmunol.* (2017) 302:1–6. doi: 10.1016/j.jneuroim.2016.12.001
24. Xie K, Liu Y, Hao W, Walter S, Penke B, Hartmann T, et al. Tenascin-C deficiency ameliorates Alzheimer's disease-related pathology in mice. *Neurobiol Aging.* (2013) 34:2389–98. doi: 10.1016/j.neurobiolaging.2013.04.013
25. Nakahara H, Gabazza EC, Fujimoto H, Nishii Y, D'Alessandro-Gabazza CN, Bruno NE, et al. Deficiency of tenascin C attenuates allergen-induced bronchial asthma in the mouse. *Eur J Immunol.* (2006) 36:3334–45. doi: 10.1002/eji.200636271
26. Carey WA, Taylor GD, Dean WB, Bristow JD. Tenascin-C deficiency attenuates TGF-ß-mediated fibrosis following murine lung injury. *Am J Physiol Lung Cell Mol Physiol.* (2010) 299:L785–93. doi: 10.1152/ajplung.00385.2009
27. Bhattacharyya S, Wang W, Morales-Nebreda L, Feng G, Wu M, Zhou X, et al. Tenascin-C drives persistence of organ fibrosis. *Nat Commun.* (2016) 7:11703. doi: 10.1038/ncomms11703
28. Brieland JK, Jackson C, Menzel F, Loebenberg D, Cacciapuoti A, Halpern J, et al. Cytokine networking in lungs of immunocompetent mice in response to inhaled Aspergillus fumigatus. *Infect Immun.* (2001) 69:1554–60. doi: 10.1128/iai.69.3.1554-1560.2001
29. Xu Y, Saegusa C, Schehr A, Grant S, Whitsett JA, Ikegami M. C/EBP{alpha} is required for pulmonary cytoprotection during hyperoxia. *Am J Physiol Lung Cell Mol Physiol.* (2009) 297:L286–98. doi: 10.1152/ajplung.00094.2009
30. Jacono FJ, Mayer CA, Hsieh YH, Wilson CG, Dick TE. Lung and brainstem cytokine levels are associated with breathing pattern changes in a rodent model of acute lung injury. *Respir Physiol Neurobiol.* (2011) 178:429–38. doi: 10.1016/j.resp.2011.04.022
31. Fahmi ANA, Shehatou GSG, Salem HA. Levocetirizine pretreatment mitigates lipopolysaccharide-induced lung inflammation in rats. *Biomed Res Int.* (2018) 2018:7019759. doi: 10.1155/2018/7019759
32. Cheng Q, Fang L, Feng D, Tang S, Yue S, Huang Y, et al. Memantine ameliorates pulmonary inflammation in a mice model of COPD induced by cigarette smoke combined with LPS. *Biomed Pharm.* (2019) 109:2005–13. doi: 10.1016/j.biopha.2018.11.002
33. Hoover-Plow JL, Gong Y, Shchurin A, Busuttil SJ, Schneeman TA, Hart E. Strain and model dependent differences in inflammatory cell recruitment in mice. *Inflamm Res.* (2008) 57:457–63. doi: 10.1007/s00011-008-7062-5
34. Kayagaki N, Warming S, Lamkanfi M, Vande Walle L, Louie S, Dong J, et al. Non-canonical inflammasome activation targets caspase-11. *Nature.* (2011) 479:117–21. doi: 10.1038/nature10558
35. Hagar JA, Powell DA, Aachoui Y, Ernst RK, Miao EA. Cytoplasmic LPS activates caspase-11: implications in TLR4-independent endotoxic shock. *Science.* (2013) 341:1250–3. doi: 10.1126/science.1240988
36. Gremlich S, Roth-Kleiner M, Equey L, Fytianos K, Schittny JC, Cremona TP. Tenascin-C inactivation impacts lung structure and function beyond lung development. *Sci Rep.* (2020) 10:5118. doi: 10.1038/s41598-020-61919-x
37. Matsumoto KI, Aoki H. The roles of tenascins in cardiovascular, inflammatory, and heritable connective tissue diseases. *Front Immunol.* (2020) 11:609752. doi: 10.3389/fimmu.2020.609752
38. Giblin SP, Schwenzer A, Midwood KS. Alternative splicing controls cell lineage-specific responses to endogenous innate immune triggers within the extracellular matrix. *Matrix Biol.* (2020). doi: 10.1016/j.matbio.2020.06.003
39. Mills JT, Schwenzer A, Marsh EK, Edwards MR, Sabroe I, Midwood KS, et al. Airway epithelial cells generate pro-inflammatory tenascin-C and small extracellular vesicles in response to TLR3 stimuli and rhinovirus infection. *Front Immunol.* (2019) 10:1987. doi: 10.3389/fimmu.2019.01987
40. Fouda GG, Jaeger FH, Amos JD, Ho C, Kunz EL, Anasti K, et al. Tenascin-C is an innate broad-spectrum, HIV-1-neutralizing protein in breast milk. *Proc Natl Acad Sci USA.* (2013) 110:18220–5. doi: 10.1073/pnas.1307336110
41. Itoh S, Yamaoka N, Kamoshida G, Takii T, Tsuji T, Hayashi H, et al. Staphylococcal superantigen-like protein 8 (SSL8) binds to tenascin C and inhibits tenascin C-fibronectin interaction and cell motility of keratinocytes. *Biochem Biophys Res Commun.* (2013) 433:127–32. doi: 10.1016/j.bbrc.2013.02.050

Conflict of Interest: The authors declare that the research was conducted in the absence of any commercial or financial relationships that could be construed as a potential conflict of interest.

frontiers in Immunology

ORIGINAL RESEARCH
published: 15 March 2021
doi: 10.3389/fimmu.2021.635166

Novel Human Tenascin-C Function-Blocking Camel Single Domain Nanobodies

*Sayda Dhaouadi[1], Rahma Ben Abderrazek[1], Thomas Loustau[2†], Chérine Abou-Faycal[2†], Ayoub Ksouri[1†], William Erne[2†], Devadarssen Murdamoothoo[2], Matthias Mörgelin[3], Andreas Kungl[4,5], Alain Jung[6], Sonia Ledrappier[6], Zakaria Benlasfar[1], Sandrine Bichet[7], Ruth Chiquet-Ehrismann[7‡], Ismaïl Hendaoui[7], Gertraud Orend[2] and Balkiss Bouhaouala-Zahar[1,8]**

[1] Laboratoire des Venins et Biomolécules Thérapeutiques, Institut Pasteur de Tunis, Université Tunis El Manar, Tunis, Tunisia, [2] Université Strasbourg, INSERM U1109 – The Tumor Microenvironment group, Hôpital Civil, Institut d'Hématologie et d'Immunologie, Fédération de Médecine Translationnelle de Strasbourg (FMTS), Strasbourg, France, [3] Colzyx AB, Lund, Sweden, [4] Institute of Pharmaceutical Sciences, Karl Franzens University Graz, Graz, Austria, [5] Antagonis Biotherapeutics GmbH, Graz, Austria, [6] Tumor Bank Centre Paul Strauss, Strasbourg, France, [7] Friedrich Miescher Institute for Biomedical Research, Basel, Switzerland, [8] Faculté de Médecine de Tunis, Université Tunis el Manar, Tunis, Tunisia

The extracellular matrix (ECM) molecule Tenascin-C (TNC) is well-known to promote tumor progression by multiple mechanisms. However, reliable TNC detection in tissues of tumor banks remains limited. Therefore, we generated dromedary single-domain nanobodies Nb3 and Nb4 highly specific for human TNC (hTNC) and characterized the interaction with TNC by several approaches including ELISA, western blot, isothermal fluorescence titration and negative electron microscopic imaging. Our results revealed binding of both nanobodies to distinct sequences within fibronectin type III repeats of hTNC. By immunofluroescence and immunohistochemical imaging we observed that both nanobodies detected TNC expression in PFA and paraffin embedded human tissue from ulcerative colitis, solid tumors and liver metastasis. As TNC impairs cell adhesion to fibronectin we determined whether the nanobodies abolished this TNC function. Indeed, Nb3 and Nb4 restored adhesion of tumor and mesangial cells on a fibronectin/TNC substratum. We recently showed that TNC orchestrates the immune-suppressive tumor microenvironment involving chemoretention, causing tethering of CD11c+ myeloid/dendritic cells in the stroma. Here, we document that immobilization of DC2.4 dendritic cells by a CCL21 adsorbed TNC substratum was blocked by both nanobodies. Altogether, our novel TNC specific nanobodies could offer valuable tools for detection of TNC in the clinical practice and may be useful to inhibit the immune-suppressive and other functions of TNC in cancer and other diseases.

Keywords: nanobody, extracellular matrix, tenascin-c, tumor biomarker, interaction modeling, diagnostic tool, therapeutic tool, fibronectin type III repeat

OPEN ACCESS

Edited by:
Manuela Mengozzi, Brighton and Sussex Medical School, United Kingdom

Reviewed by:
Bhalchandra Mirlekar, University of North Carolina at Chapel Hill, United States
Antonio Maurizi, University of L'Aquila, Italy

***Correspondence:**
Balkiss Bouhaouala-Zahar
balkiss.bouhaouala@fmt.utm.tn; balkiss.bouhaouala@pasteur.utm.tn

†These authors have contributed equally to this work

‡Deceased

Specialty section:
This article was submitted to Inflammation, a section of the journal Frontiers in Immunology

Received: *29 November 2020*
Accepted: *19 February 2021*
Published: *15 March 2021*

Citation:
Dhaouadi S, Ben Abderrazek R, Loustau T, Abou-Faycal C, Ksouri A, Erne W, Murdamoothoo D, Mörgelin M, Kungl A, Jung A, Ledrappier S, Benlasfar Z, Bichet S, Chiquet-Ehrismann R, Hendaoui I, Orend G and Bouhaouala-Zahar B (2021) Novel Human Tenascin-C Function-Blocking Camel Single Domain Nanobodies. Front. Immunol. 12:635166. doi: 10.3389/fimmu.2021.635166

INTRODUCTION

Tenascin-C (TNC), discovered over three decades ago, is one of the ECM molecules that is highly expressed in tumors such as breast, colorectal and gastric cancers (1–4). High TNC expression levels correlate with shortened lung metastasis-free survival in breast cancer and overall survival in glioma patients (5, 6). TNC is a large modular hexameric glycoprotein (7). Each TNC subunit displays a central oligomerization domain, followed by 14.5 epidermal growth factor (EGF)-like repeats (three disulfide bridges per EGF-repeat), 17 fibronectin type 3 (FNIII) repeats (eight constant and nine additional repeats domains that are subject to alternative splicing) and a globular fibrinogen domain (7). At physiological level, TNC is transiently expressed during organogenesis (8) and its expression is largely restricted to a few sites in the adult organism such as in some stem cell niches, tendons, and reticular fibers of lymphoid organs (9). Interestingly, high TNC levels are also found in milk of breast feeding HIV+ mothers (10). At pathological level, TNC was shown to act at multiple levels to promote tumor progression into cancer by enhancing survival, proliferation and invasion of tumor cells, driving the formation of new but poorly functional blood vessels and to corrupt anti-tumor immunity, altogether enhancing metastasis. In addition to tumors, TNC is also highly up-regulated in wound healing, fibrosis and chronic inflammation (11, 12). Recently, high TNC levels were also associated with more severe COVID19 symptoms (13). Using stochastic tumorigenesis models with engineered high and low levels of TNC it was formally proven that TNC indeed is a promoter of tumor progression (14). TNC is inducing and activating a wide range of cellular signaling pathways such as Wnt, Notch, JNK and TGFβ (14–17). TNC also acts on stromal and immune cells thereby promoting tumor angiogenesis and immune escape (18–22). The distinct spatio-temporal expression pattern of TNC is highly regulated (23). *In vitro* studies demonstrated that various stimuli such as EGF, TGFβ, b-FGF, and TNF-α, can induce expression of TNC in breast cancer stroma (5, 24). In cancerous breast tissues, EGF induced TNC via its receptor EGFR which activated oncogenic Ras signaling. Mammary tumor cells also produced transforming growth factor β1 (TGFβ1), which induced TNC expression in the surrounding stroma (25, 26). Due to defective autophagy TNC seems to be highly abundant in triple negative breast cancer (27). An overview of factors regulating TNC expression is presented in Giblin et al. (23).

Given its high expression in cancer tissues as well as its inflammation promoting actions, several efforts have been launched to specifically detect TNC *in situ* as well as to inhibit its main pathological effects. These approaches included down regulation of TNC expression with siRNA or aptamers (28–32) and the use of TNC-specific antibodies for the delivery of drugs or radiotherapy (33–35). Moreover, numerous monoclonal antibodies recognizing TNC have been developed. However, all generated tools have their intrinsic limitations and caveats. In particular, antibodies may not reach the target tissue or can raise an immune response and formalin fixation, usually used in routine pathology service, can impair epitope recognition (36, 37). Thus, better molecular tools are needed for specific and sensitive recognition and potential targeting of TNC. To overcome these limitations, recombinant nanobodies (Nbs) with their remarkable characteristics (i.e., high stability, solubility and specificity and low immunogenicity) may provide a solution (38–43).

Here, we have generated two "best in class" nanobodies (Nb3 and Nb4) that recognize specifically TNC with high affinity by ELISA and staining of formalin fixed and fresh frozen tissues, emphasizing novel opportunities for early diagnosis and potential monitoring of cancer progression. Therefore, these nanobodies may be useful for applications in routine cancer diagnosis and for future *in vivo* targeting of TNC in cancer. On the other hand, as TNC impairs cell adhesion on a fibronectin substratum, we determined whether the nanobodies abolished this function of TNC. Indeed Nb3 and Nb4 restored adhesion of human osteosarcoma and mesangial cells on the fibronectin/TNC substratum. Interestingly, we observed that immobilization of DC2.4 dendritic cells on a TNC substratum in context of CCL21 (22) was blocked by Nb3 and Nb4. Finally, by modeling the Nb/TNC interaction we determined the putative amino acid residues involved in complex formation. Altogether, we demonstrated that our two novel TNC-specific nanobodies display valuable characteristics for detection of TNC *in situ*, and revealed their potential as therapeutic tools for inhibition of immune-suppressive and other functions of TNC.

MATERIALS AND METHODS

Purification of Recombinantly Expressed hTNC

HEK 293/hTNC cells, previously stably transfected with the human TNC coding sequence (hTNC) were used to produce hTNC as previously described (44, 45). Briefly, cells were cultured in Dulbecco's Minimal Essential Medium (DMEM, catalog number 11995040 Gibco Life Technologies, Inc., Paisley, Scotland) supplemented with 10 % (v/v) fetal calf serum (FCS, catalog number 2-01F90-I BioConcept, Allschwil, Swizerland), 10.25 μg/mL G418 and 1.5 μg/mL puromycin under a 5% CO_2 atmosphere at 37°C. The recombinant hTNC was purified from the conditioned medium lacking FCS as previously described (44). Briefly, fibronectin was removed from the conditioned medium by gelatin-agarose affinity chromatography (46, 47), and the flow through was purified by a nickel affinity chromatography column (48). The purity of the protein was checked by Coomassie Blue stained 7% SDS-PAGE and by western-blot, under reducing and non-reducing conditions. The concentration of hTNC was determined by Bradford assay (catalog number 500-0006 Bio-Rad Laboratories, Hercules, CA, USA).

E. coli Strains and Vector

The phage display vector pMECS of 4,510 bp was utilized to construct the VHH library, hosted in *E. coli* strain TG1 (generously provided by Prof. Serge Muyldermans, VUB Brussel, Belgium). This phagemid vector contains a sequence encoding a PelB leader signal to secrete the cloned VHH-encoded Nb in

the periplasm with two C-terminal Hemagglutinin (HA) and 6X Histidine (6X His) tags for VHH-detection, when hosted in *E. coli* strain WK6 (49).

Generation of the Phage-Display VHH-Library

The anti-hTNC nanobody phage-display VHH-library was constructed as previously described with slight modifications (39, 49, 50). Briefly, 3 days after the last boost of antigen injection, 150 mL of anti-coagulated blood sample was collected from the jugular vein of the immunized dromedary as recently detailed (51). Peripheral blood mononuclear cells (PBMCs) were extracted by density gradient centrifugation using Lymphoprep (catalog number 17-829 LONZA, Basel, Switzerland). Subsequently, total RNA was extracted and purified. An amount of 40 μg of total RNA was reverse transcribed into cDNA with oligo-dT primer and the SuperScript II First-Strand Synthesis System for RT-PCR (catalog number 18064-014 Invitrogen, Carsbad, CA, USA). Thereafter, cDNA fragments were used as template to amplify heavy-chain IgG encoding variable domains using specific primers [CALL001 (5′-GTCCTGGCTGCTCTTCTACAAGG-3′) and CALL002 (5′-GGTACGTGCTGTTGAACTGTTCC-3′)]. The 700 bp PCR fragment (VHH-CH2 without CH1 exon, corresponding to heavy-chain antibodies) was purified from a 1% agarose gel using the Qiaquick gel extraction kit (catalog number 28704 Qiagen, Hilden, Germany). Subsequently, these sequences were used as template in a nested PCR to amplify VHH-only variable domains with nested-PCR primers [SM017 (5′-CCAGCCGGCC ATGGCTGCATGGTGCAGCTGGTGGAGTCTGG-3′) and PMCF (5′-CTAGTGCGGCCGCTGAGGAGACGGTGACCTG GGT-3′)], annealing at the Framework 1 and Framework 4 regions, including NcoI and NotI restriction sites, respectively (catalog numbers R0193T and R3189M New England Biolabs, UK, respectively). The PCR product was ligated into the pMECS phagemid vector (T4 DNA Ligase, catalog number 15224-041 Invitrogen, Carsbad, CA, USA) using a molar ratio 1:3 in favor of the inserts. Freshly prepared electro-competent *E. coli* TG1 cells were transformed by the ligated product and plated overnight (O/N) on selective Luria-Bertani Miller (LB) media supplemented with (100 μg/mL) ampicillin (catalog number 271896 Sigma Aldrich, MO, USA) and glucose 2% (catalog number G8270 Sigma Aldrich, MO, USA). Colonies were recovered from the overnight-incubated plates at 37°C. Library size was estimated by serial dilutions.

Selection of Anti-hTNC Nanobodies (Nbs)

A representative repertoire of the VHH library was displayed on phage particles using M13KO7 helper phage infection (catalog number 170-3578 New England, BioLabs, UK). Three consecutive rounds of immuno-affinity selection were carried out on 96-well microtiter plates (catalog number M5785-1CS Sigma Aldrich, MO, USA) pre-coated with hTNC (1 μg/panning, O/N at 4°C). After each round of biopanning, bound phage particles were eluted (100 mM triethylamine, pH 10.0, catalog number T0886 Sigma Aldrich, MO, USA) and immediately neutralized with 1 M Tris-HCl, pH 7.4 (catalog number CE234 GeneON, Germany) and used to infect exponentially growing TG1 *E. coli*. Following the third round of biopanning, individual colonies were randomly picked. VHH expression was induced with 1 mM isopropyl-D-thiogalactopyranoside (IPTG, catalog number 2900245 5PRIME, Germany) in the periplasmic bacterial compartment. Solid phase ELISA of each periplasmic extract was carried out on hTNC (1 μg/mL), using a mouse anti-HA antibody (catalog number H9658 Sigma Aldrich, MO, USA) and goat anti-mouse IgG-peroxidase antibody (catalog number A9044 Sigma Aldrich, MO, USA).

VHH Sequence Analysis

The VHH sequences of clones that scored positive in periplasmic extract-ELISA were determined using the Genomic platform of Institut Pasteur de Tunis facilities (ABI Prism 3100 genetic analyzer; Applied Biosystems, Foster City, CA, USA). The VHH nucleotide sequences were obtained using the ABI PRISM^{TM} BigDye Terminator v3.1 Cycle Sequencing Reaction Kit (catalog number 4337454 Applied Biosystems, USA).

Production, Purification, and Characterization of hTNC-Specific Nbs

Recombinant vectors of selected positive clones with highest binding capacity to hTNC were used to transform WK6 electrocompetent cells. Nb production was performed in shake flasks by growing each recombinant bacteria in Terrific Broth medium (TB, catalog number 743-29175 BD Biosciences, FL, USA) supplemented with ampicillin (100 μg/mL) and 0.1% glucose. The Nb periplasmic expression was subsequently induced with 1 mM IPTG, O/N at 28°C. The periplasmic extract obtained by osmotic shock was loaded on a His-Select column (NiNTA, catalog number 1018544 Qiagen, Hilden, Germany). The His-tagged hTNC-specific Nbs were eluted with 500 mM imidazole (catalog number I-0125 Sigma Aldrich, MO, USA) and an amount of 5 μg was checked on a 15% SDS gel upon-PAGE (Bio Rad), following dialysis towards PBS with a 12 kDa cut-off membrane (catalog number D9527-100FT Sigma Aldrich, MO, USA). The final yield was determined using Bradford assay (catalog number 500-0006 Bio-Rad Laboratories, Hercules, CA, USA) and the molar concentration was estimated using the theoretical extinction coefficient of the VHH sequence. The specificity of the purified anti-hTNC nanobodies was assessed by ELISA. Briefly, 0.5 μg/mL of hTNC was coated onto microtiter plates O/N at 4°C and unspecific sites were blocked with 1% (w/v) gelatin (catalog number 48723 Fluka Analytical, USA) supplemented with PBS/0.05% Tween-20 at 37°C for 2 h. Affinity-purified Nb was added (5 μg/mL, 1 h). Following a washing step, bound Nb was detected with a mouse anti-HA antibody (catalog number H9658 Sigma Aldrich, MO, USA) and revealed with a goat anti-mouse IgG-peroxydase conjugate (catalog number A9044 Sigma Aldrich, MO, USA).

Assessement of Nb Binding Affinity

The assessement of Nb binding affinity was performed using two methods: (i) indirect ELISA was carried out using a serial Nb dilution ranging from 5×10^{-7} to 5×10^{-12} M, as described above; (ii) Isothermal Fluorescence Titration

(IFT) was performed using recombinant murine TNC (mTNC, 700 nM, 0.01% Tween-20), as previously described with slight modifications (52). Briefly, the Nb concentration varied from 500 to 3,500 nM. The fluorescence emission spectra for mTNC/Nb complexes were collected and subsequently subtracted from emission spectra for mTNC and the resulting curves were then integrated. The mean values resulting from three independent measurements were plotted against the concentration of the added Nb. The resulting binding isotherms were analyzed by nonlinear regression using the program Origin (Microcal Inc., Northampton, MA, USA). The following equation describes the bimolecular association reaction, where Fi is the initial and Fmax is the maximum fluorescence values. The KD is the dissociation constant, and [mTNC] and [Nb] are the total concentrations of the mTNC and the Nb ligand, respectively:

$$F = F_{i+}F_{max}[KD + [mTNC] + [Nb] - \frac{\sqrt{(KD + [mTNC] + [Nb])^2 - 4[mTNC][Nb]}}{2[mTNC]}]$$

Negative Electron Microscopy Imaging

The Nb/ hTNC interaction complexes were visualized by negative staining and electron microscopy as previously described (53). Each Nb (20 nM) was conjugated with 5 nm colloidal gold particles (AuNPs) according to routinely used procedures (54). AuNP-Nb conjugates were incubated with hTNC (20 nM) for 30 minutes (min) at room temperature (RT) and subsequently negatively stained with 2% uranyl acetate. Specimens were assessed and electron micrographs were taken at 60 kV with a Phillips EM-410 electron microscope using imaging plates (Ditabis).

Western Blot Analysis of TNC Specific Nb

Cell lysates (40 μg) from HEK293, HEK293/hTNC, (20 μg) NT193 and subclone NT193-1 cells (generated by limited dilution), RAW267 macrophages (ATCC) and DC2.4 dendritic cells (22) in RIPA buffer (catalog number R0278 SIGMA Aldrich, MO, USA) or purified human hTNC (hTNC, 100 ng) and murine TNC (mTNC, 50 ng) were boiled at 100°C for 5 min, before loading on a 4–20% gradient SDS/PAGE gel (catalog number 456-8095 Mini-PROTEAN TGX^{TM}, Bio-Rad Laboratories, Hercules, CA, USA), then, transferred onto a PVDF membrane (catalog number 1620174 Bio-Rad Laboratories, Hercules, CA, USA). After blocking with 5% milk, PBS/0.1% Tween-20 (catalog number 1706404 Bio-Rad Laboratories, Hercules, CA, USA) the membrane was incubated O/N at 4°C with Nb3 or Nb4 (2 μg/mL). After three washing steps, the membrane was first incubated with a mouse anti-HA antibody (1 h 30 min at RT), and then with the anti-mouse IgG horseradish peroxidase conjugate diluted at 1:1,000 (catalog number AB_772209, NXA931, Amersham GE Helthcare, USA). Immunocomplexes were revealed with ECL (catalog number 28 980926 Amersham GE healthcare, USA). A prestained protein ladder (10–250 kDa, catalog number 06P-0211 Euromedex, France) was used. Mouse monoclonal antibody B28.13 (1 μg/mL), raised against hTNC was used as a positive control (55).

Immunofluroescence Assay

Glioblastoma cell xenografts had previously been generated by subcutaneous injection of 2 × 10^6 U87MG or U87MG-shTNC (TNC knockdown) cells into the flank of a nude mouse (56). Frozen (−80°C) sections were cut (7 μm thickness), fixed with 4% paraformaldehyde (PFA) (catalog number 30525-89-4 Sigma Aldrich, MO, USA) for 15 min at RT, and permeabilized with 0.5% Triton X-100 in PBS and blocked with 10% normal donkey serum (NDS) in PBS for 2 h at RT (catalog number 017-000-121 Jackson ImmunoResearch Inc, USA). Sections were co-stained with the Nb and B28.13 antibody diluted in PBS, 10% NDS O/N at 4°C, rabbit anti-HA antibody (ab236632 abcam, UK, 1:1,000 dilution, 90 min at RT) and, donkey anti-mouse antibody labeled with Texas Red fluorophore (catalog number PA1-28626 Invitrogen, Carsbad, CA, USA), and donkey anti-rabbit antibody labeled with Alexa Fluor 488 Green fluorophore (catalog number AB-2313584 Jackson Immuno Research Inc, USA) were used (1:1,000 dilution for 90 min at RT). After each antibody incubation, sections were washed five times with PBS. For staining of cell nuclei, sections were incubated with 4', 6-diamidino-2-phenylindole (DAPI, 0.2 μg/mL, catalog number 32670 Sigma Aldrich, MO, USA) for 10 min at RT. Slides were sealed with a polymerization medium (Fluorsave^{TM} Reagent, Calbiochem) underneath the coverslips and stored at 4°C until analysis. Pictures were taken with an AxioCam MRm (Zeiss) camera and Axiovision software.

Human Tumor Samples and Analysis by Immunohistochemistry

Surgically removed tongue tumors, Formalin-Fixed Paraffin-Embedded (FFPE) embedded in FFPE, were retrieved from the tumor bank of the Centre Paul Strauss (Strasbourg, France). The FFPE-embedded 17/18G percutaneous needle biopsy of an hepatic metastasis derived from carcinoma of the gall bladder (CGB) was collected as part of a study involving human participants approved by the Mongi Slim University Hospital (MSUH) Committee on Medical Ethics (La Marsa, Tunisia) and the Ethikkommission Nordwest-und Zentralschweiz (Switzerland). Informed consent was obtained for all subjects. Characteristics of patients with oral squamous cell carcinoma (OSCC), or CGB liver metastasis, are summarized in **Supplementary Table 1**.

Immunohistochemical staining of OSCC samples was performed on serial 5 μm deparaffinized tumor sections. For hTNC staining, intrinsic peroxidase was blocked by incubating sections with 3% hydrogen peroxide for 15 min and antigen retrieval was performed in Sodium Citrate (10 mM) buffer pH 6.0 at 95°C. Sections were blocked in 5% goat serum for 1 h, then incubated ON/4°C with rabbit anti-TNC antibody (#19011, Millipore, 1 μg/mL) or anti-hTNC Nb (2 μg/mL). After PBS rinsing, sections were incubated with biotinylated goat anti-rabbit or goat anti-lama antibodies (1 h at RT) then avidin-biotin (PK-4000, VECTASTAIN ABC Kit, Vector Lab, California, USA). Staining was revealed with 3, 3 ′-Diaminobenzidine developing solution (SK-4100, DAB, Vector Lab, California, USA) then sections were counterstained with hematoxylin.

After embedding in aqueous mounting medium, sections were examined using a Zeiss Axio Imager Z2 microscope. Pictures were taken with an AxioCam MRm (Zeiss, Axiovision) camera. The image acquisition setting (microscope, magnification, light intensity, exposure time) was kept constant per experiment and in between conditions. The origin of the tumor sample, patient gender, TNM stage, presence of metastasis and sampling date are depicted in **Supplementary Table 1**.

Immunohistochemical stainings of the CGB liver metastasis sample were performed on a Ventana Discovery Ultra instrument (Roche Diagnostics). The procedure RUO Discovery Universal was used with 40 min CC1 pre-treatment and anti-TNC B28.13 (1:5,000), Nb3 (1:100) or Nb4 (1:50) were applied manually and incubated for 1 h at 37°C. For Nb3 and Nb4, a rabbit anti-HA antibody (C29F4, Cell Signaling), used as a linker to detect the nanobodies, was applied manually (1:200) and incubated for 1 h at 37°C. Then, an anti-mouse antibody used for B28.13 (ImmPRESS reagent kit peroxidase anti-mouse Ig MP-7402, Vector Laboratories) or an anti-rabbit antibody used for Nb3 and Nb4 (ImmPRESS reagent kit peroxidase anti-rabbit Ig MP-7401, Vector Laboratories) were applied manually (200 µl) and incubated for 32 min at 37°C. Finally, the ChromoMap DAB kit (Roche Diagnostics) was used for detection and slides were counterstained with Hematoxylin II and Bluing Reagent (Roche Diagnostics) for 8 min.

Boyden Chamber Transwell Chemoretention Assay

Boyden chamber transwell chemoretention assay of DC2.4 dendritic cells toward CCL21 was carried out as described previously (22). The bottom of the chamber was filled with DMEM containing human CCL21 (200 ng/mL, catalog number 366-6C-025 R&D Systems, Minneappolis, USA). The lower surface of the transwells was coated with purified horse fibronectin (FN) (37), rat collagen type I (Col I, catalog number 354236 BD Biosciences, FL, USA) or hTNC at a final concentration of 1 $\mu g/cm^2$ and incubated O/N with blocking solution alone or with the Nb, respectively. DC2.4 (5×10^5) cells resuspended in 150 µL of 1% FBS-complemented DMEM were placed into the top chamber of the transwell system. After 5 h of incubation at 37°C in 5% CO_2, cells on the lower side of the insert were fixed with PFA and stained with DAPI before cell counting.

Adhesion Assay

The adhesion assay was carried out on human KRIB osteosarcoma and human MES mesangial cells. Precisely, 96-well plates were coated with 1 $\mu g/cm^2$ FN, hTNC or with FN and hTNC together. Nbs were added at 500 nM after the coating for 1 h at 37°C. Plates were rinsed with PBS and the non-coated plastic surface was blocked with 1% BSA for 1 h. After blocking, KRIB osteosarcoma and MES were plated for 3 and 2 h, respectively, at 37°C in a humidified atmosphere with 5% CO_2. After incubation, non adherent cells were removed by PBS washing and spread cells were stained with cristal violet and counted.

Statistical Analysis

Statistical differences were analyzed by a two-way ANOVA test or a Kruskal-Wallis t-test, Student's test and Dunn's post-test. Statistical analyses were performed using the GraphPad Prism software. p-values < 0.05 or < 0.005 were considered as statistically significant. Data are expressed as the mean ± SEM.

Structural Modeling of the Nb – TNC Interaction

For the Nb - TNC structral interaction modeling the Rosetta Antibody application (57, 58) from "ROSETTA 3.8"[1] was used. Selection of the top 10 Model was done according to Rosetta scoring based on system energy. Structural information about the 5th TNC fibronectin type III repeat (TN5) was extracted from the protein data bank deposited under the PDB code: 1TEN. The TN5 structure was refined using the ROSETTA relax application which then was used to map potential interaction sites in the selected Nb through the ZDOCK docking tool, version 3.0.2 (59). Structure and complex interactions were then visualized via the molecular visualization PyMOL software (60).

RESULTS

Generation of an Immune VHH Library to Produce hTNC- Specific Nanobodies

An immune response against hTNC had been elicited in the immunized dromedary as previously described (51). From PBMC, total RNA was extracted and cDNA was prepared. This cDNA was used as template to perform the first PCR using primers CALL001 and CALL002 specific for the variable domains of the heavy-chain isotypes (IgG1, IgG2, and IgG3), subsequently leading to the co-amplification of VH and VHH coding domains (**Supplementary Figure 1A**). As expected, because of the presence of CH1 domain in conventional antibodies (IgG1) and different hinge size in non-conventional antibodies (HCAbs), three PCR products were observed by agarose gel electrophoresis: the 900, 790, and 720 bp fragments corresponding to the VH-CH1-Hinge-CH2 of the IgG1 and the VHH-Hinge-CH2 exons of the IgG2 and IgG3, respectively (**Supplementary Figure 1A**). Selective only-VHH fragments were successfully amplified using nested PCR specific-primers and cloned in pMECS phagemid (see above). The obtained hTNC-specific VHH library was estimated to contain approximately 3×10^6 CFU/mL independent clones. The insert size of 19 randomly chosen clones was investigated by PCR. The library insertion rate with a VHH insert of the expected size was 78.94% (**Supplementary Figure 1D**).

A representative aliquot of the TG1 cells harboring the VHH antibody repertoire was rescued with the M13KO7 helper phage to produce phage particles expressing the nanobodies. Following three rounds of phage display selection on solid-phase coated hTNC, enrichment for hTNC-specific phage particles was observed from the first round of panning onwards (**Supplementary Table 2**). Twenty-five periplasmic extracts

[1]The Rosetta software, https://www.rosettacommons.org/software/license-and-download

selected from randomly picked individual clones of biopanning rounds were checked by ELISA. Only clones scoring positively by ELISA without binding to unspecific proteins (AahI and BotI toxins, respectively) were retained (**Supplementary Figure 1E**). In total, eight recombinant clones displaying highest recognition and binding to the hTNC from the sequenced VHHs were selected. Two recombinant clones displayed identical amino-acid sequences (Nb3 and Nb5). The Nb3, Nb4, and Nb29 were selected for further investigation. As illustrated in **Figure 1A**, all hTNC-specific Nb sequences (Nb3, Nb4, and Nb29) exhibit the VHH hallmark amino acid residues in the framework-2 region (FR2 Phe42, Glu49, Arg50, and Gly52) and the conserved Trp at position 118 of the anchoring region. According to their common CDR1 sequence, Nb3 and Nb4 are most likely derived from the same V-D-J rearrangement and share the same B-cell progenitor (40). The difference in CDR3 length of the Nb29 corresponding sequence is remarkable (21 amino-acid residues). Interestingly, the Nb29 has a total of six cysteins (at positions 23, 33, 103, 108, 117, and 119) and therefore harbors two additional interloop disulfide bonds, in addition to the FR1/FR3 conventional ones (Cys23/Cys103). Nevertheless, because of its moderate binding to hTNC and low yield, Nb29 was not further investigated here.

The CDR3 residue length within the Nb3 and Nb4 sequences (17 amino-acid residues) was identical and no difference was noticed. The only divergence in the Nb3 and Nb4 sequences was observed at position 2 (Leu substituted by Val in FR1), at position 52 (Gly substituted by Ala in CDR2) and at position 92 (Asp substituted by Gly in FR3), respectively, suggesting an interaction with a common epitope on TNC.

Production and Purification of hTNC Specific Nanobodies

Only clones that scored highly positive (**Supplementary Figure 1E**) were further used for flask production and Immobilized Metal Affinity Chromatography purification (IMAC), according to Hmila et al. (61). Briefly, production of each soluble anti-hTNC Nb was accomplished by transformation of *E. coli* WK6 cells with the corresponding recombinant phagemid. The amber stop codon located between the VHH insert and the gene III within the pMECS phagemid, resulted in expression of the Nb as soluble protein in the periplasm compartment of *E. coli*, leading to rapid IMAC purification of the Nb. As expected, the Coomassie-stained SDS/PAGE gel revealed the apparent molecular weight of 14 kDa (**Figure 1B**). The Nb3 and Nb4 production yields were estimated ranging from 0.6 to 0.8 mg/L, respectively, when flask cultured in TB medium. No bands indicative of contaminants or Nb degradation were detected.

Nb4 (5 μg/mL) displayed a higher ELISA binding titer toward hTNC (0.5 μg/mL, OD_{492nm} = 1.526), compared to Nb3 (5 μg/mL, OD_{492nm} = 0.913) and to the irrelevant nanobody (anti-BotI toxin nanobody, 5 μg/mL, OD_{492nm} = 0,118) (**Figure 1C**, **Supplementary Figure 2**). Furthermore, immunoblotting assays revealed that both nanobodies showed a specific recognition of not only the purified hTNC (100 ng) but also of TNC in the supernatant from HEK293/TNC cells. Parental HEK293 cells did not express TNC and also showed no signal with Nb3 nor Nb4 (**Figure 1D**).

As human and murine TNC are highly conserved (62) we used Nb3 and Nb4 for detection of murine TNC by western blot. Whereas, the monoclonal anti-TNC antibody MTn12 recognized recombinant mTNC expressed in HEK293/TNC cells indicated by the appearance of multiple bands, Nb3 and Nb4 did not recognize these TNC species (**Figure 1E**). There were several higher molecular weight bands of TNC recognized by MTn12 in recombinant TNC, NT193, and RAW267 cells. However, one or more of these bands at 250 kDa were well-recognized by Nb3 and Nb4 in NT193 cells but poorly in HEK293 and RAW267 cells. On the contrary TNC proteoforms (between 150 and 250 kDa) that were recognized by Nb3 and Nb4 in NT193-1, RAW267 and DC2.4 cells were not recognized by MTn12 (**Figure 1E**). There are several explanations for this result. First it is conceivable that the epitope recognized by MTn12 (which is not known) is different to that recognized by Nb3 and Nb4. Second Nb3 and Nb4 recognize a particular TNC conformation as epitope which is lost upon denaturation by SDS and boiling. Third, glycosylation may have an impact on the conformation of the epitope recognized by Nb3 and Nb4. Recently it was shown that N-glycosylation in TNC (in particular within TN5) impacted binding of the envelope protein of HIV (10). Apparently the conformation of the epitope recognized by Nb3 and Nb4 is still available in NT193 and the other murine cells despite denaturation as seen in **Figure 1E**. These bands are specific for TNC since unspecific anti-HA bands are below 85 kDa (63). In conclusion, Nb3 and Nb4 may recognize a conformational epitope in TNC that could be sensitive to denaturation and/or N-glycosylation which has to be further investigated in the future.

Assessment of Nb3 and Nb4 Affinities for TNC by Isothermal Fluorescence Titration

By Isothermal Fluorescence Titration (IFT), we investigated the binding of Nb3 or Nb4 to fluorescently tagged mTNC until signal saturation and determined the dissociation constant (K_D) as 711 $\times$ 10^{-9} M (Nb3) and 537 $\times$ 10^{-9} M (Nb4) that indicates a robust interaction (**Figure 1F**). In addition, ELISA assays were performed with Nb molar concentrations ranging from 5 $\times$ 10^{-7} to 5 $\times$ 10^{-12} M and revealed specific binding with a 50% Effective Concentration (EC_{50}) of both Nb3 and Nb4 binding to hTNC at 10 and 5 nM, respectively, again revealing a strong interaction (**Figure 1G**).

Detection of the Nanobody Binding Site in TNC by Negative Electron Microscopy

We investigated the location of the antigenic epitope in hTNC by negative electron microscopy where the nanobodies were coupled to gold beads. Upon incubation of hTNC with gold beads-bound nanobodies, we detected the gold particles along the length of the hTNC monomers and quantified them (**Figure 2A**). We observed a high number of Nb3 and Nb4 binding in the middle of the hTNC monomer resembling binding of several soluble factors in the fifth fibronectin type

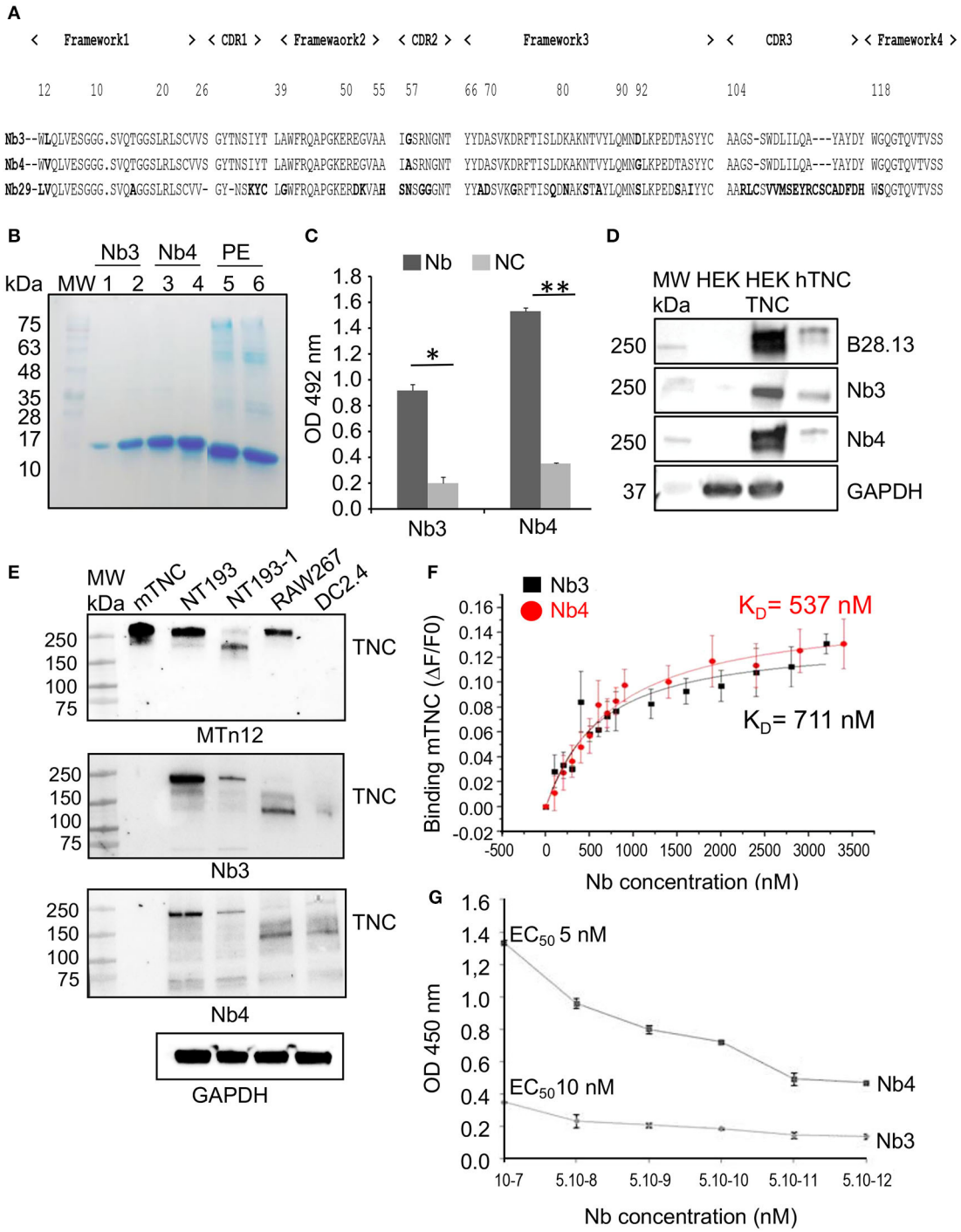

FIGURE 1 | Specificity of the purified nanobodies for hTNC **(A)** Comparative alignment of amino acid sequences of nanobodies Nb3, Nb4, and Nb29 showing four amino acid hallmark changes at positions F42, E49, R50, and G52 according to the IMGT Scientific chart analysis for the V-Domain. Positioning of CDRs1-3 and Frameworks 1–4 are indicated. **(B)** SDS-PAGE analysis of the purified nanobodies Nb3 and Nb4. The nanobodies were expressed in bacteria and purified bacterial lysate was separated on a 15 % SDS-PAGE gel that was stained with Coomassie blue. Lanes represent MW: Prestained molecular weight marker, size indicated in kDa. 1, 2: Nb3 eluates 1 and 2. 3, 4: Nb4 eluates 1 and 2. 5: Purified periplasmic extract (PE) from Nb3 after induction. 6: Purified periplasmic extract from Nb4 after induction. Nb3 and Nb4 are visible at 15 kDa, the respective molecular weight of a nanobody. **(C)** Binding specificity assessement of Nb3 and Nb4 An amount of 50 ng hTNC was coated onto microtiter plates, and 500 ng (100 µl) nanobodies were added. After incubation with a mouse anti-HA antibody and then anti-mouse HRP, absorbance at 492 nm was measured by an ELISA reader. NC, no coating. Values were the means of 3 independent experiments. Mean ± SEM, $*p < 0.05$, $**p < 0.01$, Student's t-test. **(D)** Western blot analysis of Nb3 and Nb4 An amount of 40 µg of total cell lysate from parental HEK293 (HEK) (devoid of TNC) and HEK:TNC

(Continued)

FIGURE 1 | (engineered to express hTNC) and 100 ng of purified hTNC were analyzed by Western blot for detection of TNC by B28.13 (monoclonal anti-hTNC antibody) or Nb3 and Nb4 (2 μg/mL). GAPDH was used as loading control. Representative result, $n = 3$. **(E)** Western blot of 50 ng of purified mTNC (22) and 20 μg of total cell lysate of the indicated murine cells with GAPDH as loading control. Detection of TNC with the MTn12 antibody or Nb3 and Nb4, respectively. Representative result, $n = 2$. **(F)** Determination of the effective concentration (EC50) at which 50% of epitopes in hTNC are occupied by Nb3 (*diamonds*) and Nb4 (*squares*), respectively. The experiment was done in triplicates. Mean ± SEM. $^*p < 0.05$, Two-way ANOVA test. **(G)** Binding affinities of Nb3 and Nb4 for recombinant mTNC as measured by isothermal fluorescence titration. The experiment was done three times.

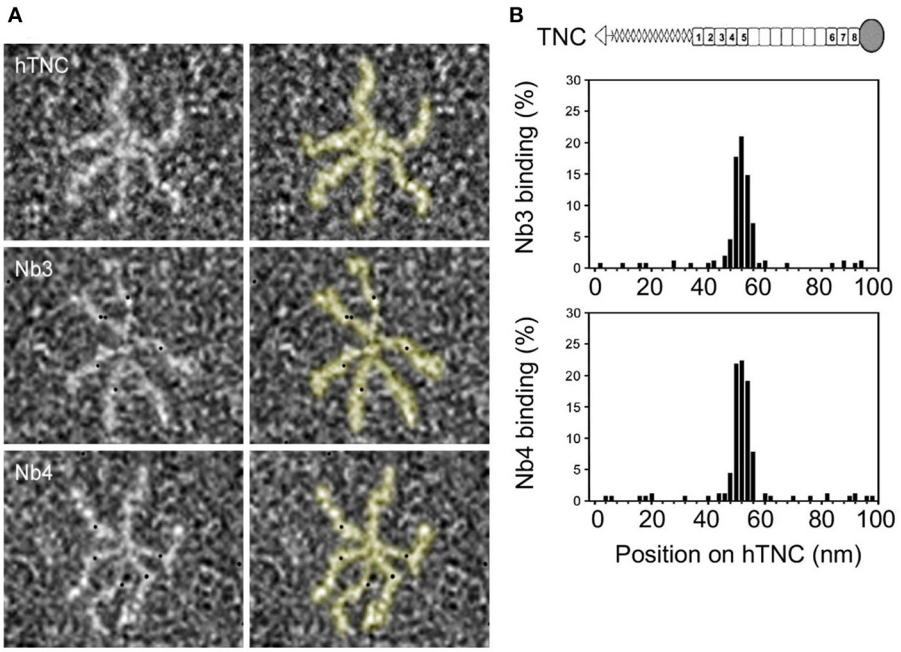

FIGURE 2 | Identification of interaction sites of Nb3 and Nb4 in hTNC. **(A)** Binding of gold-labeled Nb3 and Nb4 to hTNC was determined by negative staining and transmission electron microscopy. The hTNC molecule in the absence or presence of Nb3 or Nb4 is depicted. Black dots represent binding sites for Nb3 and Nb4 in hTNC. **(B)** Quantification of Nb3 and Nb4 binding according to the position (nm) on TNC Representation of a TNC monomer with oligomerization domain (triangle) to form hexamers as seen in **(A)**, FNIII repeats (gray boxes, constant domains, white boxes, alternative domains) and fibrinogen like domain (circle). Representative result of three independent experiments, displaying the quantification of 500 micrographs.

III repeat (FNIII) in TNC [TN5 (64)]. Nb3 and Nb4 showed a similar binding pattern suggesting that both nanobodies recognize the same or overlapping epitopes in hTNC, presumably TN5 (**Figure 2B**).

Nanobodies Nb3 and Nb4 Recognize hTNC in Fresh Frozen and Paraffin-Embedded Human Tissues

Next, we investigated whether Nb3 and Nb4 recognized hTNC in FFPA tissues. Therefore, we stained human colon tissue from an ulcerative colitis (UC) patient and noticed a staining pattern that resembled published TNC expression in this tissue (65–67), (**Supplementary Figure 3A**). We also stained tissue from human tongue tumors (OSCC) with Nb3 and Nb4 and with a commercial rabbit polyclonal anti-TNC antibody on an adjacent section, and observed similar staining patterns for TNC reminiscent of tumor matrix tracks (TMT) that have previously been described [**Figure 3A**, (22)]. We also stained a liver metastasis from a patient with a carcinoma of the gall bladder (CGB) (**Supplementary Table 1**) with Nb3 and Nb4 and observed a strong immunoreactivity of the stroma, similar to the staining observed with the anti-TNC antibody B28.13 (**Figure 3B**). This stromal staining resembled that of TNC expression in biliary tract cancers, including CGB liver metastasis as seen by conventional IHC (68).

Next we addressed recognition of murine and human TNC in tissues by IHC and IF. Therefore, we stained U87MG glioblastoma xenografted tumors where it was previously noticed that human TNC was largely more abundant than murine TNC by IHC and IF (56). We observed a fibrillar TNC signal in the U87MG tumors by IHC with Nb3 and Nb4 (**Figure 3C**) that overlapped with that of the B28.13 antibody signal, confirming specificity of the nanobodies for TNC (**Figure 3D**). As the U87MG tumors also express murine TNC but at much lower abundance (56), we stained U87MG tumors with a knockdown for human TNC in the grafted tumor cells and did not see a signal, suggesting that Nb3 and Nb4 at the chosen dilution recognize predominantly human TNC (**Figure 3E**).

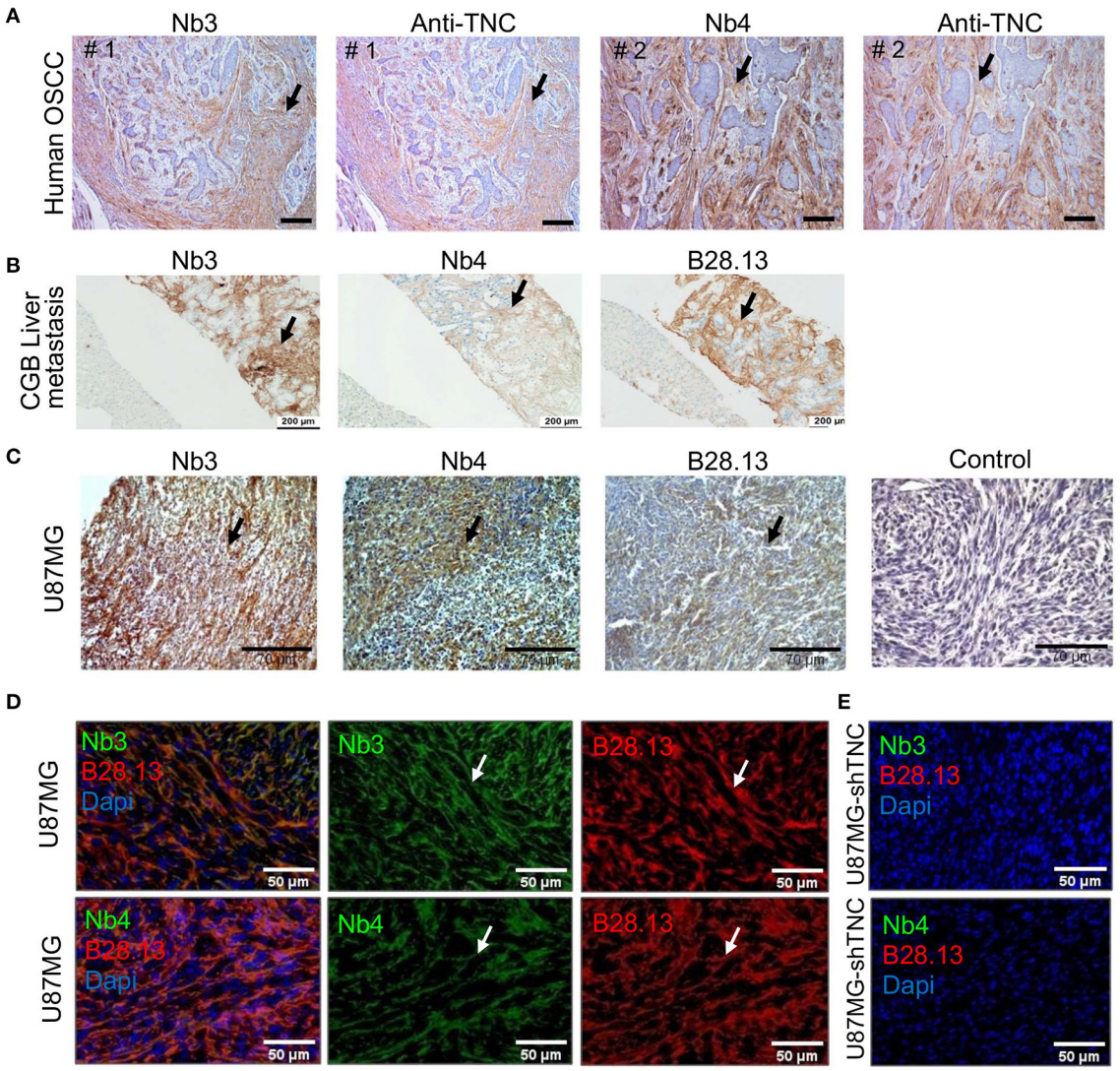

FIGURE 3 | Detection of TNC in tissues by Nb3 and Nb4 IHC **(A–C)** and IF analysis **(D,E)** with Nb3 and Nb4 **(A–E)**, B28-13 **(B–E)** and a polyclonal anti-TNC antibody (Anti-TNC) **(A)**. **(A)** Human OSCC (FFPE), **(B)** liver metastasis from a gall bladder carcinoma (FFPE), **(C–E)** U87MG tumors, **(C)** FFPE, **(D,E)** PFA fixed tissue. Scale bar, 100 µm **(A)**, 200 µm **(B)**, 70 µm **(C)** and 50 µm **(D,E)**.

Nanobody Nb4 Counteracts the Anti-adhesive Properties of TNC on a FN/TNC Substratum

By using human osteosarcoma KRIB cells, we investigated whether Nb4 had an impact on cell rounding by TNC on a FN/TNC substratum. Previously, we had shown that cells are inhibited by TNC to spread on a combined FN/TNC substratum since TNC competed syndecan-4 binding to FN (44, 69). Here, we plated KRIB cells on FN, FN/TNC and TNC, respectively with or without Nb4. By staining with pholloidin (polymerized actin) and anti-vinculin (focal adhesions), we confirmed cell spreading on FN and cell rounding on FN/TNC and TNC, respectively. While cells had some actin stress fibers and focal adhesions on FN, addition of Nb4 did not change that (**Figures 4A,B**, **Supplementary Figure 4**). However, upon addition of Nb4 to cells plated on FN/TNC we observed that cells spread in a Nb4 dose dependent manner with actin stress fibers and focal adhesions that looked similar to those in cells plated on FN (**Figures 4A,B**, **Supplementary Figure 4**). As in KRIB cells, both Nb3 and Nb4 restored adhesion of mesangial cells (MES) on a FN/TNC substratum suggesting that Nb3 and Nb4 blocked binding of TNC to FN (**Figures 4C,D**).

Nanobodies Nb3 and Nb4 Abolished DC2.4 Chemoretention by TNC/CCL21

Previously, we had shown that in combination with CCL21 TNC immobilized dendritic DC2.4 cells (22). Here we used a Boyden chamber transwell migration assay to investigate whether Nb3

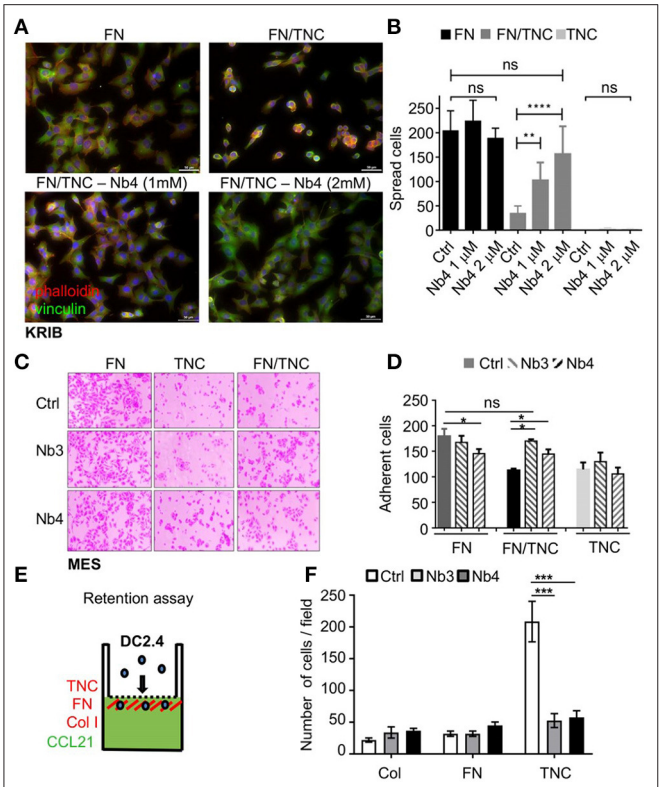

FIGURE 4 | Nb3 and Nb4 interfere with TNC functions. **(A,B)** Cell spreading assay followed by quantification of KRIB cells plated on FN, a mixture of FN and hTNC (top panels) or a mixture of FN and hTNC incubated with Nb4 (bottom panels). After 2 h, the KRIB cells were fixed and stained with phalloidin (red) to detect polymerized actin, or an anti-vinculin antibody (green) to detect focal adhesion complexes and the nuclear marker DAPI (blue). Higher magnifications are shown in **Supplementary Figure 4**. Spread cells were counted **(B)**. $N = 3$ experiments, $n = 2$ wells. $^{**}p < 0.01$, $^{***}p < 0.001$. Two-way ANOVA test. **(C,D)** Adhesion of mesangial cells (MES) 2 h after plating on FN, TNC or FN/TNC without (Ctrl) or with Nb3 and Nb4, respectively followed by quantification **(D)**. $N = 3$ experiments, $n = 2$ wells. $^{*}p < 0.05$. Two-way ANOVA test. **(E)** Schematic representation of the Boyden chamber transwell chemoretention assay with DC2.4 toward CCL21 in the bottom well. The lower surface of the insert was coated with FN, Col I, or hTNC, respectively. **(F)** Quantification of DC2.4 cells on the coated surfaces upon migration toward CCL21 (5 h after plating) and pretreatment or not (Ctrl) with Nb3 and Nb4, respectively. Note that Nb3 and Nb4 significantly abolished DC2.4 cell retention by TNC/CCL21. $N = 2$ experiments, $n = 4$ wells. Mean ± SEM, Kruskal-Wallis test and Dunn's post-test. $^{***}p < 0.005$, $^{****}p < 0.0001$.

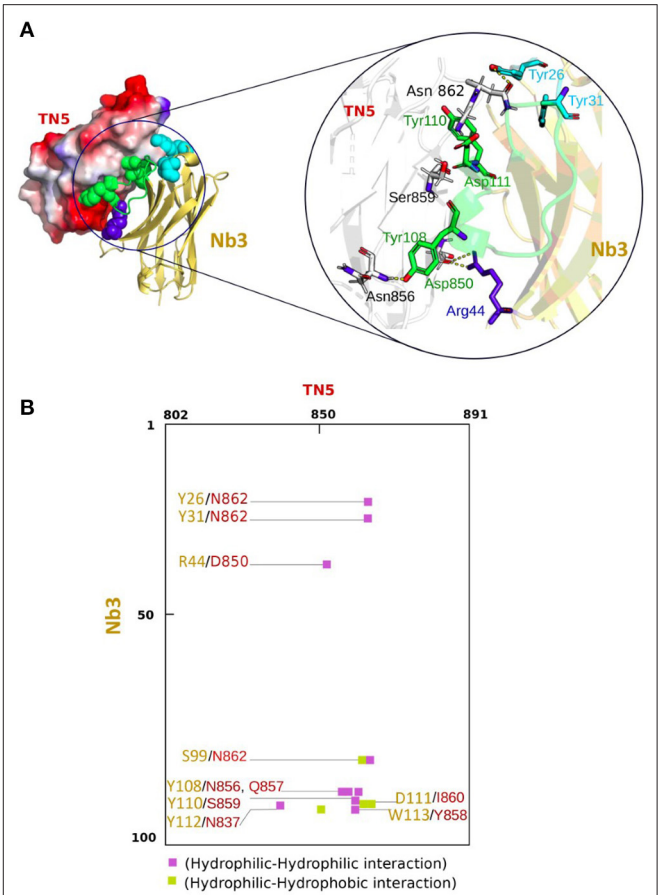

FIGURE 5 | Modeling of the three dimensional topology of the Nb3/TN5 interaction complex and information about amino acid contacts. **(A)** Model of the Nb3/TN5 complex TN5 (red) and Nb3 (yellow) are shown with contacting amino acids in blue and green (left). Magnification (circle) represents a spatial view on identified amino acid residues (three letter code, position in TN5 and Nb3 indicated by a number, respectively) generating relevant hydrophobic, electrostatic and H-bond interactions (right). TN5 is represented as white surface with electrostatic surface coloring. Nb3 is presented in transparent yellow. The most implicated amino acid residues forming H-bonds are labeled with a dashed yellow line. **(B)** Contact interaction map of TN5 with Nb3 representing amino acids 802–891 in TNC (top) and amino acids 1–100 in Nb3 (left). Violet (hydrophilic-hydrophilic), green (hydrophobic-hydrophobic) and yellow (hydrophilic-hydropholic) boxes represent the properties of the interaction.

and Nb4 impacted chemoretention by TNC. Therefore, we coated the lower surface of the insert with FN, collagen I (ColI) or TNC and added Nb3 or Nb4, respectively, and measured DC2.4 cell migration toward CCL21 placed in the lower chamber. We measured cells adhering on the coated surfaces in the presence or absence of the nanobodies and observed first a high number of cells being tethered on TNC but not the other coatings. Second, we noticed that the number of adherent cells dropped on TNC to that of the other coatings upon addition of Nb3 and Nb4 whereas no difference was seen with the other matrix coatings (**Figures 4E,F**).

Three Dimensional Topology of the Nb3/TN5 Interaction Complex

We adopted a computational structure analysis strategy in order to identify amino acid residues involved in the interaction of Nb3 with TN5. The 1f2x (chain L), 3l95 (chain B), 5ocl (chain G) and 5vak (chain B) structures were used as principal template for Nb3-frameworks, CDR1, CDR2 and CDR3, respectively. The number of generated Nb3 models was set to 1,000. The top ten model best scores, ranked according to an energy-based scoring were selected from 10 clusters composed of 100 structures per cluster then visually double checked (to detect structural anomalies) using the molecular visualization PyMOL software.

The TN5 structure (1TEN) was included in the Nb3 molecular docking simulation. The positively and negatively charged residues are in blue and red, respectively, whereas the neutral side-chains are indicated in white, showing clearly separated charges on the TN5 surface. Using the docking approach, we generated the top ten possible binding sites, ranked according to an energy-based scoring and filtered them to get an unique complex presenting the best molecular orientation with the most stable position (**Figure 5A**). In order to assess the main amino acid residues involved in the molecular Nb3-TN5 interaction, we used the COCOMAPS (bioCOmplexes COntact MAPS) web application server. A predicted intermolecular contact map of the Nb3-TN5 complex is illustrated in **Figure 5B** with a cut-off of 3 Å, highlighting the most crucial residues mainly implicated in the complex interaction. The predicted binding site residues in TN5 are as follow: N862, D850, N856-Q857, S859, I860, N837, Y858 interacting with Nb3 at position Y26, Y31, R44, S99, Y108, Y110, D111, Y112, W113. Interestingly, the CDR2 and CDR3 are predicted to dominate the interaction with TN5. Details of crucial residues involved in H bounds as proton donors or acceptors are described in **Supplementary Table 3**.

DISCUSSION

The matrix, a highly abundant component of tumors, could be considered as a good tumor biomarker as matrix is often more stable than e.g., antigens expressed by tumor cells (70, 71). Furthermore, matrix seems to be accessible to antibodies and antibody derivatives in therapy (33). Detection of abundant tumor specific matrix could be useful for monitoring tumors and their progression. In this context, TNC is an intriguing matrix molecule, as it is highly expressed not only in tumors, but also in fibrosis and chronic inflammation often correlating with disease progression (4, 11, 72, 73). Hence, detection of high TNC levels in tissues and body fluids of patients with e.g., cancer or rheumatoid arthritis is a promising strategy (21, 22, 62). The large isoform of TNC, highly abundant in cancer tissue, may even be a good address for the delivery of drugs into the tumor (1). In particular, TNC-specific antibodies were shown to be a means for tumor targeting. In the past, several TNC-specific monoclonal antibodies were developed as well as aptamers and antibody fragments (scFv) that are currently undergoing clinical evaluation (37, 74–78). The anti-human TNC G11 antibody (79) was used for targeting TNC in glioma xenografts upon coupling with ^{18}F-fluorodeoxyglucose (37). Phase I and II clinical trials were performed with the F16 anti-TNC antibody in glioma patients (80, 81), breast cancer (82, 83) and Hodgkin's lymphoma (35). Coupling the TNC specific F16 antibody to IL-2 (Teleukin®) was used to deliver IL-2 into the cancer tissue (82, 84). Moreover, since 2013, a phase II clinical trial using Teleukin® labeled with ^{131}Iodine is in progress in melanoma patients (EudraCT 2012-004018-33) (35). These antibodies did not show any adverse effects and may be useful for tumor imaging. One needs to await the outcome of the clinical studies to see whether targeting TNC with these antibodies can also reduce tumor growth and potentially tumor progression (78).

Staining of FFPE tissues remains a challenge in the clinical practice due to frequent masking of epitopes. Also access of antibodies to their epitopes used in functionalized antibody assisted drug delivery remains a challenge. Due to their intrinsic characteristics, such as small size, high stability and good specificity, nanobodies constitute promising agents to overcome some of these limitations (85). Indeed, in a recently patented study covering another group of TNC specific nanobodies (86, 87), the authors demonstrated that the radioactive coupled nanobody ^{64}Cu-NJTs detected micrometastasis in tumor mice by life imaging. These results promise that TNC specific nanobodies could be used for delivery of therapeutic compounds into tumors or into other tissues with high TNC content.

In this report we aimed at the development of nanobodies directed against hTNC to detect TNC in FFPE tissues and to block TNC functions. We purified recombinant TNC of human origin and used this molecule to elicit a potent immune response in the dromedary. A substantial proportion of polyclonal heavy chain IgG subclasses bound to TNC and recognized TNC by IF staining in tumor tissue (51). This encouraged us to generate nanobodies. A VHH library from this dromedary was generated that met the required quality control standards (88, 89) and allowed us to isolate nanobodies that specifically recognized TNC. Although, the titer of dromedary antibodies against hTNC was significantly high, the *in vitro* selection of anti-hTNC binders from this specific VHH library allowed us to retrieve only eight binders after three rounds of bio-panning. A possible explanation of this limited sequence diversity of binders might be attributed to our screening condition as we immobilized hTNC which potentially has masked the epitopes or prevented nanobodies to bind due to sterical hindrance. To retrieve nanobodies recognizing additional TNC sequences, future biopanning could be done by using soluble TNC.

In this paper, we have generated eight human TNC specific nanobodies and the two best in class candidates (Nb3, Nb4) in terms of binding strength and specificity were further characterized in more detail. The amino acid sequences of the three TNC-specific Nb revealed a high degree of identity with human VH sequences of family III; however the VHH imprints were clearly present (90, 91).

Nb3 and Nb4 recognized specifically TNC by immunoblotting, ELISA and negative EM imaging and by staining of PFA and FFPE fixed human tissues. We identified binding of Nb3 and Nb4 in the center of the TNC monomer around TN5 which may be a particularly exposed site in TNC as TN5 was shown to bind several soluble factors (22, 64). Future studies have to address whether TN5 is particular in raising an immune response. It is interesting to note N-glycosylation sites in TN5 and that N-glycosylation is important for the envelope proteins of HIV to bind TNC (10). In this context it will be interesting to learn more about the antigenic epitope properties of the NJTs nanobodies and to see whether the epitopes are different.

Both nanobodies exhibited a TNC specific staining in all tested tissues confirming the aptitude of Nb3 and Nb4 to recognize native TNC *in situ*. As our study is limited to a few examples as proof of concept, more stainings of FFPE embedded tissues have

to be done in the future. It is important to compare Nb3 and Nb4 stainings with established anti-TNC antibody staining protocols to determine whether staining patterns are similar or different. *In silico*, 3D modeling of the interaction of Nb3 with TN5 revealed the potential contribution of CDR2 and CDR3 in the interaction with critical hydrophobic amino acid residues in TN5. Future site directed mutagenesis experiments have to evaluate the predicted nanobody-TN5 interaction sites in particular taking into account a potential role of N-glycosylation.

The Nb3 and Nb4 nanobodies may be suitable for a sandwich ELISA assay. There is a need for a robust ELISA assay to detect TNC in body fluids such as blood and urine to be used as parameters for earlier diagnosis of diseases with high TNC levels (11, 12, 92, 93). Only few commercial ELISA kits are available. A frequently used one recognizes the FNIIIB domain that is not present in all TNC proteoforms and thus may miss TNC species lacking this domain (94). Thus, an advantage of using Nb3 and Nb4 for ELISA is that they recognize an epitope in the constant FNIII domains (likely in TN5) thereby potentially detecting more TNC isoforms.

To respond to the need of high Nb3 and Nb4 yields for applications mentioned above the expression conditions have to be optimized in the future as the production yields of Nb3 and Nb4 varied and were not very high.

Finally, we observed that Nb3 and Nb4 recognized not only human TNC but also murine TNC as seen by immunoblotting and IFT with a K_D value in the three digits nanomolar range comparable to other molecules binding TNC [TGF-β1, K_D = 20.3 nM (64); CCL21, K_D = 58 nM (22); FN III13, K_D =128 nM (44)]. Therefore, these nanobodies may be useful for preclinical models assessing tumor growth by life imaging, delivery of drugs into tissues with high TNC levels or even to inhibit TNC actions in tumors as we observed that both Nb3 and Nb4 inhibited TNC-induced cell rounding, and TNC specific retention of immune cells in the matrix. Thus, our nanobodies could be suitable to inhibit TNC functions in cancer cell migration and invasion and to ablate immune-suppressive functions of TNC in cancer. As a major binding site for the envelope protein in HIV was found in TN5 (10), Nb3 and Nb4 may be useful to modulate this interaction. Finally, Nb3 and Nb4 may also be useful to target TNC actions in COVID19 as high TNC levels correlated with severity of the disease symptoms (13). Our results provide a rationale for a future clinical evaluation of the hTNC-specific Nbs.

DATA AVAILABILITY STATEMENT

The raw data supporting the conclusions of this article will be made available by the authors, without undue reservation.

ETHICS STATEMENT

The Institutional Review Board of the Centre de Ressources Biologiques (Association française de normalization: 2010/39043.2) of the Hautepierre hospital (Strasbourg, France) and Centre Paul Strauss have approved the study on human Ulcerative Colitis samples and human OSCC, respectively. The patients/participants provided their written informed consent to participate in the study.

AUTHOR CONTRIBUTIONS

SD contributed by library construction, nanobody selection, characterization of the nanobodies, and writing the manuscript. RB contributed to the library construction and nanobody selection. WE, TL, CA-F, and AKs contributed by characterization of the TNC blocking functions of the nanobodies. DM, AKs, SB, and IH contributed to the characterization of the nanobodies. MM contributed to characterization of the nanobody TNC interaction by negative electron microscopy. ZB contributed to the dromedary veterinary management and immunizations. RC-E contributed by funding, supervision, and validation. GO contributed by funding, supervision, validation, manuscript writing, and review and editing. BB-Z led the project, contributed by funding, supervision, validation, manuscript writing, and review and editing. All authors contributed to the article and approved the submitted version.

FUNDING

This work was funded by grants from Institut Pasteur Tunis, PRF D4P1 project, Tunisia, to BB-Z, Friedrich Miescher Institute, Basel, Swizerland to RC-E and ANR-AngioFib, ANR-ACKITEC, INCa/Ligue contre le Cancer ECMpact, University Strasbourg and INSERM to GO and personal fellowships to WE (French Ministry of Research MRT) and DM (Association pour la recherche sur le cancer ARC).

ACKNOWLEDGMENTS

We like to thank Dr. H. Bannour, M. Vet for his invaluable help on dromedary immunization. We thank Prof. Lotfi Hendaoui and Prof. Ahlem Lahmar for providing the CGB hepatic metastasis FFPE tissue and the associated clinicopathological diagnosis. We like to acknowledge Agnes Neuville (Department of Pathology, HUS Hautepierre) for providing the UC specimens and Tristan Rupp for having generated the U87MG tumors. We are sincerely sad that we cannot share the accomplished work with RC-E who had initiated this project together with BB-Z.

SUPPLEMENTARY MATERIAL

The Supplementary Material for this article can be found online at: https://www.frontiersin.org/articles/10.3389/fimmu.2021.635166/full#supplementary-material

REFERENCES

1. Takeda A, Otani Y, Iseki H, Takeuchi H, Aikawa K, Tabuchi S, et al. Clinical significance of large Tenascin-C spliced variant as a potential biomarker for colorectal cancer. *World J Surg.* (2007) 31:388–94. doi: 10.1007/s00268-006-0328-6
2. Hancox RA, Allen MD, Holliday DL, Edwards DR, Pennington CJ, Guttery DS, et al. Tumour-associated tenascin-C isoforms promote breast cancer cell invasion and growth by matrix metalloproteinase-dependent and independent mechanisms. *Breast Cancer Res.* (2009) 11. doi: 10.1186/bcr2251
3. Alharth AS, Alyami WA. Tenascin-C (TNC) promotes breast cancer cell invasion and proliferation: functional effects of TNC knockdown in highly invasive breast cancer cell lines. *Am J Med Biol Res.* (2016) 3:55–61. doi: 10.12691/ajmbr-3-2-2
4. Shen C, Wang C, Yin Y, Chen H, Yin X, Cai Z, et al. Tenascin-C expression is significantly associated with the progression and prognosis in gastric GISTs. *Medicine.* (2019) 98:e14045. doi: 10.1097/MD.0000000000014045
5. Ishihara A, Yoshida T, Tamaki H, Sakakura T. Tenascin expression in cancer cells and stroma of human breast cancer and its prognostic significance: *Clin Cancer Res.* (1995) 9:1035–41.
6. Leins A, Riva P, Lindstedt R, Davidoff MS, Mehraein P, Weis S. Expression of tenascin-C in various human brain tumors and its relevance for survival in patients with astrocytoma. *Cancer.* (2003) 98:2430–9. doi: 10.1002/cncr.11796
7. Chiquet-Ehrismann R, Hagios C, Schenk S. The complexity in regulating the expression of tenascins. *BioEssays.* (1995) 17:873–8. doi: 10.1002/bies.950171009
8. Erickson HP, Bourdon MA. Tenascin: An extracellular matrix protein prominent in specialized embryonic tissues and tumors. *Annu Rev Cell Biol*, (1989) 5:72–92. doi: 10.1146/annurev.cb.05.110189.000443
9. Chiquet-Ehrismann R, Orend G, Chiquet M, Tucker RP, Midwood KS. Tenascins in stem cell niches. *Matrix Biol.* (2014) 37:112–23. doi: 10.1016/j.matbio.2014.01.007
10. Mangan RJ, Stamper L, Ohashi T, Eudailey JA, Go EP, Jaeger FH, et al. Determinants of Tenascin-C and HIV-1 envelope binding and neutralization. *Mucosal Immunol.* (2019) 12:1004–12. doi: 10.1038/s41385-019-0164-2
11. Chiquet-Ehrismann R, Chiquet M. Tenascins: regulation and putative functions during pathological stress: Tenascins in pathological stress. *J Pathol.* (2003) 200:488–99. doi: 10.1002/path.1415
12. Midwood KS, Orend G. The role of tenascin-C in tissue injury and tumorigenesis. *J Cell Commun Signal.* (2009) 3:287–310. doi: 10.1007/s12079-009-0075-1
13. Zeng H, Chen D, Yan J, Yang Q, Han Q, Li S, et al. Proteomic characteristics of bronchoalveolar lavage fluid in critical COVID-19 patients. *FEBS J.* (2020) 287:febs.15609. doi: 10.1111/febs.15609
14. Saupe F, Schwenzer A, Jia Y, Gasser I, Spenlé C, Langlois B, et al. Tenascin-C downregulates Wnt inhibitor Dickkopf-1, promoting tumorigenesis in a neuroendocrine tumor model. *Cell Rep.* (2013) 5:482–92. doi: 10.1016/j.celrep.2013.09.014
15. Sun Z, Velázquez-Quesada I, Murdamoothoo D, Ahowesso C, Yilmaz A, Spenlé C, et al. Tenascin-C increases lung metastasis by impacting blood vessel invasions. *Matrix Biol.* (2019) 83:26–47. doi: 10.1016/j.matbio.2019.07.001
16. Oskarsson T, Acharyya S, Zhang XH-F, Vanharanta S, Tavazoie SF, Morris PG, et al. Breast cancer cells produce tenascin C as a metastatic niche component to colonize the lungs. *Nat Med.* (2011) 17:867–74. doi: 10.1038/nm.2379
17. Lowy CM, Oskarsson T. Tenascin C in metastasis: a view from the invasive front. *Cell Adhes Migr.* (2015) 9:112–24. doi: 10.1080/19336918.2015.1008331
18. Langlois B, Saupe F, Rupp T, Arnold C, Van der Heyden M, Orend G, et al. AngioMatrix, a signature of the tumor angiogenic switch-specific matrisome, correlates with poor prognosis for glioma and colorectal cancer patients. *Oncotarget.* (2014) 18:10529–45. doi: 10.18632/oncotarget.2470
19. Bellone M, Caputo S, Jachetti E. Immunosuppression via Tenascin-C. *Oncoscience.* (2015) 2:667. doi: 10.18632/oncoscience.210
20. Jachetti E, Caputo S, Mazzoleni S, Brambillasca CS, Parigi SM, Grioni M, et al. Tenascin-C protects cancer stem-like cells from immune surveillance by arresting T-cell activation. *Cancer Res.* (2015) 75:2095–108. doi: 10.1158/0008-5472.CAN-14-2346
21. Deligne C, Murdamoothoo D, Gammage AN, Gschwandtner M, Erne W, Loustau T, et al. Matrix-targeting immunotherapy controls tumor growth and spread by switching macrophage phenotype. *Cancer Immunol Res.* (2020) 8:368–82. doi: 10.1158/2326-6066.CIR-19-0276
22. Spenlé C, Loustau T, Murdamoothoo D, Erne W, Beghelli-de la Forest Divonne S, Veber R, et al. Tenascin-C orchestrates an immune-suppressive tumor microenvironment in oral squamous cell carcinoma. *Cancer Immunol Res.* (2020) 8:1122–38. doi: 10.1158/2326-6066.CIR-20-0074
23. Giblin SP, Midwood KS. Tenascin-C: form versus function. *Cell Adhes Migr.* (2015) 9:48–82. doi: 10.4161/19336918.2014.987587
24. Dandachi N, Hauser-Kronberger C, MoreÂ E, Wiesener B, Hacker GW, Dietze O, et al. Co-expression of tenascin-C and vimentin in human breast cancer cells indicates phenotypic transdifferentiation during tumour progression: correlation with histopathological parameters, hormone receptors, and oncoproteins. *J Pathol.* (2000) 193:181–9. doi: 10.1002/1096-9896(2000)9999:99993.0.CO;2-V
25. Maschler S, Grunert S, Danielopol A, Beug H, Wirl G. Enhanced tenascin-C expression and matrix deposition during Ras/TGF-β-induced progression of mammary tumor cells. *Oncogene.* (2004) 23:3622–33. doi: 10.1038/sj.onc.1207403
26. Tucker RP, Chiquet-Ehrismann R. Tenascin-C: its functions as an integrin ligand. *Int J Biochem Cell Biol.* (2015) 65:165–8. doi: 10.1016/j.biocel.2015.06.003
27. Li Z-L, Zhang H-L, Huang Y, Huang J-H, Sun P, Zhou N-N, et al. Autophagy deficiency promotes triple-negative breast cancer resistance to T cell-mediated cytotoxicity by blocking tenascin-C degradation. *Nat Commun.* (2020) 11:3806. doi: 10.1038/s41467-020-17395-y
28. Hicke BJ, Marion C, Chang Y-F, Gould T, Lynott CK, Parma D, et al. Tenascin-C aptamers are generated using tumor cells and purified protein. *J Biol Chem.* (2001) 276:48644–54. doi: 10.1074/jbc.M104651200
29. Zukiel R, Nowak S. Suppression of human brain tumor with interference RNA specific for tenascin-C. *Cancer Biol Therapy.* (2006) 5:1002–7. doi: 10.4161/cbt.5.8.2886
30. Rolle K, Nowak S, Wyszko E, Nowak M, Zukiel R, Piestrzeniewicz R, et al. Promising human brain tumors therapy with interference RNA intervention (iRNAi). *Cancer Biol Therapy.* (2010) 9:397–407. doi: 10.4161/cbt.9.5.10958
31. Rolle K. miRNA Multiplayers in glioma. From bench to bedside. *Acta Biochim Polonica.* (2015) 62:353–65. doi: 10.18388/abp.2015_1072
32. Grabowska M, Grześkowiak BF, Szutkowski K, Wawrzyniak D, Głodowicz P, Barciszewski J, et al. Nano-mediated delivery of double-stranded RNA for gene therapy of glioblastoma multiforme. *PLoS ONE.* (2019) 14:e0213852. doi: 10.1371/journal.pone.0213852
33. Brack SS. Tumor-targeting properties of novel antibodies specific to the large isoform of tenascin-C. *Clin Cancer Res.* (2006) 12:3200–8. doi: 10.1158/1078-0432.CCR-05-2804
34. Heuveling DA, de Bree R, Vugts DJ, Huisman MC, Giovannoni L, Hoekstra OS, et al. Phase 0 microdosing PET study using the human mini antibody F16SIP in head and neck cancer patients. *J Nucl Med.* (2013) 54:397–401. doi: 10.2967/jnumed.112.111310
35. Aloj L, D'Ambrosio L, Aurilio M, Morisco A, Frigeri F, Caraco' C, et al. Radioimmunotherapy with Tenarad, a 131I-labelled antibody fragment targeting the extra-domain A1 of tenascin-C, in patients with refractory Hodgkin's lymphoma. *Eur J Nucl Med Mol Imaging.* (2014) 41:867–77. doi: 10.1007/s00259-013-2658-6
36. Petronzelli F. Improved tumor targeting by combined use of two antitenascin antibodies. *Clin Cancer Res.* (2005) 11:7137s—45s. doi: 10.1158/1078-0432.CCR-1004-0007
37. Silacci M. Human monoclonal antibodies to domain C of tenascin-C selectively target solid tumors *in vivo*. *Protein Eng Design Select.* (2006) 19:471–8. doi: 10.1093/protein/gzl033
38. Saerens D, Muyldermans S, (eds). *Single Domain Antibodies: Methods and Protocols*. Totowa, NJ: Humana Press (2012).
39. Hmila I, Saerens D, Ben Abderrazek R, Vincke C, Abidi N, Benlasfar Z, et al. A bispecific nanobody to provide full protection against lethal scorpion envenoming. *FASEB J.* (2010) 24:3479–89. doi: 10.1096/fj.09-148213
40. Conrath KE, Lauwereys M, Galleni M, Matagne A, Re J-MF, Kinne JR, et al. β-Lactamase inhibitors derived from single-domain antibody fragments elicited in the camelidae. *Antimicrob Agents Chemother.* (2001) 45:6. doi: 10.1128/AAC.45.10.2807-2812.2001

41. Chen W, Zhu Z, Feng Y, Xiao X, Dimitrov DS. Construction of a large phage-displayed human antibody domain library with a scaffold based on a newly identified highly soluble, stable heavy chain variable domain. *J Mol Biol.* (2008) 382:779–89. doi: 10.1016/j.jmb.2008.07.054
42. Ebrahimizadeh W, Mousavi Gargari S, Rajabibazl M, Safaee Ardekani L, Zare H, Bakherad H. Isolation and characterization of protective anti-LPS nanobody against *V. cholerae* O1 recognizing Inaba and Ogawa serotypes. *Appl Microbiol Biotechnol.* (2013) 97:4457–66. doi: 10.1007/s00253-012-4518-x
43. De Meyer T, Muyldermans S, Depicker A. Nanobody-based products as research and diagnostic tools. *Trends Biotechnol.* (2014) 32:263–70. doi: 10.1016/j.tibtech.2014.03.001
44. Huang W, Chiquet-Ehrismann R, Moyano JV, Garcia-Pardo A, Orend G. Interference of Tenascin-C with syndecan-4 binding to fibronectin blocks cell adhesion and stimulates tumor cell proliferation. *Cancer Res.* (2001) 61:8586–94. Available online at: https://cancerres.aacrjournals.org/content/canres/61/23/8586.full.pdf
45. Degen M, Brellier F, Kain R, Ruiz C, Terracciano L, Orend G, et al. Tenascin-W is a novel marker for activated tumor stroma in low-grade human breast cancer and influences cell behavior. *Cancer Res.* (2007) 67:9169–79. doi: 10.1158/0008-5472.CAN-07-0666
46. Ehrismann R, Chiquet M, Turner DC. Mode of action of fibronectin in promoting chicken myoblast attachment. *J Biol Chem.* (1981) 256:4056–62. doi: 10.1016/S0021-9258(19)69564-5
47. Fischer D, Brown-Lüdi M, Schulthess T, Chiquet-Ehrismann R. Concerted action of tenascin-C domains in cell adhesion, anti-adhesion and promotion of neurite outgrowth. *J Cell Sci.* (1997) 110:1513–22.
48. Fischer D, Chiquet-Ehrismann R, Bernasconi C, Chiquet M. A single heparin binding region within fibrinogen-like domain is functional in chick tenascin-C. *J Biol Chem*. (1995) 270:3378–84. doi: 10.1074/jbc.270.7.3378
49. Vincke C, Gutiérrez C, Wernery U, Devoogdt N, Hassanzadeh-Ghassabeh G, Muyldermans S. Generation of single domain antibody fragments derived from camelids generation of manifold constructs. In: Nevoltris D., Chames P. editors. *Antibody Engineering*. Totowa, NJ: Humana Press (2012). p. 145–76.
50. Abderrazek RB, Hmila I, Vincke C, Benlasfar Z, Pellis M, Dabbek H, et al. Identification of potent nanobodies to neutralize the most poisonous polypeptide from scorpion venom. *Biochem J.* (2009) 424:263–72. doi: 10.1042/BJ20090697
51. Dhaouadi S, Murdamoothoo D, Tounsi A, Erne W, Benabderrazek R, Benlasfar Z, et al. Generation and characterization of dromedary Tenascin-C and Tenascin-W specific antibodies. *Biochem Biophys Res Commun.* (2020) 530:471–8. doi: 10.1016/j.bbrc.2020.05.077
52. Gerlza T, Hecher B, Jeremic D, Fuchs T, Gschwandtner M, Falsone A, et al. A combinatorial approach to biophysically characterise chemokine-glycan binding affinities for drug development. *Molecules.* (2014) 19:10618–34. doi: 10.3390/molecules190710618
53. Westman J, Hansen FC, Olin AI, Mörgelin M, Schmidtchen A, Herwald H. p33 (gC1q receptor) prevents cell damage by blocking the cytolytic activity of antimicrobial peptides. *J Immunol.* (2013) 191:5714–21. doi: 10.4049/jimmunol.1300596
54. Baschong W, Wrigley NG. Small colloidal gold conjugated to fab fragments or to immunoglobulin g as high-resolution labels for electron microscopy: a technical overview. *J Electron Microsc Tech.* (1990) 14:313–23. doi: 10.1002/jemt.1060140405
55. Schenk S, Muser J, Vollmer G, Chiquet-Ehrismann R. Tenascin-C in serum: a questionable tumor marker. *Int J Cancer.* (1995) 61:443–9. doi: 10.1002/ijc.2910610402
56. Rupp T, Langlois B, Koczorowska MM, Radwanska A, Sun Z, Hussenet T, et al. Tenascin-C orchestrates glioblastoma angiogenesis by modulation of pro- and anti-angiogenic signaling. *Cell Rep.* (2016) 17:2607–19. doi: 10.1016/j.celrep.2016.11.012
57. Weitzner B, Jeliazkov J, Lyskov S, Marze N, Kuroda D, Frick R, et al. Modeling and docking of antibody structures with Rosetta. *Nat Protoc.* (2017) 12:401–16. doi: 10.1038/nprot.2016.180
58. Ksouri A, Ghedira K, Ben Abderrazek R, Shankar Gowri BA, Benkahla A, Bishop Tastan O, et al. Homology modeling and docking of AahII-Nanobody complexes reveal the epitope binding site on AahII scorpion toxin. *Biochem Biophys Res Commun.* (2018) 496:1025–32. doi: 10.1016/j.bbrc.2018.01.036
59. Pierce BG, Wiehe K, Hwang H, Kim BH, Vreven T, Weng Z. ZDOCK server: interactive docking prediction of protein-protein complexes and symmetric multimers. *Bioinformatics.* (2014) 30:1771–3. doi: 10.1093/bioinformatics/btu097
60. Schrödinger LLC. *The PyMOL Molecular Graphics System, Version 1.3r1*. Portland, OR: Schrödinger, LLC (2010).
61. Hmila I, Ben Abdallah R, Saerens D, Benlasfar Z, Conrath K, Ayeb ME, et al. VHH, bivalent domains and chimeric Heavy chain-only antibodies with high neutralizing efficacy for scorpion toxin AahI′. *Mol Immunol.* (2008) 45:3847–56. doi: 10.1016/j.molimm.2008.04.011
62. Chiquet-Ehrismann R. Tenascins, a growing family of extracellular matrix proteins. *Experientia.* (1995) 51:853–62. doi: 10.1007/BF01921736
63. Steel J, Lowen AC, Wang TT, Yondola M, Gao Q, Haye K, et al. Influenza virus vaccine based on the conserved hemagglutinin stalk domain. *mBio.* (2010) 1:e00018–10. doi: 10.1128/mBio.00018-10
64. De Laporte L, Rice JJ, Tortelli F, Hubbell JA. Tenascin C promiscuously binds growth factors via its fifth fibronectin type III-like domain. *PLoS ONE.* (2013) 18:e62072. doi: 10.1371/journal.pone.0062076
65. Spenlé C, Lefebvre O, Lacroute J, Méchine-Neuville A, Barreau F, Blottière HM, et al. The laminin response in inflammatory bowel disease: protection or malignancy? *PLoS ONE.* (2014) 9:e111336. doi: 10.1371/journal.pone.0111336
66. Kawamura T, Yamamoto M, Suzuki K, Suzuki Y, Kamishima M, Sakata M, et al. Tenascin-C produced by intestinal myofibroblasts promotes colitis-associated cancer development through angiogenesis. *Inflamm Bowel Dis.* (2019) 25:732–41. doi: 10.1093/ibd/izy368
67. Ning L, Li S, Gao J, Ding L, Wang C, Chen W, et al. Tenascin-C is increased in inflammatory bowel disease and is associated with response to infliximab therapy. *BioMed Res Int.* (2019) 2019:1–9. doi: 10.1155/2019/1475705
68. Hendaoui I, Lahmar A, Campo L, Mebarki S, Bichet S, Hess D, et al. Tenascin-W is a novel stromal marker in biliary tract cancers. *Front Immunol.* (2021) 11:1–12. doi: 10.3389/fimmu.2020.630139
69. Sun Z, Schwenzer A, Rupp T, Murdamoothoo D, Vegliante R, Lefebvre O, et al. Tenascin-C promotes tumor cell migration and metastasis through integrin α9β1–mediated YAP inhibition. *Cancer Res.* (2018) 78:950–61. doi: 10.1158/0008-5472.CAN-17-1597
70. Venning FA, Wullkopf L, Erler JT. Targeting ECM disrupts cancer progression. *Front Oncol.* (2015) 5:224. doi: 10.3389/fonc.2015.00224
71. Genova C, Rijavec E, Grossi F. Tumor microenvironment as a potential source of clinical biomarkers in non-small cell lung cancer: can we use enemy territory at our advantage? *J Thorac Dis.* (2017) 9:4300–4. doi: 10.21037/jtd.2017.10.66
72. Orend G, Chiquet-Ehrismann R. Tenascin-C induced signaling in cancer. *Cancer Lett.* (2006) 244:143–63. doi: 10.1016/j.canlet.2006.02.017
73. Midwood KS, Chiquet M, Tucker RP, Orend G. Tenascin-C at a glance. *J Cell Sci.* (2016) 129:4321–7. doi: 10.1242/jcs.190546
74. Akabani G, Reardon DA, Coleman RE, Wong TZ, Metzler SD, Bowsher JE, et al. Dosimetry and radiographic analysis of 131I-labeled Anti-Tenascin 81C6 murine monoclonal antibody in newly diagnosed patients with malignant gliomas: a phase II Study.11. *Int J Radiat Oncol Biol Phys.* (2000) 46:947–56. Available online at: https://jnm.snmjournals.org/content/40/4/631.long
75. Reardon DA, Zalutsky MR, Bigner DD. Antitenascin-C monoclonal antibody radioimmunotherapy for malignant glioma patients. *Exp Rev Anticancer Ther.* (2007) 7:675–87. doi: 10.1586/14737140.7.5.675
76. Schliemann C, Wiedmer A, Pedretti M, Szczepanowski M, Klapper W, Neri D. Three clinical-stage tumor targeting antibodies reveal differential expression of oncofetal fibronectin and tenascin-C isoforms in human lymphoma. *Leuk Res.* (2009) 33:1718–22. doi: 10.1016/j.leukres.2009.06.025
77. Ko HY, Choi K-J, Lee CH, Kim S. A multimodal nanoparticle-based cancer imaging probe simultaneously targeting nucleolin, integrin αvβ3 and tenascin-C proteins. *Biomaterials.* (2011) 32:1130–8. doi: 10.1016/j.biomaterials.2010.10.034
78. Spenlé C, Gasser I, Saupe F, Janssen K-P, Arnold C, Klein A, et al. Spatial organization of the tenascin-C microenvironment in experimental and human cancer. *Cell Adhes Migr.* (2015) 9:4–13. doi: 10.1080/19336918.2015.1005452
79. Carnemolla B, Castellani P, Ponassi M, Borsi L, Urbini S, Nicolo G, et al. Identification of a glioblastoma-associated tenascin-C isoform by

a high affinity recombinant antibody. *Am J Pathol.* (1999) 154:1345–52. doi: 10.1016/S0002-9440(10)65388-6
80. Paganelli G, Magnani P, Zito F, Lucignani G, Sudati F, Truci G, et al. Pre-targeted immunodetection in glioma patients: tumour localization and single-photon emission tomography imaging of [99mTc]PnAO-biotin. *Eur J Nucl Med.* (1994) 21:314–21. doi: 10.1007/BF00947966
81. Riva P, Franceschi G, Frattarelli M, Riva N, Guiducci G, Cremonini AM, et al. 131I radioconjugated antibodies for the locoregional radioimmunotherapy of high-grade malignant glioma–phase I and II study. *Acta Oncol Stockh Swed.* (1999) 38:351–9. doi: 10.1080/028418699431438
82. Catania C, Maur M, Berardi R, Rocca A, Giacomo AMD, Spitaleri G, et al. The tumor-targeting immunocytokine F16-IL2 in combination with doxorubicin: dose escalation in patients with advanced solid tumors and expansion into patients with metastatic breast cancer. *Cell Adhes Migr.* (2015) 9:14–21. doi: 10.4161/19336918.2014.983785
83. De Braud FG, Catania C, Onofri A, Pierantoni C, Cascinu S, Maur M, et al. Combination of the immunocytokine F16-IL2 with doxorubicin or paclitaxel in patients with solid tumors: results from two phase Ib trials. *J Clin Oncol.* (2011) 29:2595. doi: 10.1200/jco.2011.29.15_suppl.2595
84. Kovacs JA, Vogel S, Albert JM, Falloon J, Davey RT, Walker RE, et al. Controlled trial of interleukin-2 infusions in patients infected with the human immunodeficiency virus. *N Engl J Med.* (1996) 335:1350–6. doi: 10.1056/NEJM199610313351803
85. Behar G, Siberil S, Groulet A, Chames P, Pugniere M, Boix C, et al. Isolation and characterization of anti-Fc RIII (CD16) llama single-domain antibodies that activate natural killer cells. *Protein Eng Des Sel.* (2007) 21:1–10. doi: 10.1093/protein/gzm064
86. Jailkhani N, Ingram JR, Rashidian M, Rickelt S, Tian C, Mak H, et al. Noninvasive imaging of tumor progression, metastasis, and fibrosis using a nanobody targeting the extracellular matrix. *Proc Natl Acad Sci USA.* (2019) 116:14181–90. doi: 10.1073/pnas.1817442116
87. Hynes RO. *Nanobody Based Imaging Targeting of ECM in Disease Development*. U.S. Patent No 20190225693. Massachusetts, MA: U.S. Patent and Trademark office (2019).
88. Li T, Huang M, Xiao H, Zhang G, Ding J, Wu P, et al. Selection and characterization of specific nanobody against bovine virus diarrhea virus (BVDV) E2 protein. *PLoS ONE.* (2017) 12:e0178469. doi: 10.1371/journal.pone.0178469
89. Wan R, Liu A, Hou X, Lai Z, Li J, Yang N, et al. Screening and antitumor effect of an anti-CTLA-4 nanobody. *Oncol Rep.* (2017) 39:511–8. doi: 10.3892/or.2017.6131
90. Lefranc M-P, Pommié C, Ruiz M, Giudicelli V, Foulquier E, Truong L, et al. IMGT unique numbering for immunoglobulin and T cell receptor variable domains and Ig superfamily V-like domains. *Dev Comp Immunol.* (2003) 27:55–77. doi: 10.1016/S0145-305X(02)00039-3
91. Noël F, Malpertuy A, de Brevern AG. Global analysis of VHHs framework regions with a structural alphabet. *Biochimie.* (2016) 131:11–9. doi: 10.1016/j.biochi.2016.09.005
92. Raza K, Schwenzer A, Juarez M, Venables P, Filer A, Buckley DC, et al. Detection of antibodies to citrullinated tenascin-C in patients with early synovitis is associated with the development of rheumatoid arthritis. *RMD Open.* (2016) 2:2: e000318. doi: 10.1136/rmdopen-2016-000318
93. Ishizaki J, Takemori A, Suemori K, Matsumoto T, Akita Y, Sada K et al. Targeted proteomics reveals promising biomarkers of disease activity and organ involvement in antineutrophil cytoplasmic antibody-associated vasculitis. *Arthritis Res Ther.* (2017) 19:218. doi: 10.1186/s13075-017-1429-3
94. Giblin S, Schwenzer A, Midwood KS. Alternative splicing controls cell lineage-specific responses to endogenous innate immune triggers within the extracellular matrix. *Matrix Biol.* (2020) 93:95–114. doi: 10.1016/j.matbio.2020.06.003

Conflict of Interest: MM was employed by Colzyx AB.

The remaining authors declare that the research was conducted in the absence of any commercial or financial relationships that could be construed as a potential conflict of interest.

frontiers in Immunology

MINI REVIEW
published: 06 April 2021
doi: 10.3389/fimmu.2021.612271

Stroma Involvement in Pancreatic Ductal Adenocarcinoma: An Overview Focusing on Extracellular Matrix Proteins

Sophie Liot[1†], Jonathan Balas[1†], Alexandre Aubert[1], Laura Prigent[1], Perrine Mercier-Gouy[1], Bernard Verrier[1], Philippe Bertolino[2], Ana Hennino[2], Ulrich Valcourt[1] and Elise Lambert[1]*

[1] Laboratoire de Biologie Tissulaire et Ingénierie Thérapeutique (LBTI), UMR CNRS 5305, Université Lyon 1, Institut de Biologie et Chimie des Protéines, Lyon, France, [2] Cancer Research Center of Lyon, UMR INSERM 1052, CNRS 5286, Lyon, France

OPEN ACCESS

Edited by:
Gertraud Orend,
INSERM Immuno Rhumatologie Moléculaire (IRM), France

Reviewed by:
Rolf A. Brekken,
University of Texas Southwestern Medical Center, United States
I. Velázquez-Quesada,
Temple University, United States

***Correspondence:**
Elise Lambert
elise.lambert@ibcp.fr

[†] These authors have contributed equally to this work

Specialty section:
This article was submitted to Cancer Immunity and Immunotherapy, a section of the journal Frontiers in Immunology

Received: 30 September 2020
Accepted: 23 February 2021
Published: 06 April 2021

Citation:
Liot S, Balas J, Aubert A, Prigent L, Mercier-Gouy P, Verrier B, Bertolino P, Hennino A, Valcourt U and Lambert E (2021) Stroma Involvement in Pancreatic Ductal Adenocarcinoma: An Overview Focusing on Extracellular Matrix Proteins. Front. Immunol. 12:612271. doi: 10.3389/fimmu.2021.612271

Pancreatic cancer is the seventh leading cause of cancer-related deaths worldwide and is predicted to become second in 2030 in industrialized countries if no therapeutic progress is made. Among the different types of pancreatic cancers, Pancreatic Ductal Adenocarcinoma (PDAC) is by far the most represented one with an occurrence of more than 90%. This specific cancer is a devastating malignancy with an extremely poor prognosis, as shown by the 5-years survival rate of 2–9%, ranking firmly last amongst all cancer sites in terms of prognostic outcomes for patients. Pancreatic tumors progress with few specific symptoms and are thus at an advanced stage at diagnosis in most patients. This malignancy is characterized by an extremely dense stroma deposition around lesions, accompanied by tissue hypovascularization and a profound immune suppression. Altogether, these combined features make access to cancer cells almost impossible for conventional chemotherapeutics and new immunotherapeutic agents, thus contributing to the fatal outcomes of the disease. Initially ignored, the Tumor MicroEnvironment (TME) is now the subject of intensive research related to PDAC treatment and could contain new therapeutic targets. In this review, we will summarize the current state of knowledge in the field by focusing on TME composition to understand how this specific compartment could influence tumor progression and resistance to therapies. Attention will be paid to Tenascin-C, a matrix glycoprotein commonly upregulated during cancer that participates to PDAC progression and thus contributes to poor prognosis.

Keywords: pancreatic ductal adenocarcinoma, stroma, tumor microenvironment, extracellular matrix, tenascin

INTRODUCTION

Pancreatic cancer is relatively rare and represents 2.5% of all cancers worldwide in 2018 (1). However, the fatal outcome of this disease is almost inevitable which consequently ranks this cancer site as the most devastating one. This poor survival is mainly inherent to the fact that this cancer evolves with few specific symptoms and is therefore mostly diagnosed at an advanced stage when

the cancer presents a very aggressive behavior (4). Upon cancer detection, resection is possible in 10–20% of the cases, depending on tumor stage, and localization. Before or after surgery, or for unresectable tumors, various treatments including chemotherapeutic agents (gemcitabine, nab-paclitaxel, 5-fluorouacil, or FOLFIRINOX) and radiotherapy are generally used, but demonstrate little improvement of patient survival (4–6). Therefore, the discovery of new therapeutics and/or earlier detection of the disease before the onset of signs and symptoms is mandatory to improve patient survival rate.

Acinar cells are the predominant cell type in the pancreas and present an intrinsic plasticity enabling them to perform metaplasia to ductal-like cells. This metaplastic process called acinar-to-ductal metaplasia (ADM), is observed during acute and chronic pancreatitis and may represent the initial step toward the formation of pancreatic intraepithelial neoplasia (PanIN), which may then progress to PDAC. PanIN lesions are classified in different grades, from PanIN1A to PanIN3, characterized by the evolution of epithelial cell morphology (**Figure 1**).

Pancreatic carcinogenesis is a multi-stage process resulting primarily from the accumulation of genetic alterations (average of 63 mutations per patient) in the somatic DNA of normal cells as well as inherited mutations (7). Among the numerous referenced alterations, *KRAS*, *CDKN2A*, *TP53,* and *SMAD4* are the four most frequently mutated genes. *KRAS* proto-oncogene mutations have been detected in 92% of PDAC and are already detectable in precursor lesions, including early preinvasive intraepithelial neoplasia. Interestingly, *SMAD4* mutations are associated with tumor size, lymphatic invasion, and metastasis and no survival at 5 years (8).

Besides the dramatic modifications in epithelial tissue morphology and genome, PDAC formation is also characterized by the desmoplastic reaction induced by tumor cells, which corresponds to a profound modification of the connective tissue through (1) recruitment and activation of specific fibroblasts and (4) intense ECM deposition. Initially corresponding to around 5% of pancreas mass, the connective tissue thus largely develops up to 90% of tumor area (60% on average) (9). Changes in stroma composition also lead to modifications in local immune system and vascularization, which dramatically influence prognosis (10, 11). However, the TME also contains anti-tumor components, which could explain why strategies depleting connective tissue cells have been so ineffective or even deleterious (12, 13).

The purpose of this review will thus be to describe the changes (1) in the cellular composition of the TME, as well as (4) in the ECM composition by attempting to identify which proteins have a potential pro- or anti-tumoral role with the ultimate aim of bringing out new therapeutic targets.

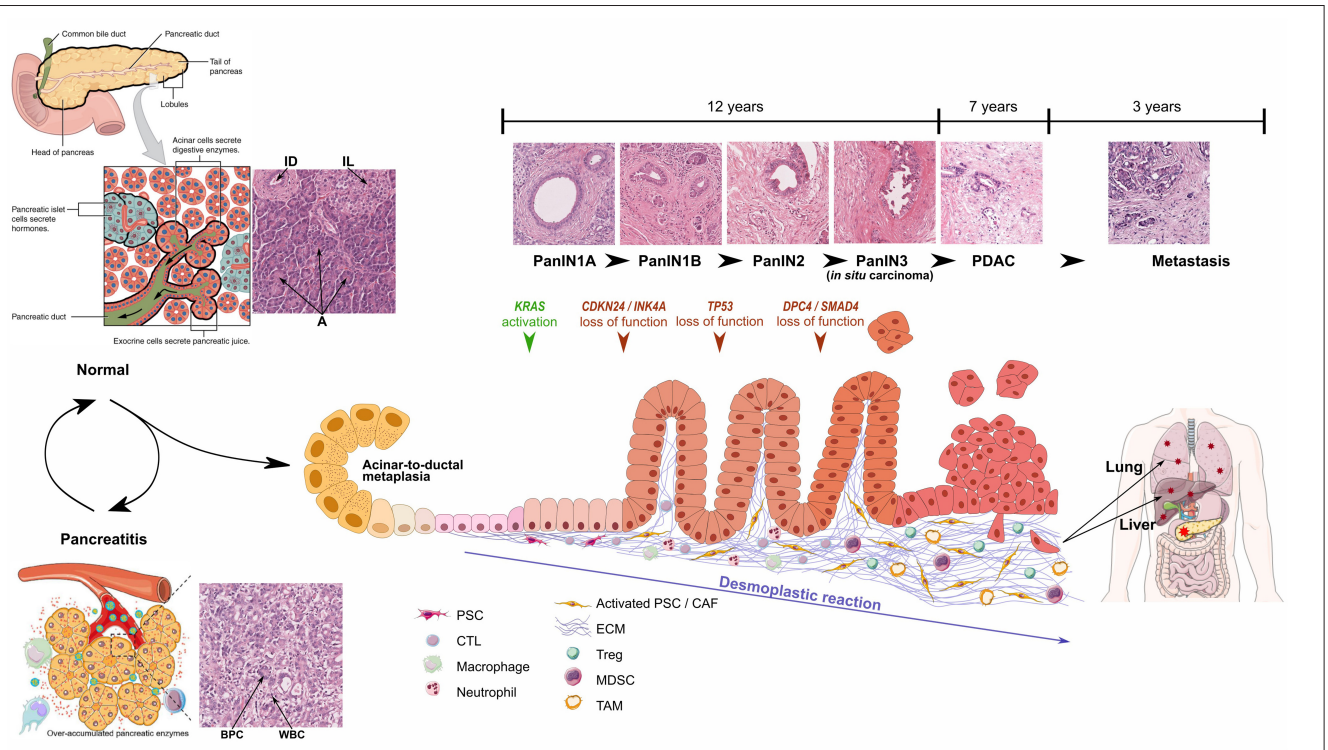

FIGURE 1 | Schematic representations and optical microscopic images of normal pancreas, pancreatitis, and progression from PanIN1 to invasive PDAC. Particular focus is made on development of desmoplastic stroma. Pancreatitis schematic representation from Yao et al. (2), PanIN progression inspired from Morris et al. (3). ID, Interlobular Duct; IL, Islet of Langerhans; A, Acini; BPC, Benign Pancreatic Cells; WBC, White Blood Cells. Healthy pancreas scheme has been obtained from OpenStax College - Anatomy & Physiology. http://cnx.org/content/col11496/1.6/.

Cellular Composition of the Stroma

Cancer-Associated Fibroblasts

Among the various PDAC stromal cell types, the Cancer-Associated Fibroblasts (CAFs) are the most abundant. The CAF population presents a high heterogeneity and diversity of functions, presumably due to the multiple origins of these cells (14). Indeed, they can originate from tissue-resident fibroblasts that are activated under the control of growth factors such as TGFβ or following genetic mutations such as TP53 or PTEN (15). Another cellular origin of CAFs, and probably the most frequent one, is the Pancreatic Stellate Cells (PSCs) (16). PSC activation occurs following pancreatic injury, or upon PDGF or TGFβ stimulation, and leads to (1) morphological changes from a star-like shape into spindle-like cells, (4) loss of vitamin-A droplets and (5) increase in cell nucleus volume (17–19). CAFs may also derive from the recruitment and differentiation of bone marrow-derived mesenchymal stem cells or from the trans-differentiation of non-fibroblastic lineages such as adipocytes or epithelial cells (12, 20, 21). Various markers can be used to distinguish the multiple subsets of CAFs, such as PDGF-receptor α and β (PDGFRα/β), α-SMA, FAP, and S100A4 (Ca^{2+}-binding protein), but none of them is exclusively expressed by CAFs, further highlighting CAF heterogeneity (21, 22). CAFs are responsible for the deposition of a dense tumor stroma, which subsequently can function as a physical barrier against immune infiltration or as a structural scaffold for cell interactions. In addition, CAFs secrete MMPs, which consequently ensure ECM degradation and the subsequent release of various factors leading to the recruitment of specific cells and/or cell dissemination. Finally, CAFs also produce many growth factors and proinflammatory cytokines such as TGFβ, vascular endothelial growth factor (VEGF), interleukin-6 (IL-6) and CXC-chemokine ligand 12 (CXCL12), thereby promoting tumor growth, angiogenesis and recruitment of immunosuppressive cells into the TME to assist in immune evasion (20, 23). In an effort to depict the fibroblast heterogeneity, 3 different CAF subpopulations have been identified according to their function or gene signature: the "inflammatory," "myofibroblastic" and "antigen-presenting" CAFs (24, 25).

Endothelial Cells

Despite the obvious production of pro-angiogenic factors by CAFs and pancreatic tumor cells, PDAC is characterized by a low microvascular density compared to other types of cancers (11). Indeed, the dense fibrotic stroma forms a physical barrier that inhibits the formation and the proper functioning of vasculature, resulting in sparse constricted blood and lymphatic vessels that are only partially functional and physically separated from the cancer cells. This feature is deleterious for patient survival since low vascularity is associated with poor patient survival due to poor anti-cancer immune cell infiltration and chemotherapeutic drug delivery (26). Consequently, addition of anti-angiogenic drug (bevacizumab) to standard chemotherapy demonstrated no improvement in PDAC outcome (27). On contrary, vascular normalization aiming at improving drug delivery could be a good strategy for this type of carcinoma (27).

Infiltrating Immune Cells

Chronic pancreatitis is a risk factor for the development of PDAC as well as of systemic diseases characterized by chronic low-grade inflammation, such as metaflammation in patients with the metabolic syndrome or diabetes (28, 29). Interestingly, chronic pancreatitis and PDAC tissues show similarities in their desmoplasia and inflammatory infiltrates, indicating overlapping inflammatory responses.

The prevention and elimination of cancer cells are dependent on the immune system around the tumor. The PDAC immune microenvironment is characterized by (1) the exhaustion of anti-cancer immune cytotoxic T lymphocytes notably due to high mechanical constraints within the tumor and (4) the infiltration of multiple types of tumor-promoting immune cells, including myeloid-derived suppressor cells, tumor-associated macrophages and regulatory T cells (10, 30). Those tumor-promoting immune cells, in combination with CAFs and cancer cells secrete various pro-inflammatory cytokines such as TGFβ, TNFα, and different interleukins which subsequently favor immune evasion, PDAC development and metastasis formation (31). Various strategies are currently developed to treat PDAC by restoring proper immune system function: enzymatic digestion of TME, vascular normalization and neutralization of immune system modulators (21).

ECM Evolution During Pancreatic Carcinogenesis

PDAC is characterized by an intense desmoplastic reaction, defined as the fibrotic response of healthy tissue to invasive carcinoma and consisting of an abnormal accumulation of ECM components, mostly collagen fibers (32). This new TME acts as a physical barrier preventing (1) proper angiogenesis, and subsequent drug delivery, and (4) anti-cancer immune infiltration (33, 34). Consequently, TME has been considered as deleterious for patient prognosis and CAFs, which are responsible for dense ECM deposition, have been the target of clinical trials. However, CAF depletion resulted in an apparent paradoxical accelerated disease progression and encouraged a more detailed analysis of the most differentially regulated ECM components in the pancreatic tumors vs. healthy tissue, in order to identify new therapeutic targets within the TME (35, 36). We hereafter describe these matrix components according to the matrisome classification [**Table 1**; (37)].

Core Matrisome

Collagens

Collagens are by far the most represented constituents of the connective tissue of normal and pathological pancreas (>90% of ECM proteins), with the type I and III fibrillar collagens accounting for >90% of all collagen mass (36, 38). Protein level for those collagens increases 2.6-fold during pancreatic tumor progression, which explains desmoplasia and justifies them as crucial targets. Additionally, the stroma undergoes intense rearrangement, leading to highly aligned collagen fibers, associated with bad prognosis for patients following pancreatic cancer resection (111). Despite their increased deposition, no ratio variation is observed for type I and III collagens

TABLE 1 | ECM proteins involved in PDAC, presented according to the matrisome classification.

Matrisome category		Name	Pro (+) or Anti (-) tumoral role in PDAC			Secreted by…	References
Part 1							
Core matrisome	Collagens	Collagen type I	+	Patients	• ↘ Patient survival (analysis of PDAC patient samples and their corresponding clinicopathological parameters	Stromal cells	(36, 38–45)
				in vivo	• Nutritive source (PKI model) • + Invasion and EMT • Mechanical constraint → hypovascularization, low immune cell infiltration, - chemotherapy delivery		
				in vitro	• + Proliferation, migration, EMT and—apoptosis (pancreatic cancer cell lines) • Nutritive source (PK4A cell line)		
		Collagen type III	+	*in vivo*	• Desmoplasia/mechanical constraint → hypovascularization, low immune cell infiltration, – chemotherapy delivery	Stromal cells	
		Collagen type IV	+	Patients	• High circulating collagen IV: ↘ survival after surgery (quick relapse) • Poor outcome	Tumor and stromal cells	(46, 47)
				in vivo	• Nutritive source (PKI model)		
				in vitro	• + Cancer cell growth, maintenance of migratory phenotype and—apoptosis (pancreatic cell lines) • Nutritive source (PK4A cell line)		
		Collagen type V	+	*in vivo*	• + Metastasis formation (orthotopic mouse models of PDAC)	Stromal cells, PSCs	(48)
				in vitro	• + Adhesion, proliferation, migration and survival (PDAC cell lines) • + Angiogenesis		
		Collagen type VI	+	*in vivo*	• + Metastasis under hyperglycemia conditions (orthotopic implantation and intravenous injection of PDAC murine cells)	Stromal cells	(36, 39)
		Collagen type XV	–	*in vitro*	• – Migratory abilities and EMT (BxPC-3 cell line)	Stromal cells	(49)
	Proteoglycans	Testican	+	Patients	• Poor patient survival	Stromal cells	(50, 51)
				in vitro	• + Collagen deposition and invasive cancer cell growth (organotypic coculture models) • + Cancer cell proliferation, survival, migration, invasion and EMT (PDAC cell lines)		
		Lumican	–	Patients	• ↗ Patient survival • ↘ Metastatic recurrence after surgery	Stromal cells	(52, 53)
				in vivo	• – Cancer cell growth (xenograft and syngeneic orthotopic mouse models)		
		Decorin	–	*in vitro*	• – Cell growth (cancer cell lines)	Stromal cells	(36, 54)
		Biglycan	–	*in vitro*	• Cell growth (PDAC cell lines) • – Cell migration / metastasis (pancreatic cell lines)	Tumor and stromal cells	(55–58)
			+	Patients	• Poor prognosis (↘ overall survival)	Stromal cells	
		Versican	+	*in vivo* and *in vitro*	• Immunosuppressive component, ↘ T cell infiltration (KPC mouse model and PDAC organotypic spheroid coculture models)	Tumor and stromal cells	(59, 60)
	ECM glycoproteins	Laminins	+	Patients	• Poor prognosis (public online databases)	Tumor cells	(61, 62)
				in vivo	• + Cancer cell proliferation, invasion and migration (+ metastasis) (subcutaneous xenograft mouse model and pancreatic cancer liver metastasis mouse model)		
				in vitro	• + Cancer cell proliferation, survival, migration, invasion and EMT (pancreatic cell lines)		
		Fibronectin	+	Patients	• Associated with advanced stages, patient short survival and poor prognosis (analysis of PDAC patient samples and their corresponding clinicopathological parameters	Tumor and stromal cells	(63–68)
				in vitro	• + Tumor growth and invasion • + Chemoresistance (cells from PDAC patients and pancreatic cancer cell lines)		
		TGFβi	+	Patients	• Poor prognosis, associated with patient short survival	Tumor and stromal cells	(69–72)
				in vivo	• + Tumor rigidity and immunosuppression (various pancreatic mouse models) • + Tumor growth		
				in vitro	• + Cancer cell migration and invasion (pancreatic cancer cell lines)		
		Tenascin-C	+	Patients	• Poor prognosis (PDAC patient samples), may depend on tumor stage • Correlated with perineural invasion, advanced stages, postoperative locoregional recurrence and metastases (resected PDAC specimens and clinicopathological features)	Stromal cells	(9, 73–77)
				in vitro	• + Perineural invasion (coculture model) • + Cancer cell proliferation, invasion and EMT (metastasis) (PDAC cell lines and primary PanIN and PDAC cells)		

(Continued)

TABLE 1 | Continued

Matrisome category		Name	Pro (+) or Anti (-) tumoral role in PDAC			Secreted by…	References
PART 2							
Matrisome-associated proteins	Secreted factors	TGFβ	+	*in vivo*	• + PSC activation, proliferation and collagen synthesis (subcutaneous and orthotopic transplantation models and transgenic mouse models) • + Metastasis (orthotopic and transgenic mouse models) • Immunosuppression and inappropriate inflammation	Tumor and stromal cells	(40, 78–81)
				in vitro	• + PSC activation, proliferation and collagen synthesis • + Cancer cell proliferation and—apoptosis (various pancreatic cancer cell lines and coculture models) • + Cancer cell EMT and invasion		
		SHH	+	*in vivo* and *in vitro*	• + PSC recruitment and activation (+ desmoplasia) (human pancreatic primary cells, PDAC cell lines, subcutaneous and orthotopic transplantation of PDAC cells and transgenic pancreatic mouse models)	Tumor cells	(82)
		FGF-2	+	*in vitro*	• + PSC activation and collagen synthesis (various PDAC cell lines)	Tumor cells	(40)
		PDGF	+	*in vitro*	• + PSC activation and collagen synthesis (various PDAC cell lines)	Tumor cells	(40)
		CXCLs	+	*in vivo*	• + Desmoplastic reaction and tumor angiogenesis (transgenic mouse models) • + Cancer cell migration/invasion • + Inflammation	Tumor cells	(36, 83, 84)
		S100 proteins	+	*in vivo*	• + Tumor growth and metastasis (various xenograft and transgenic pancreatic mouse models)	Tumor cells	(85–87)
				in vitro	• + Cancer cell survival, migration/invasion (PDAC cell lines)		
	ECM regulators	MMPs	+	Patients	• Poor prognosis (analysis of PDAC patient samples and their corresponding clinicopathological parameters)	Tumor cells	(36, 88–90)
				in vivo	• ADM induction (various KRAS mouse models) • + Tumor growth and metastasis (mice harboring orthotopic pancreatic cancers, subcutaneously injected with pancreatic cancer cell lines or several genetic Kras-driven PDAC models • + Angiogenesis (subcutaneously or orthotopically injected mice with PDAC cells)		
				in vitro	• + Cancer cell proliferation and invasion		
		ADAMs	+	Patients	• Associated with poor prognosis and invasive tumors (analysis of PDAC patient samples and their corresponding clinicopathological parameters)	Tumor and stromal cells	(91–93)
				in vivo	• + Tumor growth and metastasis (orthotopically-injected mice and KRAS mouse model) • + Angiogenesis		
				in vitro	• + Cancer cell migration/invasion (PDAC cell lines) • + Angiogenesis		
		TIMPs	–	*in vivo*	• Tumor growth and metastasis, + apoptosis (subcutaneous and orthotopic injection) • – Angiogenesis	Stromal cells	(94–96)
				in vitro	• – Cancer cell invasion,—invadopodia (co-culture models)		
			+	*in vivo*	• + Tumor growth and metastasis (KPC and subcutaneously injected mouse models) • Drug resistance	Tumor cells	
		SERPINs	+ (–)	Patients	• Poor survival / Poor prognosis (analysis of PDAC patient samples and their corresponding clinicopathological parameters)	Tumor and stromal cells	(36, 97–100)
				in vivo	• + Tumor growth, invasion and metastasis (PDAC cells transplanted mouse models)		
		LOXs	+	Patients	• Poor survival post-resection (transcriptomic analysis of patient samples)	Stromal cells	(36, 101, 102)
				in vivo	• Drug resistance: + desmoplasia,—perfusion (orthotopically transplanted mouse model) • + Cancer cell migration/invasion, + metastasis (KPC mouse model)		

(Continued)

TABLE 1 | Continued

Matrisome category		Name	Pro (+) or Anti (-) tumoral role in PDAC			Secreted by…	References
ECM-affiliated proteins		Annexins	+	Patients	• Associated with poor patient survival, tumor progression and recurrence post-resection (analysis of PDAC patient samples and their corresponding clinicopathological parameters, and TCGA public online database	Tumor and stromal cells	(103–109)
				in vivo	• + Metastasis (pancreatic transplanted mouse model)		
				in vitro	• + Cancer cell growth, - apoptosis • + Cancer cell invasion and EMT activation (PDAC cell lines) • + Chemoresistance		
		Galectins	+	*in vivo*	• Gal1: ADM induction • Gal3: + Tumor growth and immune escape • Gal9: + Immune escape	Stromal cells (Gal1) and tumor cells (Gal3 and Gal9)	(110)
				in vitro	• Gal1 and 3: + PSC activation • Gal1: + Cancer cell proliferation, migration/invasion and immunosuppression • Gal3: + Cancer cell growth/proliferation and invasion/migration		
			–	Patients	• Gal4: Associated with patient better survival and less metastases	Tumor cells	
				in vitro	• Gal4:—Cancer cell migration and invasion (PDAC primary cells and cell lines)		

Pro-(+) or anti-(–) tumoral role as well as cells responsible for their secretion are detailed. +: promotion, –: inhibition, ↗: increased, ↘: decreased. Each protein family has been classified according to the matrisome classification and is highlighted with a specific color. Tenascin-C information is highlighted in dark green.

between healthy and PDAC connective tissues, thus encouraging attention to other collagens differentially expressed during pancreatic carcinogenesis (37). Among them, type IV, V, VI, VII, XII, XIV, and XV collagens are key players in pancreatic tumorigenesis and act either as beneficial or detrimental molecules. For instance, collagen IV, which is an essential constituent of the basement membrane (BM), is produced by cancer cells, favors cancer cell growth, migration and protect them from apoptosis. Consequently, high serum level of collagen IV is associated with quick relapse after surgery and thus poor survival (46, 47). On contrary, another BM component, collagen XV, is lost during pancreatic tumorigenesis and its overexpression reduces the migratory abilities of PDAC cells in type I collagen-rich matrices (49). Interestingly, collagen VI is highly expressed during PDAC progression, induces metastatic colonization particularly in a hyperglycemic context and could therefore be targeted especially in diabetic patients (36, 39).

Besides their architectural and signaling role enabling tumor progression, collagens also serve as a nutritive source. Indeed, under PDAC specific conditions low in oxygen and nutrients, tumor cells metabolize collagen molecules, and thus collagen-derived proline enables PDAC cell proliferation (112). Therefore, this could explain the correlation between high serum collagen fragment levels in serum and significantly shorter overall survival, and prompts detailed analysis of collagen fragment role during PDAC progression (113).

Proteoglycans

Proteoglycans consist of one or more glycosaminoglycan (GAG) chain(s)—representing around 85% of the molecule mass—covalently attached to a core protein, and are categorized depending of their GAG chain nature and size (114). Among the small proteoglycans which are mainly expressed by TME, testican acts as a pro-tumoral molecule by affecting collagen deposition and thus favoring tumor cell growth and invasion, therefore leading to a poor patient survival, whereas lumican interferes with tumor progression and is associated with prolonged patient survival by limiting cancer cell growth and metastasis (50, 52, 53). Decorin is also considered as an anti-tumoral constituent by reducing tumor cell growth (36, 54) whereas the pro- or anti-tumoral status of biglycan in PDAC is still under debate. Indeed, its expression by stromal and epithelial cells (1) is induced by TGFβ, (4) has been described to inhibit pancreatic cancer cell growth and migration (55–57), but (5) is associated with poor prognosis (58). Finally, versican, which corresponds to a large proteoglycan expressed by both stromal and epithelial cells in PDAC, acts as an immunosuppressive component by reducing T cell infiltration and is thus considered as a deleterious molecule for patient survival (59).

Glycoproteins

Laminins are a family of ECM glycoproteins representing the major non-collagenous constituent in BM. Most of their subunits are over-expressed in PDAC and associated with poor outcome for patient survival (61). Fibronectin (FN1), which supports cell-ECM interactions, is essential for wound healing, development, and tissue homeostasis under physiological context. FN1 is also upregulated in PDAC which leads to tumor growth, invasion and metastasis formation and is consequently associated with poor prognosis in PDAC patients (63).

Transforming Growth Factor beta-induced (TGFβi) protein, also named βig-h3, is able to modulate cell adhesion through various integrins, including αvβ3, α1β1, and αvβ5.This glycoprotein is increased during pancreatic cancer and acts either directly on tumor $CD8^+$ T cells by reducing their proliferation and activation or on tumor cells by promoting their migration and invasion (69, 115). TGFβi could thus be regarded

for its double therapeutic potential to increase local anti-tumor immunity and subsequently induce cancer cell apoptosis or inhibit metastasis (69–72).

Among the four members of the Tenascin (TN) family, Tenascin-C (TNC) is by far the most well-characterized and is commonly described as being widely distributed in embryonic tissues, restricted in some adult tissues, such as stem cell niches and tendons (116), and *de novo* re-expressed during physio-pathological contexts such as wound healing and tumor progression (117). In PDAC, TNC protein is restrained to the tumor stroma and is not found in epithelial tumor cells or adjacent normal pancreatic tissue (9). High TNC expression, and downstream signaling through the Annexin II receptor, have been initially correlated with poor prognosis but this association is still controversial and could depend on the stage and grade of the pancreatic tumor or the specific location of TNC (9, 73, 118). So, high perineural TNC expression is associated with perineural invasion and poor prognosis with high loco-regional recurrence (74). In the same line, a recent study highlighted TNC as a prominent protein found in exosomal compartment and associated with local invasion and distant metastasis (75).

We recently demonstrated *TNXB* gene and TNX protein were significantly downregulated in the six cancers with the highest incidence and mortality worldwide (i.e., lung, breast, prostate, stomach, colorectal, and liver carcinomas) and low TNX levels were associated with poor prognosis in patients suffering from lung and breast carcinomas (119). In the same study, TNX protein expression was also decreased in tumor samples from PDAC patients (119).

Matrisome-Associated Proteins

Secreted Factors

In pancreatic cancer, Various Factors Are Mainly produced by cancer cells to favor tumor progression. Among them, TGFβ role is complex and mediates both pro- and anti-tumoral activities in cancer cells depending on their context, in space and time and their microenvironment. Indeed, in normal pancreatic cells and at early stages of pancreatic carcinogenesis, TGFβ exerts a tumor suppressive effect through SMAD4-regulated genes. However, in the late phase, SMAD4 is inactivated whereas TGFβ expression is upregulated leading to PI3K/Akt, Ras/ERK, p38MAPK, and Rho/GTPase pathway activation and subsequent tumor progression (120). Then, TGFβ invariably induces (1) proliferation and survival of PDAC cells, (4) EMT, invasion, and metastasis, (5) production of a dense fibrotic stroma and (6) deregulation of the immune microenvironment toward immunosuppression and inappropriate inflammation. Thus, various promising pre-clinical and clinical trials have already evaluated the potential of TGFβ-targeting therapies, through TGFβ regulator (losartan), TGFβ neutralizing antibodies or TGFβ receptor inhibitors (78–81, 121, 122). Other signaling factors are secreted by pancreatic cancer cells, enabling PSC recruitment and activation, and subsequent desmoplastic response inducing collagen synthesis. Thus, Sonic HedgeHog (SHH), Fibroblast Growth Factor-2 (FGF-2) and Platelet-derived Growth Factor (PDGF) are overexpressed during PDAC and interfering with their signaling corresponds to valuable strategies for PDAC treatment (40, 82). However, clinical trials using IPI-926, vismodegib and sonidegib that target the hedgehog pathway have so far been disappointing (123). PDAC cells also overexpress several CXC ligands, which are involved in desmoplastic reaction, immune modulation and tumor angiogenesis (36, 124). Thus, blocking the CXCLs-CXCR2 axis improves survival in a PDAC developing mouse model by reducing cell invasion and inflammation and could be a therapeutic approach against PDAC progression (83, 125). Finally, proteomic analyses of ECM during PDAC progression demonstrated that various members of the S100 Ca^{2+}-binding protein family, notably S100P and S100A4, are upregulated in this disease and their high levels are associated with poor prognosis, thus shedding light on their receptor, i.e., the Receptor for Advanced Glycation End products (RAGE) and the RAGE/S100 ligand axis as a promising therapeutic approach (85). Therefore, various S100 monoclonal antibodies, S100 protein inhibitors or RAGE antagonist have already demonstrated a reduction of tumor growth and metastasis formation in mouse models (85).

ECM Regulators

Many proteins overexpressed during pancreatic tumorigenesis are responsible for ECM remodeling and are therefore potential targets for pancreatic cancer treatment. Matrix MetalloProteinases (MMPs), A Disintegrin And Metalloproteinases (ADAMs), and A Disintegrin And Metalloproteinase with ThromboSpondin motifs (ADAMTSs) are zinc-dependent endopeptidases that are able to degrade all ECM proteins. Their activities are tightly regulated by proteolytic activation and inhibition *via* their natural inhibitors, Tissue Inhibitors of MetalloProteinases (TIMPs) (126). The imbalance between the expression of metalloproteinases and TIMPs is thus of crucial interest in cancer development and metastasis (127). With some exceptions, those proteases are overexpressed during pancreatic cancer progression and are the targets of numerous pre-clinical and clinical trials, which for some of them were disappointing or less powerful than expected, probably due to (1) aspecific metalloproteinase targeting (use of broad-spectrum inhibitors) or (4) compensation mechanisms set up by tumor cells (88).

Several SERPIN family members are also importantly differentially regulated during PDAC development, mainly promoting tumor growth, invasion, and are associated with poor survival, but their activities have to be analyzed individually with particular attention paid to their original cells (36, 97–99). Finally, Lysyl Oxidases (LOX), a family of extracellular copper-dependent enzymes involved in ECM cross-linking, are also important matrix regulators over-represented during pancreatic tumorigenesis (36). Their inhibition in mouse model prolonged tumor-free survival by interfering with stroma stiffness (101, 102).

ECM-Affiliated Proteins

Among the ECM-affiliated proteins significantly deregulated during PDAC development, numerous members belong to the vertebrate "A subgroup" of the annexin superfamily coding a

calcium- and membrane-binding protein (36). This subgroup consists of at least 12 members (A1-A11 and A13), all of which are suspected to be involved in tumor development (103). In PDAC, annexins are known to favor tumor cell growth, EMT, invasion and metastasis and to inhibit apoptosis. Additionally, they interact with various peri-cellular proteins such as S100 proteins and TNC, which are upregulated during PDAC progression. Therefore, annexin overexpression is associated with poor patient prognosis and could inspire new therapeutic strategies (128). Galectins, which are a family of carbohydrate-binding proteins, are also upregulated during PDAC progression (36, 110). Besides galectin-4, which has been described as a tumor suppressor by inhibiting tumor cell migration and invasion, the other galectins favor pancreatic tumor. Consequently, galectin inhibitors are considered as promising opportunities for pancreatic cancer therapeutic interventions, either alone or combined with current chemo- and/or immunotherapies (110).

CONCLUSIONS

During pancreatic tumorigenesis, important stromal modifications occur both at the cell landscape level and the matrix molecular composition in response to tumor signals. Herein, we have listed these major changes by focusing only on the proteins belonging to the matrisome. However, other extracellular components have not been underlined, but can drastically influence pancreatic tumor progression, as it is the case for hyaluronic acid (HA) (129–136). Indeed, in PDAC mouse model, HA deposition (1) was observed very early during tumor formation in an intralobular position in ADM regions and close to PanIN lesions and (4) preceded collagen deposition around lesions that will progress to PDAC (129). Besides making the ECM denser, HA deposition may be related to an inflammatory stage allowing the recruitment of immune cells in ADM areas, which further underlines the value of HA as a therapeutic target for PDAC treatment. Various drugs targeting HA have been developed such as pegylated hyaluronidase (PEGPH20) and Minnelide (132, 137). However, PEGPH20 in combination with conventional chemotherapies failed to demonstrate an improvement in median overall survival, leading to the recent discontinuation of PEGPH20 development after a phase 3 clinical trial. Minnelide, corresponding to an active substance extracted from thunder god vine is still under investigation and its mechanism of action seems multimodal (132, 138–140). Additionally, abnormal glycosylation of ECM components such as proteoglycans and glycoproteins can significantly influence tumor growth, neoplastic progression, metastasis and chemoresistance and thus should be considered for new drug design (141, 142). So far, despite promising results in preclinical models, no therapeutic strategy targeting the stroma compartment has brought conclusive results in clinical settings. This could be explained by differences in pharmacokinetics, pharmacodynamics and metabolism and the failure to accurately model the tumor microenvironment of patients using preclinical mouse models. However, a better understanding of the tumor stroma is expected to open up new possibilities for the development of new drugs.

AUTHOR CONTRIBUTIONS

SL and JB: data curation, investigation and writing—original draft. AA, LP, and PM-G: writing—review and editing. BV: funding acquisition. PB and UV: writing—review and editing and funding acquisition. AH: investigation and writing—review and editing. EL: conceptualization, supervision, and writing—original draft. All authors: contributed to the article and approved the submitted version.

FUNDING

This work was supported by the Ligue Nationale contre le Cancer, Comité du Rhône, Comité de l'Allier, Comité de Savoie, and Comité de la Drôme, Comité Régional Auvergne-Rhône-Alpes et Saône-et-Loire (2019) as well as by the Fondation ARC pour la recherche sur le cancer (PJA 20141201790), Bristol Myers Squibb Foundation (2018–2019), and Inserm Transfert (2018–2020).

REFERENCES

1. Ferlay J, Colombet M, Soerjomataram I, Mathers C, Parkin DM, Piñeros M, et al. Estimating the global cancer incidence and mortality in 2018: GLOBOCAN sources and methods. *Int J Cancer.* (2019) 144:1941–53. doi: 10.1002/ijc.31937
2. Yao Q, Jiang X, Zhai Y-Y, Luo L-Z, Xu H-L, Xiao J, et al. Protective effects and mechanisms of bilirubin nanomedicine against acute pancreatitis. *J ControlRelease.* (2020) 322:312–25. doi: 10.1016/j.jconrel.2020.03.034
3. Morris JP, Wang SC, Hebrok M. KRAS, Hedgehog, Wnt and the twisted developmental biology of pancreatic ductal adenocarcinoma. *Nat Rev Cancer.* (2010) 10:683–95. doi: 10.1038/nrc2899
4. Eibl AS G. Pancreatic Ductal Adenocarcinoma. *Pancreapedia: The Exocrine Pancreas Knowledge Base.* (2015). Available online at: /reviews/pancreatic-ductal-adenocarcinoma (accessed September 19, 2020).
5. Lambert A, Schwarz L, Borbath I, Henry A, Van Laethem J-L, Malka D, et al. An update on treatment options for pancreatic adenocarcinoma. *Ther Adv Med Oncol.* (2019) 11:1758835919875568. doi: 10.1177/1758835919875568
6. Oba A, Ho F, Bao QR, Al-Musawi MH, Schulick RD, Del Chiaro M. neoadjuvant treatment in pancreatic cancer. *Front Oncol.* (2020) 10:245. doi: 10.3389/fonc.2020.00245
7. Jones S, Zhang X, Parsons DW, Lin JC-H, Leary RJ, Angenendt P, et al. Core signaling pathways in human pancreatic cancers revealed by global genomic analyses. *Science.* (2008) 321:1801–6. doi: 10.1126/science.1164368
8. Oshima M, Okano K, Muraki S, Haba R, Maeba T, Suzuki Y, et al. Immunohistochemically detected expression of 3 major genes (CDKN2A/p16, TP53, and SMAD4/DPC4) strongly predicts survival in patients with resectable pancreatic cancer. *Ann Surg.* (2013) 258:336–46. doi: 10.1097/SLA.0b013e3182827a65
9. Leppänen J, Lindholm V, Isohookana J, Haapasaari K-M, Karihtala P, Lehenkari PP, et al. Tenascin C, Fibronectin, and tumor-stroma ratio in pancreatic ductal adenocarcinoma. *Pancreas.* (2019) 48:43–8. doi: 10.1097/MPA.0000000000001195
10. Li K-Y, Yuan J-L, Trafton D, Wang J-X, Niu N, Yuan C-H, et al. Pancreatic ductal adenocarcinoma immune microenvironment

and immunotherapy prospects. *Chronic Dis Transl Med.* (2020) 6:6–17. doi: 10.1016/j.cdtm.2020.01.002
11. Longo V, Brunetti O, Gnoni A, Cascinu S, Gasparini G, Lorusso V, et al. Angiogenesis in pancreatic ductal adenocarcinoma: A controversial issue. *Oncotarget.* (2016) 7:58649–58. doi: 10.18632/oncotarget.10765
12. Rhim AD, Oberstein PE, Thomas DH, Mirek ET, Palermo CF, Sastra SA, et al. Stromal elements act to restrain, rather than support, pancreatic ductal adenocarcinoma. *Cancer Cell.* (2014) 25:735–47. doi: 10.1016/j.ccr.2014.04.021
13. Özdemir BC, Pentcheva-Hoang T, Carstens JL, Zheng X, Wu C-C, Simpson TR, et al. Depletion of carcinoma-associated fibroblasts and fibrosis induces immunosuppression and accelerates pancreas cancer with reduced survival. *Cancer Cell.* (2014) 25:719–34. doi: 10.1016/j.ccr.2014.04.005
14. Öhlund D, Elyada E, Tuveson D. Fibroblast heterogeneity in the cancer wound. *J Exp Med.* (2014) 211:1503–23. doi: 10.1084/jem.20140692
15. Arina A, Idel C, Hyjek EM, Alegre M-L, Wang Y, Bindokas VP, et al. Tumor-associated fibroblasts predominantly come from local and not circulating precursors. *Proc Natl Acad Sci USA.* (2016) 113:7551–6. doi: 10.1073/pnas.1600363113
16. Neuzillet C, Tijeras-Raballand A, Ragulan C, Cros J, Patil Y, Martinet M, et al. Inter- and intra-tumoural heterogeneity in cancer-associated fibroblasts of human pancreatic ductal adenocarcinoma. *J Pathol.* (2019) 248:51–65. doi: 10.1002/path.5224
17. Xu Z, Pothula SP, Wilson JS, Apte MV. Pancreatic cancer and its stroma: a conspiracy theory. *World J Gastroenterol.* (2014) 20:11216–29. doi: 10.3748/wjg.v20.i32.11216
18. Moir JAG, Mann J, White SA. The role of pancreatic stellate cells in pancreatic cancer. *Surgical Oncology.* (2015) 24:232–8. doi: 10.1016/j.suronc.2015.05.002
19. Apte MV, Xu Z, Pothula S, Goldstein D, Pirola RC, Wilson JS. Pancreatic cancer: The microenvironment needs attention too!. *Pancreatology*. (2015). 15 (4. Suppl):S32–8. doi: 10.1016/j.pan.2015.02.013
20. Sun Q, Zhang B, Hu Q, Qin Y, Xu W, Liu W, et al. The impact of cancer-associated fibroblasts on major hallmarks of pancreatic cancer. *Theranostics.* (2018) 8:5072–87. doi: 10.7150/thno.26546
21. Liu T, Han C, Wang S, Fang P, Ma Z, Xu L, et al. Cancer-associated fibroblasts: an emerging target of anti-cancer immunotherapy. *J Hematol Oncol.* (2019) 12:86. doi: 10.1186/s13045-019-0770-1
22. Norton J, Foster D, Chinta M, Titan A, Longaker M. Pancreatic cancer associated fibroblasts (caf): under-explored target for pancreatic cancer treatment. *Cancers (Basel).* (2020) 12:12051347. doi: 10.3390/cancers12051347
23. Huang T-X, Guan X-Y, Fu L. Therapeutic targeting of the crosstalk between cancer-associated fibroblasts and cancer stem cells. *Am J Cancer Res.* (2019) 9:1889–904.
24. Öhlund D, Handly-Santana A, Biffi G, Elyada E, Almeida AS, Ponz-Sarvise M, et al. Distinct populations of inflammatory fibroblasts and myofibroblasts in pancreatic cancer. *J Exp Med.* (2017) 214:579–96. doi: 10.1084/jem.20162024
25. Elyada E, Bolisetty M, Laise P, Flynn WF, Courtois ET, Burkhart RA, et al. Cross-species single-cell analysis of pancreatic ductal adenocarcinoma reveals antigen-presenting cancer-associated fibroblasts. *Cancer Discov.* (2019) 9:1102–23. doi: 10.1158/2159-8290.CD-19-0094
26. Katsuta E, Qi Q, Peng X, Hochwald SN, Yan L, Takabe K. Pancreatic adenocarcinomas with mature blood vessels have better overall survival. *Sci Rep.* (2019) 9:1310. doi: 10.1038/s41598-018-37909-5
27. Li S, Xu H-X, Wu C-T, Wang W-Q, Jin W, Gao H-L, et al. Angiogenesis in pancreatic cancer: current research status and clinical implications. *Angiogenesis.* (2019) 22:15–36. doi: 10.1007/s10456-018-9645-2
28. Kirkegård J, Mortensen FV, Cronin-Fenton D. Chronic pancreatitis and pancreatic cancer risk: a systematic review and meta-analysis. *Am J Gastroenterol.* (2017) 112:1366–72. doi: 10.1038/ajg.2017.218
29. Hotamisligil GS. Inflammation, metaflammation and immunometabolic disorders. *Nature.* (2017) 542:177–85. doi: 10.1038/nature21363
30. Hosein AN, Brekken RA, Maitra A. Pancreatic cancer stroma: an update on therapeutic targeting strategies. *Nat Rev Gastroenterol Hepatol.* (2020) 17:487–505. doi: 10.1038/s41575-020-0300-1
31. Padoan A, Plebani M, Basso D. Inflammation and pancreatic cancer: focus on metabolism, cytokines, and immunity. *Int J Mol Sci.* (2019) 20:20030676. doi: 10.3390/ijms20030676
32. Nielsen MFB, Mortensen MB, Detlefsen S. Key players in pancreatic cancer-stroma interaction: Cancer-associated fibroblasts, endothelial and inflammatory cells. *World J Gastroenterol.* (2016) 22:2678–700. doi: 10.3748/wjg.v22.i9.2678
33. Feig C, Gopinathan A, Neesse A, Chan DS, Cook N, Tuveson DA. The pancreas cancer microenvironment. *Clin Cancer Res.* (2012) 18:4266–76. doi: 10.1158/1078-0432.CCR-11-3114
34. Whatcott CJ, Posner RG, Von Hoff DD, Han H. Desmoplasia and chemoresistance in pancreatic cancer. In: Grippo PJ, Munshi HG, editors. Pancreatic Cancer and Tumor Microenvironment [Internet]. Trivandrum (India): Transworld Research Network (2012) (accessws April 23, 2020). Available online at: http://www.ncbi.nlm.nih.gov/books/NBK98939/
35. Amakye D, Jagani Z, Dorsch M. Unraveling the therapeutic potential of the Hedgehog pathway in cancer. *Na Med.* (2013) 19:1410–22. doi: 10.1038/nm.3389
36. Tian C, Clauser KR, Öhlund D, Rickelt S, Huang Y, Gupta M, et al. Proteomic analyses of ECM during pancreatic ductal adenocarcinoma progression reveal different contributions by tumor and stromal cells. *Proc Natl Acad Sci USA.* (2019) 116:19609–18. doi: 10.1073/pnas.1908626116
37. Naba A, Clauser KR, Ding H, Whittaker CA, Carr SA, Hynes RO. The extracellular matrix: Tools and insights for the "omics" era. *Matrix Biol.* (2016) 49:10–24. doi: 10.1016/j.matbio.2015.06.003
38. Imamura T, Iguchi H, Manabe T, Ohshio G, Yoshimura T, Wang ZH, et al. Quantitative analysis of collagen and collagen subtypes I, III, and V in human pancreatic cancer, tumor-associated chronic pancreatitis, and alcoholic chronic pancreatitis. *Pancreas.* (1995) 11:357–64. doi: 10.1097/00006676-199511000-00007
39. Jian Z, Cheng T, Zhang Z, Raulefs S, Shi K, Steiger K, et al. Glycemic variability promotes both local invasion and metastatic colonization by pancreatic ductal adenocarcinoma. *Cell Mol Gastroenterol Hepatol.* (2018) 6:429–49. doi: 10.1016/j.jcmgh.2018.07.003
40. Bachem MG, Schünemann M, Ramadani M, Siech M, Beger H, Buck A, et al. Pancreatic carcinoma cells induce fibrosis by stimulating proliferation and matrix synthesis of stellate cells. *Gastroenterology.* (2005) 128:907–21. doi: 10.1053/j.gastro.2004.12.036
41. Provenzano PP, Cuevas C, Chang AE, Goel VK, Von Hoff DD, Hingorani SR. Enzymatic targeting of the stroma ablates physical barriers to treatment of pancreatic ductal adenocarcinoma. *Cancer Cell.* (2012) 21:418–29. doi: 10.1016/j.ccr.2012.01.007
42. Whatcott CJ, Diep CH, Jiang P, Watanabe A, LoBello J, Sima C, et al. Desmoplasia in primary tumors and metastatic lesions of pancreatic cancer. *Clin Cancer Res.* (2015) 21:3561–8. doi: 10.1158/1078-0432.CCR-14-1051
43. Weniger M, Honselmann KC, Liss AS. The extracellular matrix and pancreatic cancer: a complex relationship. *Cancers.* (2018) 10:316. doi: 10.3390/cancers10090316
44. Shintani Y, Hollingsworth MA, Wheelock MJ, Johnson KR. Collagen i promotes metastasis in pancreatic cancer by activating c-jun nh2-terminal kinase 1 and up-regulating n-cadherin expression. *Cancer Res.* (2006) 66:11745–53. doi: 10.1158/0008-5472.CAN-06-2322
45. Armstrong T, Packham G, Murphy LB, Bateman AC, Conti JA, Fine DR, et al. Type I collagen promotes the malignant phenotype of pancreatic ductal adenocarcinoma. *Clin Cancer Res.* (2004) 10:7427–37. doi: 10.1158/1078-0432.CCR-03-0825
46. Ohlund D, Lundin C, Ardnor B, Oman M, Naredi P, Sund M. Type IV collagen is a tumour stroma-derived biomarker for pancreas cancer. *Br J Cancer.* (2009) 101:91–7. doi: 10.1038/sj.bjc.6605107
47. Öhlund D, Franklin O, Lundberg E, Lundin C, Sund M. Type IV collagen stimulates pancreatic cancer cell proliferation, migration, and inhibits apoptosis through an autocrine loop. *BMC Cancer.* (2013) 13:1–11. doi: 10.1186/1471-2407-13-154
48. Berchtold S, Grünwald B, Krüger A, Reithmeier A, Hähl T, Cheng T, et al. Collagen type V promotes the malignant phenotype of pancreatic ductal adenocarcinoma. *Cancer Lett.* (2015) 356(2, Part B):721–32. doi: 10.1016/j.canlet.2014.10.020

49. Clementz AG, Mutolo MJ, Leir S-H, Morris KJ, Kucybala K, Harris H, et al. Collagen XV inhibits epithelial to mesenchymal transition in pancreatic adenocarcinoma cells. *PLoS ONE.* (2013) 8:e72250. doi: 10.1371/journal.pone.0072250
50. Veenstra VL, Damhofer H, Waasdorp C, Steins A, Kocher HM, Medema JP, et al. Stromal SPOCK1 supports invasive pancreatic cancer growth. *Mol Oncol.* (2017) 11:1050–64. doi: 10.1002/1878-0261.12073
51. Li J, Ke J, Fang J, Chen J-P. A potential prognostic marker and therapeutic target: SPOCK1 promotes the proliferation, metastasis, and apoptosis of pancreatic ductal adenocarcinoma cells. *J Cell Biochem.* (2020) 121:743–54. doi: 10.1002/jcb.29320
52. Li X, Truty MA, Kang Y, Chopin-Laly X, Zhang R, Roife D, et al. Extracellular lumican inhibits pancreatic cancer cell growth and is associated with prolonged survival after surgery. *Clin Cancer Res.* (2014) 20:6529–40. doi: 10.1158/1078-0432.CCR-14-0970
53. Li X, Kang Y, Roife D, Lee Y, Pratt M, Perez MR, et al. Prolonged exposure to extracellular lumican restrains pancreatic adenocarcinoma growth. *Oncogene.* (2017) 36:5432–8. doi: 10.1038/onc.2017.125
54. Köninger J, Giese NA, Mola FF di, Berberat P, Giese T, Esposito I, et al. Overexpressed decorin in pancreatic cancer: potential tumor growth inhibition and attenuation of chemotherapeutic action. *Clin Cancer Res.* (2004) 10:4776–83. doi: 10.1158/1078-0432.CCR-1190-03
55. Weber CK, Sommer G, Michl P, Fensterer H, Weimer M, Gansauge F, et al. Biglycan is overexpressed in pancreatic cancer and induces G1-arrest in pancreatic cancer cell lines. *Gastroenterology.* (2001) 121:657–67. doi: 10.1053/gast.2001.27222
56. Chen W-B, Lenschow W, Tiede K, Fischer JW, Kalthoff H, Ungefroren H. Smad4/DPC4-dependent regulation of biglycan gene expression by transforming growth factor-beta in pancreatic tumor cells. *J Biol Chem.* (2002) 277:36118–28. doi: 10.1074/jbc.M203709200
57. Otterbein H, Lehnert H, Ungefroren H. Negative control of cell migration by rac1b in highly metastatic pancreatic cancer cells is mediated by sequential induction of nonactivated smad3 and biglycan. *Cancers (Basel).* (2019) 11: 11121959. doi: 10.3390/cancers11121959
58. Aprile G, Avellini C, Reni M, Mazzer M, Foltran L, Rossi D, et al. Biglycan expression and clinical outcome in patients with pancreatic adenocarcinoma. *Tumour Biol.* (2013) 34:131–7. doi: 10.1007/s13277-01 2-0520-2
59. Rainiero HR, Emmerich PB, Sievers CK, Maloney CJ, Pitera RT, Payne SN, et al. Abstract 1904: Versican production is driven by both epithelial and stromal cells in pancreatic cancer. *Cancer Res.* (2019) 79(13 Supplement):1904–904. doi: 10.1158/1538-7445.AM20 19-1904
60. Skandalis SS, Kletsas D, Kyriakopoulou D, Stavropoulos M, Theocharis DA. The greatly increased amounts of accumulated versican and decorin with specific post-translational modifications may be closely associated with the malignant phenotype of pancreatic cancer. *Biochim Biophys Acta.* (2006) 1760:1217–25. doi: 10.1016/j.bbagen.2006.03.021
61. Yang C, Liu Z, Zeng X, Wu Q, Liao X, Wang X, et al. Evaluation of the diagnostic ability of laminin gene family for pancreatic ductal adenocarcinoma. *Aging (Albany NY).* (2019) 11:3679–703. doi: 10.18632/aging.102007
62. Zhang H, Pan Y-Z, Cheung M, Cao M, Yu C, Chen L, et al. LAMB3 mediates apoptotic, proliferative, invasive, and metastatic behaviors in pancreatic cancer by regulating the PI3K/Akt signaling pathway. *Cell Death Dis.* (2019) 10:230. doi: 10.1038/s41419-019-1320-z
63. Hu D, Ansari D, Zhou Q, Sasor A, Said Hilmersson K, Andersson R. Stromal fibronectin expression in patients with resected pancreatic ductal adenocarcinoma. *World J Surg Oncol.* (2019) 17:29. doi: 10.1186/s12957-019-1574-z
64. Porter RL, Magnus NKC, Thapar V, Morris R, Szabolcs A, Neyaz A, et al. Epithelial to mesenchymal plasticity and differential response to therapies in pancreatic ductal adenocarcinoma. *Proc Natl Acad Sci USA.* (2019) 16:26835–45. doi: 10.1073/pnas.1914915116
65. Hu D, Ansari D, Pawłowski K, Zhou Q, Sasor A, Welinder C, et al. Proteomic analyses identify prognostic biomarkers for pancreatic ductal adenocarcinoma. *Oncotarget.* (2018) 9:9789–807. doi: 10.18632/oncotarget.23929
66. Topalovski M, Brekken RA. Matrix control of pancreatic cancer: New insights into fibronectin signaling. *Cancer Letters.* (2016) 381:252–8. doi: 10.1016/j.canlet.2015.12.027
67. Hiroshima Y, Kasajima R, Kimura Y, Komura D, Ishikawa S, Ichikawa Y, et al. Novel targets identified by integrated cancer-stromal interactome analysis of pancreatic adenocarcinoma. *Cancer Letters.* (2020) 469:217–27. doi: 10.1016/j.canlet.2019.10.031
68. Amrutkar M, Aasrum M, Verbeke CS, Gladhaug IP. Secretion of fibronectin by human pancreatic stellate cells promotes chemoresistance to gemcitabine in pancreatic cancer cells. *BMC Cancer.* (2019) 19:596. doi: 10.1186/s12885-019-5803-1
69. Goehrig D, Nigri J, Samain R, Wu Z, Cappello P, Gabiane G, et al. Stromal protein βig-h3 reprogrammes tumour microenvironment in pancreatic cancer. *Gut.* (2019) 68:693–707. doi: 10.1136/gutjnl-2018-317570
70. Turtoi A, Musmeci D, Wang Y, Dumont B, Somja J, Bevilacqua G, et al. Identification of novel accessible proteins bearing diagnostic and therapeutic potential in human pancreatic ductal adenocarcinoma. *J Proteome Res.* (2011) 10:4302–13. doi: 10.1021/pr200527z
71. Sato T, Muramatsu T, Tanabe M, Inazawa J. Identification and characterization of transforming growth factor beta-induced in circulating tumor cell subline from pancreatic cancer cell line. *Cancer Sci.* (2018) 109:3623–33. doi: 10.1111/cas.13783
72. Costanza B, Rademaker G, Tiamiou A, De Tullio P, Leenders J, Blomme A, et al. Transforming growth factor beta-induced, an extracellular matrix interacting protein, enhances glycolysis and promotes pancreatic cancer cell migration. *Int J Cancer.* (2019) 145:1570–84. doi: 10.1002/ijc.32247
73. Yoneura N, Takano S, Yoshitomi H, Nakata Y, Shimazaki R, Kagawa S, et al. Expression of annexin II and stromal tenascin C promotes epithelial to mesenchymal transition and correlates with distant metastasis in pancreatic cancer. *Int J Mol Med.* (2018) 2:821–30. doi: 10.3892/ijmm.2018.3652
74. Furuhashi S, Sakaguchi T, Murakami T, Fukushima M, Morita Y, Ikegami K, et al. Tenascin C in the tumor-nerve microenvironment enhances perineural invasion and correlates with locoregional recurrence in pancreatic ductal adenocarcinoma. *Pancreas.* (2020) 49:442–54. doi: 10.1097/MPA.0000000000001506
75. Qian S, Tan X, Liu X, Liu P, Wu Y. Exosomal Tenascin-c induces proliferation and invasion of pancreatic cancer cells by WNT signaling. *Onco Targets Ther.* (2019) 12:3197–205. doi: 10.2147/OTT.S192218
76. Xu Y, Li Z, Jiang P, Wu G, Chen K, Zhang X, et al. The co-expression of MMP-9 and Tenascin-C is significantly associated with the progression and prognosis of pancreatic cancer. *Diagn Pathol.* (2015) 10:211. doi: 10.1186/s13000-015-0445-3
77. Cai J, Lu W, Du S, Guo Z, Wang H, Wei W, et al. Tenascin-C modulates cell cycle progression to enhance tumour cell proliferation through AKT/FOXO1 signalling in pancreatic cancer. *Journal of Cancer.* (2018) 9:4449–62. doi: 10.7150/jca.25926
78. Löhr M, Schmidt C, Ringel J, Kluth M, Müller P, Nizze H, et al. Transforming growth factor-beta1 induces desmoplasia in an experimental model of human pancreatic carcinoma. *Cancer Res.* (2001) 61:550–5.
79. Neuzillet C, Gramont A de, Tijeras-Raballand A, Mestier L de, Cros J, Faivre S, et al. Perspectives of TGF-β inhibition in pancreatic and hepatocellular carcinomas. *Oncotarget.* (2013) 5:78–94. doi: 10.18632/oncotarget.1569
80. Shen W, Tao G, Zhang Y, Cai B, Sun J, Tian Z. TGF-β in pancreatic cancer initiation and progression: two sides of the same coin. *Cell Biosci.* (2017) 7:39. doi: 10.1186/s13578-017-0168-0
81. Principe DR, Park A, Dorman MJ, Kumar S, Viswakarma N, Rubin J, et al. TGFβ blockade augments pd-1 inhibition to promote t-cell-mediated regression of pancreatic cancer. *Mol Cancer Ther.* (2019) 18:613–20. doi: 10.1158/1535-7163.MCT-18-0850
82. Bailey JM, Swanson BJ, Hamada T, Eggers JP, Singh PK, Caffery T, et al. Sonic hedgehog promotes desmoplasia in pancreatic cancer. *Clin Cancer Res.* (2008) 14:5995–6004. doi: 10.1158/1078-0432.CCR-08-0291
83. Sano M, Ijichi H, Takahashi R, Miyabayashi K, Fujiwara H, Yamada T, et al. Blocking CXCLs - CXCR2 axis in tumor-stromal interactions contributes to survival in a mouse model of pancreatic ductal adenocarcinoma through reduced cell invasion/migration and a shift of immune-inflammatory microenvironment. *Oncogenesis.* (2019) 8:1–12. doi: 10.1038/s41389-018-0117-8

84. Ijichi H, Chytil A, Gorska AE, Aakre ME, Bierie B, Tada M, et al. Inhibiting Cxcr2 disrupts tumor-stromal interactions and improves survival in a mouse model of pancreatic ductal adenocarcinoma. *J Clin Invest.* (2011) 121:4106–17. doi: 10.1172/JCI42754
85. Leclerc E, Vetter SW. The role of S100 proteins and their receptor RAGE in pancreatic cancer. *Biochim Biophys Acta.* (2015) 1852:2706–11. doi: 10.1016/j.bbadis.2015.09.022
86. Arumugam T, Ramachandran V, Sun D, Peng Z, Pal A, Maxwell DS, et al. Designing and developing S100P inhibitor 5-methyl cromolyn for pancreatic cancer therapy. *Mol Cancer Ther.* (2013) 12:654–62. doi: 10.1158/1535-7163.MCT-12-0771
87. Dakhel S, Padilla L, Adan J, Masa M, Martinez JM, Roque L, et al. S100P antibody-mediated therapy as a new promising strategy for the treatment of pancreatic cancer. *Oncogenesis.* (2014) 3:e92. doi: 10.1038/oncsis.2014.7
88. Slapak EJ, Duitman J, Tekin C, Bijlsma MF, Spek CA. Matrix metalloproteases in pancreatic ductal adenocarcinoma: key drivers of disease progression? *Biology.* (2020) 9:80. doi: 10.3390/biology9040080
89. Awasthi N, Mikels-Vigdal AJ, Stefanutti E, Schwarz MA, Monahan S, Smith V, et al. Therapeutic efficacy of anti-MMP9 antibody in combination with nab-paclitaxel-based chemotherapy in pre-clinical models of pancreatic cancer. *J Cell Mol Med.* (2019) 23:3878–87. doi: 10.1111/jcmm.14242
90. Rath N, Morton JP, Julian L, Helbig L, Kadir S, McGhee EJ, et al. ROCK signaling promotes collagen remodeling to facilitate invasive pancreatic ductal adenocarcinoma tumor cell growth. *EMBO Mol Med.* (2017) 9:198–218. doi: 10.15252/emmm.201606743
91. Oria VO, Lopatta P, Schmitz T, Preca B-T, Nyström A, Conrad C, et al. ADAM9 contributes to vascular invasion in pancreatic ductal adenocarcinoma. *Mol Oncol.* (2019) 13:456–79. doi: 10.1002/1878-0261.12426
92. Schlomann U, Koller G, Conrad C, Ferdous T, Golfi P, Garcia AM, et al. ADAM8 as a drug target in pancreatic cancer. *Nat Commun.* (2015) 6:6175. doi: 10.1038/ncomms7175
93. Veenstra VL, Damhofer H, Waasdorp C, van Rijssen LB, van de Vijver MJ, Dijk F, et al. ADAM12 is a circulating marker for stromal activation in pancreatic cancer and predicts response to chemotherapy. *Oncogenesis.* (2018) 7:87. doi: 10.1038/s41389-018-0096-9
94. Bloomston M, Shafii A, Zervos EE, Rosemurgy AS. TIMP-1 overexpression in pancreatic cancer attenuates tumor growth, decreases implantation and metastasis, and inhibits angiogenesis. *J Surg Res.* (2002) 102:39–44. doi: 10.1006/jsre.2001.6318
95. Benzing C, Lam H, Tsang CM, Rimmer A, Arroyo-Berdugo Y, Calle Y, et al. TIMP-2 secreted by monocyte-like cells is a potent suppressor of invadopodia formation in pancreatic cancer cells. *BMC Cancer.* (2019) 19:1214. doi: 10.1186/s12885-019-6429-z
96. D'Costa Z, Jones K, Azad A, van Stiphout R, Lim SY, Gomes AL, et al. Gemcitabine-Induced TIMP1 attenuates therapy response and promotes tumor growth and liver metastasis in pancreatic cancer. *Cancer Res.* (2017) 77:5952–62. doi: 10.1158/0008-5472.CAN-16-2833
97. Mardin WA, Ntalos D, Mees ST, Spieker T, Senninger N, Haier J, et al. SERPINB5 promoter hypomethylation differentiates pancreatic ductal adenocarcinoma from pancreatitis. *Pancreas.* (2016) 45:743–7. doi: 10.1097/MPA.0000000000000526
98. Harris NLE, Vennin C, Conway JRW, Vine KL, Pinese M, Cowley MJ, et al. SerpinB2 regulates stromal remodelling and local invasion in pancreatic cancer. *Oncogene.* (2017) 36:4288–98. doi: 10.1038/onc.2017.63
99. Tian C, Öhlund D, Rickelt S, Lidström T, Huang Y, Hao L, et al. Cancer cell-derived matrisome proteins promote metastasis in pancreatic ductal adenocarcinoma. *Cancer Res.* (2020) 80:1461–74. doi: 10.1158/0008-5472.CAN-19-2578
100. Bianconi D, Herac M, Spies D, Kieler M, Brettner R, Unseld M, et al. SERPINB7 expression predicts poor pancreatic cancer survival upon gemcitabine treatment. *Transl Oncol.* (2019) 12:15–23. doi: 10.1016/j.tranon.2018.08.019
101. Miller BW, Morton JP, Pinese M, Saturno G, Jamieson NB, McGhee E, et al. Targeting the LOX/hypoxia axis reverses many of the features that make pancreatic cancer deadly: inhibition of LOX abrogates metastasis and enhances drug efficacy. *EMBO Mol Med.* (2015) 7:1063–76. doi: 10.15252/emmm.201404827
102. Le Calvé B, Griveau A, Vindrieux D, Maréchal R, Wiel C, Svrcek M, et al. Lysyl oxidase family activity promotes resistance of pancreatic ductal adenocarcinoma to chemotherapy by limiting the intratumoral anticancer drug distribution. *Oncotarget.* (2016) 7:32100–12. doi: 10.18632/oncotarget.8527
103. Mussunoor S, Murray GI. The role of annexins in tumour development and progression. *J Pathol.* (2008) 216:131–40. doi: 10.1002/path.2400
104. O'Sullivan D, Dowling P, Joyce H, McAuley E, McCann A, Henry M, et al. A novel inhibitory anti-invasive MAb isolated using phenotypic screening highlights AnxA6 as a functionally relevant target protein in pancreatic cancer. *Br J Cancer.* (2017) 117:1326–35. doi: 10.1038/bjc.2017.306
105. Karanjawala ZE, Illei PB, Ashfaq R, Infante JR, Murphy K, Pandey A, et al. New markers of pancreatic cancer identified through differential gene expression analyses: claudin 18 and annexin A8. *Am J Surg Pathol.* (2008) 32:188–96. doi: 10.1097/PAS.0b013e31815701f3
106. Zheng L, Foley K, Huang L, Leubner A, Mo G, Olino K, et al. Tyrosine 23 phosphorylation-dependent cell-surface localization of annexin A2 is required for invasion and metastases of pancreatic cancer. *PLoS ONE.* (2011) 6:e19390. doi: 10.1371/journal.pone.0019390
107. Takano S, Togawa A, Yoshitomi H, Shida T, Kimura F, Shimizu H, et al. Annexin II overexpression predicts rapid recurrence after surgery in pancreatic cancer patients undergoing gemcitabine-adjuvant chemotherapy. *Ann Surg Oncol.* (2008) 15:3157–68. doi: 10.1245/s10434-008-0061-5
108. Takahashi H, Katsuta E, Yan L, Dasgupta S, Takabe K. High expression of Annexin A2 is associated with DNA repair, metabolic alteration, and worse survival in pancreatic ductal adenocarcinoma. *Surgery.* (2019) 166:150–6. doi: 10.1016/j.surg.2019.04.011
109. Zhu J, Wu J, Pei X, Tan Z, Shi J, Lubman DM. Annexin A10 is a candidate marker associated with the progression of pancreatic precursor lesions to adenocarcinoma. *PLoS ONE.* (2017) 12:e0175039. doi: 10.1371/journal.pone.0175039
110. Manero-Rupérez N, Martínez-Bosch N, Barranco LE, Visa L, Navarro P. The galectin family as molecular targets: hopes for defeating pancreatic cancer. *Cells.* (2020) 9:689. doi: 10.3390/cells9030689
111. Drifka CR, Loeffler AG, Esquibel CR, Weber SM, Eliceiri KW, Kao WJ. Human pancreatic stellate cells modulate 3D collagen alignment to promote the migration of pancreatic ductal adenocarcinoma cells. *Biomed Microdevices.* (2016) 18:105. doi: 10.1007/s10544-016-0128-1
112. Olivares O, Mayers JR, Gouirand V, Torrence ME, Gicquel T, Borge L, et al. Collagen-derived proline promotes pancreatic ductal adenocarcinoma cell survival under nutrient limited conditions. *Nat Commun.* (2017) 8:16031. doi: 10.1038/ncomms16031
113. Willumsen N, Ali SM, Leitzel K, Drabick JJ, Yee N, Polimera HV, et al. Collagen fragments quantified in serum as measures of desmoplasia associate with survival outcome in patients with advanced pancreatic cancer. *Sci Rep.* (2019) 9:19761. doi: 10.1038/s41598-019-56268-3
114. Iozzo RV, Schaefer L. Proteoglycan form and function: a comprehensive nomenclature of proteoglycans. *Matrix Biol.* (2015) 42:11–55. doi: 10.1016/j.matbio.2015.02.003
115. Patry M, Teinturier R, Goehrig D, Zetu C, Ripoche D, Kim I-S, et al. βig-h3 Represses T-cell activation in type 1 diabetes. *Diabetes.* (2015). 64:4212–9. doi: 10.2337/db15-0638
116. Chiquet-Ehrismann R, Orend G, Chiquet M, Tucker RP, Midwood KS. Tenascins in stem cell niches. *Matrix Biol.* (2014) 37:112–23. doi: 10.1016/j.matbio.2014.01.007
117. Midwood KS, Chiquet M, Tucker RP, Orend G. Tenascin-C at a glance. *J Cell Sci.* (2016) 129:4321–7. doi: 10.1242/jcs.190546
118. Esposito I, Penzel R, Chaib-Harrireche M, Barcena U, Bergmann F, Riedl S, et al. Tenascin C and annexin II expression in the process of pancreatic carcinogenesis. *J Pathol.* (2006) 208:673–85. doi: 10.1002/path.1935
119. Liot S, Aubert A, Hervieu V, Kholti NE, Schalkwijk J, Verrier B, et al. Loss of Tenascin-X expression during tumor progression: A new pan-cancer marker. *Matrix Biol Plus.* (2020) 100021. doi: 10.1016/j.mbplus.2020.100021
120. Ahmed S, Bradshaw A-D, Gera S, Dewan MZ, Xu R. The TGF-β/smad4 signaling pathway in pancreatic carcinogenesis and its clinical significance. *J Clin Med.* (2017) 6:10005. doi: 10.3390/jcm6010005
121. Murphy JE, Wo JY, Ryan DP, Clark JW, Jiang W, Yeap BY, et al. Total Neoadjuvant therapy with folfirinox in combination with losartan followed

by chemoradiotherapy for locally advanced pancreatic cancer. *JAMA Oncol.* (20190) 5:1020–7. doi: 10.1001/jamaoncol.2019.0892
122. Hauge A, Rofstad EK. Antifibrotic therapy to normalize the tumor microenvironment. *J Transl Med.* (2020) 18:207. doi: 10.1186/s12967-020-02376-y
123. Jiang B, Zhou L, Lu J, Wang Y, Liu C, You L, et al. Stroma-targeting therapy in pancreatic cancer: one coin with two sides? *Front Oncol.* (2020) 10:576399. doi: 10.3389/fonc.2020.576399
124. Susek KH, Karvouni M, Alici E, Lundqvist A. The role of CXC chemokine receptors 1-4 on immune cells in the tumor microenvironment. *Front Immunol.* (2018) 9:2159. doi: 10.3389/fimmu.2018.02159
125. Cheng Y, Ma X-L, Wei Y-Q, Wei X-W. Potential roles and targeted therapy of the CXCLs/CXCR2 axis in cancer and inflammatory diseases. *Biochim Biophys Acta Rev Cancer.* (2019) 1871:289–312. doi: 10.1016/j.bbcan.2019.01.005
126. Raeeszadeh-Sarmazdeh M, Coban M, Sankaran B, Radisky E. Engineering protein therapeutics for cancer based on the natural matrix metalloproteinase inhibitor TIMP-1. *The FASEB Journal.* (2020) 34:1. doi: 10.1096/fasebj.2020.34.s1.04889
127. Bramhall SR. The matrix metalloproteinases and their inhibitors in pancreatic cancer. *From molecular science to a clinical application. Int J Pancreatol.* (1997) 21:1–12.
128. Schloer S, Pajonczyk D, Rescher U. Annexins in translational research: hidden treasures to be found. *Int J Mol Sci.* (2018) 19:19061781. doi: 10.3390/ijms19061781
129. Johnson BL, Salazar M d'Alincourt, Mackenzie-Dyck S, D'Apuzzo M, Shih HP, Manuel ER, et al. Desmoplasia and oncogene driven acinar-to-ductal metaplasia are concurrent events during acinar cell-derived pancreatic cancer initiation in young adult mice. *PLoS ONE.* (2019) 14:e0221810. doi: 10.1371/journal.pone.0221810
130. Sato N, Kohi S, Hirata K, Goggins M. Role of hyaluronan in pancreatic cancer biology and therapy: once again in the spotlight. *Cancer Sci.* (2016) 107:569–75. doi: 10.1111/cas.12913
131. Sato N, Cheng X-B, Kohi S, Koga A, Hirata K. Targeting hyaluronan for the treatment of pancreatic ductal adenocarcinoma. *Acta Pharm Sin B.* (2016) 6:101–5. doi: 10.1016/j.apsb.2016.01.002
132. Banerjee S, Modi S, McGinn O, Zhao X, Dudeja V, Ramakrishnan S, et al. Impaired synthesis of stromal components in response to minnelide improves vascular function, drug delivery, and survival in pancreatic cancer. *Clin Cancer Res.* (2016) 22:415–25. doi: 10.1158/1078-0432.CCR-15-1155
133. Nakazawa H, Yoshihara S, Kudo D, Morohashi H, Kakizaki I, Kon A, et al. 4-methylumbelliferone, a hyaluronan synthase suppressor, enhances the anticancer activity of gemcitabine in human pancreatic cancer cells. *Cancer Chemother Pharmacol.* (2006). 57:165–70. doi: 10.1007/s00280-005-0016-5
134. Cheng X-B, Sato N, Kohi S, Yamaguchi K. Prognostic impact of hyaluronan and its regulators in pancreatic ductal adenocarcinoma. *PLoS ONE.* (2013) 8:e80765. doi: 10.1371/journal.pone.0080765
135. van Mackelenbergh MG, Stroes CI, Spijker R, van Eijck CHJ, Wilmink JW, Bijlsma MF, et al. Clinical trials targeting the stroma in pancreatic cancer: a systematic review and meta-analysis. *Cancers (Basel).* (2019) 11:588. doi: 10.3390/cancers11050588
136. Ho WJ, Jaffee EM, Zheng L. The tumour microenvironment in pancreatic cancer - clinical challenges and opportunities. *Nat Rev Clin Oncol.* (2020) 17:527–40. doi: 10.1038/s41571-020-0363-5
137. Hingorani SR, Zheng L, Bullock AJ, Seery TE, Harris WP, Sigal DS, et al. HALO 202: randomized phase ii study of pegph20 plus nab-paclitaxel/gemcitabine versus nab-paclitaxel/gemcitabine in patients with untreated, metastatic pancreatic ductal adenocarcinoma. *J Clin Oncol.* (2018) 36:359–66. doi: 10.1200/JCO.2017.74.9564
138. Banerjee S, Saluja A. Minnelide, a novel drug for pancreatic and liver cancer. *Pancreatology.* (2015) 15(4 Suppl.):S39–43. doi: 10.1016/j.pan.2015.05.472
139. Dauer P, Nomura A, Saluja A, Banerjee S. Microenvironment in determining chemo-resistance in pancreatic cancer: Neighborhood matters. *Pancreatology.* (2017) 17:7–12. doi: 10.1016/j.pan.2016.12.010
140. Jentzsch V, Davis JAA, Djamgoz MBA. Pancreatic Cancer (PDAC): introduction of evidence-based complementary measures into integrative clinical management. *Cancers (Basel).* (2020) 12:3096. doi: 10.3390/cancers12113096
141. Pan S, Brentnall TA, Chen R. Proteome alterations in pancreatic ductal adenocarcinoma. *Cancer Lett.* (2020) 469:429–36. doi: 10.1016/j.canlet.2019.11.020
142. Silsirivanit A. Glycosylation markers in cancer. *Adv Clin Chem.* (2019) 89:189–213. doi: 10.1016/bs.acc.2018.12.005

Conflict of Interest: The authors declare that the research was conducted in the absence of any commercial or financial relationships that could be construed as a potential conflict of interest.

frontiers in Immunology

MINI REVIEW
published: 12 April 2021
doi: 10.3389/fimmu.2021.663902

Did Tenascin-C Co-Evolve With the General Immune System of Vertebrates?

Gertraud Orend[1,2,3] *and Richard P. Tucker*[4*]

[1] Inserm U1109, The Tumor Microenvironment Laboratory, INSERM UMR_S 1109, Faculté de Médecine, Hopital Civil, Institut d'Hématologie et d'Immunologie, Strasbourg, France, [2] Université Strasbourg, Strasbourg, France, [3] Fédération de Médecine Translationnelle de Strasbourg (FMTS), Strasbourg, France, [4] Department of Cell Biology and Human Anatomy, University of California at Davis, Davis, CA, United States

Tenascin-C plays important roles in immunity. Toll-like receptor 4, integrin α9β1 and chemokines have already been identified as key players in executing the immune regulatory functions of tenascin-C. Tenascin-C is also found in reticular fibers in lymphoid tissues, which are major sites involved in the regulation of adaptive immunity. Did the "tool box" for reading and interpreting the immune-regulating instructions imposed by tenascins and tenascin-C co-evolve? Though the extracellular matrix is ancient, tenascins evolved relatively recently. Tenascin-like genes are first encountered in cephalochordates and urochordates, which are widely accepted as the early branching chordate lineages. Vertebrates lacking jaws like the lamprey have tenascins, but a tenascin gene that clusters in the tenascin-C clade first appears in cartilaginous fish. Adaptive immunity apparently evolved independently in jawless and jawed vertebrates, with the former using variable lymphocyte receptors for antigen recognition, and the latter using immunoglobulins. Thus, while tenascins predate the appearance of adaptive immunity, the first tenascin-C appears to have evolved in the first organisms with immunoglobulin-based adaptive immunity. While a C-X-C chemokine is present in the lamprey, C-C chemokines also appear in the first organisms with immunoglobulin-based adaptive immunity, as does the major histocompatibility complex, T-cell receptors, Toll-like receptor 4 and integrin α9β1. Given the importance of tenascin-C in inflammatory events, the co-evolution of tenascin-C and key elements of adaptive and innate immunity is suggestive of a fundamental role for this extracellular matrix glycoprotein in the immune response of jawed vertebrates.

Keywords: tenascin, immunity, evolution, phylogeny, chemokine, development

OPEN ACCESS

Edited by:
Jr-Kai Yu,
Academia Sinica, Taiwan

Reviewed by:
Benyamin Rosental,
Ben-Gurion University of the Negev, Israel
Toshiyuki Murai,
Osaka University, Japan

***Correspondence:**
Richard P. Tucker
rptucker@ucdavis.edu

Specialty section:
This article was submitted to Inflammation, a section of the journal Frontiers in Immunology

Received: *03 February 2021*
Accepted: *22 March 2021*
Published: *12 April 2021*

Citation:
Orend G and Tucker RP (2021) Did Tenascin-C Co-Evolve With the General Immune System of Vertebrates? Front. Immunol. 12:663902. doi: 10.3389/fimmu.2021.663902

INTRODUCTION

Tenascins are extracellular matrix glycoproteins with one or more epidermal growth factor-like repeats, multiple fibronectin type III (FNIII) domains, and a C-terminal fibrinogen-related domain (FReD) (1). In bony fishes and tetrapods there are four tenascins. The first tenascin to be discovered and characterized was tenascin-C (2), which is widely expressed in the embryo at sites of cell

motility and other forms of active morphogenesis but has a much more restricted distribution in adult organisms (3). Tenascin-R (4) and tenascin-W (5, 6) are primarily expressed in the developing nervous system and in developing bone, respectively, though tenascin-W is also found together with tenascin-C in certain stem cell niches in the adult (7). Tenascin-X is widely expressed in loose connective tissue during development and in the adult (8).

In addition to expression in the embryo, tenascin-C is expressed in the adult in a variety of pathologic situations, notably in the stroma of most solid tumors (9) and at other sites of inflammation (10). Midwood et al. (11) found that chronic inflammation associated with rheumatoid arthritis (RA) requires the expression of tenascin-C, and that joint damage from induced erosive arthritis is limited in mice lacking tenascin-C. These authors went on to show that tenascin-C's FReD is a ligand for Toll-like receptor 4 (TLR4), and that tenascin-C acts through TLR4-mediated signaling to initiate the production of pro-inflammatory cytokines (11). Tenascin-C is also an integrin ligand (12), and through integrin α9β1 tenascin-C can induce the expression of pro-inflammatory chemokines such as CCL2, CCL4 and CXCL5 (13). Correspondingly, the expression of CXCL2 is reduced in the absence of tenascin-C in an animal model of liver ischemia and reperfusion injury (14). Using a murine RA model of joint injury, Ruhmann et al. (15) showed that tenascin-C plays an active role in the polarization of Th17 lymphocytes, demonstrating a role for tenascin-C in inflammatory damage from the adaptive immune system. Tenascin-C can promote cancer progression in many ways (9, 16, 17). Recently tenascin-C was shown to contribute to the immune-suppressive microenvironment of the tumor stroma through integrin α9β1 inducing CCL21 (in lymphatic endothelial cells) and TLR4 regulating CCR7 (in CD11c+/dendritic cells) (18, 19). This suggests that cancer cells may be able to hijack important immune-related functions of tenascin-C in tumors.

In this mini review we will explore the possibility that tenascin-C appeared during evolution along with other critical players in the immune system, pointing to fundamental roles for this extracellular matrix glycoprotein in regulating inflammatory events. We will also consider the possibility that tenascin-C acts through some of the same players to perform similar roles during embryonic development.

THE EVOLUTION OF TENASCINS

Phylogenetic analysis can be used to predict the first appearance of a protein during evolution, and in turn this can be used to infer an explanation for the evolution of the protein. Some well-studied extracellular matrix genes encoding components like fibrillar collagens, laminins and thrombospondins are found in the genomes of sponges and sea anemones, indicating that they evolved prior to specialized connective tissues and a complex nervous system (20). Tenascins, in contrast, are not found in the genomes of animals outside the phylum Chordata (21, 22). Invertebrate members of the phylum like the cephalochordates and urochordates have a single tenascin gene (i.e., prior to the whole genome duplication events of ancestral vertebrates), but when included in the construction of phylogenetic trees these tenascins do not belong to any of the four tetrapod tenascin clades. Two tenascins are found in the genome of the Japanese lamprey *Lethenteron japonicum* and one in the genome of the sea lamprey *Petromyzon marinus*. But like the tenascins from invertebrates, the tenascins from these jawless (agnathan) fish do not sort to the tenascin-C, -R, -W or -X clades. Cartilaginous fish like the elephant shark *Chalorhincus milii*, in contrast, have tenascin-C and tenascin-R, while bony fish and tetrapods have all four tenascin paralogs (23). Thus, tenascin-C and tenascin-R evolved together with the first jawed vertebrates (gnathostomes), and additional members of the family appeared later during evolution. The evolution of tenascins is summarized in **Figure 1**.

THE EVOLUTION OF ADAPTIVE IMMUNITY

Like most protostomes and echinoderms, cephalochordates have an extremely complicated innate immune system. An early analysis of the *Branchiostoma* genome revealed 48 TLR genes and 92 nucleotide-binding oligomerization domain-like receptors, among hundreds of other genes related to innate immunity (24). A more recent examination revealed 30 additional TLRs and confirmed their expression (25). However, cephalochordates lack an adaptive immune system. In contrast, jawless vertebrates like the lamprey were first shown, over half a century ago, to have both innate and adaptive immune systems (26). The lamprey's adaptive immune system is based not on recombination-activating gene-mediated rearrangement of light chains and heavy chains to make immunoglobulins, but instead on rearrangement based on leucine-rich repeat cassettes to create variable lymphocyte receptors (VLRs) (27). The lamprey's immune cells express one VLR per cell, and secreted VLR dimers form pentamers (28), not unlike IgM. These stunning examples of convergent evolution were recently reviewed by Flajnik (29). In contrast, all jawed vertebrates, from cartilaginous fish to mammals and birds, have an adaptive immune system based on immunoglobulins, T-cell receptors, and the major histocompatibility complex (MHC). The evolution of immunoglobulin-based adaptive immunity in gnathostomes has been thoroughly reviewed by others (30–34). Thus, adaptive immunity is seen in all vertebrates, but it has evolved independently into a VLR-based system in jawless vertebrates, and into an immunoglobulin-based system in jawed vertebrates.

THE EVOLUTION OF CHEMOKINES

Chemokines are secreted factors that influence cell motility both in the embryo and in the immune system. They are classified according to the arrangement of cysteine residues found at the amino terminus of the protein (C-C, C-X-C, CX3C and XC). Their receptors are named using the same schema (CCR, CXCR, CX3CR and XCR) (35). Invertebrates, including cephalochordates and urochordates, do not have chemokines

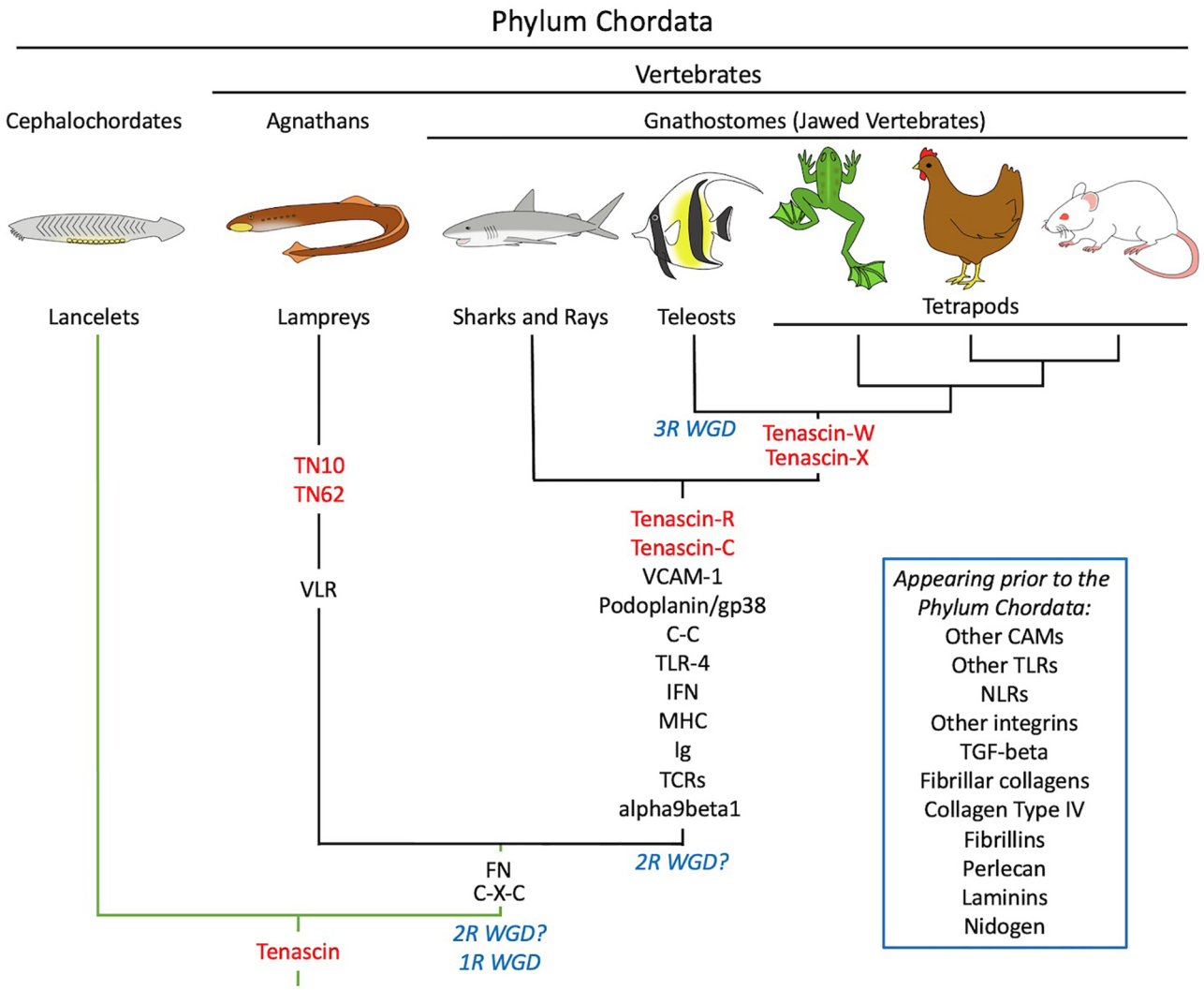

FIGURE 1 | A schematic illustration of the co-evolution of tenascins (in red) and elements of the immune systems of representative chordates. Tenascins first appeared in invertebrate members of the phylum Chordata like the cephalochordates. Branches in green indicate chordates lacking an adaptive immune system, while branches in black indicate chordates with both innate and adaptive immunity. In the vertebrates, the jawless agnathans (e.g., lamprey) evolved adaptive immunity based on variable lymphocyte receptors (VLRs); the first chemokines (C-X-C) and fibronectin (FN) appeared at this time as well. Tenascin-C first appeared in the jawed vertebrates (gnathostomes), together with immunoglobulin (Ig)-based adaptive immunity, the major histocompatibility complex (MHC), additional chemokines (C-C), interferons (IFN), T-cell receptors (TCR), Toll-like receptor 4 (TLR4) and the integrin α9β1. Podoplanin/gp38 and VCAM-1 appeared at this time as well. Many key elements of reticular fibers and vertebrate immune systems predate the evolution of chordates and are included in the inset. See text for details. 1R WGD, First round whole genome duplication; 2R WGD (with the question marks showing two proposed periods for this event), Second round whole genome duplication; 3R WGD, third round whole genome duplication; CAMs, cell adhesion molecules; TN10 and TN62, lamprey-specific tenascins; NLRs, nucleotide-binding oligomerization domain-like receptors.

(24), but a C-X-C chemokine (an IL-8 homologue) has been found in the lamprey (36), and extensive analysis of the lamprey genome reveals three CXCRs homologous to CXCRs from human (37). The same study demonstrated the presence of 6 CCRs, 5 CXCRs and a XCR in the elephant shark, and even more in bony fishes. Thus, while C-X-C chemokines evolved with the first vertebrates, the large number and diversity of chemokines found in mammalian genomes first appeared with the evolution of jawed vertebrates.

THE EVOLUTION OF THE EXTRACELLULAR MATRIX OF RETICULAR FIBERS

The presence of tenascin-C in the reticular fibers of lymphoid organs (38) and in tumor matrix tracks (39) is remarkable and may represent an ancient defense program that is reused, or perhaps better characterized as mis-used, in cancer. However, most of the other extracellular matrix molecules found in

reticular fibers appear to be more ancient than tenascin-C. For example, fibrillar collagens, collagen type IV, fibrillins, perlecan, laminins and nidogen are found in the genomes of sponges and placozoans (20). Other specific collagen types found in reticular fibers appear significantly later, but still predate the jawed vertebrates (e.g., collagen type XII is found in urochordates [Gene ID 100182938]). Fibronectin evolved in jawless vertebrates (23), i.e., after tenascins but before tenascin-C and gnathostome-specific immunity. Fibroblast reticular cells (FRCs) are an important stromal cell type that shapes the structure and function of lymph nodes (40). FRC markers such as podoplanin/gp38 and VCAM-1 appear to have co-evolved with tenascin-C in jawed fishes (41) (XM_033029124.1), though other cell adhesion molecules are quite ancient (42). Remarkably, stroma in oral squamous cell carcinomas has lymphoid properties characterized by abundant FRCs expressing extracellular matrix components of lymph nodes including tenascin-C and utilizing CCR7/CCL21 signaling for retaining CD11c+ immune cells in the tumor matrix tracks. Moreover, in the absence of tenascin-C these lymphoid properties are largely diminished suggestive of tenascin-C as an orchestrator of these tissues (19).

DISCUSSION

Tenascins appeared with the first chordates, but tenascin-C evolved with the jawed vertebrates. This coincides with the evolution of immunoglobulin-based adaptive immunity, the MHC, most chemokines, T-cell receptors, interferon Types I and II (43), and TLR-4 (**Figure 1**). Given the recently identified roles of tenascin-C in regulating inflammatory events, tenascin-C may have evolved, in part, to play a key function in adaptive and innate immunity in jawed vertebrates. The high amino acid sequence conservation in tenascin-C (44) and the absence of gross deletions of tenascin-C underscores a potential important role in the organism, perhaps related to fine-tuning adaptive immunity. Interestingly, α9β1 integrin also evolved in vertebrates even though homologues of other alpha integrin subunits are found much earlier in sponges and sea anemones (45, 46).

Not all of the hardware in the mammalian immunoglobulin-based adaptive immunity tool kit co-evolved with tenascin-C in cartilaginous fishes. As described above, some chemokines predate the appearance of tenascin-C, and other key elements appear to have evolved after. For example, the natural killer cell activating receptor NKG2D is not found in fishes, amphibians, reptiles or birds, but is limited instead to mammals, including monotremes (e.g., the platypus) (XM_029081597.1). Others, like transforming growth factor β, appeared earlier in the first deuterostomes (47).

Mucosal fluids such as breast milk have anti-HIV activity, and this activity is mimicked with exogenous tenascin-C and lost when naturally occurring tenascin-C is removed from breast milk (48). Tenascin-C is proposed to block the interaction between the HIV-1 envelope protein (Env) and the coreceptor CCR5/CXCR4 *via* binding to the HIV-1 Env V3 loop *via* the FNIII and FReD domains in tenascin-C, and appears to require oligomerization and N-linked glycosylations (49). Thus, tenascin-C can also play an important role in preventing infection through pathways independent of the traditional innate and adaptive immune systems. This may be another reason why the tenascin-C sequence is so highly conserved.

While tenascin-C is expressed during inflammation, it is also abundant in the normal embryo. For example, tenascin-C is found in the extracellular matrix surrounding neural crest cells (50), a population of migratory cells that also appears to have evolved in the first vertebrates (51). Neural crest cells themselves make tenascin-C (52), and they stop migrating if this tenascin-C expression is disrupted with antisense morpholinos (53). Tenascin-C may have similar roles during inflammation and development. For example, neural crest cell migration into the pharyngeal arches of the chicken embryo is disrupted by CXCR4 antagonists (54), and CXCR4-null mice have abnormally small dorsal root ganglia, which are formed from the neural crest (55). As the CXCR4 ligand, SDF-1/CXCL12, is also a chemoattractant for T-lymphocytes (56), tenascin-C may be acting through similar pathways in the embryo and during the immune response.

One of the places where tenascin-C is expressed in the adult organism, and in the embryo, is in stem cell niches (e.g., neural, hair follicle, dental pulp, periosteal, hematopoietic and lymphoid progenitor stem cell niches) (7). As in immunity, the many roles of chemokines in a variety of stem cell niches in regulating cell proliferation and migration are well known, suggesting the use of similar tool kits in diverse systems (57–59). Future studies can be directed toward exploring potential roles for tenascin-C and chemokine expression and functions in the stem cell niches.

What does phylogenetic analysis tell us about tenascin-C and its role as a TLR-4 ligand? While TLRs are ancient parts of the innate immune system that predate the evolution of tenascins by hundreds of millions of years (60–62), TLR-4 is a relatively new member of the family that co-evolved with tenascin-C in jawed vertebrates (63). However, interactions between the FReD of tenascin-C and TLR-4 may not be limited to this member of the tenascin family, as the binding pocket of the FReD is found in the other tenascin family members as well (64). One intriguing possibility is that the tenascin/TLR interactions may have predated the roles currently being found for tenascin-C in the immune systems of vertebrates and may indicate a fundamental role for tenascins in invertebrate chordates in regulating their innate immunity. Future studies should address in more detail the common determinators of how tenascin-C regulates innate and adaptive immunity through TRL4, integrin α9β1, chemokines and other yet-to-be-identified partners. This could also be important in the defense against microbes, as described above with HIV-1.

We have focused here on well-known elements of innate and adaptive immunity in vertebrates and especially on molecules with known connections to tenascin-C; future studies should concentrate on other players in the context of the evolution of extracellular matrix.

AUTHOR CONTRIBUTIONS

GO conceived the review topic and contributed to the manuscript's outline, editing, and literature search. RPT wrote the manuscript and prepared the figure. All authors contributed to the article and approved the submitted version.

FUNDING

GO is supported by INSERM, the University Strasbourg, Agence National de la Recherche (ANR-ACKITEC, ANR-MatrixNash), Institut National Contre le Cancer (INCa PLBIO-TENMAX), and L'Alliance nationale pour les sciences de la vie et de la santé (AVIESAN-Radio3R).

ACKNOWLEDGMENTS

GO would like to acknowledge all members of the Tumor Microenvironment laboratory for the active discussions on extracellular matrix in health and diseases.

REFERENCES

1. Chiquet-Ehrismann R, Tucker RP. Tenascins and the importance of adhesion modulation. *Cold Spring Harb Perspect Biol* (2011) 3:a004960. doi: 10.1101/cshperspect.a004960
2. Chiquet M. Tenascin-C: From discovery to structure-function relationships. *Front Immunol* (2020) 11:611789. doi: 10.3389/fimmu.2020.611789
3. Midwood KS, Chiquet M, Tucker RP, Orend G. Tenascin-C at a glance. *J Cell Sci* (2016) 129:4321–7. doi: 10.1242/jcs.190546
4. Anlar B, Gunel-Ozcan A. Tenascin-R: Role in the central nervous system. *Int J Biochem Cell Biol* (2012) 44:1385–9. doi: 10.1016/j.biocel.2012.05.009
5. Tucker RP, Degen M. The expression and possible functions of tenascin-W during development and disease. *Front Cell Dev Biol* (2019) 7:53. doi: 10.3389/fcell.2019.00053
6. Degen M, Scherberich A, Tucker RP. Tenascin-W: Discovery, evolution and future prospects. *Front Immunol* (2020) 11:623305. doi: 10.3389/fimmu.2020.623305
7. Chiquet-Ehrismann R, Orend G, Chiquet M, Tucker RP, Midwood KS. Tenascins in stem cell niches. *Matrix Biol* (2014) 37:112–23. doi: 10.1016/j.matbio.2014.01.007
8. Valcourt U, Alcaraz LB, Exposito JY, Lethias C, Bartholin L. Tenascin-X: Beyond the architectural function. *Cell Adh Migr* (2015) 9:154–65. doi: 10.4161/19336918.2014.994893
9. Lowy CM, Oskarsson T. Tenascin-C in metastasis: A view from the invasive front. *Cell Adh Migr* (2015) 9:112–24. doi: 10.1080/19336918.2015.1008331
10. Marzeda AM, Midwood KS. Internal affairs: Tenascin-C as a clinically relevant, endogenous driver of innate immunity. *J Histochem Cytochem* (2018) 66:289–304. doi: 10.1369/0022155418757443
11. Midwood K, Sacre S, Piccinini AM, Inglis J, Trebaul A, Chan E, et al. Tenascin-C is an endogenous activator of Toll-like receptor 4 that is essential for maintaining inflammation in arthritic joint disease. *Nat Med* (2009) 15:774–80. doi: 10.1038/nm.1987
12. Tucker RP, Chiquet-Ehrismann R. Tenascin-C: Its functions as an integrin ligand. *Int J Biochem Cell Biol* (2015) 65:165–8. doi: 10.1016/j.biocel.2015.06.003
13. Kanayama M, Kurotaki D, Morimoto J, Asano T, Matsui Y, Nakayama Y, et al. Alpha9 integrin and its ligands constitute critical joint microenvironments for development of autoimmune arthritis. *J Immunol* (2009) 182:8015–25. doi: 10.4049/jimmunol.0900725
14. Kuriyama N, Duarte S, Hamada T, Busuttil RW, Coito AJ. Tenascin-C: A novel mediator of hepatic ischemia and reperfusion injury. *Hepatology* (2011) 54:2125–36. doi: 10.1002/hep.24639
15. Ruhmann M, Piccinini AM, Kong PL, Midwood KS. Endogenous activation of adaptive immunity: Tenascin-C drives interleukin-17 synthesis in murine arthritic joint disease. *Arthritis Rheumatol* (2012) 64:2179–90. doi: 10.1002/art.34401
16. Orend G, Chiquet-Ehrismann R. Tenascin-C induced signaling in cancer. *Cancer Lett* (2006) 244:143–63. doi: 10.1016/j.canlet.2006.02.017
17. Yoshida T, Akatsuka T, Imanaka-Yoshida K. Tenascin-C and integrins in cancer. *Cell Adh Migr* (2015) 9:96–104. doi: 10.1080/19336918.2015.1008332
18. Deligne C, Murdamoothoo D, Gammage AN, Gschwandtner M, Erne W, Loustau T, et al. Matrix-targeting immunotherapy controls tumor growth and spread by switching macrophage phenotype. *Cancer Immunol Res* (2020) 8:368–82. doi: 10.1158/2326-6066.CIR-19-0276
19. Spenlé C, Loustau T, Murdamoothoo D, Erne W, Beghelli-de la Forest Divonne S, Veber R, et al. Tenascin-C orchestrates an immune-suppressive tumor microenvironment in oral squamous cell carcinoma. *Cancer Immunol Res* (2020) 8:1122–38. doi: 10.1158/2326-6066.CIR-20-0074
20. Ozbek S, Balasubramanian PG, Chiquet-Ehrismann R, Tucker RP, Adams JC. The evolution of extracellular matrix. *Mol Biol Cell* (2010) 21:4300–5. doi: 10.1091/mbc.E10-03-0251
21. Tucker RP, Drabikowski K, Hess JF, Ferralli J, Chiquet-Ehrismann R, Adams JC. Phylogenetic analysis of the tenascin gene family: Evidence of origin early in the chordate lineage. *BMC Evol Biol* (2006) 6:60. doi: 10.1186/1471-2148-6-60
22. Tucker RP, Chiquet-Ehrismann R. Evidence for the evolution of tenascin and fibronectin early in the chordate lineage. *Int J Biochem Cell Biol* (2009) 41:424–34. doi: 10.1016/j.biocel.2008.08.003
23. Adams JC, Chiquet-Ehrismann R, Tucker RP. The evolution of tenascins and fibronectin. *Cell Adh Migr* (2015) 9:22–33. doi: 10.4161/19336918.2014.970030
24. Huang S, Yuan S, Guo L, Yu Y, Li J, Wu T, et al. Genomic analysis of the immune gene repertoire of amphioxus reveals extraordinary innate complexity and diversity. *Genome Res* (2008) 18:1112–26. doi: 10.1101/gr.069674.107
25. Ji J, Ramos-Vicente D, Navas-Pérez E, Herrera-Úbeda C, Lizcano JM, Garcia-Fernàndez J, et al. Characterization of the TLR family in *Branchiostoma lanceolatum* and discovery of a novel TLR22-like involved in dsRNA recognition in Amphioxus. *Front Immunol* (2018) 9:2525. doi: 10.3389/fimmu.2018.02525
26. Finstad J, Good RA. The evolution of the immune response. 3. Immunologic responses in the lamprey. *J Exp Med* (1964) 120:1151–68. doi: 10.1084/jem.120.6.1151
27. Pancer Z, Amemiya CT, Ehrhardt GR, Ceitlin J, Gartland GL, Cooper MD. Somatic diversification of variable lymphocyte receptors in the agnathan sea lamprey. *Nature* (2004) 430:174–80. doi: 10.1038/nature02740
28. Herrin BR, Alder MN, Roux KH, Sina C, Ehrhardt GR, Boydston JA, et al. Structure and specificity of lamprey monoclonal antibodies. *Proc Natl Acad Sci U S A* (2008) 105:2040–5. doi: 10.1073/pnas.0711619105
29. Flajnik MF. A convergent immunological holy trinity of adaptive immunity in lampreys: Discovery of the variable lymphocyte receptors. *J Immunol* (2018) 201:1331–5. doi: 10.4049/jimmunol.1800965
30. Boehm T. Evolution of vertebrate immunity. *Curr Biol* (2012) 22:R722–32. doi: 10.1016/j.cub.2012.07.003
31. Flajnik MF, Du Pasquier L. "Chapter 4: Evolution of the immune system." In: WE Paul, editor. *Fundamental Immunology*. Philadelphia, PA: Lippincott Williams & Wilkins (2013).
32. Zhu LY, Nie L, Zhu G, Xiang LX, Shao JZ. Advances in research of fish immune-relevant genes: a comparative overview of innate and adaptive immunity in teleosts. *Dev Comp Immunol* (2013) 39:39–62. doi: 10.1016/j.dci.2012.04.001
33. Smith NC, Rise ML, Christian SL. A comparison of the innate and adaptive immune systems in cartilaginous fish, ray-finned fish, and lobe-finned fish. *Front Immunol* (2019) 10:2292. doi: 10.3389/fimmu.2019.02292

34. Antonacci R, Massari S, Linguiti G, Caputi Jambrenghi A, Giannico F, Lefranc MP, et al. Evolution of the T-Cell Receptor (TR) loci in the adaptive immune response: The tale of the TRG locus in mammals. *Genes (Basel)* (2020) 11:624. doi: 10.3390/genes11060624
35. Zlotnik A, Yoshie O. Chemokines: a new classification system and their role in immunity. *Immunity* (2000) 12:121–7. doi: 10.1016/s1074-7613(00)80165-x
36. Najakshin AM, Mechetina LV, Alabyev BY, Taranin AV. Identification of an IL-8 homolog in lamprey (*Lampetra fluviatilis*): Early evolutionary divergence of chemokines. *Eur J Immunol* (1999) 29:375–82. doi: 10.1002/(SICI)1521-4141(199902)29:02<375::AID-IMMU375>3.0.CO;2-6
37. Bajoghli B. Evolution and function of chemokine receptors in the immune system of lower vertebrates. *Eur J Immunol* (2013) 43:1686–92. doi: 10.1002/eji.201343557
38. Sobocinski GP, Toy K, Bobrowski WF, Shaw S, Anderson AO, Kaldjian EP. Ultrastructural localization of extracellular matrix proteins of the lymph node cortex: Evidence supporting the reticular network as a pathway for lymphocyte migration. *BMC Immunol* (2010) 11:42. doi: 10.1186/1471-2172-11-42
39. Spenlé C, Gasser I, Saupe F, Janssen KP, Arnold C, Klein A, et al. Spatial organization of the tenascin-C microenvironment in experimental and human cancer. *Cell Adh Migr* (2015) 9:4–13. doi: 10.1080/19336918.2015.1005452
40. Martinez VG, Pankova V, Krasny L, Singh T, Makris S, White IJ, et al. Fibroblastic reticular cells control conduit matrix deposition during lymph node expansion. *Cell Rep* (2019) 29:2810–22.e5. doi: 10.1016/j.celrep.2019.10.103
41. Renart J, San Mauro D, Agorreta A, Rutherford K, Gemmell NJ, Qintanilla M. Evolutionary history of the podoplanin gene. *Gene Rep* (2018) 13:28–37. doi: 10.1016/j.genrep.2018.08.005
42. Tucker RP, Adams JC. Adhesion networks of cnidarians: a postgenomic view. *Int Rev Cell Mol Biol* (2014) 308:323–77. doi: 10.1016/B978-0-12-800097-7.00008-7
43. Secombes CJ, Zou J. Evolution of interferons and interferon receptors. *Front Immunol* (2017) 8:209. doi: 10.3389/fimmu.2017.00209
44. Mackie EJ, Tucker RP. The tenascin-C knockout revisited. *J Cell Sci* (1999) 112:3847–53.
45. Ewan R, Huxley-Jones J, Mould AP, Humphries MJ, Robertson DL, Boot-Handford RP. The integrins of the urochordate *Ciona intestinalis* provide novel insights into the molecular evolution of the vertebrate integrin family. *BMC Evol Biol* (2005) 5:31. doi: 10.1186/1471-2148-5-31
46. Gong Q, Garvey K, Qian C, Yin I, Wong G, Tucker RP. Integrins of the starlet sea anemone *Nematostella vectensis*. *Biol Bull* (2014) 227:211–20. doi: 10.1086/BBLv227n3p211
47. Hinck AP, Mueller TD, Springer TA. Structural biology and evolution of the TGF-β family. *Cold Spring Harb Perspect Biol* (2016) 8:a022103. doi: 10.1101/cshperspect.a022103
48. Fouda GG, Jaeger FH, Amos JD, Ho C, Kunz EL, Anasti K, et al. Tenascin-C is an innate broad-spectrum, HIV-1-neutralizing protein in breast milk. *Proc Natl Acad Sci U S A* (2013) 110:18220–5. doi: 10.1073/pnas.1307336110
49. Mangan RJ, Stamper L, Ohashi T, Eudailey JA, Go EP, Jaeger FH, et al. Determinants of Tenascin-C and HIV-1 envelope binding and neutralization. *Mucosal Immunol* (2019) 12:1004–12. doi: 10.1038/s41385-019-0164-2
50. Mackie EJ, Tucker RP, Halfter W, Chiquet-Ehrismann R, Epperlein HH. The distribution of tenascin coincides with pathways of neural crest cell migration. *Development* (1988) 102:237–50.
51. Bronner ME, LeDouarin NM. Development and evolution of the neural crest: An overview. *Dev Biol* (2012) 366:2–9. doi: 10.1016/j.ydbio.2011.12.042
52. Tucker RP, McKay SE. The expression of tenascin by neural crest cells and glia. *Development* (1991) 112:1031–9.
53. Tucker RP. Abnormal neural crest cell migration after the in vivo knockdown of tenascin-C expression with morpholino antisense oligonucleotides. *Dev Dyn* (2001) 222:115–9. doi: 10.1002/dvdy.1171
54. Rezzoug F, Seelan RS, Bhattacherjee V, Greene RM, Pisano MM. Chemokine-mediated migration of mesencephalic neural crest cells. *Cytokine* (2011) 56:760–8. doi: 10.1016/j.cyto.2011.09.014
55. Belmadani A, Tran PB, Ren D, Assimacopoulos S, Grove EA, Miller RJ. The chemokine stromal cell-derived factor-1 regulates the migration of sensory neuron progenitors. *J Neurosci* (2005) 25:3995–4003. doi: 10.1523/JNEUROSCI.4631-04.2005
56. Bleul CC, Fuhlbrigge RC, Casasnovas JM, Aiuti A, Springer TA. A highly efficacious lymphocyte chemoattractant, stromal cell-derived factor 1 (SDF-1). *J Exp Med* (1996) 184:1101–9. doi: 10.1084/jem.184.3.1101
57. Staniszewska M, Słuczanowska-Głąbowska S, Drukała J. Stem cells and skin regeneration. *Folia Histochem Cytobiol* (2011) 49:375–80. doi: 10.5603/fhc.2011.0053
58. Anthony BA, Link DC. Regulation of hematopoietic stem cells by bone marrow stromal cells. *Trends Immunol* (2014) 35:32–7. doi: 10.1016/j.it.2013.10.002
59. Hocking AM. The role of chemokines in mesenchymal stem cell homing to wounds. *Adv Wound Care (New Rochelle)* (2015) 4:623–30. doi: 10.1089/wound.2014.0579
60. Brennan JJ, Gilmore TD. Evolutionary origins of Toll-like receptor signaling. *Mol Biol Evol* (2018) 35:1576–87. doi: 10.1093/molbev/msy050
61. Meijer AH, Gabby Krens SF, Medina Rodriguez IA, He S, Bitter W, Ewa Snaar-Jagalska B, et al. Expression analysis of the Toll-like receptor and TIR domain adaptor families of zebrafish. *Mol Immunol* (2004) 40:773–83. doi: 10.1016/j.molimm.2003.10.003
62. Palti Y. Toll-like receptors in bony fish: From genomics to function. *Dev Comp Immunol* (2011) 35:1263–72. doi: 10.1016/j.dci.2011.03.006
63. Liu G, Zhang H, Zhao C, Zhang H. Evolutionary history of the Toll-like receptor gene family across vertebrates. *Genome Biol Evol* (2020) 12:3615–34. doi: 10.1093/gbe/evz266
64. Zuliani-Alvarez L, Marzeda AM, Deligne C, Schwenzer A, McCann FE, Marsden BD, et al. Mapping tenascin-C interaction with toll-like receptor 4 reveals a new subset of endogenous inflammatory triggers. *Nat Commun* (2017) 8:1595. doi: 10.1038/s41467-017-01718-7

Conflict of Interest: The authors declare that the research was conducted in the absence of any commercial or financial relationships that could be construed as a potential conflict of interest.

frontiers in Immunology

REVIEW
published: 26 April 2021
doi: 10.3389/fimmu.2021.671485

Extracellular Vesicles: An Emerging Mechanism Governing the Secretion and Biological Roles of Tenascin-C

Lucas Albacete-Albacete[†], *Miguel Sánchez-Álvarez and Miguel Angel del Pozo*[*]

Mechanoadaptation and Caveolae Biology Lab, Area of Cell and Developmental Biology, Centro Nacional de Investigaciones Cardiovasculares (CNIC), Madrid, Spain

OPEN ACCESS

Edited by:
Kyoko Imanaka-Yoshida, Mie University, Japan

Reviewed by:
Yasunori Miyamoto, Ochanomizu University, Japan
Thomas N. Wight, Benaroya Research Institute, United States

***Correspondence:**
Miguel Angel del Pozo
madelpozo@cnic.es

[†]Present address:
Lucas Albacete-Albacete, Cell Biology Division, MRC Laboratory of Molecular Biology, Cambridge, United Kingdom

Specialty section:
This article was submitted to Inflammation, a section of the journal Frontiers in Immunology

Received: *23 February 2021*
Accepted: *08 April 2021*
Published: *26 April 2021*

Citation:
Albacete-Albacete L, Sánchez-Álvarez M and del Pozo MA (2021) Extracellular Vesicles: An Emerging Mechanism Governing the Secretion and Biological Roles of Tenascin-C. Front. Immunol. 12:671485. doi: 10.3389/fimmu.2021.671485

ECM composition and architecture are tightly regulated for tissue homeostasis. Different disorders have been associated to alterations in the levels of proteins such as collagens, fibronectin (FN) or tenascin-C (TnC). TnC emerges as a key regulator of multiple inflammatory processes, both during physiological tissue repair as well as pathological conditions ranging from tumor progression to cardiovascular disease. Importantly, our current understanding as to how TnC and other non-collagen ECM components are secreted has remained elusive. Extracellular vesicles (EVs) are small membrane-bound particles released to the extracellular space by most cell types, playing a key role in cell-cell communication. A broad range of cellular components can be transported by EVs (e.g. nucleic acids, lipids, signalling molecules and proteins). These cargoes can be transferred to target cells, potentially modulating their function. Recently, several extracellular matrix (ECM) proteins have been characterized as *bona fide* EV cargoes, exosomal secretion being particularly critical for TnC. EV-dependent ECM secretion might underpin diseases where ECM integrity is altered, establishing novel concepts in the field such as ECM nucleation over long distances, and highlighting novel opportunities for diagnostics and therapeutic intervention. Here, we review recent findings and standing questions on the molecular mechanisms governing EV–dependent ECM secretion and its potential relevance for disease, with a focus on TnC.

Keywords: tenascin C, extracellular matrix (ECM), exosomes, fibronectin (FN), tumor progression, cardiovascular disease, inflammation

INTRODUCTION

Multicellularity drove the emergence of cell differentiation and functional specialization, changing the continuous communication cells establish with their surrounding environment. A connective substance among tissues ensuring nurturing and functional coordination between cells evolved, giving rise to the extracellular matrix (ECM) (1, 2). In addition to providing a physical scaffold, the ECM actively participates of several biochemical and biomechanical processes related to morphogenesis, differentiation and homeostasis. A meshwork generally composed of water, proteins, glycoproteins and proteoglycans, the ECM exhibits tissue-specific matrix composition and architecture, which provide unique physicochemical properties (3, 4). Importantly, the ECM is constantly remodelled by cells to

maintain tissue and organismal homeostasis across conditions (5–7). Apart from the regulated secretion of specific structural components, ECM architectural remodeling is orchestrated by secreted modifying enzymes (metalloproteinases (MMPs) (8) and their inhibitors (TIMPs) (9), and other enzymes controlling ECM modification and crosslinking—such as lysyl oxidases (LOX) (10) or transglutaminases—, and a reciprocal biomechanical crosstalk with resident cells (11). Several growth factors and cytokines are bound to the ECM and modulate cell adhesion, differentiation, growth and migration (12) and its architecture and physical properties can modulate cell function (13). Conversely, cell proliferation, spatial arrangement and contractility drives ECM remodeling (14–16).

The broad functional relevance of the ECM is reflected by the numerous pathological conditions associated with ECM alteration or dysfunction. Some of these diseases are related to genetic abnormalities that imply a decrease in the expression, or post-translational modification, of certain ECM proteins (17–20). On the other hand, desmoplasia—an increase in bulk ECM deposition and/or dysregulated expression of certain ECM components—(21), causes architectural and biomechanical alterations driving different pathologies, including cardiovascular diseases, chronic inflammation or cancer.

Tenascins are a family of extracellular matrix (ECM) glycoproteins composed of five members (Tenascin-C (TnC), R, W, X and Y), TnC being the best characterized among them (22). TnC is a hexameric protein which contributes to regulate cell substrate adhesion through the modulation of focal adhesion (FA) binding to other ECM components such as fibronectin (FN) (23), and downstream events such as cell activation, apoptotic cascades, and migration. TnC is expressed abundantly during development, especially in the neural system. However, expression levels of TnC in adults are substantially reduced and its presence is virtually limited to stem cell niches and tendons. Increased TnC expression in adult, differentiated tissues is commonly associated with tissue damage and repair, as well as with pathological conditions such as dysregulated inflammation (as occurs, for example, in atherosclerotic lesions) or tumorigenesis (24–31).

Despite their physiopathological relevance, our understanding of the intracellular mechanisms regulating the trafficking and secretion of TnC and many other ECM components is limited (32). Notably, recent studies support that extracellular vesicles (EVs), including exosomes and microvesicles (MVs), can act as carriers of ECM components, including TnC and FN, a well-known, evolutionarily related partner of TnC (33, 34). Here, we review our current knowledge on the role of EVs on TnC secretion and ECM deposit, and their potential relevance for inflammation and disease.

PHYSIOPATHOLOGICAL ROLES OF TnC AND THEIR MOLECULAR BASIS

Certain features of tumor progression and metastasis are currently considered subverted, aberrant wound repair programs (35), where ECM deposit and remodeling by resident fibroblast is dysregulated. This altered stromal ECM can in turn promote several cancer hallmarks (36). For example, sustained proliferation requires cell adhesion to ECM and growth factor-dependent activation of Erk and PI3K, to promote G1/S transition. The ECM can also promote the induction of hypoxia-triggered angiogenesis acting as a reservoir of angiogenesis regulators, activate cell invasion through the regulation of cell adhesion and invadopodia formation, or modulate the immune response (13, 37). Several ECM components exhibiting differential expression and/or arrangement in tumors play relevant roles in the progression of the disease. Altered deposition of different collagen types can regulate cell growth, differentiation and cell migration. An excessive deposition of collagen I in many solid tumor types confers rigidity to the tumor stroma, and its altered assembly and crosslinking, mechanical properties and architectural features such as anisotropy, affect tumor cell biology (3, 5). Other key ECM components also exhibit altered expression in cancer. FN is considered a major building block in ECM fibre assembly and remodeling, and can bind to other molecules including heparin, collagens, tenascins or fibrin to modulate their assembly and their interaction with cells (38, 39).

During development, TnC is expressed robustly and contributes to physiological epithelial-to-mesenchymal transitions (EMT) and morphogenesis (25). In contrast, in normal adult tissues TnC expression is usually low, except for stem cell niches and tendons. Upon tissue damage, TnC can be rapidly upregulated and contributes to physiological inflammation and repair. Owing to its capacity to promote proinflammatory and activated states in different cell types, increased TnC deposition is associated with several pathological conditions. Persistent high levels of TnC can promote chronic inflammation and desmoplasia, driving pathological events such as fibrosis or oncogenesis.

TnC was initially characterized as a modulator of cell adhesion, either through its interaction with other ECM components (23) or through direct binding to specific cell receptors. Its binding to integrins such as α9β1, αVβ3, α8β1 and αVβ6 (27, 28) can induce EMT in several cancer models (40–42), modulate the dynamics of focal adhesions (43, 44) or reduce apoptosis. These characteristics support its potential as a marker of poor prognosis, underpinned by its impact on cell motility and invasion, aberrant angiogenesis (45) and immunomodulation (31, 46, 47). Importantly, TnC modulates the activation state of immune cells such as macrophages and lymphocytes; this appears to be an important aspect of its contribution to both physiological tissue repair, as well as pathological conditions involving tissue remodeling (48–50).

Several mouse models reveal the importance of TnC in tumor progression and its implication in tumor cell survival, proliferation, invasion and metastasis (51, 52). TnC can influence fibroblasts and differentiation of epithelial cells onto myofibloblasts through the tumor growth factor-β (TGF-β) signalling pathway (53), regulate inflammatory signalling by an activation of Toll-like receptor 4 (TLR4) (54) or modulate epidermal growth factor (EGF)-receptor driven cell proliferation cell proliferation (55). As part of the AngioMatrix (56), TnC can participate in the angiogenic switch,

and generate an aberrant vasculature within tumours. Both as a result of this promotion of aberrant angiogenesis, as well as through direct modulation of immune cell populations, TnC is likely an important contributor to the emerging role of stromal ECM composition and architecture as central regulators of antitumor immunity (57–60). An intriguing feature that may be particularly relevant for the rationalization of TnC as a biomarker, or even therapeutic target, in the context of antitumor immunotherapy is its potential to selectively determine macrophage polarity towards M1-like, cytokine-releasing phenotypes (mainly through its interaction with α9β1, αVβ3 and TLR4 receptors); and promote an anergic state in T-cells (presumably by interfering with integrin signalling) (61, 62). Recent studies have shown the beneficial effects of targeting TnC in antitumor immunotherapy in breast (63) and oral squamous cell carcinoma (64) mouse models. Combinational therapy with monoclonal antibodies that inhibited TnC-mediated TLR4 activation and anti-PD-L1 treatment significantly reduced tumor growth and lung metastasis *in vivo* (63). In line with these results, ablation of TnC or its effector CCR7 implied inhibition of the lymphoid immune-suppressive stromal properties, reducing tumor progression and metastasis in oral squamous cell carcinoma (64), indicating a relevant approach in the therapy of head and neck tumors.

TnC has a prominent role in cardiovascular tissue remodeling. Almost invariably, TnC re-expression is associated with cardiovascular pathological processes coursing with inflammation, such as myocardial infarction, hypertensive cardiac fibrosis, myocarditis or dilated cardiomyopathy (65–67). Upregulation of TnC is also a hallmark of the proatherogenic vessel remodeling, driving the progression of atherosclerotic disease (AS) (68–70); however, TnC deficiency in mouse models of genetic hypercholesterolemia exacerbate atherosclerosis and promote lesions prone to rupture, reflecting the delicate balance between the physiological roles of TnC in tissue homeostasis (71).

TnC can play a role in several diseases derived from a fibrotic state generated upon tissue damage (50, 52, 72, 73). For example, in neuroinflammation (29), brain injury (74) or glioma (59), where ECM deposition is enhanced, TnC accumulation is found associated with blood-brain barrier disruption, neuronal apoptosis and activation of inflammatory pathways (mitogen-activated protein kinases and NF-kB). Finally, TnC is implicated in other fibrotic diseases such as kidney and liver damage through orchestration of the fibrotic niche and is considered as a biomarker of poor prognosis (75, 76).

THE STANDING QUESTION OF TnC SECRETION

ECM component biogenesis, intracellular trafficking and export pathways are tightly controlled, but our current mechanistic understanding of these processes, particularly regarding non-collagen ECM components, is rather limited. Collagens, a family of large fibrillar ECM proteins, constitute over 30% of the total protein mass in multicellular organisms (77–79). These proteins are initially synthesized as an immature form, known as preprocollagen, in the endoplasmic reticulum (ER). These polypeptides undergo hydroxylation of proline and lysine residues and are assembled as triple helices, yielding procollagens (80). Procollagens must then be trafficked to the Golgi apparatus for further posttranslational modification. The coat complex type II (COPII) vesicle transport machinery facilitates the regulated transfer of proteins from the ER to the ER-Golgi intermediate compartment (ERGIC) and cis-Golgi (81, 82), and is strictly required for procollagen trafficking and secretion: mutation or genetic ablation of core COPII components such as SAR1B, SEC23A, SEC24A/C or SEC13 profoundly affect the secretion of collagens and lead to their accumulation in the ER (32). In contrast with smaller cargoes, procollagen units are too big (~300nm in length) to be incorporated into conventional ~80-nm COPII (83), and additional regulators (transport and Golgi organization protein 1 (TANGO1), cutaneous T-cell lymphoma-associated antigen 5 (cTAGE5), trafficking From ER To Golgi Regulator (TFG), or the KHLH12-cullin-3 ubiquitin E3 ligase complex) (84–87) have been identified as required for nascent COPII vesicles to accommodate and carry these rigid fibrillar molecules. Finally, procollagens are transported in tubular structures emanating from the Golgi to the plasma membrane (PM) and secreted to the extracellular space, where they will be cleaved to generate tropocollagens and assembled in crosslinked fibrils (**Figure 1**).

While this canonical route is relatively well characterized for collagens, several of its regulators, including core components of the COPII machinery, appear to be dispensable for the secretion of other ECM components. Indeed, the mechanisms governing the trafficking and secretion of a majority of non-collagen ECM proteins have remained puzzlingly elusive (32, 88). Soluble FN, which assembles in fibrillar structures upon secretion to the extracellular space and binding exposed integrins (38), is initially synthesized in the ER (32, 89). Current models describe its transport to the extracellular space through the secretory pathway (90–93), as it reaches the Golgi apparatus (94–98) to undergo further glycosylation (39). However, FN secretion seems to be unaffected by mutation or genetic ablation of core COPII components that severely impair collagen transport from the ER, such as SEC23A (99), SEC24D (100) or TANGO1 (32, 101), and its trafficking remains incompletely explored. Proteins such as periostin (89) and transmembrane P24 Trafficking Protein 2 (TMED2; the human homolog of *emp24*) (102) are proteins potentially associated with the export of FN from the ER.

TnC has a six arm-structure termed hexabrachion, consisting of six 320kDa monomers stabilized by amino-terminal disulphide bonds. In contrast to FN, oligomerization of TnC is a rapid process that takes place cotranslationally in the ER, and two models have been proposed. In one model, the six monomers are simultaneously assembled into a single hexabrachion, as suggested by pulse-chase approaches which found no apparent intermediate species (103). In the second model, oligomerization is a two-step process (104), whereby two intermediate trimers are first formed through the stabilization of alpha-helical coiled-coil interactions at their amino-terminal

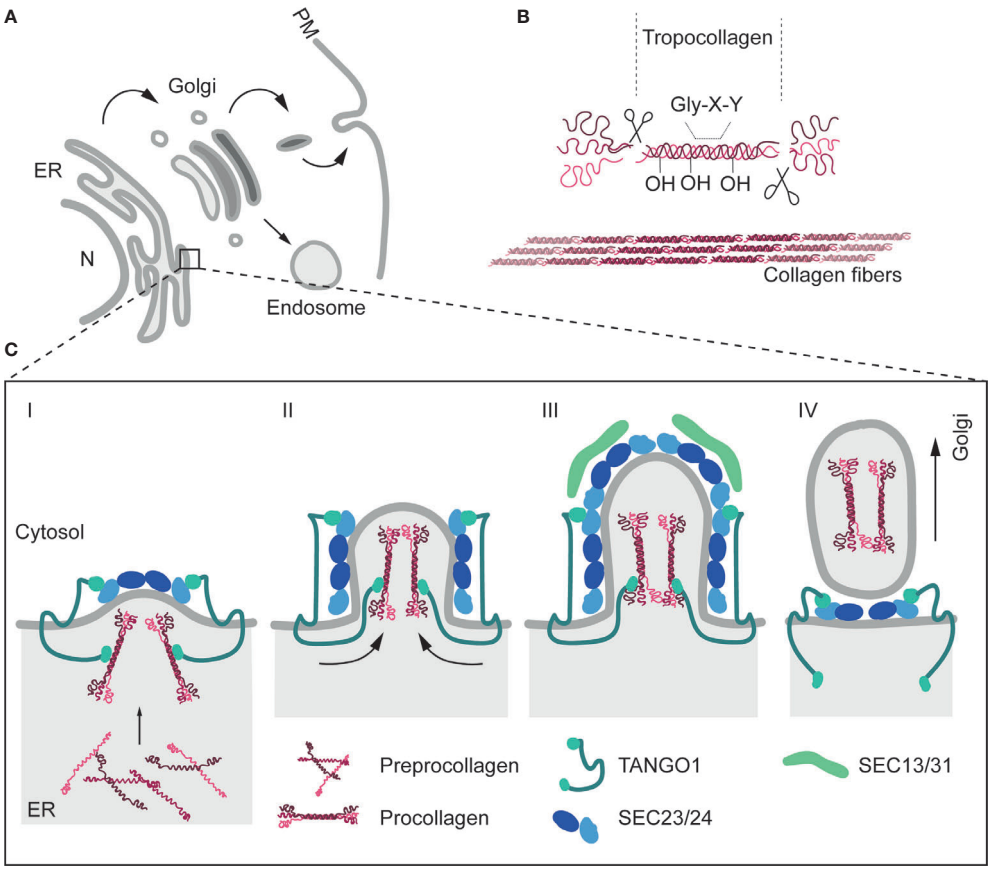

FIGURE 1 | The secretory pathway and collagen secretion. **(A)** Schematic representation of cell secretion routes. The ER constitutes the main protein factory in the cell. ER-associated ribosomes translate proteins that can be subsequently inserted onto the membrane, or released into the ER lumen. After translation, several modifications can be added to proteins bydifferent enzymatic activities. Proteins are then transported to the Golgi apparatus, mainly through the COPII-dependent pathway. Within the Golgi, further modifications are carried out. Finally, proteins will be sorted into vesicles and transported to their final destination, including the plasma membrane (PM) (receptors, adhesion proteins and extracellular proteins) or endosomes. **(B)** Collagens are initially secreted as procollagens. Once in the extracellular space, terminal peptides are cleaved by the procollagen peptidase to form tropocollagen. Finally, collagen fibrils are assembled *via* covalent cross-linking by lysyl oxidases, which link hydroxylysine and lysine residues. Multiple collagen fibrils assemble into collagen fibers. **(C)** In addition to COPII machinery, other regulators are necessary for the proper export of procollagen from the ER. TANGO1 participates in the sorting of procollagen in vesicles through a direct binding through Hsp47 in the lumen of the ER. Preprocollagen peptides are synthesised and assembled in the lumen of the ER. Once procollagens are formed, TANGO1, previously recruited trough the interaction to Sec23 (Sec23/24 complex), position the collagen fibrils in the budding vesicle (Stage I). Later, as the vesicle grow, TANGO1 pushes procollagen molecules towards the lumenal face of the ER (Stage II). In stage III, ER vesicles are big enough to accommodate collagens. TANGO1 separates its SH3-like domain from Hsp47/collagens. This is the followed by the release of TANGO1 from Sec23 and the recruitment of Sec13/31 to the ER membrane. Finally, in stage IV, fission of the collagen-containing vesicles is undertaken and TANGO1 return to interact with the Sec23/24 complex (84).

domains. Then, hexabrachion assembly is favoured by an increase in homophylic binding affinity between the two trimers. Similar to FN, evidence supporting TnC transit through (105), and glycosylation at (24), the Golgi, suggests that TnC is trafficked from the ER to the Golgi apparatus. This transfer appears to be a rate-limiting step for secretion output (103) and is affected in cells treated with brefeldin-A, an inhibitor of ER-Golgi vesicle transport (106). However, like for many other ECM components, the precise mechanisms regulating TnC trafficking and secretion remain incompletely characterized. An unexpected, emerging mechanism for the secretion of these and other non-collagen components, is extracellular vesicle (EV) secretion.

EV BIOGENESIS AND GENERAL FUNCTIONS

Recent studies show that extracellular vesicles (EVs) can export ECM components to the extracellular environment (107), constituting alternative mechanisms for ECM secretion and deposition and implying specific regulatory principles for their trafficking (108, 109). EVs are a heterogeneous group of cell-derived membranous structures that include exosomes and MVs, which defer on their intracellular origin (110).

Exosome biogenesis takes place in the endosomal compartment through endosome membrane budding (111–113). Several mechanisms have been implicated in this process. One of the

most studied mechanisms is dependent on the ESCRT (Endosomal Sorting Complexes Required for Transport) machinery, whose four conserved complexes (ESCRT-0, -I, -II and -III) (114–116) assemble sequentially on the cytosolic surface of the endosomal membrane. Ubiquitylation is an important event not only for ESCRT-dependent vesicle formation, but also for the specification of cargo to be sorted onto exosomes (113, 117). Additionally, evidence for an ESCRT-independent mechanism for exosome biogenesis has been described (118). Specific lipid species such as ceramides (derived from sphingomyelinases-mediated hydrolysis of sphingomyelin) (119), LBPA (lyso-bis-phosphatidic acid) (120) or cholesterol, as well as proteins that modulate membrane organization, including tetraspanins (121) and caveolin-1 (108, 122, 123), have been recently identified as important regulators of ESCRT-independent endosome dynamics and exosome biogenesis.

On the other hand, MVs are derived from scission of small plasma membrane-derived vesicles (110). This process—termed ectocytosis—shares many similar steps to exosome formation. The ESCRT machinery, as well as cytoskeletal elements and their regulators, such as RHO family of GTPases and ROCK, are important for the formation of MVs together with other membrane-associated proteins, including tetraspanins and membrane cargos (124) (**Figure 2**).

Virtually every cell type can release EVs, and these structures are abundant in the extracellular space and body fluids such as plasma, urine and saliva. A broad spectrum of cargoes (e.g. nucleic acids, proteins or signalling molecules) can be sorted onto these vesicles and subsequently exported and transferred to target cells. Many cargoes have been related to the modulation of the biology of acceptor cells in multiple physiologic and pathologic scenarios.

Immune responses are exquisitely regulated to ensure defence from external pathogens or physicochemical insults as well as internal alterations such as tumor cell growth, while avoiding damage of the self. EVs are crucial in the intricate cell-cell communication involved. EVs are frequently described as pro-inflammatory mediators and participate in the propagation of inflammatory signals during infections and chronic inflammatory diseases among components of innate immunity. Mechanistically, several cargoes such as cytokines, receptors and microRNAs can modulate the activation state and function of macrophages, neutrophilic granulocytes and natural killer (NK) cells (125). EVs also participate of several steps of acquired immunity and antigen presentation. Antigen presenting cells (APCs), including B lymphocytes, dendritic cells (DCs) and macrophages can release major histocompatibility complex II (MHC-II) through exosomes enabling antigen presentation to $CD4^+$ T lymphocytes at distance (126). EVs released by tumor cells or several pathogens can constitute a relevant source of antigens for APCs for their processing and presentation to $CD4^+$ T lymphocytes (127, 128).

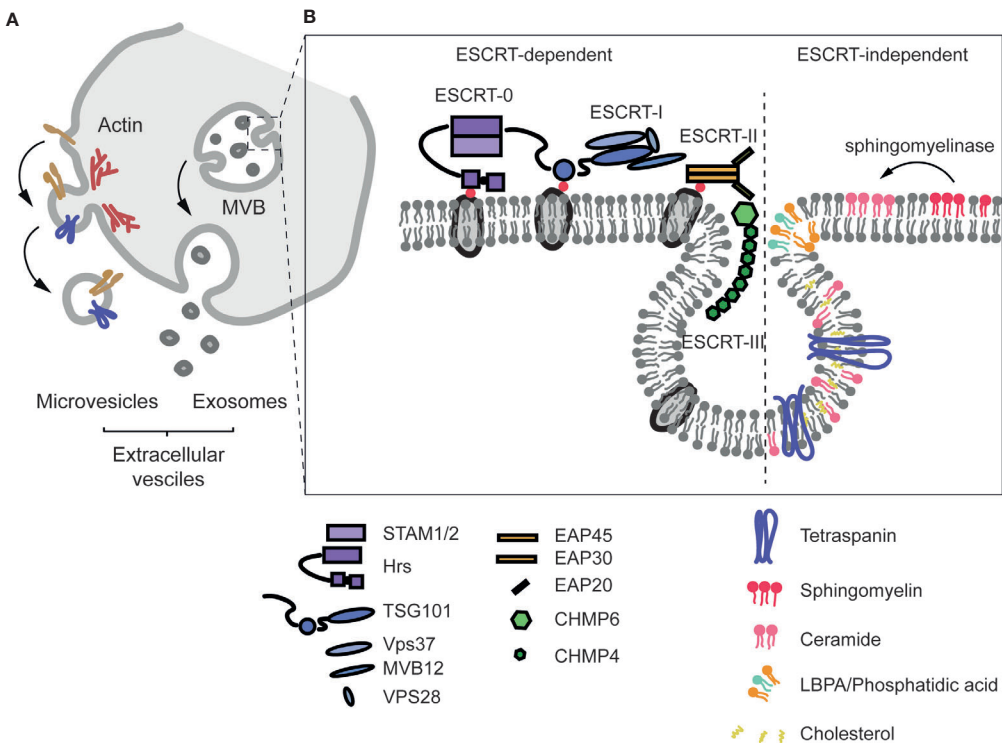

FIGURE 2 | Extracellular vesicle formation. **(A)** Extracellular vesicles are classified according to their origin. Microvesicles are formed from the PM in a process called ectocytosis that depends on the ESCRT machinery and the actin cytoskeleton. Exosomes are derived from the budding process on the membrane of the endosome/multivesicular body, and released to the extracellular space upon fusion of the endosome with the PM. **(B)** Diagram of the structure of the ESCRT machinery and of ESCRT-independent mechanisms implicated in exosome formation.

EVs also actively participate of the immune synapse between lymphocytes and APCs, and lymphocytes specifically relocalize multivesicular bodies (MVBs) towards the contact site, leading to a localized increase in exosome secretion and unidirectional transfer of microRNAs that modulate downstream responses. Highlighting the key role of EV communication in this process, inhibition of exosomes formation/secretion dysregulates gene expression in APCs (129) and reduces antibody production in activated B-cells (130, 131).

Immune cell-derived EVs are also involved in other inflammatory processes such as tissue fibrosis, where an increase in ECM deposition has been described to impact cell behaviour, including cell proliferation, migration and differentiation, and subsequently participating in the development of several pathologies. A prominent EVs profibrotic cargo is interleukin-1β (IL-1β) (132), which is released by DCs upon binding of ATP to P2X purinoceptor 7 (P2X7R) (133) and can act on several IL-1β) receptor-expressing cell types (134, 135). IL-1β can, in turn, induce vesicular secretion of interleukin-6 (IL-6) in mast cells, amplifying inflammation (136). Other ligands that induce fibrosis such as TGF-β or TNFα have also been described as EVs cargoes.

EVs-dependent secretion and inter-tissue communication is also involved in vascular physiopathology (137–140). EVs-mediated communication can be involved in either AS progression or lesion prevention. Krüppel-like factor 2 (KLF2)-expressing endothelial cells (ECs) (an atheroprotective hallmark) can load miR-143/145 in exosomes to control smooth muscle cell (SMC) activation and reduce AS lesion formation (141). In contrast, proinflammatory cues on ECs repress the presence of Ten-eleven translocation 2 (TET2) dioxygenase in exosomes, promoting plaque formation (142). SMCs can influence back endothelial function through EVs: SMC-derived E cargo miR-155 increases endothelial permeability (143). EVs also play a role in the development of an inflammatory environment in the progressing atherosclerotic plaque (144–146). EVs may also directly contribute to subendothelial matrix remodeling and lesion progression, either through recently discovered ECM deposition (see below), as well as sphingomyelin phosphodiesterase 3 (SMPD3)-dependent calcification (147).

Myocardial injury engages mechanisms to repair and maintain cardiac function, including cardiac fibrosis by activation of resident fibroblasts through TGF-β, EDN-1, PDGF, CCN2 and AGTII ligands, which can be released through EVs derived from cardiomyocytes and ECs. Reflecting a role in events after myocardial injury, miRNAs cargo signatures on EVs (including miR-1, -208, -214) (148, 149) emerge as good biomarkers of myocardial infarction detection and prognosis from plasma samples.

Tumor cells (TCs) usually secrete large amounts of EVs, which can influence different aspects of tumor progression and behaviour, including tumour-associated fibroblast activation, angiogenesis, immunomodulation, matrix remodeling or the establishment of pre-metastatic niches. TC populations are heterogeneous (150–152). TCs communicate inside the tumor and can transfer part of their unique characteristics to other surrounding cancer cells. For example, tumour-derived EVs can modulate local growth *via* autocrine transfer of mutant KRAS proto-oncogene to wild type KRAS-expressing colon cancer cells (153). Similarly, glioblastoma microvesicles transport specific RNAs that promote neighbour proliferation (154). EVs can also transmit their capacity to adapt to the characteristic tumor stresses such as hypoxia, changes in pH and nutrient deprivation (155).

Tumor angiogenesis and abnormal vascularization determines its behaviour and response to therapy (156, 157). Many pro-angiogenic factors are tumoral EV cargoes, such as the vascular endothelial growth factor (VEGF), platelet-derived growth factor (PDGF), TGF-b, TNF-a or fibroblast growth factor (FGF) (158). Tumour-derived exosomes can also induce vascular permeability in distant organs in breast, melanoma and colorectal cancers (159–161).

Antitumor immunity and its suppression by tumors are another major focus of research and therapeutic intervention, and EVs also play a role in this process. DCs induce T-cell and NK cell activation in an EV-dependent manner to mount an antitumor response (126, 162–164). As the tumor progresses, TCs deploy mechanisms such as attenuation of NK cell cytotoxicity (block of NKG2D pathway), reduction of T-cell-mediated killing or activation of myeloid-derived suppressor cells (TC-derived EVs can contain PGE2, TGF-b and HSP72) (127).

Under physiological conditions, fibroblasts are in a quiescent state. Upon tissular damage, they can enter an activated state, whereby a "secretory phenotype"—to produce both paracrine signals and new ECM components—and contractile activity—for the biomechanical remodeling of tissue—are acquired. Dysregulated persistent activation is a hallmark of tumour-associated fibroblasts (TAFs) (165) and other pathological conditions coursing with fibrosis and desmoplasia. Tumour-derived EVs can induce fibroblast activation (166), by virtue of microRNA cargo subsets modulating motility, collagen contraction or proliferation (167). TC-derived exosomes can also induce secretion of specific ECM components, such as FN (168, 169), as well as ECM remodeling enzymes (170, 171).

Evidence suggests that EVs can actively participate of ECM sculpting (172, 173), through ECM remodeling cargoes such as MMPs (174) or lysyl oxidases (175, 176). Active MMPs such as MMP-1, -13, -2, -3 or -14 are detected on the surface of EVs derived from several tumor cell types. Moreover, ADAMs family (regulators of cell adhesion and migration) components and more specifically the two most notorious members of this family (ADAM10 and ADAM17) have been described as EVs cargoes (177, 178).

EVs AS ECM CARRIERS: IMPLICATIONS IN ECM SECRETION

Recent studies support that some ECM components are EVs cargoes themselves, implying that trafficking and export mechanisms could coexist with canonical secretion pathways, modulating ECM composition and architecture and

subsequently impacting on cell behaviour. Additionally, EV function could also be linked to ECM remodelling in the sense that ECM fiber components might influence the retention of EVs at specific regions through discrete subsets of receptors in their surface (168), therefore contributing to their selectivity for cell type targeting and favouring a specific evolving composition and architecture of the ECM during its remodeling.

Early observations hinting at the involvement of EVs in matrix secretion and deposition described "matrix vesicles" (179, 180), as a relevant mechanism for osteoblast-mediated primary bone mineralization (181, 182). Secreted matrix vesicles initiate the nucleation of calcium phosphate crystals by an influx of Ca^{2+} and PO_4^{3-} through their membrane transporters and the action of several intraluminal enzymes such as tissue-nonspecific alkaline phosphatase (TNSALP), ectonucleotide pyrophosphatase/phosphodiesterase 1 (ENPP1) or phosphoethanolamine/phosphocholine phosphatase 1 (PHOSPHO1) (182). Interestingly, a role for matrix vesicles has been also described in vascular SMC-driven calcification during AS progression (147).

Our understanding of the implication of EVs in the secretion and deposition of specific ECM components has since considerably lagged. Recent studies have shown that ECM proteins are exported and deposited by EVs (183, 184) (www.vesiclepedia.org, www.exocarta.org) and animal models in which exosome production has been abrogated through disruption of neutral sphingomyelinase (NSMase) activities show marked alterations in ECM deposition and architecture (185, 186). FN is a prominent ECM cargo in EVs from different cell types, and the blockade of exosome secretion partially alters, although does not completely impair, FN fiber deposit (108). Other groups have recently described that FN is transported by EVs. FN accumulates at the surface of exosomes through its binding to heparan-sulfate (187, 188) and that upon beta1 integrin endocytosis (189), FN can be redeposited from the endosomal compartment at the basal cell surface in epithelial cells (cortactin-dependent) (190) and in epicardial cells (mediated by Bves and NDRG4) (191). Moreover, Weaver and colleagues suggested that exosome secretion plays a key role in autocrine deposition of FN at the leading edge of the cells: Golgi secreted FN would be in an inactive form previous to its assembly at the cell surface (38), exosomal FN, presumably sourced from the endosomal compartment (109, 189, 191) would constitute a rapid alternative pathway for competent adhesive substrate deposition (**Figure 3**).

FN-containing EVs have been associated with tumor progression. Certain features of tumor cells can be altered by the presence of FN-positive EVs in the media. Weaver and coworkers have characterized that exosome secretion in invadopodia is essential for FN resecretion, and regulates cell adhesion, directional motility and invasion in tumor cells (109, 192, 193). Invasiveness of fibroblasts is positively regulated by FN-positive EVs treatment (194). Exosomal FN can modulate other functional programmes such as proliferation (195), signal

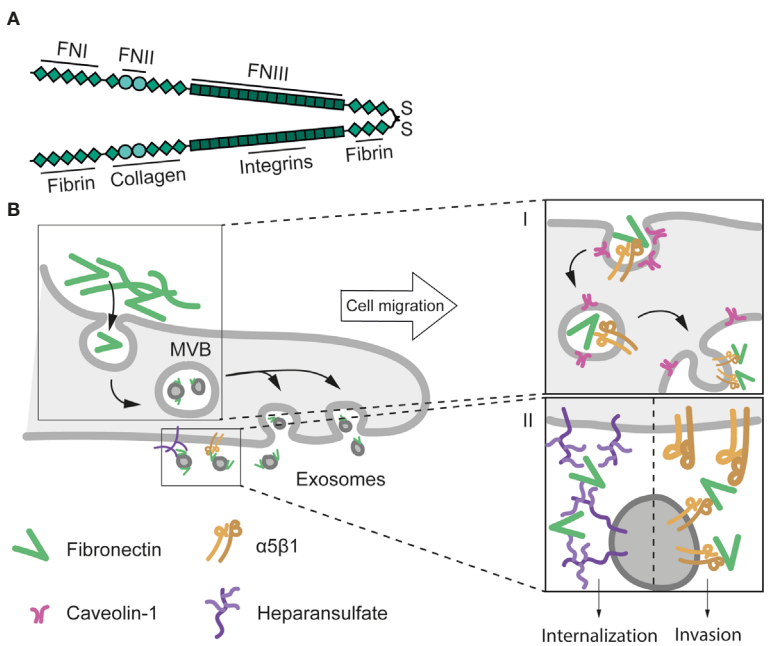

FIGURE 3 | Structure and exosomal secretion of FN. **(A)** Structure of a FN dimer stabilised by a di-sulphide bond. Basic domains (FNI, II, and II) and the main binding sites to other ECM proteins and receptors are depicted. **(B)** Exosome-mediated FN secretion and cell migration. Caveolin-1-dependent β1 integrin endocytosis is implicated in the internalization of extracellular FN. Upon endocytosis, FN is transported to endosomes, where exosomes are formed (stage I) (189). Exosomal FN is then released at invadopodia, and induces cell migration and invasion through its internalization (138) or *via* activation of integrin-mediated pathways (192) (stage II).

transduction (138, 196), endocytosis (197) or cell survival (198). Finally, exosomal FN can modulate tumor immunity. Secretion of FN-containing EVs can be induced by tumour-associated leukocytes (199), but these FN pools can also induce pro-inflammatory IL-1β) production by macrophages (200). FN interacts with acceptor cells through plasma membrane heparansulfate and α5 integrin receptor (109, 187, 200). However, the mechanism of action of exosomal FN seems to require its internalization (138). This apparent discrepancy may indicate that exosomal ECM could be activating several pathways depending on the mechanism by which they interact with acceptor cells (**Table 1**).

EV SECRETION: AN INTEGRAL ASPECT OF TnC BIOLOGICAL ROLES

Recent studies demonstrate that exosome secretion is strictly required for appropriate extracellular TnC deposition by both tumor cells and different fibroblast types (108, 122) (**Figure 4**). Circulating exosomes from cancer patients frequently carry TnC (24), and several cancer cell types secrete TnC in EVs *in vitro* (183, 184) (www.microvesicle.org, www.exocarta.org). Disruption of exosome secretion by pharmacological inhibition or RNAi-mediated depletion of NSMase 2 led to accumulation of TnC at the ER and decreased extracellular TnC fibre formation. These studies excluded internalization of extracellular TnC and established that exosome-secreted TnC is synthesized *de novo*. Mechanistically, caveolin-1 [Cav1; a pivotal regulator of membrane organization, mechanoadaptation, ECM remodeling and cholesterol efflux (16, 203–205)] is strictly required for the appropriate biogenesis of exosome subpopulations of different sizes, and the sorting onto them of specific ECM components, through the control of cholesterol content in endosomal compartments. Interestingly, this effect varies across ECM exosome cargoes, suggesting that the extent of dependency on different secretion routes may be specific for each ECM component; for example, in contrast with TnC, FN deposition is only partially decreased upon disruption of exososomal secretion. Cav1 deficiency, exogenous cholesterol loading or pharmalogical inhibition of cholesterol trafficking from endosomes all markedly impaired exosomal secretion of TnC. Cholesterol homeostasis emerges as an as yet poorly understood mechanism by which membrane trafficking and metabolism potentially feed onto functions allocated at the endosomal compartment, including cell signalling regulation (206, 207) and exosome secretion (108).

The involvement of Cav1 as a central regulator of this process is not trivial. Cav1 is a central node simultaneously regulating the transduction of information on ECM composition and physical properties (204), and the coordinated remodeling of both aspects (16, 108, 208). This reciprocal crosstalk [first discussed by Bissell and Hall as stromal dynamic reciprocity (209)] is key to understand both physiological and pathological processes pertaining different tissues. Furthermore, collagens are not a class of ECM components correlating with TnC in their Cav1-dependent sorting onto exosomes; in fact, Cav1 might regulate oppositely COPII-dependent deposition of collagen, and exosome-mediated secretion of other ECM components (210). It remains to be studied whether other components of caveolae such as PTRF—which does appear to modulate exosome-mediated secretion (211)—also regulate the sorting of ECM components to exosomes. Cav1-dependent regulation of tissue architecture and cell function is relevant for several conditions in

TABLE 1 | Literature contributing evidence of FN as an EV secreted cargo. EVs origin: cell type/tissue from which EVs containing TnC were detected; WB: western blotting.

FN EVs origin	Target cell	Detection approach	Result	Ref.
Myeloma RPMI-8226 and CAG)	Human bone marrow stroma (HS-5), Human umbilical vein endothelial cells	WB and light microscopy	Exosome-cell interaction and internalization Myeloma tumour growth and progression (p38 and pERK activation) Increased endothelial cell invasion	(187)
Fibrosarcoma (HT1080)	Fibrosarcoma (HT1080)	WB and sucrose gradient	Increased motility	(192)
HIV-1 infected dendritic cells	T-lymphocyte	WB	Viral trans-infection Increased IFN-γ, TNF-α, IL-1β and RANTES Activation of p38/Stat pathways	(201)
Human trabecular meshwork cells	N/A	WB	Dexamethasone reduces exosomal FN levels	(188)
Fibrosarcoma (HT1080)	Fibrosarcoma (HT1080)	WB and sucrose gradient	Tumour cell migration	(109)
Transplantation patient serum	N/A	WB	Allograft rejection biomarker	(202)
Human trophoblast	Macrophage	WB	Increased IL-1β production	(200)
Mesenchymal stem cells	Bone marrow (SH-SY5Y)	WB and Proteomics	Increased mitosis and growth factor secretion	(195)
Endothelial cells	Hepatic stellate cell	WB and electron microscopy	Increased AKT phosphorylation Increased cell migration	(138)
Tumour-associated leukocytes	Breast cancer (AT-3) Colon cancer (4T1, CT26)	WB and FACS	Increased exosomal FN Increased tumour cell invasion	(199)
Fibroblast (IMR90)	Fibroblast (IMR90)	Proteomics, FACS	Fibroblast invasion	(194)
Primary melanocyte	Primary melanocyte	WB, proteomics, light microscopy	Increased melanocyte survival after UVB radiation	(198)
Microvascular endothelial cells	Oligodendrocyte precursor cell (OPC)	Proteomics, enzyme-linked immunosorbent assay	OPCs survival and proliferation	(197)

which TnC has a prominent role, such as tumor progression or cardiovascular remodeling (16, 212, 213). An additional standing question is whether Cav1 expression (both during exosome biogenesis as well as at destination) may determine the specificity of exosome-mediated communication, given the prominent role integrins appear to have in this process (168).

Exosome secretion appears to account for the major share (if not the totality) of TnC extracellular release and deposition (108); thus, virtually all biological/physiopathological roles of TnC should be framed by the specific features of exosomal communication. Exosomes enable the transport of cargoes across interorgan distances, and TnC-containing exosomes can nucleate ECM beds in different organs of TnCKO mice such as liver and lungs upon intravenous injection (108); these observations suggest that exosomal deposit of TnC and associated ECM components contributes significantly to pre-metastatic niche formation (169). These pools of exosomal TnC are fully functional and apart from fostering ECM fiber nucleation, efficiently induce proinflammatory states and features compatible with EMT in breast cancer cells in 2D and 3D culture models (108, 122). Exosomal TnC levels also correlate with invasiveness in pancreatic ductal adenocarcinoma (184, 214), and induce invasion through WNT/β-catenin signaling, a crucial pathway in EMT modulation, and activation of the NF/κB pathway (214). Exosomes have also recently emerged as efficient platforms for immunomodulation in the tumor microenvironment and other tissue contexts (131, 215); it is likely that the prominent roles TnC has as a regulator of immune cell function (see first section) are exerted at least in part through exosomes. Interestingly, exosomes released by SARS-CoV2-infected cells are significantly enriched in TnC and could promote the propagation of inflammation to distant sites (216). Serum TnC levels have been explored as diagnostic/prognostic markers in different pathologies (24), but whether all circulating TnC is exclusively trafficked through EVs is yet to be determined. Other examples of paracrine secretion of TnC in exosomes include osteoblasts (217), airway epithelial cells (218) and several tumor cells (183, 184), where exosomal TnC has been associated to alterations of pre-existing ECM, impacting collagen and alkaline phosphatase activity. Yong and co-workers also described that brain tumour-initiating cells can secrete TnC in exosomes and suppress T-cell activation, enabling tumor progression and metastasis through the modulation of antitumor immunity (219). Mechanistically, TnC could inhibit T-cell activation and proliferation through the well-established TnC receptors α5β1 and αvβ6 integrins, reducing mTOR signaling (**Figure 5** and **Table 2**).

Additionally, it may be considered that TnC fibers at a given ECM niche could act as efficient receptors for the homing of

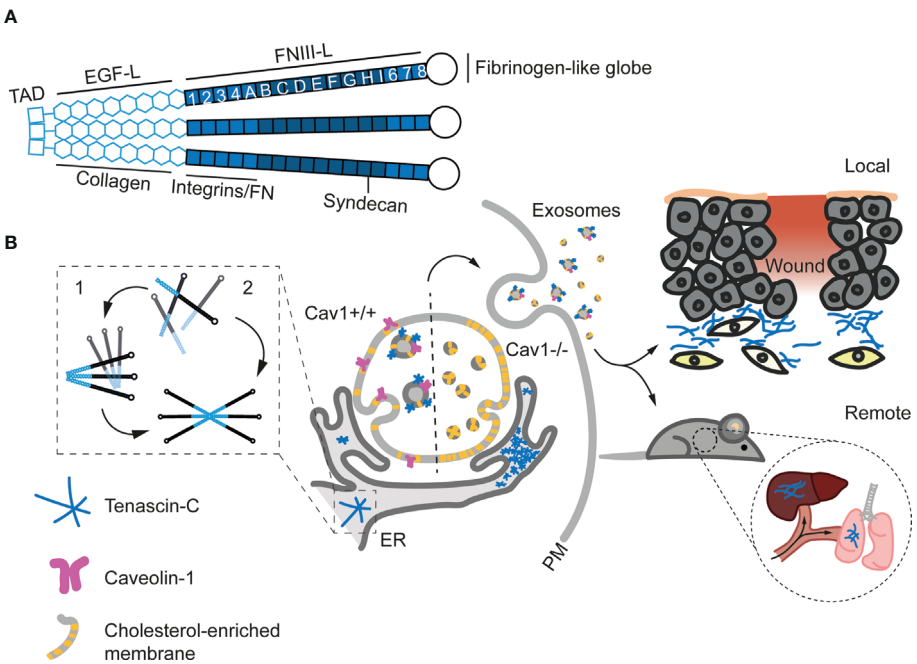

FIGURE 4 | Structure and exosomal secretion of TnC. **(A)** Structure of a trimer of TnC. Tenascin monomers bind *via* the tenascin assembly domain (TAD) located at the N-terminus. Basic domains (EGF-Like and FNIII-Like) and the main binding sites to other ECM proteins and receptors are depicted. **(B)** Models for TnC biosynthesis. In model 1, hexabrachions are formed in a very rapid co-translational process where six monomers are simultaneously assembled. In model 2, the hexabrachion assembly take place in two steps. First, monomers form an intermediary trimer through α-helical coiled-coil interactions in the TAD. Subsequently, two trimers assemble in a hexamer that is stabilized by di-sulphide bonds. **(C)** Exosome-mediated TnC secretion. After biosynthesis in the ER, TnC is transported to multivesicular bodies (MVBs) in a Cav1 dependent manner ($Cav1^{+/+}$). The absence of Cav1 ($Cav1^{-/-}$) increases the levels of cholesterol at MVBs and alters exosome formation, preventing the sorting of TnC onto exosomes and leading to the accumulation of TnC in the ER. Upon secretion, exosomal TnC can be locally deposited, or modulate the behavior of surrounding cells. On the other hand, exosomes can eventually reach the blood stream and generate new TnC nucleation points at distant organs and tissues (108).

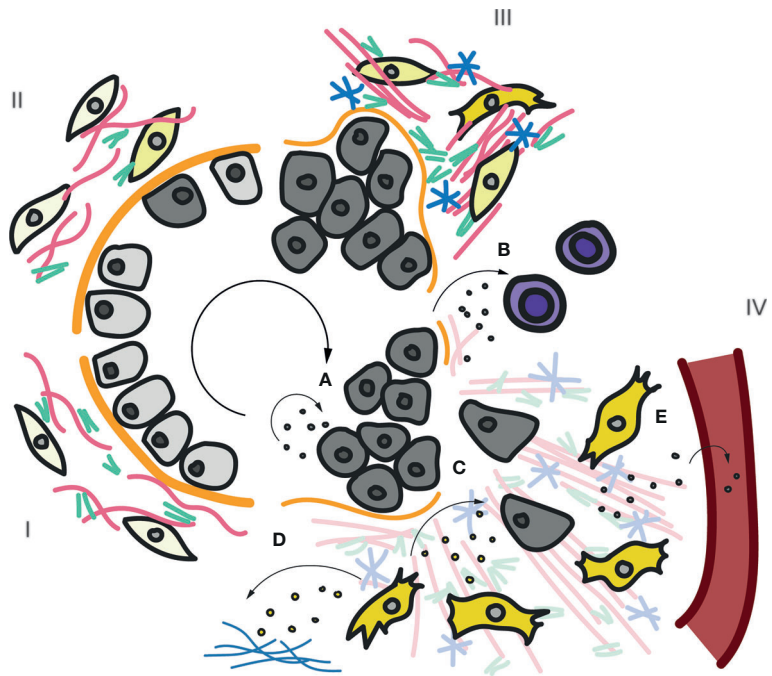

FIGURE 5 | Roles of exosomal TnC in cancer progression and immunomodulation. Scheme of the main stages (I-IV) in carcinoma tumor progression. In stage I a normal epithelium is shown, composed by epithelial cells located on a basal membrane. Underneath, the interstitial matrix deposited by stromal cells provides support. Insults promote transformation of epithelial cells onto tumoral cells, which lose polarity and adhesion (Stage II). In stage III, continuously activated fibroblasts increase the production and secretion of ECM, including collagens, FN and TnC. Tumor cells start invading neighbouring tissues and degrading the basal membrane. Finally, in stage IV, a highly remodelled ECM favors tumor cell migration through the interstitial space towards blood and lymphatic vessels, to metastasize. The previously described roles of exosomal TnC in tumor progression are depicted **(A–E)**. **(A)** Paracrine/autocrine secretion of TnC-loaded exosomes induce tumor cell proliferation and invasion (122). **(B)** Exosomal TnC derived from brain tumour-initiating cells suppresses mTOR activity and T-cell activity (219)(Mirzaei et al). Activated fibroblasts can also secrete exosomes carrying TnC that can **(C)** modulate tumor cells and/or deposit new TnC matrix (108) **(D)**. Finally, TnC-positive exosomes can be released into the bloodstream to deposit TnC at distant organs **(E)**. An increase in TnC in plasma has been proposed as poor prognosis marker in many cancers and inflammatory diseases (24).

TABLE 2 | Literature contributing evidence of TnC as an EV secreted cargo. EVs origin: cell type/tissue from which EVs containing TnC were detected; WB: western blotting.

TnC EVs origin	Target cell	Detection approach	Result	Ref.
Fibroblast	Breast cancer (MDA-MB-468)	WB, sucrose gradient and proteomics	Matrix deposition in 2D, 3D and *in vivo* increased migration and invasion	(108)
Breast cancer (MDA-MB-231)	Breast cancer (MDA-MB-231, T47-D)	WB, proteomics	increased migration and invasion	(122)
Brain tumor-initiating cells Glioblastoma patients	T-lymphocyte	WB	Inhibition of mTOR signalling and inhibition of T-cell proliferation, activation and cytokine secretion	(219)
Osteoblast-like cells (SaOS2)	N/A	WB	Bone mineralization	(217)
Pancreatic cancer (PC-1, PC-1.0, AsPC-1, Capan-2)	Pancreatic cancer	WB	Increased migration and invasion Increased proliferation through activation of the NF/kB	(214)
Metastatic colorectal cancer (SW480, SW620)	N/A	Proteomics	Increased exosomal TnC in metastatic cell lines	(183)
Pancreatic ductal adenocarcinoma patients (pancreatic duct fluid)	N/A	Proteomics	Increased exosomal TnC correlates with stromal TnC matrix	(184)

exosome subsets exposing TnC-binding receptors, a mechanism that may contribute to ECM remodeling and its coordination with cell modulation. Finally, the consideration of features derived from exosomal secretion might be highly relevant for biomedical applications aiming at tissue repair and regeneration: exosomes would potentially enable for accurate "dosage" and target specificity (220), and might hold the key for leveraging on the tissue remodeling and repair activities of TnC (221) through

very controlled time frames, bypassing uncontrolled chronic inflammation states.

CONCLUDING REMARKS AND PERSPECTIVES

The characterization of mechanisms driving ECM deposit and of antifibrotic agents (72, 222, 223) aiming at intervening or preventing diseases such as chronic hepatitis (224), kidney diseases (225), systemic sclerosis, pulmonary fibrosis (226, 227) or cancer and tumor progression (228) has been intensive. Throughout the past decade, the study of EV-associated ECM components has expanded our understanding of ECM biology. EVs have been suggested as integral components of stromal environments (172, 173), and enable the impact of ECM-secreting cell populations on distant organismal locations. These insights have opened several key questions. We do not know whether EV-mediated transport of certain ECM components specifies their function at destiny. Mechanistically, we have a very limited understanding as to how ECM components are routed for sorting onto exosomes, instead of being targeted for degradation at the endosomal compartment; whether and how cells use different potential mechanisms for the secretion of a given ECM component; and how these processes are integrated with the complex reciprocal regulation established between ECM and stromal cells. Finally, the principles by which target cell specificity (168) correlates with this ECM secretion activity remain unexplored. The potential interplay of EV-carried TnC with other cargoes regarding their impact on target cells is also a key question. Given the potential of EV-trafficked TnC levels as serum diagnosis/prognosis biomarkers, and the ability of EVs to nucleate novel ECM niches at specific organs, the biology of exosomal TnC secretion holds the promise to explore potential novel theranostic applications.

AUTHOR CONTRIBUTIONS

LA-A, MS-Á, and MP conceived and wrote the article. LA-A created all infographics, and led bibliographical revision with support from MS-Á. MP coordinated the review. All authors contributed to the article and approved the submitted version.

FUNDING

The authors acknowledge the grant support to MP from the Spanish Ministerio de Ciencia e Innovación (CSD2009-0016, SAF2014-51876-R, SAF2017-83130-R, BFU2016-81912-REDC, and IGP-SO-MINSEV1512-07-2016), Fundació La Marató de TV3 (674/C/2013 and 201936-30-31), Worldwide Cancer Research Foundation (# 15-0404), Asociación Española Contra el Cáncer (PROYE20089DELP), and Fondo Europeo de Desarrollo Regional *"Una manera de hacer Europa"*. MP received funding from the European Union Horizon 2020 research and innovation program under Marie Sklodowska-Curie grant agreement no. 641639, and is member of the Tec4Bio consortium (ref. S2018/NMT4443; Actividades de I+D entre Grupos de Investigación en Tecnologías, Comunidad Autónoma de Madrid/FEDER, Spain). LA-A was supported by a Ministerio de Ciencia, Innovación y Universidades predoctoral fellowship associated with the Severo Ochoa Excellence program (ref. SVP-2013-06789). The Centro Nacional de Investigaciones Cardiovasculares Carlos III is supported by the Ministerio de Ciencia e Innovación and the Pro CNIC Foundation and is a Severo Ochoa Center of Excellence (SEV-2015-0505).

ACKNOWLEDGMENTS

We thank members of the del Pozo lab for insightful discussions and suggestions.

REFERENCES

1. Hynes RO. The Evolution of Metazoan Extracellular Matrix. *J Cell Biol* (2012) 196:671–9. doi: 10.1083/jcb.201109041
2. Ozbek S, Balasubramanian PG, Chiquet-Ehrismann R, Tucker RP, Adams JC. The Evolution of Extracellular Matrix. *Mol Biol Cell* (2010) 21:4300–5. doi: 10.1091/mbc.e10-03-0251
3. Frantz C, Stewart KM, Weaver VM. The Extracellular Matrix At a Glance. *J Cell Sci* (2010) 123:4195–200. doi: 10.1242/jcs.023820
4. Cox TR, Erler JT. Remodeling and Homeostasis of the Extracellular Matrix: Implications for Fibrotic Diseases and Cancer. *Dis Model Mech* (2011) 4:165–78. doi: 10.1242/dmm.004077
5. Egeblad M, Rasch MG, Weaver VM. Dynamic Interplay Between the Collagen Scaffold and Tumor Evolution. *Curr Opin Cell Biol* (2010) 22:697–706. doi: 10.1016/j.ceb.2010.08.015
6. Kass L, Erler JT, Dembo M, Weaver VM. Mammary Epithelial Cell: Influence of Extracellular Matrix Composition and Organization During Development and Tumorigenesis. *Int J Biochem Cell Biol* (2007) 39:1987–94. doi: 10.1016/j.biocel.2007.06.025
7. Bonnans C, Chou J, Werb Z. Remodelling the Extracellular Matrix in Development and Disease. *Nat Rev Mol Cell Biol* (2014) 15:786–801. doi: 10.1038/nrm3904
8. Mott JD, Werb Z. Regulation of Matrix Biology by Matrix Metalloproteinases. *Curr Opin Cell Biol* (2004) 16:558–64. doi: 10.1016/j.ceb.2004.07.010
9. Arpino V, Brock M, Gill SE. The Role of Timps in Regulation of Extracellular Matrix Proteolysis. *Matrix Biol* (2015) 44–46:247–54. doi: 10.1016/j.matbio.2015.03.005
10. Trackman PC. Functional Importance of Lysyl Oxidase Family Propeptide Regions. *J Cell Commun Signal* (2018) 12:45–53. doi: 10.1007/s12079-017-0424-4
11. Alexander J, Cukierman E. Stromal Dynamic Reciprocity in Cancer: Intricacies of Fibroblastic-ECM Interactions. *Curr Opin Cell Biol* (2016) 42:80–93. doi: 10.1016/j.ceb.2016.05.002
12. Hynes RO. The Extracellular Matrix: Not Just Pretty Fibrils. *Science (80-)* (2009) 326:1216–9. doi: 10.1126/science.1176009
13. Pickup MW, Mouw JK, Weaver VM. The Extracellular Matrix Modulates the Hallmarks of Cancer. *EMBO Rep* (2014) 15:1243–53. doi: 10.15252/embr.201439246
14. Calvo F, Ege N, Grande-Garcia A, Hooper S, Jenkins RP, Chaudhry SI, et al. Mechanotransduction and YAP-Dependent Matrix Remodelling is Required for the Generation and Maintenance of Cancer-Associated Fibroblasts. *Nat Cell Biol* (2013) 15:637–46. doi: 10.1038/ncb2756
15. Mohammadi H, Sahai E. Mechanisms and Impact of Altered Tumour Mechanics. *Nat Cell Biol* (2018) 20:766–74. doi: 10.1038/s41556-018-0131-2

16. Goetz JG, Minguet S, Navarro-Lérida I, Lazcano JJ, Samaniego R, Calvo E, et al. Biomechanical Remodeling of the Microenvironment by Stromal Caveolin-1 Favors Tumor Invasion and Metastasis. *Cell* (2011) 146 (1):148–63. doi: 10.1016/j.cell.2011.05.040
17. Valcourt U, Alcaraz LB, Exposito JY, Lethias C, Bartholin L. Tenascin-X: Beyond the Architectural Function. *Cell Adh Migr* (2015) 9:154–65. doi: 10.4161/19336918.2014.994893
18. Marini JC, Forlino A, Cabral WA, Barnes AM, San Antonio JD, Milgrom S, et al. Consortium for Osteogenesis Imperfecta Mutations in the Helical Domain of Type I Collagen: Regions Rich in Lethal Mutations Align With Collagen Binding Sites for Integrins and Proteoglycans. *Hum Mutat* (2007) 28:209–21. doi: 10.1002/humu.20429
19. Pober BR. Williams-Beuren Syndrome. *N Engl J Med* (2010) 362:239–52. doi: 10.1056/NEJMra0903074
20. Jarvelainen H, Sainio A, Koulu M, Wight TN, Penttinen R. Extracellular Matrix Molecules: Potential Targets in Pharmacotherapy. *Pharmacol Rev* (2009) 61:198–223. doi: 10.1124/pr.109.001289
21. Wynn TA, Ramalingam TR. Mechanisms of Fibrosis: Therapeutic Translation for Fibrotic Disease. *Nat Med* (2012) 18:1028–40. doi: 10.1038/nm.2807
22. Jones FS, Jones PL. The Tenascin Family of ECM Glycoproteins: Structure, Function, and Regulation During Embryonic Development and Tissue Remodeling. *Dev Dyn* (2000) 218:235–59. doi: 10.1002/(SICI)1097-0177(200006)218:2<235::AID-DVDY2>3.0.CO;2-G
23. Huang W, Chiquet-Ehrismann R, Moyano JV, Garcia-Pardo A, Orend G. Interference of Tenascin-C With Syndecan-4 Binding to Fibronectin Blocks Cell Adhesion and Stimulates Tumor Cell Proliferation. *Cancer Res* (2001) 61:8586–94.
24. Giblin SP, Midwood KS. Tenascin-C: Form Versus Function. *Cell Adh Migr* (2015) 9:48–82. doi: 10.4161/19336918.2014.987587
25. Midwood KS, Chiquet M, Tucker RP, Orend G. Tenascin-C At a Glance. *J Cell Sci* (2016) 129:4321–7. doi: 10.1242/jcs.190546
26. Midwood KS, Hussenet T, Langlois B, Orend G. Advances in Tenascin-C Biology. *Cell Mol Life Sci* (2011) 68:3175–99. doi: 10.1007/s00018-011-0783-6
27. Tucker RP, Chiquet-Ehrismann R. Tenascin-C: its Functions as an Integrin Ligand. *Int J Biochem Cell Biol* (2015) 65:165–8. doi: 10.1016/j.biocel.2015.06.003
28. Yoshida T, Akatsuka T, Imanaka-Yoshida K. Tenascin-C and Integrins in Cancer. *Cell Adh Migr* (2015) 9:96–104. doi: 10.1080/19336918.2015.1008332
29. Wiemann S, Reinhard J, Faissner A. Immunomodulatory Role of the Extracellular Matrix Protein Tenascin-C in Neuroinflammation. *Biochem Soc Trans* (2019) 47:1651–60. doi: 10.1042/BST20190081
30. Imanaka-Yoshida K. Inflammation in Myocardial Disease: From Myocarditis to Dilated Cardiomyopathy. *Pathol Int* (2020) 70(1):1–11. doi: 10.1111/pin.12868
31. Udalova IA, Ruhmann M, Thomson SJ, Midwood KS. Expression and Immune Function of Tenascin-C. *Crit Rev Immunol* (2011) 31:115–45. doi: 10.1615/CritRevImmunol.v31.i2.30
32. Unlu G, Levic DS, Melville DB, Knapik EW. Trafficking Mechanisms of Extracellular Matrix Macromolecules: Insights From Vertebrate Development and Human Diseases. *Int J Biochem Cell Biol* (2014) 47:57–67. doi: 10.1016/j.biocel.2013.11.005
33. Chiquet-Ehrismann R. What Distinguishes Tenascin From Fibronectin? *FASEB J* (1990) 4:2598–604. doi: 10.1096/fasebj.4.9.1693347
34. Adams JC, Chiquet-Ehrismann R, Tucker RP. The Evolution of Tenascins and Fibronectin. *Cell Adh Migr* (2015) 9:22–33. doi: 10.4161/19336918.2014.970030
35. Schafer M, Werner S. Cancer as an Overhealing Wound: An Old Hypothesis Revisited. *Nat Rev Mol Cell Biol* (2008) 9:628–38. doi: 10.1038/nrm2455
36. Hanahan D, Weinberg RA. Hallmarks of Cancer: The Next Generation. *Cell* (2011) 144:646–74. doi: 10.1016/j.cell.2011.02.013
37. Quail DF, Joyce JA. Microenvironmental Regulation of Tumor Progression and Metastasis. *Nat Med* (2013) 19:1423–37. doi: 10.1038/nm.3394
38. Singh P, Carraher C, Schwarzbauer JE. Assembly of Fibronectin Extracellular Matrix. *Annu Rev Cell Dev Biol* (2010) 26:397–419. doi: 10.1146/annurev-cellbio-100109-104020
39. Pankov R, Yamada KM. Fibronectin At a Glance. *J Cell Sci* (2002) 115:3861–3. doi: 10.1242/jcs.00059
40. Katoh D, Nagaharu K, Shimojo N, Hanamura N, Yamashita M, Kozuka Y, et al. Binding of Alphavbeta1 and Alphavbeta6 Integrins to Tenascin-C Induces Epithelial-Mesenchymal Transition-Like Change of Breast Cancer Cells. *Oncogenesis* (2013) 2:e65. doi: 10.1038/oncsis.2013.27
41. Bates RC, Bellovin DI, Brown C, Maynard E, Wu B, Kawakatsu H, et al. Transcriptional Activation of Integrin Beta6 During the Epithelial-Mesenchymal Transition Defines a Novel Prognostic Indicator of Aggressive Colon Carcinoma. *J Clin Invest* (2005) 115:339–47. doi: 10.1172/JCI200523183
42. Ramos DM, Dang D, Sadler S. The Role of the Integrin Alpha V Beta6 in Regulating the Epithelial to Mesenchymal Transition in Oral Cancer. *Anticancer Res* (2009) 29:125–30.
43. Nagaharu K, Zhang X, Yoshida T, Katoh D, Hanamura N, Kozuka Y, et al. Tenascin C Induces Epithelial-Mesenchymal Transition-Like Change Accompanied by SRC Activation and Focal Adhesion Kinase Phosphorylation in Human Breast Cancer Cells. *Am J Pathol* (2011) 178:754–63. doi: 10.1016/j.ajpath.2010.10.015
44. Yokosaki Y, Monis H, Chen J, Sheppard D. Differential Effects of the Integrins Alpha9beta1, Alphavbeta3, and Alphavbeta6 on Cell Proliferative Responses to Tenascin. Roles of the Beta Subunit Extracellular and Cytoplasmic Domains. *J Biol Chem* (1996) 271:24144–50. doi: 10.1074/jbc.271.39.24144
45. Saupe F, Schwenzer A, Jia Y, Gasser I, Spenle C, Langlois B, et al. Tenascin-C Downregulates Wnt Inhibitor Dickkopf-1, Promoting Tumorigenesis in a Neuroendocrine Tumor Model. *Cell Rep* (2013) 5:482–92. doi: 10.1016/j.celrep.2013.09.014
46. Lowy CM, Oskarsson T. Tenascin C in Metastasis: A View From the Invasive Front. *Cell Adh Migr* (2015) 9:112–24. doi: 10.1080/19336918.2015.1008331
47. Shao H, Kirkwood JM, Wells A. Tenascin-C Signaling in Melanoma. *Cell Adh Migr* (2015) 9:125–30. doi: 10.4161/19336918.2014.972781
48. Kimura T, Tajiri K, Sato A, Sakai S, Wang Z, Yoshida T, et al. Tenascin-C Accelerates Adverse Ventricular Remodelling After Myocardial Infarction by Modulating Macrophage Polarization. *Cardiovasc Res* (2019) 115(3):614–24. doi: 10.1093/cvr/cvy244
49. Manrique-Castano D, Dzyubenko E, Borbor M, Vasileiadou P, Kleinschnitz C, Roll L, et al. Tenascin-C Preserves Microglia Surveillance and Restricts Leukocyte and, More Specifically, T Cell Infiltration of the Ischemic Brain. *Brain Behav Immun* (2020) 91:639–48. doi: 10.1016/j.bbi.2020.10.016
50. Ummarino D. Systemic Sclerosis: Tenascin C Perpetuates Tissue Fibrosis. *Nat Rev Rheumatol* (2016) 12:375. doi: 10.1038/nrrheum.2016.99
51. Sun Z, Velazquez-Quesada I, Murdamoothoo D, Ahowesso C, Yilmaz A, Spenle C, et al. Tenascin-C Increases Lung Metastasis by Impacting Blood Vessel Invasions. *Matrix Biol* (2019) 83:26–47. doi: 10.1016/j.matbio.2019.07.001
52. Kasprzycka M, Hammarstrom C, Haraldsen G. Tenascins in Fibrotic Disorders-From Bench to Bedside. *Cell Adh Migr* (2015) 9:83–9. doi: 10.4161/19336918.2014.994901
53. Katoh D, Kozuka Y, Noro A, Ogawa T, Imanaka-Yoshida K, Yoshida T. Tenascin-C Induces Phenotypic Changes in Fibroblasts to Myofibroblasts With High Contractility Through the Integrin αvβ1/Transforming Growth Factor β/SMAD Signaling Axis in Human Breast Cancer. *Am J Pathol* (2020) 190(10):2123–35. doi: 10.1016/j.ajpath.2020.06.008
54. Midwood K, Sacre S, Piccinini AM, Inglis J, Trebaul A, Chan E, et al. Tenascin-C is an Endogenous Activator of Toll-Like Receptor 4 That is Essential for Maintaining Inflammation in Arthritic Joint Disease. *Nat Med* (2009) 15:774–80. doi: 10.1038/nm.1987
55. Yeo SY, Lee KW, Shin D, An S, Cho KH, Kim SH. A Positive Feedback Loop Bi-Stably Activates Fibroblasts. *Nat Commun* (2018) 9:3016. doi: 10.1038/s41467-018-05274-6
56. Langlois B, Saupe F, Rupp T, Arnold C, van der Heyden M, Orend G, et al. Angiomatrix, a Signature of the Tumor Angiogenic Switch-Specific Matrisome, Correlates With Poor Prognosis for Glioma and Colorectal Cancer Patients. *Oncotarget* (2014) 5:10529–45. doi: 10.18632/oncotarget.2470
57. Mhaidly R, Mechta-Grigoriou F. Fibroblast Heterogeneity in Tumor Micro-Environment: Role in Immunosuppression and New Therapies. *Semin Immunol* (2020) 48:101417. doi: 10.1016/j.smim.2020.101417

58. Schmid P, Cortes J, Pusztai L, McArthur H, Kümmel S, Bergh J, et al. Pembrolizumab for Early Triple-Negative Breast Cancer. *N Engl J Med* (2020) 382:810–21. doi: 10.1056/NEJMoa1910549
59. Yalcin F, Dzaye O, Xia S. Tenascin-C Function in Glioma: Immunomodulation and Beyond. *Adv Exp Med Biol* (2020) 1272:149–172. doi: 10.1007/978-3-030-48457-6_9
60. Li ZL, Cortes J, Pusztai L, McArthur H, Kümmel S, Bergh J, et al. Autophagy Deficiency Promotes Triple-Negative Breast Cancer Resistance to T Cell-Mediated Cytotoxicity by Blocking Tenascin-C Degradation. *Nat Commun* (2020) 11(1):3806. doi: 10.1038/s41467-020-17395-y
61. Hauzenberger D, Bergström SE, Klominek J, Sundqvist KG. Spectrum of Extracellular Matrix Degrading Enzymes in Normal and Malignant T Lymphocytes. *Anticancer Res* (1999) 19(3A):1945–52.
62. Benbow JH, Thompson KJ, Cope HL, Brandon-Warner E, Culberson CR, Bossi KL, et al. Diet-Induced Obesity Enhances Progression of Hepatocellular Carcinoma Through Tenascin-C/Toll-Like Receptor 4 Signaling. *Am J Pathol* (2016) 186(1):145–58. doi: 10.1016/j.ajpath.2015.09.015
63. Deligne C, Murdamoothoo D, Gammage AN, Gschwandtner M, Erne W, Loustau T, et al. Matrix-Targeting Immunotherapy Controls Tumor Growth and Spread by Switching Macrophage Phenotype. *Cancer Immunol Res* (2020) 8:368–82. doi: 10.1158/2326-6066.CIR-19-0276
64. Spenlé C, Loustau T, Murdamoothoo D, Erne W, Beghelli-de la Forest Divonne S, Veber R, et al. Tenascin-C Orchestrates an Immune-Suppressive Tumor Microenvironment in Oral Squamous Cell Carcinoma. *Cancer Immunol Res* (2020) 8:1122–38. doi: 10.1158/2326-6066.CIR-20-0074
65. Golledge J, Clancy P, Maguire J, Lincz L, Koblar S. The Role of Tenascin C in Cardiovascular Disease. *Cardiovasc Res* (2011) 92:19–28. doi: 10.1093/cvr/cvr183
66. Imanaka-Yoshida K, Aoki H. Tenascin-C and Mechanotransduction in the Development and Diseases of Cardiovascular System. *Front Physiol* (2014) 5:283. doi: 10.3389/fphys.2014.00283
67. Imanaka-Yoshida K, Tawara I, Yoshida T. Tenascin-C in Cardiac Disease: A Sophisticated Controller of Inflammation, Repair, and Fibrosis. *Am J Physiol Physiol* (2020) 319(5):C781–C796. doi: 10.1152/ajpcell.00353.2020
68. Gao W, Li J, Ni H, Shi H, Qi Z, Zhu S, et al. Tenascin C: A Potential Biomarker for Predicting the Severity of Coronary Atherosclerosis. *J Atheroscler Thromb* (2019) 26(1):31–8. doi: 10.5551/jat.42887
69. Liu R, He Y, Li B, Liu J, Ren Y, Han W, et al. Tenascin-C Produced by Oxidized LDL-Stimulated Macrophages Increases Foam Cell Formation Through Toll-Like Receptor-4. *Mol Cells* (2012) 34(1):35–41. doi: 10.1007/s10059-012-0054-x
70. Steffensen LB, Mortensen MB, Kjolby M, Hagensen MK, Oxvig C, Bentzon JF, et al. Disturbed Laminar Blood Flow Vastly Augments Lipoprotein Retention in the Artery Wall: A Key Mechanism Distinguishing Susceptible From Resistant Sites. *Arterioscler Thromb Vasc Biol* (2015) 35:1928–35. doi: 10.1161/ATVBAHA.115.305874
71. Wang L, Wang W, Shah PK, Song L, Yang M, Sharifi BG. Deletion of Tenascin-C Gene Exacerbates Atherosclerosis and Induces Intraplaque Hemorrhage in Apo-E-Deficient Mice. *Cardiovasc Pathol* (2012) 21(5):398–413. doi: 10.1016/j.carpath.2011.12.005
72. Distler JHW, Gyorfi AH, Ramanujam M, Whitfield ML, Konigshoff M, Lafyatis R. Shared and Distinct Mechanisms of Fibrosis. *Nat Rev Rheumatol* (2019) 15:705–30. doi: 10.1038/s41584-019-0322-7
73. Mack M. Inflammation and Fibrosis. *Matrix Biol* (2018) 68–69:106–21. doi: 10.1016/j.matbio.2017.11.010
74. Suzuki H, Fujimoto M, Kawakita F, Liu L, Nakano F, Nishikawa H, et al. Toll-Like Receptor 4 and Tenascin-C Signaling in Cerebral Vasospasm and Brain Injuries After Subarachnoid Hemorrhage. *Acta Neurochir Suppl* (2020) 127:91–6. doi: 10.1007/978-3-030-04615-6_15
75. El-Karef A, Yoshida T, Gabazza EC, Nishioka T, Inada H, Sakakura T, et al. Deficiency of Tenascin-C Attenuates Liver Fibrosis in Immune-Mediated Chronic Hepatitis in Mice. *J Pathol* (2007) 211(1):86–94. doi: 10.1002/path.2099
76. Zhu H, Liao J, Zhou X, Hong X, Song D, Hou FF, et al. Tenascin-C Promotes Acute Kidney Injury to Chronic Kidney Disease Progression by Impairing Tubular Integrity Via $α$V$β$6 Integrin Signaling. *Kidney Int* (2020) 97(5):1017–31. doi: 10.1016/j.kint.2020.01.026
77. Ricard-Blum S. The Collagen Family. *Cold Spring Harb Perspect Biol* (2011). doi: 10.1101/cshperspect.a004978
78. Kadler KE, Baldock C, Bella J, Boot-Handford RP. Collagens At a Glance. *J Cell Sci* (2007) 120(Pt 12):1955–8. doi: 10.1242/jcs.03453
79. Gordon MK, Hahn RA. Collagens. *Cell Tissue Res* (2010) 339:247–57. doi: 10.1007/s00441-009-0844-4
80. Gelse K, Pöschl E, Aigner T. Collagens - Structure, Function, and Biosynthesis. *Adv Drug Deliv Rev* (2003) 55(12):1531–46. doi: 10.1016/j.addr.2003.08.002
81. Gomez-Navarro N, Melero A, Li XH, Boulanger J, Kukulski W, Miller EA. Cargo Crowding Contributes to Sorting Stringency in COPII Vesicles. *J Cell Biol* (2020) 219(7):e201806038. doi: 10.1083/JCB.201806038
82. Gomez-Navarro N, Miller EA. COP-Coated Vesicles. *Curr Biol* (2016). doi: 10.1016/j.cub.2015.12.017
83. McCaughey J, Stephens DJ. ER-to-Golgi Transport: A Sizeable Problem. *Trends Cell Biol* (2019) 29:940–53. doi: 10.1016/j.tcb.2019.08.007
84. Malhotra V, Erlmann P. The Pathway of Collagen Secretion. *Annu Rev Cell Dev Biol* (2015) 31:109–24. doi: 10.1146/annurev-cellbio-100913-013002
85. Raote I, Ortega Bellido M, Pirozzi M, Zhang C, Melville D, Parashuraman S, et al. TANGO1 assembles into rings around COPII coats at ER exit sitess. *J Cell Biol* (2017) 216:901–9. doi: 10.1083/jcb.201608080
86. Tanabe T, Maeda M, Saito K, Katada T. Dual Function of Ctage5 in Collagen Export From the Endoplasmic Reticulum. *Mol Biol Cell* (2016) 27(13):2008–13. doi: 10.1091/mbc.E16-03-0180
87. Jin L, Pahuja KB, Wickliffe KE, Gorur A, Baumgärtel C, Schekman R, et al. Ubiquitin-Dependent Regulation of COPII Coat Size and Function. *Nature* (2012) 482(7386):495–500. doi: 10.1038/nature10822
88. Al-Yafeai Z, Yurdagul A, Peretik JM, Alfaidi M, Murphy PA, Orr AW, et al. Endothelial FN (Fibronectin) Deposition by α5β1 Integrins Drives Atherogenic Inflammation. *Arterioscler Thromb Vasc Biol* (2018) 38:2601–14. doi: 10.1161/ATVBAHA.118.311705
89. Kii I, Nishiyama T, Kudo A. Periostin Promotes Secretion of Fibronectin From the Endoplasmic Reticulum. *Biochem Biophys Res Commun* (2016) 470:888–93. doi: 10.1016/j.bbrc.2016.01.139
90. Choi MG, Hynes RO. Biosynthesis and Processing of Fibronectin in NIL.8 Hamster Cells. *J Biol Chem* (1979) 254:12050–5. doi: 10.1016/S0021-9258(19)86426-8
91. Mosher DF, Fogerty FJ, Chernousov MA, Barry EL. Assembly of Fibronectin Into Extracellular Matrix. *Ann N Y Acad Sci* (1991) 614:167–80. doi: 10.1111/j.1749-6632.1991.tb43701.x
92. Uchida N, Smilowitz H, Ledger PW, Tanzer ML. Kinetic Studies of the Intracellular Transport of Procollagen and Fibronectin in Human Fibroblasts. Effects of the Monovalent Ionophore, Monensin. *J Biol Chem* (1980) 255:8638–44. doi: 10.1016/S0021-9258(18)43547-8
93. Pizzey JA, Bennett FA, Jones GE. Monensin Inhibits Initial Spreading of Cultured Human Fibroblasts. *Nature* (1983) 305:315–7. doi: 10.1038/305315a0
94. Villiger B, Kelley DG, Engleman W, Kuhn C 3rd, Mcdonald JA. Human Alveolar Macrophage Fibronectin: Synthesis, Secretion, and Ultrastructural Localization During Gelatin-Coated Latex Particle Binding. *J Cell Biol* (1981) 90:711–20. doi: 10.1083/jcb.90.3.711
95. Hedman K. Intracellular Localization of Fibronectin Using Immunoperoxidase Cytochemistry in Light and Electron Microscopy. *J Histochem Cytochem* (1980) 28:1233–41. doi: 10.1177/28.11.7000891
96. Ledger PW, Uchida N, Tanzer ML. Immunocytochemical Localization of Procollagen and Fibronectin in Human Fibroblasts: Effects of the Monovalent Ionophore, Monensin. *J Cell Biol* (1980) 87:663–71. doi: 10.1083/jcb.87.3.663
97. Yamada SS, Yamada KM, Willingham MC. Intracellular Localization of Fibronectin by Immunoelectron Microscopy. *J Histochem Cytochem* (1980) 28:953–60. doi: 10.1177/28.9.6997370
98. Anderson RG, Pathak RK. Vesicles and Cisternae in the Trans Golgi Apparatus of Human Fibroblasts are Acidic Compartments. *Cell* (1985) 40:635–43. doi: 10.1016/0092-8674(85)90212-0
99. Zhu M, Tao J, Vasievich MP, Wei W, Zhu G, Khoriaty RN, et al. Neural Tube Opening and Abnormal Extraembryonic Membrane Development in SEC23A Deficient Mice. *Sci Rep* (2015) 5:15471. doi: 10.1038/srep15471
100. Sarmah S, Barrallo-Gimeno A, Melville DB, Topczewski J, Solnica-Krezel L, Knapik EW. Sec24D-Dependent Transport of Extracellular Matrix Proteins

is Required for Zebrafish Skeletal Morphogenesis. *PLoS One* (2010) 5:e10367. doi: 10.1371/journal.pone.0010367
101. Wilson DG, Phamluong K, Li L, Sun M, Cao TC, Liu PS, et al. Global Defects in Collagen Secretion in a Mia3/TANGO1 Knockout Mouse. *J Cell Biol* (2011) 193:935–51. doi: 10.1083/jcb.201007162
102. Hou W, Jerome-Majewska LA. TMED2/Emp24 is Required in Both the Chorion and the Allantois for Placental Labyrinth Layer Development. *Dev Biol* (2018) 444:20–32. doi: 10.1016/j.ydbio.2018.09.012
103. Redick SD, Schwarzbauer JE. Rapid Intracellular Assembly of Tenascin Hexabrachions Suggests a Novel Cotranslational Process. *J Cell Sci* (1995) 108:1761–9.
104. Kammerer RA, Schulthess T, Landwehr R, Lustig A, Fischer D, Engel J. Tenascin-C Hexabrachion Assembly is a Sequential Two-Step Process Initiated by Coiled-Coil Alpha-Helices. *J Biol Chem* (1998) 273:10602–8. doi: 10.1074/jbc.273.17.10602
105. Caubit X, Riou JF, Coulon J, Arsanto JP, Benraiss A, Boucaut JC, et al. Tenascin Expression in Developing, Adult and Regenerating Caudal Spinal Cord in the Urodele Amphibians. *Int J Dev Biol* (1994) 38:661–72 doi: 10.3402/jev.v4.27066.
106. Teng J, Zhang PL, Russell WJ, Zheng LP, Jones ML, Herrera GA. Insights Into Mechanisms Responsible for Mesangial Alterations Associated With Fibrogenic Glomerulopathic Light Chains. *Nephron Physiol* (2003) 94:28–38. doi: 10.1159/000071288
107. Becker A, Thakur BK, Weiss JM, Kim HS, Peinado H, Lyden D. Extracellular Vesicles in Cancer: Cell-to-Cell Mediators of Metastasis. *Cancer Cell* (2016) 30(6):836–48. doi: 10.1016/j.ccell.2016.10.009
108. Albacete-Albacete L, Navarro-Lérida I, López JA, Martín-Padura I, Astudillo AM, Ferrarini A, et al. ECM Deposition is Driven by Caveolin-1–Dependent Regulation of Exosomal Biogenesis and Cargo Sorting. *J Cell Biol* (2020) 219 (11):e202006178. doi: 10.1083/jcb.202006178
109. Sung BH, Ketova T, Hoshino D, Zijlstra A, Weaver AM. Directional Cell Movement Through Tissues is Controlled by Exosome Secretion. *Nat Commun* (2015) 6:7164. doi: 10.1038/ncomms8164
110. van Niel G, D'Angelo G, Raposo G. Shedding Light on the Cell Biology of Extracellular Vesicles. *Nat Rev Mol Cell Biol* (2018) 19:213–28. doi: 10.1038/nrm.2017.125
111. Colombo M, Raposo G, Théry C. Biogenesis, Secretion, and Intercellular Interactions of Exosomes and Other Extracellular Vesicles. *Annu Rev Cell Dev Biol* (2014) 30:255–89. doi: 10.1146/annurev-cellbio-101512-122326
112. Mathieu M, Martin-Jaular L, Lavieu G, Théry C. Specificities of Secretion and Uptake of Exosomes and Other Extracellular Vesicles for Cell-to-Cell Communication. *Nat Cell Biol* (2019) 21:9–17. doi: 10.1038/s41556-018-0250-9
113. Villarroya-Beltri C, Baixauli F, Gutiérrez-Vázquez C, Sánchez-Madrid F, Mittelbrunn M. Sorting it Out: Regulation of Exosome Loading. *Semin Cancer Biol* (2014) 28:3–13. doi: 10.1016/j.semcancer.2014.04.009
114. Henne WM, Buchkovich NJ, Emr SD. The Escrt Pathway. *Dev Cell* (2011) 21 (1):77–91. doi: 10.1016/j.devcel.2011.05.015
115. Williams RL, Urbé S. The Emerging Shape of the ESCRT Machinery. *Nat Rev Mol Cell Biol* (2007) 8:355–68. doi: 10.1038/nrm2162
116. Raiborg C, Stenmark H. The ESCRT Machinery in Endosomal Sorting of Ubiquitylated Membrane Proteins. *Nature* (2009) 458:445–52. doi: 10.1038/nature07961
117. Vietri M, Radulovic M, Stenmark H. The Many Functions of Escrts. *Nat Rev Mol Cell Biol* (2020) 21:25–42. doi: 10.1038/s41580-019-0177-4
118. Stuffers S, Sem Wegner C, Stenmark H, Brech A. Multivesicular Endosome Biogenesis in the Absence of Escrts. *Traffic* (2009) 10:925–37. doi: 10.1111/j.1600-0854.2009.00920.x
119. Trajkovic K, Hsu C, Chiantia S, Rajendran L, Wenzel D, Wieland F, et al. Ceramide Triggers Budding of Exosome Vesicles Into Multivesicular Endosomes. *Science (80-)* (2008). doi: 10.1126/science.1153124
120. Gruenberg J. Life in the Lumen: The Multivesicular Endosome. *Traffic* (2020) 21(1):76–93. doi: 10.1111/tra.12715
121. Andreu Z, Yáñez-Mó M. Tetraspanins in Extracellular Vesicle Formation and Function. *Front Immunol* (2014) 5(442):442. doi: 10.3389/fimmu.2014.00442
122. Campos A, Salomon C, Bustos R, Diaz J, Martinez S, Silva V, et al. Caveolin-1-Containing Extracellular Vesicles Transport Adhesion Proteins and Promote Malignancy in Breast Cancer Cell Lines. *Nanomedicine (Lond)* (2018) 13:2597–609. doi: 10.2217/nnm-2018-0094
123. Ni K, Wang C, Carnino JM, Jin Y. The Evolving Role of Caveolin-1: A Critical Regulator of Extracellular Vesicles. *Med Sci (Basel Switzerland)* (2020) 8(4):46. doi: 10.3390/medsci8040046
124. Li B, Antonyak MA, Zhang J, Cerione RA. Rhoa Triggers a Specific Signaling Pathway That Generates Transforming Microvesicles in Cancer Cells. *Oncogene* (2012) 31(45):4740–9. doi: 10.1038/onc.2011.636
125. Yanez-Mo M, Siljander PR, Andreu Z, Zavec AB, Borras FE, Buzas EI, et al. Biological Properties of Extracellular Vesicles and Their Physiological Functions. *J Extracell Vesicles* (2015) 4:27066.
126. Raposo G, Nijman HW, Stoorvogel W, Liejendekker R, Harding CV, Melief CJ, et al. B Lymphocytes Secrete Antigen-Presenting Vesicles. *J Exp Med* (1996) 183:1161–72. doi: 10.1084/jem.183.3.1161
127. Greening DW, Gopal SK, Xu R, Simpson RJ, Chen W. Exosomes and Their Roles in Immune Regulation and Cancer. *Semin Cell Dev Biol* (2015) 40:72–81. doi: 10.1016/j.semcdb.2015.02.009
128. Thery C, Amigorena S. The Cell Biology of Antigen Presentation in Dendritic Cells. *Curr Opin Immunol* (2001) 13:45–51. doi: 10.1016/S0952-7915(00)00180-1
129. Mittelbrunn M, Gutiérrez-Vázquez C, Villarroya-Beltri C, González S, Sánchez-Cabo F, González MÁ, et al. Unidirectional Transfer of Microrna-Loaded Exosomes From T Cells to Antigen-Presenting Cells. *Nat Commun* (2011) 2(282). doi: 10.1038/ncomms1285
130. Fernandez-Messina L, Rodriguez-Galan A, de Yebenes VG, Gutierrez-Vazquez C, Tenreiro S, Seabra MC, et al. Transfer of Extracellular Vesicle-Microrna Controls Germinal Center Reaction and Antibody Production. *EMBO Rep* (2020) 21:e48925. doi: 10.15252/embr.201948925
131. Fernandez-Messina L, Gutierrez-Vazquez C, Rivas-Garcia E, Sanchez-Madrid F, de la Fuente H. Immunomodulatory Role of Micrornas Transferred by Extracellular Vesicles. *Biol Cell* (2015) 107:61–77. doi: 10.1111/boc.201400081
132. MacKenzie A, Wilson HL, Kiss-Toth E, Dower SK, North RA, Surprenant A. Rapid Secretion of Interleukin-1beta by Microvesicle Shedding. *Immunity* (2001) 15:825–35. doi: 10.1016/S1074-7613(01)00229-1
133. Pizzirani C, Ferrari D, Chiozzi P, Adinolfi E, Sandona D, Savaglio E, et al. Stimulation of P2 Receptors Causes Release of IL-1beta-Loaded Microvesicles From Human Dendritic Cells. *Blood* (2007) 109:3856–64. doi: 10.1182/blood-2005-06-031377
134. Dower SK, Kronheim SR, Hopp TP, Cantrell M, Deeley M, Gillis S, et al. The Cell Surface Receptors for Interleukin-1 Alpha and Interleukin-1 Beta are Identical. *Nature* (1986) 324:266–8. doi: 10.1038/324266a0
135. Borthwick LA. The IL-1 Cytokine Family and its Role in Inflammation and Fibrosis in the Lung. *Semin Immunopathol* (2016) 38:517–34. doi: 10.1007/s00281-016-0559-z
136. Kandere-Grzybowska K, Letourneau R, Kempuraj D, Donelan J, Poplawski S, Boucher W, et al. IL-1 Induces Vesicular Secretion of IL-6 Without Degranulation From Human Mast Cells. *J Immunol* (2003) 171:4830–6. doi: 10.4049/jimmunol.171.9.4830
137. Femmino S, Penna C, Margarita S, Comita S, Brizzi MF, Pagliaro P. Extracellular Vesicles and Cardiovascular System: Biomarkers and Cardioprotective Effectors. *Vasc Pharmacol* (2020) 135:106790. doi: 10.1016/j.vph.2020.106790
138. Wang R, Ding Q, Yaqoob U, de Assuncao TM, Verma VK, Hirsova P, et al. Exosome Adherence and Internalization by Hepatic Stellate Cells Triggers Sphingosine 1-Phosphate-Dependent Migration. *J Biol Chem* (2015) 290:30684–96. doi: 10.1074/jbc.M115.671735
139. Lawson C, Vicencio JM, Yellon DM, Davidson SM. Microvesicles and Exosomes: New Players in Metabolic and Cardiovascular Disease. *J Endocrinol* (2016) 228:R57–71. doi: 10.1530/JOE-15-0201
140. Vanhaverbeke M, Gal D, Holvoet P. Functional Role of Cardiovascular Exosomes in Myocardial Injury and Atherosclerosis. *Adv Exp Med Biol* (2017) 998:45–58. doi: 10.1007/978-981-10-4397-0_3
141. Hergenreider E, Heydt S, Treguer K, Boettger T, Horrevoets AJ, Zeiher AM, et al. Atheroprotective Communication Between Endothelial Cells and Smooth Muscle Cells Through Mirnas. *Nat Cell Biol* (2012) 14:249–56. doi: 10.1038/ncb2441
142. Li B, Zang G, Zhong W, Chen R, Zhang Y, Yang P, et al. Activation of CD137 Signaling Promotes Neointimal Formation by Attenuating TET2 and Transferrring From Endothelial Cell-Derived Exosomes to Vascular Smooth Muscle Cells. *BioMed Pharmacother* (2020) 121:109593. doi: 10.1016/j.biopha.2019.109593

143. Zheng B, Yin WN, Suzuki T, Zhang XH, Zhang Y, Song LL, et al. Exosome-Mediated Mir-155 Transfer From Smooth Muscle Cells to Endothelial Cells Induces Endothelial Injury and Promotes Atherosclerosis. *Mol Ther* (2017) 25:1279–94. doi: 10.1016/j.ymthe.2017.03.031
144. Huang C, Han J, Wu Y, Li S, Wang Q, Lin W, et al. Exosomal MALAT1 Derived From Oxidized Low-Density Lipoprotein-Treated Endothelial Cells Promotes M2 Macrophage Polarization. *Mol Med Rep* (2018) 18:509–15. doi: 10.3892/mmr.2018.8982
145. Gao H, Wang X, Lin C, An Z, Yu J, Cao H, et al. Exosomal MALAT1 Derived From Ox-LDL-Treated Endothelial Cells Induce Neutrophil Extracellular Traps to Aggravate Atherosclerosis. *Biol Chem* (2020) 401:367–76. doi: 10.1515/hsz-2019-0219
146. Tang N, Sun B, Gupta A, Rempel H, Pulliam L. Monocyte Exosomes Induce Adhesion Molecules and Cytokines Via Activation of NF-Kappab in Endothelial Cells. *FASEB J* (2016) 30:3097–106. doi: 10.1096/fj.201600368RR
147. Kapustin AN, Chatrou ML, Drozdov I, Zheng Y, Davidson SM, Soong D, et al. Vascular Smooth Muscle Cell Calcification is Mediated by Regulated Exosome Secretion. *Circ Res* (2015) 116:1312–23. doi: 10.1161/CIRCRESAHA.116.305012
148. Cheng Y, Wang X, Yang J, Duan X, Yao Y, Shi X, et al. A Translational Study of Urine Mirnas in Acute Myocardial Infarction. *J Mol Cell Cardiol* (2012) 53:668–76. doi: 10.1016/j.yjmcc.2012.08.010
149. Aurora AB, Mahmoud AI, Luo X, Johnson BA, van Rooij E, Matsuzaki S, et al. Microrna-214 Protects the Mouse Heart From Ischemic Injury by Controlling Ca(2)(+) Overload and Cell Death. *J Clin Invest* (2012) 122:1222–32. doi: 10.1172/JCI59327
150. Prasetyanti PR, Medema JP. Intra-Tumor Heterogeneity From a Cancer Stem Cell Perspective. *Mol Cancer* (2017) 16:41. doi: 10.1186/s12943-017-0600-4
151. McGranahan N, Swanton C. Clonal Heterogeneity and Tumor Evolution: Past, Present, and the Future. *Cell* (2017) 168:613–28. doi: 10.1016/j.cell.2017.01.018
152. Meacham CE, Morrison SJ. Tumour Heterogeneity and Cancer Cell Plasticity. *Nature* (2013) 501:328–37. doi: 10.1038/nature12624
153. Demory Beckler M, Higginbotham JN, Franklin JL, Ham AJ, Halvey PJ, Imasuen IE, et al. Proteomic Analysis of Exosomes From Mutant KRAS Colon Cancer Cells Identifies Intercellular Transfer of Mutant KRAS. *Mol Cell Proteomics* (2013) 12:343–55. doi: 10.1074/mcp.M112.022806
154. Skog J, Wurdinger T, van Rijn S, Meijer DH, Gainche L, Sena-Esteves M, et al. Glioblastoma Microvesicles Transport RNA and Proteins That Promote Tumour Growth and Provide Diagnostic Biomarkers. *Nat Cell Biol* (2008) 10:1470–6. doi: 10.1038/ncb1800
155. Khan S, Jutzy JM, Aspe JR, McGregor DW, Neidigh JW, Wall NR. Survivin is Released From Cancer Cells Via Exosomes. *Apoptosis* (2011) 16:1–12. doi: 10.1007/s10495-010-0534-4
156. Kalluri R. Basement Membranes: Structure, Assembly and Role in Tumour Angiogenesis. *Nat Rev Cancer* (2003) 3:422–33. doi: 10.1038/nrc1094
157. De Palma M, Biziato D, Petrova TV. Microenvironmental Regulation of Tumour Angiogenesis. *Nat Rev Cancer* (2017) 17:457–74. doi: 10.1038/nrc.2017.51
158. Mashouri L, Yousefi H, Aref AR, Ahadi AM, Molaei F, Alahari SK, et al. Exosomes: Composition, Biogenesis, and Mechanisms in Cancer Metastasis and Drug Resistance. *Mol Cancer* (2019) 18:75. doi: 10.1186/s12943-019-0991-5
159. Zhou W, Fong MY, Min Y, Somlo G, Liu L, Palomares MR, et al. Cancer-Secreted Mir-105 Destroys Vascular Endothelial Barriers to Promote Metastasis. *Cancer Cell* (2014) 25:501–15. doi: 10.1016/j.ccr.2014.03.007
160. Peinado H, Aleckovic M, Lavotshkin S, Matei I, Costa-Silva B, Moreno-Bueno G, et al. Melanoma Exosomes Educate Bone Marrow Progenitor Cells Toward a Pro-Metastatic Phenotype Through MET. *Nat Med* (2012) 18:883–91. doi: 10.1038/nm.2753
161. Zeng Z, Li Y, Pan Y, Lan X, Song F, Sun J, et al. Cancer-Derived Exosomal Mir-25-3p Promotes Pre-Metastatic Niche Formation by Inducing Vascular Permeability and Angiogenesis. *Nat Commun* (2018) 9:5395. doi: 10.1038/s41467-018-07810-w
162. Viaud S, Terme M, Flament C, Taieb J, Andre F, Novault S, et al. Dendritic Cell-Derived Exosomes Promote Natural Killer Cell Activation and Proliferation: A Role for NKG2D Ligands and IL-15Ralpha. *PLoS One* (2009) 4:e4942. doi: 10.1371/journal.pone.0004942
163. Obregon C, Rothen-Rutishauser B, Gerber P, Gehr P, Nicod LP. Active Uptake of Dendritic Cell-Derived Exovesicles by Epithelial Cells Induces the Release of Inflammatory Mediators Through a TNF-Alpha-Mediated Pathway. *Am J Pathol* (2009) 175:696–705. doi: 10.2353/ajpath.2009.080716
164. Gastpar R, Gehrmann M, Bausero MA, Asea A, Gross C, Schroeder JA, et al. Heat Shock Protein 70 Surface-Positive Tumor Exosomes Stimulate Migratory and Cytolytic Activity of Natural Killer Cells. *Cancer Res* (2005) 65:5238–47. doi: 10.1158/0008-5472.CAN-04-3804
165. Kalluri R. The Biology and Function of Fibroblasts in Cancer. *Nat Rev Cancer* (2016) 16:582–98. doi: 10.1038/nrc.2016.73
166. Wortzel I, Dror S, Kenific CM, Lyden D. Exosome-Mediated Metastasis: Communication From a Distance. *Dev Cell* (2019) 49:347–60. doi: 10.1016/j.devcel.2019.04.011
167. Yang F, Ning Z, Ma L, Liu W, Shao C, Shu Y, et al. Exosomal Mirnas and Mirna Dysregulation in Cancer-Associated Fibroblasts. *Mol Cancer* (2017) 16:148. doi: 10.1186/s12943-017-0718-4
168. Hoshino A, Costa-Silva B, Shen TL, Rodrigues G, Hashimoto A, Tesic Mark M, et al. Tumour Exosome Integrins Determine Organotropic Metastasis. *Nature* (2015) 527:329–35 doi: 10.1038/nature15756.
169. Costa-Silva B, Aiello NM, Ocean AJ, Singh S, Zhang H, Thakur BK, et al. Pancreatic Cancer Exosomes Initiate Pre-Metastatic Niche Formation in the Liver. *Nat Cell Biol* (2015) 17:816–26 doi: 10.1038/ncb3169.
170. Xu G, Zhang B, Ye J, Cao S, Shi J, Zhao Y, et al. Exosomal Mirna-139 in Cancer-Associated Fibroblasts Inhibits Gastric Cancer Progression by Repressing MMP11 Expression. *Int J Biol Sci* (2019) 15:2320–9. doi: 10.7150/ijbs.33750
171. Chen Z, Wang H, Xia Y, Yan F, Lu Y. Therapeutic Potential of Mesenchymal Cell-Derived Mirna-150-5p-Expressing Exosomes in Rheumatoid Arthritis Mediated by the Modulation of MMP14 and VEGF. *J Immunol* (2018) 201:2472–82. doi: 10.4049/jimmunol.1800304
172. Rilla K, Mustonen AM, Arasu UT, Harkonen K, Matilainen J, Nieminen P. Extracellular Vesicles are Integral and Functional Components of the Extracellular Matrix. *Matrix Biol* (2019) 75–76:201–19. doi: 10.1016/j.matbio.2017.10.003
173. Manou D, et al. The Complex Interplay Between Extracellular Matrix and Cells in Tissues. *Methods Mol Biol* (2019) 1952:1–20. doi: 10.1007/978-1-4939-9133-4_1
174. Ramteke A, Caon I, Bouris P, Triantaphyllidou IE, Giaroni C, Passi A. Exosomes Secreted Under Hypoxia Enhance Invasiveness and Stemness of Prostate Cancer Cells by Targeting Adherens Junction Molecules. *Mol Carcinog* (2015) 54:554–65. doi: 10.1002/mc.22124
175. Li R, Wang Y, Zhang X, Feng M, Ma J, Li J, et al. Exosome-Mediated Secretion of LOXL4 Promotes Hepatocellular Carcinoma Cell Invasion and Metastasis. *Mol Cancer* (2019) 18:18. doi: 10.1186/s12943-019-0948-8
176. de Jong OG, van Balkom BW, Gremmels H, Verhaar MC. Exosomes From Hypoxic Endothelial Cells Have Increased Collagen Crosslinking Activity Through Up-Regulation of Lysyl Oxidase-Like 2. *J Cell Mol Med* (2016) 20:342–50. doi: 10.1111/jcmm.12730
177. Shimoda M. Extracellular Vesicle-Associated Mmps: A Modulator of the Tissue Microenvironment. *Adv Clin Chem* (2019) 88:35–66. doi: 10.1016/bs.acc.2018.10.006
178. Nawaz M, Shah N, Zanetti B, Maugeri M, Silvestre R, Fatima F, et al. Extracellular Vesicles and Matrix Remodeling Enzymes: The Emerging Roles in Extracellular Matrix Remodeling, Progression of Diseases and Tissue Repair. *Cells* (2018) 7(10):167. doi: 10.3390/cells7100167
179. Ali SY, Sajdera SW, Anderson HC. Isolation and Characterization of Calcifying Matrix Vesicles From Epiphyseal Cartilage. *Proc Natl Acad Sci U S A* (1970) 67:1513–20. doi: 10.1073/pnas.67.3.1513
180. Bonucci E. Fine Structure and Histochemistry of 'Calcifying Globules' in Epiphyseal Cartilage. *Z Zellforsch Mikrosk Anat* (1970) 103:192–217. doi: 10.1007/BF00337312
181. Shapiro IM, Landis WJ, Risbud MV. Matrix Vesicles: Are They Anchored Exosomes? *Bone* (2015) 79:29–36. doi: 10.1016/j.bone.2015.05.013
182. Hasegawa T. Ultrastructure and Biological Function of Matrix Vesicles in Bone Mineralization. *Histochem Cell Biol* (2018) 149:289–304. doi: 10.1007/s00418-018-1646-0
183. Ji H, Greening DW, Barnes TW, Lim JW, Tauro BJ, Rai A, et al. Proteome Profiling of Exosomes Derived From Human Primary and Metastatic Colorectal Cancer Cells Reveal Differential Expression of Key Metastatic

Factors and Signal Transduction Components. *Proteomics* (2013) 13:1672–86. doi: 10.1002/pmic.201200562
184. Zheng J, Hernandez JM, Doussot A, Bojmar L, Zambirinis CP, Costa-Silva B, et al. Extracellular Matrix Proteins and Carcinoembryonic Antigen-Related Cell Adhesion Molecules Characterize Pancreatic Duct Fluid Exosomes in Patients With Pancreatic Cancer. *HPB* (2018) 20:597–604. doi: 10.1016/j.hpb.2017.12.010
185. Manickam G, Moffatt P, Murshed M. Role of SMPD3 During Bone Fracture Healing and Regulation of its Expression. *Mol Cell Biol* (2019) 39(4):e00370–18. doi: 10.1128/MCB.00370-18
186. Stoffel W, Hammels I, Jenke B, Schmidt-Soltau I, Niehoff A. Neutral Sphingomyelinase 2 (SMPD3) Deficiency in Mice Causes Chondrodysplasia With Unimpaired Skeletal Mineralization. *Am J Pathol* (2019) 189:1831–45. doi: 10.1016/j.ajpath.2019.05.008
187. Purushothaman A, Bandari SK, Liu J, Mobley JA, Brown EE, Sanderson RD. Fibronectin on the Surface of Myeloma Cell-Derived Exosomes Mediates Exosome-Cell Interactions. *J Biol Chem* (2016) 291:1652–63. doi: 10.1074/jbc.M115.686295
188. Dismuke WM, Klingeborn M, Stamer WD. Mechanism of Fibronectin Binding to Human Trabecular Meshwork Exosomes and its Modulation by Dexamethasone. *PLoS One* (2016) 11:e0165326. doi: 10.1371/journal.pone.0165326
189. Shi F, Sottile J. Caveolin-1-Dependent Beta1 Integrin Endocytosis is a Critical Regulator of Fibronectin Turnover. *J Cell Sci* (2008) 121:2360–71. doi: 10.1242/jcs.014977
190. Sung BH, Zhu X, Kaverina I, Weaver AM. Cortactin Controls Cell Motility and Lamellipodial Dynamics by Regulating ECM Secretion. *Curr Biol* (2011) 21:1460–9. doi: 10.1016/j.cub.2011.06.065
191. Benesh EC, Miller PM, Pfaltzgraff ER, Grega-Larson NE, Hager HA, Sung BH, et al. Bves and NDRG4 Regulate Directional Epicardial Cell Migration Through Autocrine Extracellular Matrix Deposition. *Mol Biol Cell* (2013) 24:3496–510. doi: 10.1091/mbc.e12-07-0539
192. Sung BH, Weaver AM. Exosome Secretion Promotes Chemotaxis of Cancer Cells. *Cell Adh Migr* (2017) 11:187–95. doi: 10.1080/19336918.2016.1273307
193. Hoshino D, Kirkbride KC, Costello K, Clark ES, Sinha S, Grega-Larson N, et al. Exosome Secretion is Enhanced by Invadopodia and Drives Invasive Behavior. *Cell Rep* (2013) 5:1159–68. doi: 10.1016/j.celrep.2013.10.050
194. Chanda D, Otoupalova E, Hough KP, Locy ML, Bernard K, Deshane JS, et al. Fibronectin on the Surface of Extracellular Vesicles Mediates Fibroblast Invasion. *Am J Respir Cell Mol Biol* (2019) 60:279–88. doi: 10.1165/rcmb.2018-0062OC
195. Yuan O, Lin C, Wagner J, Archard JA, Deng P, Halmai J, et al. Exosomes Derived From Human Primed Mesenchymal Stem Cells Induce Mitosis and Potentiate Growth Factor Secretion. *Stem Cells Dev* (2019) 28:398–409. doi: 10.1089/scd.2018.0200
196. Antonyak MA, Li B, Boroughs LK, Johnson JL, Druso JE, Bryant KL, et al. Cancer Cell-Derived Microvesicles Induce Transformation by Transferring Tissue Transglutaminase and Fibronectin to Recipient Cells. *Proc Natl Acad Sci U S A* (2011) 108:4852–7. doi: 10.1073/pnas.1017667108
197. Osawa S, Kurachi M, Yamamoto H, Yoshimoto Y, Ishizaki Y. Fibronectin on Extracellular Vesicles From Microvascular Endothelial Cells is Involved in the Vesicle Uptake Into Oligodendrocyte Precursor Cells. *Biochem Biophys Res Commun* (2017) 488:232–8. doi: 10.1016/j.bbrc.2017.05.049
198. Bin BH, Kim DK, Kim NH, Choi EJ, Bhin J, Kim ST, et al. Fibronectin-Containing Extracellular Vesicles Protect Melanocytes Against Ultraviolet Radiation-Induced Cytotoxicity. *J Invest Dermatol* (2016) 136:957–66. doi: 10.1016/j.jid.2015.08.001
199. Deng Z, Cheng Z, Xiang X, Yan J, Zhuang X, Liu C, et al. Tumor Cell Cross Talk With Tumor-Associated Leukocytes Leads to Induction of Tumor Exosomal Fibronectin and Promotes Tumor Progression. *Am J Pathol* (2012) 180:390–8. doi: 10.1016/j.ajpath.2011.09.023
200. Atay S, Gercel-Taylor C, Taylor DD. Human Trophoblast-Derived Exosomal Fibronectin Induces Pro-Inflammatory IL-1beta Production by Macrophages. *Am J Reprod Immunol* (2011) 66:259–69. doi: 10.1111/j.1600-0897.2011.00995.x
201. Kulkarni R, Prasad A. Exosomes Derived From HIV-1 Infected Dcs Mediate Viral Trans-Infection Via Fibronectin and Galectin-3. *Sci Rep* (2017) 7(1):14787. doi: 10.1038/s41598-017-14817-8
202. Sharma M, Kaur H, Roy S. Tissue-Associated Self-Antigens Containing Exosomes: Role in Allograft Rejection. *Hum Immunol* (2018) 79:653–8. doi: 10.1016/j.humimm.2018.06.005
203. Parton RG, Del Pozo MA. Caveolae as Plasma Membrane Sensors, Protectors and Organizers. *Nat Rev Mol Cell Biol* (2013) 14(2):98–112. doi: 10.1038/nrm3512
204. Moreno-Vicente R, Pavón DM, Martín-Padura I, Català-Montoro M, Díez-Sánchez A, Quílez-Álvarez A, et al. Caveolin-1 Modulates Mechanotransduction Responses to Substrate Stiffness Through Actin-Dependent Control of YAP. *Cell Rep* (2018) 25(6):1622–1635.e6. doi: 10.1016/j.celrep.2018.10.024
205. Pol A, Morales-Paytuví F, Bosch M, Parton RG. Non-Caveolar Caveolins - Duties Outside the Caves. *J Cell Sci* (2020) 133(9):jcs241562. doi: 10.1242/jcs.241562
206. Enrich C, Rentero C, Grewal T, Futter CE, Eden ER. Cholesterol Overload: Contact Sites to the Rescue! *Contact* (2019). doi: 10.1177/2515256419893507
207. Höglinger D, Burgoyne T, Sanchez-Heras E, Hartwig P, Colaco A, Newton J, et al. NPC1 Regulates ER Contacts With Endocytic Organelles to Mediate Cholesterol Egress. *Nat Commun* (2019) 10(1):4276. doi: 10.1038/s41467-019-12152-2
208. Strippoli R, Burgoyne T, Sanchez-Heras E, Hartwig P, Colaco A, Newton J, et al. Caveolin1 and YAP Drive Mechanically Induced Mesothelial to Mesenchymal Transition and Fibrosis. *Cell Death Dis* (2020) 11(8):647. doi: 10.1038/s41419-020-02822-1
209. Bissell MJ, Hall HG, Parry G. How Does the Extracellular Matrix Direct Gene Expression? *J. Theor Biol* (1982) 99:31–68. doi: 10.1016/0022-5193(82)90388-5
210. Strippoli R, Sandoval P, Moreno-Vicente R, Rossi L, Battistelli C, Terri M, et al. Molecular Mechanisms Underlying Peritoneal EMT and Fibrosis. *Stem Cells Int* (2016) 2016:3543678. doi: 10.1155/2016/3543678
211. Inder KL, Ruelcke JE, Petelin L, Moon H, Choi E, Rae J, et al. Cavin-1/PTRF Alters Prostate Cancer Cell-Derived Extracellular Vesicle Content and Internalization to Attenuate Extracellular Vesicle-Mediated Osteoclastogenesis and Osteoblast Proliferation. *J Extracell Vesicles* (2014) 3(1):23784. doi: 10.3402/jev.v3.23784
212. Cao J, Navis A, Cox BD, Dickson AL, Gemberling M, Karra R, et al. Single Epicardial Cell Transcriptome Sequencing Identifies Caveolin 1 as an Essential Factor in Zebrafish Heart Regeneration. *Development* (2016) 143:232–43. doi: 10.1242/dev.130534
213. Fernández-Hernando C, Yu J, Suárez Y, Rahner C, Dávalos A, Lasunción MA, et al. Genetic Evidence Supporting a Critical Role of Endothelial Caveolin-1 During the Progression of Atherosclerosis. *Cell Metab* (2009) 10:48–54. doi: 10.1016/j.cmet.2009.06.003
214. Qian S, Tan X, Liu X, Liu P, Wu Y. Exosomal Tenascin-C Induces Proliferation and Invasion of Pancreatic Cancer Cells by WNT Signaling. *Onco Targets Ther* (2019) 12:3197–205. doi: 10.2147/OTT.S192218
215. Daassi D, Mahoney KM, Freeman GJ. The Importance of Exosomal PDL1 in Tumour Immune Evasion. *Nat Rev Immunol* (2020) 20:209–15. doi: 10.1038/s41577-019-0264-y
216. Sur S, Kaur H, Roy S. Exosomes From COVID-19 Patients Carry Tenascin-C and Fibrinogen-β in Triggering Inflammatory Signals in Cells of Distant Organ. *Int J Mol Sci* (2021) 22. doi: 10.1101/2021.02.08.430369
217. Li C, Cui Y, Luan J, Zhou X, Li H, Wang H, et al. Tenascin C Affects Mineralization of Saos2 Osteoblast-Like Cells Through Matrix Vesicles. *Drug Discovery Ther* (2016) 10:82–7. doi: 10.5582/ddt.2016.01009
218. Mills JT, Schwenzer A, Marsh EK, Edwards MR, Sabroe I, Midwood KS, et al. Airway Epithelial Cells Generate Pro-Inflammatory Tenascin-C and Small Extracellular Vesicles in Response to TLR3 Stimuli and Rhinovirus Infection. *Front Immunol* (2019) 10:1987. doi: 10.3389/fimmu.2019.01987
219. Mirzaei R, Sarkar S, Dzikowski L, Rawji KS, Khan L, Faissner A, et al. Brain Tumor-Initiating Cells Export Tenascin-C Associated With Exosomes to Suppress T Cell Activity. *Oncoimmunology* (2018) 7:e1478647. doi: 10.1080/2162402X.2018.1478647
220. Wei W, Ao Q, Wang X, Cao Y, Liu Y, Zheng SG, et al. Mesenchymal Stem Cell-Derived Exosomes: A Promising Biological Tool in Nanomedicine. *Front Pharmacol* (2020) 11:590470. doi: 10.3389/fphar.2020.590470
221. Sharma P, Kaur H, Roy S. Designing a Tenascin-C-Inspired Short Bioactive Peptide Scaffold to Direct and Control Cellular Behavior. *ACS Biomater Sci Eng* (2019) 5:6497–510. doi: 10.1021/acsbiomaterials.9b01115

222. Rosenbloom J, Macarak E, Piera-Velazquez S, Jimenez SA. Human Fibrotic Diseases: Current Challenges in Fibrosis Research. *Methods Mol Biol* (2017) 1627:1–23. doi: 10.1007/978-1-4939-7113-8_1
223. Zhao X, Kwan JYY, Yip K, Liu PP, Liu FF. Targeting Metabolic Dysregulation for Fibrosis Therapy. *Nat Rev Drug Discov* (2020) 19:57–75. doi: 10.1038/s41573-019-0040-5
224. Schuppan D, Ashfaq-Khan M, Yang AT, Kim YO. Liver Fibrosis: Direct Antifibrotic Agents and Targeted Therapies. *Matrix Biol* (2018) 68–69:435–51. doi: 10.1016/j.matbio.2018.04.006
225. Meng XM, Nikolic-Paterson DJ, Lan HY. Tgf-β: The Master Regulator of Fibrosis. *Nat Rev Nephrol* (2016). doi: 10.1038/nrneph.2016.48
226. Somogyi V, Chaudhuri N, Torrisi SE, Kahn N, Müller V, Kreuter M. the Therapy of Idiopathic Pulmonary Fibrosis: What is Next? *Eur Respir Rev* (2019) 28(153):190021. doi: 10.1183/16000617.0021-2019
227. Maher TM, Strek ME. Antifibrotic Therapy for Idiopathic Pulmonary Fibrosis: Time to Treat. *Respir Res* (2019) 20:205. doi: 10.1186/s12931-019-1161-4
228. Hauge A, Rofstad EK. Antifibrotic Therapy to Normalize the Tumor Microenvironment. *J Trans Med* (2020) 18(1):207. doi: 10.1186/s12967-020-02376-y

Conflict of Interest: The authors declare that the research was conducted in the absence of any commercial or financial relationships that could be construed as a potential conflict of interest.

frontiers in Immunology

ORIGINAL RESEARCH
published: 13 May 2021
doi: 10.3389/fimmu.2021.613438

Latent TGF-β Activation Is a Hallmark of the Tenascin Family

*Alexandre Aubert[1], Perrine Mercier-Gouy[1], Stéphanie Aguero[1], Laurent Berthier[1], Sophie Liot[1], Laura Prigent[1], Lindsay B. Alcaraz[2], Bernard Verrier[1], Raphaël Terreux[1], Catherine Moali[1], Elise Lambert[1] and Ulrich Valcourt[1]**

[1] Laboratoire de Biologie Tissulaire et Ingénierie Thérapeutique (LBTI), UMR CNRS 5305, Université Lyon 1, Institut de Biologie et Chimie des Protéines, Lyon, France, [2] Institut de Recherche en Cancérologie de Montpellier (IRCM), INSERM U1194, Université de Montpellier, Institut du Cancer de Montpellier (ICM), Montpellier, France

Transforming growth factor-β (TGF-β) isoforms are secreted as inactive complexes formed through non-covalent interactions between bioactive TGF-β entities and their N-terminal pro-domains called latency-associated peptides (LAP). Extracellular activation of latent TGF-β within this complex is a crucial step in the regulation of TGF-β activity for tissue homeostasis and immune cell function. We previously showed that the matrix glycoprotein Tenascin-X (TN-X) interacted with the small latent TGF-β complex and triggered the activation of the latent cytokine into a bioactive TGF-β. This activation most likely occurs through a conformational change within the latent TGF-β complex and requires the C-terminal fibrinogen-like (FBG) domain of the glycoprotein. As the FBG-like domain is highly conserved among the Tenascin family members, we hypothesized that Tenascin-C (TN-C), Tenascin-R (TN-R) and Tenascin-W (TN-W) might share with TN-X the ability to regulate TGF-β bioavailability through their C-terminal domain. Here, we demonstrate that purified recombinant full-length Tenascins associate with the small latent TGF-β complex through their FBG-like domains. This association promotes activation of the latent cytokine and subsequent TGF-β cell responses in mammary epithelial cells, such as cytostasis and epithelial-to-mesenchymal transition (EMT). Considering the pleiotropic role of TGF-β in numerous physiological and pathological contexts, our data indicate a novel common function for the Tenascin family in the regulation of tissue homeostasis under healthy and pathological conditions.

Keywords: tenascins, transforming growth factor (TGF)-β, latent TGF-β activation, tissue homeostasis, tumor microenvironment, immune cell modulation

OPEN ACCESS

Edited by:
Gertraud Orend, INSERM Immuno Rhumatologie Moléculaire (IRM), France

Reviewed by:
Kim Midwood, University of Oxford, United Kingdom
Shizuya Saika, Wakayama Medical University Hospital, Japan
Joanne Murphy-Ullrich, University of Alabama at Birmingham, United States

***Correspondence:**
Ulrich Valcourt
ulrich.valcourt@ibcp.fr

Specialty section:
This article was submitted to Inflammation, a section of the journal Frontiers in Immunology

Received: *02 October 2020*
Accepted: *16 April 2021*
Published: *13 May 2021*

Citation:
Aubert A, Mercier-Gouy P, Aguero S, Berthier L, Liot S, Prigent L, Alcaraz LB, Verrier B, Terreux R, Moali C, Lambert E and Valcourt U (2021) Latent TGF-β Activation Is a Hallmark of the Tenascin Family. Front. Immunol. 12:613438. doi: 10.3389/fimmu.2021.613438

INTRODUCTION

The Tenascin family is a group of large extracellular matrix (ECM) glycoproteins composed of four members, Tenascin-C (TN-C), Tenascin-R (TN-R), Tenascin-W (TN-W, also known as Tenascin-N) and Tenascin-X (TN-X), sharing a common modular structure. Tenascins are composed of heptad repeats at the amino terminus, followed by several Epidermal Growth Factor (EGF)-like domains, different numbers of Fibronectin type III (FNIII) repeats and a C-terminal globular domain resembling Fibrinogen (FBG-like domain) (1). The amino-terminal cysteine-rich region with

heptad repeats, forming the Tenascin assembly domain, allows individual subunits to oligomerize into disulfide-linked trimers, permitting TN-R and TN-X to form structures called "tri-brachions" (2, 3). TN-C and TN-W are able to form hexamers, also known as "hexa-brachions", due to the presence of an additional cysteine residue within this domain forming an extra disulfide bridge between two trimers (4, 5).

Tenascin family members have very specific expression patterns. TN-R (160-180 kDa), which is restricted to the nervous system, is expressed by oligodendrocytes and subtypes of neurons in the central nervous system and by Schwann cells in the peripheral nervous system. TN-R plays a major role in the regulation of neural stem cell progenitor proliferation and differentiation (6), and its expression is upregulated during axonal myelinization (7). Mutations found in the TN-R encoding gene (*TNR*) are associated with predisposition for neurodevelopmental pathologies, such as attention deficit hyperactivity disorder (8) and non-progressive form of spastic disorders (9). TN-X (450 kDa), encoded by the *TNXB* gene, is the largest member of the Tenascin family and is constitutively present in adult connective tissues, including tendons, ligaments, digestive tract and dermis. TN-X interacts with fibrillar (types I, III and V) collagens, fibril-associated (types XII and XIV) collagens and other matrix components (Decorin) (3, 10), and is believed to regulate the spacing between collagen fibrils (11). Through this architectural function, TN-X might provide the connective tissue with appropriate biomechanical properties to support tissue and organ functions (12). Consequently, TN-X deficiency causes classical-like Ehlers-Danlos Syndrome (EDS) in Human (13), a rare and hereditary connective tissue disorder characterized by generalized joint hypermobility, skin hyperlaxity and easy bruising (14). TN-C (220 kDa) and TN-W (180 kDa), which are mainly expressed during embryonic development, remain barely detectable in adult tissues, with a very restricted expression in several stem cell niches. Indeed, TN-C has been found in neural and epithelial stem cell niches, whereas TN-W has been associated with the osteogenic one (15).

Nevertheless, TN-C and TN-W levels are often up-regulated under physio-pathological stresses, including fibrosis, angiogenesis, wound healing and tumor progression (16–18). Indeed, TN-C and TN-W are often *de novo* expressed in different types of cancer, in which they display well characterized pro-tumoral activities by promoting tumor cell proliferation (19), cell migration and invasiveness (20), and metastasis formation (21). Consequently, these two glycoproteins have been proposed as biomarkers for most solid tumors (*i.e.* breast, colorectal and pancreatic cancers) (22, 23), in which TN-C has been often associated with poor clinical outcome (22, 24). While far less studied, TN-R and TN-X have also been identified as being involved in tumor progression. Due to its specific localization, TN-R expression has been tightly related to brain cancer development. Indeed, TN-R was described as down-regulated in glioblastomas, medulloblastomas, ependymomas and meningiomas, while up-regulated in gangliogliomas, suggesting that its role as either a tumor-promoting or tumor-suppressing factor is highly context-dependent (25, 26). In contrast to TN-C and TN-W, we recently demonstrated that (*i*) TN-X is down-regulated at both mRNA and protein levels in the six cancers with the highest incidence and mortality worldwide (*i.e.* lung, breast, colorectal, prostate, stomach and liver cancers) and (*ii*) a low level of *TNXB* transcripts is correlated with a worse overall survival in patients suffering from breast or lung cancers (27). Even if the molecular mechanisms involved are still unknown, these observations suggest that TN-X might exert tumor-suppressive properties.

In addition to its architectural function within the ECM, we also identified a novel role for the TN-X in the regulation of cell signaling. Thanks to its C-terminal FBG-like domain, TN-X was found to regulate Transforming Growth factor (TGF)-β bioavailability (28). The three TGF-β isoforms (TGF-β1, 2 and 3) are pleiotropic cytokines secreted by a broad range of cell types in an inactive form. Indeed, they are synthesized as pro-proteins and form disulfide-linked homodimers that are proteolytically processed before secretion. Upon cleavage, the pro-domain, called latency-associated peptide (LAP), remains non-covalently bound to the mature (bioactive) TGF-β moiety, maintaining it in a latent state by preventing its exposure to cell-surface receptors. Latent TGF-β can be found as a soluble entity, called the small latent complex (SLC), but also as a large latent complex (LLC), in which the SLC is covalently bound to a Latent TGF-β Binding Proteins (LTBP), thus maintaining a reservoir of latent TGF-β into the matrix (29). In order to exert its physiological roles, latent TGF-β has to be activated, meaning that the mature TGF-β entity has to be released from the SLC. Depending on the cell and/or tissue context, latent TGF-β activation may result from (*i*) a proteolytic cleavage within the LAP pro-domain and the subsequent release of the mature TGF-β and/or (*ii*) a conformational change in the LAP, allowing exposure of the TGF-β entity (30). During the latter process, mature TGF-β remains in interaction with its LAP pro-domain, but the bioactive sites of the cytokine are unmasked and able to bind to TGF-β type II receptor (TβRII) at the cell surface (31). Activated TβRII then recruits and activates the TGF-β type I receptor (TβRI) by trans-phosphorylation. In the canonical TGF-β signaling pathway, TβRI phosphorylates Smad2 and Smad3, allowing them to interact with Smad4 in order to enter the nucleus and act as transcription factors that regulate a large set of TGF-β-responsive genes (32). These genes are involved in key biological mechanisms, such as embryonic development, tissue homeostasis and repair, through stem cell fate orientation, cell cycle arrest (cytostasis), epithelial-to-mesenchymal transition (EMT), cell motility and immuno-modulation. TGF-β cytokines also play a dual role during cancer development, acting either as oncogenic or tumor-suppressing factors depending on the cellular context (32, 33).

Based on the conserved modular structure between the four members of the Tenascin family, we speculated that TN-C, TN-R and TN-W share with TN-X the ability to regulate latent TGF-β activation through their C-terminal globular domain. Indeed, amino-acid sequence alignment revealed that FBG-like domains of the four Tenascins are highly conserved, sign of a potential functional redundancy. Herein, we demonstrated that full-length

Tenascins, and their respective FBG-like domains, are produced and purified in association with SLC components (*i.e.* TGF-β1 and its LAP pro-domain). Interestingly, recombinant FBG-like domains, presented to cells in either immobilized or soluble form, have the ability to induce the canonical TGF-β/Smad intracellular pathway in epithelial cells, suggesting that the molecular association between the C-terminal part of the Tenascins and latent TGF-β promotes the activation of the cytokine. Consequently, epithelial cells cultured onto immobilized FBG-like domains underwent cell cycle arrest (cytostasis) and partial EMT, two cellular programs induced by active TGF-β. Altogether, our results indicate that latent TGF-β activation is a common feature of the Tenascin family, providing new insights into the mechanisms by which these glycoproteins may regulate tissue homeostasis under healthy and pathological conditions.

MATERIALS AND METHODS

Cell Culture and Reagents

Normal Murine Mammary Gland (NMuMG) epithelial cells were obtained from ATCC (American Type Culture Collection) and cultured in complete Dulbecco modified Eagle's medium (DMEM), containing 10% (v/v) Fetal Bovine Serum (FBS, Gibco), 1% (v/v) Penicillin-Streptomycin (PS, Gibco), and supplemented with 10 µg/mL Insulin (Roche). Human Embryonic Kidney (HEK)-293 cells expressing Epstein-Barr Nuclear Antigen 1 (EBNA1) were purchased from Invitrogen and maintained in the same complete medium in the presence of 250 µg/mL of G418 (Geneticin, PAA) as recommended by the manufacturer.

HEK-293 EBNA1 cells stably transfected with pCEP4-BM40-6HIS/Puromycin encoding full-length human TN-C and TN-W, respectively donated by G. Orend (U1109 INSERM, Strasbourg, France) and R. Chiquet-Ehrismann (Friedrich Miescher Institute for Biomedical Research, Basel, Switzerland), were cultured in complete DMEM containing 2.5 µg/mL of Puromycin (Gibco). HEK-293 cells stably transfected with pSecTag2/hygromycin expression vector (Invitrogen) encoding either full-length bovine TN-X (from Gly^{23} to $Gly^{4,135}$ residues according to the GenBank reference NM_174703) or its TN-$X^{\Delta E\Delta F}$ derivative (consisting of FNIII modules only, from Gly^{745} to $Thr^{3,910}$ residues) (3, 34), were cultured in complete DMEM containing 400 µg/mL of Hygromycin B (Thermo Fischer Scientific).

Recombinant human TGF-β1 was purchased from PeproTech and dissolved in 4mM HCl containing 0.1% (w/v) Bovine Serum Albumin (BSA, Euromedex) for cell culture experiments. For neutralization experiments, mouse monoclonal IgG1 anti-TGF-β1/β2/β3 (Clone 1D11) antibody was purchased from R&D Systems and isotype-matched mouse Gamma Globulin used as negative control from Jackson ImmunoResearch. In both cases, cells were incubated for 10 min at 37°C in presence of 5 or 10 µg/mL of either anti-pan-TGF-β or isotype-matched antibody before stimulation.

Plasmids, Cloning and Cell Transfection

For recombinant protein production in mammalian cells, FBG-like sequences of human TN-X (from $Gly^{4,048}$ to $Gly^{4,272}$ residues according to GenBank ID 7148), TN-C (from $Gly^{1,338}$ to $Ala^{1,564}$; GenBank ID 3371), TN-W (from Val^{990} to $Phe^{1,229}$; GenBank ID 63923) and TN-R (from $Gly^{1,027}$ to $Phe^{1,257}$; GenBank ID 7143) were cloned between NheI and BamHI restriction sites into the pCEP4-BM40-8HIS/Puromycin expression plasmid (gift from M. Koch, University of Cologne, Germany) using the One-Step Sequence- and Ligation- independent Cloning (SLIC) method (35) and specific oligonucleotides (**Table 1**). cDNAs encoding the FBG-like domains of human TN-C and TN-W were amplified using full-length protein-encoding plasmids (36) as templates. Prior to SLIC cloning, the cDNA encoding the FBG-like domain of human TN-R was amplified from human brain mRNA (Clontech) by RT-PCR using the PrimeStar HS DNA Polymerase (Takara Bio Inc.) and the following forward 5'-GGAGGCCGGGTGTTCCCTCATC-3' and reverse 5'-CTCAGAACTGTAAGGACTGCCG-3' oligonucleotides. Similarly, the cDNA encoding the FBG-like domain of TN-X was obtained by RT-PCR from human primary fibroblast mRNA using the following forward 5'-GGTGGGCTGCGGATC CCCTTC-3' and reverse 5'-GCCTCCCCCCGCTGGGGAGC-3' primers. The integrity of the cloned sequences was assessed by direct sequencing (Eurofins Genomics).

A cleavage site attributed to the Furin-like family of pro-protein convertases was identified at the C-terminal sequence of human FBG-W domain, thus allowing the removal of the histidine tag during biochemical purification of the recombinant protein. Consequently, site-directed mutagenesis was performed on the FBG-W-encoding pCEP4-BM40-8HIS

TABLE 1 | Oligonucleotide primers used for the cloning of the FBG-like domains in the pCEP4-BM40-8HIS/Puromycin vector using the SLIC method.

Primer name	Primer Sequence
pCEP4-hFBGC-Forward	5'-**CTTTGCCTGGCCGGGAGGGCTCTGGCAGCCCC**GCTAGCAGGACTCCTGTACCCCTTCCCC-3'
pCEP4-hFBGC-Reverse	5'-**GGATCATTAATGGTGGTGATGATGGTGGTGGTG**GGATCCTGCCCGTTTGCGCCTGCCTTC-3'
pCEP4-hFBGR-Forward	5'-**CTTTGCCTGGCCGGGAGGGCTCTGGCAGCCCC**GCTAGCAGGAGGCCGGGTGTTCCCTCAT-3'
pCEP4-hFBGR-Reverse	5'-**GGATCATTAATGGTGGTGATGATGGTGGTGGTG**GGATCCGAACTGTAAGGACTGCCGTTT-3'
pCEP4-hFBGW-Forward	5'-**CTTTGCCTGGCCGGGAGGGCTCTGGCAGCCCC**GCTAGCAGTTGGTGCCCGTTTCCCACAC-3'
pCEP4-hFBGW-Reverse	5'-**GGATCATTAATGGTGGTGATGATGGTGGTGGTG**GGATCCGAACGTTCGCAGCCTTCCTCT-3'
pCEP4-hFBGX-Forward	5'-**CTTTGCCTGGCCGGGAGGGCTCTGGCAGCCCC**GCTAGCAGGTGGGCTGCGGATCCCCTTC-3'
pCEP4-hFBGX-Reverse	**5'-TGGATCATTAATGGTGGTGATGATGGTGGTGGTG**GGATCCGCCTCCCCCCGCTGGGGAGC-3'

Vector tail sequences are indicated by bold face. Restriction sites are underlined.

plasmid to substitute the $Arg^{1,220}$ amino-acid by an alanine residue, using the QuikChange II XL Site-Directed Mutagenesis Kit (Agilent Technologies) and the following forward 5'-TGTCCTGGGCAGAAAGAAGGCGACGCT GAGAGGAAGGCTG-3' and reverse 5'-CAGCCTTCC TCTCAGCGTCGCCTTCTTTCTGCCCAGGACA-3' oligonucleotides. The recombinant FBG-W^{RKKA} domain was used throughout the study.

HEK293-EBNA1 cells at 70-90% confluency in 6-well plate were transfected with 4 µg of pCEP4-BM40-8HIS/Puromycin plasmid encoding FBG-like domain using Lipofectamine 2000 (Invitrogen), in serum- and antibiotic-free DMEM for 48 hours. Mock-transfected cells, corresponding to HEK-293 EBNA1 cells transfected with empty pCEP4-BM40-8HIS/Puromycin vector were used as a negative control. Once transfected, the G418 antibiotic was replaced by 2.5 µg/mL of Puromycin (Gibco) in the culture medium.

For recombinant protein production in bacteria, cDNAs encoding FBG-like domains of the four human Tenascins were amplified by PCR (Taq Platinum HF polymerase, TermoFisher), flanked with appropriate restriction sites (**Table 2**) and ligated into the linearized and dephosphorylated pT7.7 vector (United States Biochemical Corp.) using Rapid DNA ligation kit (Roche). Integrity of the cloned sequences was assessed by direct sequencing (Eurofins Genomics). Chemically ultracompetent *E.coli* BL21-DE (3) bacteria (New England Biolabs) were transformed using heat-chock method and selected on LB-agar plates containing 100 µg/mL ampicillin (Sigma-Aldrich).

Recombinant Protein Production, Purification and Adsorption

For protein production in mammalian cells, stably transfected HEK-293 or HEK-293 EBNA1 cells were cultured over confluence for 3 weeks under serum deprivation and culture medium was collected 3 times a week. Conditioned media enriched in recombinant proteins or collected from mock-transfected cells were cleared from cellular debris by centrifugation for 10min at 400g at 4°C and stored at -80°C.

Full-length TN-X and TN-$X^{\Delta E\Delta F}$ were purified by mean of two chromatographic steps as described previously (3). Briefly, a first affinity chromatography was performed on Heparin-Sepharose column (GE Healthcare). After two washes with 50 mM Tris-HCl, pH 8.0, proteins were eluted using 0.5 M NaCl in 50 mM Tris-HCl, pH 8.0, dialyzed 3 times against 50 mM Tris-HCl pH 8.0 (twice for 2 hours and once overnight) and applied on a Q-Sepharose column (GE Healthcare). Elution was performed using linear NaCl gradient (from 0 M to 1 M) in 50 mM Tris-HCl, pH 8.0 and fractions enriched in recombinant proteins were pooled.

Full-length TN-C and TN-W were purified as described by Giblin et al. (2018) (37). Before purification, histidine-tagged full-length TN-C and TN-W were precipitated from conditioned medium by stirring 2h at 4°C in presence of 2.2 M ammonium sulfate (Sigma-Aldrich), pelleted by centrifugation at 12,000g, for 20 min at 4°C, resuspended in 50 mL of Phosphate-Buffered Saline (PBS, Euromedex) containing 0.01% Tween-20 (VWR) and dialyzed 3 times (twice for 2h and once overnight) at 4°C in PBS containing 0.01% Tween-20. In order to remove Fibronectin (FN), a first gelatin-Agarose column (Sigma-Aldrich) was performed, in which FN stayed attached to the gelatin beads while TN-C or TN-W passed to the flow-through. This flow-through containing TN-C or TN-W was then applied on a Ni-Nitriloacetic acid agarose (Ni-NTA, Qiagen) column, which was subsequently washed twice using PBS containing 20 mM imidazole. TN-C or TN-W were then eluted using 300 mM imidazole diluted in PBS.

Prior purification, mock-conditioned medium or conditioned media enriched in human FBG-X, FBG-C, FBG-W or FBG-R were dialyzed using MWCO 6,000-8,000 Da dialysis tubing (SpectrumLabs) in 300 mM NaCl, 50 mM NaH_2PO_4, 5 mM imidazole (Sigma-Aldrich), overnight at 4° C. Thanks to the presence of eight histidine residues at the C-terminal end of recombinant FBG-like domains, a single Ni-NTA affinity column was performed. Column was washed twice using 300 mM NaCl, 50 mM NaH_2PO_4, 5 mM imidazole, and proteins were eluted with 200 mM imidazole (diluted in the washing buffer).

After an initial overnight dialysis against PBS, fractions enriched in recombinant proteins were dialyzed overnight against sterile PBS containing 0.2% (v/v) chloroform (Sigma-Aldrich) to prevent contamination, followed by a last overnight dialysis against sterile PBS before storage at -80°C. The homogeneity of recombinant proteins was assessed by SDS-PAGE coupled with R250 Coomassie Blue staining (Biorad), and protein concentration was determined using the QuantiPro™ BCA Assay kit (Sigma-Aldrich).

Recombinant CUB1CUB2 (C1C2) fragment of human Procollagen C-proteinase enhancer-1 (PCPE-1) containing

TABLE 2 | Oligonucleotide primers used for the cloning of the FBG-like domains in the pT7.7 vector using standard method.

Primer name	Primer sequence	Restriction site
pT7-7-hFBGC-Forward	5'-CGCGGATCCGGACTCCTGTACCCCTTCCCC-3'	*BamHI*
pT7-7-hFBGC-Reverse	5'-CCCCTGCAGTGCCCGTTTGCGCCTGCC-3'	*PstI*
pT7-7-hFBGR-Forward	5'-GCTAGAATTCGCGGAGGCCGGGTGTTCCCT-3'	*EcoRI*
pT7-7-hFBGR-Reverse	5'-CCCCTGCAGGAACTGTAAGGACTGCCGTTT-3'	*PstI*
pT7-7-hFBGW-Forward	5'-CGCGGATCCGTTGGTGCCCGTTTCCCACAC-3'	*BamHI*
pT7-7-hFBGW-Reverse	5'-CCCGTCGACGAACGTTCGCAGCCTTCC-3	*SalI*
pT7-7-hFBGX-Forward	5'-GCTAGAATTCGCGGTGGGCTGCGGATCCCC-3'	*EcoRI*
pT7-7-hFBGX-Reverse	5'-CCCCTGCAGGCCTCCCCCCGCTGGGGAGCG-3'	*PstI*

Restriction sites are underlined.

eight histidine residues at its C-terminal end was produced in HEK-293 T cells, as previously described (38).

Recombinant proteins were diluted in PBS and adsorbed onto cell culture dishes or coverslips overnight at 4°C. When full-length Tenascins were used within the same experiment, the quantity of coated recombinant protein was 22.2 pmol/cm^2, while FBG-like domains were coated either at 333 pmol/cm^2 (corresponding to 10 µg/cm^2), 666 pmol/cm^2 (20 µg/cm^2) or 999 pmol/cm^2 (30 µg/cm^2), depending on the experiments. Following passive protein adsorption, non-specific interaction sites were saturated using 1% (w/v) BSA diluted in PBS for 1h at 37°C.

For protein production in bacteria, transformed BL21-DE (3) cells were cultured in LB medium containing 100 µg/mL ampicillin until the 600nm absorbance was comprised between 0.6 and 0.8. Protein production was then induced by 1 mM Isopropyl β-D-1-thiogalactopyranoside (IPTG, Sigma) for 3h at 37°C. Bacteria were pelleted by centrifugation at 5,000g for 20min and insoluble FBG-like domains were extracted from inclusion bodies by stirring 1h at room temperature with 100 mM CAPS (Sigma) pH 11.0 containing 8 M urea (Promega). Protein lysate was cleared from bacteria debris by centrifugation at 5,000g for 20min and supernatant containing solubilized proteins were incubated for 1h at room temperature with Ni-NTA beads. Once loaded onto an empty column, histidine-tagged FBG-like domains bound to the Ni-NTA beads were washed and refolded using a linear decreasing urea gradient (concentration from 8 M to 0 M) diluted in 100 mM CAPS, each time using 10 column volumes. Elution was performed using 200 mM imidazole diluted in 100 mM CAPS, pH 8.0, and dialyzed twice overnight against sterile PBS at 4°C before storage at -80°C. Purity and concentration of recombinant proteins produced in bacteria was assessed as described earlier for proteins produced in mammalian cells. Recombinant FBG-like domains produced in bacteria were noted FBG* to distinguish them with those produced in mammalian cells.

The level of LPS in each recombinant protein preparation was assessed using the *Limulus amaebocyte* lysate assay (Pierce LAL Chromogenic Endotoxin Quantitation Kit) according to the manufacturer's instructions. The levels of LPS in recombinant proteins purified from mammalian cell conditioned medium were below 50 pg/mL, whereas they were ranging between 100 and 500 pg/mL in the FBG-like domains purified from bacteria.

Immunoblotting

For cell signaling analyses, either 10^6 NMuMG cells were seeded and cultured for 3h in the presence of immobilized recombinant proteins or 5.10^5 cells were seeded on plastic dishes, and stimulated the day after with soluble recombinant FBG-like domains for 1h prior to cell lysis. Total proteins were extracted from stimulated NMuMG cells using radioimmunoprecipitation assay (RIPA) extraction buffer (Thermo Scientific) containing EDTA-free protease inhibitor and phosphatase inhibitor cocktails (Roche) for 20min on ice. After centrifugation at 13,200g for 10min at 4°C, supernatant containing solubilized proteins were stored at -20°C prior to Western blot analyses. 20 µg of total proteins were resolved by SDS-PAGE in Tris-Glycine buffer containing Sodium-Dodecyl-Sulfate (TG-SDS, Euromedex) and then transferred onto Polyvinylidene Fluoride membrane (PVDF, Milipore) at 0.4 A during 2h in TG-SDS buffer containing 20% Ethanol. Membrane was saturated using 5 or 10% (w/v) non-fat dry milk diluted in Tris-buffered saline (TBS, Euromedex) containing 0.1% (v/v) Tween-20 (T-TBS, VWR) for 1h at room temperature prior overnight incubation with primary antibody (at 4°C). Rabbit monoclonal antibody anti-phospho-Smad2 (Ser465/467, diluted at 1/1,000 in T-TBS containing 5% (w/v) BSA) and rabbit polyclonal antibody anti-Smad2/3 (diluted at 1/500 in T-TBS containing 5% (w/v) BSA) were purchased from Cell Signaling Technology, goat polyclonal antibody anti-human LAP (TGF-β1) was purchased from R&D System (diluted at 1/100 in T-TBS containing 5% (w/v) non-fat dry milk), rat monoclonal antibody anti-TGF-β1 (diluted at 1/500 in T-TBS containing 5% (w/v) non-fat dry milk) was purchased from BD Pharmigen™, mouse monoclonal anti-6X His tag (diluted at 1/1,000 in T-TBS) was purchased from Abcam, monoclonal mouse antibody anti-GAPDH (diluted at 1/1,000 in T-TBS) was purchased from Abcam, and rabbit antibody anti-actin (diluted at 1/1,000 in T-TBS) was purchased from Sigma-Aldrich. Secondary anti-mouse IgG (Abcam, diluted at 1/10,000 in T-TBS containing 5% (w/v) non-fat dry milk), anti-rabbit IgG (Abcam, diluted at 1/5,000 or 1/2,500 in T-TBS containing 5% (w/v) non-fat dry milk), anti-goat IgG (ImmunoResearch Laboratories, diluted at 1/2,000 in T-TBS containing 10% (w/v) non-fat dry milk) and anti-rat IgG (ImmunoResearch Laboratories, diluted at 1/2,000 in T-TBS containing 10% (w/v) non-fat dry milk) antibodies coupled with Horseradish Peroxidase (HRP) were added for 1h at room temperature prior to signal detection using the enhanced chemiluminescence technique with the ECL™ prime Western Blotting Detection Reagent (GE Healthcare) and the FX Fusion CCD camera (Vilber Lourmat). Signals were quantified using FIJI software (SciJava).

Cell Reporter Assay

100,000 NMuMG cells were seeded on 24-well culture plates on day 1. On day 2, cells were co-transfected with the pGL3-basic reporter plasmid (Promega) encoding firefly luciferase under control of TGF-β-responsive elements ((CAGA)$_{12}$-Luc) (39) together with the pRL-CMV vector (Promega) encoding Renilla luciferase under the control of the cytomegalovirus ubiquitous promoter to determine the transfection efficiency and to normalize firefly luciferase activity. Transfection was carried out for 4h to 6h using lipofectamine 2000 (Invitrogen) according to manufacturer recommendations, using a 20:1 plasmid ratio corresponding to 0.8 µg of pGL3-MLP-(CAGA)$_{12}$ and 0.04 µg of pRL-CMV per condition. Cells were then cultured in complete medium and stimulated for 16h using the amount of proteins described in figure legends. On day 3, cell lysates were obtained using Passive Lysis Buffer (Promega) for 15min at room temperature under shaking and were then kept frozen at -20°C. Luciferase assay was performed in Costar 96-well flat bottom white polystyrol plates using the Dual Glo luciferase reporter assay system (Promega) according to the recommendations of the manufacturer. Briefly, luciferase activity was measured for 7s per well using 20 µL of cell lysate

and 100 µL of LAR II buffer. Then, luciferase activity was quenched and Renilla was activated by adding 100 µL of Stop&Glo solution per well, followed by a reading of Renilla activity for 7 seconds. Luminescence measurements were performed on Tecan i-control Infinite M1000 (Tecan Group).

MTT Test

MTT test was performed on 5,000 NMuMG cells cultured in complete medium for 48h onto 96-well plates coated or not (PBS) with 333 pmol/cm^2 (corresponding to 10 µg/cm^2), 666 pmol/cm^2 (20 µg/cm^2) or 999 pmol/cm^2 (30 µg/cm^2) of purified recombinant human FBG-like domains. Cells were then incubated for 2h with 0.5 mg/mL MTT (3-(4,5-dimethylthiazol-2-yl)-2,5-diphenyltetrazolium bromide; Sigma-Aldrich) dissolved in culture medium, allowing NAD(P)H-dependent mitochondrial oxido-reductase enzymes to reduce MTT into formazan. Formazan was then solubilized from intracellular compartment using 10% (v/v) Triton X-100 in 0.1M HCl (Euromedex) and absorbance was measured by spectrophotometry at 570nm (Tecan M1000 PRO, infinite).

Direct Fluorescence and Indirect Immunofluorescence Microscopy

100,000 NMuMG cells cultured in complete medium for 72h onto coverslips coated with purified recombinant human FBG-like domains (666 pmol/cm^2) were fixed for 20min using 4% (w/v) paraformaldehyde, permeabilized for 10min using 0.5% (v/v) Triton X-100 in PBS and non-specific sites were saturated for 1h using 5% (v/v) SVF in PBS. All steps were performed at ambient temperature. Actin direct fluorescence analyses were performed using Tetramethylrhodamine isothiocyanate-labelled phalloidin (Sigma-Aldrich). Indirect immunofluorescence experiments were performed using mouse monoclonal anti-E-Cadherin (1/200; BD Transduction Laboratories™) and Alexa Fluor 488-conjugated goat anti-mouse IgG (1/1,000; Life Technologies) antibodies. DNA was stained with DAPI contained in the Vectashield mounting medium (Vector Laboratories). Observations were conducted using an ECLIPE Ti-E inverted microscope (Nikon) equipped with a DS-Fi2 color camera and the NIS element imaging software.

Homology Modeling and Protein-Protein Docking

The four FBG-like domains of the human Tenascins, FBG-C, FBG-R, FBG-W and FBG-X, were modeled by homology using SWISS-MODEL web service. The PDB structure of the FGB-like domain of human TN-C (PDB code 6QNV chain A) was chosen as fold for the four models. The coverage for FBG-C starts at amino-acid #1979 to 2194 with 96% of identity, the FGB-R starts at amino-acid #1133 to 1358 with 60% of identity, FGB-W starts at amino-acid #1065 to 1280 with 52% of identity and for FBG-X starts at amino-acid #4025 to 4240 with 54% of identity. The high identity and the alignment quality of the FBG-like domain sequences with the fold were enough to create reliable models. All resulting models were checked, then charged and minimized using the MOE molecular modeling software (version 2019) with AMBER14:ETH force-field under pH 7. For latent TGF-β (pro-TGF-β1), PDB structure labeled 3RJR was used. This structure was checked, charged and minimized with the same protocol as for FGB-like domains.

Each FBG-like domain with pro-TGF-β1 were submitted to ClusPro webserver to perform protein-protein docking. No constraint in term of binding residue was set. 1,000 trials with rigid docking algorithms were selected and 30 cluster structures were constructed. Ten complexes optimized with charm force-field were output from the server. As complex is not mainly hydrophobic or hydrophilic, "balanced" score results were selected. For each FBG-like domain, the ten structures were checked, charged and minimized with MOE software using AMBER14:EHT force-field at pH 7.

Molecular Dynamics and Trajectory Analysis

The twelve complexes were inserted in a TIP3P box, with a minimal distance of 12Å to the box limit, were prepared for molecular dynamic simulations. All simulations were performed using the molecular dynamics program AMBER18 (40) using the AMBER 14SB force-field. The simulation systems were kept under isothermal/isobaric (NPT) conditions except for the heating phase. Energy minimization was performed to obtain a low energy starting conformation for the subsequent MD simulation. The solvated complexes were minimized for a total of 5,000 cycles, using the steepest descent method for 2,500 cycles, followed by 2,500 cycles of a conjugate gradient. Then, a 1ns heating phase was performed from 0 to 300K at constant pressure and temperature. The equilibration/production was performed for 100ns. The time step of the simulations was 0.002ps.

The VMD software (41) was used to visualize trajectories generated during the simulation. Root Mean Square Deviation (RMSD) was used to determine structure stability. RMSDs were calculated for every simulation. Analysis of all RMSD reveals than the value of each dynamics is stabilized around 3Å and parameters of simulation reveal that simulations have reach equilibrium around 10 ns of simulation time. On the last 50ns of the trajectory 100 frames were sampled, one every 0.5ns.

Affinity Binding Calculation and Alanine Scanning

For each simulation, the 100 sampled complexes without water were sent to Prodigy binding energy calculation. For each frame, the binding energy was computed and the mean energy was calculated. For each FBG, the three complexes conformation with the lowest binding energy were selected for additional analyzes. To investigate which residues of the structures were involved in the interaction, an alanine scanning simulation was performed. The last frame of MD for all three complexes was sent to MOE to do alanine scanning simulation. Each simulation will mutate to alanine all Tenascin amino-acid that may interact with latent TGF-β (pro-TGF-β1) or *vice versa*. Alanine scanning method was performed with a "rotamer explorer" algorithm with a conformation limit set to 50. The affinity was computed by GBVI/WSA algorithm between latent TGF-β and each FBG-like domain.

Surface Plasmon Resonance (SPR) Analyses

The interaction between recombinant human mature TGF-β1 (dissolved in 10 mM citric acid; Peprotech) or human latent TGF-β1 (LTGF-β1, dissolved in PBS with 50% glycerol; ref. 299-LT-CF; BioTechne) and the four FBG-like domains or human Thrombospondin (TSP)-1 [purified from platelets as described (42)] was studied by surface plasmon resonance (SPR) using a Biacore T200 instrument. The four FBG domains and LTGF-β1 were immobilized on Series S CM5 sensorchips using amine coupling chemistry at pH 7.0 (in 10 mM HEPES) while FBG-X which was diluted in 10 mM sodium acetate pH 5.0. The control channels were prepared with the same activation/deactivation procedure except that the protein solution was replaced by buffer alone. The experiments were run in PBS buffer (Gibco) supplemented with 0.05% P-20 and sensorgrams were recorded at 25°C with a flow rate of 30 µl/min. Signals from control flow cells were automatically subtracted from signals in active flow cells. Regeneration of active and control channels was performed using 2 M NaCl. Kinetic data were analyzed using the Biacore T200 Evaluation software 3.2.

Data and Statistical Analysis

The GraphPad Prism 8 software was used for graphical representations of data and statistical analyses. Each result shown is from an experiment representative of at least three independently repeated experiments. For MTT test, statistical analyses were performed using non-parametric ANOVA (Kruskal-Wallis test), and each condition was compared to the control condition (N-C) using Dunn's multiple comparisons test. p values < 0.05 were considered as statistically significant (p values were indicated in the figure legends).

RESULTS

Amino-Acid Sequence Conservation Between Tenascin FBG-Like Domains Suggests a Functional Redundancy in Latent TGF-β Activation

To evaluate sequence conservation between the four human Tenascin FBG-like domains (hereafter called FBG-C, FBG-R, FBG-W and FBG-X), their amino-acid sequences were aligned using the CLUSTALW software (**Figure 1A**). Sequence comparison showed that the FBG-like domains of the four Tenascins share a high degree of identity (35 %) and similarity (55 %) when compared all together (**Figure 1A**). This high degree of sequence homology may also imply a structural similarity, because the cysteine residues responsible for the formation of two disulfide bounds are strictly conserved between the four domains (**Figure 1A**, highlighted in yellow). In order to perform a deeper analysis, we also compared the sequences of FBG-like domains in pairs (**Figure 1B**). When compared two by two, the degree of similarity is strongly increased, showing that FBG-like domains share more than 50% of sequence identity and at least 65% of similarity, except for FBG-X and FBG-W, which appeared to be the most divergent ones. Consequently, FBG-C seems to be closer to FBG-R and FBG-W, and FBG-X seems to be the most distant domain of the Tenascin family (still with >47% identity with its counterparts), as previously suggested by Chiquet-Ehrismann (43). Nevertheless, this high degree of homology between FBG-like domains strengthens the idea that latent TGF-β activation might be a common property to all members of the Tenascin family.

Recombinant Full-Length Tenascins and Their Respective FBG-Like Domains Are Produced and Purified in Association With the Small Latent Complex

We first wanted to determine whether human TN-C and TN-W could be associated with latent TGF-β, as previously observed for TN-X (28). To do so, recombinant full-length TN-C (220 kDa), TN-W (180 kDa) and TN-X (450 kDa) were produced in mammalian cells and purified from conditioned media using specific chromatographic steps as detailed in the "Materials and Methods" section (**Figures 2A, B**). Full-length TN-R was not included in this study because, to our knowledge, no recombinant human TN-R has been cloned and characterized yet. As negative control, we also included a recombinant TN-X fragment called TN-X$^{\Delta E \Delta F}$ (380 kDa), which does not contain EGF-like repeats and FBG-like domain (**Figure 2A**) (3). This truncated TN-X fragment is used to indicate the basal level of contaminating TGF-β1 in our purified recombinant proteins (28). We then decided to analyze the presence of SLC components (*i.e.* TGF-β and LAP(β) entities) in purified protein fractions. Immunoblotting performed on equimolar quantity of purified TN-X, TN-C and TN-W confirmed the presence of both TGF-β1 moiety and LAP(β1) pro-domain in all recombinant full-length protein preparations (**Figure 2C**), showing that these three glycoproteins co-purify with the endogenously synthesized latent TGF-β1. As previously described, TN-X$^{\Delta E \Delta F}$ purification fraction does not contain any component of the SLC (**Figure 2C**), thus confirming that latent TGF-β1 is not associated with TN-X FNIII repeats.

To confirm the implication of the C-terminal globe of Tenascin family members in this association, FBG-like domains of human TN-X, -C, -W, and -R were cloned, produced in mammalian cells, and purified from conditioned medium using nickel-chelating chromatography (**Figures 2A, D**). As negative control, we used a purification fraction of CUB1CUB2 (C1C2), a recombinant histidine-tagged fragment derived from the Procollagen C-proteinase enhancer-1 (PCPE-1) extracellular protein. The recombinant C1C2 fragment was produced using similar conditions as for the FBG-like domains (mammalian host cells and purification method) (38) and has a comparable molecular mass (≈30 kDa). After protein purity assessment by Coomassie Blue staining on SDS-PAGE (**Figure 2D**), we performed immunoblotting on equimolar quantity of purified FBG-like domains or C1C2 protein to analyze the presence of SLC components. As shown in **Figure 2E**, both TGF-β1 and LAP(β1) entities were detected in each

A

```
FBG-X   GGLRIPFPRDCGEEMQNGAGASRTSTIFLNGNRERPLNVFCDMETDGGGWLVFQRRMDGQ
FBG-C   IGLLYPFPKDCSQAMLNGDTTSGLYTIYLNGDKAQALEVFCDMTSDGGGWIVFLRRKNGR
FBG-W   VGARFPHPSDCSQVQQNSNAASGLYTIYLHGDASRPLQVYCDMETDGGGWIVFQRRNTGQ
FBG-R   GGRVFPHPQDCAQHLMNGDTLSGVYPIFLNGELSQKLQVYCDMTTDGGGWIVFQRRQNGQ
         *   *.* **.:   *.   *   .*:*:*:  : *:*:*** :*****:** **  *:

FBG-X   TDFWRDWEDYAHGFGNISGEFWLGNEALHSLTQ--AGDYSMRVDLRAGDEAVFAQYDSFH
FBG-C   ENFYQNWKAYAAGFGDRREEFWLGLDNLNKITA--QGQYELRVDLRDHGETAFAVYDKFS
FBG-W   LDFFKRWRSYVEGFGDPMKEFWLGLDKLHNLTTGTPARYEVRVDLQTANESAYAIYDFFQ
FBG-R   TDFFRKWADYRVGFGNVEDEFWLGLDNIHRITS--QGRYELRVDMRDGQEAAFASYDRFS
         :*:: *  *  ***:   ***** : :: :*    . *.:***::   *:.:* ** *

FBG-X   VDSAAEYYRLHLEGYHGTAGDSMSYHSGSVFSARDRDPNSLLISCAVSYRGAWWYRNCHY
FBG-C   VGDAKTRYKLKVEGYSGTAGDSMAYHNGRSFSTFDKDTDSAITNCALSYKGAFWYRNCHR
FBG-W   VASSKERYKLTVGKYRGTAGDALTYHNGWKFTTFDRDNDIALSNCALTHHGGWWYKNCHL
FBG-R   VEDSRNLYKLRIGSYNGTAGDSLSYHQGRPFSTEDRDNDVAVTNCAMSYKGAWWYKNCHR
         * .:   *:* :  * *****:::**.*  *:: *:* :  : .**::::*.:**:***

FBG-X   ANLNGLYGSTVDHQGVSWYHWKGFEFSVPFTEMKLRP--RNFRSPAGG----------
FBG-C   VNLMGRYGDNNHSQGVNWFHWKGHEHSIQFAEMKLRP--SNFRNLEGRRKRA--------
FBG-W   ANPNGRYGETKHSEGVNWEPWKGHEFSIPYVELKIRPHGYSREPVLGRKKRTLRGRLRTF
FBG-R   TNLNGKYGESRHSQGINWYHWKGHEFSIPFVEMKMRP--YNHRLMAGRKRQSLQ-----F
         .*  * **.. . :*:.*  ***.*.*: :.*:*:**   . .   *
```

B

Amino-acid sequence identity (%)				
	FBG-X	FBG-C	FBG-W	FBG-R
FBG-X		52.2	47.1	53.5
FBG-C	52.2		50.8	59.3
FBG-W	47.1	50.8		55.0
FBG-R	53.5	59.3	55.0	

Amino-acid sequence similarity (%)				
	FBG-X	FBG-C	FBG-W	FBG-R
FBG-X		68.9	64.2	69.7
FBG-C	68.9		72.5	81.4
FBG-W	64.2	72.5		76.3
FBG-R	69.6	81.4	76.3	

FIGURE 1 | Sequence alignment and homology degree between the Tenascin family FBG-like domains. **(A)** Multiple sequence alignment analysis of the FBG-like domains of human TN-X, -C, -W and -R (FBG-X, -C, -W, -R) performed with CLUSTALW software. Red (*) labelled residues are identical between the four FBG-like domains, green labelled (:) residues are highly conserved and blue labelled (.) residues are poorly conserved. The four conserved cysteine residues are highlighted in yellow. **(B)** Percentages of identity and similarity amongst the amino-acid sequences of the FBG-like domains of the human Tenascins performed with paired comparisons using CLUSTALW software.

purified FBG-like domain fraction, and were absent from C1C2 fraction, confirming the specificity of the molecular association between latent TGF-β1 and Tenascin FBG-like domains. Altogether, these results indicated that the Tenascin family members might be specifically associated with latent TGF-β1 through their FBG-like domains.

During the course of the experiments, we identified a cleavage site located within the C-terminal sequence of the human FBG-W domain that is responsible for the removal of the histidine tag during the biochemical purification of the recombinant protein (**Figure S1**). Indeed, this domain harbors a cationic tail with the following sequence $Arg^{1,217}$-Lys-Lys-$Arg^{1,220}$ (RKKR), which corresponds to the consensus sequence (Arg-Xaa-(Lys/Arg)-Arg-Xaa) for the Furin-like family of pro-protein convertases. Using site-directed mutagenesis, we abolished the C-terminal cleavage site by substituting the $Arg^{1,220}$ amino-acid by an alanine residue. Compared to the FBG-W^{RKKR} domain, the molecular mass of the FBG-W^{RKKA} protein is higher and the histidine-tag is henceforth detectable (**Figure S1**). As this substitution does not prevent the co-purification of the modified FBG-W domain with the latent TGF-β (**Figure 2E**), this recombinant version was used throughout the study. This result also suggests that the molecular association between the FBG-like domains and the LAP–TGF-β complex does not involve the very C-terminal extremity of the FBG knob.

The Recombinant FBG-Like Domains of the Four Tenascins Physically Interact With TGF-β

To confirm a physical interaction between the four FBG-like domains and the small latent (LAP–TGF-β) complex, surface plasmon resonance analyses (SPR) were performed using commercially available recombinant human latent TGF-β1 (LTGF-β1). Although we previously demonstrated that LAP (β1) co-immunoprecipitated with FBG-X (28), we failed to detect an interaction between the four FBG-like domains of Tenascins and recombinant LTGF-β1 by SPR (**Figure S2**). As we did not succeed either to show the binding of LTGF-β1 with purified human TSP-1 (**Figure S2B**), a well-established partner and activator of latent TGF-β (44), it remains questionable whether the purified recombinant LTGF-β1 was in a favorable conformation to enable such an interaction using this biochemical approach. In contrast, we demonstrated a direct interaction between mature TGF-β1 and the four FBG-like

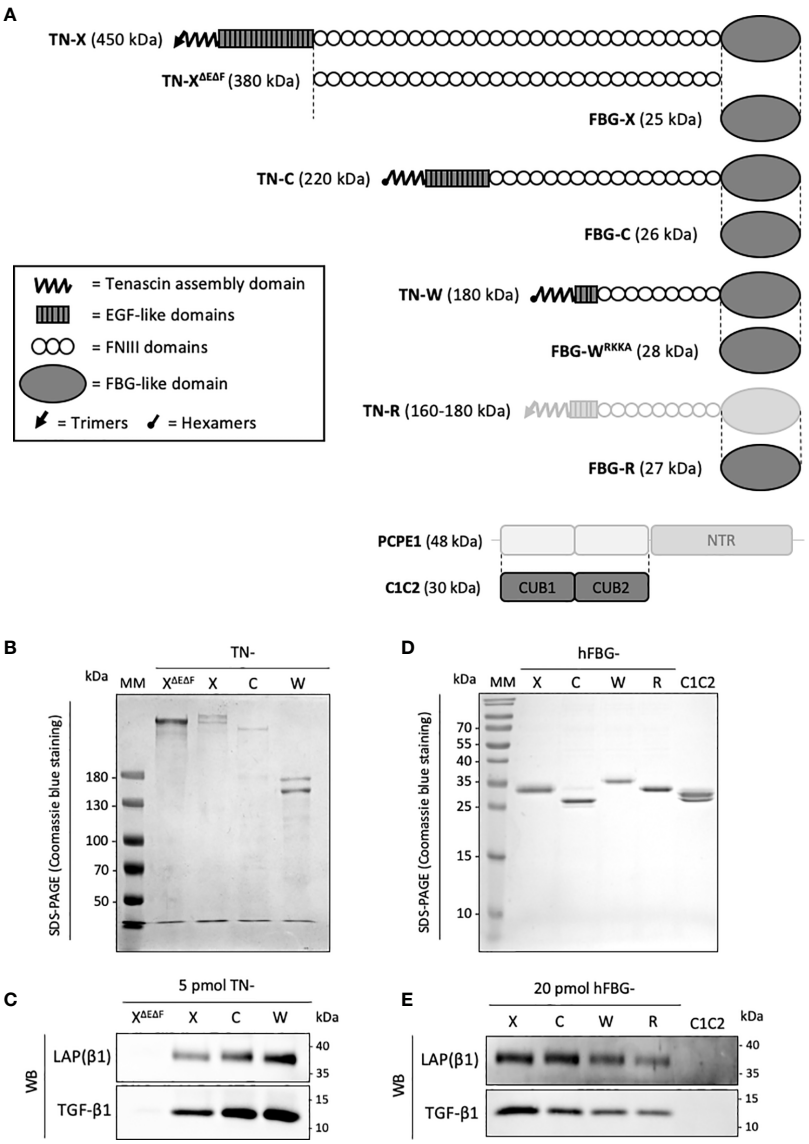

FIGURE 2 | Recombinant full-length Tenascins and their respective FBG-like domains co-purify with latent TGF-β1. **(A)** Schematic representation of the recombinant proteins used in this study (dark grey). Structural modules of Tenascins are depicted in the inset. **(B, D)** SDS-PAGE analysis of the purified recombinant proteins and stained with Coomassie blue. MM, molecular mass markers. **(B)** Purified full-length TN-X, TN-C, TN-W and the TN-$X^{\Delta E\Delta F}$ fragment (1 μg each) were loaded on 6% acrylamide gels under reducing conditions. **(D)** Purified recombinant FBG-like domains of the four human Tenascins and the recombinant CUB1CUB2 (C1C2) domain (2 μg) were resolved on 15% acrylamide gels under reducing conditions. **(C, E)** Western blot analysis indicating the level of human mature TGF-β1 and LAP (β1) pro-domain associated with equimolar quantity of purified recombinant full-length TN or TN-$X^{\Delta E\Delta F}$ fragment (5 pmol each) **(C)** and recombinant Tenascin FBG-like domains or CUB1CUB2 (C1C2) protein (20 pmol) **(E)**.

domains (**Figures 3A–D**). The association and dissociation curves obtained with different concentrations of TGF-β1 were best fitted with the heterogenous ligand model to determine the apparent equilibrium dissociation constants (K_D) between the different entities (**Table 3**). Bioactive TGF-β1 binds with higher affinity to FBG-X (K_{D1} = 342 nM and K_{D2} = 407 nM) than to FBG-W (K_{D1} = 1.9 μM and K_{D2} = 6.5 μM). Curves derived from the interaction between TGF-β1 and immobilized FBG-C and FBG-R could not be fitted due to weak signals at the lower TGF-β1 concentrations and aggregation occurring when higher concentrations were injected.

Molecular Docking of the Small Latent Complex With the FBG-Like Domains of the Tenascins

The latter result prompted us to model the association of pro-TGF-β1 (31) with the four human Tenascin FBG-like domains using modeling and molecular dynamic approaches. Thanks to the high

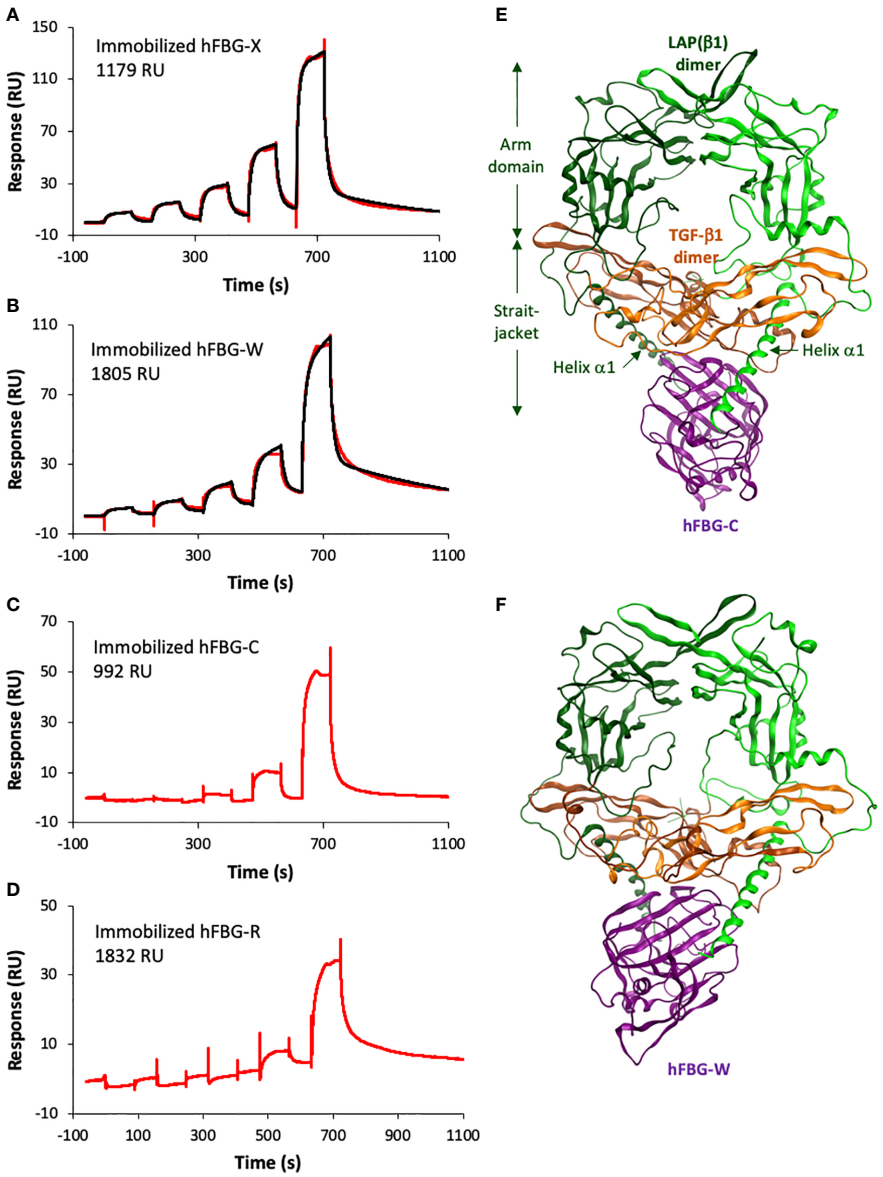

FIGURE 3 | The recombinant FBG-like domains of Tenascins interact with TGF-β1. **(A–D)** Interactions of TGF-β1 with FBG-like domains analyzed by SPR. Increasing concentrations of TGF-β1 were injected in single-cycle mode over immobilized FBG-X **(A)**, FBG-W **(B)**, FBG-C **(C)** and FBG-R **(D)**. The experimental curves are shown in red and the best fits with the heterogeneous ligand model in black. The concentrations of TGF-β1 were as follows: **(A)** 15.6 – 31.2 – 62.5 – 125 – 250 nM; **(B)** 7.8 – 15.6 – 31.25 – 62.5 – 125 nM; **(C)** 20.2 – 40.5 – 81 – 162 – 324 nM; **(D)** 9.4 – 18.8 – 37.5 – 75 – 150 nM. **(E, F)** Homology models showing the predicted docking between the FBG-like domain of TN-C **(E)** or TN-W **(F)** and the pro-TGF-β1. The dimeric LAP(β1) pro-domain is shown in green, the TGF-β1 dimer in orange and the FBG-like domains in purple. 'Straitjacket' and arm domains of the LAP(β1) dimer are indicated.

TABLE 3 | Kinetic and dissociation constants derived from SPR analysis.

	k_{a1} ($M^{-1}s^{-1}$)	k_{d1} (s^{-1})	K_{D1} (μM)	k_{a2} ($M^{-1}s^{-1}$)	k_{d2} (s^{-1})	K_{D2} (μM)	Chi^2 (RU^2)
hFBG-X	8085	0.00276	**0.342**	2.074 10^5	0.0845	**0.407**	5.27
hFBG-C	*NA*	*NA*	*NA*	*NA*	*NA*	*NA*	*NA*
hFBG-W	1036	0.00196	**1.89**	1.430 10^4	0.0926	**6.48**	4.21
hFBG-R	*NA*	*NA*	*NA*	*NA*	*NA*	*NA*	*NA*

*See legend of **Figure 3** for experimental conditions. Best fits for the interactions of TGF-β1 with FBG-X and FBG-W were obtained with the heterogeneous ligand model. NA, not applicable.*

sequence identity observed between the four FBG-like domains, it was possible to generate reliable models of the FBG-R, -W and -R from the known X-ray structure of FBG-C (PDB code 6QNV). Indeed, homology models predict that each FBG-like domain exhibits similar subdomain organization and folding. Then, protein-protein docking simulations for the complexes involving FBG-like domains and pro-TGF-β1 were performed with ClusPro. For each FBG-like domain, three poses with the best score affinity were selected (**Figures 3E, F** and **S3A**). Binding energies between the four domains revealed some differences, FBG-X displaying the highest (14.2, 14.8, and 13.2 kcal.mol^{-1}), FBG-W (13.2, 11.9 and 13.1) and FBG-C (12.8, 11.1, and 12.4 kcal.mol^{-1}) intermediate, and FBG-R (10.7, 11.2, and 11.7 kcal.mol^{-1}) the lowest values. These energy scores suggested that FBG-X should bind with a higher affinity to pro-TGF-β1 than FBG-W and FGB-C, themselves having a better affinity than FBG-R. The twelve selected complexes were submitted to an alanine scanning simulation and resulting binding energies were further calculated. For each protein domain, residues were considered to play a critical role in the interaction if the ΔΔG affinity between the wild-type FBG and the corresponding virtual mutant was higher than 2 kcal.mol^{-1} and if they came out in the three simulations performed with a specific FBG-like domain. These simulations predicted a limited number of key residues (four to six residues per domain) involved in the interaction with the FBG-like domains. These are mostly located in the loop 9 of the four FBG-like domains, a region located at the C-terminal part of the domains, but upstream of the cationic tail of FBG-W, FBG-C and FBG-R (**Figure S3B**). These residues are predicted to play a critical role in the interaction with pro-TGF-β1 mostly through hydrogen bonds and steric modification of the interface. In addition, the pro-TGF-β1 is suggested to interact with the FBG-like domains not only through the LAP pro-domain (helix α1 from the straightjacket domain) but also with the N-terminal region of the mature TGF-β1 moiety (**Figures 3E, F**, **S3A**, **S4**). Pro-TGF-β1 was also submitted to an alanine scanning simulation and critical residues predicted to be involved in the interaction with each FBG-like domain were also determined (**Figure S4**).

FBG-Like Domains of the Tenascin Family Members Activate the Canonical TGF-β/Smad Intracellular Signaling Pathway

Because of their association with latent TGF-β1, we investigated the ability of full-length Tenascins and FBG-like domains to stimulate the canonical TGF-β/Smad intracellular signaling pathway. In the first set of experiments, we analyzed the phosphorylation of Smad2 in Normal Murine Mammary Gland (NMuMG) epithelial cells seeded for 3h onto non-coated (N-C) dishes, or dishes coated with equimolar quantity of recombinant proteins (22,2 pmol/cm^2 for full-length Tenascins or 333 pmol/cm^2 for FBG-like domains). Because cells were not able to adhere properly onto full-length TN-C due to its anti-adhesive property (45), detached NMuMG cells were harvested and pelleted from culture medium prior to protein extraction. While NMuMG cells cultured onto N-C dishes or dishes coated with TN-X$^{\Delta E \Delta F}$ displayed basal levels of phosphorylated Smad2, cells cultured onto full-length TN-X, TN-C and TN-W exhibited a marked phosphorylation of Smad2 (**Figure 4A**). Smad2 phosphorylation is comparable to that obtained with TGF-β1 stimulation for cells cultured onto TN-X and slightly less intense (but still strong) for cells cultured onto immobilized TN-C and TN-W (**Figures 4A, B**). Level of Smad2 phosphorylation was also increased when NMuMG cells were seeded onto equimolar quantity of immobilized FBG-like domain of the four Tenascins (**Figures 4C, D**).

Because Tenascins are known to modulate cell adhesion, we next decided to analyze Smad activity in NMuMG cells stimulated with soluble, instead of immobilized, recombinant proteins. Results obtained with equimolar concentration of soluble FBG-like domains were similar to those obtained using coated proteins, resulting in Smad2 phosphorylation in NMuMG cells (**Figure 4E**). As a negative control, we used the conditioned medium obtained from mock-transfected cells that was submitted to a nickel-chelating column (MOCK), as done for the FBG-like domains. NMuMG stimulation using this mock fraction induced a near to basal Smad2 phosphorylation (**Figure 4E**). Similarly, the CUB1CUB2 protein fragment failed to induce an activation of the Smad signaling pathway in NMuMG cells (**Figure 4F**), thus confirming that Smad2 phosphorylation can be attributed to the Tenascin-derived proteins, but not to an irrelevant protein domain.

As a readout of Smad2 transcriptional activity, we performed Luciferase analyses in NMuMG cells. Cells were transiently transfected with the $(CAGA)_{12}$-Luc synthetic reporter construct containing twelve repeats of the Smad-binding element (39) and were stimulated with soluble recombinant FBG-like domains. Recombinant human TGF-β1 and MOCK or vehicle (PBS) were respectively used as positive and negative controls. Stimulation with soluble FBG-like domains induced a marked increase of luciferase activity in transiently transfected NMuMG cells, in comparison with MOCK or PBS treatment (**Figure 4G**). Altogether, these results indicated that the FBG-like domains of the four Tenascins induced a canonical TGF-β/Smad intracellular pathway in epithelial cells, resulting in a functional Smad transcriptional activity.

Tenascins Are Able to Activate Latent TGF-β Thanks to Their FBG-Like Domains

Then, we planned to determine whether TN-X ability to activate latent TGF-β through its C-terminal knob was shared by TN-C and TN-W. We first analyzed the impact of full-length Tenascins on the canonical TGF-β signaling pathway in the presence of an anti-TGF-β1/2/3 neutralizing antibody directed against mature TGF-β entities. In NMuMG cells, this antibody significantly inhibited Smad2 phosphorylation induced by either soluble mature TGF-β1 or immobilized full-length Tenascins, as compared with control IgG (**Figure 5A**). Similarly, the neutralizing antibody abolished Smad2 phosphorylation provoked by coated FBG-like domains (**Figure 5B**). These results suggest that FBG-like domains of the four Tenascins are able to induce Smad signaling by increasing mature TGF-β bioavailability.

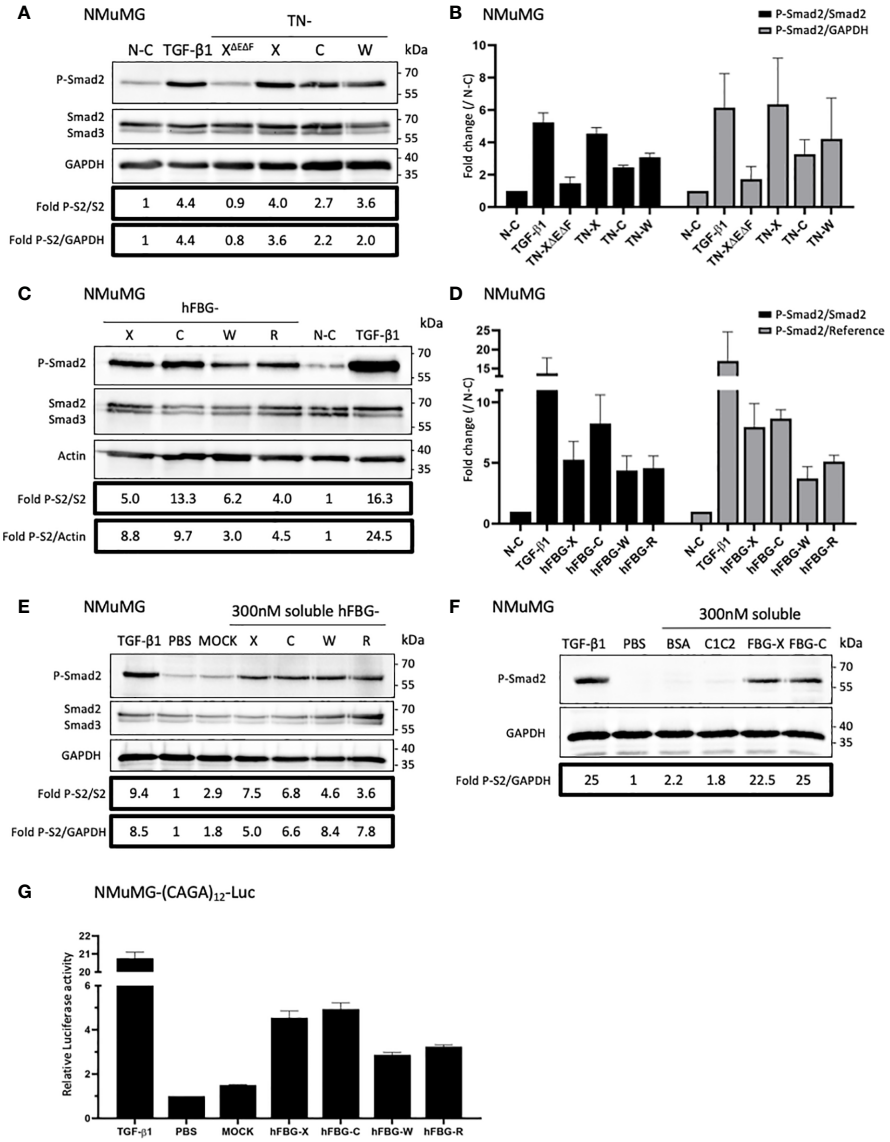

FIGURE 4 | Full-length Tenascins and their respective FBG-like domains stimulate TGF-β/Smad intracellular signaling pathway in epithelial cells. **(A)** Western Blot analysis showing phosphorylated Smad2 (P-Smad2), total Smad2/3 and GAPDH levels in NMuMG cells cultured for 3h onto control non-coated (N-C) dishes or dishes coated with equimolar quantity (22,2 pmol/cm^2) of full-length Tenascins (TN) or central TN-X fragment (TN-X$^{\Delta E \Delta F}$), or stimulated with soluble active TGF-β1 (2 ng/mL). **(B)** Fold changes of P-Smad2 to total Smad2 levels or to GAPDH levels. Graph shows means ± SD of n = 3 independent experiments. **(C)** Western Blot analysis showing P-Smad2, total Smad2/3 and Actin levels in NMuMG cultured for 3h onto equimolar quantity of FBG-like domains (333 pmol/cm^2) or stimulated with soluble active TGF-β1 (2 ng/mL). **(D)** Fold changes of P-Smad2 to total Smad2 levels or to reference protein levels. Graph shows means ± SD of n = 3 independent experiments. **(E)** Western-blot analysis showing P-Smad2, Smad2/3 and GAPDH levels in NMuMG cells stimulated for 1h in the presence of active TGF-β1 (2 ng/mL), stimulated or not (PBS) with soluble FBG-like domains (300 nM) or MOCK-CM. "MOCK-CM" referred to the conditioned media of MOCK-transfected HEK293 EBNA cells, submitted to Nickel-affinity chromatography and eluted from the column as for the FBG-like domains. **(F)** Immunoblotting analysis showing P-Smad2 and GAPDH levels in NMuMG cells stimulated for 1h in the presence of active TGF-β1 (2 ng/mL), stimulated or not (PBS) with soluble CUB1CUB2 protein fragment (C1C2), bovine serum Albumin (BSA) or FBG-like domains (300 nM each). **(G)** Relative Luciferase activity of NMuMG cells transiently transfected with the Smad-responsive (CAGA)$_{12}$-Luc reporter construct and treated for 16h with soluble FBG-like domains (600 nM), MOCK-CM or TGF-β1 (2 ng/mL). Graph shows one representative result from 3 independent experiments.

The FBG-like domains produced in mammalian cells are associated with latent TGF-β1 (**Figure 2E**). To get rid of this source of endogenous TGF-β and to determine whether FBG-like domains are able to activate exogenous latent TGF-β (*i.e.* secreted by the cells or from the serum), we produced these recombinant domains in a prokaryotic system. As shown by SDS-PAGE coupled with Coomassie blue staining (**Figure 5C**), the FBG-like domains produced in bacteria (noted FBG*)

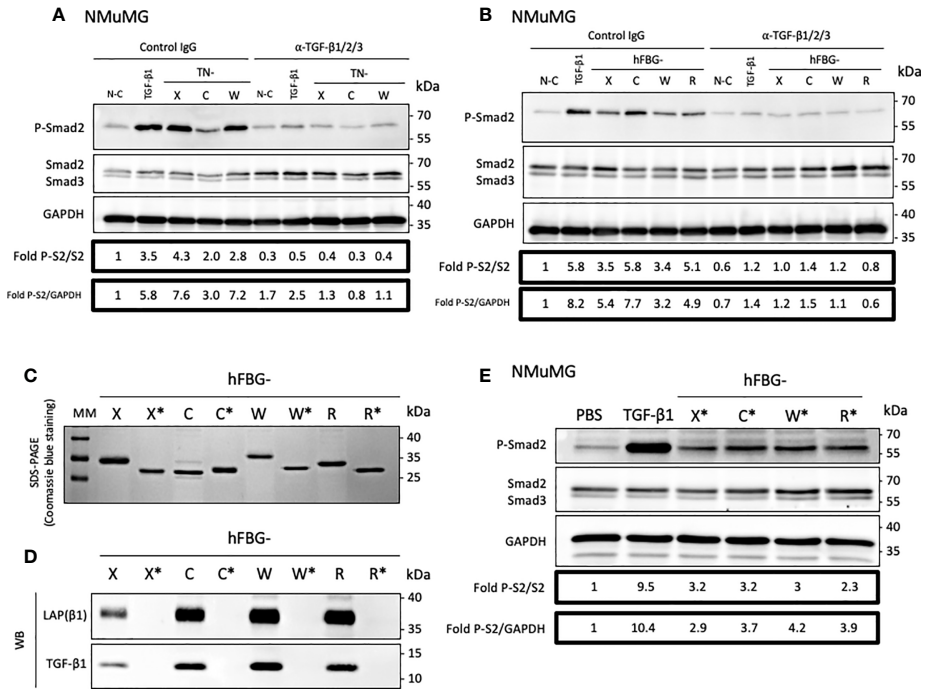

FIGURE 5 | The FBG-like domain of the Tenascin family members activates the latent TGF-β in epithelial cells. **(A)** Western-blot analysis showing P-Smad2, total Smad2/3 and GAPDH levels in NMuMG cultured for 3h onto Non-Coated (N-C) dishes, dishes coated with 22,2 pmol/cm^2 full-length Tenascins (TN) or stimulated with 2 ng/mL TGF-β1, in presence of anti-pan-TGF-β antibody or isotype-matched control IgG (10 µg/mL). **(B)** Western Blot analysis showing P-Smad2, total Smad2/3 and GAPDH levels in NMuMG cells cultured for 3h in presence of 333 pmol/cm^2 of FBG-like domains as described in **(A)**. **(C)** SDS-PAGE analysis of purified recombinant FBG-like domains produced in mammalian cells (FBG) and *E. coli* (FBG*) resolved on 15% acrylamide gels under reducing conditions (2 µg each). MM, molecular mass markers. **(D)** Western-Blot analysis of the levels of mature TGF-β1 and LAP(β1) pro-domain associated with 20 pmol of FBG-like domains produced in mammalian cells (FBG) and *E coli* (FBG*). **(E)** Western-blot analysis showing P-Smad2, Smad2/3 and GAPDH levels in NMuMG cells stimulated for 1h with active TGF-β1 (2 ng/mL), soluble purified FBG-like domains produced in *E Coli* (720 nM) or vehicle (PBS).

displayed lower molecular masses than those produced in mammalian cells, most likely due to the absence of post-translational modifications in the proteins produced in prokaryotic systems. Although purified recombinant FBG-X*, FBG-C*, FBG-W* and FBG-R* did not contain any TGF-β1 and LAP(β1) (**Figure 5D**), they retained their ability to induce Smad2 phosphorylation when presented to NMuMG cells in a soluble form (**Figure 5E**). To ensure that Smad2 phosphorylation was solely attributed to FBG-like domains, but not to bacterial contaminants such as lipopolysaccharides (LPS) and LPS-associated molecules, we confirmed that increasing doses of LPS (1-100 ng/mL) did not induce Smad2 phosphorylation in NMuMG cells (**Figure S5**). These experiments definitively showed that the FBG-like domains produced in bacteria and devoid of TGF-β kept their ability to activate the pool of latent TGF-β that is either secreted by cells or available from the serum, resulting in the induction of a TGF-β/Smad intracellular pathway.

FBG-Like Domain of Tenascins Trigger EMT and Cytostasis in Epithelial Cells

Cytostasis and epithelial-to-mesenchymal transition (EMT) are two cellular programs promoted by bioactive TGF-β (46–48). Firstly, to determine whether the activation of latent TGF-β mediated by the four FBG-like domains was sufficient to regulate epithelial cell plasticity, we compared actin and E-Cadherin localizations in NMuMG cells cultured onto N-C dishes (control) or dishes coated with the FBG-like domains. In control condition, NMuMG cells displayed a cuboidal shape, with cortical actin cytoskeleton distribution and E-Cadherin localization at the cell-cell junctions, two typical features of an epithelial cell morphology (**Figure 6A**). As expected, NMuMG cells stimulated with soluble mature TGF-β1 or cultured onto immobilized FBG-X underwent EMT, characterized by a cellular scattering, a reorganization of actin cytoskeleton into stress fibers and a loss of E-Cadherin signal. Interestingly, epithelial cells cultured onto dishes coated with recombinant FBG-C, FBG-W or FBG-R also displayed EMT features, but at different degrees. Even if a pool of actin remained cortically located, a fraction of F-actin reorganized to form stress fibers, whereas E-Cadherin disappeared from the cell-cell junctions. This phenotypical switch was partially observed in NMuMG cultured onto coated FBG-R, in which some cellular islets still exhibited epithelial features, while others underwent partial EMT (**Figure 6A**). Concomitantly, quantitative gene expression analyses revealed a decrease of epithelial cell marker (*E-cadherin*) and a gain of

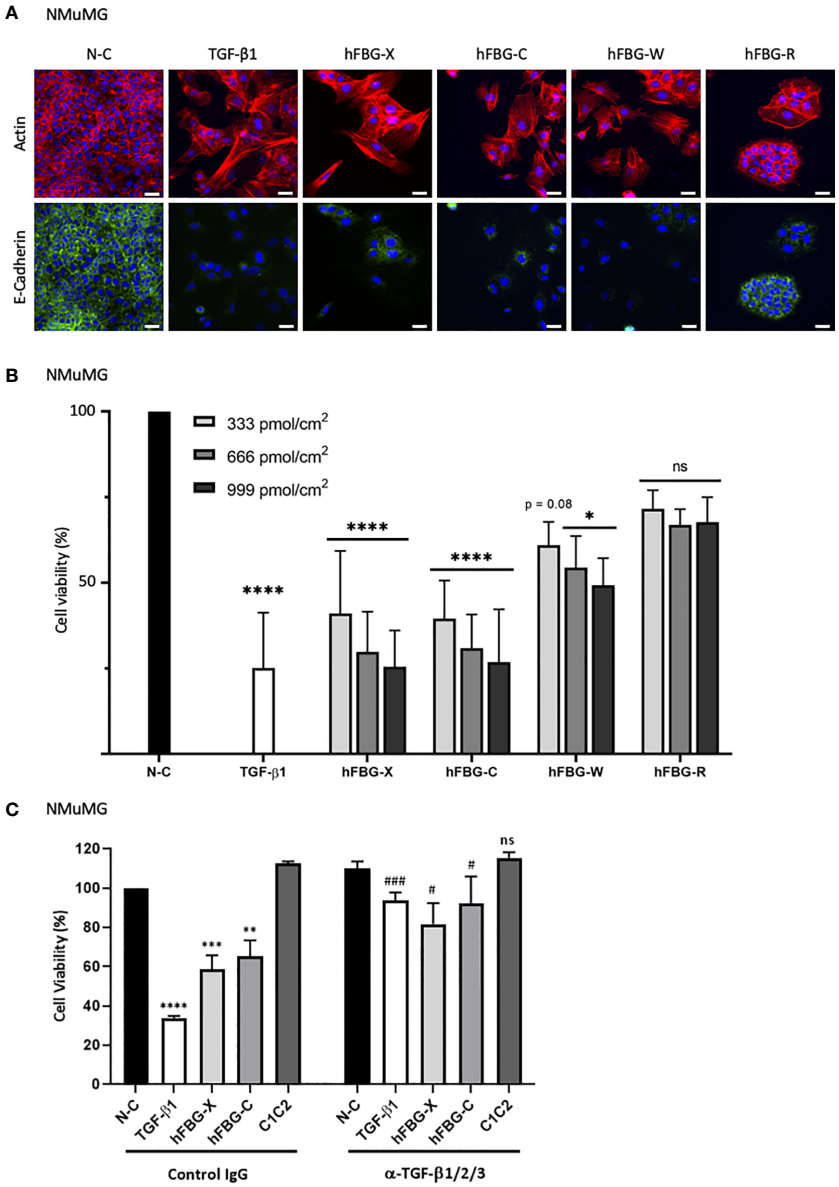

FIGURE 6 | The FBG-like domains of Tenascins trigger EMT and cytostasis in epithelial cells. **(A)** F-actin direct fluorescence (red) and E-Cadherin indirect immunofluorescence (green) performed on NMuMG cells cultured for 72h onto N-C dishes, dishes coated with 666 pmol/cm^2 FBG-like domains or stimulated with soluble TGF-β1 (5 ng/mL). Cell nuclei were counterstained with DAPI (blue). Bars, 15 µm. **(B)** Percentage of cell viability in NMuMG cells cultured for 48h onto N-C dishes, dishes coated with 333, 666 or 999 pmol/cm^2 FBG-like domains, or stimulated with 5 ng/mL TGF-β1. Error bars are means ± SD from 3 independent experiments. *$p < 0.05$ compared to N-C condition. ****$p < 0.0001$ compared to N-C condition. ns, not significant. **(C)** Percentage of cell viability in NMuMG cells cultured for 48h onto N-C dishes, dishes coated with 666 pmol/cm^2 FBG-like domains (FBG-X and FBG-C) or CUB1CUB2 protein fragment (C1C2), or stimulated with 5 ng/mL TGF-β1, in the presence of anti-pan-TGF-β antibody or isotype-matched control IgG (5 µg/mL). Error bars are means ± SD from 3 independent experiments. **, *** and **** respectively correspond to $p < 0.01$, $p < 0.001$ and $p < 0.0001$ compared to N-C condition. # and ### respectively correspond to $p < 0.05$ and $p < 0.001$ *versus* their control IgG-treated counterpart. ns, not significant.

mesenchymal cell markers (*Vimentin* and *Fibronectin-1*), as well as of EMT inducers (*Hmga2*, *Snail1*, and *Zeb1*), when cells were cultured onto immobilized FBG-like domains. Once again, transcriptional responses varied among the FBG domain, the strongest being observed with the FBG-X and the lowest with FBG-R (**Figure S6A**). The EMT transcriptional program induced by the FBG-like domain is abolished in the presence of a neutralizing antibody, thus confirming that this cell response is dependent on TGF-β activation (**Figure S6B**).

A concomitant observation with EMT was the marked decrease in cell number, as judged by nuclei staining (**Figure 6A**), when NMuMG cells were cultured onto immobilized

recombinant FBG-like domains or stimulated with active TGF-β1. We then assessed whether the activation of latent TGF-β mediated by the four FBG-like domains was able to induce a cytostatic program in epithelial cells. As a readout of cell number, we performed a MTT assay in NMuMG cells stimulated with recombinant active TGF-β1 or cultured onto dishes coated with increasing quantities of FBG-like domains (*i.e.* 333, 666 and 999 pmol/cm^2) (**Figure 6B**). While FBG-X and FBG-C induced a strong reduction of living cell number comparable to TGF-β1 for the highest quantity (999 pmol/cm^2), FBG-W and FBG-R led to a lower but still significant reduction of cell number. The decrease in numbers of living cells was proportional to the quantity of proteins used in this experiment (**Figure 6B**). The reduction of cell number in the presence of the FBG-like domains was not the consequence of a cytotoxic effect due to the cell exposure to an exogenous protein domain, as the irrelevant CUB1CUB2 protein fragment did not modify cell viability (**Figure 6C**). Finally, the decrease in living cell number could be attributed to the cytostatic effect of bioactive TGF-β, as the neutralizing anti-mature TGF-β1/2/3 antibody significantly reverted the effects mediated by the FBG-like domains (**Figure 6C**).

Altogether, these results indicated that the canonical Smad intracellular pathway induced by the FBG-like domains of the four Tenascins resulted in the activation of TGF-β cell programs in mammary epithelial cells, such as EMT and growth arrest.

DISCUSSION

Because of its central role in tissue homeostasis and integrity, extracellular activation of latent TGF-β is a crucial mechanism that needs to be tightly regulated (49, 50). By interacting with several ECM components, the small (SLC) and the large (LLC) latent complexes are trapped within the matrix compartment, creating a pool of latent cytokine that can be activated upon requirement. Even if a growing number of ECM proteins are referenced as TGF-β partners (29), only a few have the ability to promote its activation. To our knowledge, Thrombospondin-1 (TSP-1), Connective Tissue Growth Factor (CTGF, also known as CCN2) and TN-X have been so far the only three ECM macromolecules described as latent TGF-β activators, both *in vitro* (28, 51, 52) and *in vivo* (52, 53).

In this study, we confirmed the TN-X ability to activate latent TGF-β and identified human TN-C, TN-W and possibly TN-R, as new activators of the latent cytokine *in vitro*, thanks to their highly conserved C-terminal FBG-like domain. Indeed, we found that the FBG-like domains of TN-C, TN-W and TN-R are associated with TGF-β1 SLC *in vitro* and that this molecular association promotes the presentation of the mature cytokine to cells. This conclusion first relies on the fact that FBG-like domains of the four Tenascins co-purified with both entities of the SLC, *i.e.* TGF-β1 and its LAP pro-domain (**Figure 2**). Second, the globular domains of TN-C, TN-W and TN-R physically interact with TGF-β1 *in vitro* (**Figure 3**). Third, the FBG-like domains are able to unravel the mature TGF-β1, as they induce a Smad intracellular signaling pathway activation when presented to cells (either in an immobilized or a soluble form, **Figure 4**). This activation leads to the induction of TGF-β-responsive programs, such as EMT and cytostasis in epithelial cells, two processes that are abolished by the presence of a neutralizing anti-mature TGF-β1/2/3 antibody (**Figure 6** and **S6**). Finally, FBG-like domains produced in bacteria and free from endogenous TGF-β are able to activate the latent cytokine from an exogenous source, either present in the serum or secreted by cells (**Figure 5**).

Although the concomitant binding of the LAP pro-domain to the TGF-β–FGB protein complex remains to be confirmed experimentally for TN-C, TN-W and TN-R, molecular modeling and dynamic analyses predicted the interaction of the small latent (LAP–TGF-β) complex with the FBG-like domain of the four Tenascins (**Figures 3E, F** and **S3**). More specifically, alanine scanning analyses predict that the dimeric latent TGF-β 'sits' on the C-terminal portion of the FBG globes, through interactions with both the LAP pro-domain and the mature TGF-β moiety (**Figures 3E, F** and **S3**), thus giving insight into the biochemical association observed between these two entities and the FBG-like domains. The dimeric LAP(β1) pro-domain is predicted to bind to the FBG-like domain, through several amino acids from the first α-helix that are located immediately upstream of the latency lasso, which maintains mature TGF-β1 in a latent form through non-covalent interactions (31). In addition, the dimeric mature TGF-β1 is suggested to bind to the FBG-like globes through three stretches of sequences located upstream or surrounding the interchain disulfide bond (Cys^{355}). In turn, five to six key amino-acid residues mostly located to the loop9 of the FBG-like domains are predicted to bind with pro-TGF-β1 mostly through hydrogen bonds and steric modifications of the interface. The involvement of these candidate amino acids in the interaction needs further validation not only *in vitro* using mutated recombinant FBG-like domains, but also *in vivo* with the analysis of inherited variants occurring in the globular domains. Indeed, Morissette and collaborators identified a novel *TNXB* c.12174C>G mutation that reduces the binding affinity of latent TGF-β to the native TN-X (54). This mutation, resulting in the p.C4058W amino-acid substitution within the FBG-like knob of TN-X, is not located in the loop9, but resides in its N-terminal portion. This cysteine residue, which is involved in the formation of a first disulfide bond within the FBG-like domain, is conserved not only in TN-X proteins from different species, but also in other members of the human Tenascin family (cysteine in position 11, **Figure 1A**). The first disulfide bridge is predicted to maintain the correct orientation of the FBG-like domain downstream of the FNIII modules. The absence of this disulfide bond in TN-X^{C4058W} might result in an inappropriate folding of the FBG-like domain over the FNIII modules, thus preventing an optimal presentation of this domain towards its molecular partner. Further molecular dynamic analyses are needed to confirm this hypothesis.

SPR analyses confirmed the direct interaction between mature TGF-β1 and the four FBG-like domains (**Figures 3A–D**). For both FBG-X and FBG-W, kinetics sensorgrams were best fitted with the heterogenous ligand model, indicating that TGF-β1 interaction may result from two conformations of the globular domain on the sensor

chip or may occur with at least two binding sites on the FBG-like domains. Notably, the two binding sites display similar dissociation constants for one FBG but result from kinetic constants that differ by one log. This model is also compatible with a putative conformational change triggered by the FBG-like domain on the latent cytokine, as explained hereafter. The kinetics data indicate that TGF-β1 binds to FBG-X with a higher affinity than to FBG-W. This experimental observation correlates with the calculated binding energies for the four domains. Indeed, *in silico* analyses predict that FBG-X displays the highest affinity for pro-TGF-β1, then followed by FBG-W and FBG-C, with FBG-R having the lowest value. These relative affinities, obtained in biochemically defined environment (SPR) or from *in silico* analyses (molecular modelling), are rather consistent with the intensity of the cellular responses obtained *in vitro* for each FBG-like domain. Indeed, FBG-X mostly exhibited the strongest TGF-β-dependent response, compared to FBG-W and FBG-C, while FBG-R was the recombinant domain displaying the weaker effect. In line with this, the binding parameters of FBG-C and FBG-R could not be determined because of the weak signals obtained with the lowest TGF-β1 concentrations, indicating a weaker affinity of these two FBG-like domains for the mature cytokine. Moreover, kinetics analyses were also limited in the high concentration range by the fact that mature TGF-β1 tended to form aggregates at higher concentrations.

These observations raise further questions regarding the exact role(s) of full-length Tenascins in the regulation of TGF-β bioavailability in a complex tissue environment. Are full-length molecules only involved in the storage of the latent cytokine within the ECM or do they also participate in the activation of latent TGF-β *in vivo*? In our *in vitro* assays we noticed that FBG-like domains appeared to be less effective at inducing Smad2 phosphorylation than full-length Tenascin proteins (**Figure 4**). Although it is conceivable that a hexameric molecule (TN-C or TN-W) might offer a 2-fold higher probability to bind to and to activate latent TGF-β compared to a trimeric protein (TN-X or TN-R) *in vivo*, it is unlikely the case in our *in vitro* assays. Indeed, cells were seeded onto equimolar quantity of molecules (with regard to the molecular mass of each monomeric chain), *i.e.* onto similar number of FBG-like domains, whatever the length (intact or solely the C-terminal portion of Tenascin) or the assembly (oligomeric or monomeric) of the immobilized protein. However, the oligomeric nature of the proteins might help in the activation process, by offering multiple and cooperative binding sites to latent TGF-β. Although less compatible with the molecular modeling analyses, it is possible that two FBG-like domains from independent chains within an oligomer might cooperate in binding to and activating latent TGF-β (or presenting activated TGF-β to cell-surface receptors). While analyzing the interaction between FBG-like domains and mature TGF-β1 using SPR, the bivalent analyte model also gave good fits of the experimental curves (**Table S1**). These observations suggest that a single dimeric mature TGF-β molecule might bind to two FBG-like domains simultaneously. Alternatively, it is also possible to propose a cooperation between the FBG-SLC complex with another TGF-β-binding site within the full-length molecule in the process of latent TGF-β activation. For instance, the fifth FNIII domain of TNC has also been shown to interact with TGF-β1 (55). One can speculate that in an hexameric TN-C protein, one FBG-like domain from one chain may cooperate with a fifth FNIII domain (from the same or an independent chain) in the activation of the latent cytokine. However, this hypothesis in unlikely true for TN-X as the central region of this glycoprotein (the TN-X$^{\Delta E \Delta F}$ fragment only composed of FNIII domains) does not interact neither with the LAP(β1) pro-domain nor with the mature TGF-β1 (this study and (28)). Finally, we cannot exclude in our experiments that the small globular FBG-like proteins may be less efficiently adsorbed to plastic culture dishes than to the full-length Tenascin molecules in regards with their intrinsic physicochemical properties and/or structural parameters.

Extracellular activation of latent TGF-β has been shown to require numerous actors, such as various proteases and/or cell-surface receptors (such as RGD-dependent integrins), whose involvements are context- and tissue-dependent (30). Among the ECM molecules, TSP-1 was the first glycoprotein shown to activate latent TGF-β (51). TSP-1 is a trimeric protein which interacts non-covalently with latent TGF-β. The activation process involves the disruption of these non-covalent binding between the mature TGF-β cytokine and its LAP pro-domain through competing interactions between discrete sequences in TSP-1 and both components of the latent TGF-β complex (56). Firstly, the KRFK sequence located at the beginning of the second Thrombospondin type 1 repeat (TSR) can efficiently replace the RKPK sequence in mature TGF-β to interact with the LSKL sequence in LAP (bold sequences in **Figure S4**). This LSKL sequence is located in the first α-helix, just upstream the latency lasso (**Figure S4A**). Secondly, a repeated WXXW motif (where X is any amino acid residue) within TSP-1 has been shown to interact with the VLAL sequence in mature TGF-β (**Figure S4B**). It is assumed that these combined interactions subsequently induce a conformational change in the SLC and lead to the exposure of TGF-β, which otherwise remains buried within the straightjacket. Like TSP-1, TN-X is a trimeric glycoprotein, whose FBG-like domain interacts non-covalently with the SLC. After having excluded the involvement of proteases and RGD-dependent integrins, we deduced that latent TGF-β activation by TN-X most-likely occurred through a conformational change within the SLC (28). Even if a deeper analysis of the involved molecular mechanism is required, it is tempting to speculate that FBG-like domain of TN-C, TN-W and TN-R might also induce a conformational switch in this complex, thus leading to the exposure of mature TGF-β and its presentation to cell-surface receptors. Interestingly, like TSP-1, the FBG-like domain of the four Tenascins contains a conserved WXXW motif located in the loop 9, whose amino acids have been predicted to interact with the mature TGF-β1 (*, **Figure S3B**). As, from *in silico* analyses, the VLAL sequence in the bioactive TGF-β1 is unlikely to bind to the FBG-like domains (**Figure S4B**), the involvement of this tryptophan-rich motif will have to be confirmed experimentally following site-directed mutagenesis in the FBG globes. We also previously identified

that α11β1 integrin was required for TN-X-mediated latent TGF-β activation (28). The exact role played by α11β1 integrin in latent TGF-β activation is still not clear. This cell-surface receptor might serve as a docking site for the FBG–LAP–TGF-β complex at the membrane, or might have an active role in the activation process by assisting the FBG-X domain to trigger the conformational change of the latent complex. Consequently, we cannot exclude the involvement of cell-surface receptor(s) for the activation of latent TGF-β1 by FBG-C, FBG-W and FBG-R. This question needs to be answered using RNA interference or neutralizing antibody approach, starting with αvβ3 integrin, a cell-surface receptor for the TN-C FBG-like domain (57). Nevertheless, this screening is challenged by the absence of identified cell-surface receptor for the FBG-like domain of TN-W and TN-R. Herein, by showing that latent TGF-β activation is a hallmark of the Tenascin family, we provide new evidences that these ECM glycoproteins are able to regulate cytokine activity and cellular signaling. Whether FBG-R retains the ability to regulate latent TGF-β1 activation within the full-length protein is an open question that will have to be answered in the future.

Tenascins are complex glycoproteins that appeared early in the chordate lineage and evolved into four conserved members in Coelacanth and Tetrapod (58). This degree of conservation suggests a crucial function in all Vertebrates. Because of its location at the very C-terminal end of Tenascin, the FBG-like globe is supposed to be more prone to be lost during evolution. However, this domain has been conserved, indicating the presence of a selective pressure to maintain it (59). This hypothesis becomes more and more attractive since the FBG knob function has been better characterized, although still underestimated. FBG-like domain function probably involves interactions with cell-surface receptors, other ECM components or signaling molecules. For instance, the FBG-like domain of TN-C, TN-W and TN-R, but not of TN-X, have been shown to interact with Toll-like receptor 4 (TLR4) to drive inflammatory cytokine synthesis *in vitro* and *in vivo* (60). Three distinct sites within the FBG-C domain contribute to TLR4 activation: (*i*) a cationic ridge made up of residues from loops 5–7, close to which sits (*ii*) a triad of hydrophobic/polar residues from loop 7 and (*iii*) a C-terminal cationic tail in loop 10. Whereas the cationic tail and the hydrophobic/polar residues seem non-essential; the cationic ridge is the dominant inflammatory epitope. To determine whether the binding of the LAP–TGF-β complex to the FBG-C domain might interfere with its ability to interact with TLR4, we highlighted key residues involved in TLR4 interaction in our molecular model (**Figure S7**). Latent TGF-β is predicted to lie on FBG-C in an opposite region from the three TLR4-binding sites. Although this has to be confirmed functionally, this observation suggests that the interaction of FBG-C with the latent TGF-β might not interfere with its ability to activate TLR4.

TGF-β has a dual role during carcinogenesis. Indeed, in normal or pre-malignant epithelial cells, it exerts tumor-suppressive activities by triggering apoptosis and cytostasis, thereby preventing malignant transformation (47, 48). In contrast, at later stages of tumor progression, TGF-β acts more as an oncogene by inducing EMT and immune evasion, thus promoting cancer cell invasion, dissemination and metastatic colonization. Interestingly, TN-X and TN-C/TN-W have opposite expression patterns in healthy and tumor tissues. Whereas TN-X is constitutively present in most adult connective tissues, we recently demonstrated a marked reduction of TN-X in the six most prevalent and lethal cancers worldwide (27). On the opposite, TN-C and TN-W are barely detectable in adult healthy tissues, but are often *de novo* expressed in cancers (23, 61), in which their ability to promote proliferation, migration and invasiveness have been extensively studied in the past decade (18, 22). More importantly, TN-C has been recently shown to promote EMT through activation of TGF-β canonical signaling pathway in breast cancer cells established using a mouse mammary tumor virus (MMTV) model (62). Up to date, molecular mechanisms underlying these processes are still not elucidated. Here, we show that the FBG-like domains of the four Tenascins induce cytostatic and EMT response in normal murine mammary gland epithelial cells *in vitro*. Based on opposite Tenascin expression patterns, it is tempting to speculate that TN-X might exert a TGF-β-dependent growth arrest in normal tissues or early malignant cells, whereas TN-C and TN-W induce latent TGF-β activation to trigger EMT at later stages of malignant transformation. Thus, this shared mechanism, at two different stages of cancer development, may have opposite impact on tumor progression. Strikingly, TN-C and TN-W have also been described as TGF-β responsive genes, that could lead to a positive retro-control loop (63, 64). Consequently, TN-C and TN-W, by their ability to activate latent TGF-β, can promote their own expression, resulting in a sustained TGF-β activation over time. In well-established tumors, this constant source of activated TGF-β may promotes tumor progression, increasing cancer invasiveness, aggressiveness and lethality. Indeed, even if Sun *et al.* also observed an increased TGF-β1 secretion in TN-C-stimulated murine breast cancer cells (62), this attractive hypothesis will require further investigation using established *in vivo* models.

Finally, TGF-β exerts a central role in tumor immune evasion (30). Indeed, this cytokine is produced by cancer cells but also by other cell types in the tumor microenvironment, including activated fibroblasts, macrophages, platelets and regulatory T cells (Tregs). High level of active TGF-β blocks naive T cell differentiation toward a Th1 effector phenotype, promotes their conversion toward the Treg subset and abolishes antigen-presenting functions of dendritic cells. Interestingly, the involvement of TN-C in the regulation of anti-tumor immunity has recently gained more attention. Tumor-initiating cells arising from prostate intraepithelial neoplasia or glioblastoma have been shown to secrete TN-C to protect themselves from immune surveillance, through an α5β1 or αvβ6 integrin-dependent inhibition of T cell activation and proliferation (65, 66). More recently, TN-C has also been shown to favor an immune-suppressive tumor microenvironment in oral squamous cell carcinoma, through the induction of a CCR7 signaling in dendritic cells, thus promoting the recruitment of T regulatory cells and the expression of anti-inflammatory cytokines (67). Knowing the role of TGF-β in tumor immune evasion, it would

be relevant to investigate whether the immune-suppressive functions of TN-C (and maybe TN-W) might also depend on its ability to regulate TGF-β activity within these tumor microenvironments.

Considering the pleiotropic role of TGF-β in numerous physiological and pathological contexts, our data showing that latent TGF-β activation is a hallmark of the TN family shed light on a novel function for this ECM proteins in the regulation of tissue homeostasis and during pathological dysregulations.

DATA AVAILABILITY STATEMENT

The raw data supporting the conclusions of this article will be made available by the authors, without undue reservation.

AUTHOR CONTRIBUTIONS

AA: Conceptualization, Methodology, Investigation, Formal analysis; Writing – Original draft. PM-G: Validation, Writing – Review and Editing. LB: Software, Formal Analysis. SA: Software, Formal Analysis. RT: Software, Formal analysis, Writing – Review and Editing. SL: Writing – Review and Editing. LP: Writing – Review and Editing. LA: Writing – Review and Editing. BV: Funding acquisition. CM: Investigation, Formal analysis; Writing – Review & Editing. EL: Writing – Review and Editing. UV: Conceptualization, Writing – Original draft, Supervision, Funding Acquisition. All authors contributed to the article and approved the submitted version.

FUNDING

This work was supported by the Centre National de la Recherche Scientifique (CNRS), the Ligue Nationale Contre le Cancer, Comité du Rhône (to UV), Comité de l'Allier (to UV) and Comité de la Saône-et-Loire (to BV), the Fondation ARC pour la Recherche sur le Cancer" (PJA 20141201790) (to UV), the French Association of Ehlers-Danlos Syndromes (AFSED) (to UV), and fellowships from the Ministère de l'Enseignement Supérieur, de la Recherche et de l'Innovation (MESRI) of France (LP) and from the Ecole Normale Supérieure de Lyon (AA and SL). The authors declare no competing financial interests.

ACKNOWLEDGMENTS

We thank R. Chiquet-Ehrismann and G. Orend for valuable reagents. We acknowledge the contribution of SFR Biosciences (UMS3444/CNRS, US8/Inserm, ENS de Lyon, UCBL) facilities and particularly V. Gueguen-Chaignon from the Protein Science Facility (SPF) for valuable advice regarding protein purification, and past members of our research group for their help in this work.

SUPPLEMENTARY MATERIAL

The Supplementary Material for this article can be found online at: https://www.frontiersin.org/articles/10.3389/fimmu.2021.613438/full#supplementary-material

REFERENCES

1. Chiquet-Ehrismann R, Tucker RP. Tenascins and the Importance of Adhesion Modulation. *Cold Spring Harb Perspect Biol* (2011) 3(5):a004960. doi: 10.1101/cshperspect.a004960
2. Nörenberg U, Wille H, Wolff JM, Frank R, Rathjen FG. The Chicken Neural Extracellular Matrix Molecule Restrictin: Similarity With EGF-, Fibronectin Type III-, and Fibrinogen-Like Motifs. *Neuron* (1992) 8:849–63. doi: 10.1016/0896-6273(92)90199-N
3. Lethias C, Carisey A, Comte J, Cluzel C. Exposito J-Y. A Model of Tenascin-X Integration Within the Collagenous Network. *FEBS Lett* (2006) 580:6281–5. doi: 10.1016/j.febslet.2006.10.037
4. Erickson HP, Taylor HC. Hexabrachion Proteins in Embryonic Chicken Tissues and Human Tumors. *J Cell Biol* (1987) 105:1387–94. doi: 10.1083/jcb.105.3.1387
5. Scherberich A, Tucker RP, Samandari E, Brown-Luedi M, Martin D, Chiquet-Ehrismann R. Murine tenascin-W: A Novel Mammalian Tenascin Expressed in Kidney and At Sites of Bone and Smooth Muscle Development. *J Cell Sci* (2004) 117:571–81. doi: 10.1242/jcs.00867
6. Liao H, Huang W, Schachner M, Guan Y, Guo J, Yan J, et al. Beta 1 Integrin-Mediated Effects of Tenascin-R Domains EGFL and FN6-8 on Neural Stem/Progenitor Cell Proliferation and Differentiation In Vitro. *J Biol Chem* (2008) 283:27927–36. doi: 10.1074/jbc.M804764200
7. Jung M, Pesheva P, Schachner M, Trotter J. Astrocytes and Neurons Regulate the Expression of the Neural Recognition Molecule Janusin by Cultured Oligodendrocytes. *Glia* (1993) 9:163–75. doi: 10.1002/glia.440090302
8. Hawi Z, Yates H, Pinar A, Arnatkeviciute A, Johnson B, Tong J, et al. A Case-Control Genome-Wide Association Study of ADHD Discovers a Novel Association With the Tenascin R (TNR) Gene. *Transl Psychiatry* (2018) 8:284. doi: 10.1038/s41398-018-0329-x
9. Wagner M, Lévy J, Jung-Klawitter S, Bakhtiari S, Monteiro F, Maroofian R, et al. Loss of TNR Causes a Nonprogressive Neurodevelopmental Disorder With Spasticity and Transient Opisthotonus. *Genet Med* (2020) 22:1061–8. doi: 10.1038/s41436-020-0768-7
10. Elefteriou F, Exposito JY, Garrone R, Lethias C. Binding of Tenascin-X to Decorin. *FEBS Lett* (2001) 495:44–7. doi: 10.1016/s0014-5793(01)02361-4
11. Bristow J, Carey W, Egging D, Schalkwijk J. Tenascin-X, Collagen, Elastin, and the Ehlers-Danlos Syndrome. *Am J Med Genet C Semin Med Genet* (2005) 139C:24–30. doi: 10.1002/ajmg.c.30071
12. Valcourt U, Alcaraz LB, Exposito J-Y, Lethias C, Bartholin L. Tenascin-X: Beyond the Architectural Function. *Cell Adh Migr* (2015) 9:154–65. doi: 10.4161/19336918.2014.994893
13. Burch GH, Gong Y, Liu W, Dettman RW, Curry CJ, Smith L, et al. Tenascin-X Deficiency is Associated With Ehlers-Danlos Syndrome. *Nat Genet* (1997) 17:104–8. doi: 10.1038/ng0997-104
14. Malfait F, Francomano C, Byers P, Belmont J, Berglund B, Black J, et al. The 2017 International Classification of the Ehlers-Danlos Syndromes. *Am J Med Genet C Semin Med Genet* (2017) 175:8–26. doi: 10.1002/ajmg.c.31552
15. Chiquet-Ehrismann R, Orend G, Chiquet M, Tucker RP, Midwood KS. Tenascins in Stem Cell Niches. *Matrix Biol* (2014) 37:112–23. doi: 10.1016/j.matbio.2014.01.007
16. Jones FS, Jones PL. The Tenascin Family of ECM Glycoproteins: Structure, Function, and Regulation During Embryonic Development and Tissue Remodeling. *Dev Dyn* (2000) 218:235–59. doi: 10.1002/(SICI)1097-0177(200006)218:2<235::AID-DVDY2>3.0.CO;2-G
17. Midwood KS, Chiquet M, Tucker RP, Orend G. Tenascin-C At a Glance. *J Cell Sci* (2016) 129:4321–7. doi: 10.1242/jcs.190546

18. Tucker RP, Degen M. The Expression and Possible Functions of Tenascin-W During Development and Disease. *Front Cell Dev Biol* (2019) 7:53. doi: 10.3389/fcell.2019.00053
19. Qian S, Tan X, Liu X, Liu P, Wu Y. Exosomal Tenascin-c Induces Proliferation and Invasion of Pancreatic Cancer Cells by WNT Signaling. *Onco Targets Ther* (2019) 12:3197–205. doi: 10.2147/OTT.S192218
20. Scherberich A, Tucker RP, Degen M, Brown-Luedi M, Andres A-C, Chiquet-Ehrismann R. Tenascin-W is Found in Malignant Mammary Tumors, Promotes Alpha8 Integrin-Dependent Motility and Requires p38MAPK Activity for BMP-2 and TNF-alpha Induced Expression In Vitro. *Oncogene* (2005) 24:1525–32. doi: 10.1038/sj.onc.1208342
21. Oskarsson T, Acharyya S, Zhang XH-F, Vanharanta S, Tavazoie SF, Morris PG, et al. Breast Cancer Cells Produce Tenascin C as a Metastatic Niche Component to Colonize the Lungs. *Nat Med* (2011) 17:867–74. doi: 10.1038/nm.2379
22. Orend G, Chiquet-Ehrismann R. Tenascin-C Induced Signaling in Cancer. *Cancer Lett* (2006) 244:143–63. doi: 10.1016/j.canlet.2006.02.017
23. Brellier F, Martina E, Degen M, Heuzé-Vourc'h N, Petit A, Kryza T, et al. Tenascin-W is a Better Cancer Biomarker Than Tenascin-C for Most Human Solid Tumors. *BMC Clin Pathol* (2012) 12:14. doi: 10.1186/1472-6890-12-14
24. Lowy CM, Oskarsson T. Tenascin C in Metastasis: A View From the Invasive Front. *Cell Adh Migr* (2015) 9:112–24. doi: 10.1080/19336918.2015.1008331
25. Bi B, Li F, Guo J, Li C, Jing R, Lv X, et al. Label-Free Quantitative Proteomics Unravels the Importance of RNA Processing in Glioma Malignancy. *Neuroscience* (2017) 351:84–95. doi: 10.1016/j.neuroscience.2017.03.023
26. Anlar B, Gunel-Ozcan A. Tenascin-R: Role in the Central Nervous System. *Int J Biochem Cell Biol* (2012) 44:1385–9. doi: 10.1016/j.biocel.2012.05.009
27. Liot S, Aubert A, Hervieu V, Kholti NE, Schalkwijk J, Verrier B, et al. Loss of Tenascin-X Expression During Tumor Progression: A New Pan-Cancer Marker. *Matrix Biol Plus* (2020) 6–7:100021. doi: 10.1016/j.mbplus.2020.100021
28. Alcaraz LB, Exposito J-Y, Chuvin N, Pommier RM, Cluzel C, Martel S, et al. Tenascin-X Promotes Epithelial-to-Mesenchymal Transition by Activating Latent TGF-β. *J Cell Biol* (2014) 205:409–28. doi: 10.1083/jcb.201308031
29. Robertson IB, Rifkin DB. Regulation of the Bioavailability of TGF-β and TGF-β-Related Proteins. *Cold Spring Harb Perspect Biol* (2016) 8(6):a021907. doi: 10.1101/cshperspect.a021907
30. Lodyga M, Hinz B. Tgf-β1 - A Truly Transforming Growth Factor in Fibrosis and Immunity. *Semin Cell Dev Biol* (2020) 101:123–39. doi: 10.1016/j.semcdb.2019.12.010
31. Shi M, Zhu J, Wang R, Chen X, Mi L, Walz T, et al. Latent TGF-β Structure and Activation. *Nature* (2011) 474:343–9. doi: 10.1038/nature10152
32. David CJ, Massagué J. Contextual Determinants of Tgfβ Action in Development, Immunity and Cancer. *Nat Rev Mol Cell Biol* (2018) 19:419–35. doi: 10.1038/s41580-018-0007-0
33. Massagué J. Tgfβ Signalling in Context. *Nat Rev Mol Cell Biol* (2012) 13:616–30. doi: 10.1038/nrm3434
34. Lethias C, Elefteriou F, Parsiegla G, Exposito JY, Garrone R. Identification and Characterization of a Conformational Heparin-Binding Site Involving Two Fibronectin Type III Modules of Bovine Tenascin-X. *J Biol Chem* (2001) 276:16432–8. doi: 10.1074/jbc.M010210200
35. Jeong J-Y, Yim H-S, Ryu J-Y, Lee HS, Lee J-H, Seen D-S, et al. One-Step Sequence- and Ligation-Independent Cloning as a Rapid and Versatile Cloning Method for Functional Genomics Studies. *Appl Environ Microbiol* (2012) 78:5440–3. doi: 10.1128/AEM.00844-12
36. Degen M, Brellier F, Kain R, Ruiz C, Terracciano L, Orend G, et al. Tenascin-W is a Novel Marker for Activated Tumor Stroma in Low-Grade Human Breast Cancer and Influences Cell Behavior. *Cancer Res* (2007) 67:9169–79. doi: 10.1158/0008-5472.CAN-07-0666
37. Giblin SP, Murdamoothoo D, Deligne C, Schwenzer A, Orend G, Midwood KS. How to Detect and Purify Tenascin-C. *Methods Cell Biol* (2018) 143:371–400. doi: 10.1016/bs.mcb.2017.08.022
38. Bourhis J-M, Vadon-Le Goff S, Afrache H, Mariano N, Kronenberg D, Thielens N, et al. Procollagen C-proteinase Enhancer Grasps the Stalk of the C-propeptide Trimer to Boost Collagen Precursor Maturation. *Proc Natl Acad Sci USA* (2013) 110:6394–9. doi: 10.1073/pnas.1300480110
39. Dennler S, Itoh S, Vivien D, ten Dijke P, Huet S, Gauthier JM. Direct Binding of Smad3 and Smad4 to Critical TGF Beta-Inducible Elements in the Promoter of Human Plasminogen Activator Inhibitor-Type 1 Gene. *EMBO J* (1998) 17:3091–100. doi: 10.1093/emboj/17.11.3091
40. Case DA, Ben-Shalom IY, Brozell SR, Cerutti DS, Cheatham TE, Cruzeiro VWD, et al. *Amber 2018*. San Francisco: University of California (2018).
41. Humphrey W, Dalke A, Schulten K. VMD: Visual Molecular Dynamics. *J Mol Graph* (1996) 14:33–38, 27–28. doi: 10.1016/0263-7855(96)00018-5
42. Anastasi C, Rousselle P, Talantikite M, Tessier A, Cluzel C, Bachmann A, et al. BMP-1 Disrupts Cell Adhesion and Enhances TGF-β Activation Through Cleavage of the Matricellular Protein Thrombospondin-1. *Sci Signal* (2020) 13 (639):eaba3880. doi: 10.1126/scisignal.aba3880
43. Chiquet-Ehrismann R. Tenascins. *Int J Biochem Cell Biol* (2004) 36:986–90. doi: 10.1016/j.biocel.2003.12.002
44. Schultz-Cherry S, Ribeiro S, Gentry L, Murphy-Ullrich JE. Thrombospondin Binds and Activates the Small and Large Forms of Latent Transforming Growth Factor-Beta in a Chemically Defined System. *J Biol Chem* (1994) 269 (43):26775–82.
45. Huang W, Chiquet-Ehrismann R, Moyano JV, Garcia-Pardo A, Orend G. Interference of Tenascin-C With Syndecan-4 Binding to Fibronectin Blocks Cell Adhesion and Stimulates Tumor Cell Proliferation. *Cancer Res* (2001) 61 (23):8586–94.
46. Valcourt U, Kowanetz M, Niimi H, Heldin C-H, Moustakas A. TGF-Beta and the Smad Signaling Pathway Support Transcriptomic Reprogramming During Epithelial-Mesenchymal Cell Transition. *Mol Biol Cell* (2005) 16:1987–2002. doi: 10.1091/mbc.E04-08-0658
47. Bartholin L, Vincent DF, Valcourt U. TGF-β as Tumor Suppressor: In Vitro Mechanistic Aspects of Growth Inhibition. In: Moustakas A, Miyazawa K. (eds). *TGF-β in Human Disease*. Springer, Tokyo: Aristidis Moustakas & Keiji Miyazawa. (2013). p. 113–38. doi: 10.1007/978-4-431-54409-8_5
48. Valcourt U, Vincent DF, Bartholin L. TGF-β as Tumor Suppressor: Lessons from Mouse Models. In: A Moustakas, K Miyazawa. (eds). *Tgf-β in Human Disease*. Tokyo: Springer Japan. (2013). p. 139–68. doi: 10.1007/978-4-431-54409-8_6
49. Annes JP, Munger JS, Rifkin DB. Making Sense of Latent TGFbeta Activation. *J Cell Sci* (2003) 116:217–24. doi: 10.1083/jcb.200312172
50. Derynck R, Budi EH. Specificity, Versatility, and Control of TGF-β Family Signaling. *Sci Signal* (2019) 12(570):eaav5183. doi: 10.1126/scisignal.aav5183
51. Schultz-Cherry S, Murphy-Ullrich JE. Thrombospondin Causes Activation of Latent Transforming Growth Factor-Beta Secreted by Endothelial Cells by a Novel Mechanism. *J Cell Biol* (1993) 122:923–32. doi: 10.1083/jcb.122.4.923
52. Tang X, Muhammad H, McLean C, Miotla-Zarebska J, Fleming J, Didangelos A, et al. Connective Tissue Growth Factor Contributes to Joint Homeostasis and Osteoarthritis Severity by Controlling the Matrix Sequestration and Activation of Latent Tgfβ. *Ann Rheum Dis* (2018) 77:1372–80. doi: 10.1136/annrheumdis-2018-212964
53. Crawford SE, Stellmach V, Murphy-Ullrich JE, Ribeiro SM, Lawler J, Hynes RO, et al. Thrombospondin-1 is a Major Activator of TGF-beta1 In Vivo. *Cell* (1998) 93:1159–70. doi: 10.1016/s0092-8674(00)81460-9
54. Morissette R, Chen W, Perritt AF, Dreiling JL, Arai AE, Sachdev V, et al. Broadening the Spectrum of Ehlers Danlos Syndrome in Patients With Congenital Adrenal Hyperplasia. *J Clin Endocrinol Metab* (2015) 100: E1143–52. doi: 10.1210/jc.2015-2232
55. De Laporte L, Rice JJ, Tortelli F, Hubbell JA. Tenascin C Promiscuously Binds Growth Factors Via its Fifth Fibronectin Type III-like Domain. *PloS One* (2013) 8:e62076. doi: 10.1371/journal.pone.0062076
56. Murphy-Ullrich JE, Poczatek M. Activation of Latent TGF-beta by thrombospondin-1: Mechanisms and Physiology. *Cytokine Growth Factor Rev* (2000) 11:59–69. doi: 10.1016/S1359-6101(99)00029-5
57. Yokoyama K, Erickson HP, Ikeda Y, Takada Y. Identification of Amino Acid Sequences in Fibrinogen Gamma -Chain and Tenascin C C-Terminal Domains Critical for Binding to Integrin Alpha Vbeta 3. *J Biol Chem* (2000) 275:16891–8. doi: 10.1074/jbc.M000610200
58. Adams JC, Chiquet-Ehrismann R, Tucker RP. The Evolution of Tenascins and Fibronectin. *Cell Adh Migr* (2015) 9:22–33. doi: 10.4161/19336918.2014.970030
59. Erickson HP. Evolution of the Tenascin Family–Implications for Function of the C-terminal Fibrinogen-Like Domain. *Perspect Dev Neurobiol* (1994) 2:9–19. doi: 10.1080/0907676x.1994.9961218

60. Zuliani-Alvarez L, Marzeda AM, Deligne C, Schwenzer A, McCann FE, Marsden BD, et al. Mapping Tenascin-C Interaction With Toll-Like Receptor 4 Reveals a New Subset of Endogenous Inflammatory Triggers. *Nat Commun* (2017) 8:1595. doi: 10.1038/s41467-017-01718-7
61. Midwood KS, Hussenet T, Langlois B, Orend G. Advances in Tenascin-C Biology. *Cell Mol Life Sci* (2011) 68:3175–99. doi: 10.1007/s00018-011-0783-6
62. Sun Z, Velázquez-Quesada I, Murdamoothoo D, Ahowesso C, Yilmaz A, Spenlé C, et al. Tenascin-C Increases Lung Metastasis by Impacting Blood Vessel Invasions. *Matrix Biol* (2019) 83:26–47. doi: 10.1016/j.matbio.2019.07.001
63. Maschler S, Grunert S, Danielopol A, Beug H, Wirl G. Enhanced Tenascin-C Expression and Matrix Deposition During Ras/TGF-beta-induced Progression of Mammary Tumor Cells. *Oncogene* (2004) 23:3622–33. doi: 10.1038/sj.onc.1207403
64. Chiovaro F, Martina E, Bottos A, Scherberich A, Hynes NE, Chiquet-Ehrismann R. Transcriptional Regulation of Tenascin-W by TGF-beta Signaling in the Bone Metastatic Niche of Breast Cancer Cells. *Int J Cancer* (2015) 137:1842–54. doi: 10.1002/ijc.29565
65. Jachetti E, Caputo S, Mazzoleni S, Brambillasca CS, Parigi SM, Grioni M, et al. Tenascin-C Protects Cancer Stem-like Cells From Immune Surveillance by Arresting T-Cell Activation. *Cancer Res* (2015) 75:2095–108. doi: 10.1158/0008-5472.CAN-14-2346
66. Mirzaei R, Sarkar S, Dzikowski L, Rawji KS, Khan L, Faissner A, et al. Brain Tumor-Initiating Cells Export Tenascin-C Associated With Exosomes to Suppress T Cell Activity. *Oncoimmunology* (2018) 7:e1478647. doi: 10.1080/2162402X.2018.1478647
67. Spenlé C, Loustau T, Murdamoothoo D, Erne W, Beghelli-de la Forest Divonne S, Veber R, et al. Tenascin-C Orchestrates an Immune-Suppressive Tumor Microenvironment in Oral Squamous Cell Carcinoma. *Cancer Immunol Res* (2020) 8(9):1122–38. doi: 10.1158/2326-6066.CIR-20-0074

Conflict of Interest: The authors declare that the research was conducted in the absence of any commercial or financial relationships that could be construed as a potential conflict of interest.

frontiers in Immunology

ORIGINAL RESEARCH
published: 05 July 2021
doi: 10.3389/fimmu.2021.636108

Impact of Tenascin-C on Radiotherapy in a Novel Syngeneic Oral Squamous Cell Carcinoma Model With Spontaneous Dissemination to the Lymph Nodes

Caroline Spenlé[1,2,3†], Thomas Loustau[2,3,4†], Hélène Burckel[5‡], Gilles Riegel[2,3,4‡], Chérine Abou Faycal[2,3,4‡], Chengbei Li[2,3,4‡], Alev Yilmaz[1,2,3,4‡], Luciana Petti[6], Fanny Steinbach[2,3,4], Constance Ahowesso[1,2,3], Camille Jost[1,2,3], Nicodème Paul[2,3,7], Raphael Carapito[2,3,7], Georges Noël[5,8], Fabienne Anjuère[6], Nathalie Salomé[2,3,4] and Gertraud Orend[1,2,3,4*]*

[1] INSERM U1109-MN3T, The Microenvironmental Niche in Tumorigenesis and Targeted Therapy, Strasbourg, France, [2] Université de Strasbourg, Strasbourg, France, [3] Fédération de Médecine Translationnelle de Strasbourg (FMTS), Strasbourg, France, [4] INSERM U1109, The Tumor Microenvironment Group, Strasbourg, France, [5] Institut de Cancérologie de Strasbourg Europe (ICANS), UNICANCER, Paul Strauss Comprehensive Cancer Center, Radiobiology Laboratory, Université de Strasbourg, Strasbourg, France, [6] Université Côte d'Azur, CNRS, IPMC, Valbonne-Sophia Antipolis, France, [7] Platform GENOMAX, INSERM UMR_S 1109, Faculté de Médecine, Fédération Hospitalo-Universitaire OMICARE, LabEx TRANSPLANTEX, Strasbourg, France, [8] Institut de Cancérologie Strasbourg Europe (ICANS), UNICANCER, Department of Radiation Oncology, Strasbourg, France

Radiotherapy, the most frequent treatment of oral squamous cell carcinomas (OSCC) besides surgery is employed to kill tumor cells but, radiotherapy may also promote tumor relapse where the immune-suppressive tumor microenvironment (TME) could be instrumental. We established a novel syngeneic grafting model from a carcinogen-induced tongue tumor, OSCC13, to address the impact of radiotherapy on OSCC. This model revealed similarities with human OSCC, recapitulating carcinogen-induced mutations found in smoking associated human tongue tumors, abundant tumor infiltrating leukocytes (TIL) and, spontaneous tumor cell dissemination to the local lymph nodes. Cultured OSCC13 cells and OSCC13-derived tongue tumors were sensitive to irradiation. At the chosen dose of 2 Gy mimicking treatment of human OSCC patients not all tumor cells were killed allowing to investigate effects on the TME. By investigating expression of the extracellular matrix molecule tenascin-C (TNC), an indicator of an immune suppressive TME, we observed high local TNC expression and TIL infiltration in the irradiated tumors. In a TNC knockout host the TME appeared less immune suppressive with a tendency towards more tumor regression than in WT conditions. Altogether, our novel syngeneic tongue OSCC grafting model, sharing important features with the human OSCC disease could be relevant for future anti-cancer targeting of OSCC by radiotherapy and other therapeutic approaches.

Keywords: radiotherapy, oral squamous carcinoma, tumor microenvironment, tenascin-C, syngeneic animal model, immune suppression

OPEN ACCESS

Edited by:
Joanne Murphy-Ullrich, University of Alabama at Birmingham, United States

Reviewed by:
Tomer Cooks, Ben-Gurion University of the Negev, Israel
Michal Amit Rahat, Technion-Israel Institute of Technology, Israel
Andreas Faissner, Ruhr University Bochum, Germany

***Correspondence:**
Gertraud Orend
gertraud.orend@inserm.fr
Caroline Spenlé
cspenle@unistra.fr

†These authors have contributed equally to this work and share first authorship

‡These authors have contributed equally to this work and share second authorship

Specialty section:
This article was submitted to Inflammation, a section of the journal Frontiers in Immunology

Received: *30 November 2020*
Accepted: *11 June 2021*
Published: *05 July 2021*

Citation:
Spenlé C, Loustau T, Burckel H, Riegel G, Abou Faycal C, Li C, Yilmaz A, Petti L, Steinbach F, Ahowesso C, Jost C, Paul N, Carapito R, Noël G, Anjuère F, Salomé N and Orend G (2021) Impact of Tenascin-C on Radiotherapy in a Novel Syngeneic Oral Squamous Cell Carcinoma Model With Spontaneous Dissemination to the Lymph Nodes. Front. Immunol. 12:636108. doi: 10.3389/fimmu.2021.636108

INTRODUCTION

Head and neck squamous cell carcinoma (HNSCC) is the 7th most frequent cancer with a low percentage of 5-year survival (1). HNSCC in the oral cavity, lip, tongue and upper throat, coined oral squamous cell carcinoma (OSCC), can metastasize to regional lymph nodes and the lung (2). Exposure to tobacco, bethel nut and alcohol represent high risk factors for developing OSCC (1, 3).

Apart from surgical removal of cancer tissue in OSCC, radiotherapy is the most common treatment (4, 5). Radiotherapy is used in 70% of cancer patients and includes high energy rays (photons, protons or charged particles) where the total dose varies between 50 and 70 Gy, with a daily fractionation of 1.8–2 Gy (5). Absorption of these rays induces DNA double strand breaks and reactive oxygen species causing a tumoricidal effect that is largely dependent on an anti-tumor immune response (6, 7). Dying tumor cells can generate neoantigens that activate the immune system involving dendritic cells (DC), macrophages and other immune subtypes (8). Radiotherapy can act as a two-edged sword by activating and inhibiting the immune defense against tumor cells, respectively (9, 10).

The extracellular matrix (ECM) molecule tenascin-C (TNC) is highly expressed in malignant tumors including HNSCC and plays multiple roles in the tumor microenvironment (TME) promoting cancer progression and metastasis (11–13). TNC promotes tumor cell survival, proliferation, invasion, formation of leaky blood vessels and lung metastasis as demonstrated in spontaneous tumor models with high TNC in comparison to engineered low TNC (14–16). Moreover, TNC forms local niches within the tumor where stromal and immune cells are enriched, regulating cell behavior (14, 15, 17). Recently, by using mice expressing or lacking TNC, we have shown that TNC orchestrates an immune-suppressive TME in the carcinogen 4-nitroquinoline-1-oxide (4NQO)-induced OSCC model (18).

In the past several OSCC tumor grafting models have been established from 4NQO-induced tongue, lip and esophageal squamous cell carcinomas that were used in drug targeting (19–23). Some of these models showed high resemblance with human papilloma virus (HPV)-negative OSCC which was recently confirmed at mutation level (24). However, in none of these models the impact of radiotherapy on the TME has been addressed.

Here, we established a novel syngeneic OSCC model derived from a 4NQO-induced OSCC in the tongue that showed similarities with HPV-negative HNSCC by recapitulating mutations seen in human tumors, constitutive transforming growth factor beta (TGFβ) signaling, abundant TIL in TNC-rich stroma, and spontaneous tumor cell dissemination to the local lymph nodes. Most importantly, this model was sensitive to radiotherapy and revealed an impact of TNC on tumor regression. This model does allow not only to investigate tumor regression by radiotherapy but could be useful for assessing effects of radiotherapy on the TME. Finally, our model could be relevant for future anti-cancer targeting of OSCC by radiotherapy and/or other therapeutic approaches.

MATERIAL AND METHODS

Cell Culture

OSCC2 cells were established from a murine 4NQO induced tongue tumor arising in a female C57Bl/6J mouse (18) and cultured in DMEM-F12 with 4.5 g/L glucose, 10% FBS, 1% penicillin–streptomycin (Sigma, P4333), 40 µg/ml gentamicin (Dutscher, L0012-100) and 0.4 µg/ml hydrocortisone (Sigma, H4001). Cells were checked for the absence of mycoplasms (once every two months, PlasmoTest, Invivogen, rep-pt1). OSCC2 cells (5×10^6) were subcutaneously engrafted into the back of a C57Bl/6J mouse for 4 weeks before extraction of the tumor, treatment with collagenase as described (18) and explanting cells into cell culture dishes. After three passages *in vitro*, 5×10^6 cells were again grafted into the neck of a C57Bl/6J mouse which induced a tumor from which cells were explanted in cell culture as described, giving rise to the cell line OSCC13. For bioluminescence experiments, OSCC13 cells were infected with lentiviral particles carrying a luciferase reporter gene. In brief, lentiviral particles were established with ViraPower™ Lentiviral Expression Systems (Invitrogen) and the plasmid pLenti-CMV-LUC (Addgene, #21474) in HEK293T cells (ATCC). OSCC13 cells were then infected with the lentiviral particles and cells stably expressing the luciferase reporter were established by selection with 10 µg/ml of blasticidin (InvivoGen) giving rise to the OSCC13-LUC cell line.

Orthotopic Grafting of OSCC13 Cells in the Tongue and Bioluminescence Detection

Nude mice (8 weeks of age) or WT and TNCKO (C57Bl/6J) mice (bred in house) were grafted in the first third part of the tongue. In particular, 3×10^6 OSCC13 cells in 10 µl PBS were injected using a U-100 insulin syringe (BD Micro-Fine) in C57Bl/6J mice. Some 1×10^6 cells OSCC13-LUC (luciferase expression vector expressing cells) were similarly grafted. Tumors were visible 2 weeks upon engraftment and mice were sacrificed for analysis at 3 weeks (bioluminescence experiment), 2 and 4 weeks (NIR) or 4 weeks (IR). For irradiation analysis, a 2 Gy unique dose of photons was delivered two weeks after tumor cell engraftment (3×10^6 cells). Mice were sacrificed two weeks later and tissue was analyzed by staining. For bioluminescence detection, a RediJect D-Luciferin Ultra Bioluminescent Substrate

Abbreviations: 4NQO, 4-nitroquinoline-1-oxide; AUF, arbitrary units of fluorescence; CBA, cytometry bead array; CCL21, Chemokine (C–C motif) ligand 21; CCR7, C–C chemokine receptor type 7; CXCR4, C-X-C chemokine receptor type 4; DC, dendritic cells; ECM, the extracellular matrix; EMT, epithelial-to-mesenchymal transition; FNIII, fibronectin type III; FRC, fibroblast reticular cells; H&E, hematoxylin and eosin; HNSCC, head and neck squamous cell carcinoma; HPV, human papillomavirus; IF, immunofluorescence; IFNγ, Interferon γ; IL1β, Interleukin 1β; IR, irradiated; LM, Laminin; NIR, non-irradiated; ORA, over-representation analysis; OSCC, oral squamous cell carcinomas; PE, plating efficiency; PFA, paraformaldehyde; SF, surviving fraction; TGFβ, transforming growth factor beta; TIL, tumor infiltrating leukocytes; TLR4, Toll Like Receptor 4; TME, tumor microenvironment; TMT, tumor matrix tracks; TNC, tenascin-C; TNFα, tumor necrosis factors α.

(Perkinelmer 770505) solution at 30 mg/ml was injected intraperitoneally 7 min before imaging. Images were acquired for 5 min using a live imager (NightOwl, Berthold). All mice were housed and handled according to the guidelines of INSERM and the ethical committee of Alsace, France (CREMEAS) (Directive 2010/63/EU, 01386.02, C-67-482-033 on the protection of animals used for scientific purposes).

Immune Cell Preparation From Tumors and Cytokine Production

OSCC13 tumor tissues were cut in small pieces and then treated with a solution of collagenase IV (1 mg/ml; Sigma-Aldrich, France) and DNase (0.2 mg/ml; Roche Diagnostics, France) at 37°C for 20 min under constant shaking. Cell suspensions from the OSCC13 tongue tumors (400,000 cells/well) were stimulated with anti-CD3/CD28 dynabeads (Gibco #11452D) at a bead-to-cell ratio of 1:1 for 24 h according to the provider's instructions (Becton Dickinson). Supernatants were collected and assessed for the indicated cytokines using the CBA technology (BD Biosciences, France).

Immunostaining

For immunofluorescence staining (IF), unfixed frozen 8 µm tumor sections or cells fixed with 2% paraformaldehyde (PFA) followed by permeabilization in 0.1% TritonX-100/PBS for 10 min were directly incubated overnight with the primary antibodies (**Supplementary Table S1**). Secondary antibodies conjugated with Alexa 488, Cy3 or Cy5 were used (**Supplementary Table S1**). Dapi (Sigma D9542) was used to visualize nuclei. After embedding in FluorSave Reagent (Calbiochem, 345789), sections were examined using a Zeiss Axio Imager Z2 microscope. Pictures were taken with an AxioCam MRm (Zeiss) camera and were analyzed using the Axiovision software. Control sections were processed as mentioned above with omission of the primary antibodies. The image acquisition setting (microscope, magnification, light intensity, exposure time) was kept constant per experiment and in between experimental conditions (comparison NIR with IR tumors) or was adjusted to get the best image (all other stainings).

Real-Time Quantitative PCR

Cells were dissolved in the TRIzol reagent (Invitrogen, 12044977) for total RNA extraction. RNA quality was confirmed by optical density measurement. cDNA was synthesized from 1 µg of total RNA using random primers and Moloney murine leukemia virus reverse transcriptase (MultiScribe, Applied Biosystems, 10117254). The cDNA was used for qRTPCR in an Mx3005P Real-Time PCR System (ThermoFisher Scientific). Reactions were carried out in duplicate for all conditions using a Sybr Green Master mix (ThermoFisher Scientific, 4344463) or Fast Taqman mix (ThermoFisher Scientific, 4444557) and expression of mouse Gapdh mRNA (Life Technology, 433764T) was used as endogenous control in the comparative cycle threshold method ($2^{-}\Delta\Delta^{Ct}$). Primer sequences used are listed in **Supplementary Table S2**.

RNAseq Analysis

RNA from OSCC13 cells (grown for 24 h in DMEM/10% FCS, N = 2) was isolated using the RNeasy Mini Kit (Qiagen). For each sample, quality control was carried out and assessed with the NGS Core Tools FastQC (http://www.bioinformatics.babraham.ac.uk/projects/fastqc/). Sequence reads were mapped using STAR (25). The total mapped reads were finally available in a BAM (Binary Alignment Map) format for variant calling. Variant calling was performed using the ultra-sensitive variant caller VarDict (26) where only variants with a PASS status were selected. At last, the variants were annotated by the Ensembl Variant Effect Predictor tool (27). Mutation signatures were obtained using the computational framework SigProfiler (https://www.mathworks.com/matlabcentral/fileexchange/38724-sigprofiler). Gene mutation analyses were performed by comparing data from OSCC13 cells with that from publicly available HNSCC dataset from the TCGA consortium (28) and 4MOQ cell lines previously described (24). In addition, p53 mutation patterns observed in the characterized HNSCC samples from TCGA and OCSS13 cell lines were represented and compared using the "lolipop" mutation pattern generator (29). From the list of genes expressed by OSCC13 cells, an over-representation analysis (ORA) was performed in order to determine the gene sets statistically over-represented (**Supplementary Table S3**). Visualization of genes and GO terms was performed using Webgestalt program (30) and Gene Ontology database (31). Multiple testing Benjamini–Hochberg correction was performed and an False-discovery rate threshold was applied (FDR ≤0.05). The original data are available at ArrayExpress accession *E-MTAB-10614*.

Irradiation of Tumor Cells and Tumor Mice

Cells seeded in 6-well plates (Falcon, 353046) were exposed, at room temperature, to gamma irradiation, with single doses of 2, 4, 6, 8 or 10 Gy. A ^{137}Cs γ-irradiator (Biobeam GM 8000, GSM GmbH, Leipzig, Germany) was used in the Paul Strauss Center/Institut de Cancérologie Strasbourg Europe (Strasbourg, France) at a dose rate of 2.5 Gy/min. Cells in control flasks were sham irradiated. Tumor bearing (WT and TNCKO) mice, 2 weeks after engrafting of 3×10^6 OSCC13 cells in the tongue, were irradiated under anesthesia (ketamine 100 mg/kg and xylazine 10 mg/kg) with the irradiator Biobeam GM 8000 with a single fraction of 2 Gy at dose rate of 2.5 Gy/min. The whole body of the mouse, apart from the front of the head, was protected with a lead shield to avoid radiation toxicity. Eyes were protected with a moisturizing cream. No toxic effect was seen in non-tumor bearing mice as assessed by quantification of white and red blood cells numbers, respectively.

Cell Proliferation Assay

In vitro determination of OSCC2 and OSCC13 cell growth was performed using a resazurin assay (Interchim (UP669413 Uptiblue, Montluçon, France). Cells were seeded in 96-well plates at a density of 1×10^3 cells per well in 100 µl and incubated for 24 h. Subsequently, cells were irradiated with single irradiation doses and incubated at 37°C for 1, 2, 3 or 6 days. Subsequently, 20 µl

(10% of final volume) of resazurin were added to each well and cells were incubated at 37°C for four additional hours. The fluorescence of each well was measured at 560–590 nm using a Synergy™ microplate reader (Biotek, Winooski, USA). Results were expressed in arbitrary units of fluorescence (AUF) after subtraction of the blank value (medium only). All experiments were repeated at least three times independently.

Clonogenic Survival Assay

Cells were seeded in 6-well plates (Falcon, 353046) at a density of 2×10^5 cells per well and allowed to adhere overnight in standard culture conditions (DMEM with 10% FBS). Cells were then exposed to irradiation and collected 24 h after irradiation. Cells were trypsinized and enumerated using a Countess® cell counter (Countess, Invitrogen, Carlsbad, USA). Then, cells were seeded in fresh medium and plated at two different dilutions into 6-well plates. The seeding densities used were 100 and 200 cells for the control non-irradiated condition, 200 and 400 cells after 2 Gy, 400 and 800 after 4 Gy, 750 and 1500 after 6 Gy, 1,500 and 3,000 after 8 Gy and 3,000 and 6,000 cells after 10 Gy. Thirteen days later, clones were stained using 0.05% crystal violet (Sigma-Aldrich, C0775) in a 5% ethanol solution and positive colonies containing more than 50 cells were scored. The plating efficiency (PE) and then the surviving fractions (SF) were calculated. The plating efficiency (PE) is defined as the ratio of the number of colonies formed for each condition to the number of cells seeded for each condition. Furthermore, the surviving fraction (SF) is expressed as the ratio of the plating efficiency after treatment to plating efficiency without treatment (non-irradiated control). Survival curves were plotted using surviving fractions for the different doses. Treatments were performed in triplicate and the experiments were repeated four times independently.

Statistical Analysis

For all data, Gaussian distribution was tested. When data followed a Gaussian distribution, statistical differences were analyzed by unpaired t-test (with Welch's correction in case of unequal variance) or ANOVA one-way with Tukey post-test. Otherwise, the Mann–Whitney test or a non-parametric ANOVA followed by Dunns post-test were used to verify significance of the observed differences. For clonogenic survival assay, data were compared pairwise with a Student–Newman–Keuls test. All statistical analyses were performed using the GraphPad Prism 5.02 software. Mean ± SEM. p values <0.05 were considered as statistically significant, *p <0.05; **p <0.01; ***p <0.001.

RESULTS

Establishment of the OSCC13 Cell Line From a 4NQO-Induced Tongue Tumor

We established a murine OSCC tumor by exposing a C57Bl/6J mouse to the carcinogen 4-nitroquinoline-1-oxide (4NQO) in the drinking water for 20 weeks as recently described (18). Then cells were explanted giving rise to the epithelioid cell line OSCC2 as seen by phase contrast imaging and immunofluorescence (IF) staining for E-cadherin (**Figure 1A**). As OSCC2 cells generated tumors in the tongues of 60% of mice we sought to increase the grafting efficiency to 100% which was accomplished by a two times sub-cutaneous grafting of OSCC2 cells in the upper neck of C57Bl/6J mice. The arising OSCC13 cells were phenotypically indistinguishable from the OSCC2 cells as seen by phase contrast imaging and E-cadherin IF staining (**Figure 1A**). To compare the genetic differences and similarities between OSCC13 cells and human HNSCC tumors, we performed RNAseq analysis. By using SigProfiler program we compared the mutation rate in OSCC13 cells with that in tobacco smoking associated human HNSCC (32) and in 4NQO-induced tongue tumors (24). As described previously, cells extracted from 4NQO-induced tumors show remarkable similarity to human cancer cells (24). The mutational patterns induced by 4NQO and tobacco have similar higher mutation rate in translated than in untranslated regions and substitution type rates on each nucleotide. Only the T to A transition, frequently mutated in the tobacco signature is barely found in the 4NQO signature. Interestingly the OSCC13 signature presented nucleotide substitution rates recapitulating tobacco and 4NQO signatures with both high T to A and C to T substitution frequencies (**Figure 1B**). Investigation of mutations in 18 genes that are frequently mutated in human HPV-negative HNSCC and in the 4NQO-induced 4MOSC cells, revealed also high mutation rates in the OSCC13 cells (except for Fat4 and Keap1 that did not show mutations). Moreover, six other genes frequently affected in human OSCC, but not found to be altered in the 4MOSC cells, were also mutated in the OSCC13 cells (Pik3cd, Fat1, Notch2, Cdh10, Nf1 and Pten) suggesting that OSCC13 cells phenocopy characteristics described for human HNSCC (**Figure 1C**). TP53 encoding the tumor suppressor molecule p53 is frequently mutated in human tumors (84.8% of HPV-negative HNSCC (TGCA cohort)). We investigated hotspots of mutations in TP53 and observed seven mutations in the DNA binding domain with four in common to HPV-negative HNSCC (**Figure 1D**). Next, by over-representation analysis (ORA) we investigated gene expression of the cultured OSCC13 cells. We observed several immune modulating molecules such as *Cd274, Ctla4* and *Irf7* to be expressed by the cultured OSCC13 cells, mimicking HNSCC, 4NQO-induced tumors and the 4MOSC1-4 cells [**Supplementary Table S3** (18, 24, 33)]. Moreover, many molecules involved in the TGFβ (46 genes) and Wnt signaling pathways (68 genes) were significantly expressed suggesting intrinsic activation of these pathways again recapitulating features of human HNSCC [**Figure 1E** and **Supplementary Table S3** (34, 35)]. Altogether, we propose that the OSCC13 cells could be a relevant novel cellular model that recapitulates properties of human tobacco smoking associated HNSCC.

OSCC13 Cells Induce Tumors Upon Grafting in the Tongue of Syngeneic Mice

Grafting OSCC13 cells underneath the mucosa induced tongue tumors that were collected and characterized by tissue staining

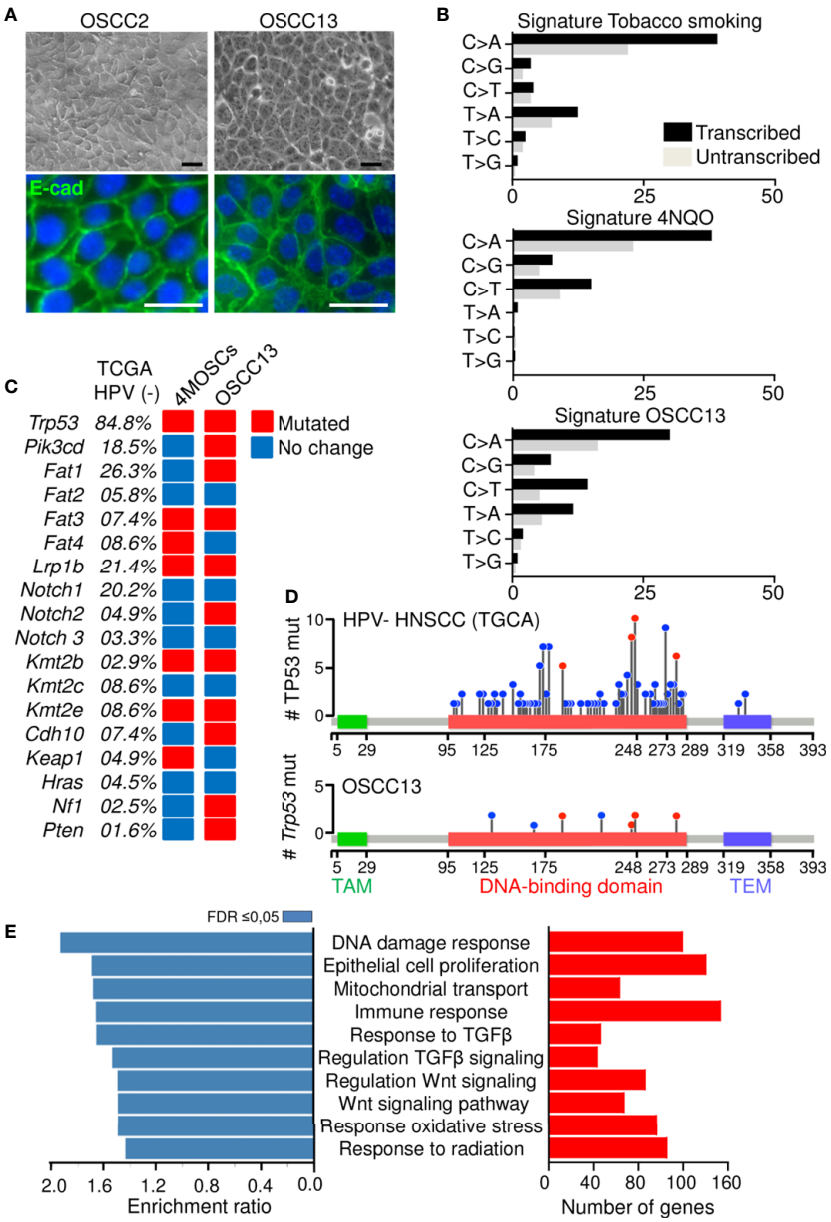

FIGURE 1 | Phenotype of a new OSCC model. **(A)** Phase contrast and IF imaging of E-cadherin in OSCC2 and OSCC13 cells. Scale bar, 25 µm. **(B)** Percentage of somatic substitutions located in the translated or untranslated genome regions in patients with smoking-associated HNSCC (top (32), in 4NQO-derived lesions (middle (24); and in OSCC13 cells (bottom). **(C)** Graphical matrix representation of individual mutations in OSCC13 compared to 4MOSCs and smoking-associated HNSCC (24, 32). The most frequently observed alterations in the indicated genes of human HPV negative HNSCC (TGCA database) and the corresponding percentage of mutations in 4MOSCs and OSCC13 are shown. The presence (red) or absence (blue) of mutations are indicated for OSCC13 and the 4MOSC1–4 cells when at least two of the four cells showed the same phenotype. **(D, E)** RNA data analysis of cultured OSCC13 cells 24 h after plating. **(D)** Lollipop mutational plot of TP53 mutations in human HNSCC (HPV-negative) tumor samples from TCGA database (top) and mouse HNSCC cell line (OSCC13) (bottom). The frequency of mutations is represented by the height of the lollipop. The blue circles indicate mutations specific to human or mouse, and the red circles illustrate mutations common to human and mouse HNSCCs. TAM, Transactivation motif; TEM, Tetramerisation motif. **(E)** Over-represented gene ontology terms as determined by the Webgestalt program and Geneontology database. Bar charts show the enrichment ratio (blue) and expressed gene numbers (red) of the 10 most over-represented GO processes associated with FDR ≤ 0.05.

with hematoxylin and eosin (H&E), and IF with antibodies against specific markers. We observed that tumors highly expressed TNC (**Supplementary Figures S1A, B**). Human OSCC tumors and 4NQO-induced tumors are highly vascularized (18, 36), therefore we stained for lymphatic (LYVE1) and blood vessels (CD31). We observed a high staining of LYVE1 and CD31 around but not inside the tumors which indicates that the angiogenic switch may not

have occurred yet (**Figure 2A**). As the RNA seq analysis revealed constitutive TGFβ signaling in the tumor cells we investigated phosphorylation of Smad3 as indicator of pathway activation. Indeed, P-Smad3 was highly abundant however mostly cytoplasmic (**Figure 2B**). As TGFβ signaling can be activated in stromal, immune and cancer cells (34), future studies have to determine in which stromal cells this pathway is preactivated in the OSCC13 tumors. OSCC tongue tumors are mainly of epithelial origin (two over three patients) (37). We investigated the cellular properties by combined staining for CK8/18 and vimentin and noticed that the majority of cells inside the tumor mass expressed CK8/18 (**Figure 2C**). In addition, streaks of vimentin+ cells were seen to separate CK8/18+ tumor cell nests (**Figure 2C**). Vimentin+ cells likely represent carcinoma associated fibroblasts. Future studies have to reveal whether vimentin+ cells also derive from tumor cells having undergone epithelial-to-mesenchymal transition (EMT). As ERTR7+ fibroblast reticular cells (FRC) were numerous in 4NQO-induced tumors (18) we investigated their abundance by staining for gp38 and ERTR7 (and the lack of LYVE1 staining). Indeed we observed FRC to be highly abundant in the OSCC13 tumors (**Figure 2D**). We noticed that ERTR7 +/gp38+ cells surrounded the tumors and that the ERTR7 signal showed a continuation from the tumor border into the tumor mass reminiscent of FRC migrating from outside tissue into the tumor mass. FRC are an important source of matrix as demonstrated in the 4NQO-induced tumors (18). Here, we stained for TNC and saw a similar staining pattern as for ERTR7, separating tumor cells (p63+), supportive of FRC also expressing TNC in this model (**Figure 2E**). TNC was arranged in fibrillar matrix alignments resembling tumor matrix tracks (TMT) like in 4NQO-induced tongue and other tumors (12, 18, 38) (**Figure 2E**).

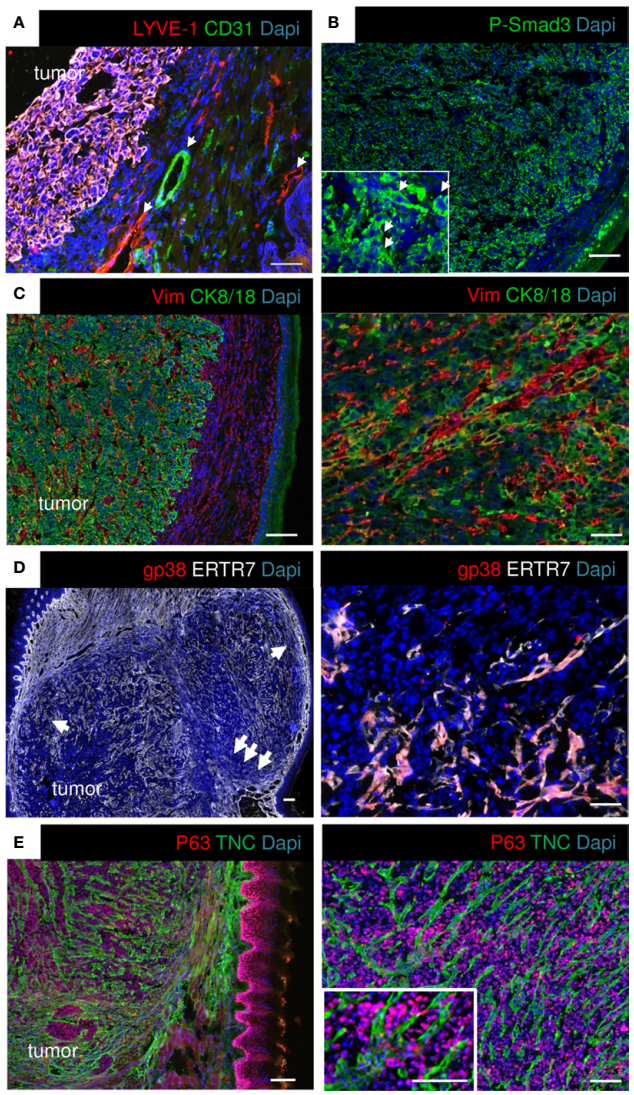

FIGURE 2 | Characterization of OSCC13 tumors by immunostaining. 4 weeks syngeneic tongue tumors derived from 1 × 10^6 engrafted OSCC13 cells were stained for the indicated molecules. Representative images are shown (N = 3). Scale bar, 100 µm. Arrows point at LYVE+ lymphatic and CD31+ blood vessels in the surroundings of the tumor mass **(A),** at P-Smad3+ cells (higher magnification inlet in **B**), and at ERTR7+ cells invading the tumor mass from the surrounding tissue **(D)**. **(C–E)**, scale bar, 500 µm (left). Right panels, higher magnification, scale bar, 100 µm **(C, E)**, 50 µm **(D)**.

Immune Suppressive TME in OSCC13 Tumors

As the RNA seq analysis showed that the cultured OSCC13 cells expressed *Cd274* we stained the OSCC13 tumors for PDL-1 and indeed found an ubiquitous expression, resembling high PDL-1 in human OSCC, 4NQO-induced OSCC and other OSCC grafted tumors [**Figure 3A** (24)]. Human OSCC and 4NQO-induced tumors are known to be highly invaded by tumor-infiltrating leucocytes (TIL). To address the immune status also in the OSCC13 tumors we stained for the leukocyte marker CD45+ and noticed an accumulation of leukocytes around and inside the tumors with close vicinity to TNC and laminin (LM) matrix tracks which is again similar to the 4NQO-induced OSCC [**Figure 3B** and **Supplementary Figure S1C** (18)]. Staining for CD11c+ myeloid/dendritic cells revealed localization inside the TNC-rich stroma, like in the 4NQO-induced OSCC [**Figure 3C** (18)]. By staining for Col12 (another prominent matrix molecule in OSCC) together with C–C chemokine receptor type 7 (CCR7) we observed a TMT-like organization of Col12 similar to the 4NQO tumors (18). Moreover, we noticed CCR7+ cells [dendritic cells, macrophages and naïve T cells (39)] invading the tumors (**Figure 3D**). Staining for CD206 and F4/80 revealed high colocalization of both markers inside the tumors, indicating abundance of macrophages with a M2 phenotype (**Figure 3E**). Finally, we assessed the potential presence of immune suppressive Treg by Foxp3 staining. Indeed, FoxP3+ cells were present in vicinity to Col12 (**Figure 3F**). In summary, engrafted OSCC13 cells gave rise to tumors with a TME comprising TNC, LM and Col12 matrix, abundant fibroblasts and immune cells that shared an immune suppressive phenotype with 4NQO-induced tumors and human HNSCC (18).

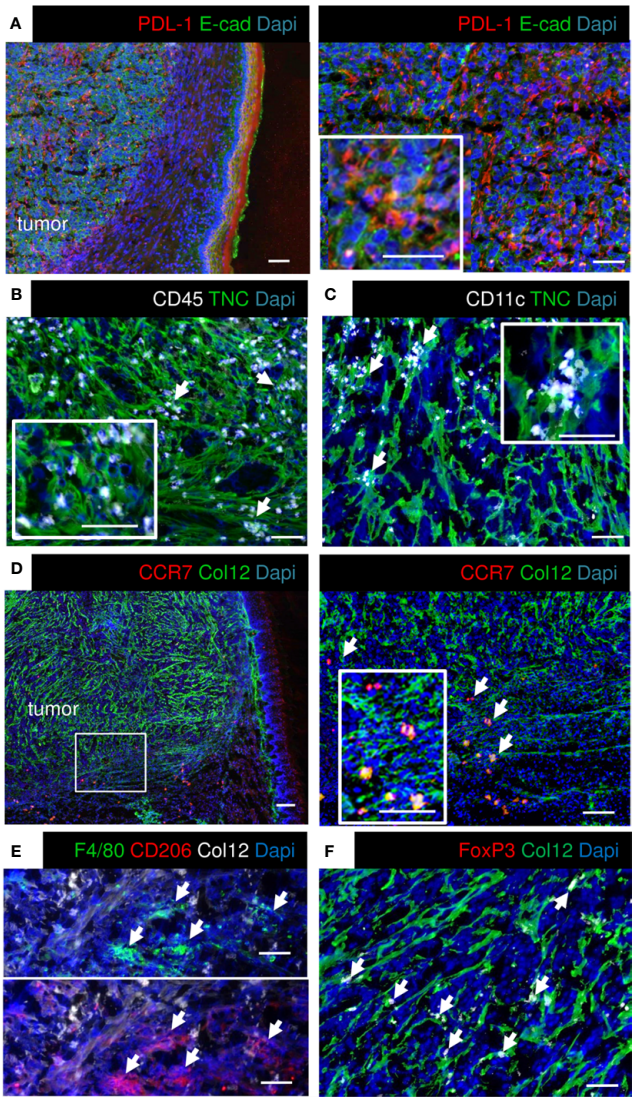

FIGURE 3 | Characterization of immunity markers in OSCC13 tumors by immunostaining. About 4 weeks syngeneic tongue tumors derived from 1 × 10^6 engrafted OSCC13 cells were stained for the indicated molecules. Representative images are shown (N = 3). Scale bar, 100 µm. Arrows point at CD45+ **(B)**, CD11c+ **(C)**, CCR7+ **(D)**, F4/80 and CD206+ **(E)** and Foxp3+ cells **(F)** that are in close vicinity to matrix. **(A, D)**, scale bar, 500 µm (left). Right panels, higher magnification. Scale bar, 50 µm **(A)**, 100 µm **(D)**.

OSCC13 Tumor Cells Spontaneously Disseminate and Home to the Local Lymph Nodes

As tumor cells were found in the local lymph nodes of mice with 4NQO-induced tumors (18), we wondered whether OSCC13 cells were also able to spontaneously disseminate. First, we used a bioluminescence approach to detect OSCC13 cells engineered to express luciferase and monitored luciferin in tumors and local lymph nodes upon grafting of OSCC13 cells underneath the tongue mucosa of nude mice. We saw a bioluminescence signal in the primary tumor one week after grafting that increased with time (but was hidden at 3 weeks behind the anesthesia cap) (**Figure 4A**). More importantly, we also saw a small luciferin signal in the lymph nodes already one week after grafting that further increased by week 2 and was highly prominent at week 3. A strong luciferin signal was confirmed by imaging of the extracted lymph nodes demonstrating that the OSCC13 tumor cells had spontaneously homed to the lymph nodes and expanded there (**Figure 4A**). Next, we investigated potential lymph node metastasis in the immune competent condition by grafting OSCC13 cells into the tongue mucosa of a C57Bl/6J mouse followed by tissue staining of the lymph nodes 4 weeks after grafting. As we had seen P-Smad3 expression in OSCC13 tumors [**Figure 2B** (18)], we stained the lymph nodes for p63, in addition to other markers. Indeed in the lymph nodes of all investigated tumor mice (3/3) we saw numerous p63+ cells inside the lymph nodes (**Figure 4B**). Co-staining with TNC revealed that the p63+ tumor cells were present in association with TNC that was expressed in short fibrillar networks resembling TNC-rich reticular fibers in lymph nodes [**Figure 4C** (18)]. As tumor cells expressed P-Smad3 (**Figure 2B**) we used this marker together with CK8/18 and observed cells that were positive for both markers, further supporting the presence of OSCC13 tumor cells in the lymph nodes (**Figure 4D**). Next, we addressed whether tumor cells expanded in this model as seen in nude mice (**Figure 4A**) and used staining for the proliferation marker Ki67 in combination with CK8/18+. Indeed, we noticed CK8/18+ cells in the lymph nodes that also expressed Ki67 confirming that disseminated tumor cells could expand in the lymph nodes (**Figure 4E**). We wondered whether tumor cells potentially also homed to the lung in the grafting model, the second most frequent site of metastasis in the human OSCC patient (40). However, the experiment had to be discontinued after 4 weeks as the tumors had reached the ethically accepted size, thus a potential metastasis to the lung could not be addressed rigorously. Interestingly, in one tumor mouse we observed a macroscopical metastasis on the outer surface of the lung, suggesting that potentially tumor cells may also disseminate to the lung. Future studies have to address the lung metastatic potential of OSCC13 cells in more detail.

Altogether, these results strongly suggest that tumor cells from the OSCC13 engrafted tongue tumors spontaneously disseminated and homed to the local lymph nodes where some tumor cells proliferated demonstrating their metastatic potential.

Response of OSCC13 Cells and Derived Tumors to Radiotherapy

Radiotherapy cannot only kill tumor cells but also triggers inflammation and changes in the tumor bed that may counteract tumor regression (41). So far immune competent murine grafting models with a relevant TME to address the roles of radiotherapy in OSCC were not described. To investigate radiosensitivity we exposed OSCC13 cells (in comparison to OSCC2 cells) to increasing single doses of irradiation and determined subsequent tumor cell proliferation and survival in clonogenic assays. We observed a significant reduction in proliferation of OSCC13 cells 6 days after

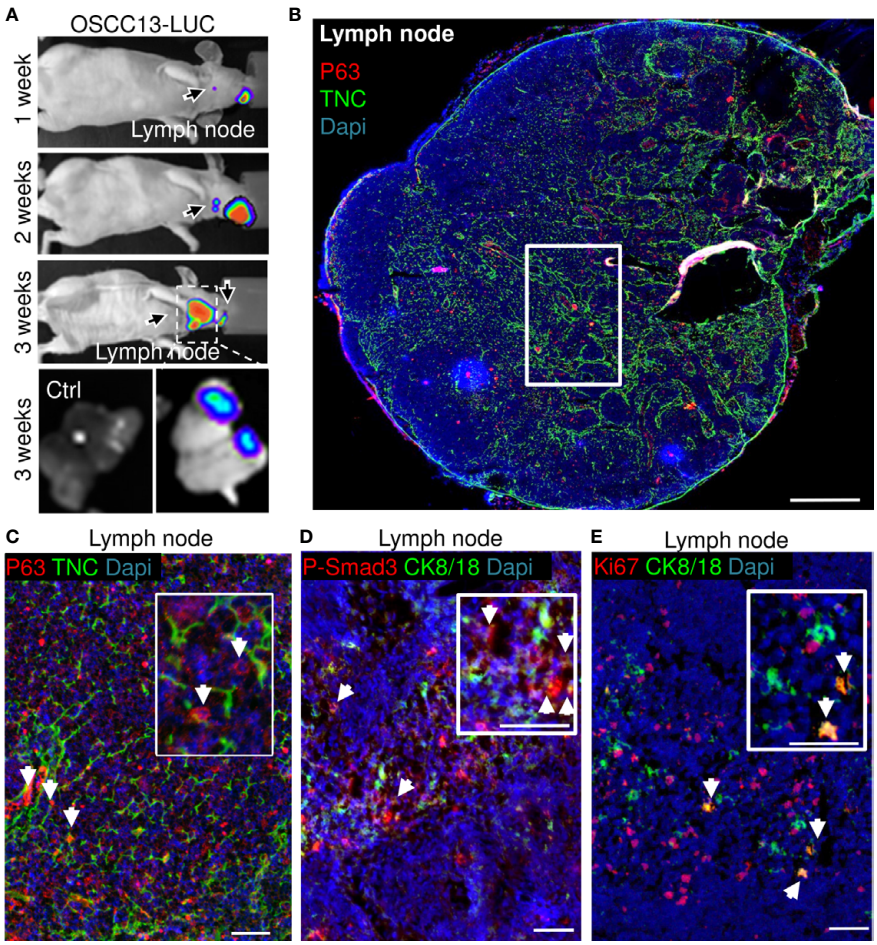

FIGURE 4 | OSCC13 tumor cells home to the local lymph nodes and expand. **(A)** Detection of luciferase expressing OSCC13 cells in the lymph node by a Nightowl imaging machine in a nude mouse and in the dissected lymph nodes. Luciferin signal in the tumor and, expanding in the lymph node from 1–3 weeks. N = 3 mice. **(B–D)**, OSCC13 cells were engrafted in a C57Bl/6J mouse. **(B)** Representative result (N = 3) of disseminated OSCC13 cells in the lymph node by p63 **(C)** and P-Smad3 **(D)** staining and proliferating CK8/18+ tumor cells by Ki67 staining **(E).** Note tumor cells (p63+) to be placed in TNC+ matrix (inlet of **C**) and proliferation of tumor cells (CK8/18+) **(E)**, confirming tumor cell expansion in the lymph nodes presumably forming metastasis in the immune competent context like in nude mice **(A)**. N = 3 mice. Scale bar, 500 µm **(B)** and 50 µm **(C–E)**. Arrows point at tumor cells.

irradiation already at 2 Gy (only 68% living cells) with a pronounced dose-dependent effect up to 10 Gy, respectively rendering only 10% cells alive after exposure to 10 Gy (**Figure 5A**). In comparison, a 2 Gy irradiation dose had no effect on proliferation of OSCC2 cells 6 days post-radiotherapy (**Supplementary Figure S2**). Cell survival of OSCC13 cells at 2 Gy was already significantly reduced compared to OSCC2 cells (surviving fraction at 2 Gy (SF2) was 0.38 and 0.94, respectively for OSCC13 and OSCC2) and decreased further, down to 0.2% and 0.9% for OSCC13 and OSCC2, respectively after 10 Gy (**Figure 5B** and **Supplementary Figure S2**). This experiment revealed that OSCC13 cells were more radiosensitive than OSCC2 cells. Therefore, we used OSCC13 cells in the following grafting and irradiation experiments.

Non-tumor bearing mice were irradiated with 2 Gy before collection of blood and enumeration of white and red blood cells 2 weeks later that indicated the absence of irradiation-induced toxicity (**Supplementary Figure S3A**). Therefore we used 2Gy to irradiate mice with OSCC13 cell (submucosal) engrafted tumors, collected the tongues 2 weeks later and investigated a potential impact of radiotherapy by tissue staining. Indeed, H&E staining revealed that a 2 Gy irradiation dose destroyed large tumor areas indicated by an altered tumor appearance and lower tumor cell density as seen by reduced H&E, p63 and DAPI staining (**Figure 5C**). We also noticed high CD45+ leukocyte abundance with different distribution patterns showing an accumulation at the tumor rim or, within the tumor center as clusters or as single cells (**Figure 5C**). Upon irradiation TIL appeared locally densely packed by a strong CD45+ signal (**Figure 5C** and **Supplementary Figure S3B**). As TNC can be induced by radiotherapy (42) we wondered whether 2 Gy irradiation had an impact on TNC expression. Whereas, TNC appeared as a regular and homogenous fibrillar network in non-irradiated (NIR) tumors as seen before (**Figure 2**), upon

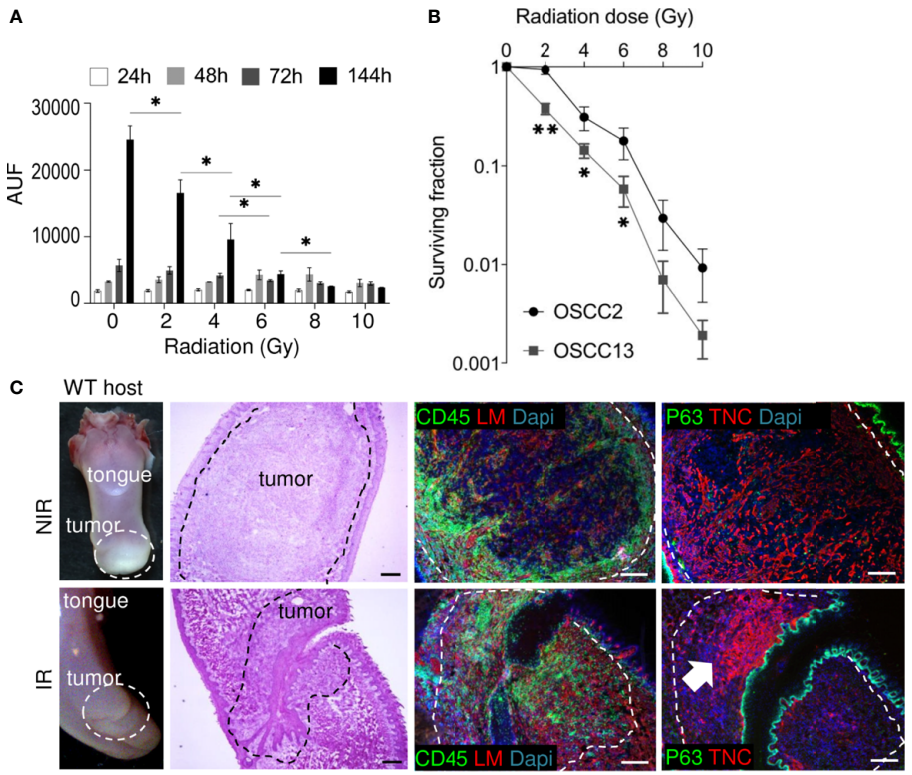

FIGURE 5 | Impact of irradiation on cultured OSCC13 cells and tumors. **(A)** OSCC13 cell proliferation upon exposure to the indicated irradiation doses after the indicated time points (hours, h) using a resazurin assay. Data are represented as mean ± SEM of at least three independent experiments. Student–Newman–Keuls test. *p < 0.05. **(B)** Clonogenic survival assessment upon exposure to the indicated irradiation doses. The surviving fractions are represented. Mean ± SD of four independent experiments. ANOVA test. **p <0.001, *p < 0.005. **(C)** Representative (N = 5) macroscopical images of H&E stained tongue tissue from OSCC13 tumors in a WT host and upon immunostaining with specific antibodies against laminin (LM, red) or TNC (red) together with CD45 (green)or p63 (green). Scale bar, 100 µm. Arrow points at dense TNC matrix seen upon irradiation. IR, irradiated; NIR, non-irradiated.

irradiation the TNC signal was largely gone (in destroyed tissue) or appeared locally as condensed matrix together with dense nuclei. We propose that thick TNC matrix and cell dense areas represent tissue that has not been killed by irradiation (**Figure 5C** and **Supplementary Figures S3B, C**).

Impact of TNC on Immunity and Radiotherapy-Induced Tumor Regression

In a tumor TNC is mostly expressed by stromal cells, but can also be expressed by immune and tumor cells (43). We used OSCC13 tumor cell grafting into a WT or TNCKO host, respectively to address the origin of TNC. We observed no TNC in tumors of a TNCKO host indicating that tumor cells poorly express TNC. Upon irradiation with 2 Gy, TNC levels increased in the irradiated tumors both in the TNCKO and WT context, however much less in the TNCKO host suggesting that the stromal cells were the major source of TNC (**Figure 6A**). Apparently, 2 Gy radiotherapy also triggered some TNC expression in the tumor cells as seen by a TNC signal in the TNCKO tumors (**Figure 6A**). As TNC can be expressed in different isoforms, we used exon junction specific primers to determine by qRTPCR whether radiotherapy had an impact on the TNC isoforms expressed by the tumor cells. Indeed cultured OSCC13 cells expressed some higher molecular weight TNC isoforms 24 h after irradiation as all primers amplified the respective alternatively spliced fibronectin type III (FNIII) domains, however the short form of TNC without the extra FNIII domains was the prominent form (**Figure 6B**). As in tumors the large isoform of TNC is highly expressed and was shown to be associated with an inflammatory pro-tumorigenic function (44) future studies have to address the potential roles of the different forms of TNC in the irradiated tumor tissue.

Next we investigated whether TNC had an impact on immunity. Therefore we investigated the abundance of different immune subtypes by flow cytometry. We observed that CD4+ and CD8+ TIL were more abundant than NK and B cells. However, no difference between tumor genotypes was seen (**Supplementary Figure S4A**). Next, we lysed the tumors and triggered T cells with a mixture of CD3 and CD28 antibodies and determined expression of cytokines 24 and 72 h later, using a cytokine cytometry bead array (CBA) assay, respectively. This analysis revealed an induction at both time points and a clear difference between tumor genotypes. Stimulated T cells from

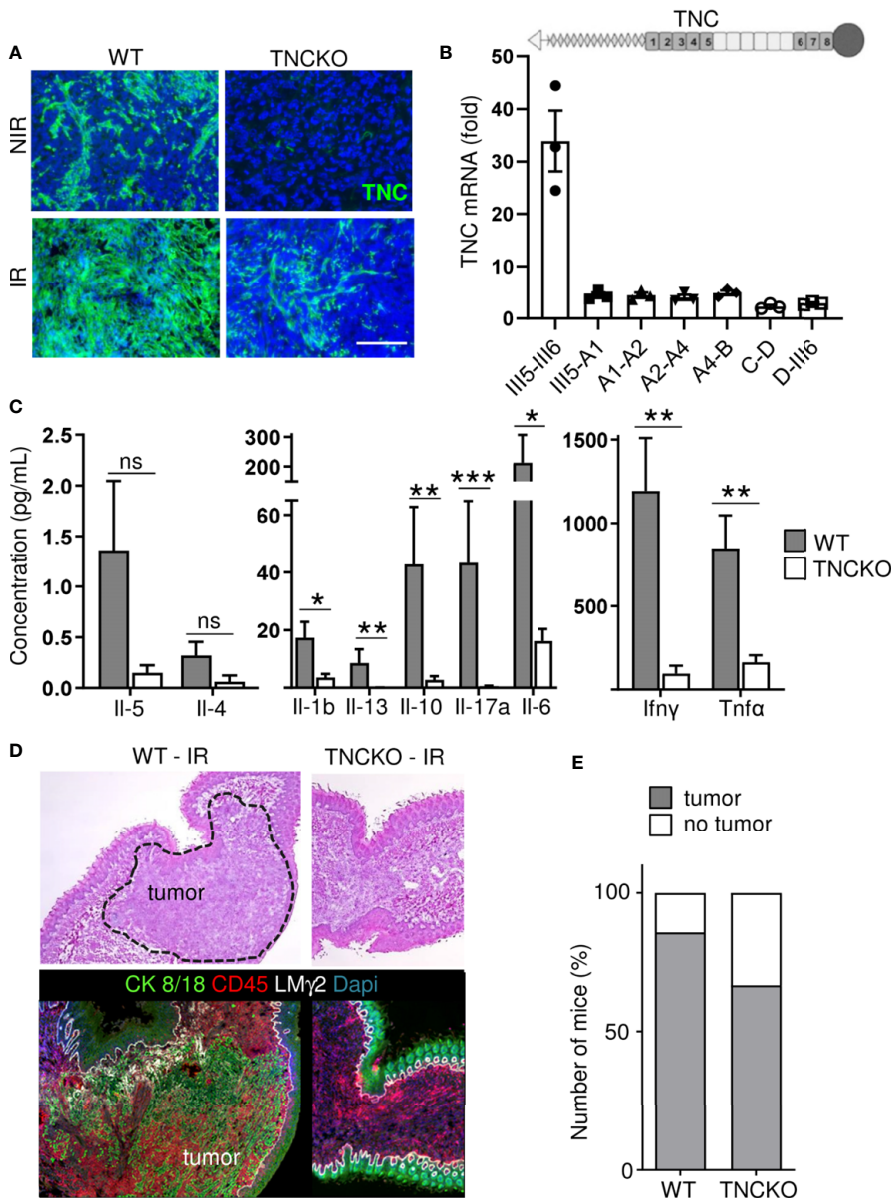

FIGURE 6 | Impact of TNC on T cell stimulation and on OSCC13 tumor abundance upon irradiation. **(A)** TNC immunostaining of non-irradiated (NIR) and irradiated (IR) tumors from WT and TNCKO mice 2 weeks upon irradiation with 2 Gy. Scale bar 100 µm. WT, N = 6, TNCKO, N = 9. **(B)** Gene expression analysis (qRTPCR) of different TNC FNIII domains (exon junctions) in OSCC13 cells 24 h upon 2 Gy irradiation (normalized to GAPDH). N = three experiments. The domain organization of TNC is schematically depicted on top with heptad oligomerization domain (triangle), FNIII domains (dark, constant, light, alternatively spliced) and fibrinogen globe (circle). **(C)** Expression of cytokines in T cells present in OSCC13 tumors from WT and TNCKO mice (2 weeks upon engraftment), 24 h after stimulation with CD3/CD28 beads, with a cytokine cytometry bead array (CBA) assay. Mean ± SEM, Mann–Whitney test, *$p < 0.05$, **$p < 0.01$, ***$p < 0.05$. **(D)** Representative H&E and immunostaining images for CK8/18 and CD45 (N = 5) of a non-irradiated and irradiated tongue from a OSCC13 tumor bearing mouse (WT or TNCKO). **(E)** Detection of tumors (by CK8/18 signal) in irradiated WT (N = 6/7) and TNCKO mice (N = 6/9); ns, not significant. Note that whereas all engrafted mice developed tumors in both genotypes, upon irradiation there was a partial regress.

TNCKO tumors expressed less Interleukin 1 beta (IL1β), IL10, IL17A, IL6, IFNγ and tumor necrosis factors α (TNFα) whereas no difference for IL4 nor IL5 was seen that were poorly expressed (**Figure 6C** and **Supplementary Figure S4B**). These results indicated that the TME in tumors of a TNCKO host may have a less inflammatory TME with less active T cells.

To address whether TNC impacted irradiation-induced tumor regression, we applied 2 Gy to OSCC13 tumors grown in a WT or TNCKO host. By staining for Dapi and CK8/18 we investigated the irradiated tissue and noticed that in the TNCKO host 30% of mice showed complete tumor regression which was less prominent in the WT host (14%) (**Figures 6D, E**). In all

other tumors we determined the tumor areas by H&E staining before and after irradiation. We noticed that tumors of both genotypes partially regressed upon irradiation but that the host genotype did not have an impact on the tumor size (measured as surface) in the given short time frame of the experiment (**Supplementary Figure S4C**).

Impact of Irradiation and TNC on CD45+ and CD206+ Immune Cell Infiltration

We compared the localization and abundance of leukocytes in OSCC13 tumors upon growth in a TNCKO host with that in a WT host by IF imaging. This showed abundant CD45+ leukocytes also in the TNCKO context within the tumors and in their direct vicinity (**Supplementary Figures S4B, D**). Upon irradiation CD45+ leukocytes also infiltrated the TNCKO tumors. In contrast to this broad infiltration in the TNCKO tumors this appeared to be more local in the WT tumors (**Supplementary Figure S4D**).

As we previously described an impact of TNC on CD206+ pro-tumoral M2 macrophages in the syngeneic NT193 breast cancer grafting model (45) we investigated the abundance and spatial distribution of CD206+ by tissue staining and subsequent quantification (**Figures 7A–D**). This experiment revealed numerous CD206+ macrophages inside the tumors and in direct tumor vicinity (**Figures 7A, B**). Whereas no difference in CD206+ macrophages was seen in WT tumors with and without irradiation TNCKO tumors showed a tendency towards less CD206+ cells after irradiation (**Figure 7C**). Determining the spatial distribution of CD206+ cells we noticed a higher inside-to-outside ratio of CD206+ macrophages in WT than TNCKO tumors. Irradiation did not impact this ratio in the given time frame (**Figure 7D**).

Altogether we have established a novel syngeneic OSCC grafting model derived from a 4NQO-induced tongue tumor that showed similarities with human OSCC by recapitulating mutations seen in human tumors, constitutive TGFβ signaling, abundant TIL within TNC-rich stroma and, spontaneous tumor cell dissemination to and expansion in the local lymph nodes. Most importantly, this model was sensitive to a 2 Gy dose of irradiation and allows not only to investigate tumor cell killing by radiotherapy but may be also useful to investigate potential rebound effects where induction of TNC could function as marker for adverse responses.

DISCUSSION

Radiotherapy is the most frequent treatment of patients with OSCC apart from surgery. Although radiotherapy kills the tumor cells, tumors relapse frequently and patients manifest with secondary tumors causing high morbidity and frequent metastasis to the local lymph nodes and lung, altogether resulting in a low 5-year survival (1). Radiotherapy and immune checkpoint therapy applied in human HNSCC cancer patients are important however, they often have either low efficiency or strong side effects (46). Therefore, novel immune competent tumor models recapitulating HNSCC-specific mutations and HNSCC-specific TME parameters are needed to better understand the targeting actions, to improve established targeting regimens and to develop novel targeting approaches.

Here we have developed a novel immune competent tongue OSCC tumor grafting model that we have investigated in detail by mutation and gene expression analysis, flow cytometry, cytokine expression analysis, extensive tissue staining and loss of function analysis. This comprehensive information on the TME and mutation phenotype has not been provided on previously published models. Mutation analysis revealed that our OSCC13 cells present mutational patterns and nucleotide substitution exchanges that recapitulate both the characteristics of tobacco- and 4NQO-induced tumor signatures. Moreover, OSCC13 cells present mutations on genes also frequently mutated in human tumors and in particular mutations in the Trp53 gene common to human HNSCC. Transcriptomic analysis of OSCC13 cells also revealed similarities in activation of signaling pathways (including TGFβ) like in many human HNSCC. Altogether the mutation pattern and gene expression profile of the OSCC13 cells is more similar to human HNSCC than other published models (24).

Although we did not detect tumor vascularization presumably due to the short duration of the experiment, important events seen in 4NQO-induced tumors were recapitulated in this model such as the development of a structured stroma with abundant matrix and TIL infiltration. We noticed effects on tumor immunity that can be considered to be anti-tumorigenic (e.g. abundant infiltration of macrophages, CD11c+ myeloid/dendritic cells, CD4+ and CD8+ TIL cells) but also pro-tumorigenic (e.g. high abundance of FRC as potential source for deposited matrix, co-localization of immune subtypes with matrix (reminiscent of retention by the matrix), numerous immune suppressive CD206+ M2 macrophages and Foxp3+ T reg cells and high PDL-1). Thus, this model could be suitable to investigate immune evolution in context of radiotherapy and/or drug targeting. Moreover, the OSCC13 tumor cells spontaneously disseminated to the local lymph nodes where they expanded demonstrating a high metastatic capacity. Whereas metastatic properties of murine OSCC cells were previously documented in a nude mouse model (47) here we described tumor cell dissemination and proliferation in the lymph nodes of immune competent OSCC13 tumor mice.

As the tumor cells expressed high PDL-1 and CTLA4 the syngeneic OSCC13 grafting model may be amenable for targeting immune checkpoints in particular in combination with radiotherapy as we have shown that OSCC13 cells and tumors are radiosensitive. Whereas irradiation experiments with human OSCC cells have previously been published in immunodeficient mice (48) to our knowledge OSCC grafting models in an immune competent host have not yet been developed for radiotherapy research. In our novel model, we have shown that OSCC13 tumors partially regressed upon exposure to 2 Gy. This model is also useful to address the effects of radiotherapy on tumor immunity as tumor cells are

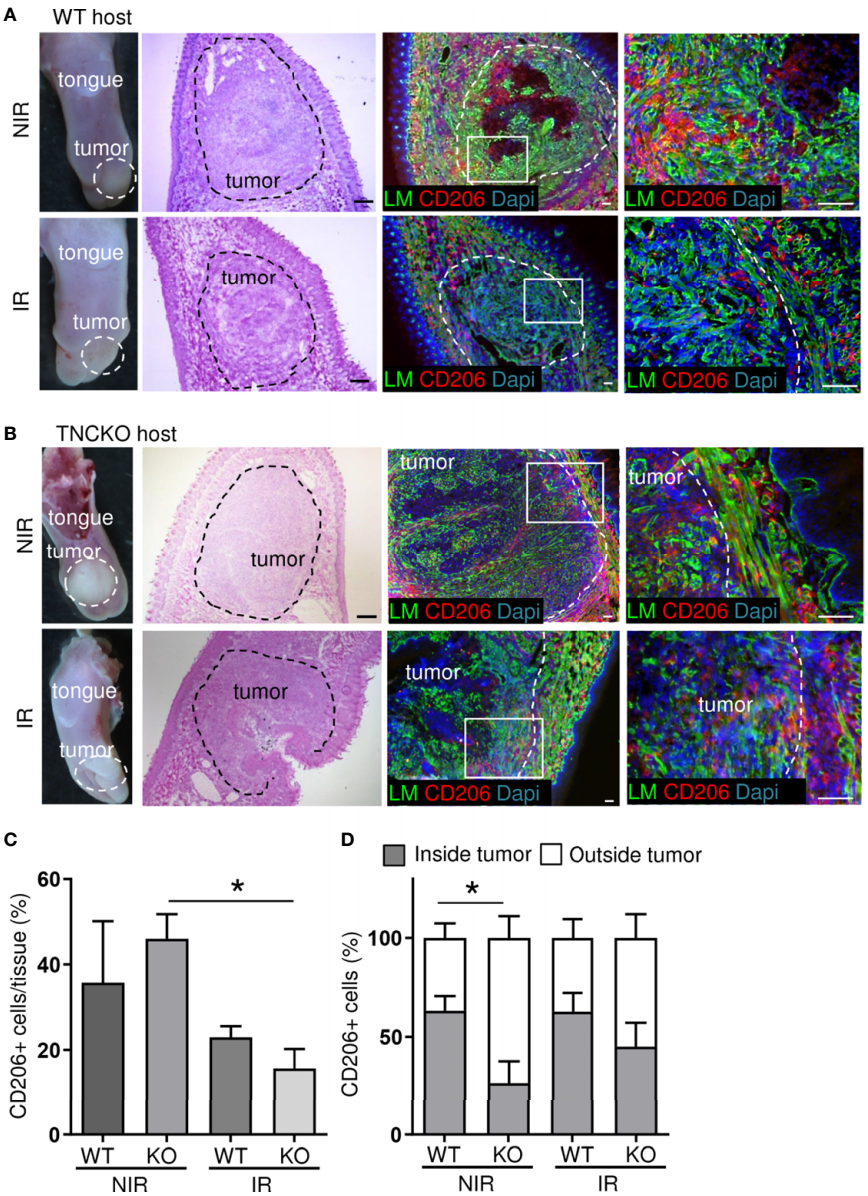

FIGURE 7 | Irradiation effects on CD206+ macrophages in OSCC13 tumors. Representative (N = 5) macroscopical images of H&E stained tongue tissue and immunostaining with specific antibodies against laminin (LM, green) and CD206 (red) in OSCC13 tumors from WT **(A)** and TNCKO mice **(B)**. Scale bar, 100 µm. **(C)** Quantification of CD206+ cells in the tongue (referenced to DAPI signal) in percentage. N = 3, mean ± SEM, non-parametric ANOVA followed by Dunns post-test, *p < 0.05. **(D)** Relative distribution of CD206+ cells inside or outside the tumor of WT and TNCKO mice in non-irradiated (NIR) and irradiated (IR) conditions, respectively. N = 3, mean ± SEM, non-parametric ANOVA followed by Dunns post-test, *p <0.05. NIR, non-irradiated mice; IR, irradiated mice.

grafted in the tongues of immune competent mice. We propose that this model may be useful for a future investigation of rebound effects (potentially enhancing lymph node metastasis) as we have seen that 2 Gy upregulated TNC. As we saw an impact of radiotherapy on dense TNC matrix expression and TIL infiltration, we speculate that TNC could serve as indicator for an immune-suppressive TME enforced by irradiation, potentially promoting tumor regrowth in the future. Here, several pathways could be involved as we saw that TNC promoted conversion of macrophages into a pro-tumoral M2 phenotype involving Toll Like Receptor 4 (TLR4) and activated C-X-C chemokine receptor type 4 (CXCR4) signaling causing immobilization of CD8+ T cells in the stroma thereby inhibiting anti-tumor immunity (17, 45, 49). Moreover, TNC profoundly shaped the TME enhancing Chemokine (C–C motif) ligand 21 (CCL21)/CCR7 signaling thereby immobilizing CD11c+ myeloid cells thus impairing their function. As inhibition of TLR4, CXCR4 and CCR7 impacted anti-tumor immunity and reduced tumorigenesis (tumor numbers, growth and metastasis) (17, 18, 45), our novel OSCC13 grafting model may be suitable to

investigate these and other alternative targeting approaches in particular in combination with radiotherapy.

Altogether, we have generated a novel immune competent OSCC grafting model recapitulating important properties of human HNSCC including HNSCC-relevant mutations, an immune-suppressive TME and radiosensitivity which opens novel opportunities for future targeting the TME and in particular the matrix in conjunction with radiotherapy and perhaps immune checkpoint targeting drugs.

DATA AVAILABILITY STATEMENT

The original contributions presented in the study are included in the article/**Supplementary Material**. Further inquiries can be directed to the corresponding authors.

ETHICS STATEMENT

The animal study was reviewed and approved by CREMEAS.

AUTHOR CONTRIBUTIONS

CS, TL, HB, CL, LP, AY, GR, CJ, CA-F, CA, FS, and NP performed experiments and analyzed data. CS, TL, HB, and GO wrote the manuscript. GN, FA, and RC supervised experiments. CS and GO designed the study, analyzed data, and revised the manuscript. NS assisted the manuscript revision. All authors contributed to the article and approved the submitted version.

FUNDING

This work was supported by INCa (FITMANET, PAIR-VADS11-023) and INCa/LNCC ECMpact (AAP2017.LNCC), ANR (AngioFib), Ligue contre le cancer (CCIRGE), University Strasbourg and INSERM to GO, Aviesan ITMO cancer (Radio-3R) to GO and GN, AAP2017.LNCC (FA), MRT fellowship to AY and fellowship from the Chinese Scholarship Council to CL.

ACKNOWLEDGMENTS

We acknowledge technical support by O. Lefebvre, A. Klein, C. Arnold, the animal facility of INSERM U1109 and the Genomax facility of INSERM U1109.

SUPPLEMENTARY MATERIAL

The Supplementary Material for this article can be found online at: https://www.frontiersin.org/articles/10.3389/fimmu.2021.636108/full#supplementary-material

REFERENCES

1. Chow LQM. Head and Neck Cancer. *New Engl J Med* (2020) 382:60–72. doi: 10.1056/NEJMra1715715
2. Argiris A, Karamouzis MV, Raben D, Ferris RL. Head and Neck Cancer. *Lancet* (2008) 371:1695–709. doi: 10.1016/S0140-6736(08)60728-X
3. Chi AC, Day TA, Neville BW. Oral Cavity and Oropharyngeal Squamous Cell Carcinoma–an Update. *CA Cancer J Clin* (2015) 65:401–21. doi: 10.3322/caac.21293
4. Castelli J, Simon A, Lafond C, Perichon N, Rigaud B, Chajon E, et al. Adaptive Radiotherapy for Head and Neck Cancer. *Acta Oncol* (2018) 57:1284–92. doi: 10.1080/0284186X.2018.1505053
5. Caudell JJ, Torres-Roca JF, Gillies RJ, Enderling H, Kim S, Rishi A, et al. The Future of Personalised Radiotherapy for Head and Neck Cancer. *Lancet Oncol* (2017) 18:e266–73. doi: 10.1016/S1470-2045(17)30252-8
6. Ray S, Cekanaviciute E, Lima IP, Sørensen BS, Costes SV. Comparing Photon and Charged Particle Therapy Using DNA Damage Biomarkers. *Int J Part Ther* (2018) 5:15–24. doi: 10.14338/IJPT-18-00018.1
7. Azzam EI, Jay-Gerin J-P, Pain D. Ionizing Radiation-Induced Metabolic Oxidative Stress and Prolonged Cell Injury. *Cancer Lett* (2012) 327:48–60. doi: 10.1016/j.canlet.2011.12.012
8. Lamberti MJ, Nigro A, Mentucci FM, Rumie Vittar NB, Casolaro V, Dal Col J. Dendritic Cells and Immunogenic Cancer Cell Death: A Combination for Improving Antitumor Immunity. *Pharmaceutics* (2020) 12:256. doi: 10.3390/pharmaceutics12030256
9. Russell JS, Brown JM. The Irradiated Tumor Microenvironment: Role of Tumor-Associated Macrophages in Vascular Recovery. *Front Physiol* (2013) 4:157. doi: 10.3389/fphys.2013.00157
10. Moeller BJ, Cao Y, Li CY, Dewhirst MW. Radiation Activates HIF-1 to Regulate Vascular Radiosensitivity in Tumors: Role of Reoxygenation, Free Radicals, and Stress Granules. *Cancer Cell* (2004) 5:429–41. doi: 10.1016/s1535-6108(04)00115-1
11. Sundquist E, Kauppila JH, Veijola J, Mroueh R, Lehenkari P, Laitinen S, et al. Tenascin-C and Fibronectin Expression Divide Early Stage Tongue Cancer Into Low- and High-Risk Groups. *Br J Cancer* (2017) 116:640–8. doi: 10.1038/bjc.2016.455
12. Midwood KS, Hussenet T, Langlois B, Orend G. Advances in Tenascin-C Biology. *Cell Mol Life Sci* (2011) 68:3175–99. doi: 10.1007/s00018-011-0783-6
13. The Extracellular Matrix and Cancer | iConcept Press, in: *The Extracellular Matrix and Cancer: Regulation of Tumor Cell Biology by Tenascin-C*. Available at: https://www.iconceptpress.com/book/the-extracellular-matrix-and-cancer–regulation-of-tumor-cell-biology-by-tenascin-c/11000138/ (Accessed August 4, 2018).
14. Langlois B, Saupe F, Rupp T, Arnold C, van der Heyden M, Orend G, et al. AngioMatrix, a Signature of the Tumor Angiogenic Switch-Specific Matrisome, Correlates With Poor Prognosis for Glioma and Colorectal Cancer Patients. *Oncotarget* (2014) 5:10529–45. doi: 10.18632/oncotarget.2470
15. Saupe F, Schwenzer A, Jia Y, Gasser I, Spenlé C, Langlois B, et al. Tenascin-C Downregulates Wnt Inhibitor Dickkopf-1, Promoting Tumorigenesis in a Neuroendocrine Tumor Model. *Cell Rep* (2013) 5:482–92. doi: 10.1016/j.celrep.2013.09.014
16. Sun Z, Velázquez-Quesada I, Murdamoothoo D, Ahowesso C, Yilmaz A, Spenlé C, et al. Tenascin-C Increases Lung Metastasis by Impacting Blood Vessel Invasions. *Matrix Biol* (2019) 83:26–47. doi: 10.1016/j.matbio.2019.07.001
17. Murdamoothoo D, Sun Z, Yilmaz A, Riegel G, Abou-Faycal C, Deligne C, et al. Tenascin-C Immobilizes Infiltrating T Lymphocytes Through CXCL12 Promoting Breast Cancer Progression. *EMBO Mol Med* (2021) n/a:e13270. doi: 10.15252/emmm.202013270
18. Spenlé C, Loustau T, Murdamoothoo D, Erne W, Beghelli-de la Forest Divonne S, Veber R, et al. Tenascin-C Orchestrates an Immune Suppressive Tumor

Microenvironment in Oral Squamous Cell Carcinoma. *Cancer Immunol Res* (2020) 8:1122–38. doi: 10.1158/2326-6066.CIR-20-0074
19. Czerninski R, Amornphimoltham P, Patel V, Molinolo AA, Gutkind JS. Targeting Mammalian Target of Rapamycin by Rapamycin Prevents Tumor Progression in an Oral-Specific Chemical Carcinogenesis Model. *Cancer Prev Res (Phila)* (2009) 2:27–36. doi: 10.1158/1940-6207.CAPR-08-0147
20. Vitale-Cross L, Czerninski R, Amornphimoltham P, Patel V, Molinolo AA, Gutkind JS. Chemical Carcinogenesis Models for Evaluating Molecular-Targeted Prevention and Treatment of Oral Cancer. *Cancer Prev Res (Phila)* (2009) 2:419–22. doi: 10.1158/1940-6207.CAPR-09-0058
21. Tang X-H, Urvalek AM, Osei-Sarfo K, Zhang T, Scognamiglio T, Gudas LJ. Gene Expression Profiling Signatures for the Diagnosis and Prevention of Oral Cavity Carcinogenesis-Genome-Wide Analysis Using RNA-Seq Technology. *Oncotarget* (2015) 6:24424–35. doi: 10.18632/oncotarget.4420
22. Badarni M, Prasad M, Balaban N, Zorea J, Yegodayev KM, Joshua B-Z, et al. Repression of AXL Expression by AP-1/JNK Blockage Overcomes Resistance to PI3Ka Therapy. *JCI Insight* (2019) 4. doi: 10.1172/jci.insight.125341
23. Elkabets M, Pazarentzos E, Juric D, Sheng Q, Pelossof RA, Brook S, et al. AXL Mediates Resistance to PI3Kα Inhibition by Activating the EGFR/PKC/mTOR Axis in Head and Neck and Esophageal Squamous Cell Carcinomas. *Cancer Cell* (2015) 27:533–46. doi: 10.1016/j.ccell.2015.03.010
24. Wang Z, Wu VH, Allevato MM, Gilardi M, He Y, Luis Callejas-Valera J, et al. Syngeneic Animal Models of Tobacco-Associated Oral Cancer Reveal the Activity of in Situ Anti-CTLA-4. *Nat Commun* (2019) 10:5546. doi: 10.1038/s41467-019-13471-0
25. Dobin A, Davis CA, Schlesinger F, Drenkow J, Zaleski C, Jha S, et al. STAR: Ultrafast Universal RNA-seq Aligner. *Bioinformatics* (2013) 29:15–21. doi: 10.1093/bioinformatics/bts635
26. Lai Z, Markovets A, Ahdesmaki M, Chapman B, Hofmann O, McEwen R, et al. VarDict: A Novel and Versatile Variant Caller for Next-Generation Sequencing in Cancer Research. *Nucleic Acids Res* (2016) 44:e108. doi: 10.1093/nar/gkw227
27. McLaren W, Gil L, Hunt SE, Riat HS, Ritchie GRS, Thormann A, et al. The Ensembl Variant Effect Predictor. *Genome Biol* (2016) 17:122. doi: 10.1186/s13059-016-0974-4
28. Lawrence MS, Sougnez C, Lichtenstein L, Cibulskis K, Lander E, Gabriel SB, et al. Comprehensive Genomic Characterization of Head and Neck Squamous Cell Carcinomas. *Nature* (2015) 517:576–82. doi: 10.1038/nature14129
29. Jay JJ, Brouwer C. Lollipops in the Clinic: Information Dense Mutation Plots for Precision Medicine. *PloS One* (2016) 11:e0160519. doi: 10.1371/journal.pone.0160519
30. Liao Y, Wang J, Jaehnig EJ, Shi Z, Zhang B. WebGestalt 2019: Gene Set Analysis Toolkit With Revamped UIs and Apis. *Nucleic Acids Res* (2019) 47:W199–205. doi: 10.1093/nar/gkz401
31. Harris MA, Clark J, Ireland A, Lomax J, Ashburner M, Foulger R, et al. The Gene Ontology (GO) Database and Informatics Resource. *Nucleic Acids Res* (2004) 32:D258–261. doi: 10.1093/nar/gkh036
32. Alexandrov LB, Ju YS, Haase K, Van Loo P, Martincorena I, Nik-Zainal S, et al. Mutational Signatures Associated With Tobacco Smoking in Human Cancer. *Science* (2016) 354:618–22. doi: 10.1126/science.aag0299
33. Ma H, Yang W, Zhang L, Liu S, Zhao M, Zhou G, et al. Interferon-Alpha Promotes Immunosuppression Through IFNAR1/STAT1 Signalling in Head and Neck Squamous Cell Carcinoma. *Br J Cancer* (2019) 120:317–30. doi: 10.1038/s41416-018-0352-y
34. White R, Malkoski S, Wang X-J. Tgfβ Signaling in Head and Neck Squamous Cell Carcinoma. *Oncogene* (2010) 29:5437–46. doi: 10.1038/onc.2010.306
35. Paluszczak J. The Significance of the Dysregulation of Canonical Wnt Signaling in Head and Neck Squamous Cell Carcinomas. *Cells* (2020) 9:E723. doi: 10.3390/cells9030723
36. Michikawa C, Uzawa N, Kayamori K, Sonoda I, Ohyama Y, Okada N, et al. Clinical Significance of Lymphatic and Blood Vessel Invasion in Oral Tongue Squamous Cell Carcinomas. *Oral Oncol* (2012) 48:320–4. doi: 10.1016/j.oraloncology.2011.11.014
37. Kinouchi M, Izumi S, Nakashiro K, Haruyama Y, Kobashi G, Uchida D, et al. Determination of the Origin of Oral Squamous Cell Carcinoma by Microarray Analysis: Squamous Epithelium or Minor Salivary Gland? *Int J Cancer* (2018) 143:2551–60. doi: 10.1002/ijc.31811
38. Spenlé C, Gasser I, Saupe F, Janssen K-P, Arnold C, Klein A, et al. Spatial Organization of the Tenascin-C Microenvironment in Experimental and Human Cancer. *Cell Adh Migr* (2015) 9:4–13. doi: 10.1080/19336918.2015.1005452
39. Bjorkdahl O, Barber KA, Brett SJ, Daly MG, Plumpton C, Elshourbagy NA, et al. Characterization of CC-Chemokine Receptor 7 Expression on Murine T Cells in Lymphoid Tissues. *Immunology* (2003) 110:170–9. doi: 10.1046/j.1365-2567.2003.01727.x
40. Noguti J, Moura CFGD, Jesus GPPD, Silva VHPD, Hossaka TA, Oshima CTF, et al. Metastasis From Oral Cancer: An Overview. *Cancer Genomics Proteomics* (2012) 9:329–35.
41. Spenlé C, Saupe F, Midwood K, Burckel H, Noel G, Orend G. Tenascin-C: Exploitation and Collateral Damage in Cancer Management. *Cell Adh Migr* (2015) 9:141–53. doi: 10.1080/19336918.2014.1000074
42. Sugyo A, Tsuji AB, Sudo H, Takano K, Kusakabe M, Higashi T. Proof of Concept Study for Increasing Tenascin-C-Targeted Drug Delivery to Tumors Previously Subjected to Therapy: X-Irradiation Increases Tumor Uptake. *Cancers (Basel)* (2020) 12:E3652. doi: 10.3390/cancers12123652
43. Yoshida T, Akatsuka T, Imanaka-Yoshida K. Tenascin-C and Integrins in Cancer. *Cell Adh Migr* (2015) 9:96–104. doi: 10.1080/19336918.2015.1008332
44. Hancox RA, Allen MD, Holliday DL, Edwards DR, Pennington CJ, Guttery DS, et al. Tumour-Associated Tenascin-C Isoforms Promote Breast Cancer Cell Invasion and Growth by Matrix Metalloproteinase-Dependent and Independent Mechanisms. *Breast Cancer Res* (2009) 11:R24. doi: 10.1186/bcr2251
45. Deligne C, Murdamoothoo D, Gammage AN, Gschwandtner M, Erne W, Loustau T, et al. Matrix-Targeting Immunotherapy Controls Tumor Growth and Spread by Switching Macrophage Phenotype. *Cancer Immunol Res* (2020) 8:368–82. doi: 10.1158/2326-6066.CIR-19-0276
46. Qian JM, Schoenfeld JD. Radiotherapy and Immunotherapy for Head and Neck Cancer: Current Evidence and Challenges. *Front Oncol* (2021) 10:608772. doi: 10.3389/fonc.2020.608772
47. Chen Y-F, Liu C-J, Lin L-H, Chou C-H, Yeh L-Y, Lin S-C, et al. Establishing of Mouse Oral Carcinoma Cell Lines Derived From Transgenic Mice and Their Use as Syngeneic Tumorigenesis Models. *BMC Cancer* (2019) 19:281. doi: 10.1186/s12885-019-5486-7
48. Shintani S, Li C, Mihara M, Terakado N, Yano J, Nakashiro K, et al. Enhancement of Tumor Radioresponse by Combined Treatment With Gefitinib (Iressa, ZD1839), an Epidermal Growth Factor Receptor Tyrosine Kinase Inhibitor, is Accompanied by Inhibition of DNA Damage Repair and Cell Growth in Oral Cancer. *Int J Cancer* (2003) 107:1030–7. doi: 10.1002/ijc.11437
49. Murdamoothoo D, Sun Z, Yilmaz A, Deligne C, Velazquez-Quesada I, Erne W, et al. Immobilization of Infiltrating Cytotoxic T Lymphocytes by Tenascin-C and CXCL12 Enhances Lung Metastasis. *EMBO Mol Med* (2021) 13(6):e13270. doi: 10.15252/emmm.202013270

Conflict of Interest: The authors declare that the research was conducted in the absence of any commercial or financial relationships that could be construed as a potential conflict of interest.

Advantages of publishing in Frontiers

OPEN ACCESS
Articles are free to read for greatest visibility and readership

FAST PUBLICATION
Around 90 days from submission to decision

HIGH QUALITY PEER-REVIEW
Rigorous, collaborative, and constructive peer-review

TRANSPARENT PEER-REVIEW
Editors and reviewers acknowledged by name on published articles

Frontiers
Avenue du Tribunal-Fédéral 34
1005 Lausanne | Switzerland

Visit us: www.frontiersin.org
Contact us: frontiersin.org/about/contact

REPRODUCIBILITY OF RESEARCH
Support open data and methods to enhance research reproducibility

DIGITAL PUBLISHING
Articles designed for optimal readership across devices

FOLLOW US
@frontiersin

IMPACT METRICS
Advanced article metrics track visibility across digital media

EXTENSIVE PROMOTION
Marketing and promotion of impactful research

LOOP RESEARCH NETWORK
Our network increases your article's readership